Engineering living materials: development of functional hybrid living materials with advanced capabilities

Anna Nikolaidou, DPhil

"Published work and a critical commentary submitted in partial fulfilment of the requirements of the University of the West of England, Bristol for the degree of Doctor of Philosophy by publication (DPhil)"

School of Architecture and Environment
College of Arts, Technology and Environment,
University of the West of England, Bristol
December 8, 2024

Abstract

The field of materials is constantly evolving. Recently, there has been a growing interest in the development of advanced materials that, upon exposure to environmental, chemical, mechanical, and electrical stimulation, exhibit capabilities such as sensing, information processing, learning, and decision-making. Advancements towards this direction include the development of advanced materials through conventional sensing technologies or the integration of biological components with synthetic components. The production of such materials presents significant challenges, including limited renewability, degradability, longevity, and durability. This research work investigates the development of materials with advanced functionalities from living components as a sustainable alternative to conventional advanced materials. It leverages the electrochemical properties and living attributes of the living cells, including self-growth, self-regulation, self-repair, and self-replication, and employs functionalisation as a method to enhance their performance. Kombucha cellulose and fungal cultures were selected as the living components due to their scalability, customisation potentials, abundance, easy accessibility, and previously reported biosensing potentials. For the fabrication of the Kombucha cellulose and fungal hybrids, the methods of fermentation and multi-organism pairing were employed. A multimodal electrical and morphological analysis was conducted, including the investigation of electrical spiking dynamics and memfractive behaviours, to provide a comprehensive understanding of the cognitive capabilities of the hybrid living materials. The experimental results demonstrated that the fungal and Kombucha hybrids present neuron–like behaviours and distinct spiking dynamics when exposed to stimulation, enabling autonomous information processing, learning, and unconventional computing. The programmable, tunable, and transformative potential of the materials makes this research work specifically original. Finally, a research framework was developed that can be applied to the creation of advanced materials from a wide range of living cells, allowing the replicability of the experiments in a structured and systematic manner. The research work has the potential to transform a diverse range of sectors, with applications spanning across a range of fields such as smart buildings, wearables, robotics, and living electronics.

Acknowledgements

I would like to express my sincere thanks and deepest gratitude to my Director of Studies, Prof Andy Adamatzky, for his continuous support and guidance in developing this work. His guidance, advice, passion for the field, expertise, constructive comments, and availability made this DPhil journey possible and have been a catalyst for my research growth and development. I would also like to thank my Supervisor, Prof Janice Kiely, for her valuable suggestions and guidance. I would like to extend my thanks to my colleagues, technical staff, and all the internal and external collaborators for their continuous support and assistance. Special thanks to my collaborators: Panagiotis Mougkogiannis, Alessandro Chiolerio, Mohammad Mahdi Dehshibi, Neil Phillips, Michail AntisthenisTsompanas, Antoni Gandia, Mona Ashtari-Majlan, Richard Mayne, and Tavs Jorgensen. Their support has been invaluable. I am grateful to David Patton for his assistance with SEM imaging. Finally, I would like to thank the University of the West of England for supporting me throughout this journey.

Contents

Page

1 Declaration **4**

2 List of Abbreviations **11**

3 Section A Outputs **12**

3.1 Bibliography of Outputs 12

4 Section B The Research Programme **15**

4.1 Introduction- Functional Materials Design 15

4.2 Aims of Research Work and Hypothesis 25

4.3 Research Question 26

4.4 Objectives 26

4.5 Hypothesis Testing 27

4.6 Scope 28

4.7 Rationale for material selection 28

4.8 Methodology and Methods 30

4.9 Limitations and mitigating risks 39

5 Section C **43**

5.1 Kombucha Cellulose [Outputs 1,2] 43

5.2 Fungal Hybrids [Outputs 3-5] 82

6 Section D - Conclusions and Outlook **98**

6.1 Key Findings and significance of work 98

6.2 Originality and Contribution to Knowledge 99

6.3 Considerations for further research 100

6.4 Possible future research directions 101

7 Publications **110**

8 Appendix **177**

Bibliography **244**

1 Declaration

The candidate declares that no parts of this submission have been submitted for another academic award or qualification at this or any other university or institute of learning. This submission is based on publications and follows the format of a DPhil submission, which includes a critical commentary and the publications submitted. The individual contribution to the research work has been reported in the publications (author's contributions statement) and includes (but not limited) conceptualisation, investigation, methodology, collection of data, data analysis, visualisation, validation, and paper writing. The required training has been completed according to the university's regulations, and the 60-credit learning has been met. The author of this thesis owns any copyright in it and has granted the University of the West of England the right to use it for any administrative, promotional, educational, and/or teaching purposes. Copies of this thesis, either in full or in extracts, may only be made available in accordance with the regulations of the library of the University of the West of England.

Word count: 21744

List of Figures

4.1 Main components of advanced materials 16
4.2 Challenges and limitations of advanced materials with conventional sensor technologies 17
4.3 Characterisation and examples of advanced bio-hybrid materials and advanced living hybrid materials 22
4.4 Properties and features of classes of advanced materials 24
4.5 Objectives and Hypothesis of research project. 27
4.6 Schematic representation of methodology and methods employed for the research work. 31
4.7 A.Fungal species *Pleurotus ostreatus* colonising substrate from hemp mat. A white mycelium network is observed. B.Culture of *Pleurotus ostreatus* fungal species inoculated on an insole from capillary matting. The insole is colonised by white and homogeneous mycelial growth. 32
4.8 Schematic representation of BC hybrids synthesised via in situ fermentation using encapsulation and injection. This method allows the entrapment of the nanoparticles and multi-species cells. 35
4.9 Plot showing sample of spikes. Adamatzky, 2018. 37
4.10 A.Example of data obtained from the recordings of the electrical activity of Kombucha and functionalised Kombucha cellulose mats using a high-resolution data logger. B.Recording of electrical activity of a Kombucha-Chlorella sample with inserted pairs of iridium-coated stainless steel sub- dermal needle electrodes. 39
4.11 Fungal hybrids and functionalised with hydrocortisone fungal hybrids subjected to X-rays and MRI scans to investigate changes in the fungal tissue before and after exposure to the chemical stimulant. 40

5.1 A.Sugared tea infusion medium where fermentation takes place. B. Formation of cellulosic film. The concentration of tea and sugar will impact the composition, density, and growth of the films. 44
5.2 Brewing of Kombucha; formation of Kombucha cellulosic films in a sugared tea solution via fermentation. 45
5.3 Growth of Kombucha-Chlorella film in sterilised Petri dish. 46
5.4 A.Glu-Arg proteinoid solution was injected into the Kombucha and Kombucha-Chlorella biofilms. B.Functionalised Kombucha-Proteinoid film section in solution to allow further growth and integration of proteinoid spheres into the film. 48

5.5 Fermentation of Kombucha film functionalised with graphene and zeolite nanoparticles. 50
5.6 A.Folded graphene-zeolite-coated Kombucha film. B.Kombucha-graphene-zeolite hybrid living film. 51
5.7 A. I-V curves measurements taken from functionalised Kombucha mat during load application of 300 g weight of cylinder form. B. I-V curves measurements taken from functionalised Kombucha mat during load application of 100 g weight of square form. 52
5.8 Diagram showing process of multi-organism pairing, functionalisation, and stimulation 53
5.9 Experimental setup and recordings of electrical spiking activity of pure Kombucha mat under 100 g square form weight application. Four pairs of iridium-coated, stainless steel subdermal needle electrodes inserted in the sample were used to record the difference of the electrical potential between the electrodes. 54
5.10 A.Capacitance, resistance, and impedance measurements taken from pure Kombucha mat prior to load application. A pair of iridium-coated stainless steel subdermal needle electrodes, with twisted cables, was inserted into the sample to allow the recording of measurements. B.Capacitance, resistance, and impedance measurements taken from pure Kombucha mat during load application of 100 g weight in cylinder form. A pair of iridium-coated stainless steel subdermal needle electrodes, with twisted cables, was inserted into the sample to allow the recording of measurements. 55
5.11 A.Current-voltage (I–V) profiling of a pure Kombucha cellulosic film B.Sweep settings used. 55
5.12 C. Current-voltage (I–V) profiling of Kombucha-Chlorella- GluArg solution. D.Graph of I-V sample profiling. 56
5.13 A.Measurements of impedance, capacitance, and resistance taken from pure Kombucha film under 600 g load application B.Measurements obtained from functionalised Kombucha-GluArg proteinoids film. 56
5.14 A.Function generator used to supply input electrical stimulants for the performance of input-output mappings. B.Experimental setup for recordings of electrical spiking activity of Kombucha film under 300 g load compression. C and D.Recordings of patterns of electrical activity using pairs of subdermal electrodes inserted into Kombucha-Chlorella films and Kombucha-Chlorella solutions. 57
5.15 SEM images of pure Kombucha film. A.The presence of multiple size yeast cells is identified, with lengths ranging from 1.93 μm to 7.76 μm. Cell bud scars, birth scars, multipolar budding, and bud-parent sites are marked in the image with red circles, yellow and red arrows, and yellow circles, respectively. Image magnification is 8000x. B.A network of cellulosic fibres with branching structure. Image magnification is 20000x. 58

5.16 SEM images of pure Kombucha film depicting microbial community of yeast and bacteria. A.Image magnification is 7000x. B.Image magnification is 7000x. C.Image magnification is 3902x. D.Image magnification is 3856x 59
5.17 SEM images of functionalised Kombucha mat. A. Clusters of zeolite crystals entangled with microbes. Image magnification is 10000x. B. Graphene-zeolite assembly formations where graphene flakes attached to zeolite crystals and yeast cells are observed. Image magnification is 10000x. C. Lower magnification image showing distribution of nanoparticles. Image magnification is 1300x. D. Yeast cells integrated into zeolite-graphene nanoparticles. Image magnification is 7000x. 61
5.18 EDS graphs of two samples collected from different sites of the functionalised Kombucha mat, showing the distribution of elements. The graphs reveal the presence of silicon (Si), aluminium (Al), and carbon (C) peaks, indicating the integration of the zeolite and graphene nanoparticles within the Kombucha mat. Additionally, the presence of fluorine (F) is observed and can be attributed to the use of PTFE solvent for the achievement of good interfacial bonding between the graphene and zeolite molecules. The gold (Au) peaks are attributed to the gold coating applied to the sample to increase its conductivity, for improved Scanning Electron Microscopy imaging. The peaks of elements in both EDS graphs follow a similar trend, indicating a homogeneous distribution of the graphene and zeolite nanoparticles in both samples and therefore, incorporation within the Kombucha matrix. 62
5.19 A.Graphene flakes integrated into zeolite crystals. Image magnification is 2500x. B.Wrinkle structural formations.Image magnification is 600x 62
5.20 Light Microscopy of Kombucha and functionalised Kombucha samples. A.Surface of functionalised Kombucha film depicting zeolite crystals and graphene flakes. Crystal size measured of 26.55 μm length. Lens: E500:X500 and E500:X2500. B.Structure of surface of pure Kombucha film. Lens: E500:X2500 and E100:X200. 63
5.21 A.Chlorella microsphere with a diameter of 4.76 μm integrated in a matrix of proteinoids and microbial cells. Image magnification is 10000x. B.Matrix of Chlorella microalgae, yeast, and bacteria cells entangled with L-Glu and L-Arg proteinoids. Image magnification is 10000x. C.Chlorella microsphere with a diameter of 3.54 μm encapsulated by proteinoids. Image magnification is 20000x. D.Chlorella microsphere with a 3.64 μm diameter encapped into a dense network of proteinoids with neuron-like formations. Image magnification is 25000x. 64
5.22 A.and B.Matrix of yeast and bacteria cells entangled with L-Glu and L-Arg proteinoids, injected into the Kombucha cellulosic film. Image magnification is 10000x. C.Proteinoid microspheres with diameter of 2.08 μm encapsulating a yeast cell of length 2.8 μm. Image magnification is 41517x. D.Image magnification is 26909x. 65

5.23 A.0.76 μm proteinoid growth identified on a yeast cell, presenting identical morphology to Kombucha yeast cell's bud-parent junctions and birth scars. Image magnification is 80000x. B.Bud-parent junctions and birth scars of diameters 1.33 μm, 0.93 μm, and 0.95 μm. Image magnification is 7000x. 66
5.24 A.Chlorella microsphere measuring 2.78 μm in diameter integrated within a network of cellulose fibers. Image magnification is 20000x. B.Chlorella microsphere measuring 3.25 μm in diameter observed in close proximity, at a distance of 0.24 μ, to a yeast cell. Image magnification is 20000x. 67
5.25 ESEM of Kombucha-Chlorella sample. Image magnification is 2000x. 67
5.26 Morphological characterisation process 68
5.27 Relationship between input and output potential for the samples. A.40% proteinoids-60% Kombucha-Chlorella. B.40% proteinoids- 60% Kombucha. C.25% proteinoids-75% Kombucha-Chlorella. D.25% proteinoids- 75% Kombucha. Samples A and C, which contain Kombucha-Chlorella, exhibit steeper slopes compared to samples B and D, which consist solely of Kombucha. Samples A and C can generate higher output potentials for the same given input potentials. The plot showcases how proteinoids-Kombucha biofilms can be optimised to improve signal transmission under various input conditions. 69
5.28 The capacitance as a function of frequency is measured for the Kombucha, Kombucha-Chlorella, Kombucha-Chlorella-proteinoids, Kombucha- proteinoids, and proteinoids samples. The capacitance of all samples decreases in a linear manner as the frequency increases. 71
5.29 Impedance measurements obtained from Kombucha, Kombucha-Chlorella, Kombucha-Chlorella-proteinoids, Kombucha-proteinoids, and proteinoids samples. Plot depicts a linear decrease in impedance until stabilised at 1.02 kHz, indicating frequency-independent impedance above 1 kHz for all samples. An exception is observed for the pure proteinoids, which exhibit a significant increase in impedance from 189.5 to 821.1 Ω within the frequency range of 34–278 kHz. 72
5.30 Boxplot comparison analysis of conductivity values for Kombucha, Kombucha-Chlorella, Kombucha-Chlorella-proteinoids, Kombucha-proteinoids, and proteinoids samples. The samples consisting of proteoinoids with Kombucha-Chlorella showed higher conductivity compared to samples containing Kombucha alone. 73
5.31 Capacitance as a function of frequency A.Kombucha response prior and under load application of 100 g, 200 g, 300 g, and 600 g. B.Kombucha-graphene-zeolite response prior and under load application of 100 g, 200 g, 300 g, and 600 g. 74

5.32 Current-voltage (I–V) profiles produced from measurements performed in the -1 V to 1 V voltage range (20 cycles) for Kombucha-Chlorella, Kombucha, Kombucha–Chlorella-proteinoids, Kombucha–proteinoids, and proteinoids samples. The I–V curves indicate 'curved'pinched hysteresis loops that are characteristic of memristive systems. 76
5.33 Hysteresis cycles showing the I-V response of the mats. Measurements taken in the -1 V to 1 V voltage range and for 20 cycles. (A)Kombucha response to the different loads and (B)functionalised Kombucha response to the different loads. 77
5.34 Statistical analysis of oscillation patterns of Kombucha-Chlorella-proteinoids sample. (a) Time-lapse voltage trace with rhythmic spikes in mV. (b) Histogram of oscillation times in seconds, with a mean of 4240.65 seconds and a median of 4068.50 seconds. (c) Histogram of spike amplitude peaks in mV, with a mean of -48.58 mV, a median of -43.25 mV, and a standard deviation of 11.09 mV. (d) Fourier transform examination of the oscillatory signal revealed prominent frequencies. 77
5.35 The dynamics of spiking after a depolarisation pulse of 50 mV. The voltage trace exhibits repeated spikes over time. 78
5.36 Analysis of a spike in terms of action potential. Adamatzky, 2018, On spiking behaviour of oyster fungi *Pleurotus djamor* 83
5.37 Examples of spike trains. (a) High frequency. (b) Low frequency. Adamatzky, 2018, On spiking behaviour of oyster fungi *Pleurotus djamor* 84
5.38 Schematic representation of methodological approach for fungal hybrid living materials. 85
5.39 A.Inoculation of hemp bedding substrate with *Pleurotus ostreatus* B.SSF and inoculation are conducted under controlled conditions. The samples are sealed in containers with air ventilation and kept in darkness at ambient room temperature. 86
5.40 A.Fungal colonisation on capillary mat. B.Fungal colonisation on hemp mat. C.Fungal hybrid living materials formed. 87
5.41 Contamination and pathogen development observed from the use of liquid culture of oyster fungi. 87
5.42 Digital visualisation and real-life image showing the experimental setup 88
5.43 Pure fungal-hemp samples and fungal-hemp-hydrocortisone samples. 89
5.44 Images depicting the experimental setup for the application and shifting of load. 90
5.45 CT scan image of fungal composite samples showing composites that received no stimulus and composites that received hydrocortisone and ethanol 2 hours before being irradiated with the beam. 91
5.46 CT scan image of fungal composite identifying segments that received hydrocortisone and ethanol. 92

5.47 A.Experimental setup of electrical activity recordings of fungal composite exposed to malt extract, dextrose, ethanol, and attachment of 50 g and 200 g. B.Experimental setup of spiking activity recordings of fungal-capillary mat insole before exposure to load compression and weight shifting. C.Experimental setup of electrical potential recordings of fungal-capillary mat insole during three modes of loading; toe, heel, and uniformly distributed. 93
5.48 Graph showing the response to application of malt extract. 93
5.49 Graphs showing potential differences under no load, even load, heel-biased, and toe-biased load. A.Spiking dynamics of Channels 1-2. B.Spiking dynamics of Channels 13-14. 95

6.1 Research framework 100
6.2 A. Inoculated lichen- substrate samples. *Flovoparmelia caperata*, *Parmotrema perlatum*, and *Xanthoria parietina* lichen species were used for the inoculation. Photograph by Simon Regan 2023. B. Exposure of lichen composites to gas emissions. 102
6.3 Statistical analysis of changes in pigmentation distribution to investigate substrate-lichen correlations and metabolic activity changes over time. 103
6.4 Fungal wearable prototype. Photo by Irina Petrova 104
6.5 Fungal wearable prototype. Photo by Irina Petrova 105
6.6 Fungal wearable prototype. Photo by Irina Petrova 106
6.7 Fungal wearable prototype. Photo by Irina Petrova 107
6.8 Digital fabrication of bio-receptive substrates that can support and sustain the growth of living communities. The images show the robotic 3D printing test system used for paste printing. In collaboration with Centre for Print Research, UWE, Bristol. 108
6.9 Robotic 3D printing of bioreceptive substrate for lichen inoculation. In collaboration with Centre for Print Research, UWE, Bristol. 109

2 List of Abbreviations

A. aceti *Acetobacter aceti*
AI Artificial Intelligence
ANNs Artificial Neural Networks
BC Bacterial Cellulose
CNNs Convolutional Neural Networks
CNT Yeast–carbon nanotubes
C. reinhardtii *Chlamydomona reinhardtii*
CT Computed tomography
EDS Energy Dispersive Spectroscopy
ELMs Engineered Living Materials
EPS Extracellular Polymeric Substances
ESEM Environmental Electron Scanning Microscopy
FFT Fast Fourier Transform
Glu-Arg L-glutamic acid and L-arginine amino acids
HOC Higher Order Complexity
MMs Mycelium Materials
MRI Magnetic resonance imaging
PANI Polyaniline
PCL Polycaprolactone
PDMS Polydimethylsiloxane
PEDOT Poly(3,4-ethylenedioxythiophene)
PEG Polyethylene glycol
PGS Polyglycerol-co-sebacate
PLA Polylactic acid
PLGA Polylactic-co-glycolic acid
PPy Polypyrrole
PTFE Polytetrafluoroethylene
PVA Polyvinyl alcohol
SCOBY Symbiotic culture of bacteria and yeast
SEM Electron Scanning Microscopy
SNNs Spiking Neural Networks
S.oneidensis *Shewanella oneidensis*

3 Section A Outputs

3.1 Bibliography of Outputs

Output 1-Journal paper

Nikolaidou, A., Mougkogiannis, P. and Adamatzky, A. (2024) **Electroactive Composite Biofilms Integrating Kombucha, Chlorella and Synthetic Proteinoid Proto–Brains**. Royal Society Open Science, 11:240238.[https://doi.org/10.1098/rsos.240238].

Output 2-Journal paper

Nikolaidou A., Chiolerio, A., Dehshibi M.M. and Adamatzky, A (2024) **Functionalising the electrical properties of Kombucha zoogleal mats for biosensing applications**. ACS Omega 2024, 9(28), 30308-30320. [https://doi.org/10.1021/acsomega.4c01227].

Output 3-Journal paper

Nikolaidou, A., Phillips, N., Tsompanas, A. and Adamatzky, A (2023) **Responsive fungal insoles for pressure detection**. Nature Scientific Reports, 13, 4595. [https://doi.org/10.1038/s41598-023-31594-9].

Output 4-Journal paper

Adamatzky, A., Nikolaidou, A., Antoni, G., Chiolerio, A. and Dehshibi, M. M. (2021) **Reactive fungal wearable**. Biosystems 199: 104304. [https://doi.org/10.1016/j.biosystems.2020.104304].

Output 5-Journal paper

Dehshibi, M. M., Chiolerio, A., Nikolaidou, A., Mayne, R., Gandia, A., Ashtari-Majlan, M., and Adamatzky, A. (2021). **Stimulating fungi *Pleurotus ostreatus* with hydrocortisone**. ACS Biomaterials Science and Engineering, 7(8), 3718-3726. [https://doi.org/10.1021/acsbiomaterials.1c00752].

Exhibition

Fungal Architectures, Arts Exhibition. 13-19 DECEMBER 2021, The Island, Bristol

Supporting Outputs- [In Appendix- Not to be assessed]

Supporting Output 1

Nikolaidou, A., Mougkogiannis, P. and Adamatzky, A. (2023) **Living Kombucha Electronics with Proteinoids**. PREPRINT available at Research Square: [https://www.researchsquare.com/article/rs-3665052/v1]. Submitted for publication to Nature Scientific Reports journal, under review.

Supporting Output 2

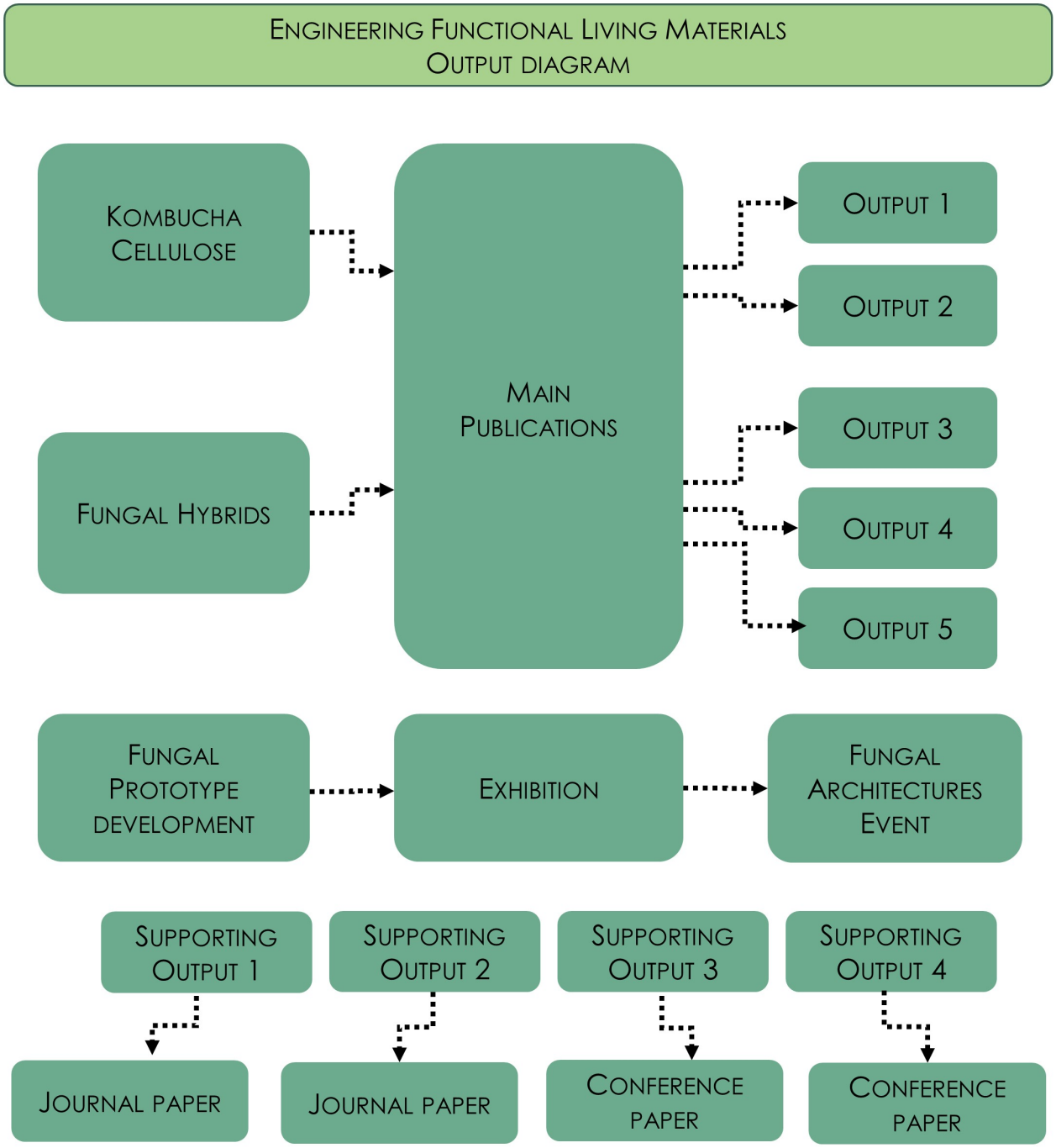
Adamatzky, A., Nikolaidou, A., Gandia, A., and Chiolerio, A. (2021). **Living wearables from slime mould and fungi**. LINKs-series, 93-98.

Supporting Output 3

Nikolaidou, A. and Jorgensen, T. (2023) **Robotic additive manufacturing of lichen composites for air quality monitoring**. Proceedings of the 37th International Conference, PLEA Rethinking Resilience, Sustainable Architecture and Urban Design, pp. 1331-1336, 24-26 June, WrocławUniversity of Science and Technology, Wrocław, Poland. ISBN 978-83-7493-275-2. [https://doi.org/10.37190/PLEA_2024]

Supporting Output 4

Nikolaidou, A. and Adamatzky, A. (2022) **Rethinking Living Matter: animate behaviours of fungal composites**. Sustainable Ecological Engineering Design for Society conference (SEEDS), Leeds Sustainability Institute.


ENGINEERING FUNCTIONAL LIVING MATERIALS
OUTPUT DIAGRAM
KOMBUCHA CELLULOSE
FUNGAL HYBRIDS
MAIN PUBLICATIONS
OUTPUT 1
OUTPUT 2
OUTPUT 3
OUTPUT 4
OUTPUT 5
FUNGAL PROTOTYPE DEVELOPMENT
EXHIBITION
FUNGAL ARCHITECTURES EVENT
SUPPORTING OUTPUT 1
SUPPORTING OUTPUT 2
SUPPORTING OUTPUT 3
SUPPORTING OUTPUT 4
JOURNAL PAPER
JOURNAL PAPER
CONFERENCE PAPER
CONFERENCE PAPER

4 Section B The Research Programme

4.1 Introduction- Functional Materials Design

The field of materials is constantly evolving. In recent years, there has been a growing interest in the development of advanced materials that exhibit capabilities that surpass the properties of conventional materials. These materials can display not only enhanced physical and mechanical properties but also unique 'intelligent' functionalities such as sensing, responsiveness to a stimulus or multiple stimulants, learning, decision-making, and adaptation. In this research work, the term advanced/functional materials refers to materials with some or all of the above capabilities. To enable sensing, memory, and information processing functionalities, the development of advanced materials usually involves the integration of electronics such as conventional sensors, actuators, and data storage systems. These materials usually incorporate a substrate, electrodes or interconnect materials, and functional or active layers (Li et al., 2020a).

The functional layers contain the active elements where primary activities, such as electrical processes, occur. The substrate serves as a solid base upon which the functional layers are deposited (Piro, Tran, and Thu, 2020; Cao and Uhrich, 2019)(Figure 4.1).

While the production of these materials has enabled advances in a plethora of fields, including personal healthcare (e.g., medical diagnostics and therapeutics), robotics, wearables, and building applications, and has accelerated the performance of complex tasks, it presents significant limitations and introduces unprecedented challenges.

4.1.1 Research problem and gap

Costs, durability, longevity, and compatibility are still factors that make materials integrated with sensor technologies challenging. Another obstacle is achieving targeted or multiple functionalities within large-area materials (Hammock et al., 2013). Flexibility and stretchability, essential for accommodating various movements, are also ongoing concerns that are being addressed in the development of highly functional materials. The most critical challenge is the substantial environmental impact of these materials, driven by issues such as low availability, limited recyclability, lack of renewability, and insufficient (bio)degradability. These factors contribute to the depletion of natural resources and the accumulation of electronic waste in the environment.

A renewable material is a substance that nature can replace at a relatively fast rate compared to the rate that it is consumed through natural processes. In contrast, a degradable material will eventually

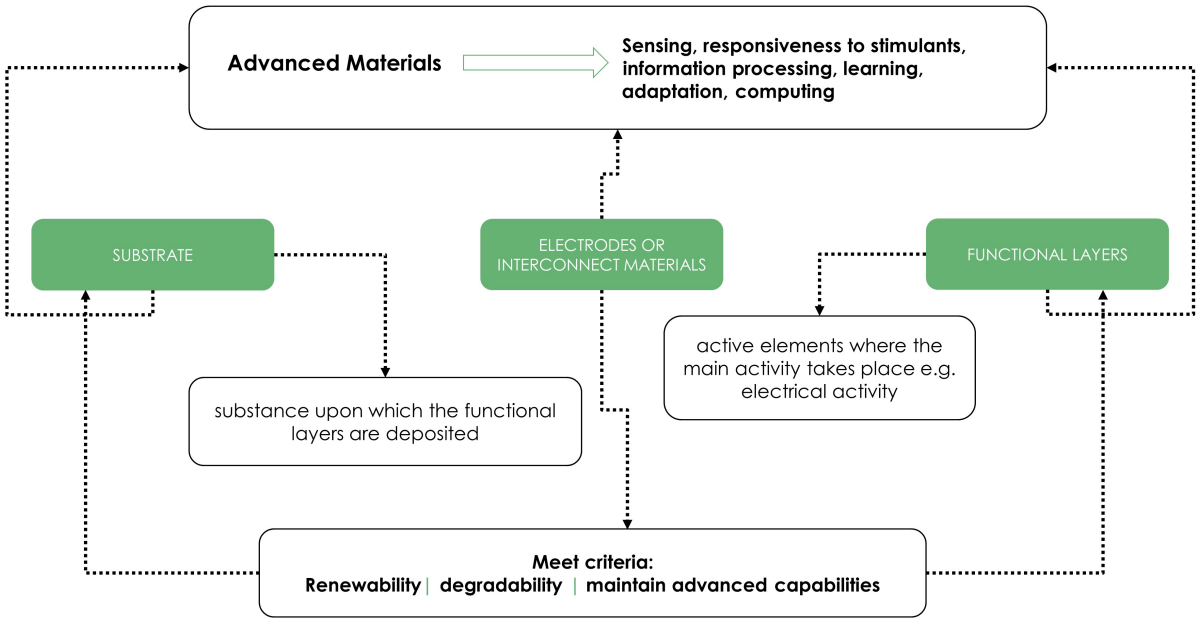


Figure 4.1: Main components of advanced materials

break down into its basic components under specific physicochemical conditions, such as temperature, pressure, and pH. Ideally, the by-products of degration should not be toxic, though this is not always the case, as some materials degrade into harmful sub-products (Piro, Tran, and Thu, 2020). Biodegradation, on the other hand, refers specifically to degradation caused by enzymatic processes resulting from cellular activity (Vert et al., 2012). The first stage of biodegradation, known as biodeterioration, occurs on the surface of materials when they are abandoned in an outdoor environment where various abiotic factors exist. The second stage, biofragmentation, involves the break down of chemical bonds, producing fragments such as oligomers or monomers. This process is classified as aerobic or anaerobic digestion, depending on the presence of oxygen. Both processes generate common by-products such as carbon dioxide and water. The third stage, assimilation, begins to occur within microbial cells (Li et al., 2020a). In Europe, the term biodegradation is defined by the EN 13432 standard, which specifies that at least 90% of a material needs to be converted to CO2 and H2O through biological actions (Costenoble, 2016).

The continued consumption and transformation of raw materials has been taking place under the assumption of a near-limitless availability of resources. Similarly, the impact of waste and pollution on climate and biodiversity was largely unaccounted for until the last decades (Nations, 1998). It has been reported that the growth in the generation of e-waste far outpaces its rate of recycling. Between 2010 and 2019, global e-waste generation increased from 5.3 to 7.3 kilograms per capita annually, while environmentally sound recycling grew at a much slower pace, from 0.8 to 1.3 kilograms per capita

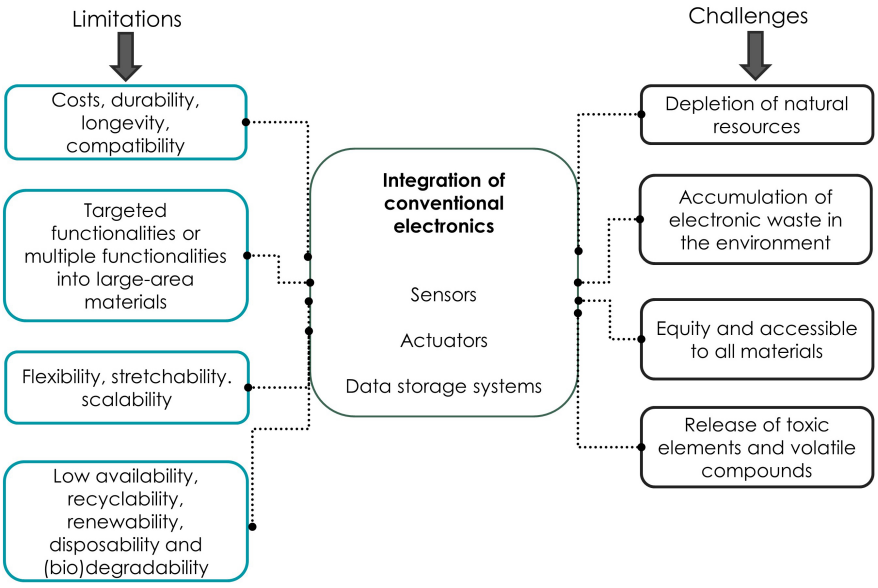


Figure 4.2: Challenges and limitations of advanced materials with conventional sensor technologies

annually (Nations, 2020). The Environmental Protection Agency estimates that only 15%–20% of electronic waste is recycled (Hileman, 2002). In addition to this, materials integrated with conventional electronics contain significant amounts of toxic elements, including mercury, arsenic, chromium, and lead. These substances can leach into soils and waterways. The incineration of plastics from e-waste can lead to the release of volatile compounds such as dioxin derivatives, polychlorinated dibenzofuran, and polychlorinated biphenyls, which are known as group 1 carcinogens (Puangprasert and Prueksasit, 2019; Guo et al., 2020)(Figure 4.2).

To lessen the environmental impact, advanced materials need to be abundant, truly renewable, and degradable while maintaining their targeted advanced functionalities and performance. Recently, there has been a growing recognition of the importance of producing such materials. Therefore, there is an urgent need for the discovery and commercialisation of innovative functional materials that allow switching current technologies to ethical and truly sustainable material choices.

4.1.2 Advanced Bio-Hybrid Materials - Non Living

Advancements towards this direction involve the development of advanced materials through biohybrid systems. Biohybrid materials are typically referred to as materials that integrate a biological component or components with a synthetic component, fabricated to selectively interact with the biological component to create a biohybrid system (Feinberg, 2015). They incorporate components from at least two distinct classes of molecules, interconnected either covalently or non-covalently, often leading to novel materials with properties superior to those of their individual components (Kopeček and Yang, 2012). The synergistic combination of two or more types of structures, deriving for example from assemblies

between materials of biological origin and inorganic materials, may produce new materials that exhibit new levels of structural organisation, novel properties, and advanced functionalities (Vandermeulen and Klok, 2004; Ruiz-Hitzky et al., 2010).

Overview on Bio-Hybrid Materials

Natural biopolymers (Choi et al., 2016; Yuan et al., 2016; Agate et al., 2018; Li et al., 2020b) and chemically synthesised polymers (Li et al., 2020b) have been utilised as substrates and/or functional layers for the production of biohybrid materials with advanced functionalities and sustainable properties. Biopolymers containing natural bioactive components offer robust mechanical properties, excellent biocompatibility, biodegradability, and multiple active binding sites, providing unique advantages for the fabrication of advanced hybrid materials (Li et al., 2020b). They can exhibit unique electrical properties, including strong electrical conductivity, high dielectric breakdown resistance, and excellent ion conduction (Li et al., 2020b). These characteristics make them ideal components for applications such as sensors, actuators, and memory devices.

Polysaccharides, proteins, polyesters, and nucleic acids, such as chitosan, cellulose, silk fibroin, keratin, and RNA, have been used as key components for the production of hybrid biomaterials for memory and sensor applications (Hosseini and Lee, 2015; Sadasivuni et al., 2015; Zhu et al., 2016; Ko et al., 2017; Jasinski et al., 2017). For example, functional polysaccharide films have been utilised as humidity sensors due to their high humidity sensitivity. This sensitivity is attributed to the formation of hydrogen bond networks between water molecules and polysaccharides, which accelerates proton transfer under humid conditions (Wang et al., 2020).

Bacterial cellulose (BC) is a versatile biomaterial used in supercapacitors as electrodes or electrolytes (Wang et al., 2016). Through pyrolysis and activation, oxygen-containing groups can be introduced on the surface of BC, enhancing its conductivity when used as electrode materials (Li et al., 2020b). Several research groups have explored the combination of BC with conducting polymers, aiming for renewable, biodegradable, and electroconductive composites (Li et al., 2014). Cellulose can be produced by pressing together moist fibers of cellulose and drying them into flexible sheets, making it an inexpensive, easily available, lightweight, and easy to process biopolymer (Cao and Uhrich, 2019). This makes it a strong candidate for substrates in advanced materials (Fortunato et al., 2008; Zschieschang et al., 2011; Peng et al., 2014; Leonat et al., 2014; Barr et al., 2011).

Keratin contains a large number of functional groups on its side chains, which enhance the chemisorption of water molecules and supports proton transfer under high humidity, making it a good biopolymer for humidity sensing (Natali et al., 2019; Hamouche et al., 2018). Chicken feathers, which consist of 90% keratin protein, are often considered waste in the food industry. However, they can make a good gate dielectric layer in biodegradable organic field-effect transistors (OFETs) (Singh et al., 2017), which are key components of many organic electronic devices (Surya et al., 2019; Kyaw et al., 2016a; Kyaw et al., 2016b).

Numerous organic semiconductors, including conjugated polymers such as polyaniline (PANI), polypyrrole (PPy), polythiophene, and poly(3,4-ethylenedioxythiophene) (PEDOT), have been developed as functional layers, interconnects or electrodes (Higgins et al., 2012; Li, Wang, and Yin, 2018) in hybrid biomaterials. Polymers with sensing capabilities- such as polyvinyl alcohol (PVA), polylactic acid (PLA), polycaprolactone (PCL), polyglycerol-co-sebacate (PGS), polyethylene glycol (PEG), polylactic-co-glycolic acid (PLGA), and polydimethylsiloxane (PDMS)- are frequently integrated as substrates into hybrid materials due to their biocompatibility and biodegradability (Cao and Uhrich, 2019).

Shellac, a natural resin originated from the secretion of female lac bug and harvested from several species of trees in India, Thailand, and China, is primarily composed of aleuritic, shellolic, and jalaric acids. It has been used as a substrate for advanced materials with electrical properties (Sharma, Shukla, Vaid, et al., 1983). Other biomaterials include carbon-based substrates, such as macroporous carbonaceous materials (Wang et al., 2014) and carbon fibers (Li et al., 2017), which are employed in applications like gas sensors (Han et al., 2019), capacitive or resistive humidity sensors (Tulliani, Inserra, and Ziegler, 2019), pressure and strain sensors (Yan, Wang, and Pan, 2018), and electrochemical sensors (Asadian, Ghalkhani, and Shahrokhian, 2019). Additionally, carbon nanotubes have been used as organic electrodes for advanced materials due to their metallic, semiconducting, and superconducting electron transport (Wang, 2005).

Silicon-based nanomaterials have been used as thin films in advanced hybrid biomaterials due to their ability to fully degrade via hydrolysis in biofluids (Kang et al., 2018). Organic materials such as textiles, paper, silk, and *Aloe vera* derivatives have also been used as substrates for electronics (Piro, Tran, and Thu, 2020; Baumgartner et al., 2017). Silk is a particular promising organic substrate material for the integration of thin-film silicon devices, as it offers great mechanical resistance, water dissolution, and biocompatibility rates (Kim et al., 2009a) that can be tuned from minutes to days through appropriate modification (Li et al., 2020a). Melanin, a naturally occurring polymer, has been shown to exhibit electronic behaviour (Cao and Uhrich, 2019). It has been reported as a biodegradable semiconducting material with good biocompatibility, making it suitable for tissue engineering applications (Bettinger et al., 2009). Indigo, a dye obtained from the plants *Indigofera tinctoria* and *Isatis tinctoria*, has been cultivated for over 4000 years in China, India, and Egypt for textile colouring. It is an intrinsically ambipolar organic semiconductor, demonstrating great potential for green organic electronics (Irimia-Vladu et al., 2012).

Integrating synthesised biodegradable active materials or electrodes with natural biodegradable substrates and -vice versa-could be a useful method to construct fully biodegradable materials with high performance. Biological hybrid materials can, therefore, serve as the foundation for a broad class of advanced materials with a wide range of functionalities. Although the above developments have led to increasingly rapid advances in the field of sensor technologies and constitute an important step towards more sustainable advanced functional materials, there are still important challenges to overcome. To

date, the use of such materials has primarily been implemented in nano- and micro-scale biomedical and bioanalytical applications, including implantable devices (Mani et al., 2007; Wang et al., 2019), health monitoring (Jayanthi, Das, and Saxena, 2017; Salek-Maghsoudi et al., 2018), drug release monitoring (Peláez et al., 2018), and forensic analysis (Yáñez-Sedeño et al., 2014; Gooch et al., 2017; Yáñez-Sedeño et al., 2019). The degradation of some of these materials requires particular conditions, which can sometimes be harsh. For instance, PLA only degrades at temperatures above 60 degrees and in a humidity-saturated environment. Consequently, if left in the environment, it will not degrade. True degradability should therefore be a point of vigilance (Piro, Tran, and Thu, 2020). Additionally, although this class of advanced materials integrates biological components, they present limited renewability, longevity, and durability. Since these materials are non-living, they cannot grow, replicate, repair, or self-assemble. Their operation spans within a precise lifetime, and maintenance or component replacement may be necessary during their functional lifetime.

4.1.3 Living Hybrid Materials

Over the last 4.5 billion years, living systems have developed materials with advanced capabilities, creating biological structures for the modification of their environment and survival (Nguyen et al., 2018). Living cells carry out their biological functions by sensing and responding to a wide variety of signals. These signals include nutrients, attractants and repellents, environmental stressors, and many other biological stimuli (Inda and Lu, 2020). A complex network of signal transduction pathways within the cell ensures that these signals are relayed to downstream regulators, which then trigger appropriate responses (Cantley et al., 2014). There are trillions of living biological computers on, inside, and around the human body: microbes. The term microbe, or microorganism, refers to micron-scale living organisms, including bacteria, yeast, and fungi (Pataranutaporn et al., 2020).

Natural biological systems are capable of sensing environmental conditions and responding to them on multiple scales (Teague, Guye, and Weiss, 2016). Living systems also possess distinctive features that endow them with intrinsic advantages for the manufacture of advanced materials. These include their capacity to grow autonomously into structured bulk materials without human intervention, to self-regenerate and degrade the components that they produce, thereby possessing a sustainable life cycle for the entire material, and to provide complex responses to environmental stimuli (Wang et al., 2022). In addition to the above features, they exhibit living attributes such as self-growth, self-regulation, self-repair, and self-replication, making them excellent candidates for the development of materials with reduced environmental impact compared to conventional materials.

Living systems usually adopt an intelligent combination of numerous parallel functional processes to respond to their environment. These processes are mutually and dynamically connected to each other in optimised harmony (Ruiz-Hitzky et al., 2010). One of the most striking molecular-scale differences between living and inanimate materials lies in the nature of their chemical bonding. In living sys-

tems, molecules are generally dynamic in their conformation and interact with other molecules through weak interactions such as hydrogen bonding and hydrophobic forces. This enables information to be transmitted from place to place and allows molecular entities to be assembled and disassembled on demand (Ball, 2021).

The above exceptional properties and capabilities make living cells highly attractive as functional components for the development of advanced materials.

Engineered Living Materials

An emerging area of living hybrid materials that has attracted interest in the scientific community is Engineered Living Materials (ELMs). ELMs are defined as materials composed of living cells that either form or assemble the material itself, or modulate its functional performance in some manner (Nguyen et al., 2018). ELMs can exhibit animate capabilities similar to those of advanced bio-hybrid materials mentioned above, such as being active- they can change their properties or perform actions- and adaptive- they can sense changes in their environment and respond to them (Miodownik, Morris, et al., 2021). In addition to the above functionalities, because ELMs are living, they can also be autonomous, capable of initiating a response without external control, and allow for significant programmed stimulus-responsive changes over the viable lifetime of the cellular components (Miodownik, Morris, et al., 2021). Living cells can act as stimulus-responsive elements, recognising environmental signals to activate pre-designed functions (Rivera-Tarazona, Campbell, and Ware, 2021). Environmental and self-generated signals can therefore provide the inputs for networks that operate like algorithms within living cells, producing outputs that enable the organism to survive or adapt (Bray, 2009). This process is analogous to conventional computing and can be referred to as unconventional computing, as computation can be defined as a physical process with the purpose of processing information (Adamatzky, 2021a).

A key difference between ELMs and other bio-hybrid materials lies in the role of living cells. In ELMs, living cells act as materials factories, drawing upon energy feedstocks from their environment to create biopolymeric building blocks and direct the formation or maintenance of the desired material (Nguyen et al., 2018).

Living hybrid materials are ELMs that contain both living organisms and abiotic components. They retain the living attributes of living systems, while the abiotic components enhance the material performance in terms of mechanical strength, physicochemical, and electrical properties (Wang et al., 2022)(Figure 4.3). The incorporation of exogenous materials with distinct features into cells provides an attractive method for upgrading living systems with characteristics that are neither inherent nor naturally achievable. This approach improves material properties and enhances or supplements the intrinsic functions of living cells (Wang et al., 2022)(Figure 4.4).

In recent years, there has been a growing body of work within the scientific community that recognises the potential of living cells as functional layers and/or substrates for the development of materials

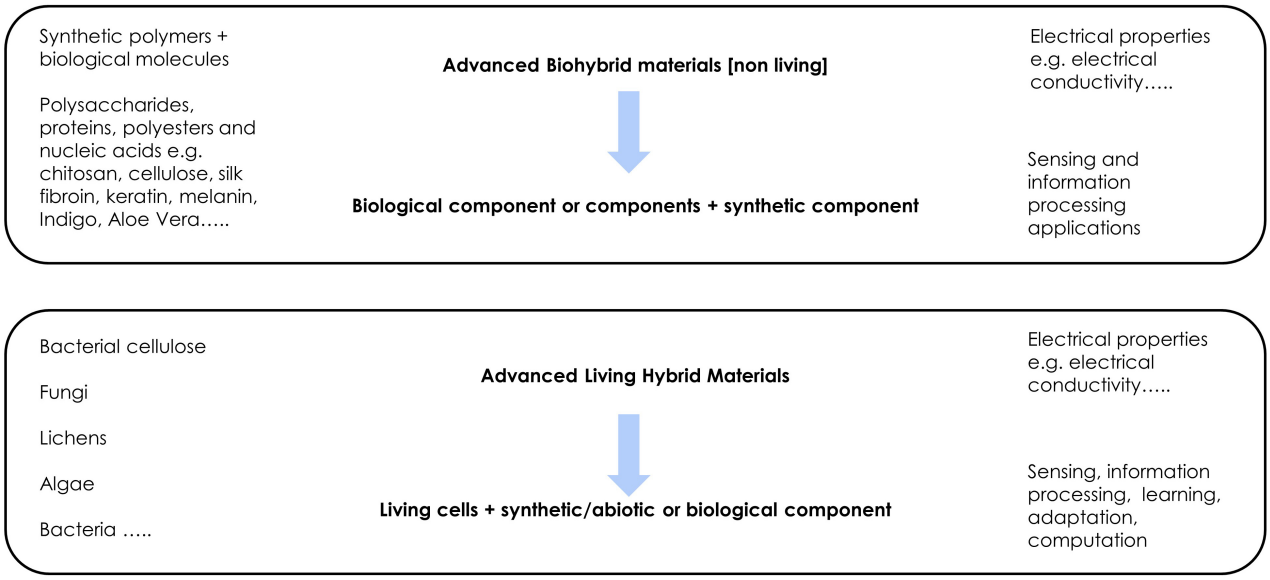


Figure 4.3: Characterisation and examples of advanced bio-hybrid materials and advanced living hybrid materials

with advanced capabilities. These include sensing external stimuli, information processing, unconventional computing, learning, and adaptation, enabling applications across diverse fields. A summary of the main breakthroughs in living hybrid materials is presented below.

Overview on Living Hybrid Materials

The use of living bacteria for the development of advanced hybrid living materials is an emerging field of research with great potential. Examples include the development of biofilms from Gram-positive bacteria, Gram-negative bacteria, and yeast, which act as humidity-triggered actuators for wearable devices actuated by the sweat of the wearer (Wang and Yao, 2017). Electroactive bacteria such as *Shewanella oneidensis (S.oneidensis)* MR-1 have received considerable attention due to their capacity to interact with electrodes and generate bioelectricity by transporting electrons to extracellular electrodes without an exogenous mediator (Hu et al., 2020; Su et al., 2021; Bird et al., 2021). Additionally, *S.oneidensis* bacteria have been used to bind and reduce graphene oxide in solution, forming an electroactive thin film from the synergistic effects between the living cells and the graphene, resulting in improved charge storage (Yuan et al., 2013). Self-healing concrete has also been developed from living bacteria to improve the longevity of concrete structures through the repair of crack formation. Spore-forming bacteria from the Bacillus genus, including *Sporosarcina pasteurii, Bacillus cohnii, Bacillus halodurans, and Bacillus pseudofirmus* naturally secrete enzymes that break down calcium lactate and drive a reaction that precipitates calcium carbonate, effectively filling cracks (De Belie and Wang, 2016). Further advancements of this approach encapsulates the spores of the bacteria (Reekst-

ing et al., 2020; Paine et al., 2016; Davies et al., 2018) e.g.in a porous clay scaffold, which protects them from compression-induced death during the concrete drying process (Jonkers et al., 2010), in silica gel and polyurethane (Wang et al., 2012), and in metakaolin and aluminosilicate geopolymers, before incorporation into the concrete to minimise decreases in mechanical properties (Koster et al., 2015). Furthermore, bacterially produced calcium carbonate has been used as a binding material in brick fabrication to enhance structural performance (Raut, Sarode, and Lele, 2014). The combination of electroactive bacteria such as *S. oneidensis* and *Geobacter sulfurreducens* with carbon-based materials, including carbon dots (Yang et al., 2020), carbon black (Freyman et al., 2020), and graphene (Yong et al., 2014), has led to materials with enhanced conductivity.

Polymers are among the most common materials used to create matrices with living microorganisms (Nguyen et al., 2018). For instance, microorganisms have been incorporated into hydrogels during the polymerisation phase (Amao et al., 2012). Living surfaces that produce, release, or metabolise molecules in response to external stimuli represent another application of living cells for targeted functionalities. For example, self-cleaning living surfaces have been developed from fungi using a three-layer structure, including a base polymeric layer used as a mechanical support for the living cells, a living layer consisting of the habitat for the living fungi cells, and a porous top layer which allows the diffusion of nutrients and gases required for the living layer and acts as protection against the external environment (Gerber et al., 2012). Living cells have also been used for the detection of pollutants such as heavy metals (Wan et al., 2019), toxicants (Kuncová et al., 2016), hormones (Gilbert et al., 2021), and explosives (Belkin et al., 2017).

In the robotics and biomedical drug transport fields, the combination of biological living material and nonliving biomaterials has facilitated the development of biosensors and biohybrid robots (also known as biobots) (Lin, Jiang, and Shang, 2022). Biological living actuators with nonliving biomaterials can better recapitulate the microstructures and motion patterns of living organisms, with remarkable advantages such as high controllability, output force, and power density at the millimeter and smaller scales, accompanied by the potential of self-assembly, self-repair, and self-replication capabilities (Yang et al., 2018; Ceylan et al., 2017; Feinberg, 2015; Ricotti and Fujie, 2017; Shimizu et al., 2013). Living material deriving from microorganisms such as algae (Arrieta et al., 2017; Xie et al., 2016) and bacteria (Zhuang, Park, and Sitti, 2017; Barroso et al., 2015; Singh and Sitti, 2016; Park et al., 2015), have been employed for actuating biobots (Shi et al., 2016; Edwards, Wright Carlsen, and Sitti, 2013; Molaei et al., 2014; Schwarz, Medina-Sánchez, and Schmidt, 2017; Park et al., 2013), enabling responses to physicochemical stimuli (Lin, Jiang, and Shang, 2022).

An important component of bio-hybrid robots is the substrate material (Distler et al., 2020; Sun et al., 2020b; Kim and Hayward, 2012; Anand, Ali, and Saif, 2015) which provides structural support and the environment for cell growth (Lin, Jiang, and Shang, 2022). The cells are either attached to or embedded in the substrate material (Lin, Jiang, and Shang, 2022). Bioinert polymers (Tanaka et al., 2019; Vannozzi et al., 2015; Lind et al., 2017; Abadi et al., 2018) such as PDMS elastomer (Lin, Jiang,

Properties	Conventional Materials [sensor technologies]	Biological Hybrid Materials [non-living]	Living Hybrid Materials
Biocompatibility	Limited	Depending on biological & synthetic components	Excellent
Biodegradability	Limited	Depending on biological & synthetic components	Excellent; self-degrade, self-dissolve
Renewability	Limited	Low	Self-grow, self-replicate, self-assembly
Durability & Longevity	Low; short lifespan, battery-powered	Medium; operation with precisely defined lifetime, maintenance required	High; self-heal, self-repair, self-regulate, functional lifetime can be controlled, enhanced lifespan
Cost	High Cost	High to low cost	Cost-effective synthesis and fabrication methods, material abundance
Scalability	Micro to macro scale	Nano to micro scale	Nano to macro scale
Sourcing	Limited; dependence on raw materials	Availability depending on materials	Unlimited; easily available, abundant
Potential applications	Buildings, biomedical, bioanalytical, diagnostics, robotics, wearables	Biomedical, bioanalytical, diagnostics, soft robotics, wearables	Buildings, biomedical, bioanalytical, diagnostics, robotics, wearables

Figure 4.4: Properties and features of classes of advanced materials

and Shang, 2022) and styrene-blockbutadiene-block-styrene (SBS) microgroove membrane (Hasebe et al., 2019), hydrogels (Distler et al., 2020; Sun et al., 2020b; Lam et al., 2019; Roshanbinfar et al., 2019; Annabi et al., 2013; Ramón-Azcón et al., 2013), artificial hydrogels (Hahn et al., 2006; Suh et al., 2004) and tissue-harvested biomaterials (Li et al., 2019; Morimoto, Onoe, and Takeuchi, 2019; Cvetkovic et al., 2017; Raman et al., 2017), have been used as substrate materials for microbial robots. Biologically active hydrogels, such as fibrinogen and gelatin derivatives, can provide many biological properties of natural extracellular matrices and with significantly higher availability due to their origin from living organisms. As a result, they are widely used for the fabrication of biobots (Lin, Jiang, and Shang, 2022). The microstructures of hydrogels facilitate the exchange of nutrients and gases, which are essential for cell survival, proliferation, and differentiation (Davidson et al., 2020).

Living material-based bio-hybrid robots can encapsulate sensors, drivers, actuators, and control systems into a single unit. They feature not only advantageous controllability and output force compared to conventional rigid bots but also intriguing capabilities such as self-assembly, self-repair, multi-degree of freedom, intelligent sensing, and efficient energy conversion (Lin, Jiang, and Shang, 2022).

Standard procedures for the encapsulation of living cells include sol–gel processes, which support the viability of microorganisms due to their mild conditions and the inertness of the formed silica-based materials (Avnir et al., 2006; Shea et al., 2004). Sol-gel techniques are used to encapsulate a wide variety of biological material, such as enzymes, antibodies, yeasts, lichens, plant cells, and bacteria, resulting in functional biomaterials for various biotechnological and analytical applications (Avnir

et al., 2006; Sexton et al., 2007; Kandimalla, Tripathi, and Ju, 2006). To enhance the viability of encapsulated species, the optimisation of the sol–gel process is performed by keeping a partially hydrated environment, similarly to hydrogels, or by incorporating glycerol in the silica matrix, as reported by Livage's group (Nassif et al., 2003). Freeze-drying offers an alternative to sol–gel encapsulation, enabling bio-immobilisation within the pores of materials while allowing the passage of nutrients and other fluids (Ruiz-Hitzky et al., 2010). For example, bionanocomposites with a cellular structure introduced via freeze-drying provide macroporosity, allowing the colonisation of microalgae such as *Chlorella vulgaris* and *Anabaena sp.PCC7120* (Ruiz-Hitzky et al., 2010). Diverse inorganic supports, including biologically modified ceramics (bioser), have also been used to assemble microorganisms like bacteria, yeast cells, and algae for functional applications such as biosensing. For instance, immobilising *Bacillus sphaericus* and *Saccharomyces cerevisiae* cells in a glycerol-modified biocer material that shows a macro-porous cellular structure (Böttcher et al., 2004) for the viability of cells. The electrospinning process has been used to produce fibrous materials containing living cells, offering a favourable environment for cell viability by entrapping the cells within the pores of a fiber matrix (Eroglu et al., 2012). Examples include yeast and bacterial cells encapsulated in core–shell electrospun fibers (Letnik et al., 2015; Knierim et al., 2015).

The development of hybrid living materials allows harvesting the functional properties from both the living and artificial components, leading to a wide range of advanced capabilities, including sensing, information processing, programmability, and computation for a diverse range of applications. This research project explores living materials for the development of a new class of advanced bio-hybrid material systems that harness the unique properties of living cells. These next-generation biological hybrid systems feature novel properties and advanced functionalities, derived from the synergistic characteristics of their components.

Data reported from the above studies suggest that utilising living cells for the production of truly sustainable material systems with advanced capabilities is a much fertile field of inquiry with transformative potential. To date, the existing body of research has predominately focused on micro-scale living material systems (nano-to micrometer scale), with very little research carried out on the use of living cells in macro-scale applications (meter-long scalability potential). This indicates the need to identify living materials that exhibit scaling up potential for the fabrication of hybrid living materials with advanced capabilities.

4.2 Aims of Research Work and Hypothesis

By leveraging the properties and electrochemical performance of living cells, and through their functionalisation and integration with targeted biological and synthetic materials, this research work aims to investigate the development of novel hybrid living materials with advanced functionalities upon exposure to environmental, electrical, chemical, and mechanical stimulation. The hypothesis is that

adopting this approach could enable the creation of materials capable of performing sensing, information processing, memory functions, and learning, thereby supporting computing. This advancement could unlock exciting opportunities for applications across a wide range of scales and fields.

4.3 Research Question

The overreaching research question that this work seeks to address is:

How can novel material systems be developed from living cells to generate adaptive, responsive, and autonomous functionalities when exposed to environmental, chemical, electrical, and mechanical stimulation?

The following measurable objectives are met(Figure 4.5).

4.4 Objectives

1.Fabrication and functionalisation

To test and establish protocols and fabrication approaches for the in situ development and assembly of hybrid materials using living cells.

1.1 Identify valorisation opportunities of interactions between microbial/fungal cells and biocompatible substrates.

1.2 Develop procedures for in situ material formation, establishing the breadth of conditions and optimal fabrication parameters that support the growth of the living hybrids (e.g. composition, concentrations, temperature, pH, light).

1.3 Deploy targeted nanoparticles for functionalisation and identify methods of functionalisation during cell growth.

2. Characterisation and performance of electrical activity assessment

2.1 Develop an experimental setup and establish protocols for data generation and collection.

2.2 Perform morphological and electrochemical characterisation of hybrid materials, both before and after functionalisation.

2.3 Implement electrical activity measurements.

2.4 Analyse data and interpret electrical properties to assess advanced capabilities, including sensing, information processing, decision-making, and computing functions.

3. Exposure to stimulation

3.1 Identify suitable stimuli agents for exposure and develop a detailed experimental setup for exposure procedures.

3.2 Record electrical responses and perform electrochemical characterisation of hybrids upon exposure to multiple stimuli, including environmental, chemical, and mechanical stimuli.

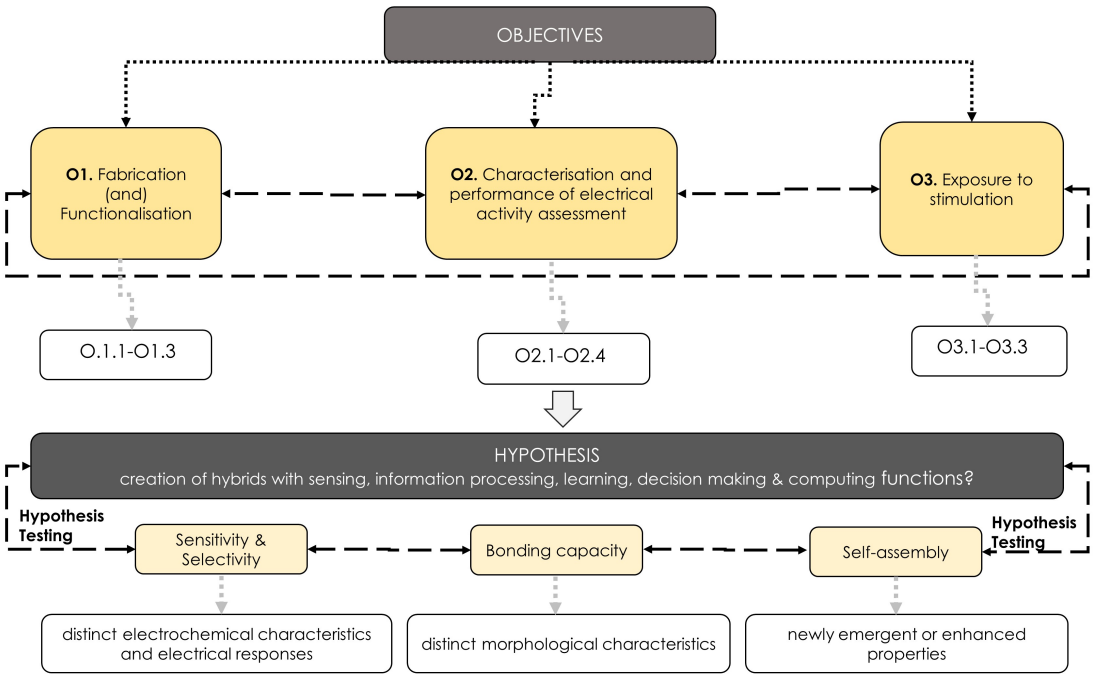


Figure 4.5: Objectives and Hypothesis of research project.

3.3 Analyse performance data to assess advanced capabilities, including sensing, information processing, learning, decision-making, and computing functions.

4.5 Hypothesis Testing

For the evaluation of the data and validation of the hypothesis, the below criteria are used:

1. Sensitivity and selectivity; evidence of distinct electrochemical characteristics and electrical responses via electrical spiking dynamics and memfractive behaviour assessment.

2. Bonding capacity; evidence of distinct morphological characteristics following functionalisation or inoculation phases, demonstrating the creation of a hybrid material through the coalesce of components (e.g.,living cells with biological or synthetic components).

3. Self-assembly; evidence of newly emergent or enhanced properties attributed to the introduction of additional components to the living cells, leading to the formation of structures with unique properties that emerge from the union of their constituent parts (Nguyen et al., 2018).

Hybrid living materials meeting the above criteria may enable the creation of material systems that exhibit dynamic behaviours and nontrivial emergent properties, akin to natural morphogenetic processes (Teague, Guye, and Weiss, 2016). The strategies that are employed in nature for morphogenesis are classified into four motifs: the French Flag model, phase separation, rule-based mechanisms, and Turing pattern models (Scholes and Isalan, 2017). For the phase separation motif, cells self-organise

based on their propensity to associate or adhere (Steinberg, 2007). Also referred to as differential adhesion, different cell types coalesce and separate to form diffuse granular patterns (Teague, Guye, and Weiss, 2016). Rule-based mechanisms encompass those mechanisms in which simple rules, such as cell morphology, growth dynamics, or death, lead to large-scale, self-generated patterns (Teague, Guye, and Weiss, 2016). For example, fractal formation of bacterial populations (Rudge et al., 2013; Ben-Jacob et al., 1994; Ben-Jacob et al., 1995), branching of colonies (Sánchez et al., 2004; Nieminen et al., 2013), and wrinkling architectures in biofilms (Asally et al., 2012).

4.6 Scope

The purpose of this research programme is to explore the development of hybrid materials from living communities and contribute to a deeper understanding of their cognitive potentials, including sensing, information processing, learning, and decision-making functionalities. It is important for the reader to note that the scope of this work is not limited to a specific discipline or field of application. However, the selection of the living communities (please refer to the section below for the rationale) was conducted on a scalability basis, providing opportunities for applications across a wide range of disciplines, including architecture, wearables, robotics, and healthcare. As a result, this program adopts a highly interdisciplinary and curiosity-driven approach with transformative potential, an approach that could unlock new material forms and functions.

4.7 Rationale for material selection

Given that living cells are unlimited and display the unprecedented complexity that biology is capable of producing, the selected living materials in this body of research work had to conform with the following fundamental principles:

1. must fabricate or direct the assembly of the bulk material.
2. must be abundant and provide easy accessibility.
3. must exhibit scalability potential, enabling production across various scales, from micro-sised to meter-scale systems.
4. can be grown and molded into various self-standing shapes and sizes.
5. must provide potential for biosensing.
6. the self-growing material may be fabricated close to its final form, requiring minimal processing.

Cellulose and Fungi meet all the above criteria and were therefore selected for conducting the research experiments.

Cellulose is the most abundant renewable organic material available in nature (Klemm et al., 2011; Moon, 2011; Tobjörk and Österbacka, 2011; Schnepp, 2013). It is produced by a wide range of living organisms, from bacteria to plants (Iguchi, Yamanaka, and Budhiono, 2000; Abeer, Mohd Amin, and

Martin, 2014; Thomas et al., 2018). BC shares the same molecular formula as plant cellulose, but with unique and sophisticated three-dimensional porous network structures (Hu et al., 2014). The bacteria secrete and assemble extracellular matrix components, in the form of polysaccharides, proteins, and DNA, during the formation of a biofilm (Branda et al., 2005). Most species of bacteria produce exopolysaccharides as an ECM components, with cellulose being one of the exopolysaccharides produced by bacteria. BC exhibits distinguished structural features and properties, including high purity, a high degree of polymerisation (up to 8000), high crystallinity (70–80%), high water content (up to 99%), and high mechanical stability, characteristics that distinguish it significantly from the plant cellulose (Barud et al., 2011).

In addition, the shape, size, and molecular structure of BC can be controlled through the alteration of the cultivation conditions, such as the type of strain, carbon source, and additives during the process of fermentation (Heßler and Klemm, 2009; Klemm et al., 2006). Existing studies have demonstrated the potential to manipulate the biogenesis of BC to produce modified BC nanofibers with controlled composition, morphology, and properties (Barud et al., 2011). Another notable feature of BC is its high aspect ratio and abundant active hydroxyl groups, which enable strong interactions with surrounding species, making it suitable for integration with various nanostructures such as inorganic and polymeric nanoparticles and nanowires (Huang and Gu, 2011). Therefore, BC offers versatile options in surface modification, a high production rate of cellulose, low production costs, flexibility, shape conformability and the ability to self-grow. Additionally, it can be produced across customised scales, including various sizes and thicknesses, making it an excellent scaffold material for biocomposite production. The electrical activity of bacterial films was reported as early as 1964 (Parker and Snyder, 1964), indicating sensing and information processing potential. Subsequent studies demonstrated that ion channels conduct long-range electrical signals within bacterial biofilms via travelling waves of potassium (Prindle et al., 2015).

Fungal materials, or mycelium materials (MMs), are considered an emerging family of environmentally friendly composites and natural polymers of fungal origin. They are primarily composed of chitin and glucan fractions, the main components of the fungal cell walls (Jones et al., 2020). They are fully biodegradable, and their production process is simple and economical, requiring a minimal knowledge of fungal biology and a basic set of tools normally used in other fungal biotechnological activities, such as kitchen fermentation processes or mushroom cultivation operations (Grimm and Wösten, 2018). Fungi can rapidly grow in situ, offering 'free' material sourcing while being renewable, abundant, and capable of decomposing quickly to return to full ecological use at the end of their lifecycle. Due to their ability to self-grow and self-repair, they display simple maintenance and low production costs.

Over the last decade, the vegetative growth of filamentous fungi, known as mycelium, has attracted increasing academic and commercial interest as a new form of low energy biofabrication and waste upcycling (Jones et al., 2017; Holt et al., 2012; Pelletier et al., 2013; Nawawi et al., 2019). Mycelium can

be cultivated from agricultural waste and molded into various shapes. Due to its rapid growth compared to other multicellular tissues, mycelium allows for easy control of its final form while also offering the potential to modify its physicochemical properties. Additionally, fungi employ excitation dynamics, manifested in calcium waves and action-potential-like spikes, as part of their decision-making processes (Adamatzky, 2018; Slayman, Long, and Gradmann, 1976). Decision-making through calcium waves propagating in living substrates strongly relates to the theory and practice of reaction–diffusion computing (Adamatzky, 2019a). A reaction–diffusion computer is a spatially extended chemical system that processes information by transforming an input concentration profile into an output concentration profile in a deterministic and controlled manner. In reaction–diffusion computers, the data are represented by the concentration profiles of reagents, while information is transferred by propagating diffusive and phase waves. Computation is implemented via the interaction of these traveling patterns (diffusive and excitation waves), and the results are recorded as a final concentration profile. Chemical reaction–diffusion computing is among the leaders in providing experimental prototypes in the fields of unconventional and nature-inspired computing (Adamatzky, Costello, and Asai, 2005; Adamatzky, 2011; Adamatzky et al., 2012; Adamatzky, 2019a).

4.8 Methodology and Methods

The research work is scientific and the mode of inquiry is characterised by an experimental approach of testing, data collection, synthesis, evaluation, and processing protocols. It employs elements of experimental research, including the design of the specific conditions to test theories or propositions, the control of the experiments, and the collection of data to isolate the relationships between defined independent variables and dependent variables (Swanson and Holton, 2005). It seeks measurable relationships among variables to test and verify the hypotheses (Swanson and Holton, 2005). Validity and reliability are ensured throughout the project by employing specific protocols to eliminate errors regarding inferences of the experimental designs. The work is conducted under controlled conditions (laboratory setting) to ensure the validity of quantitative results. Data-driven and practice-based research methods are employed, focusing on physical experimentation and methods of monitoring. This positions the research programme within a positivist philosophical framework, where results are objective and verifiable (Salama, 2019).

The methods deployed and the rationale for the selection of methods are described below(Figure 4.6).

4.8.1 Bio-fabrication

Bio-fabrication can be defined as the production of complex living or non-living biological products from raw materials such as living cells or molecules (Adamatzky et al., 2021). For the fabrication of the advanced hybrid living materials, the approach of in situ synthesis was employed, using monoculture or

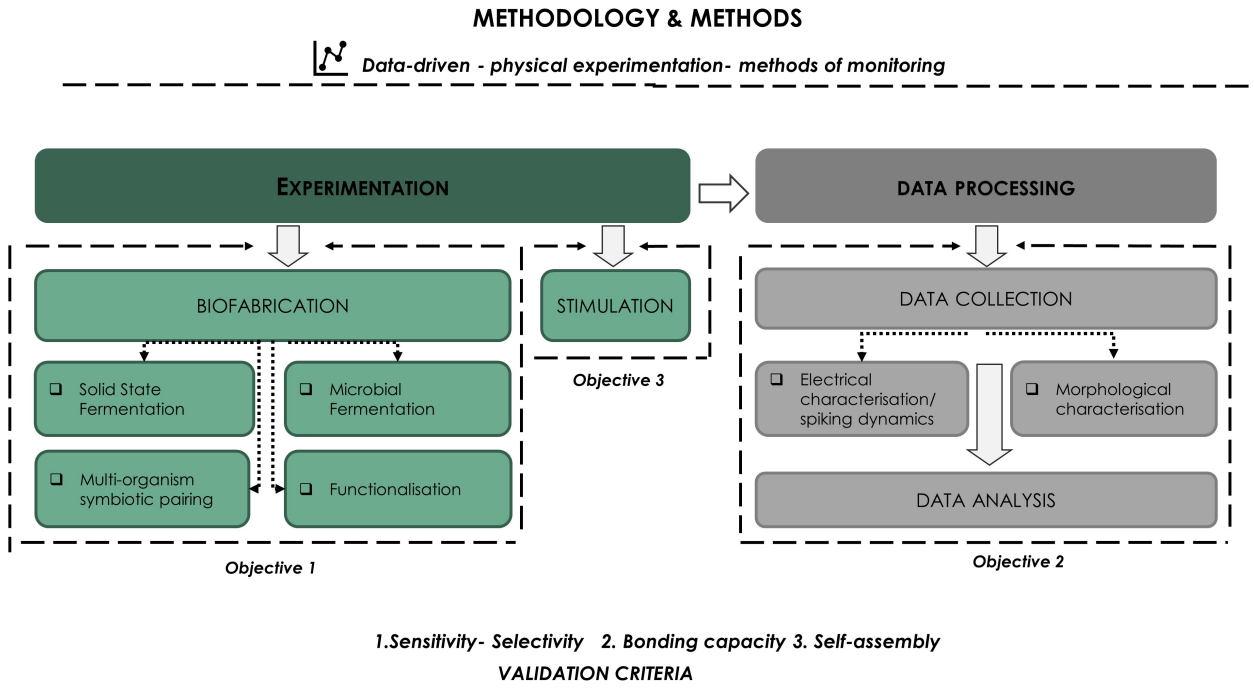


Figure 4.6: Schematic representation of methodology and methods employed for the research work.

multiculture approaches. To enhance the material's properties and achieve the desired functionalities, functionalisation processes were applied.

The below sections describe the methods and the benefits of this approach used to meet Objective 1: Fabrication and Functionalisation, and Hypothesis Validation criteria 2: Bonding capacity.

Fermentation

Fermentation is a sustainable biofabrication process that leverages the ability of microorganisms to digest nutrients and can be performed using widely accessible materials. Additionally, this method allows the growth of materials across scales and forms. As a result, the process of fermentation offers great potential for the production of the fungal and cellulosic materials and has been employed in this research work.

Solid state fermentation-Inoculation for fungal materials

Inoculation was used as a method for the in situ growth of fungal species on different substrates for the advanced fungal materials development. The fungal inoculum was deposited onto the surface of selected substrates and cultured until an homogeneous coating of white mycelial growth was observed (approximately in 3 weeks)(Figure 4.7). The formed fibrous matrix, the mycelium, formed a composite solid foamy material that surrounded, covered, and bound all the substrate particles to-

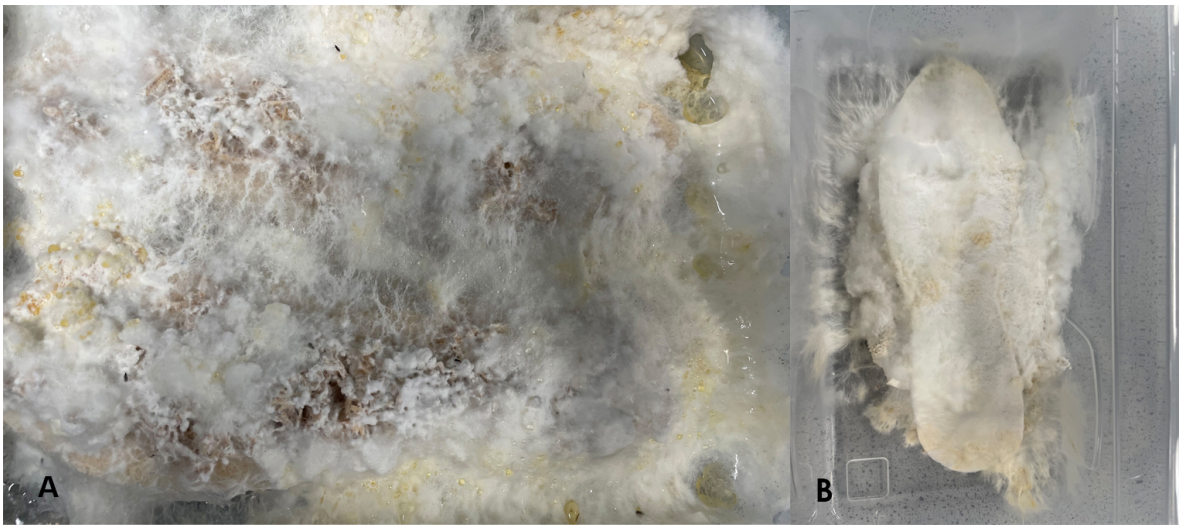


Figure 4.7: A.Fungal species *Pleurotus ostreatus* colonising substrate from hemp mat. A white mycelium network is observed. B.Culture of *Pleurotus ostreatus* fungal species inoculated on an insole from capillary matting. The insole is colonised by white and homogeneous mycelial growth.

gether (Adamatzky et al., 2021). Cultivation protocols and optimisation processes were developed through experimentation, including the inoculation of pure fungal cultures on the substrates, colonisation ability, and the establishment of the breadth of environmental conditions that support the growth (temperature, humidity and light). These measures ensured the viability of the cultures and eliminated contamination risks.

Microbial Fermentation for cellulose materials

Microbial fermentation is a biogenic process that can offer in situ fabrication of cellulosic materials, leading to new levels of structural organisation among the molecules of the material components. This process can facilitate possible self-assembly, binding, and synergetic behaviours, leading to enhanced and optimised properties.

The origins of fermentation are lost in ancient history, but it is known that both the ancient Egyptians and Sumerians had knowledge of the techniques used to convert starchy grains into alcohol (McNeil and Harvey, 2008). The fermentation process has been used for thousands of years with the fundamental purpose of making alcoholic beverages, bread, and related by-products. It is defined as a process of central metabolism in which an organism converts a carbohydrate, such as starch or sugar, into alcohol or acid (Maicas, 2020). In the 1850s and 1860s, French chemist and microbiologist Louis Pasteur became the first scientist to study fermentation, demonstrating that the process was performed by living cells (Maicas, 2020).

This method is particularly suitable for the growth of BC films. The rationale is that the films produced by the bacteria, or a combination of yeast and bacteria, present high productivity rate and

exceptional properties, making them suitable for the development of advanced living materials. Such properties include high purity, an ultra fine and highly crystalline network structure, superior mechanical strength, biodegradability, biocompatibility, large water-holding capacity, and good chemical stability (Albu et al., 2014; Shah et al., 2013). BC is also characterised by having a high water holding capacity, resulting from its very porous network that retains the water via hydrogen bonding (Gelin et al., 2007). Moreover, the structure of the cellulosic film consists of micro- and nanopores that are potentially able to hold a variety of nanoparticles, enabling the formation of interesting nanocomposites for a wide range of applications (Vitta and Thiruvengadam, 2012). Consequently, microbial fermentation can be used as a method for the immobilisation of the cellulosic films with the integration of other functional molecules during the fermentation and growth process. This approach enables in situ functionalisation and the potential assembly of new structures with novel properties that surpass those of their individual components. Finally, this method allows for the tuning of the properties of the cellulosic films, such as their composition, scale, thickness, and structure, by adjusting parameters including the fermentation time, culture medium, nutrients, temperature, oxygen availability, and pH (Hu et al., 2014; Lee and Bismarck, 2012; Ul-Islam et al., 2013).

To date, a limited number of studies have examined this method for the development of hybrid living materials, although there is an emergent number of studies leveraging the synergistic effects of microbial fermentation to create non-living advanced bio-hybrid materials from the byproducts of the process. For example, yeast fermentation has been utilised to fabricate nanocomposites with intractable polymers by harnessing the bubbles formed during the fermentation process of *Saccharomyces cerevisiae* yeast (Valentini, Bon, and Pugno, 2016). Fermentation has also been used to produce yeast–carbon nanotube (CNT) composites with improved mechanical, electrical, and optical properties compared to yeast and CNTs simply blended together. Through fermentation, *Saccharomyces cerevisiae* cells were thought to internalise and encapsulate CNTs (Valentini et al., 2016b). Yeast–graphene bionic composites with synergistic mechanical and electrical properties were successfully produced using fermentation. Graphene sheets formed an electrically conductive layer encasing the yeast cells. The composite containing living yeast cells was able to self-repair when placed back into growth medium (Valentini et al., 2016a). Synthesised BC-*Aloe vera* composite films have been developed by adding various quantities of *Aloe vera* into BC synthetic media under static conditions. The *Aloe vera* components were entrapped within the BC fibrils, resulting in a composite with superior physico-mechanical properties (Saibuatong and Phisalaphong, 2010). Similarly, multi-walled carbon nanotubes (CNTs) were added to synthetic media and incubated for two weeks. Structural analysis revealed that the CNTs were trapped between the BC fibrils (Yan et al., 2008). Several other examples of BC composite materials synthesised through the in situ fermentation strategy are also available (Chen et al., 2011; Yano et al., 2008).

The development of composite materials through the addition of nanoparticles to static BC culture presents difficulties because the particles only remain suspended in the BC synthetic media for a short

time (Shah et al., 2013). In static culture, a BC sheet is formed at the air-medium interface (Cheng, Catchmark, and Demirci, 2009). Once precipitated or settled lower in the medium, the particles can no longer be entrapped within the surface BC fibers (Shah et al., 2013). To overcome this limitation, in this research project, the nanoparticles were not added to the solution medium directly. Instead, they were inserted into the cellulose sheet via injection or encapsulation to ensure their entrapment, and the sheet was then placed into the solution to allow the continuation of the fermentation process(Figure 4.8).

Multi-organism symbiotic pairing

This method uses the division of metabolic tasks between different cells or species to simplify the production of the material as a whole via their mutualistic and complementary functions (Nguyen et al., 2018). The rationale for the selection of this method is that by co-culturing and using the dynamics of microbial consortia, the symbiotic synergies between the individual living components can unlock new material functionalities. This approach can allow the fabrication of multifunctional systems and facilitate a step-change in material development. Symbiosis refers to the relationship between two or more organisms to create conditions favourable for mutual growth and proliferation of each other, with important implications in the ecology of the system (Leavitt et al., 2015).

Examples of this method include the co-culturing of bacteria and microalgae, such as *Acetobacter aceti* and the photosynthetic microalgae *Chlamydomonas reinhardtii*. *A. aceti* produces cellulose mats at the air-water interface when grown in liquid cultures, while *C. reinhardtii* thrives in an acetate-rich medium and produces oxygen as a byproduct. By growing these two microorganisms together, researchers were able to create composite materials where the cellulose produced by *A. aceti* acts as a matrix which supports the growth and entrapment of the microalgal cells. In return, the microalgae produce oxygen, which the bacteria utilise to form cellulose uniformly within the culture medium. This mutualistic relationship results in the in situ formation of a soft biomaterial (Das et al., 2016).

Although this method exhibits very promising potential for the development of advanced hybrid living materials by leveraging the strengths of the different organisms and species, it presents some challenges that need particular attention. One of them is the control of the population size of each organism to avoid the emergence of antagonistic relationships.

Functionalisation

In situ functionalisation was used as a method for the modification, enhancement, and expansion of the electrochemical properties of the living materials by deploying targeted nanoparticles. Immobilising living microorganisms with nanomaterials is an emerging method used to form bionic composites, or in other words, composite materials that combine the advantages of both the living and nonliving worlds. When combined, living organisms provide metabolic pathways and self-organisation properties that can interact with nanomaterials, while the nanomaterials give additional functionalities to the compos-

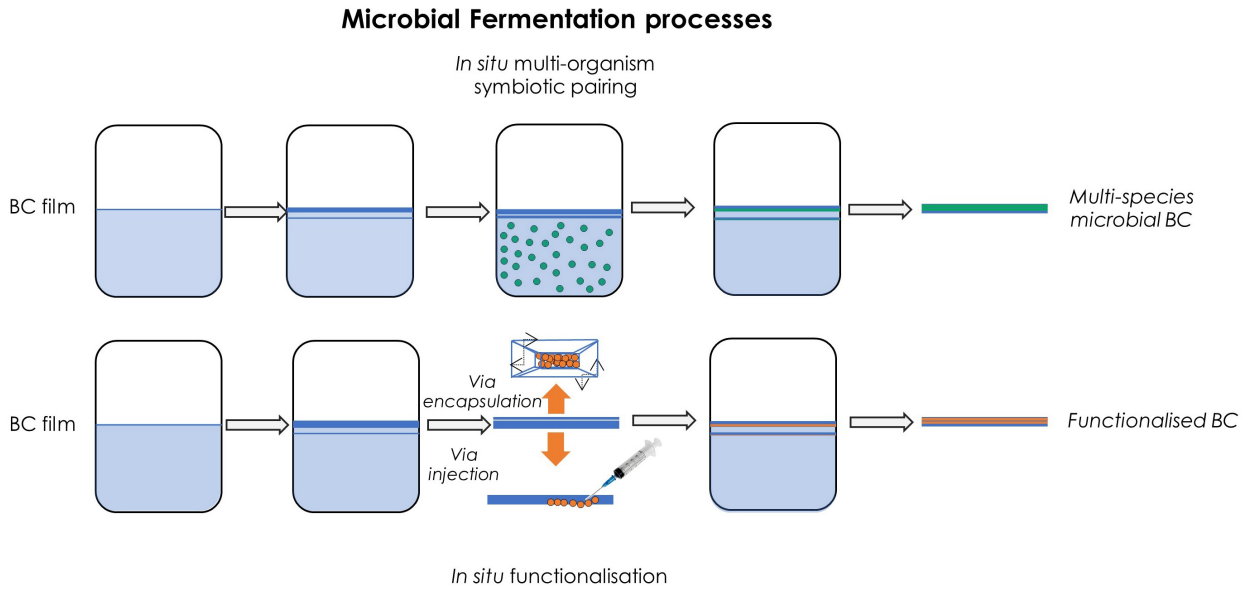


Figure 4.8: Schematic representation of BC hybrids synthesised via in situ fermentation using encapsulation and injection. This method allows the entrapment of the nanoparticles and multi-species cells.

ites, such as electronic properties (Nguyen et al., 2018). The establishment of the procedures for the synthesis of the functionalised material, binding of the particles, morphological and functional modifications was investigated in this research work. This method was used to meet Objective 1: Fabrication and Functionalisation, as well as to address Hypothesis Validation criteria 2: Bonding capacity and 3: Self-assembly.

4.8.2 Stimulation

Stimulation was used to test the materials' sensing capabilities upon exposure to environmental, chemical, electrical, and mechanical stress. Typically, the external stimuli that mediates cellular behaviour includes temperature (Piraner et al., 2017), humidity (Wang and Yao, 2017), gas molecules (Chen et al., 2021), light (Fernandez-Rodriguez et al., 2017; Zhou et al., 2022), chemicals (Liu et al., 2017; Liu et al., 2018), mechanical forces (Morales and McClean, 2017), and electrical signals (Krawczyk et al., 2020). This method was used to meet Objective 3: Exposure to stimulation, and Hypothesis Validation criteria 1: Sensitivity and Selectivity. It allowed the exploration of possible cognitive characteristics and controllability pathways, which could lead to the performance of desirable tasks.

4.8.3 Data collection and analysis

Data acquisition and analysis was performed via electrochemical characterisation, morphological characterisation, and electrical activity recordings. This approach meets Objective 2 of this research pro-

gramme and addresses Hypothesis Validation criteria 1, 2, and 3. The rationale for the selection of these methods for data collection is explained below.

Statistical analysis tools were employed to analyse the data, allowing the interpretation of the results based on the statistical significance determined (Swanson and Holton, 2005). Signal processing and measurement methods, focusing on parameters such as amplitude, hysteresis cycles, frequency, and duration of spiking activity, were deployed to extract characteristics and patterns from the electrical signal recordings and to evaluate responses both before and under varying exposure conditions. Input-output data were used for the implementation of fundamental logic operations, assessing the material's capability to perform computation and information processing functions.

Electrical characterisation and recordings of electrical activity

A multi-modal electrical analysis of the samples contributed to a comprehensive understanding of the hybrid living materials capabilities and properties. Impedance, capacitance, resistance, and current-voltage sweep measurements were taken for the electrical characterisation to assess memfractance features of the materials and evaluate possible memcapacitors, meminductors, and memristors behaviours. Additionally, recordings of electrical potential and spiking activity patterns were performed. This approach provided a unique fingerprint of electrical features and spiking dynamics before and after exposure to stimulation and was adopted to capture potential cognitive behaviours of the materials, including sensing, information processing, learning, and computing.

The reasoning is explained below:

Electrical spiking dynamics

The human brain is the best-known intelligent system, performing functions such as perception, reasoning, and control with a power consumption of nearly 20 W (Cox and Dean, 2014). Many artificial intelligence (AI) models are inspired by the brain (Yi et al., 2023). For example, Rosenblatt developed a theory for a hypothetical nervous system called a perceptron to realise binary classification of input patterns. He used this theory to address questions such as how information about the physical world is sensed, in what form it is remembered, and how information retained in memory influences recognition and behaviour (Rosenblatt, 1958). Convolutional neural networks (CNNs) have been applied to handwritten digit recognition (LeCun et al., 1998), and more recently, neural networks based on attention mechanisms using simple network architecture, dispensing with recurrence and convolutions entirely (Vaswani et al., 2017), have been researched. Although artificial neural networks (ANNs) have achieved great success in many fields (Goodfellow, Bengio, and Courville, 2016), they present drawbacks such as the consumption of huge amounts of energy (Strubell, Ganesh, and McCallum, 2019), poor robustness, and catastrophic forgetting (Chakraborty et al., 2021).

These limitations do not exist in the brain, where neurons have complex spatiotemporal dynamics,

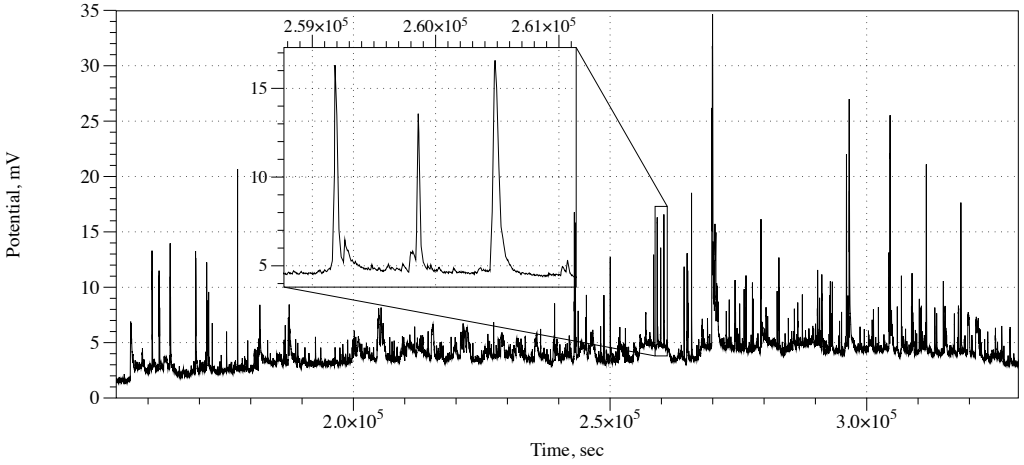


Figure 4.9: Plot showing sample of spikes. Adamatzky, 2018.

communicating and processing information through discrete spikes (Yi et al., 2023). Spiking neural networks (SNNs) mimic the way the human brain process information by taking advantage of discrete and asynchronous spikes, thus they are believed to have the capability to process spatiotemporal information efficiently (Zhu et al., 2022; Gallego et al., 2020; Paredes-Vallés, Scheper, and De Croon, 2019). Spikes of electrical potential are typically considered to be key attributes of neurons (Andres, 2015; Baslow, 2009; Pruszynski and Zylberberg, 2019), although almost all creatures without nervous system produce spikes of electrical potential (Adamatzky, 2022b), including Protozoa (Bingley, 1966; Eckert, Naitoh, and Friedman, 1972; Ooyama and Shibata, 2011), Hydrozoa (Hanson, 2021), slime moulds (Iwamura, 1949; Kamiya and Abe, 1950), plants (Fromm and Lautner, 2007; Trebacz, Dziubinska, and Krol, 2006; Zimmermann and Mithöfer, 2013), and fungi (Slayman, Long, and Gradmann, 1976).

From an information processing point of view, one of the most interesting phenomena of bioelectricity is neural spiking (Adamatzky et al., 2023). Spikes of electrical potential are the most well-known attributes of neurons linked to learning and decision-making mechanisms (Baslow, 2009; Andres, 2015; Pruszynski and Zylberberg, 2019). A train of spikes is defined as a sequence of spikes where the distance between two neighbouring spikes does not exceed the width/duration of a spike (Adamatzky, 2022a)(Figure 4.9).

Therefore, studying the generation of electrical potential and spiking activity of the hybrid living materials(Figure 4.10) can lead to conclusions regarding cognitive behaviours, such as the performance of information processing and other advanced capabilities, including computing, decision-making, and sensorial fusion functions.

Electrical characterisation

The cognitive features described above can also be found in memfractive elements. Therefore, investigating possible memfractive properties of the hybrid living materials can lead to conclusions about advanced functionalities. Memfractance can be defined as circuit elements with memory (Abdelouahab, Lozi, and Chua, 2014). Neurons are believed to be both the seat of memory and the processor of the brain; hence, memfractive elements, by combining memory with processing, could behave similarly (Gale, Lacy Costello, and Adamatzky, 2014). Neuromorphic computing is the concept of using computer components to mimic biological neural architectures, primarily the mammalian brain (Gale, Lacy Costello, and Adamatzky, 2014). In 1971, Leon Chua inferred from symmetry arguments that there should be a fourth basic circuit element to the already identified resistor, capacitor, and inductor elements, the memristor, because it behaves like a nonlinear resistor with memory (Chua, 1971). This element shows many interesting features when describing electrical phenomena, especially at small (molecular or cellular) scales, and does not depend on any particular material or physical mechanism (Abdelouahab, Lozi, and Chua, 2014).

Memristors can process many types of signals deriving from exposure to stimuli, generate various waveforms, and can be used for switching as well as for delaying signals (Chua, 1971). Additionally, a memristor's response to voltage looks similar in shape to neural responses, giving rise to emergent brain-like dynamics. (Noback and Demarest, 1981; Adamatzky et al., 2012; Gale, Costello, and Adamatzky, 2012). Memristors are similar to braincells because they also involve ionic conduction, have a short-term memory, and possess spiking dynamics. However, they differ in that memristors give current spikes in response to voltage, whereas the brain operates on (ionic) current-controlled voltage spikes. Additionally, memristors are simpler in operation than the components of the brain (Gale, Lacy Costello, and Adamatzky, 2014). Memristance is the measure of the electrical resistance in a memristor, which is capable of changing depending on the past passage of current through the device (Chua and Kang, 1976), making its resistance a function of its previous resistance (Beasley et al., 2020). The model of an optimal memristor exhibits a number of key features: (1) lobes in the positive and negative half of the cycle, and (2) a 'pinch' (or crossing) point at 0 V (Beasley et al., 2020). Memristive properties have already been reported in skin (GK et al., 2010), blood (Kosta et al., 2011), plants (Volkov et al., 2014) (including fruits (Volkov and Markin, 2017)), and slime mould (Gale, Adamatzky, and Lacy Costello, 2015).

The notion of memristive systems was later extended to capacitive and inductive elements (memcapacitors and meminductors), whose properties depend on the state and history of the system. These devices are common at the nanoscale, where the dynamical properties of electrons and ions are likely to depend on the history of the system, at least within certain time scales (Di Ventra, Pershin, and Chua, 2009).These elements (memristor, memcapacitor, and meminductor), and their combination (memfractive elements), open up new exciting functionalities that may find applications to stimulate learning,

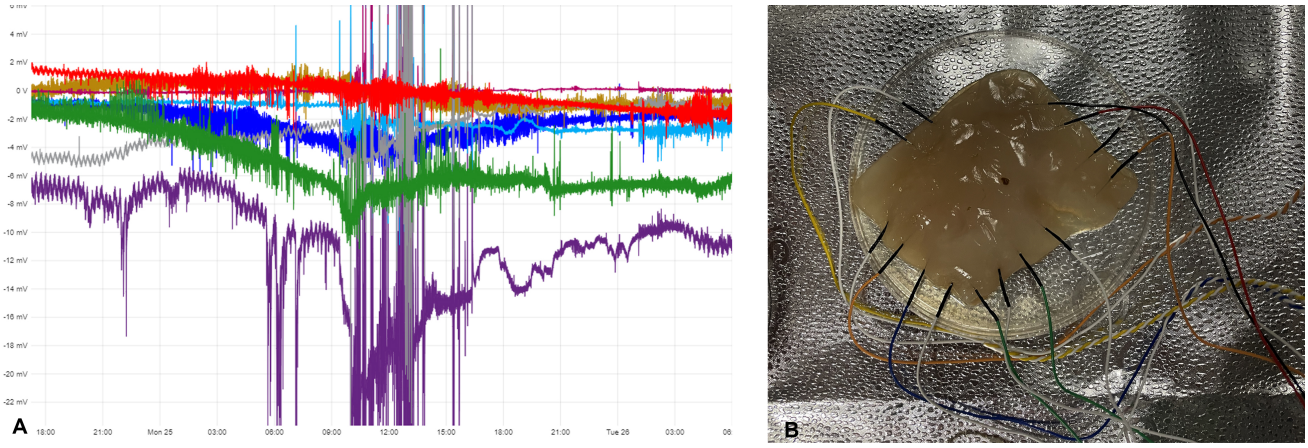


Figure 4.10: A.Example of data obtained from the recordings of the electrical activity of Kombucha and functionalised Kombucha cellulose mats using a high-resolution data logger. B.Recording of electrical activity of a Kombucha-Chlorella sample with inserted pairs of iridium-coated stainless steel subdermal needle electrodes.

adaptation, and spontaneous behaviour (Abdelouahab, Lozi, and Chua, 2014).

Morphohological and Physical characterisation

To gain a better understanding on the morphology of the materials, microstructural changes after functionalisation, the effect of the stimulants, and assess the bonding capacity of the different components, various methods of morphological and physical characterisation were employed. These included the use of X-rays, CT scans, MRI scans, Electron Scanning Microscopy (SEM), Environmental Electron Scanning Microscopy (ESEM), Digital light microscopy, and Energy Dispersive Spectroscopy (EDS). These methods are particularly useful for identifying and characterising the newly formed materials, as well as understanding the structural behaviour of their components. For each researched material, the most suitable of the above methods was used(Figure 4.11).

4.9 Limitations and mitigating risks

4.9.1 Methodological Limitations:

The potential biases or inaccuracies that the above methods may introduce are discussed below:

Living cultures and microbial consortia: The research programme relies on the use of living cultures and microbial consortia (fungal, Kombucha, and algal), which exhibit natural variability and can present slight variations in their composition (e.g., the yeast and bacteria populations in the Kombucha samples). Some inhomogeneity may be observed in the visual appearance of the samples and is a typical feature of materials produced by microorganisms. The non-uniformity observed in the growth can



Figure 4.11: Fungal hybrids and functionalised with hydrocortisone fungal hybrids subjected to X-rays and MRI scans to investigate changes in the fungal tissue before and after exposure to the chemical stimulant.

be attributed to their ongoing interactions and metabolic activities of the microbial communities. These differences may lead to subtle variations in their behaviour, such as fermentation behaviour, which can impact the properties of the material.

Environment: Minor changes in environmental conditions, such as temperature, humidity, and the type of container used for the cultivation of the samples, may influence the activity of the living communities.

Substrates: The selection of the substrates and their chemical properties for the fermentation/ inoculation phase may limit the applicability of the results. For example, a substrate used for fungal inoculation may have undergone chemical processing that can affect the fungal colonisation behaviour. A highly porous substrate might promote increased BC production or fungal growth, and potentially impact the electrical conductivity of the developed material. Additionally, findings obtained from specific substrates may not be directly transferable to other substrate types.

Contamination and pathogen development: The development of hybrid living materials is a process that involves various living microorganisms and can lead to the introduction of unwanted contaminants.

4.9.2 Empirical limitations:

The variability of the microbial systems may impact the consistency and accuracy of the results.

The above limitations may affect the reliability and generalisability of the research work. Therefore,

mitigation measures were employed to overcome them.

4.9.3 Addressing limitations and mitigating risks

To address the above limitations and minimise the risks, the below measures were taken:

- Systematic experimentation was implemented, and all experimental work was conducted under controlled laboratory conditions.
- Effective sterilisation techniques were employed to minimise the risk of contamination and ensure consistent colonisation and growth of the samples. For example, the cultivation of the samples was undertaken in sterilised containers or petri dishes within a controlled environment (hydroponic tent).
- Control experiments were performed to establish biofabrication protocols, including optimal temperature, humidity, and pH levels, which support and sustain the inoculation, colonisation, and growth of the samples. This phase also included all critical steps leading to the identification of optimisation protocols, such as substrate preparation and conditioning, extended life-support, and troubleshooting strategies to enhance stability and reliability.
- Systematic monitoring of the samples was undertaken for the early detection of any contamination and pathogen development.
- Thorough testing of substrates was employed to assess suitability for optimal growth and material formation. The integration of living cells with a diverse range of substrates was investigated to assess the generalisability of the observed effects and to identify potential substrate-specific functionalities.
- Extensive testing of living cultures and species was performed to address variability and maximise consistency. Additionally, potential variations in the density, size, and porosity of the samples could be utilised to enhance the distinct functions of the material, enabling tailored and controlled properties, such as improved interactions with functional nanomaterials. Microstructural characterisation techniques, such as Scanning Electron Microscopy, Fourier Transformed Infrared Spectroscopy Analysis, as well as further analysis of the mat's properties, could offer valuable information on correlations between inhomogeneity in growth, composition, and variations in the structure (Ramírez Tapias et al., 2020).
- The consistency of the data and accuracy of the materials' distinct responses were evaluated via repeatability of experiments and replicability tests.

- To effectively differentiate the electrical responses caused intrinsically by the living materials from those caused by external input stimuli, control recordings were conducted to evaluate the origin of the spiking activity.
- Testing and calibration of experimental setup were performed to ensure the accuracy of recordings.

The viability of the hybrid living materials, as well as the maintenance of their properties and capabilities under different environmental conditions, remains a significant limitation. This challenge needs to be addressed in future work, which falls outside the scope of this research programme.

5 Section C

Engineering functional living materials

5.1 Kombucha Cellulose [Outputs 1,2]

5.1.1 Introduction

BC is a carbohydrate polymer produced by many bacterial species (*Acetobacter xylinum, Pseudomonas, Rhizobium, E. coli*, etc.) as a structural element of their biofilm (Walker et al., 2019), and consists of ribbon-shaped ultra fine nanofibers with widths less than 100 nm (Schnepp, 2013; Bao and Li, 2012; Gao et al., 2013; Xie et al., 2012; Nyholm et al., 2011; Schnepp, 2013; Weng et al., 2015). BC inherently has a high water-retention capacity and is ultra-pure compared to plant cellulose (Hrymak and Margaritis, 2017; Fijałkowski et al., 2017). Moreover, compared to cellulose produced by plants, BC exhibits higher mechanical strength, chemical stability, and biological adaptability due to its lack of lignin, pectin, and hemicellulose polymers (Gelin et al., 2007; Tapias et al., 2022). When a community of bacteria, including acetic acid bacteria, and yeast form a symbiotic relationship, the production of cellulose is enhanced due to their synergistic microbial metabolism (Tapias et al., 2022). Such synergy can be found in Kombucha cellulose, which emerges from the fermentation of Kombucha tea.

Kombucha is a multispecies system derived from natural symbiotes and is obtained by fermenting sugared tea using a culture of bacteria and yeast, called SCOBY (Delatorre et al., 2020). It is reported to have originated in Northeast China in around 220 BC and was widely consumed during the Qin Dynasty (Dimidi et al., 2019). During the fermentation process, the microorganisms consume sucrose as the main carbon source, while the tea extract provides the nitrogen source. In the presence of oxygen, SCOBY produces organic acids, carbon dioxide, and a cellulosic floating biofilm composed of cellulose (Torgbo and Sukyai, 2018). Kombucha cellulose shows high biocompatibility due to its enhanced cell-matrix interactions, cell signaling pathways, and its ability to maintain cellular homeostasis (Patra et al., 2022).

The exact composition of the SCOBY, the type and concentration of tea and sugar used (Fu et al., 2014; Gaggıa et al., 2018), oxygen concentrations, fermentation time (Lončar et al., 2006; Chen and Liu, 2000), and temperature (Lončar et al., 2006; De Filippis et al., 2018) can all influence the composition and properties of the Kombucha cellulose films(Figure 5.1). For example, the thickness of the film may vary depending on the nutrients and breeding time (Torgbo and Sukyai, 2018).

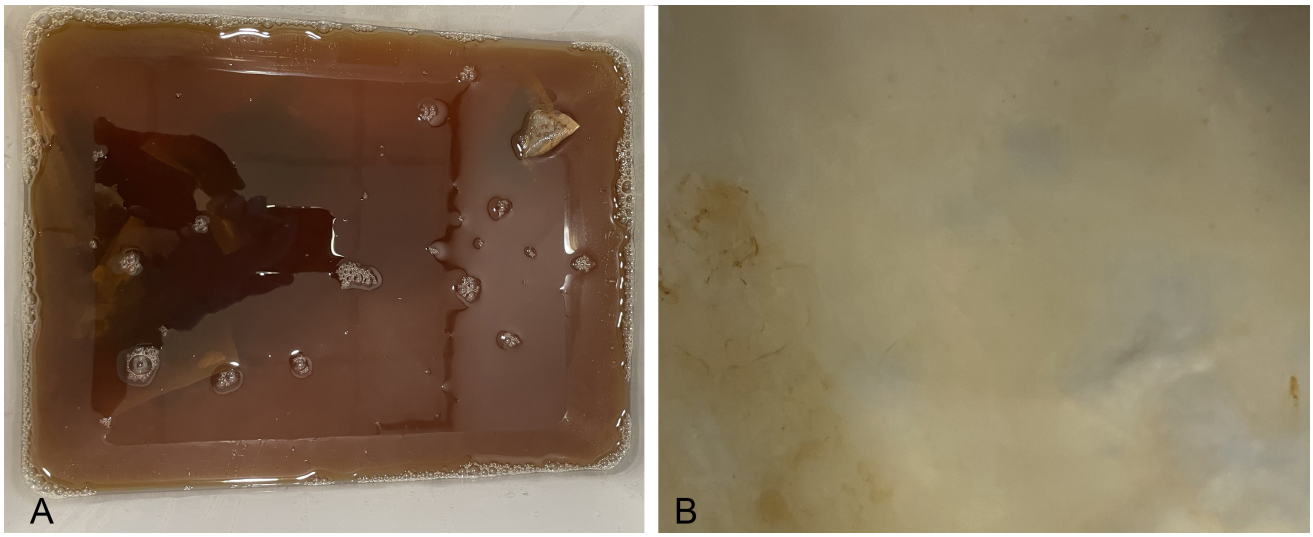


Figure 5.1: A.Sugared tea infusion medium where fermentation takes place. B. Formation of cellulosic film. The concentration of tea and sugar will impact the composition, density, and growth of the films.

Kombucha cellulose films have shown dynamics of electrical activity, represented by spikes of electrical potential, opening up exciting opportunities for the development of hybrid living materials with advanced capabilities (Adamatzky, 2023). This spiking activity may be attributed to the waves of depolarisation traveling in the films, emerging from metabolically triggered release of potassium (Adamatzky, 2022a).

5.1.2 Methods

For the fabrication of the Kombucha cellulose materials, the methods of microbial fermentation, multi-organism pairing, and functionalision were employed. Mechanical pressure and electrical stimulation were used for stimulation. To assess the materials' advanced capabilities, electrochemical and morphological characterisation was performed, along with recordings of electrical activity, as described below.

Kombucha Microbial Fermentation

For the growth of the Kombucha cellulosic films, the process of microbial fermentation was used. A commercially obtained microbial community of yeast and bacteria was cultured in an infusion of sugared tea (black tea and white granulated sugar) in sterilised plastic containers. The initial concentration of the infusion components was based on already existing Kombucha brewing protocols `https://biofabforum.org/t/manual-for-growing-bacterial-leather-kombucha/210`). Extensive brewing testings were conducted to investigate optimal concentrations of components and environmental conditions that support the growth of the films, until a thickness above 2mm was achieved.



Figure 5.2: Brewing of Kombucha; formation of Kombucha cellulosic films in a sugared tea solution via fermentation.

The acquired protocol was used for the performance of all experiments. A concentration of 5 L boiled tap water, 500 g of white granulated sugar, and 10 black tea bags was used for the fermentation. The containers were stored at room temperature (19-22°C) in the absence of light. Small openings (1 cm diameter) on the lid of the containers allowed for oxygen exposure. Every 10-14 days, the solution was replaced to allow the continuation of the fermentation and further growth of the films(Figure 5.2).

Multi-organism symbiotic pairing - Kombucha & *Chlorella vulgaris*

Chlorella vulgaris is a widely used microalgae with a spherical microscopic cell of 2–10 μm diameter (Yamamoto et al., 2004; Illman, Scragg, and Shales, 2000; Yamamoto, Kurihara, and Kawano, 2005). It exhibits great potential due to its robustness to changing environmental conditions, high growth rate (Guo and Tong, 2014), and its ability to photosynthesise (Safi et al., 2014).

The rationale for the selection of *Chlorella vulgaris* was based on already existing evidence that it can act as a living biosensor media by exhibiting periodic electrical activity in the form of spikes (Phillips, Mayne, and Adamatzky, 2022). In addition to this, the presence of specific interaction mechanisms that benefit both the microalgae and the bacteria, enabling their coexistence in the same habitat, has been reported (Jasti et al., 2005). An example includes the symbiotic co-culturing of *Pseudomonas sp.*, a Gram-negative bacterium, with *Chlorella vulgaris* (Guo and Tong, 2014). Another example includes

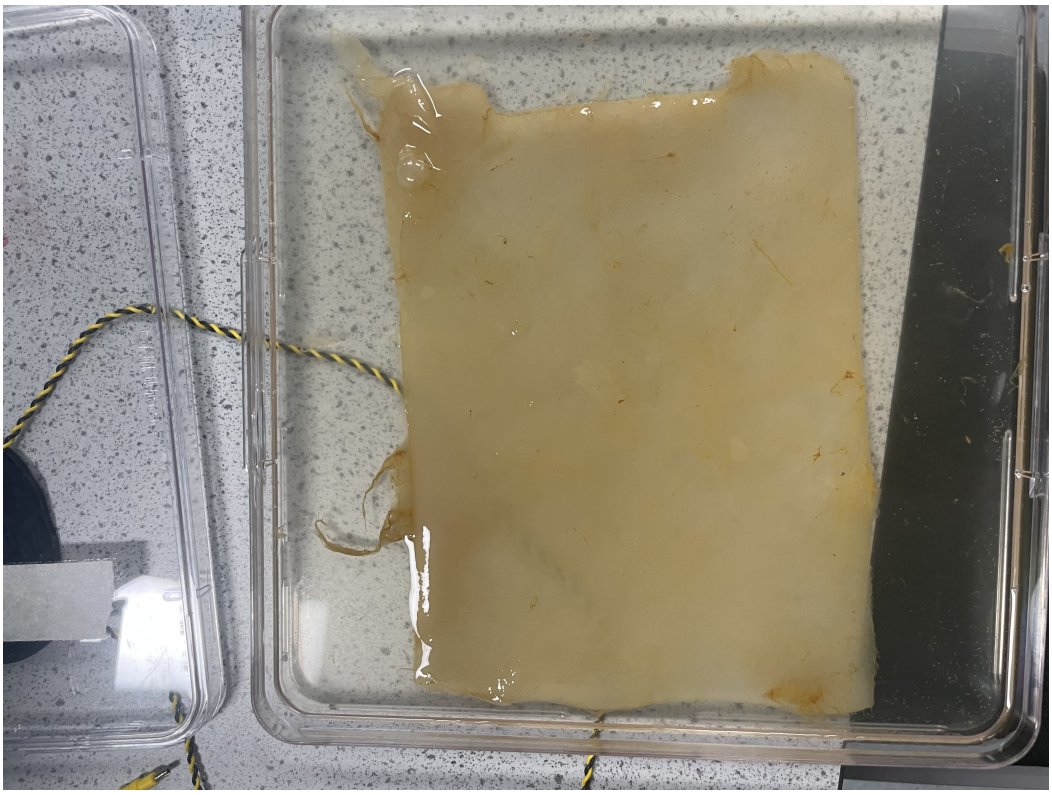


Figure 5.3: Growth of Kombucha-Chlorella film in sterilised Petri dish.

the immobilisation of the photosynthesising microalgae *C. reinhardtii* with bacterial cellulose produced by Acetobacter cells. This bacterial cellulose matrix was simultaneously used as a substrate for the growth of the microalgae *C. reinhardtii*. In turn, the microalgae provided oxygen, which was passed on to the cellulose-producing bacteria in the the surrounding environment, enabling Acetobacter to produce cellulose not only at the air–water interface but also around the photosynthetic microalgae, which became integrated into the cellulose gel (Das et al., 2016). The hypothesis was based on the assumption that since Acetobacter and photosynthetic microalgae can form synergistic interactions, and the microbial consortium of Kombucha cellulose includes Acetobacter, the photosynthetic microalgae *Chlorella vulgaris* could be a suitable candidate for symbiotic growth. A new living hybrid biofilm could be produced from the two different unicellular microorganisms, microalgae and bacterial cellulose, with potential new functionalities.

A Kombucha cellulosic film was transferred to a 240x240 mm Petri dish containing sucrose black tea solution, as described above, to allow the microbial fermentation process to continue. *Chlorella vulgaris* was introduced in the Kombucha solution medium during the fermentation process, allowing the two microbial communities to interact and enabling the assessment of synergistic interactions and the creation of favorable microenvironments.(Figure 5.3).

Functionalisation- Kombucha films & Proteinoids

For modulating the electrical properties of Kombucha cellulosic films, proteinoids were used for in situ functionalisation.

Thermal proteinoids are abiotic polypeptides that were initially synthesised by Sidney Fox in early 1970s. They are formed by heating mixtures of amino acids, leading to the formation of sequences that are not directly coded by genes (Fox, Jungck, and Nakashima, 1974). The rationale for the selection of proteinoids was based on their excellent electrical properties, such as conductivity, memristive, and memcapacitive behaviours (Mougkogiannis et al., 2023; Chua, Sirakoulis, and Adamatzky, 2019). These properties could lead to the development of materials with enhanced electrical properties through synergistic interactions between their components. Electrical membrane potentials, oscillations, and action potentials were reported when micro-electrodes were inserted into the proteinoid microspheres (Mougkogiannis and Adamatzky, 2023). Additionally, certain protein families bind specifically to polysaccharides, providing a viable way for polysaccharide-based materials to achieve additional functions. By fusing with these polysaccharide-binding domains, functional proteins can be integrated into the polysaccharide matrix to perform functions such as sensing (Gilbert et al., 2021).

Proteinoids were synthesised through the process of thermal polymerisation of amino acids. The amino acids used were L-glutamic acid and L-arginine, both with a purity level of 99%. The amino acids were heated to a temperature of 180 °C for a duration of 60 minutes, resulting in the formation of a homogeneous mixture of polypeptide chains. Afterwards, the mixture was dissolved in water to achieve a concentration of 10 mg/ml. The proteinoids were dried using lyophilisation. The proteinoids that were obtained were used without undergoing any additional purification steps. For the functionalisation, a $3 \times 3\,\mathrm{cm}^2$ section of Kombucha and Kombucha-Chlorella biofilms was used. Both sections were injected and surface-attached with 2 ml Glu-Arg proteinoid solution and then placed back into their Petri dishes to allow the continuation of the fermentation process and further growth(Figure 5.4).

Functionalisation- Kombucha films & Graphene- Zeolite Y

Another in situ functionalisation was carried out using graphene and zeolite. The hypothesis was that by combining the distinct individual properties of the two materials and integrating them into the Kombucha pellicles, new emergent or enhanced functionalities could be attained. The rationale for the selection of graphene and zeolite as cell carriers within the Kombucha zoogleal mat was based on their distinct yet complementary characteristics (Bai and Shi, 2007; Adhikari and Majumdar, 2004; Ahuja, Kumar, et al., 2009), leading to the improvement of the mat's electrical properties, such as conductivity, sensitivity, and stability.

Cellulose can strongly bind with carbon materials, such as graphene and carbon nanotubes (Bao and Li, 2012; Gao et al., 2013; Xie et al., 2012; Nyholm et al., 2011), making it a good candidate for functionalisation. Graphene, a two-dimensional sheet of sp^2-hybridised carbon arranged in a hexagonal

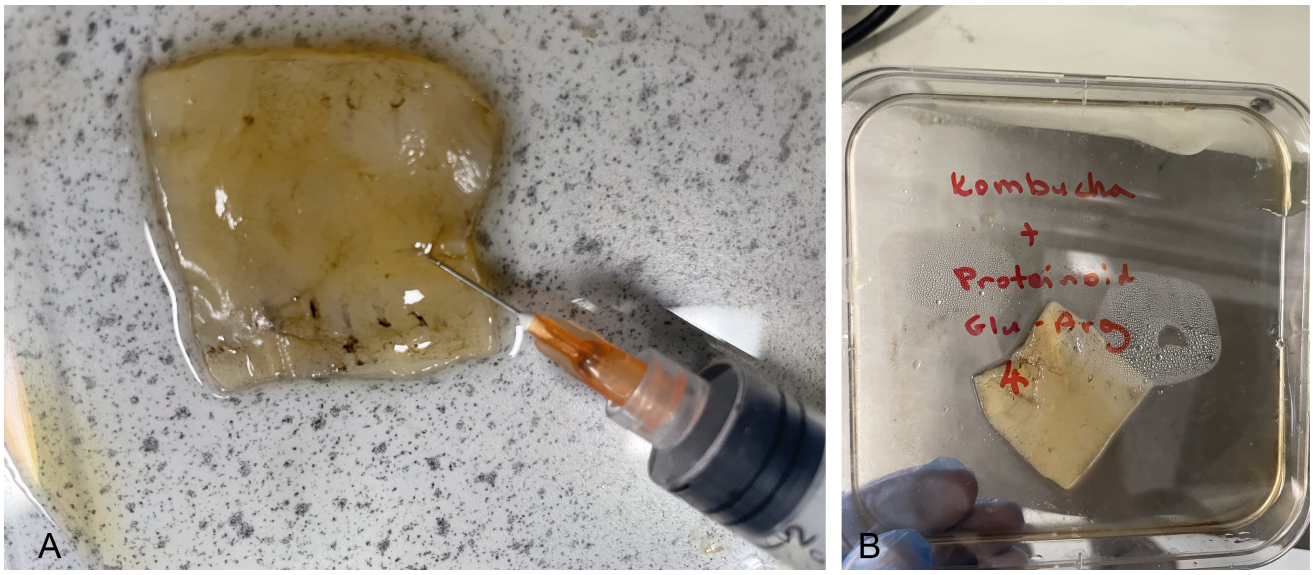


Figure 5.4: A.Glu-Arg proteinoid solution was injected into the Kombucha and Kombucha-Chlorella biofilms. B.Functionalised Kombucha-Proteinoid film section in solution to allow further growth and integration of proteinoid spheres into the film.

lattice, has revealed a variety of mechanical and electrical properties that qualify it for the reinforcement of polymer matrixes (Feng et al., 2012). Graphene exhibits excellent electrical conductivity, mechanical flexibility, thermal conductivity, and low coefficient of thermal expansion behaviour (Novoselov et al., 2004; Suk et al., 2010; Wang et al., 2008; Li et al., 2008; Blake et al., 2008). It has been used as an alternative carbon-based nanofiller in the preparation of polymer nanocomposites (Ansari and Giannelis, 2009; Ramanathan et al., 2008; Stankovich et al., 2006; Fan et al., 2010; Zhang et al., 2010; Zhao et al., 2010; Kuila et al., 2011; Bose et al., 2010). for the fabrication of nano-electronic and bio-electronic devices (Geim and Novoselov, 2007), and to replace metal conductors in electronic and electrical devices (Li et al., 2009; Kim et al., 2009b; Bae et al., 2010). The integration of graphene into the cellulose matrix enables the formation of electrical conductive pathways, facilitating effective electron transfer and improving the overall electrical conductivity of the material. Additionally, because of the many hydroxyl groups in the BC units, effective interactions between BC and graphene, such as electrostatic interaction and hydrogen bonding, are potentially achievable (Feng et al., 2012). Therefore, the attention is focused on graphene, as interfacing living cells with graphene has been proven to be effective for the integration of cellular physiology with electrical readouts (Kempaiah, Chung, and Maheshwari, 2011).

Zeolites are crystalline aluminosilicates with pores and channels of molecular dimensions (Auerbach, Carrado, and Dutta, 2003; Auerbach, Carrado, and Dutta, 2004; Cejka et al., 2007; Mintova, Tsapatsis, and Valtchev, 2009; Cejka, Corma, and Zones, 2010; Kulprathipanja, 2010) that exhibit ion-exchange properties, absorbing and reacting with molecules within their cages. Equally to graphene, zeolites present a multitude of benefits for functionalisation. Due to their structure, they have a large

surface area, high adsorption capacity, and high selectivity, enabling the absorption of various components (Kadja et al., 2021; Maghfirah et al., 2020; Azhari et al., 2022). Consequently, they can provide an expanded surface area which facilitates particle and cell immobilisation and attachment. Additionally, zeolites facilitate a suitable environment for encapsulation, enabling immobilised biomolecules to have enhanced stability (Kucherenko et al., 2022), ensuring the material's durability and functionality. Zeolites have been used to improve the performance of existing sensors or as the sensing medium itself, due to their absorption, diffusion, and catalytic properties. These characteristics make them excellent physical and chemical filters for enhancing selectivity (Zheng, Li, and Dutta, 2012).The adsorption properties of zeolites have also been exploited in conducting polymer-zeolite composites (Chuapradit et al., 2005; Ma et al., 2006; Wannatong and Sirivat, 2008; Phumman, Niamlang, and Sirivat, 2009).

Employing zeolites as a functional element and combining it with graphene has great potential to achieve enhanced sensing functionalities. Graphene contributes to exceptional electrical conductivity and mechanical strength, whereas the zeolite nanoparticles provide an expanded surface area that facilitates immobilisation, adherence, and improved stability. Their unique combination into the cellulose fibres of the Kombucha mat allows for enhanced sensitivity, stability, and electrical responses.

For the functionalisation of the Kombucha cellulosic film, a film formed from the inoculation of a SCOBY culture of yeast and bacteria in the sucrose tea infusion for 8 weeks was transferred to a 240x240 mm Petri dish. 30 ml of newly made sucrose black tea solution were added to the Petri dish, instigating the fermentation process and allowing for continuation of film growth. After 7 days of inoculation, the film was obtained for functionalisation. On removal from the Petri dish, a high intensity of yellow and brown colour was observed. The yellowness can be attributed to the Maillard reactions taking place during the fermentation and film conditioning, occurring between the sugars and amino acids, in addition to coloured phytochemicals (Tapias et al., 2022). The brown colour has been reported to be caused by melanoidins, which are coloured, nitrogen-containing compounds (Azeredo et al., 2019; Dima et al., 2017). The thickness of the film was 3.3 mm and was measured with an electronic digital caliper. The pH was monitored starting from 6.49 and decreasing to 3.02, using a digital pH-meter. Some inhomogeneity observed in the visual appearance of the functionalised Kombucha film is a typical feature of materials produced by microorganisms. Kombucha zoogleal films are multispecies systems synthesised by variable natural symbiotes, yeast and bacteria. During the process of fermentation, cooperative and competitive interactions occur among the microbes. The non-uniformity observed in the growth of the modified Kombucha film can be attributed to their ongoing interactions and metabolic activities.

5.372 g of graphene powder were mixed with 1.289 g of Zeolite Y powder. The thickness of graphene powder ranged from 1 to 3 layers, with a lateral size of 0.5 to 5 μm, a surface area of 500 m2/g, and an electrical conductivity >104 S/m. The surface area of zeolite Y was 927 m2 /g. To achieve good interfacial bonding between the graphene and zeolite molecules, PTFE solvent was used. The mixture was stirred until a homogeneous solution was attained (total weight of mixture was 12.965 g). The

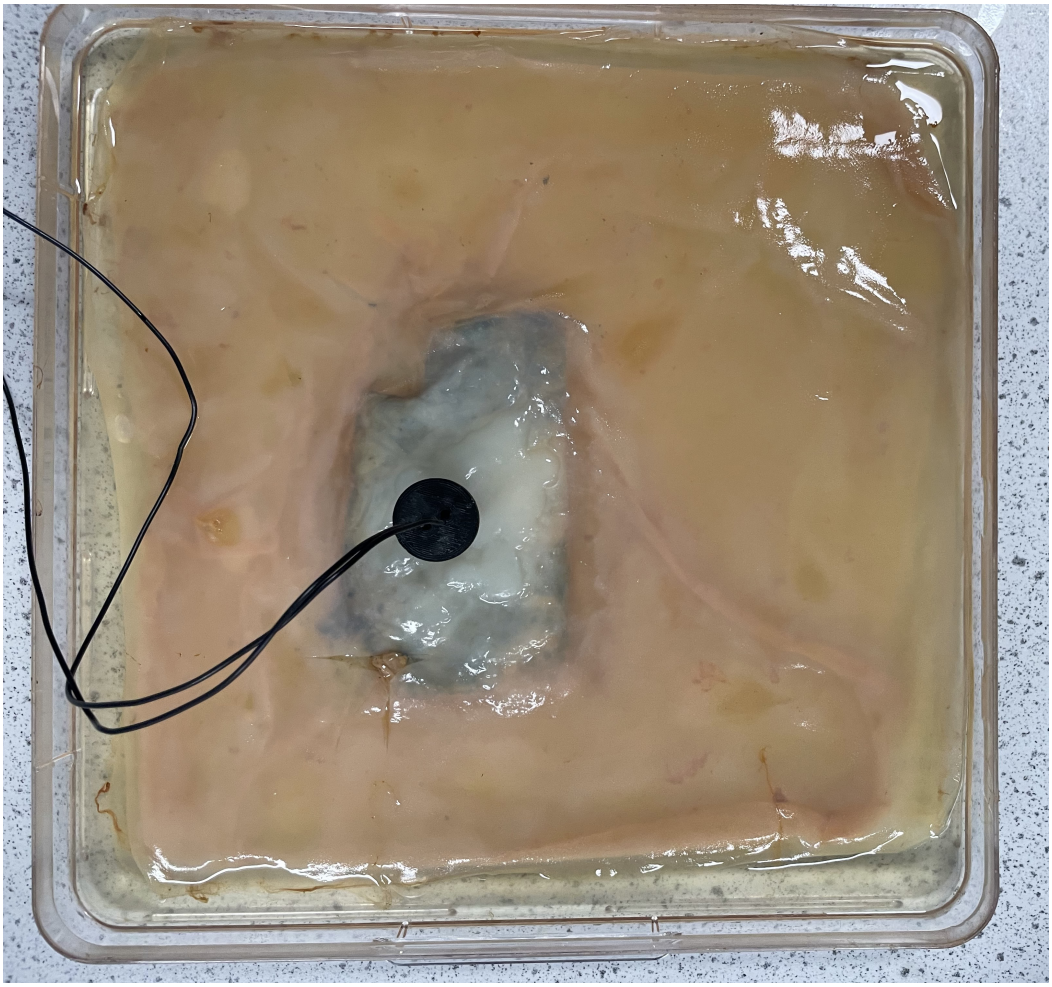


Figure 5.5: Fermentation of Kombucha film functionalised with graphene and zeolite nanoparticles.

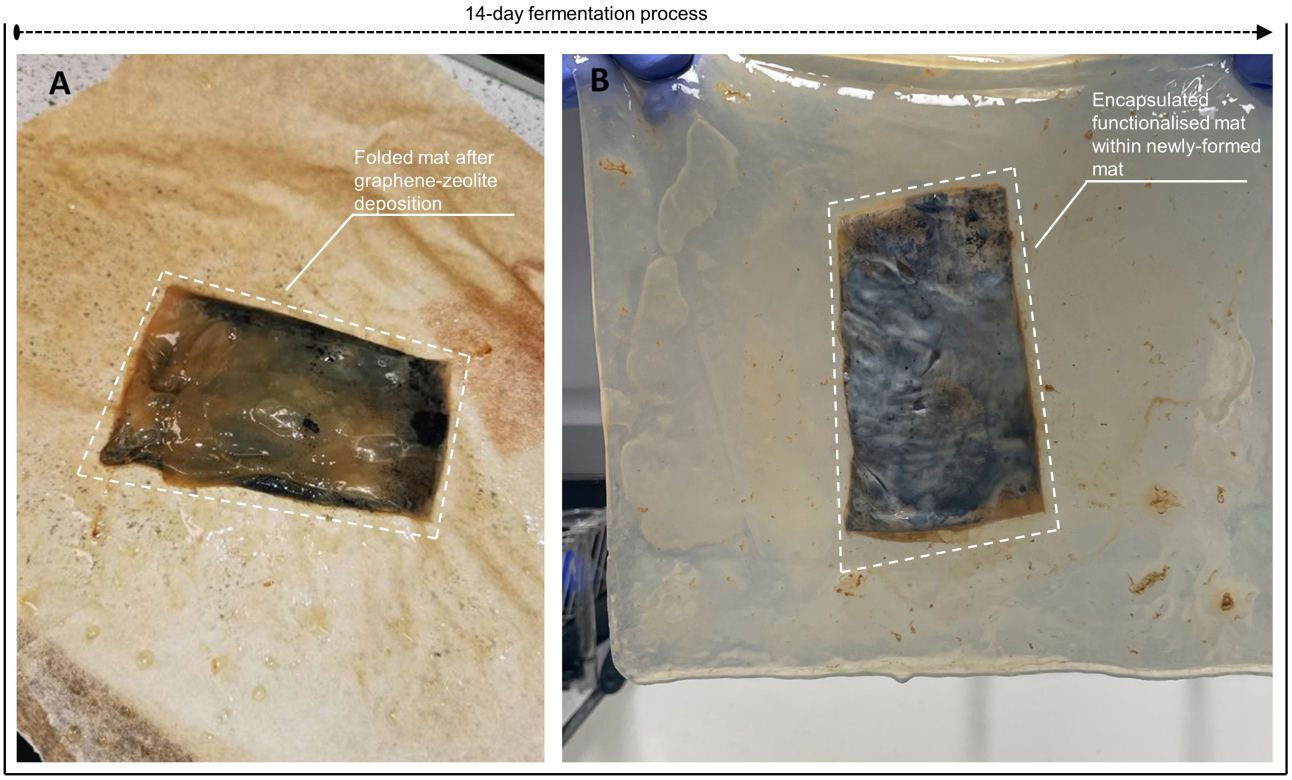


Figure 5.6: A.Folded graphene-zeolite-coated Kombucha film. B.Kombucha-graphene-zeolite hybrid living film.

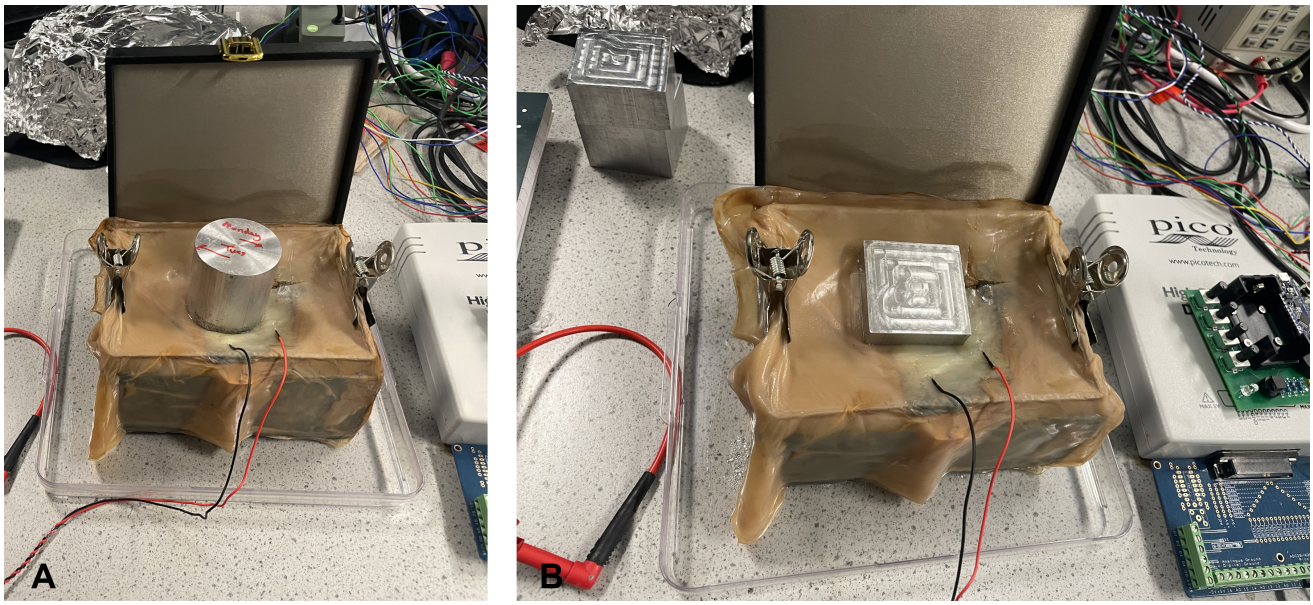


Figure 5.7: A. I-V curves measurements taken from functionalised Kombucha mat during load application of 300 g weight of cylinder form. B. I-V curves measurements taken from functionalised Kombucha mat during load application of 100 g weight of square form.

graphene-zeolite Y mixture was then deposited on the surface of the Kombucha cellulose film using a razor blade and dispersed homogeneously until fully coated. After coating the top surface, the film was folded in such a manner that the mixture remained enclosed within the film. For the in situ fabrication of the Kombucha-graphene-zeolite hybrid living material, the method of microbial fermentation was used, and the film was placed back again into the Petri dish to allow further growth(Figure 5.5). After 14 days of fermentation, a new 240x240 mm cellulose film was formed, fully encapsulating the functionalised cellulose film(Figure 5.6).

Exposure to stimulation

To assess the response of Kombucha and Kombucha-graphene-zeolite mats to mechanical stimulation, load application of manually cut square aluminium weights of 100 g (W51 × L51 × H14.2 mm), 200 g (W51 × L51 × H28.4 mm), 300 g (W51 × L51 × H42.7 mm), and circular aluminium weights of 100 g (D51 × H18.1 mm), 200 g (D51 × H36 mm), and 300 g (D51 × H54.4 mm) were employed. The weights were applied to both samples in different combinations to attain loads of 100 g, 200 g, 300 g, 400 g, and 600 g(Figure 5.7).

Electrical stimulation was applied to the Kombucha, Kombucha- proteinoids, and Kombucha-Chlorella-proteinoids samples at different concentrations, by supplying input waveforms as described in the section 'Characterisation' below. The samples were 40% Glu-Arg proteinoids- 60% Kombucha- Chlorella, 40% Glu-Arg proteinoids- 60% Kombucha, 25% Glu-Arg proteinoids- 75% Kombucha- Chlorella, and

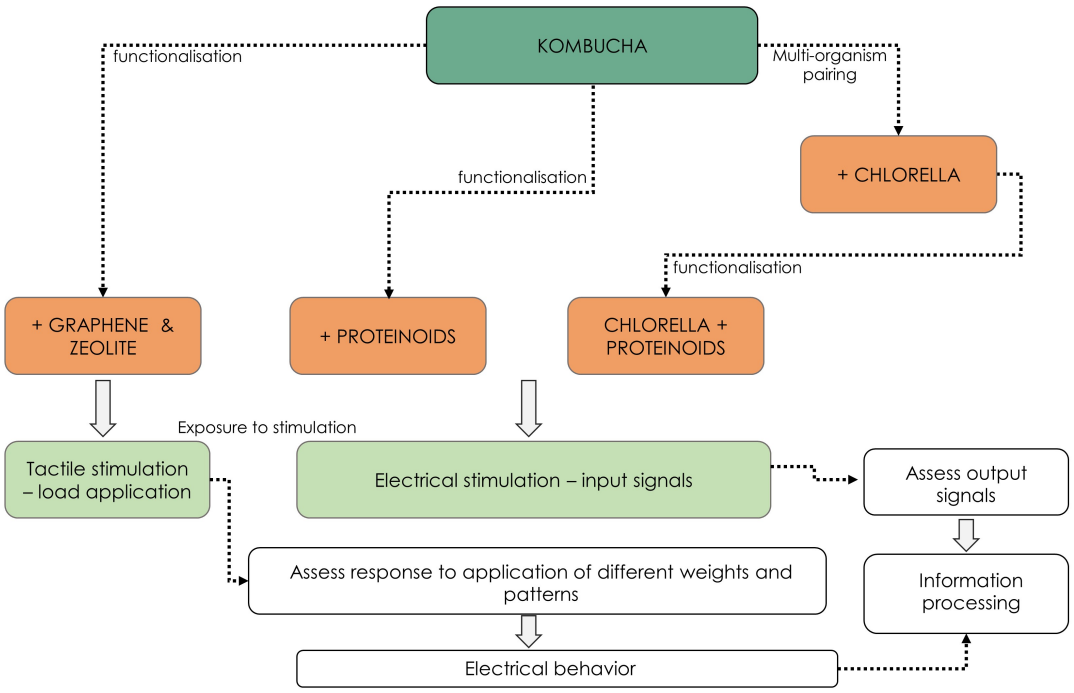


Figure 5.8: Diagram showing process of multi-organism pairing, functionalisation, and stimulation

25% Glu-Arg proteinoids- 75% Kombucha. They were subjected to input signals of 10 mV amplitude and 0.055 Hz frequency to assess output signals, thereby evaluating their capacity for information processing(Figure 5.8).

Characterisation and recordings of electrical activity

Morphological

SEM was performed for the morphological characterisation. The following samples were subjected to the characterisation with an FEI Quanta 650 field emission SEM.

1. Kombucha film
2. Kombucha & Chlorella film
3. Kombucha & Poteinoids [Glu-Arg] film
4. Kombucha & Chlorella & Poteinoids [Glu-Arg] film
5. Kombucha & Graphene and zeolite film
6. Kombucha & Poteinoids [Glu-Arg] solution

For the preparation prior to imaging, the samples were air dried, or an HMDS agent was used, followed by coating with a gold layer using an Emscope SC500 gold sputter coating unit. Images were acquired with a magnification range of 1300x - 20000x and a high voltage of 2 kV. For further imaging of the surface of the samples, some samples were subjected to digital microscopy (Keyence,

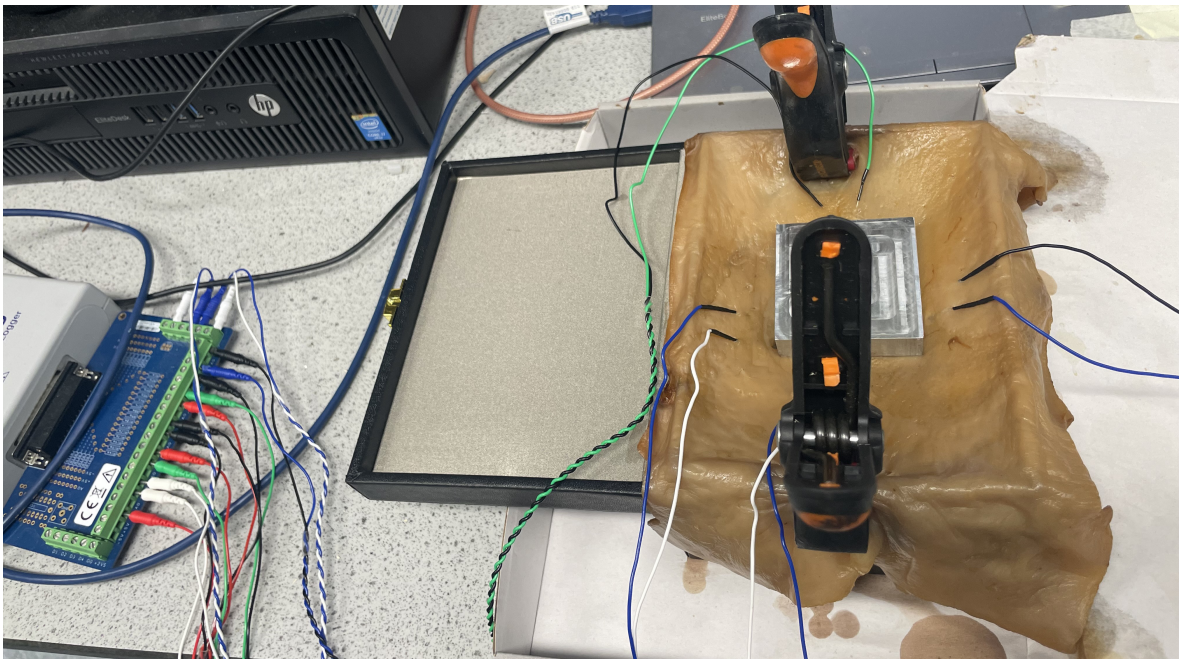


Figure 5.9: Experimental setup and recordings of electrical spiking activity of pure Kombucha mat under 100 g square form weight application. Four pairs of iridium-coated, stainless steel subdermal needle electrodes inserted in the sample were used to record the difference of the electrical potential between the electrodes.

VHX- 7000 series). Additionally, for the graphene-zeolite functionalised sample, EDS was used to investigate the distribution of inorganic materials, and Light Microscopy (Keyence, VHX- 7000 series) was employed for further surface imaging.

Electrical

The electrical properties of the samples were subjected to systematic characterisation using the methods below. For the samples exposed to stimulants, the characterisation was performed prior, during, and/or after stimulation to assess the impact of the stimulants on the behaviour of the samples(Figure 5.10)(Figure 5.9).

High precision current-voltage (I–V) sweep measurements and cyclic voltammetry were performed over voltage ranges of 0 V-5 V and -1 V to 1 V (linear dual type, voltage range from -1 V to 1 V, step 10 mV, count finite 20, source limit 1 A) using a Keithley 2450 SourceMeter(Figure 5.11)(Figure 5.12). Impedance, capacitance, and resistance measurements were taken using a BK Precision LCR Meter (model 891) within a frequency range of 20 Hz and 300 kHz(Figure 5.13). A BK Precision 4053B 10 MHz dual-channel function generator was used to supply input waveforms for the purpose of conducting experiments on frequency-dependent capacitance and resistance (input-output mappings). A pair of iridium-coated stainless steel subdermal needle electrodes, with twisted cables, was inserted into the samples to ensure direct contact with the material for measurement purposes.

Electrical activity recordings

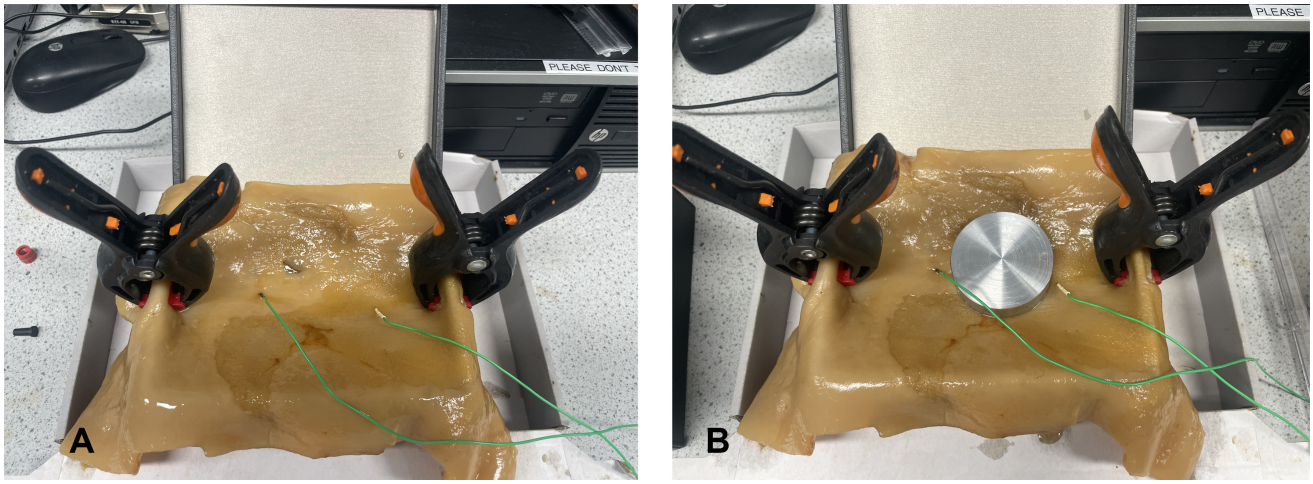


Figure 5.10: A.Capacitance, resistance, and impedance measurements taken from pure Kombucha mat prior to load application. A pair of iridium-coated stainless steel subdermal needle electrodes, with twisted cables, was inserted into the sample to allow the recording of measurements. B.Capacitance, resistance, and impedance measurements taken from pure Kombucha mat during load application of 100 g weight in cylinder form. A pair of iridium-coated stainless steel subdermal needle electrodes, with twisted cables, was inserted into the sample to allow the recording of measurements.

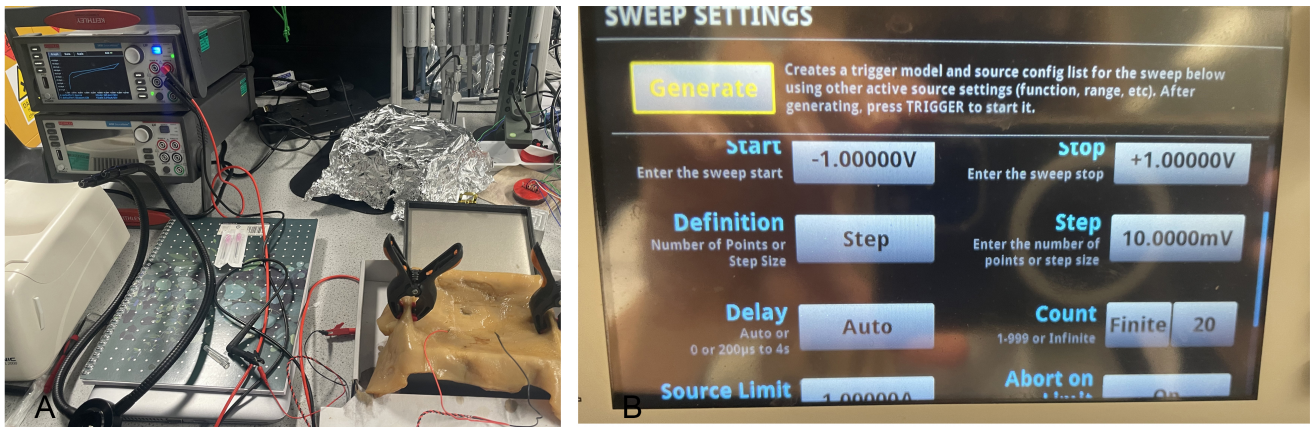


Figure 5.11: A.Current-voltage (I–V) profiling of a pure Kombucha cellulosic film B.Sweep settings used.

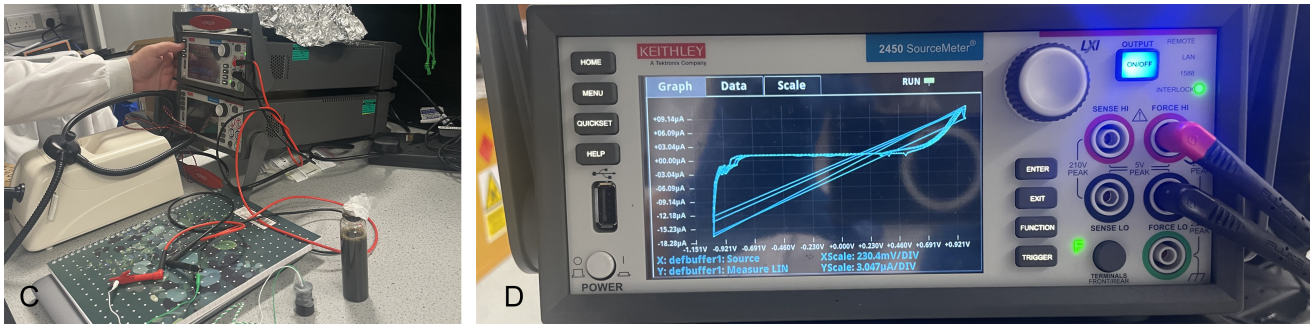


Figure 5.12: C. Current-voltage (I–V) profiling of Kombucha-Chlorella- GluArg solution. D.Graph of I-V sample profiling.

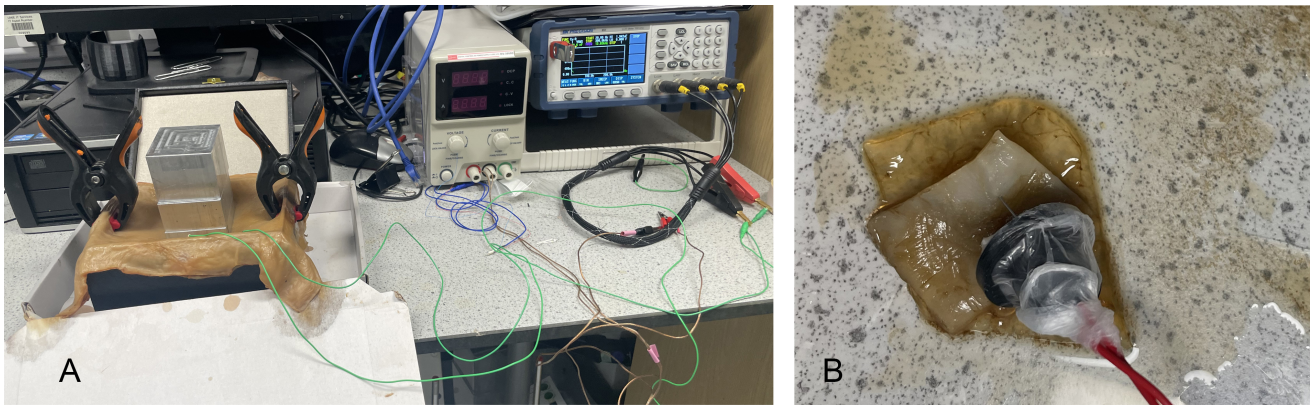


Figure 5.13: A.Measurements of impedance, capacitance, and resistance taken from pure Kombucha film under 600 g load application B.Measurements obtained from functionalised Kombucha-GluArg proteinoids film.

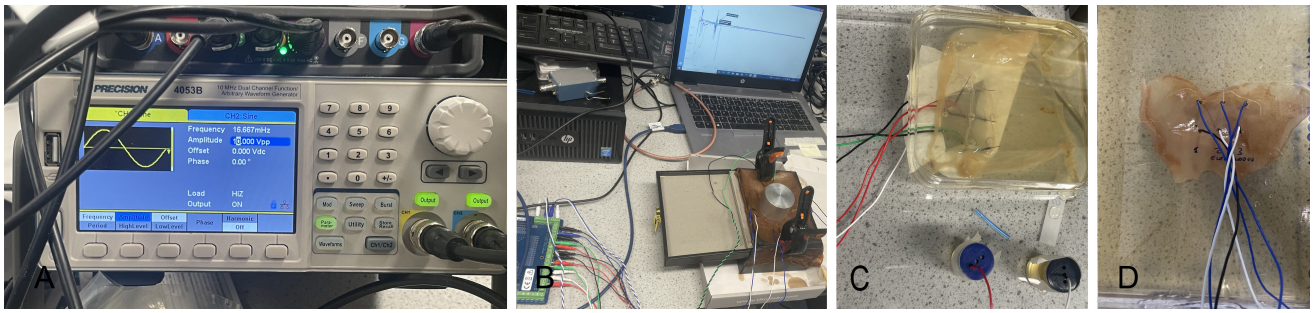


Figure 5.14: A.Function generator used to supply input electrical stimulants for the performance of input-output mappings. B.Experimental setup for recordings of electrical spiking activity of Kombucha film under 300 g load compression. C and D.Recordings of patterns of electrical activity using pairs of subdermal electrodes inserted into Kombucha-Chlorella films and Kombucha-Chlorella solutions.

A high impedance data logger was used to analyse the electrical activity of the samples. For the recordings of the electrical activity, a Picolog ADC-24 high-resolution data logger with a 24-bit A/D converter was used. The electrical activity was recorded using pairs of iridium-coated stainless steel sub- dermal needle electrodes inserted into the samples. Measurements were taken at a rate of one sample per second, with each pair of electrodes reporting the electrical potential difference between them. During the recordings, the logger undertook as many measurements as possible (typically up to 600 per second) and saved the average value. The distance between electrodes was 10-20 mm(Figure 5.14). All measurements were conducted at room temperature and the experiments were repeated to ensure error elimination.

The rationale for the selection of the above methods is described in the previous section (Section B). Valuable insights into conductivity, memfractive bahavior, spiking dynamics, responses to alternating current, and the ability to store charge could be attained. Therefore, it is possible to make conclusions regarding advanced and cognitive characteristics such as sensing, information processing, learning, logical operations, and computation. The characterisation of the electrical properties across various operating conditions also uncovers valuable insights into the relationships between stimulus and the behaviours of the hybrid living materials.

5.1.3 Key findings

Bonding capacity

SEM imaging performed to unmodified Kombucha, functionalised Kombucha-graphene-zeolite, Kombucha-proteinoids, and Kombucha-Chlorella-proteinoids samples demonstrated that the structure of the pure Kombucha film changes significantly with the integration of the nanoparticles and microalgae.

More specifically, the morphological features of pure Kombucha reveal that the microbial community of yeast and bacterial cells present mostly ellipsoidal structures, are compactly and uniformly

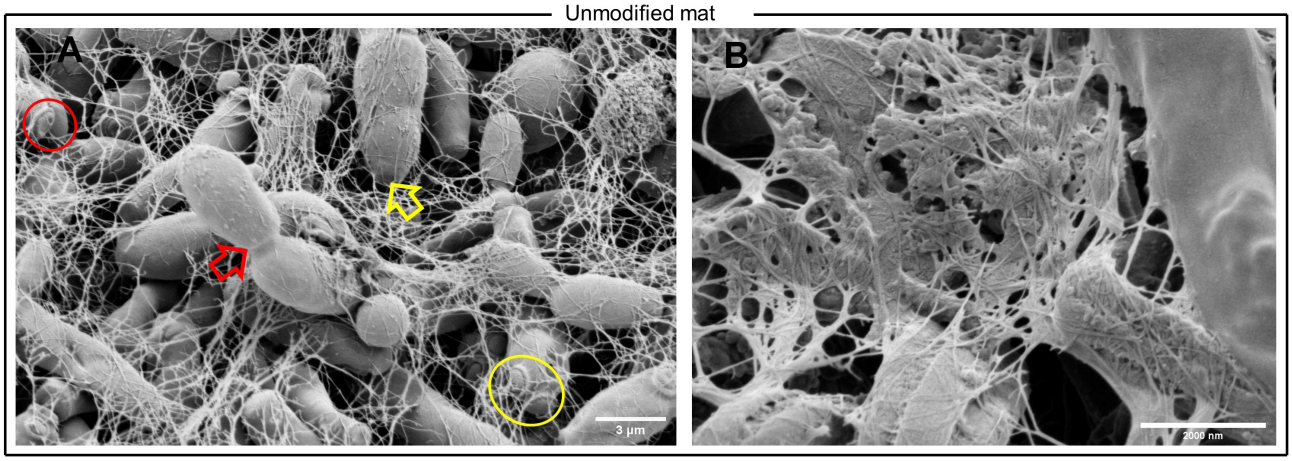


Figure 5.15: SEM images of pure Kombucha film. A.The presence of multiple size yeast cells is identified, with lengths ranging from 1.93 μm to 7.76 μm. Cell bud scars, birth scars, multipolar budding, and bud-parent sites are marked in the image with red circles, yellow and red arrows, and yellow circles, respectively. Image magnification is 8000x. B.A network of cellulosic fibres with branching structure. Image magnification is 20000x.

dispersed, and are entangled into a dense mesh of cellulosic fibres that form three dimensional web-like structures(Figure 5.16). The presence of multiple size yeast cells is observed, spanning from to 1.93 μm to 7.76 μm in length. Chain yeast elongations are visible and protrusions on the cell surfaces show cell budding mechanisms (Watson and Arthur, 1977). Figure (Figure 5.15) shows bud and birth scars, as well as bud-parent junctions (marked with red circles and yellow and red arrows, respectively). Multipolar budding is also clearly identified on some cells (marked with a yellow circle).

Images of the graphene-zeolite functionalised Kombucha film sample revealed dense aggregations of zeolite Y crystals, displaying morphologies of spherical agglomerates of tiny crystals next to larger polyhedrons, surrounded by typical flakes of graphene particles (Khenfouch et al., 2014), and integrated with scattered Kombucha microbes. The crystal structure of zeolite Y aligns with the morphological characterisation of commercial zeolites Y (Yokoi, 2016). The presented high-density configurations may be attributed to the high microporocity of zeolite active sites, which provide space for the adsorption and exchange of cations, facilitating the attachment of the graphene molecules. This connection could favour electron transport, contributing to the electrochemical performance of the functionalised Kombucha film. In addition to this, the cellulose fiber network appears to be less dense and finer where the graphene-zeolite formations are present. The measured cluster assemblies have a diameter of 9.61 μm and 7.75 μm(Figure 5.17). In comparison to unmodified Kombucha, microbial cells appear in lower densities in the functionalised Kombucha images; however, elongations and birth scars are still visible, suggesting that growth and replication mechanisms continue to take place after functionalisation.

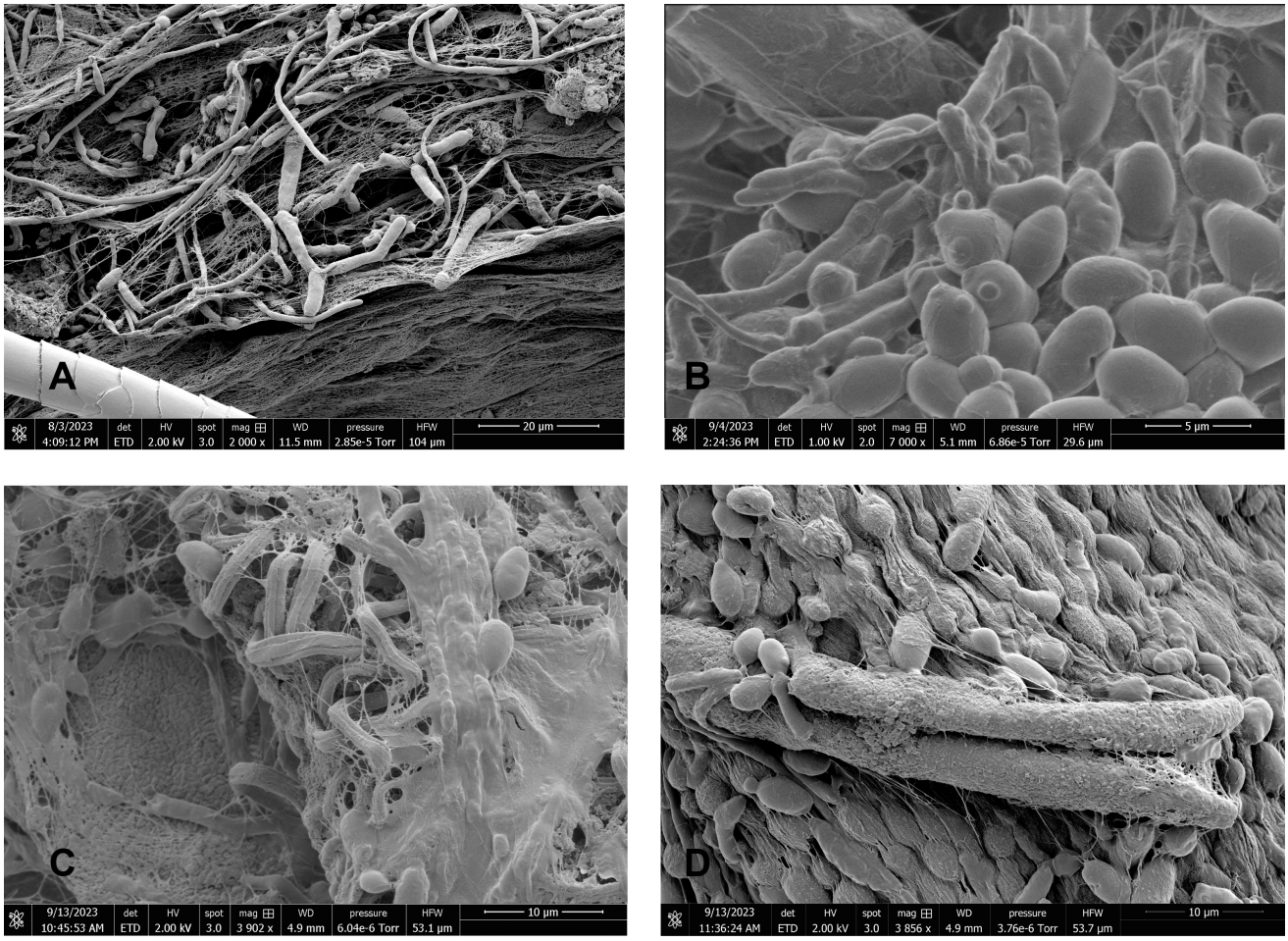


Figure 5.16: SEM images of pure Kombucha film depicting microbial community of yeast and bacteria. A.Image magnification is 7000x. B.Image magnification is 7000x. C.Image magnification is 3902x. D.Image magnification is 3856x

The above findings indicate that the new structural formations may involve the microscopic movement of the microbial population due to the mechanical and physical forces built up from the graphene-zeolite encapsulation during the in situ functionalisation process. Moreover, it is observed that the graphene-zeolite particles are found entangled and linked to the microbial cells, and in parts enveloped by the cells, suggesting bonding capacity and integration between the living biological and synthetic components. This may open up remarkable opportunities for the in situ development of functionalised hybrid materials that can self-assemble, self-replicate, self-generate, and self-grow following the fusion of living and synthetic components.

Additionally, the images depict wrinkle formations. This could be due to the microbial communities diverse cellular behaviours and complex spatial organization, including replication, that could give rise to complex 3D wrinkle structures (Webb, Givskov, and Kjelleberg, 2003; Branda et al., 2001; Wood, Hong, and Ma, 2011; Markx, Andrews, and Mason, 2004; López and Kolter, 2010; Vlamakis et al., 2008)(Figure 5.19). It is also possible that the forces generated during the biofilm growth and expansion may cause localised cell death, triggering vertical buckling and subsequent wrinkling (Asally et al., 2012).

EDS shows the distribution of elements within the functionalised Kombucha film(Figure 5.18). In the material distribution analysis, very low Al content is observed, demonstrating high hydrothermal stability (Yokoi, 2016). Figure 5.20 depicts the structure of the surface of the Kombucha and functionalised Kombucha films.

SEM performed to the functionalised with L-Glu and L-Arg proteinoids Kombucha and Kombucha-Chlorella films revealed the presence of yeast cells measuring 1.4 μm in diameter, in close proximity to bigger Chlorella microspheres. The Chlorella microspheres identified in the images measure 3.54 μm, 3.64 μm, and 4.76 μm in diameter. The proteinoids nanoparticles measure 105 nm and 243 nm. They were distributed densely and uniformly, with higher concentration observed in the vicinity of yeast cells, displaying neuron-like formations. The results indicate that the proteinoids are not simply located on the surface of the Kombucha biofilm, but are closely integrated with the microbial and microalgal components(Figure 5.21).

The integration observed can be attributed to several intermolecular interactions. These include electrostatic interactions between glutamate, arginine, and the anionic functional groups found in the extracellular polymeric substances (EPS) of the Kombucha matrix, which are rich in polysaccharides (Albano, Cavallieri, and Nicoletti, 2019). Additionally, the non-polar domains of the proteinoids may embed themselves in the hydrophobic regions of microbial cell walls or penetrate the EPS matrix (Subbiahdoss, Osmen, and Reimhult, 2022). The proteinoid-Kombucha interface exhibits several hydrogen bonding possibilities, which stem from the hydroxyl, carboxyl, and amino groups present on both proteinoid and Kombucha components. It is also possible that the proteinoids and the biofilm morphological features may exhibit conformational compatibility, enhancing multivalent binding and promoting increased surface networking (Van Oss, Good, and Chaudhury, 1986).

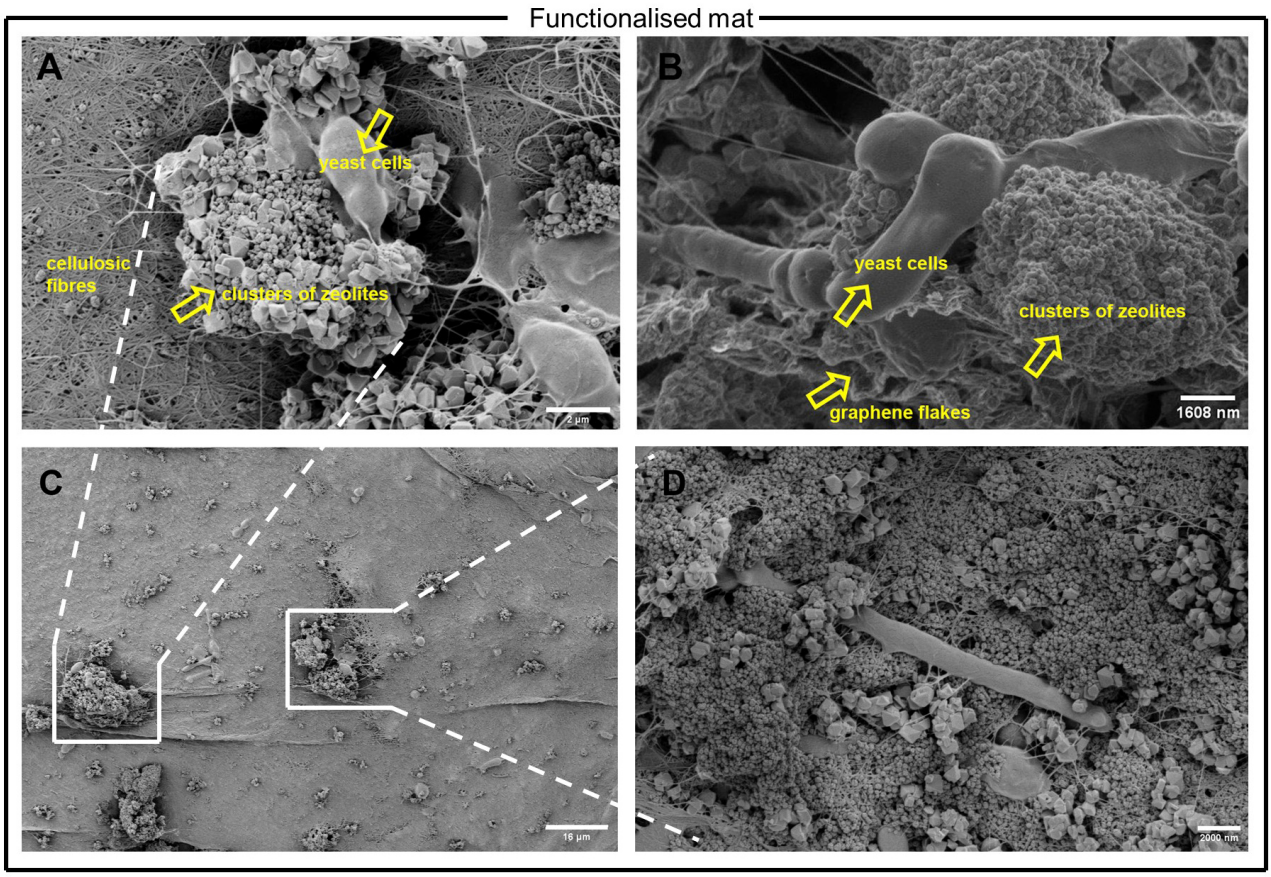


Figure 5.17: SEM images of functionalised Kombucha mat. A. Clusters of zeolite crystals entangled with microbes. Image magnification is 10000x. B. Graphene-zeolite assembly formations where graphene flakes attached to zeolite crystals and yeast cells are observed. Image magnification is 10000x. C. Lower magnification image showing distribution of nanoparticles. Image magnification is 1300x. D. Yeast cells integrated into zeolite-graphene nanoparticles. Image magnification is 7000x.

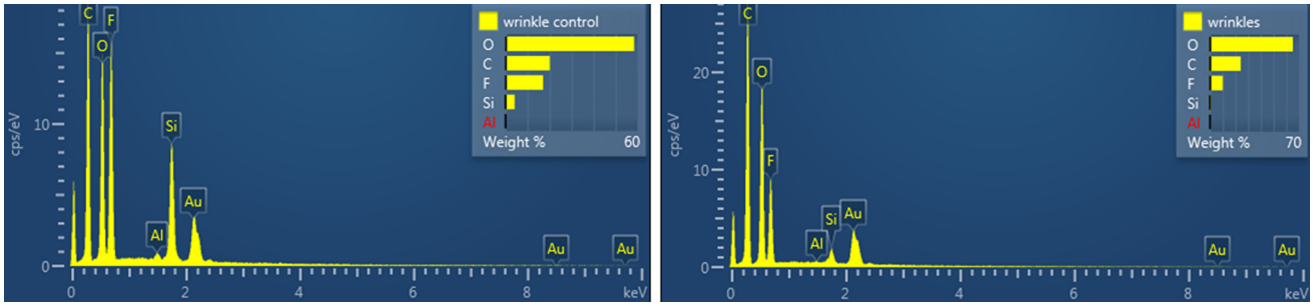


Figure 5.18: EDS graphs of two samples collected from different sites of the functionalised Kombucha mat, showing the distribution of elements. The graphs reveal the presence of silicon (Si), aluminium (Al), and carbon (C) peaks, indicating the integration of the zeolite and graphene nanoparticles within the Kombucha mat. Additionally, the presence of fluorine (F) is observed and can be attributed to the use of PTFE solvent for the achievement of good interfacial bonding between the graphene and zeolite molecules. The gold (Au) peaks are attributed to the gold coating applied to the sample to increase its conductivity, for improved Scanning Electron Microscopy imaging. The peaks of elements in both EDS graphs follow a similar trend, indicating a homogeneous distribution of the graphene and zeolite nanoparticles in both samples and therefore, incorporation within the Kombucha matrix.

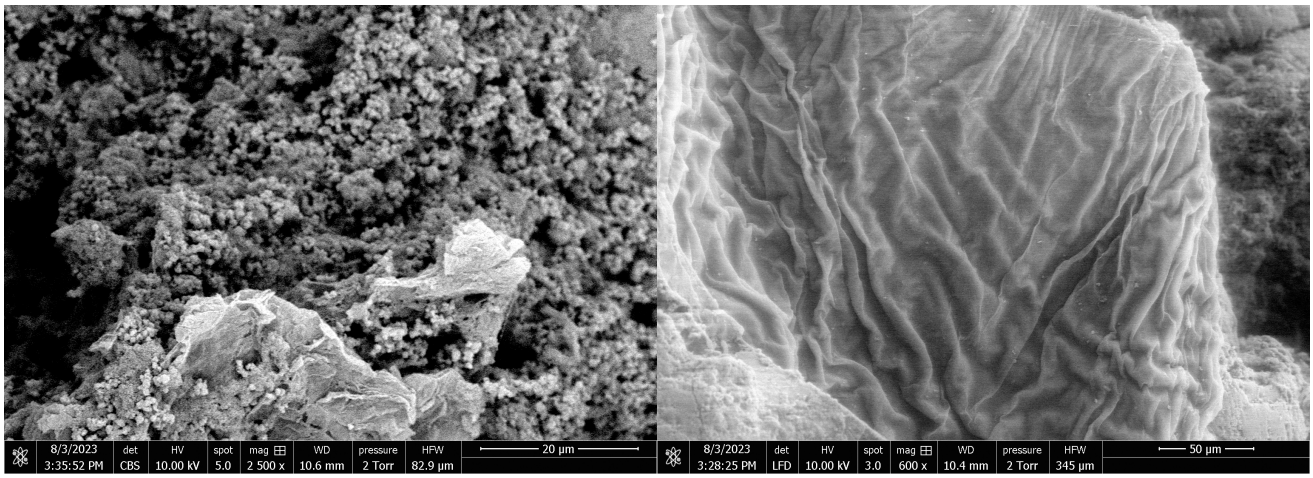


Figure 5.19: A.Graphene flakes integrated into zeolite crystals. Image magnification is 2500x. B.Wrinkle structural formations.Image magnification is 600x

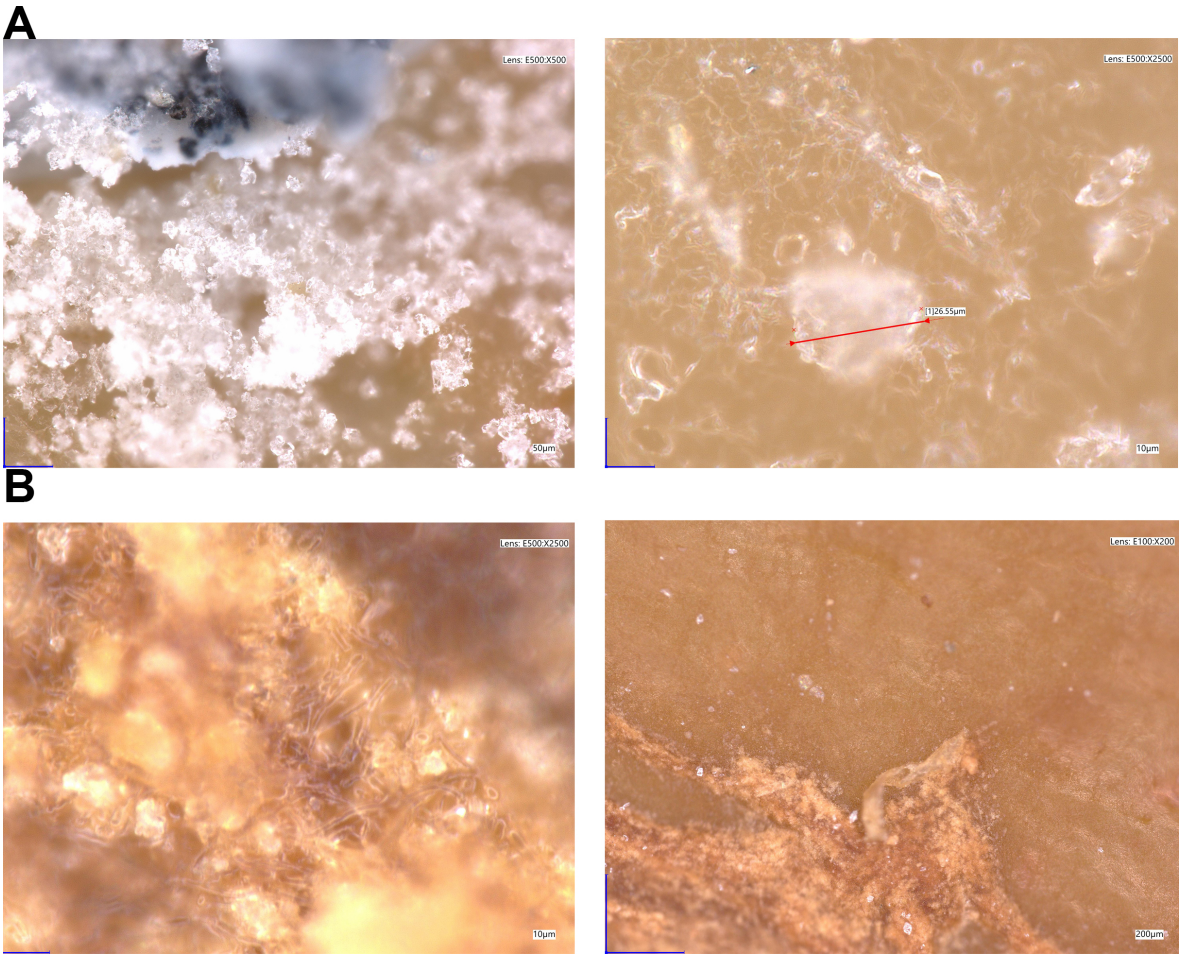


Figure 5.20: Light Microscopy of Kombucha and functionalised Kombucha samples. A.Surface of functionalised Kombucha film depicting zeolite crystals and graphene flakes. Crystal size measured of 26.55 μm length. Lens: E500:X500 and E500:X2500. B.Structure of surface of pure Kombucha film. Lens: E500:X2500 and E100:X200.

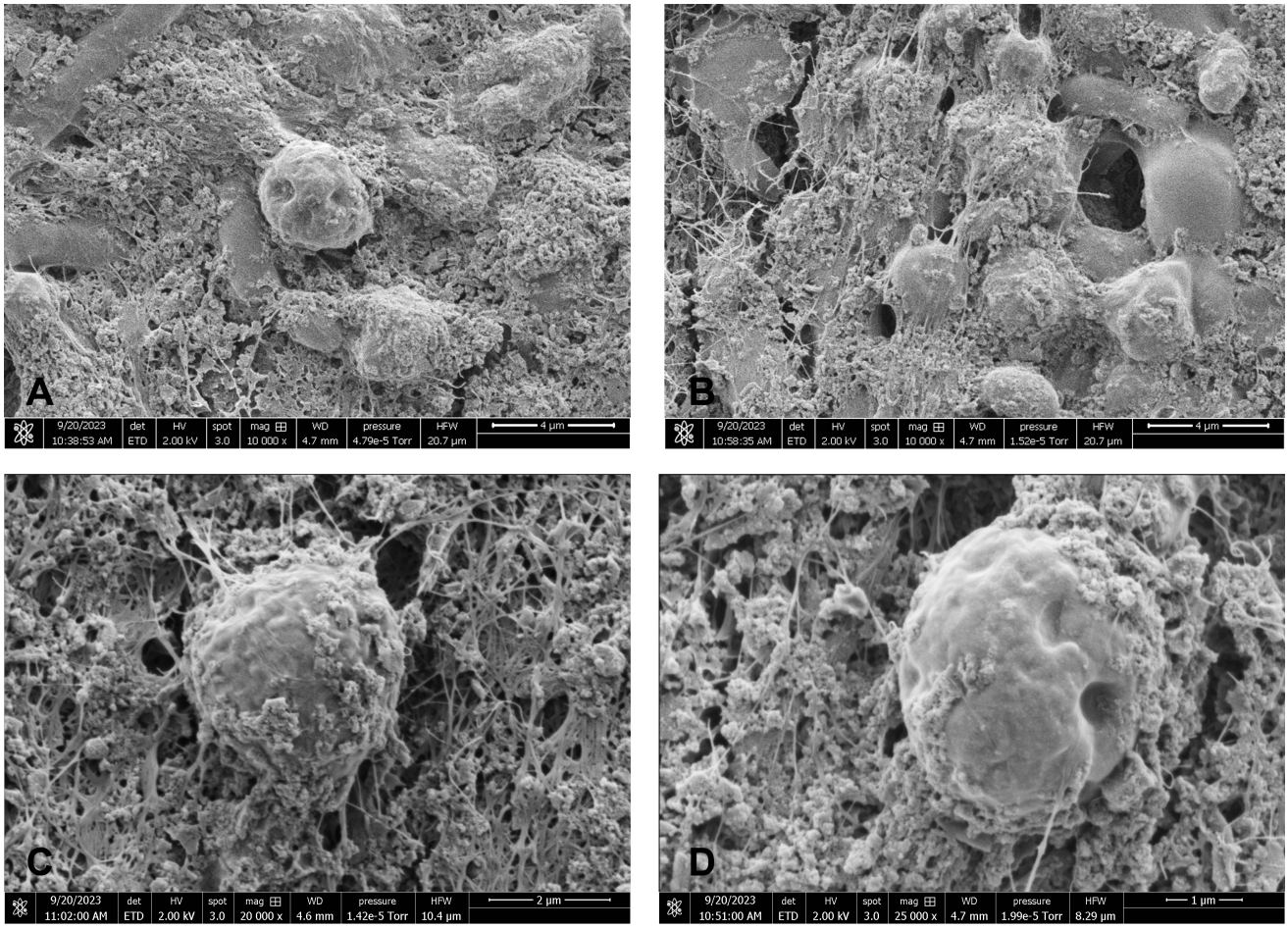


Figure 5.21: A.Chlorella microsphere with a diameter of 4.76 μm integrated in a matrix of proteinoids and microbial cells. Image magnification is 10000x. B.Matrix of Chlorella microalgae, yeast, and bacteria cells entangled with L-Glu and L-Arg proteinoids. Image magnification is 10000x. C.Chlorella microsphere with a diameter of 3.54 μm encapsulated by proteinoids. Image magnification is 20000x. D.Chlorella microsphere with a 3.64 μm diameter encapped into a dense network of proteinoids with neuron-like formations. Image magnification is 25000x.

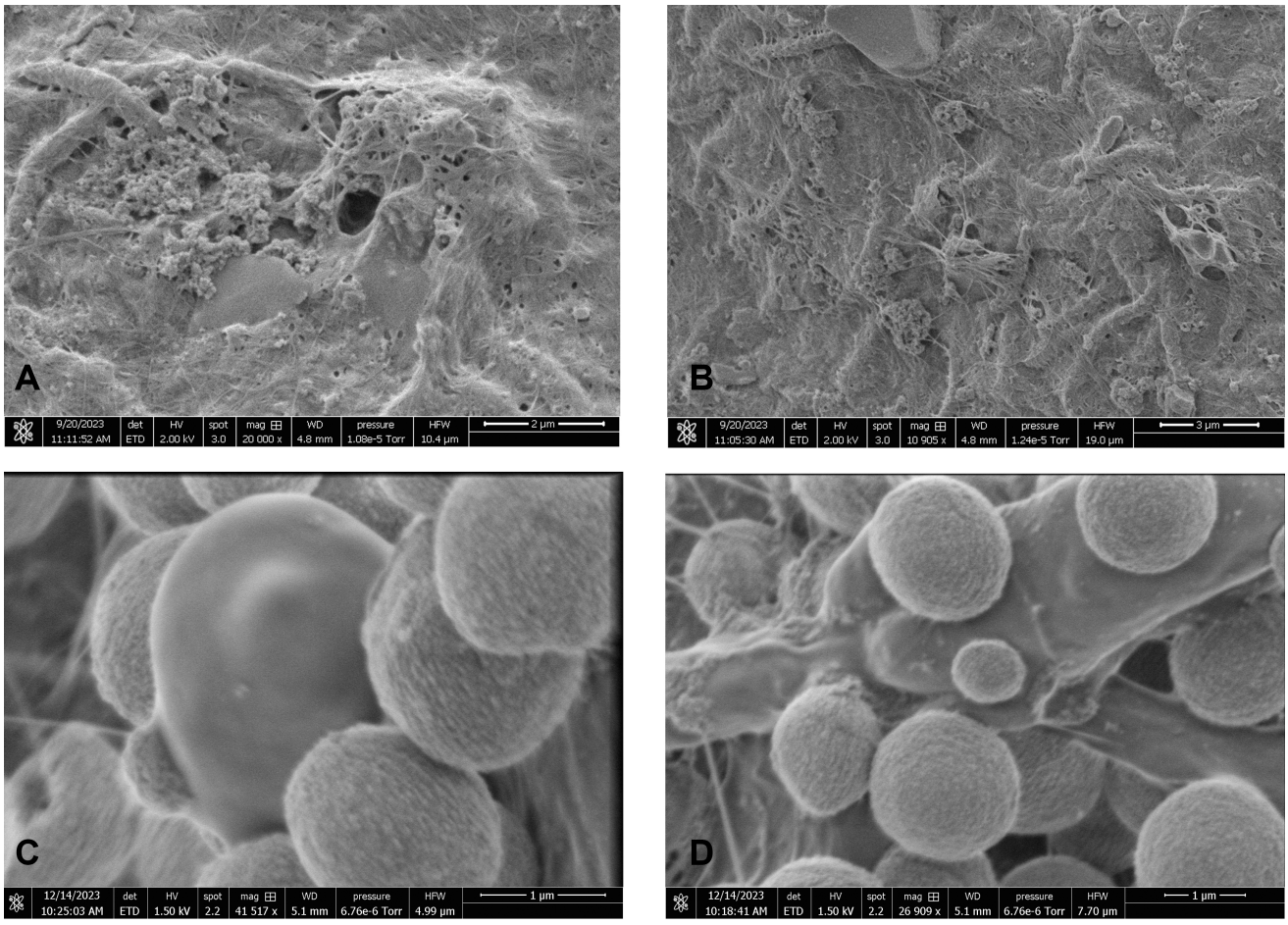


Figure 5.22: A.and B.Matrix of yeast and bacteria cells entangled with L-Glu and L-Arg proteinoids, injected into the Kombucha cellulosic film. Image magnification is 10000x. C.Proteinoid microspheres with diameter of 2.08 μm encapsulating a yeast cell of length 2.8 μm. Image magnification is 41517x. D.Image magnification is 26909x.

SEM performed on the Kombucha film injected with L-Glu and L-Arg proteinoids, as well as Kombucha solution containing L-Glu and L-Arg proteinoids, revealed similar features of integration. It is worth noting that when proteinoids are immersed in an aqueous solution at moderate temperature, they form microspheres (Fox, 1992), as evident in the images C & D of (Figure 5.22), where the proteinoids were mixed with Kombucha microbial solution. This contrasts with the neuron-like proteinoid formations observed in the images A & B of (Figure 5.22) of the Kombucha film injected with L-Glu and L-Arg proteinoids. In image C, proteinoid microspheres with diameter of 2.08 μm encapsulating a yeast cell of length 2.8 μm are observed. A 0.76 μm proteinoid growth on the yeast cell is identified, exhibiting identical morphology to Kombucha yeast cell's bud-parent junctions and birth scars. It is therefore possible that Kombucha functionalised with proteinoids can display life-like properties such as hybrid budding, self-growth, self-assembly, and self-replication through the integration of its components(Figure 5.23).

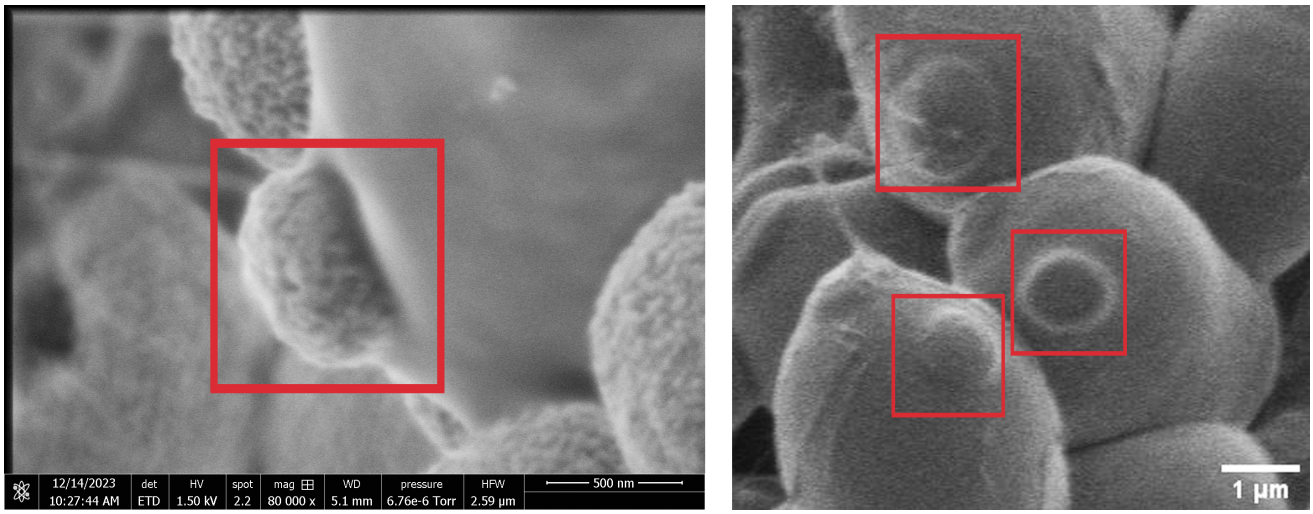


Figure 5.23: A.0.76 μm proteinoid growth identified on a yeast cell, presenting identical morphology to Kombucha yeast cell's bud-parent junctions and birth scars. Image magnification is 80000x. B.Bud-parent junctions and birth scars of diameters 1.33 μm, 0.93 μm, and 0.95 μm. Image magnification is 7000x.

The Kombucha & *Chrlorella vulgaris* mat, grown through in situ fermentation, was also subjected to SEM and ESEM (Figure 5.25) to investigate the structural properties of the new material formation resulting from the multi-organism symbiotic pairing of the Kombucha microbial community and the microalgae, as described above. Chlorella microspheres identified in the images measure 2.78 μm and 3.25 μm in diameter and can be reported in close proximity to the yeast cells, with a distance of approximately 0.24 μm, entangled in a mesh of dense cellulose fibers. This may indicate the restructuring and reorganisation of the yeast and bacteria cells, leading to the formation of a new structure that integrates both microbial and microalgal components(Figure 5.24).

The above investigations indicate that functionalisation and multi-species pairing of the Kombucha cellulose films may lead to the development of hybrid living materials that display new structural formations with distinct structures through the reorganisation and the integration of their components. Additionally, the newly formed hybrid materials continue to exhibit life-like properties such as self-growth, self-replication, self-assembly, and self-regeneration mechanisms following functionalisation and multi-species pairing with the use of fermentation process(Figure 5.26). Further research can be undertaken to investigate how the properties can be tuned by controlling the concentrations of the components. An example includes the integration of Chlorella into the Kombucha solution. The acidity of the Kombucha solution medium (pH below 3), due to the presence of yeast activity, can inhibit the development of hybrid Kombucha cellulose and microalgae materials since algae's survival rate in such acidic environment could be low. Despite this hypothesis, high-magnification SEM performed on the hybrid Kombucha- Chlorella samples revealed microalgae Chlorella beads enveloped in a mesh of bacterial cellulose fibres. This entanglement of the microalgae is likely a result of their oxygen release,

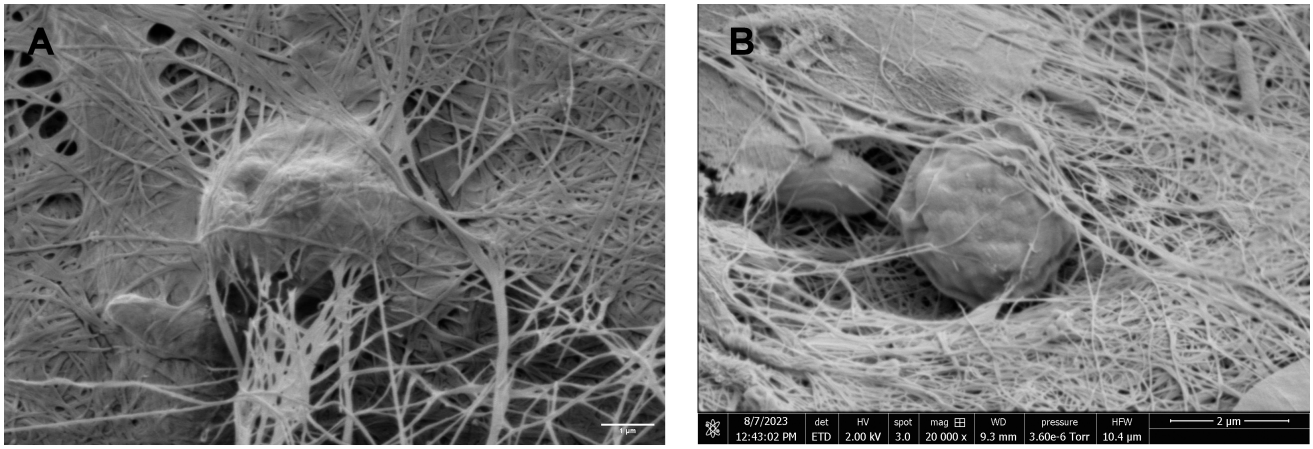


Figure 5.24: A.Chlorella microsphere measuring 2.78 μm in diameter integrated within a network of cellulose fibers. Image magnification is 20000x. B.Chlorella microsphere measuring 3.25 μm in diameter observed in close proximity, at a distance of 0.24 μ, to a yeast cell. Image magnification is 20000x.

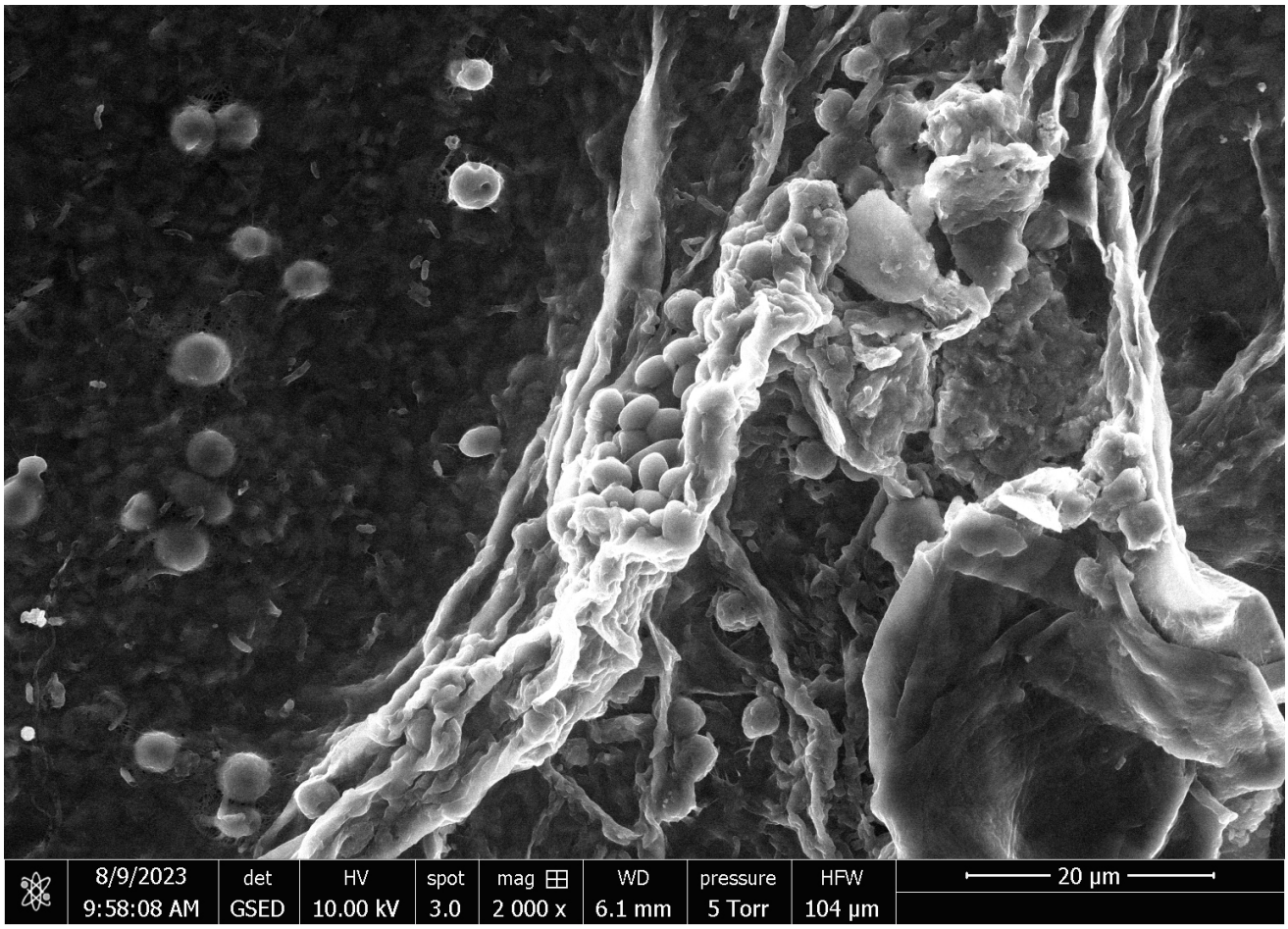


Figure 5.25: ESEM of Kombucha-Chlorella sample. Image magnification is 2000x.

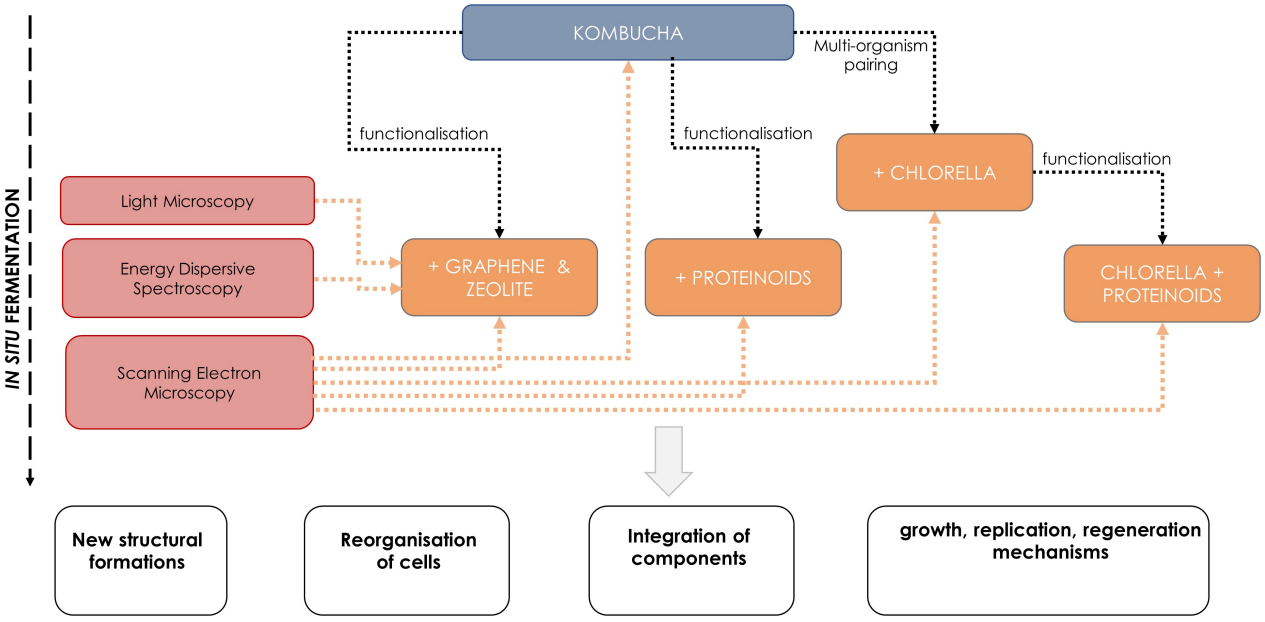


Figure 5.26: Morphological characterisation process

which attracts the bacteria, enabling the production of cellulose (Das et al., 2016). Further research is required to establish the specific conditions, such as the concentration of yeast-bacteria-microalgae solution, fermentation time, and medium acidity, for retaining both microorganisms in a living state.

Evaluating functional capabilities- sensitivity, selectivity, and self-assembly

Transmission of information

For the functionalised with proteinoids Kombucha and Kombucha-Chlorella samples, exposure to electrical input signals (input amplitudes of 10 mV $\pm$0.1 and input frequency of 0.055 Hz) resulted in increased output signals. It is worth noting that the proteinoids-Kombucha-Chlorella samples generated significantly higher output potentials compared to the proteinoids-Kombucha samples when subjected to the same input potentials, despite minor frequency swifts.

In specific, the 40% proteinoids- 60% Kombucha-Chlorella sample showed an increase in amplitude from 10.04 mV to 352.28 mV, while the 25% proteinoids- 75% Kombucha-Chlorella sample demonstrated a similar increase from 10.06 mV to 360.59 mV, with the input frequency remaining constant. On the other hand, the 40% proteinoids- 60% Kombucha sample generated an increase in amplitude from 9.96 mV to 26.13 mV, and the 25% proteinoids- 75% Kombucha sample presented an increase from 9.98 mV to 27.41 mV. A pure proteinoids sample demonstrated a decrease in amplitude observed at higher input amplitudes. The 40% proteinoids- 60% Kombucha-Chlorella sample generated an in-

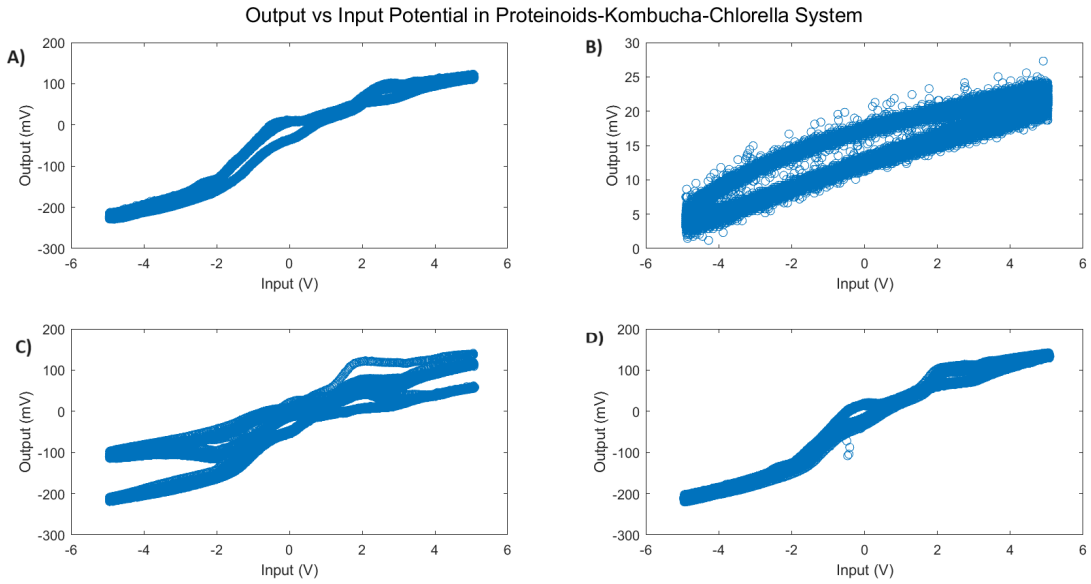


Figure 5.27: Relationship between input and output potential for the samples. A.40% proteinoids- 60% Kombucha-Chlorella. B.40% proteinoids- 60% Kombucha. C.25% proteinoids- 75% Kombucha-Chlorella. D.25% proteinoids- 75% Kombucha. Samples A and C, which contain Kombucha-Chlorella, exhibit steeper slopes compared to samples B and D, which consist solely of Kombucha. Samples A and C can generate higher output potentials for the same given input potentials. The plot showcases how proteinoids-Kombucha biofilms can be optimised to improve signal transmission under various input conditions.

crease in frequency from 0.055 Hz to 0.114 Hz, and the 25% proteinoids- 75% Kombucha-Chlorella sample showed a similar increase from 0.055 Hz to 0.120 Hz. The 40% proteinoids- 60% Kombucha sample generated an increase in frequency from 0.055 Hz to 0.256 Hz, and the 25% proteinoids- 75% Kombucha sample exhibited an increase from 0.056 Hz to 0.272 Hz(Figure 5.27).

It is therefore possible that there are synergistic interactions taking place between proteinoids, the microbial community, and the microbial-microalgae components. These interactions could be attributed to the establishment of interconnected pathways between the microbial community, microalgae, and proteinoid nanostructures, allowing electron transfer throughout the Kombucha hybrid structure. This facilitates the efficient transmission of input signals with increased amplification, demonstrating the Kombucha hybrid material's ability to process inputs effectively.

Memfractive behaviour

Capacitance measurements across a range of input frequencies (1 and 300 kHz) were taken for the Kombucha, Kombucha-Chlorella, Kombucha-Chlorella-proteinoids, Kombucha-proteinoids, and proteinoids samples. The results demonstrated voltage-dependent characteristics, showing an overall de-

crease in capacitance as the frequency increased. Irregular peaks were observed(Figure 5.28), indicating the occurrence of distinct channels for charge transfer within the architecture of the Kombucha hybrid material, activated at specific frequency resonances. Spikes in capacitance were observed for the Kombucha-Chlorella and Kombucha samples, and capacitance wells for the Kombucha-Chlorella-proteinoids, Kombucha-proteinoids, and proteinoids samples. The Kombucha samples demonstrated the lowest capacitance median value of 73.4 nF, while the proteinoids sample displayed the greatest median value of 658.6 nF. These findings suggest that incorporating proteinoids with microbial components enhances the material's dielectric permittivity.

Capacitance modulation in response to varied input frequencies shows that the Kombucha-proteinoid network actively adapts and reconfigures its structure and characteristics dependent on the stimuli. The Kombucha hybrid material undergoes molecular and morphological adaptations as the input frequency changes, resulting in changes to its dielectric properties and charge storage capacity.

In addition to the capacitance measurements, impedance measurements across a range of input frequencies were taken for the Kombucha, Kombucha-Chlorella, Kombucha-Chlorella-proteinoids, Kombucha-proteinoids, and proteinoids samples. Similarly to the capacitance measurements, a decrease in impedance was observed. The decrease was followed by the attainment of plateau values, suggesting the presence of a frequency threshold beyond which the passive electrical properties remain stable. The Kombucha sample displayed the maximum median impedance of 2655.5 Ω, indicating greater resistive properties. In contrast, the Kombucha–proteinoid sample exhibited the lowest median impedance at 945.5 Ω, suggesting complexes more conducive to charge transport(Figure 5.29).

The conductivity profiles of the Kombucha, Kombucha-Chlorella, Kombucha-Chlorella-proteinoids, and Kombucha- -proteinoids samples provided further information regarding the reorganisation of conductive components within the proteinoid-microbial-algal matrix and the ability to effectively transport charge(Figure 5.30). The conductivity σ was determined by using the measured capacitance values and applying the following relation:

$$\sigma = \frac{1}{\omega C \sqrt{1+\tan^2(\phi)}} \tag{5.1}$$

The symbol ω represents the angular frequency, C represents the capacitance, and ϕ represents the phase angle between the current and voltage. The combination of proteinoids with the microbial components resulted in increased conductivity compared to the pure Kombucha, Kombucha-Chlorella, and proteinoids samples. The Kombucha-Chlorella, Kombucha-proteinoids-Chlorella, and proteinoids samples exhibited the highest conductivity across a wide range of frequencies, indicating a higher level of charge mobility. The samples showed a decrease in conductivity as the frequency increased.

Capacitance measurements across a range of frequencies (1 and 300 kHz) were taken for the unmodified Kombucha and functionalised with graphene-zeolite Kombucha samples. The measurements were performed before and during the exposure to different loads. The results revealed that the capacitance of the unloaded functionalised mat was nearly double of the unloaded unmodified mat. The

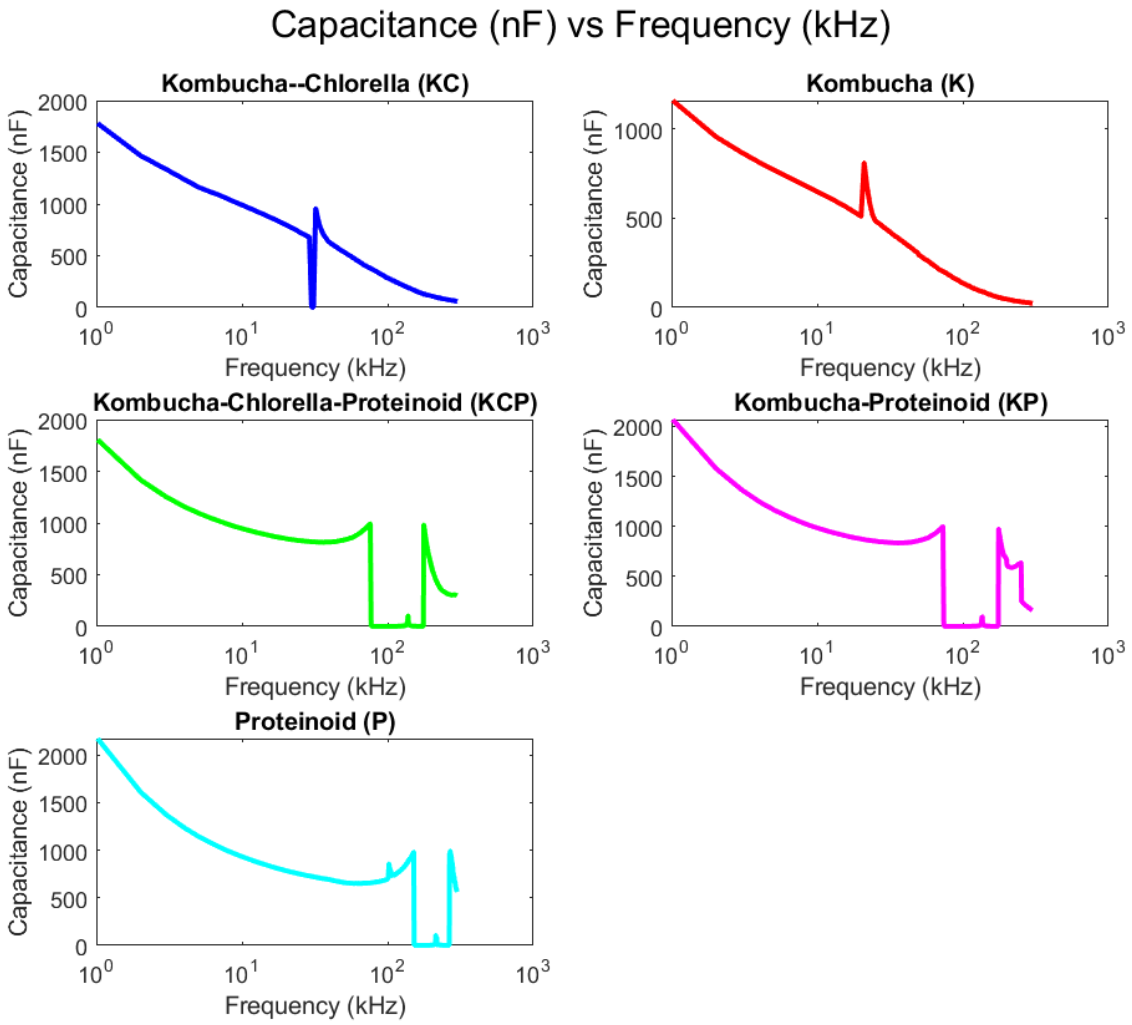


Figure 5.28: The capacitance as a function of frequency is measured for the Kombucha, Kombucha-Chlorella, Kombucha-Chlorella-proteinoids, Kombucha- proteinoids, and proteinoids samples. The capacitance of all samples decreases in a linear manner as the frequency increases.

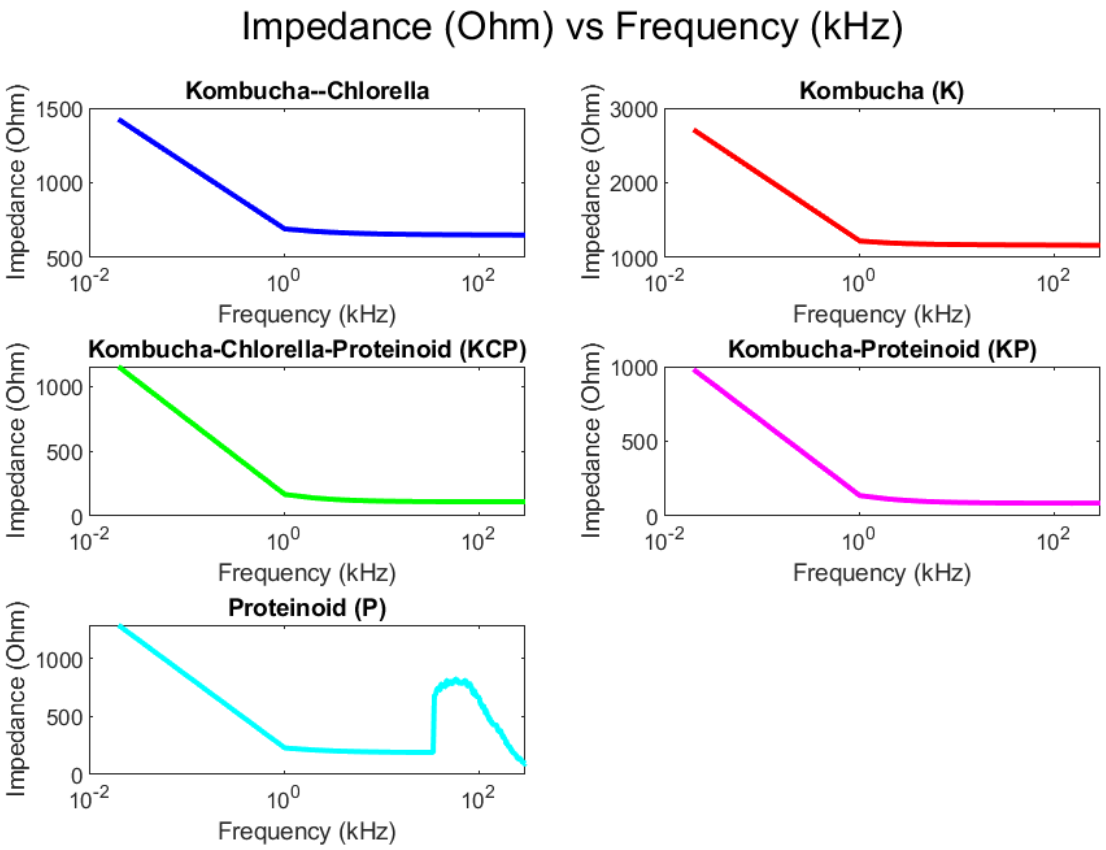


Figure 5.29: Impedance measurements obtained from Kombucha, Kombucha-Chlorella, Kombucha-Chlorella-proteinoids, Kombucha-proteinoids, and proteinoids samples. Plot depicts a linear decrease in impedance until stabilised at 1.02 kHz, indicating frequency-independent impedance above 1 kHz for all samples. An exception is observed for the pure proteinoids, which exhibit a significant increase in impedance from 189.5 to 821.1 Ω within the frequency range of 34–278 kHz.

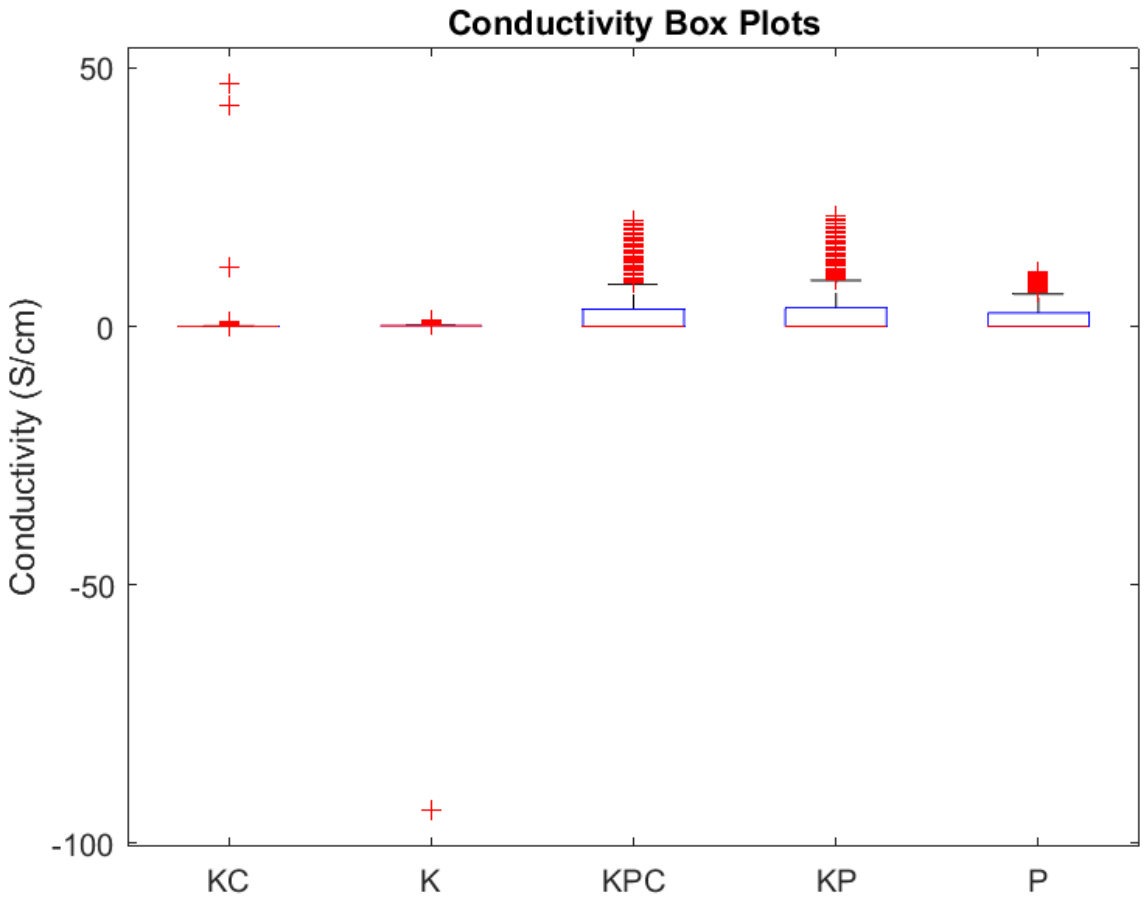


Figure 5.30: Boxplot comparison analysis of conductivity values for Kombucha, Kombucha-Chlorella, Kombucha-Chlorella-proteinoids, Kombucha-proteinoids, and proteinoids samples. The samples consisting of proteoinoids with Kombucha-Chlorella showed higher conductivity compared to samples containing Kombucha alone.

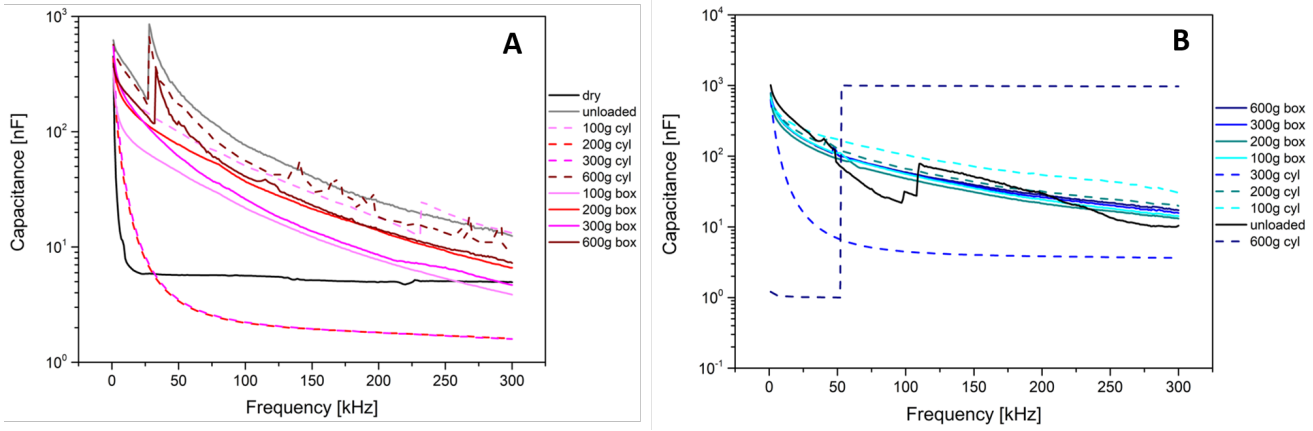


Figure 5.31: Capacitance as a function of frequency A.Kombucha response prior and under load application of 100 g, 200 g, 300 g, and 600 g. B.Kombucha-graphene-zeolite response prior and under load application of 100 g, 200 g, 300 g, and 600 g.

capacitance curves of the unmodified mat under various loads did not show any correlation with the load amount or shape of the applied load. On the contrary, the functionalised mat curves showed a more controlled behaviour. The deformation induced by 100 g and 200 g loads led to a reduction in capacitance(Figure 5.31).

Resistance measurements taken from the pure Kombucha and the functionalised graphene- zeolite Kombucha samples, in both dry and living conditions, showed that the dry functionalised mat featured a lower resistance compared to the pure Kombucha mat, attributed to the conductivity enhancement provided by the graphene addition. The consecutive loading of the mat resulted in a reduction of resistance, reaching a maximum with the intermediate loading of 200 g, then recovering back, and eventually becoming even higher than the unloaded state for the loading of 600 g. Similarly, for the functionalised Kombucha mat, the 100 g and 200 g loads reduced the resistance, while the 300 g and 600 g loads increased it, but to values lower than the unloaded state.

Current-voltage (I-V) measurements were collected for the Kombucha, Kombucha-Chlorella, Kombucha-Chlorella-proteinoids, Kombucha- proteinoids, proteinoids, and Kombucha-graphene-zeolite samples. Cyclic voltammetry (20 cycles) over 0 V to 5 V and -1 V to 1 V voltage ranges was performed for the Kombucha, Kombucha-Chlorella, Kombucha-Chlorella-proteinoids, Kombucha- proteinoids, and proteinoids samples. For the larger voltage range, the maximum conducted current was expected to be far greater (Beasley et al., 2020). Distinct 'curved' (Gale et al., 2014), non–zero-crossing (Sun et al., 2020a), pinched hysteresis loops, which are characteristic of memristive systems, were observed in the current-voltage characterisation of the Kombucha, Kombucha-Chlorella, Kombucha-Chlorella-proteinoids, and Kombucha- proteinoids samples. The extent of pinching observed in the I-V curves of the Kombucha-Chlorella-proteinoids, Kombucha- proteinoids, and proteinoids samples was greater compared to the Kombucha and Kombucha-Chrlorella samples, indicating memory functionalities de-

riving from the proteinoids, microbial, and algae consortium. In addition, the Kombucha-Chlorella-proteinoids, Kombucha- proteinoids, and proteinoids samples produced higher currents for both 0 V to 5 V and -1 V to 1 V voltage ranges, and therefore exhibited lower resistances than the Kombucha and Kombucha-Chlorella samples, suggesting greater conductivity. The proteinoids sample displayed a reduced average current in comparison to the Kombucha–proteinoids during the recorded voltage sweeps, suggesting that the addition of the Kombucha contributes to enhanced conductivity(Figure 5.32).

I-V measurements taken from the pure Kombucha and the Kombucha-graphene-zeolite samples showed that for the unmodified Kombucha sample, distinct 'curved', (Gale et al., 2014) non–zero-crossing (Sun et al., 2020a) curves were observed, which were very close. Additionally, the loading did not provide any strong variation. For the functionalised sample, the loaded curves had five times bigger current than the unloaded. Therefore,loading the functionalised mat produces higher currents (lower resistances and higher conductivity), whereas loading the pristine mat produces lower currents (higher resistances and lower conductivity)(Figure 5.33).

Spiking dynamics

To draw conclusions regarding spiking activity and spiking dynamics, the voltage oscillation patterns of the Kombucha-Chlorella-proteinoids samples were studied (Figure 5.34). Rhythmic spiking activity was observed over time, and the periodicity analysis revealed a mean surge interval of approximately 4000 seconds, or 1 hour. The amplitude histogram showed a normal distribution of spike peaks, with a mean value of –45 mV. Fourier Transform analysis of the oscillatory signal revealed prominent frequencies. Exposure to a depolarising pulse of 50 mV showed the ability to regulate the activity of spiking through stimuli. Rapid depolarisation of 50 mV induced repetitive spikes with a regular period of 6 minutes. The shape of the spike exhibited rapid rise and slower decline dynamics, with an amplitude of 25 mV(Figure 5.35).

The voltage oscillations and spike statistics findings suggest that the Kombucha-Chlorella-proteinoids nanostructures exhibit neuron–like signaling behaviours. The ability to regulate the activity of the spiking through stimuli, such as rapid depolarisation, indicates their potential for transmitting information.

In addition to the analysis of the electrical activity recordings for the Kombucha-Chlorella-proteinoids sample, the activity of the pure Kombucha and the Kombucha functionalised with graphene-zeolite samples was also analysed. The results showed increased spiking activity with a large baseline fluctuation compared to a spontaneous activity range (approximately 20 mV). Fast Fourier Transform (FFT) and Higher Order Complexity (HOC) metrics were used to gain a clearer understanding of the behaviour under different loading conditions for the two samples and to interpret their spontaneous oscillations over long timescales. The FFT analysis showed the distribution of the noise spectrum across the mat sensors over various frequencies. For 100 g load application, a broad peak spanning 0.1 to 0.2 Hz was observed in the functionalised mat data, but not in the pure Kombucha mat data. For 200 g load application, cleaner oscillation profiles were observed in the pure Kombucha mat, while the function-

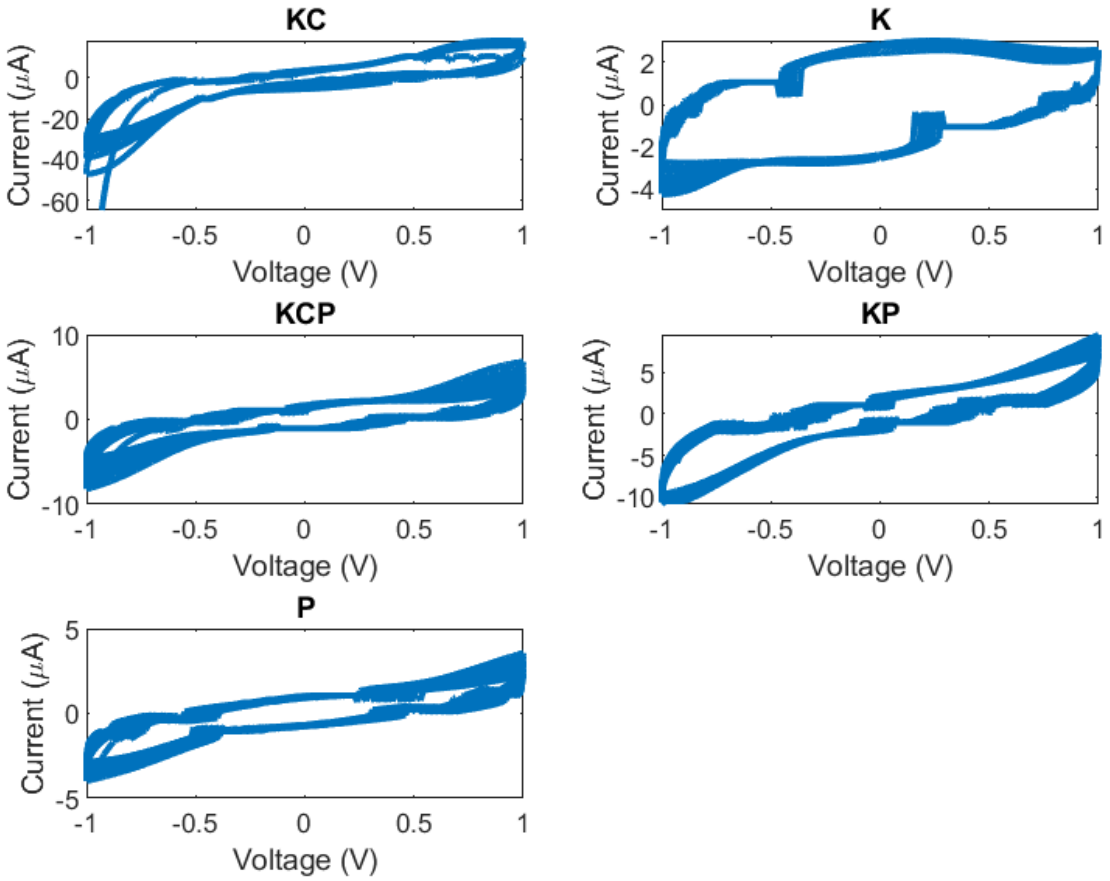


Figure 5.32: Current-voltage (I–V) profiles produced from measurements performed in the -1 V to 1 V voltage range (20 cycles) for Kombucha-Chlorella, Kombucha, Kombucha–Chlorella-proteinoids, Kombucha–proteinoids, and proteinoids samples. The I–V curves indicate 'curved'pinched hysteresis loops that are characteristic of memristive systems.

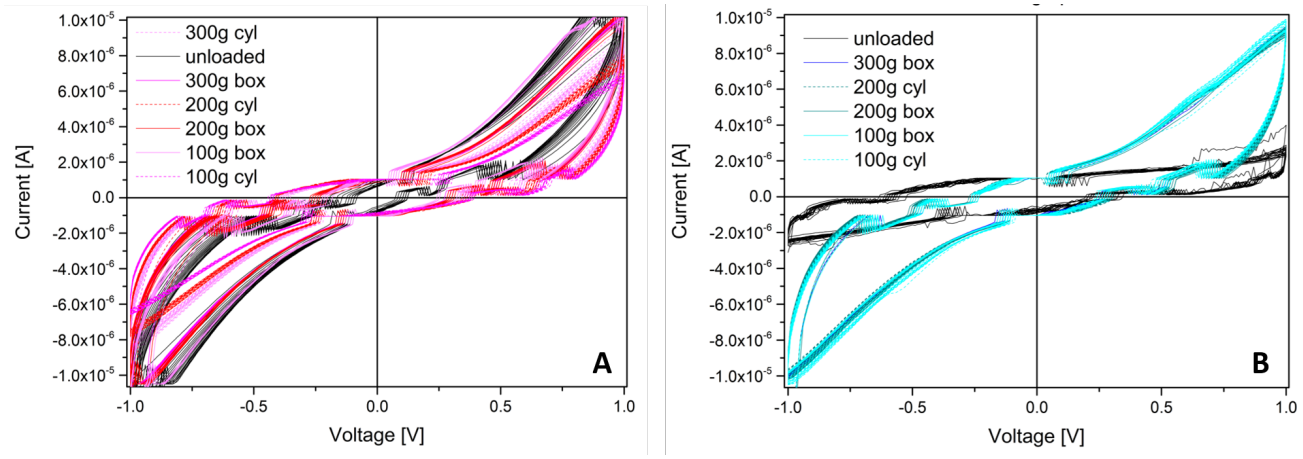


Figure 5.33: Hysteresis cycles showing the I-V response of the mats. Measurements taken in the -1 V to 1 V voltage range and for 20 cycles. (A)Kombucha response to the different loads and (B)functionalised Kombucha response to the different loads.

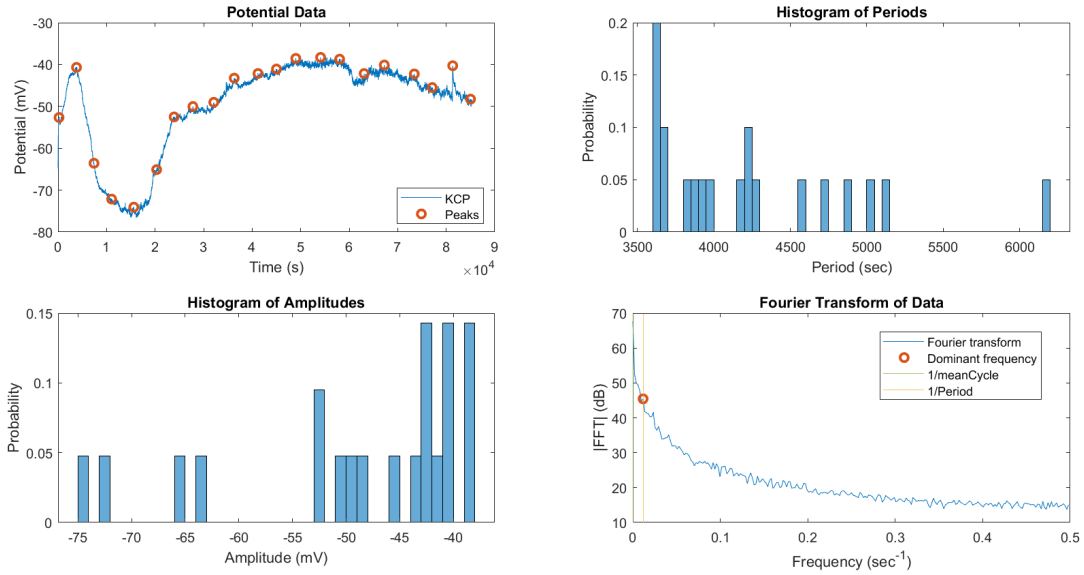


Figure 5.34: Statistical analysis of oscillation patterns of Kombucha-Chlorella-proteinoids sample. (a) Time-lapse voltage trace with rhythmic spikes in mV. (b) Histogram of oscillation times in seconds, with a mean of 4240.65 seconds and a median of 4068.50 seconds. (c) Histogram of spike amplitude peaks in mV, with a mean of -48.58 mV, a median of -43.25 mV, and a standard deviation of 11.09 mV. (d) Fourier transform examination of the oscillatory signal revealed prominent frequencies.

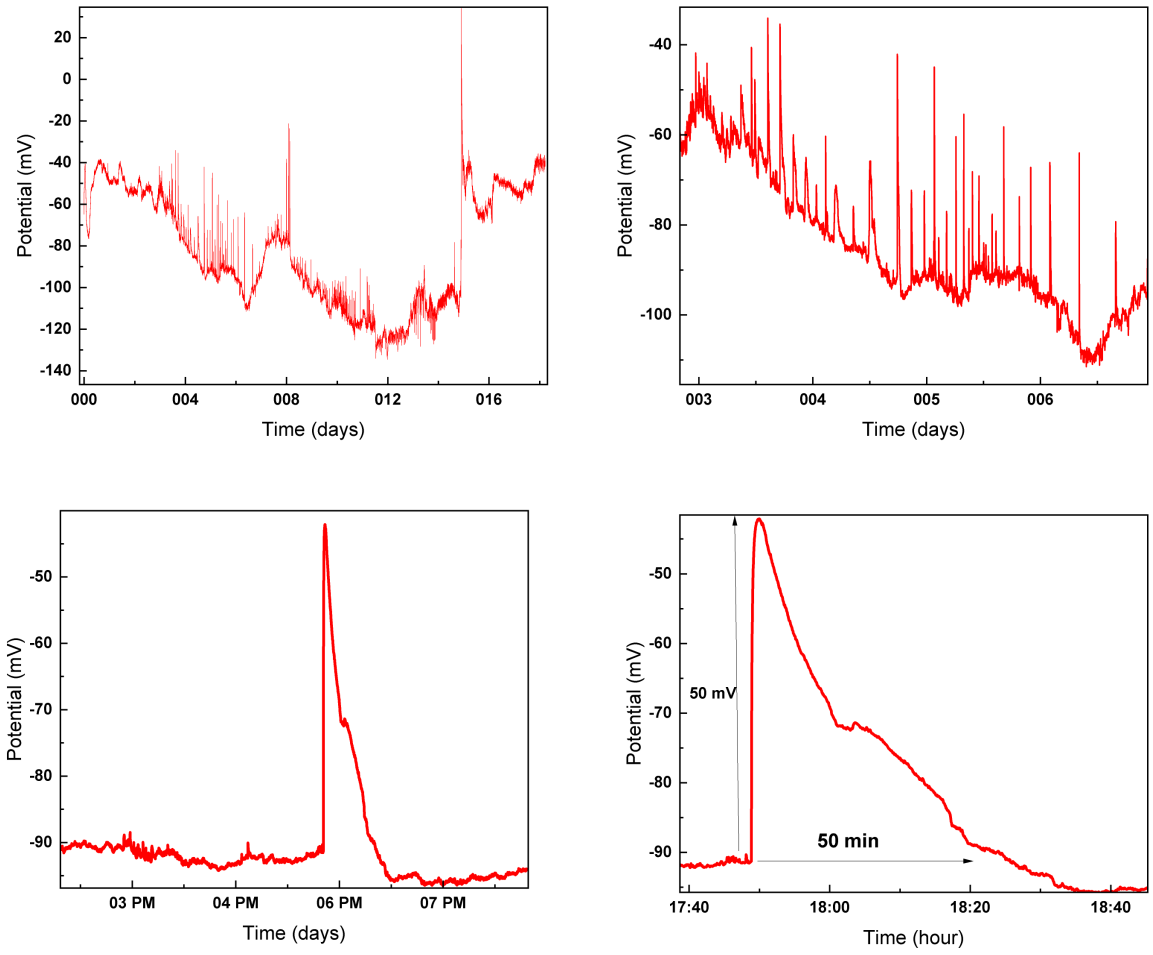


Figure 5.35: The dynamics of spiking after a depolarisation pulse of 50 mV. The voltage trace exhibits repeated spikes over time.

alised mat exhibited similar modes at slightly shifted frequencies, potentially indicative of increased conductivity.

Building Logic

In digital computing, logic gates have a binary output, either 0 or 1, in response to one or more inputs. Fundamental logical operations were implemented, and the input-output data from the Kombucha-Chlorella-proteinoids samples were processed to generate AND, OR, XOR, XNOR, NAND, and NOR logic gates, demonstrating the Kombucha hybrids' ability to execute signal processing and perform logic operations. The applied voltages for the input signals ranged from -4 to +4 V.

Molecular origins of the observed behaviour

The above results demonstrate that the Kombucha-based ELMs exhibit unique spiking dynamics, generating and transmitting electrical signals. The variations in the spiking patterns and electrical responses may be attributed to their distinct chemical composition and cell-to-cell biochemical communication processes. Kombucha biofilms are aggregates of microorganisms, yeasts and bacteria, embedded in a self-produced matrix of extracellular polymeric substances (EPS) (Vert et al., 2012). This pellicle system is fundamental for the microbial community, performing functions such as limiting the diffusion of toxins, mitigating the impact of extreme conditions in environmental parameters such as pH and temperature, and facilitating access to oxygen and nutrients (Flemming et al., 2016; Davies et al., 1998; Carlier, Pessi, and Eberl, 2015). The formation of the biofilms is a regulating mechanism that can be modulated by certain bacteria, including species of acetic acid bacteria (AAB), through the use of signaling molecules (Gullo et al., 2018). It is, therefore, possible that AAB, which are part of the Kombucha microbial consortium, contribute to the coordination of the biofilm's behaviour by detecting changes in local cell distribution and density. In other words, the biofilms may exhibit quorum sensing mechanisms, functioning through the secretion and detection of autoinducer molecules that accumulate in a cell density-dependent manner. When autoinducer concentrations reach a threshold level, quorum-sensing cells respond, allowing them to modulate behaviours whose efficacy and fitness benefits depend on the presence or absence of other cells (Nadell et al., 2008).

During the functionalisation process and the introduction of the proteinoids, microalgae, and graphene-zeolite nanoparticles, the dynamics of cell distribution and density within the ELM system are affected, potentially activating quorum sensing mechanisms that influence the structure and behaviour of the biofilms. Additionally, the yeasts in the Kombucha microbial consortium enhance the formation of the biofilm and the secretion of EPS (Tran et al., 2021), which creates the matrix in which the microbial cells and nanoparticles are embedded. Quorum sensing may enable the bacteria to turn on and off the secretion of EPS, increasing their competitive ability against the other species and strains within biofilms (Nadell et al., 2008). This mechanism may influence the distribution of the different compo-

nents within the Kombucha hybrids, their biochemical interactions, and ultimately be responsible for the varying intensities and durations observed in their spiking activity.

In bacterial biofilms, changes in membrane potential involve the movement of charged species across the cellular membrane. Biofilms can generate collective metabolic oscillations, which result from long-range metabolic interactions between interior and peripheral cells (Liu et al., 2015). Bacteria also employ active potassium transport mechanisms and potassium ion-channel-mediated electrical signals to coordinate metabolism within the biofilm (Prindle et al., 2015). It is likely that Kombucha ELMs utilise specific ion channels and transporters for signaling. Additionally, the acetic acid production by AAB creates pH gradients, which may contribute to membrane potential differences and the generation of electrical signals within the Kombucha biofilms (Clementi et al., 2014; Humphries et al., 2017). The conductive properties and large surface area of graphene-zeolite nanoparticles enhance electron transfer, potentially creating localised conductive pathways within the EPS matrix. Additionally, proteinoids, due to their amphiphilic nature, can interact with cell membranes to form ion channels or alter membrane permeability. These processes may collectively modify the system's electrical properties (Fox and Nakashima, 1980; Khurana et al., 2019).

The distinct spiking behaviours observed in Kombucha-based ELMs may be attributed to the interactions between ionic currents and cell membrane potential dynamics. In these systems, microbial cells and the biofilm matrix can function as an interconnected network of electrical components, where ion channels and redox processes facilitate ion movement across cell membranes. The complex interactions among microbial species, metabolites, and the extracellular matrix can influence the membrane potential, leading to the varied spiking patterns observed (Mougkogiannis, Nikolaidou, and Adamatzky, 2024). The functionalisation of the Kombucha films with proteinoids, microalgae and graphene-zeolite nanoparticles may create additional pathways for charge transfer, modifying the local electrical environment within the Kombucha matrix. This process could lead to the emergence of the unique spike patterns and memfractive behaviours. By adjusting the composition, concentration, and growth conditions of the components within the Kombucha matrix, it may be possible to enhance the system's transducing and signal-processing capabilities, tailoring it for various applications.

5.1.4 Contribution of findings to answering research questions- validation of hypothesis

The above key findings from the electrical and morphological characterisation, as well as the analysis of the electrical activity of the samples, suggest that:

- The functionalised Kombucha samples presented high sensitivity and selectivity characteristics through distinct electrical potential oscillations and electrical spiking dynamics, which exhibited variability in speed. Equally, it was possible to extract a unique fingerprint of spiking activity and

conductivity both before and after exposure to stimulation. These attributes are linked to learning and decision-making mechanisms, suggesting adaptive and autonomous capabilities.

- Efficient transmission and processing of information was observed. Additionally, it is possible to tune the properties of the Kombucha hybrid materials by regulating the stimulation.

- Memfractive behaviour was observed, resembling the spiking dynamics and excitability present in biological neural networks, thus indicating learning, memory, and information processing functionalities.

- Functionalised Kombucha hybrids showed enhanced properties, such as improved electrical conductivity, attributed to the introduction of additional components with the living cells (self-assembly). This could allow the modulation and tuning of the material's properties.

- The electrical characterisation of the immobilised Kombucha biofilms showed significant current fluctuations, including spiking patterns and memristive switching characteristics. These fluctuating characteristics create time-dependent behaviours in biofilms, allowing them to store historical information, adapt their electrical properties to new inputs based on past states, and evolve based on the timing and order of the stimuli inputs. This stimuli-dependent adaptability, or plasticity, is a fundamental feature of brain synapses. It enables cellular mechanisms of learning, memory formation, and other cognitive processes (Warraich and Kleim, 2010). The mechanisms that alter neuronal excitability can lead to plasticity in responses to synaptic stimulation. Intrinsic excitability refers to a neuron's tendency to fire action potentials when exposed to an input signal. This signal can come from presynaptic activity or a direct sensory input. The intrinsic excitability of neurons is responsible for the translation of synaptic input to into a neuron's output and is key to many functions of the nervous system (Schulz, 2006). Repeated stimulation can strengthen synapses over the long term (Abbott and Nelson, 2000). Biofilm plasticity is similar to synaptic plasticity in neural systems. Kombucha biofilms can adapt, presenting opportunities for use in bio-computing and adaptive sensors (Adamatzky, 2019b). The observed memristive traits suggest that the biofilms are like memory devices, their state depending on both current and past inputs (Chua, 2014).

- External stimuli could be employed to train Kombucha hybrids, presenting an opportunity for the integration of machine learning and enabling advanced computing functionalities.

- The functionalised Kombucha samples displayed distinct morphological characteristics. Their bonding capacity is evidenced by the formation of new structures through the integration of their components.

5.2 Fungal Hybrids [Outputs 3-5]

5.2.1 Introduction

Fungi are fascinating examples of complex, self-organising systems. Mycelium, the vegetative lower part of fungi, has been identified as the largest living organism on earth (a mycelium network occupies nearly $10km^2$) in Oregon's Blue Mountains) (Hawksworth, 2001; Haneef et al., 2017). It is abundant, easily accessible, and grows due to its symbiotic relationship with the materials that feed it, forming entangled networks of branching fibers (Bonfante and Genre, 2010). The filaments of the fibrous mycelium are called hyphae and consist of elongated cells. These cells are separated from each other by internal porous cross-walls, named septa, and are all enclosed within a tubular cell wall. The cell wall plays several physiological roles in fungi morphogenesis, protecting the hyphae (Thomson et al., 2015; Papagianni, 2004), and providing mechanical strength to the whole mycelium (Vega, Kalkum, et al., 2012). Mycelium is primarily composed of natural polymers such as chitin, cellulose, and proteins, making it a natural polymeric composite fibrous material (Haneef et al., 2017). Mycelium can be considered a heterogeneous material. Hyphae at the outer part of the colony grow and colonise the substrate, while most hyphae in the central zone of the mycelium do not grow.

The hyphae of some fungi have been shown to be sensitive to electrical fields, growing either toward or away from the cathode or anode (Adamatzky et al., 2021). In addition, hyphal branching could be increased by an electrical field (McGILLIVRAY and Gow, 1986). Conductivity of a mycelium happens mostly in the form of electrolytic conductivity. Living mycelium exhibits almost 13 times lower resistance than dehydrated mycelium (Adamatzky et al., 2021), thus much higher conductivity, making it a promising candidate for the development of mycelium hybrid living materials. Additionally, the collective behaviour of fungi, which emerges from the interactions of individual fungal cells, leads to intriguing phenomena such as spiking activity (Adamatzky et al., 2023). Action potential-like spiking activity in mycelium was first documented in 1976 (Slayman, Long, and Gradmann, 1976). Four types of action potential were identified: (1) spontaneous quasi-sinusoidal fluctuations with an amplitude of 10–20 mV and a period of 3–4 minutes, (2) as previous but with a shorter period of 20–30 seconds, (3) cyanide-induced oscillations with a progressively lengthening period, starting with an initial depolarisation of 20–60 mV, and (4) damped sinusoidal oscillations with an amplitude of 50–100 mV and a period 0.2–2 minutes (Adamatzky, 2018). Moreover, bursts of spiking within trains of spikes were observed, which were similar to the ones observed in the central nervous system (Cocatre-Zilgien and Delcomyn, 1992; Legendy and Salcman, 1985), indicating the possibility that mycelium networks transform information through the interaction of spikes and trains of spikes in a manner homologous to neurons (Adamatzky, 2022b).

The electrical activity was later confirmed in 1995 through intracellular recordings, showing amplitude of spikes from 5 to 50 mV, a duration from 20 to 500 ms, and a frequency between 0.5 and

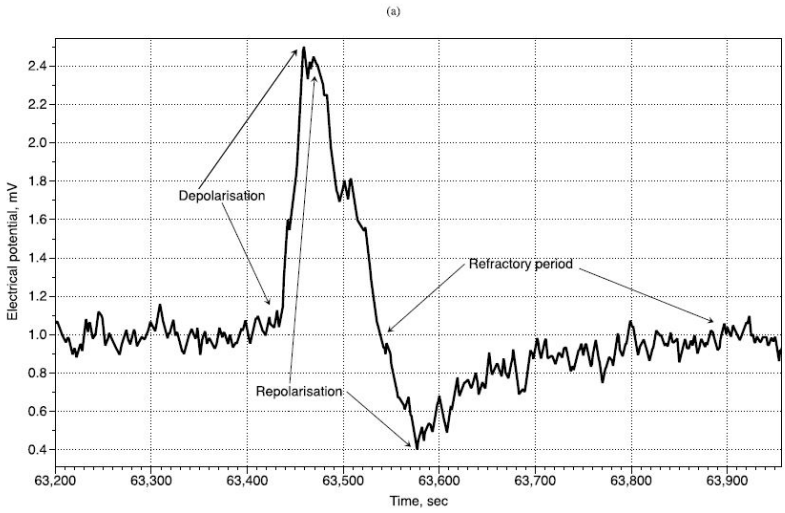


Figure 5.36: Analysis of a spike in terms of action potential. Adamatzky, 2018, On spiking behaviour of oyster fungi *Pleurotus djamor*

.

5 Hz (Olsson and Hansson, 1995). Recently, it was discovered that oscillations can be equally well recorded extracellularly by inserting electrodes into fruiting bodies and colonised substrates. These recordings revealed a rich combination of slow (hours) drift in base electrical potential combined with relatively fasts (minutes) oscillations of the potential. Trains of spikes of electrical potential were observed(Figure 5.37), and each spike resembled an action potential, where all parts were found: depolarisation, repolarisation, and the refractory period(Figure 5.36). In particular, two types of spike trains were identified: high-frequency, with approximately a spike every 2.6 minutes, and low-frequency, with approximately a spike every 14 minutes (Adamatzky, 2018). Therefore, extracellular signals that surpass a certain amplitude threshold with depolarization, repolarisation, and refractory cycles can be referred to as spike events. This method of extracellular recordings by electrode insertion has been employed in this research work to record the electrical potential and spiking activity of the mycelium living hybrid materials.

Fungi can sense diverse environmental, mechanical, and chemical cues through reception, transduction, and response mechanisms, as well as through the display of simple signal- transduction pathways, often equivalent to those present in multicellular eukaryotic organisms. They possess almost all the senses used by humans and can sense light, chemicals, gases, gravity, and electric fields (Bahn et al., 2007). Drawing upon fungi's ability to generate action potential-like impulses of electrical potential in the form of trains of spikes (Adamatzky, 2018; Beasley, Powell, and Adamatzky, 2020), and their capacity to sense environmental, chemical, and mechanical stimulation, this research project aims to investigate the potential to develop fungal hybrid living materials. These materials produce distinct patterns of electrical activity when exposed to targeted stimulants, enabling observations about their autonomous sensing, information processing, learning, logical operations, and computation abilities.

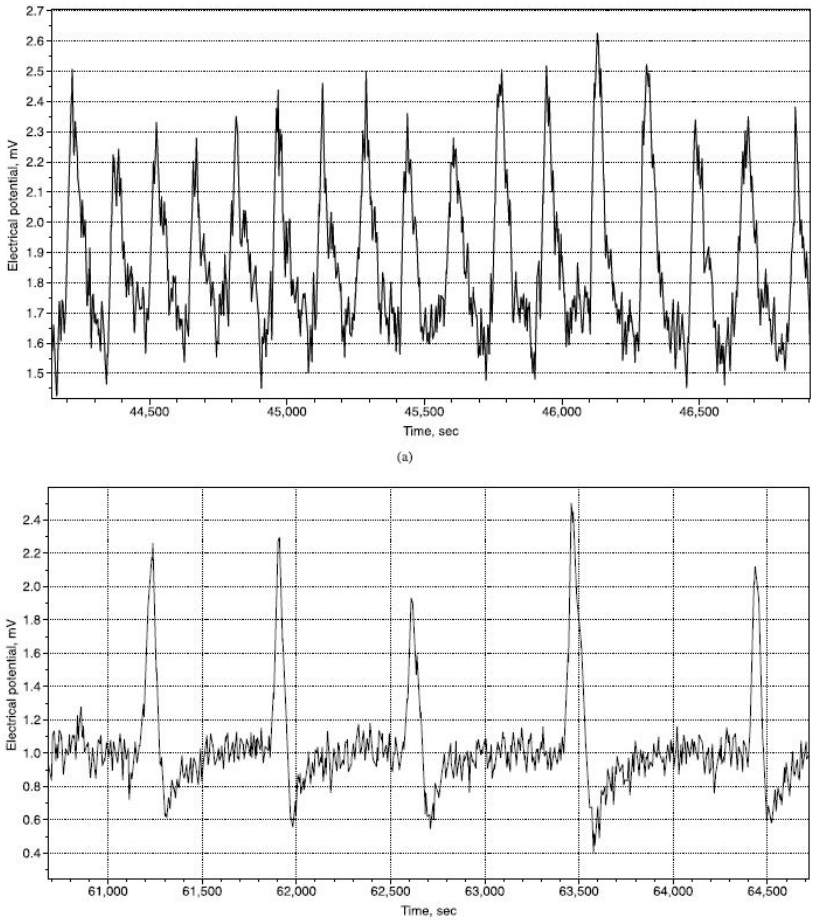


Figure 5.37: Examples of spike trains. (a) High frequency. (b) Low frequency. Adamatzky, 2018, On spiking behaviour of oyster fungi *Pleurotus djamor*

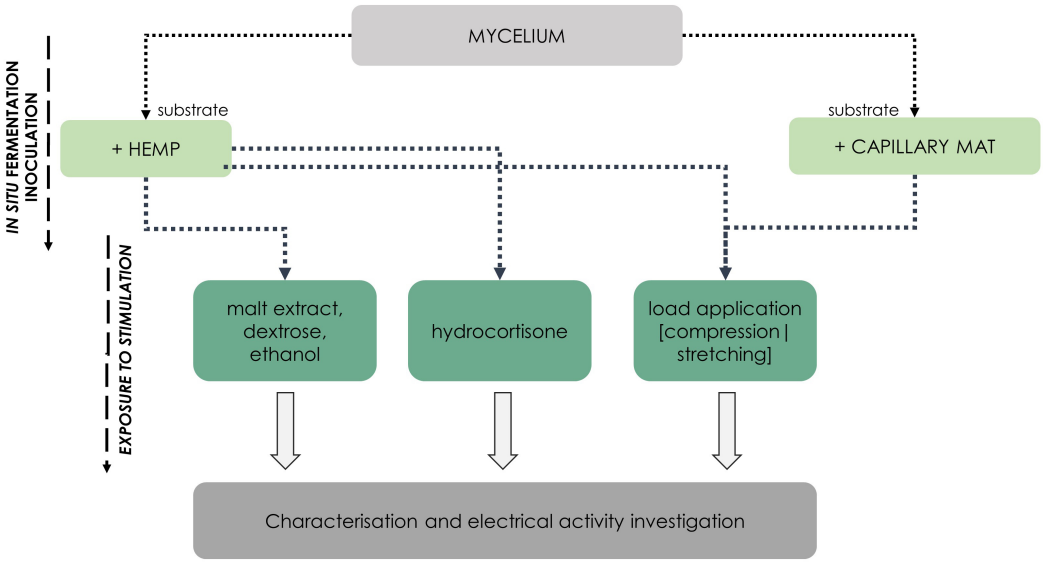


Figure 5.38: Schematic representation of methodological approach for fungal hybrid living materials.

5.2.2 Methods

For the fabrication of fungal hybrid materials, the method of solid state fermentation and inoculation were used. For the stimulation, the samples were subjected to environmental, chemical, and mechanical stimuli. To assess the materials advanced capabilities, data acquisition was performed via recordings of electrical activity and morphological characterisation(Figure 5.38).

Solid State Fermentation-Inoculation

Mycelium binds organic matter through a network of hyphal micro-filaments in a natural biological process (Jones et al., 2017; Holt et al., 2012; Pelletier et al., 2013; Nawawi et al., 2019), utilising biological growth rather than expensive, energy-intensive manufacturing processes to convert low-cost substrates such as hemp, wood-chips, and straw into environmentally friendly material composites. The fungal hyphae grow on these substrates, forming a fibrous mycelium matrix that surrounds, covers, and binds together all the substrate particles, forming a composite solid material (Adamatzky et al., 2021).

To fabricate the fungal hybrids for the performance of the experiments, commercial strains of fungi, including *Pleurotus ostreatus*, were inoculated on a range of substrates. *P.ostreatus* represents an ideal candidate for use due to its rapid growth rate and tolerance to environmental conditions. For the inoculation, hemp was selected based on existing fungal composite development protocols and substrate testing. A series of control experiments were performed to establish protocols that support the optimal growth of mycelium, including variations in hemp types, humidity levels, temperature, and lighting. This process resulted in the selection of the favourable conditions that promoted growth while elimi-

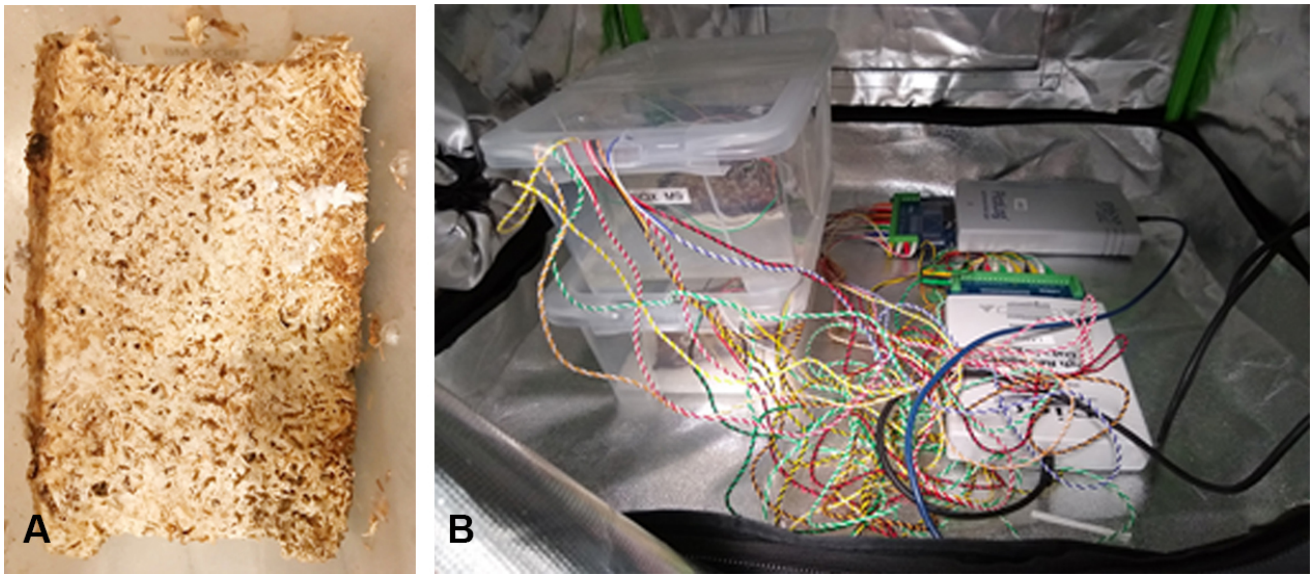


Figure 5.39: A.Inoculation of hemp bedding substrate with *Pleurotus ostreatus* B.SSF and inoculation are conducted under controlled conditions. The samples are sealed in containers with air ventilation and kept in darkness at ambient room temperature.

nating the appearance of contamination and the development of pathogens.

To achieve this, the samples were placed in plastic boxes with fitted air filter patches and kept in darkness at ambient room temperature. The inoculated substrates were placed in a hydroponic growing tent with a light-proof inner lining(Figure 5.39). When the substrates were fully colonised and a coating of white mycelial growth was observed, particles of the colonised fungus substrates were spread on fragments of moisturised hemp fibre mats and multi-layered, absorbent capillary-action matting made from bonded, non-toxic wool and acrylic fibres. The hemp and capillary mats were sealed in plastic containers and bags fitted with air filter patches, then placed again in the hydroponic tent in darkness at ambient room temperature to allow for colonisation.

The mats were checked for growth every three days, and additional moisture was added as required via a manual spray bottle with de-ionised water from a distance of approximately 10 cm to maintain the required humidity levels for keeping them healthy. The mats were kept within the sterile tent at all times, and any sources of contamination were kept away from the tent. After approximately 3-4 weeks, uniform mycelium growth throughout the hemp and capillary matting was observed.

Leveraging the self-growth and binding ability of fungal mycelium, the addition of hemp and capillary mat as substrate nutrients enabled the renewable production of medium to large scale fungal hybrid living materials(Figure 5.40). The use of liquid culture of oyster fungi was also trialed and cultured on hemp mats to monitor the growth rate but proved unsuccessful due to contamination tendencies(Figure 5.41).

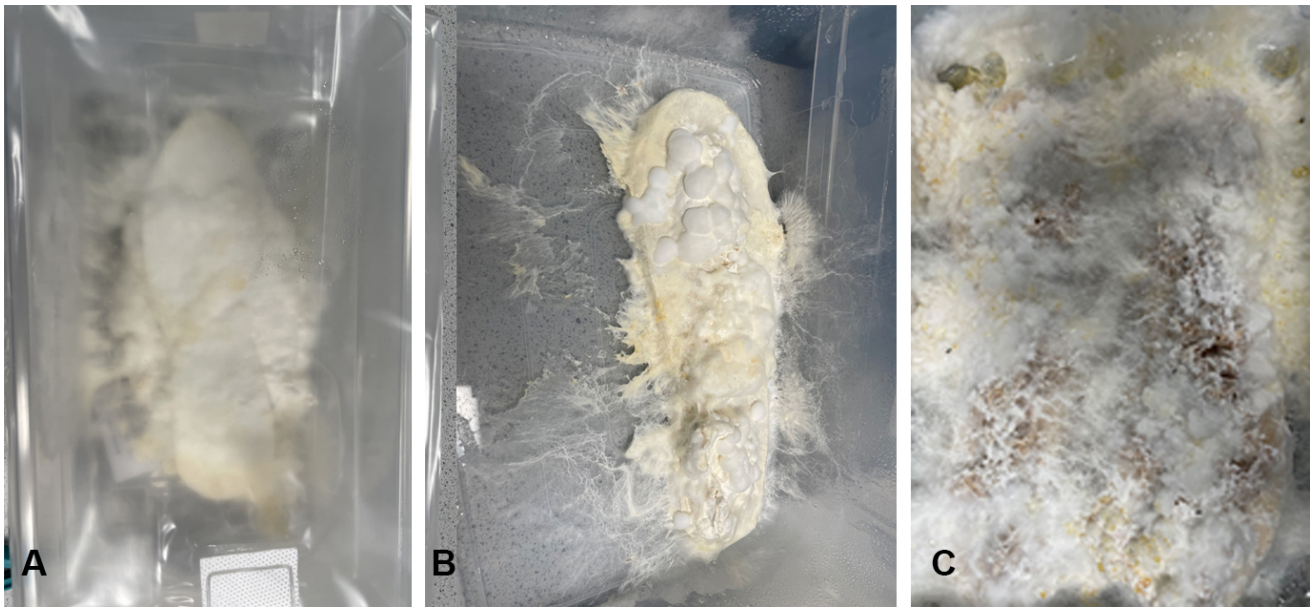


Figure 5.40: A.Fungal colonisation on capillary mat. B.Fungal colonisation on hemp mat. C.Fungal hybrid living materials formed.



Figure 5.41: Contamination and pathogen development observed from the use of liquid culture of oyster fungi.



Figure 5.42: Digital visualisation and real-life image showing the experimental setup

Exposure to stimulation

For stimulation, environmental, chemical, and mechanical stimulants were used. More specifically, malt extract powder, dextrose, ethanol, hydrocortisone, and load application were employed for the performance of the experiments. The rationale for the selection of the stimulants is described below:

Chemo-attractants & mechanical stretching

Malt extract, dextrose, and ethanol were used to assess the response capabilities of the fungal materials to chemo-attractant and mechanical stretching exposure. For exposure to malt extract, dextrose, ethanol, and mechanical stretching, the colonised fungal-hemp hybrid was attached to a cloth, which in turn was placed on a mannequin. The mannequin was covered with a plastic sheet to prevent rapid moisture loss from the fungal fabric, which was sprayed with distilled water once per two days. The humidity of the fungal fabric was 70%–80% and the illumination 30–150 LUX. The stimulation was performed with 96% ethanol, malt extract powder dissolved in distilled water, dextrose, and by attaching weights of 50 g and 200 g to the bottom part of the fabric colonised by the fungus, using clips attached to the hemp pads(Figure 5.42).

Hormone exposure

To assess their capability to report human chemical secretions, such as hormones, and therefore



Figure 5.43: Pure fungal-hemp samples and fungal-hemp-hydrocortisone samples.

address whether fungi can sense human biofluids, the samples were subjected to hydrocortisone. Hydrocortisone is a medical replacement hormone, similar to the natural stress hormone cortisol. Changes in cortisol levels released by the body indicate the presence of disease and stress. Therefore, it was investigated whether fungal hybrid materials can sense, report, and process human hormone changes and disease. For the exposure to hydrocortisone, 2 ml of the solution was applied to the surface of the colonised substrate. The rationale behind the dosage selection was that an average human patient weighing 80 kg is typically given 20 mg of synthetic cortisol per day for a variety of diseases. As a result, 20 mg divided by 80 kg yields 0.25 mg/kg. The fungal-hemp mats weighed around 100 g to 200 g each, and therefore a 2 ml dose of 250 μg was needed(Figure 5.43).

Compression- weight shifting

For mechanical stimulation, the application of compressive loading to insoles was employed. The rationale behind the selection of insoles for this series of experiments was that if it was possible to develop fungal insoles that could sense, process, and compute information regarding multiple pressure points, then it would be feasible to detect impairments in balance, gait, posture, muscle strength, and cognition, providing valuable information about a user's physical and mental health. By integrating living sensor technologies into insoles, patterns and strategies for executing different functional tasks could be assessed, capturing data that can form the basis for use in areas such as rehabilitation, prehabilitation, monitoring elderly people with mobility problems, mitigating slipping and falling, as well



Figure 5.44: Images depicting the experimental setup for the application and shifting of load.

as assessing long-term chronic conditions such as Dementia, Parkinson's disease, and stroke (Munoz-Organero et al., 2016).

Therefore, by assessing the performance and spiking activity of the fungal insoles when exposed to weight shifting (shifting of weight from toe to heel), real-time monitoring and activity recognition could be enabled.

For the application and shifting of the compressive loading from toe to heel, a bespoke test rig was developed. A flat prosthetic foot was 3D printed in acrylonitrile butadiene styrene, and a pivot joint (with an integrated locking mechanism) was positioned between the weight and aluminium plate on top of the prosthetic foot to provide control over how the compressive load was distributed across the insole. The test rig frame was assembled with a 35 kg steel bar (representing an average female with size 10 feet standing on two feet; 2 x 35 kg can replicate standing on one foot). The weight could be raised and locked in the retracted position to enable the insole to be changed. To prevent the colonised insole from dehydrating over time, a capillary matting sheet was placed under the insole. The test rig was sterilised with 80% ethanol and placed in a sterilised hydroponic growing tent with a light-proof inner lining(Figure 5.44).Three modes of compressive loading were explored: (i) toe, (ii) heel, and (iii) uniformly distributed.

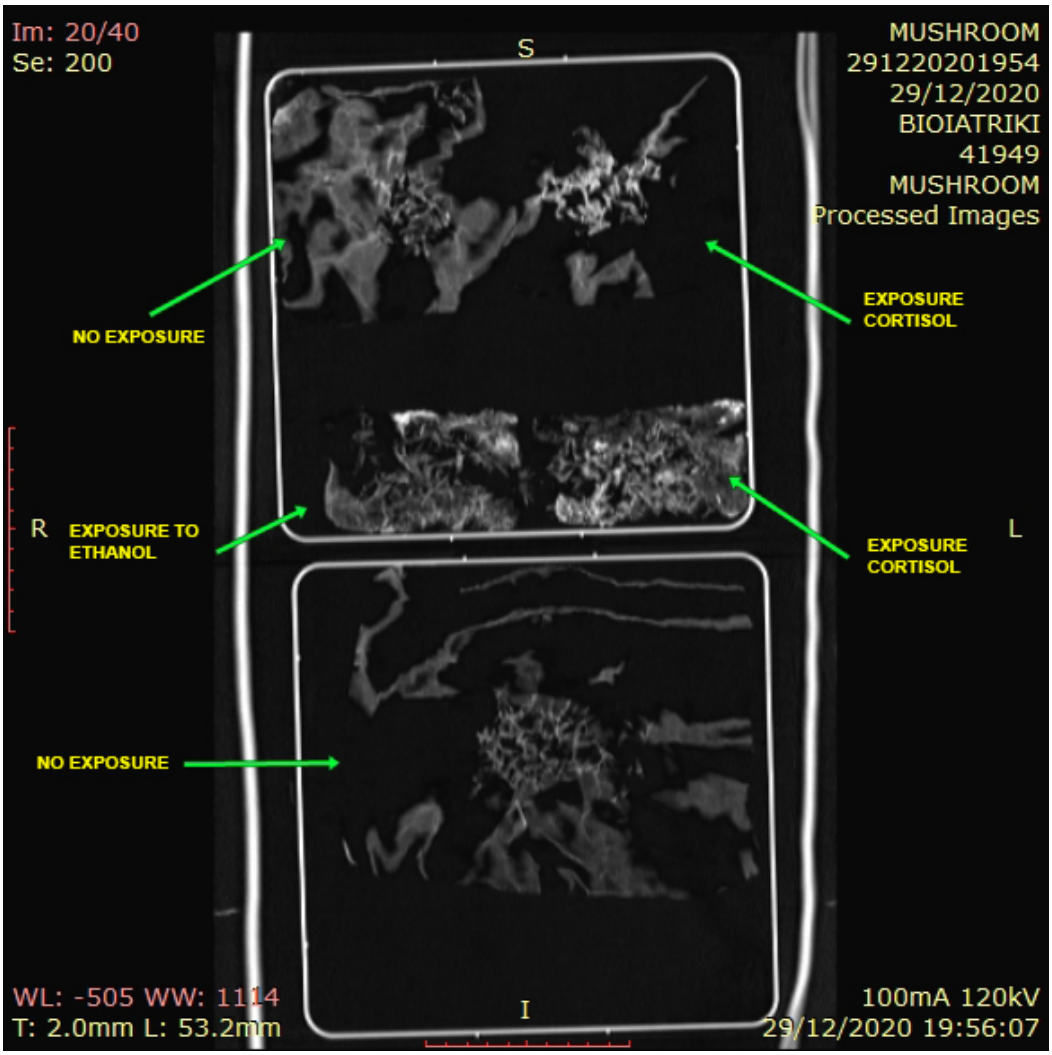


Figure 5.45: CT scan image of fungal composite samples showing composites that received no stimulus and composites that received hydrocortisone and ethanol 2 hours before being irradiated with the beam.

Characterisation and recordings of electrical activity

Morphological

X-ray, CT scans, and MRI scans were employed for the morphological and physical characterisation of the fungal materials before and after exposure to hydrocortisone and ethanol, to better understand how it affected the tissue of the fungal material. The hydrocortisone-exposed samples were subjected to the X-rays and scans 2 hours after the deposition of the hydrocortisone solution(Figure 5.45), (Figure 5.46).

Electrical activity recordings

Similarly to the Kombucha recordings, the electrical activity of all samples prior, during, and after exposure to stimulation (malt extract, dextrose, ethanol, hydrocortisone, and load application) was recorded using pairs of iridium-coated, stainless steel subdermal needle electrodes with twisted cables,

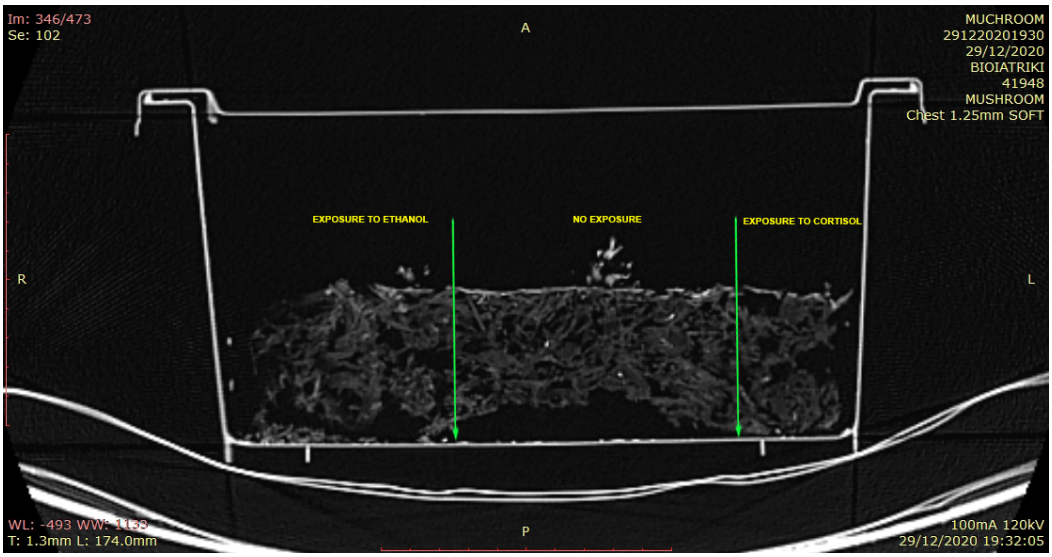


Figure 5.46: CT scan image of fungal composite identifying segments that received hydrocortisone and ethanol.

via an ADC-24 high-resolution data logger with galvanic isolation. The electrodes were inserted at a distance of 1-2 cm.

For each study, the electrical activity was recorded using five to eight electrode pairs simultaneously. Each pair of electrodes, referred to as a Channel (Ch), reported the difference in electrical potential between the electrodes. The electrical activity was recorded at a rate of one sample per second (1 Hz). Throughout the recordings, the logger took as many samples as it could (typically up to 600 per second) and saved the average value(Figure 5.47). Depending on the experiments, the electrode pairs were positioned either linearly or perimetrically.

5.2.3 Key findings

Bonding capacity and tissue changes

Analysis of the CT scans provided a better understanding of the presence of stimuli. The reconstructed computed tomography images of the fungal composite samples, both without and with hydrocortisone exposure, revealed that the impact of hydrocortisone on the fungal tissue was visible in the distribution of energy levels. The images were analysed in the frequency domain by looking at the rate at which the pixel values in the spatial domain changed, transforming the input CT image from the spatial domain to the frequency domain, and dividing the image into spectral sub-bands of varying significance. This approach provided a better understanding of the underlying distribution of changes and complexities. The substrate that was not exposed to hydrocortisone exhibited a higher energy frequency to the cortisol-exposed segment and the non-exposed segment adjacent to the cortisol-exposed segment.

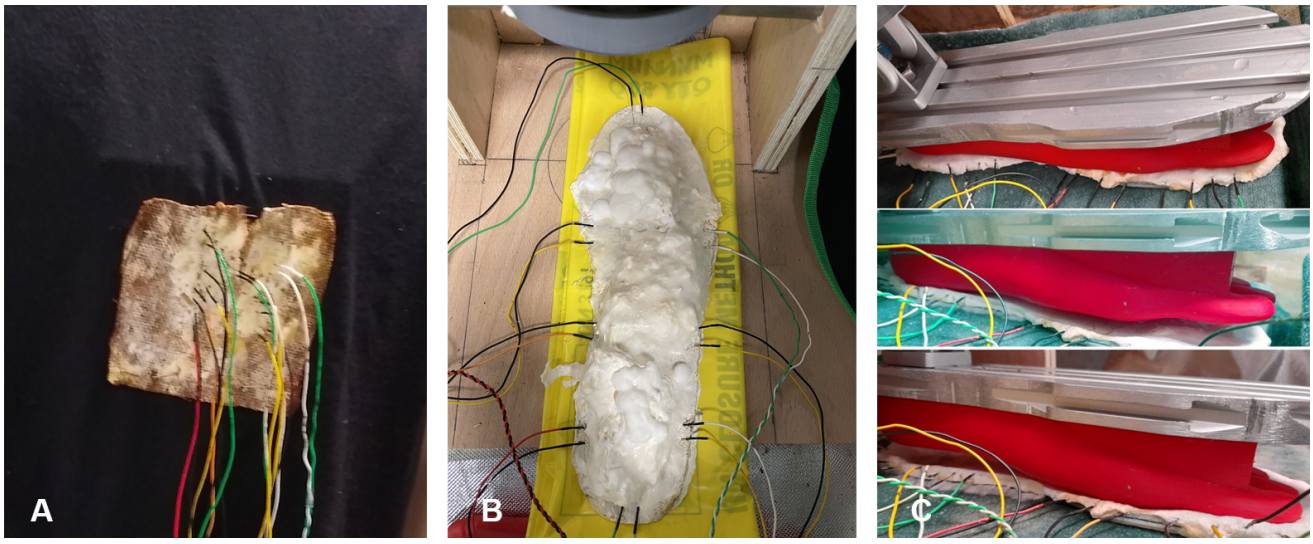


Figure 5.47: A.Experimental setup of electrical activity recordings of fungal composite exposed to malt extract, dextrose, ethanol, and attachment of 50 g and 200 g. B.Experimental setup of spiking activity recordings of fungal-capillary mat insole before exposure to load compression and weight shifting. C.Experimental setup of electrical potential recordings of fungal-capillary mat insole during three modes of loading; toe, heel, and uniformly distributed.

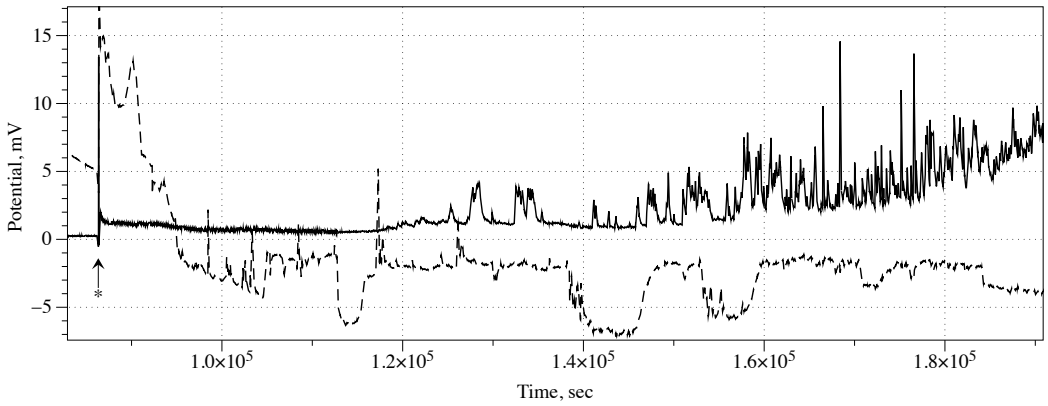


Figure 5.48: Graph showing the response to application of malt extract.

Evaluating functional capabilities- sensitivity, selectivity, & self-assembly

The fungal hybrid's response to malt extract stimuli showed distinct spiking dynamics, characterised by trains of spikes with amplitudes exceeding 2 mV in each train. Initially, the response was marked by low-frequency trains of spikes, starting with average distance between spikes in each train of 291 s, σ = 90, and an average spike amplitude of 2.6 mV, σ = 0.15. The average amplitude of the spike trains was 4.6 mV, σ = 2.5. Spikes of up to 15 mV and duration of up to 140 min were observed in the first 3 hours, attributed to the sudden increase in substrate humidity caused by the malt extract application(Figure 5.48).

A similar trend can be observed with dextrose stimulation. The findings showed low-frequency oscillatory activity before stimulation, with an average amplitude of 0.3 mV, σ = 0.2, and an average distance between the spikes of 197 min, σ = 13.9. In first 5 hours after the dextrose application, the amplitude increased to an average of 0.43 mV, σ = 0.27, and the average distance between spikes became 22 min, σ = 13. Finally, in the next 5 hours, the average amplitude of spikes increased to 1.3 mV, σ = 0.35, and the distance between spikes was 20 min, σ = 7. The above findings show that as time passes, the amplitude increased, and the distance between the spikes decreased.

Exposure to ethanol showed a drop by nearly 8 mV, followed by a further drop in the electrical potential by nearly 8 mV. The drop in potential was followed by a repolarisation phase, which lasted approximately 14 seconds. The potential remained approximately 11 mV lower than that before stimulation.

Exposure to weight attachment showed average response amplitudes of 1.3 mV, σ= 0.74 mV, for 50 g weight application. Most of the response spikes show action potential-like depolarisation, repolarisation, and hyperpolarisation phases. The response to the application of 200 g weight showed an average amplitude of 1.56 mV, σ =1.24 mV. The differential electrode pairs were arranged in a line from the top to the bottom, with Ch1 being closest to the top of the fabric and Ch13 to the bottom part. The attachment of the weights was undertaken on the bottom part of the fabric colonised by the fungus.

Exposure to hydrocortisone stimulant showed the formation of an electrical activity fingerprint that corresponds to the specific exposure event, inducing a strong response. The identification of spiking events was conducted via three stages: (1) splitting signal into chunks, (2) smoothing the chunk by mapping the constant amplitude to an instantaneous amplitude, and (3) detecting spike events. Complexity metrics were used to understand the spiking dynamics of the mycelium hybrid and to create a graphical representation of the excitatory or inhibitory state before, during, and after hydrocortisone exposure, as well as to monitor peak evolution over time. The hydrocortisone stimulus induced a much stronger response in the application locus. Following the stimulus, some excitation events could be seen propagating in the substrate at much lower potentials.

Exposure to load compression and shifting of weight across different regions of the fungal hybrid insole (toe, heel, and uniform distribution of load) showed changes in oscillatory activity.

The recordings were implemented as follow:

- The electrical activity was recorded for 30 minutes immediately before, 30 minutes during, and 30 minutes immediately after 35 kg was evenly distributed across the insole.
- The electrical activity was recorded for 24 hours immediately before 35 kg was evenly distributed across the insole.
- The prosthetic foot was then tilted back to shift the weight onto the heel region of the insole for 24 hours.

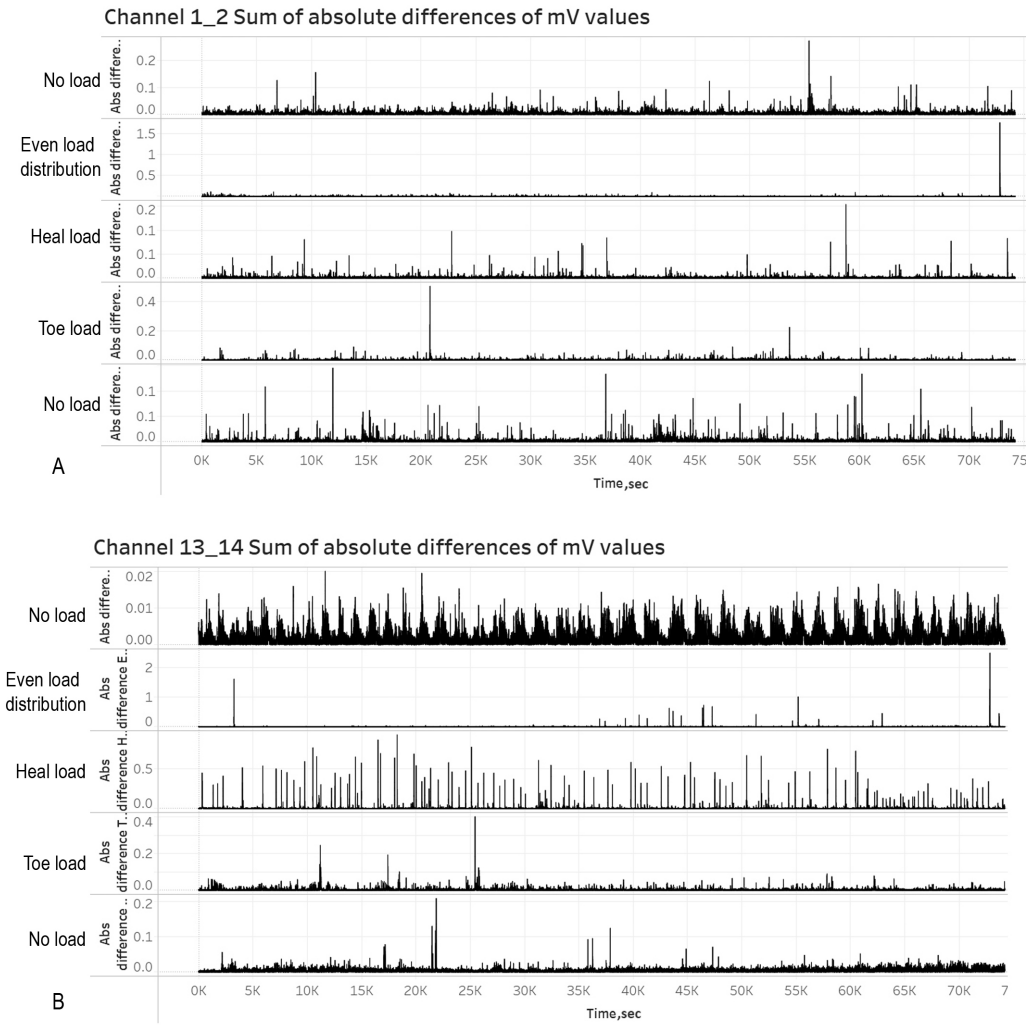


Figure 5.49: Graphs showing potential differences under no load, even load, heel-biased, and toe-biased load. A.Spiking dynamics of Channels 1-2. B.Spiking dynamics of Channels 13-14.

- The prosthetic foot was then tilted forward to shift the weight onto the toe region of the insole for 24 hours.
- The weight was removed for 24 hours.

The recordings showed that the number of spikes increased under compressive load. Additionally, the response to removing weight was different from applying weight. It was also observed that the periodicity of electrical spikes changed when the mycelium was under compressive load. The amplitude of spikes decreased under even load application compared to no load application, but no conclusions could be made regarding the electrical activity under heel-biased and toe-biased load(Figure 5.49).

The findings show that the number and periodicity of electrical spikes changed when the insoles were subjected to compressive loading in different areas, indicating possible information processing

functions when exposed to varying mechanical stimulation. This may allow for unique mappings of pressure application and weight shifting to patterns of spiking activity, suggesting possibilities for learning and computing.

Molecular origins of the observed behaviour

Similarly to the Kombucha-based ELMs, fungal ELMs display biochemical behaviours that influence their electrical properties and spiking behaviours. When exposed to external stimuli, such as mechanical pressure, the distinct fungal electrical activity may be an indicator of the information communicated between parts of the fungal colonies (Adamatzky, 2021b). It is also possible that quorum sensing mechanisms are taking place, involving the synthesis of signals that are released outside the cell via active transport or diffusion (Mehmood et al., 2019), and are translated into changes of electrical activity.

Calcium plays a major role as an intracellular signaling molecule and is involved in the transduction of a wide variety of external signals through numerous stimulus-response pathways within the cellular signal transduction network (Berridge, Bootman, and Roderick, 2003). Fungal cells use specific voltage-gated calcium channels for calcium signaling (Nakajima-Shimada et al., 1991; Nelson et al., 2004). These channels, along with mechanosensitive ion channels, may contribute to the observed electrical responses. The information is communicated through the network of hyphae, which are compartmentalised by cross walls called septa. These septa have pores that allow the streaming of cytosol and even organelles from one compartment to the other and from one hypha to another (Adamatzky et al., 2021). Septal pores also help electrical signals pass through their unique structure. Their 50-500 nm diameter allows for rapid ion movement, and this flow can be regulated by Woronin bodies (Teichert et al., 2014). The periodic translocation of water and metabolites within the mycelium, guided by calcium waves propagating at speeds of 0.3-0.5 mm/s through the hyphal network (Zelter et al., 2004), may contribute to the distinct spiking activity and electrical behaviours (Adamatzky, Chiolerio, and Sirakoulis, 2020; Almeida and Brand, 2017). Metabolite translocation is coordinated by action potential-like signals. Additionally, the cell wall and cell membrane may influence the electrical properties of the fungal composites (Adamatzky et al., 2021).

5.2.4 Contribution of findings to answering research questions- validation of hypothesis

The findings show that the fungal hybrid materials exhibit distinctive sets of responses to chemical and mechanical stimulation. Moreover, the responses indicate that it may be possible to differentiate the nature of stimuli from the spiking activity, enabling learning and decision-making functionalities.

- The fungal composite samples presented high sensitivity and selectivity characteristics via distinct electrical potential oscillations and electrical spiking dynamics.

- Similar to the Kombucha hybrid materials, the findings suggest that fungal hybrids exhibit unique electrical responses with the form of distinct spiking dynamics when exposed to different mechanical forces of compression and stretching. It is worth noting, that under stretching and as the weight increases (from 50 g to 200 g), the amplitude of the spikes increased. On the contrary, under compression, the amplitude of the spikes decreased under even load application compared to no load application. Further research on mechanical stimulation in the form of compression and stretching is needed to validate these observations.
- It may be possible to tune the properties of the fungal hybrid materials by regulating the stimulation.
- External stimuli may be used to train the fungal hybrids, presenting an opportunity for the integration of machine learning and enabling computing.
- The fungal composites displayed distinct morphological characteristics. Their bonding capacity is evidenced by new structural formations with distinct structures via integration of their components.

6 Section D - Conclusions and Outlook

6.1 Key Findings and significance of work

This research programme investigated the development of novel hybrid materials from living cells and assessed their cognitive features and advanced capabilities, such as sensing, information processing, learning, and computing. Exposure to environmental, electrical, chemical, and mechanical stimulation was employed to understand the behaviour of the novel living materials under different stimuli. Functionalisation was also deployed as a method to enhance the properties and capabilities of the newly formed materials. Two key living materials were used for the implementation of the experimental work: Kombucha cellulose and fungi. Both materials are abundant, easily accessible, display scalability potentials, and can self-grow, self-repair, and regenerate.

These important attributes can lead to the development of materials that are truly sustainable, can be grown into tailored forms and sizes, and do not require significant processing, making a significant contribution towards sustainability and circular biodiversity.

The experimental results demonstrated that the fungal and Kombucha hybrid materials present neuron–like behaviours and distinct spiking dynamics when exposed to stimulation, enabling them to perform autonomous information processing, learning, and decision-making. Additionally, they can be used as scaffolds for immobilisation with nanoparticles to enhance properties such as electron mobility, charge transfer, and conductivity, allowing them to be tailored and tuned according to specific demands. Tuning of the properties and electrical activity can be achieved by adjusting the composition and concentrations of the living communities to improve signaling behaviours such as transmission under various input conditions and increase amplification. Finally, stimuli can be mapped onto patterns of electrical activity, providing opportunities for the integration of machine learning and enabling unconventional computation.

The above findings are significant as they open up exciting opportunities for the development of a versatile technology that integrates living communities, has the ability to process information, and acts as a living computer. Moreover, due to its capacity to be developed across different scales, this unique programme of research has transformative potential. Finally, as it leverages the natural, distinct features and unique sensing and adaptive strategies employed by fungi and Kombucha microbial communities, it opens up new pathways towards the investigation of other targeted living communities that may also present distinct cognitive behaviours.

The research work led to the establishment of an innovative framework that allows the replicability of the experiments, data collection, and analysis in a structured and systematic manner, ensuring

validity, rigorousness, and reliability. This framework can be applied for the development of hybrid living materials from a wide range of living cells, making a significant contribution to an emergent and transdisciplinary field of research that leverages the animate properties of living materials.

The framework includes a design-fabrication-testing-analysis-evaluation-validation cycle approach as follows(Figure 6.1):

1. In situ biofabrication methods [microbial fermentation, solid-state fermentation, and multi-organism symbiotic pairing]
2. Functionalisation approaches [in situ functionalisation via fermentation; injection and encapsulation]
3. Establishment of experimental setups for stimulant exposure [mechanical stimulation via load application, weight shifting, compression and stretching; chemical stimulation via injection and deposition of chemicals; electrical exposure via electrical input potential]
4. Execution of experiments and data collection methods [capacitance, impedance, resistance, and current-voltage (I-V) measurements; recordings of electrical potential; morphological characterisation using CT scans, MRI scans, X-rays, SEM, ESEM, EDS, and Light Microscopy]
5. Data analysis [spiking dynamics, including amplitude, hysteresis cycles, frequency, and duration of spiking activity; memfractive behaviour, including conductivity and fundamental logic operations]
6. Evaluation of behaviour and capabilities [sensing, information processing, learning, decision-making, and computing]
7. Validation strategies [specificity and selectivity, bonding capacity, and self-assembly]

6.2 Originality and Contribution to Knowledge

This original and unique work is looking to develop truly environmentally friendly and accessible hybrid living materials with cognitive characteristics by utilising the animate attributes of living cells for real-time monitoring of various environmental, chemical, mechanical, and electrical parameters through their electrochemical performance. It represents a fundamental change in materials production and performance and has the potential to transform a diverse range of sectors. It can, therefore, have applications in a wide range of disciplines, such as:

- Smart buildings and cities: Integration into building materials for cladding systems that act as real-time reporters of environmental changes, such as air quality monitoring.

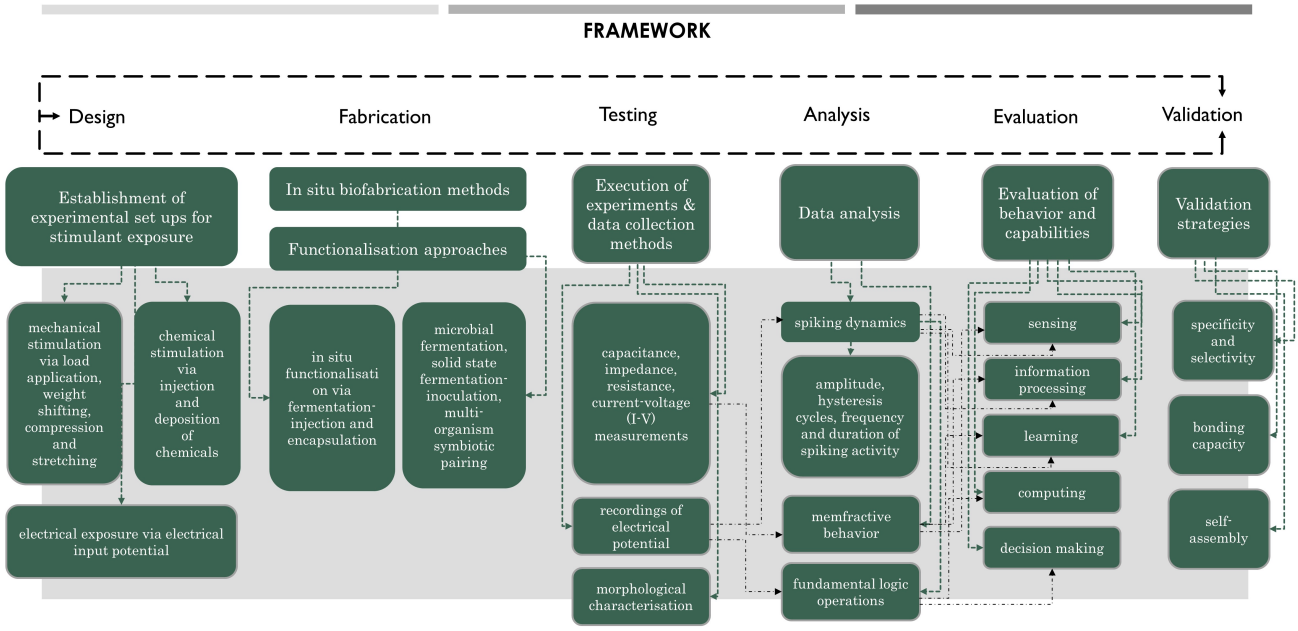


Figure 6.1: Research framework

- Wearables: Integration into wearables that facilitate real-time detection of physiological changes in the human body or other biological systems, with potential applications in real-time health monitoring.
- Robotics, living electronics, and computing devices: Development of living circuits for robots and electronic devices. Additionally, external stimulus patterns can be used to train the living hybrids, presenting opportunities for the integration of machine learning and enabling unconventional and biologically inspired information processing.
- Space exploration and other extreme environments applications: Integration into materials with self-healing and energy storage properties.

Furthermore, the programmable and tunable potential of the materials makes this research work specifically original. It is possible to program the desired responses and properties by adjusting the stimulation parameters and material composition, establishing a unique correlation between structure and function. The understanding of stimulus-response mechanisms, signal transmission modes, and programmable behaviours could lead to customisation and tuning of the hybrid materials' properties.

6.3 Considerations for further research

Elements of the research work that need to be considered for further investigation are as follows:

Wettability: As fermentation is used as a method for growing and sustaining the living hybrids, the wettability of the material may impact the flow of electrical current, affecting its electrical properties.

Re-swelling performance: The ability of the materials to transition between living and non-living/dry states, and vice versa, along with its impact on electrical performance, warrants exploration.

Longevity: Investigating the longevity of the living hybrids without the need for a power supply, as well as finding innovative ways to extend their use and maintain their activity, should be further explored.

Efficacy and stability: These are crucial factors in determining the potential of commercialisation and widespread use of green electronics in the future, and hence merit further consideration.

Maintenance: The maintenance of the living organisms requires a nutrient-rich environment, which may not be feasible in many practical applications due to potential biohazard threats posed by the cells.

Bioreceptiveness: Exploring materials that can host and support the natural growth and colonisation of surfaces by environmentally beneficial microbes, without the need for additional layers of support (Armstrong, 2023), holds promise for further investigation.

Porosity Control: Further exploration into controlling the porosity of materials and its effects on binding capacity and electrochemical performance is recommended.

Evolvability and real-time feedback implementation: This includes mechanisms such as storing the history of exposure to desired signals and should be considered for implementation to enhance the functionality of the materials.

6.4 Possible future research directions

Introduction of other targeted living communities for desirable functionalities

The properties and performance of other living species could be explored to achieve specific functionalities.

Initial work in this direction has been conducted through the integration of lichen species into abiotic biological substrates for air quality monitoring. Lichens are symbiotic organisms composed of a fungal partner and one or more photosynthetic partners (Kranner et al., 2008), and they are excellent biomonitors for air pollutants, making them good indicators of pollutant presence. The objectives of the research work were:

- To assess bonding capacity and establish protocols for lichen/substrate colonisation for the development of the hybrids.
- To 3D print substrates that present optimal colonisation behaviour using a digitally-driven paste delivery system.



Figure 6.2: A. Inoculated lichen- substrate samples. *Flovoparmelia caperata*, *Parmotrema perlatum*, and *Xanthoria parietina* lichen species were used for the inoculation. Photograph by Simon Regan 2023. B. Exposure of lichen composites to gas emissions.

- To evaluate gas absorption of hybrid materials upon exposure to a range of pollutants.
- To develop a framework for deploying lichen hybrid material systems for air quality monitoring.

Further work is currently being undertaken to better understand if, upon exposure to gas emissions, it is possible for the lichen matrices to differentiate air pollutants. Initial studies can be found in the Appendix section/ Supporting Output 3(Figure 6.2), (Figure 6.3).

Wearable sensors and large-scale prototype development

Incorporating Kombucha and fungal biohybrid systems into wearable devices or implantable sensors could facilitate real-time detection of physiological changes in the human body or other biological systems, with potential applications in real-time health monitoring. For example, monitoring hormonal secretions like cortisol could allow the detection of stress levels and disease states (Parlak, 2021). Sweat composition analysis might be achievable through the detection and processing of distinct electrical activity patterns induced by changes in electrolytes, glucose, or other biomarkers in sweat (Gao et al., 2016). This could provide valuable information about hydration levels and metabolic processes. Additionally, electrical activity patterns and memfractive properties could be used to infer patterns of muscle activation, providing important information about muscle movement and fatigue (Ray et al., 2019).

With distinct sensing and stimuli-responsive actions when exposed to environmental stimulation, the integration of Kombucha and fungal biohybrid systems into wearable sensors can also facilitate environmental monitoring (Kang et al., 2022) and enable temporal information processing and learning from the environment (Mei et al., 2022). These functionalities allow the creation of tailored wearable sensors that evolve into self-learning systems, optimising their behaviour over time. Examples include

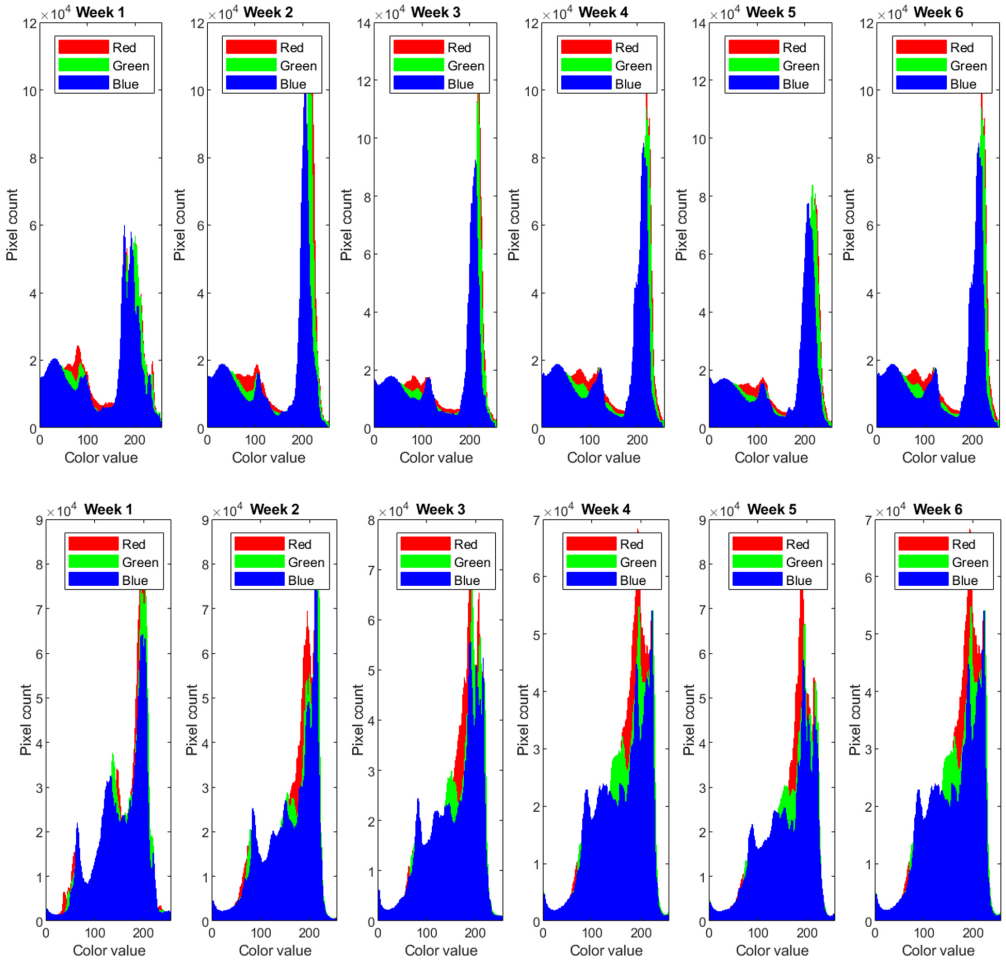


Figure 6.3: Statistical analysis of changes in pigmentation distribution to investigate substrate-lichen correlations and metabolic activity changes over time.

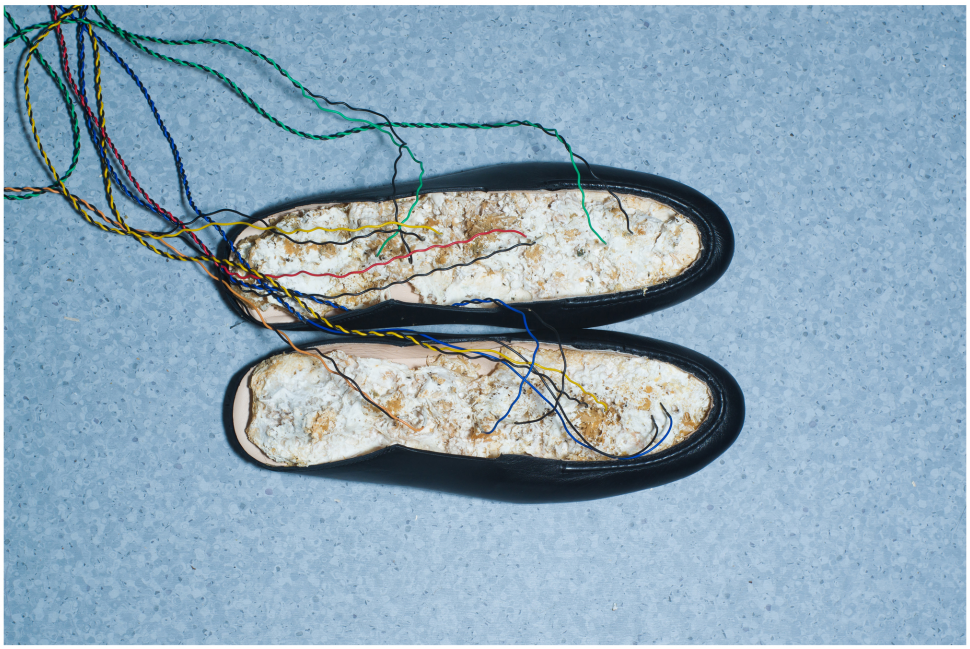


Figure 6.4: Fungal wearable prototype. Photo by Irina Petrova

detecting pollutants, gases, and particulate matter to assess environmental safety and air quality; monitoring external conditions such as temperature, light, and humidity to adapt wearable functionality or provide user feedback; and identifying harmful chemicals or toxins in the immediate surroundings.

Information about motion and shifts in body weight is also possible to be obtained, providing valuable insights into mobility, activity recognition, and rehabilitation. Electrical spikes can contribute to creating activity profiles, contributing to the identification of changes in cognitive behaviours. Furthermore, identifying specific pressure points and load distribution through distinct electrical spiking activity can provide critical data about gait, posture, and balance. It is also possible for the systems to self- evaluate their performance by detecting mechanical degradation or stress in the wearable device itself, enhancing their reliability and longevity.

The electrical spiking activity could also be explored for energy harvesting purposes. If the spiking can be converted into a usable form of energy, it could help power small electronic devices or sensors. This capability would allow for obtaining a wide range of information in remote or hard-to-reach locations, significantly broadening the application potential of these living biohybrid systems.

Initial prototyping in this direction has been conducted with the fabrication of large-scale wearables for environmental and health monitoring. The images below show the prototypes, which were exhibited as art installations (Fungal Architectures, Bristol, 2021) (Figure 6.4), (Figure 6.5), (Figure 6.6), (Figure 6.7).



Figure 6.5: Fungal wearable prototype. Photo by Irina Petrova



Figure 6.6: Fungal wearable prototype. Photo by Irina Petrova

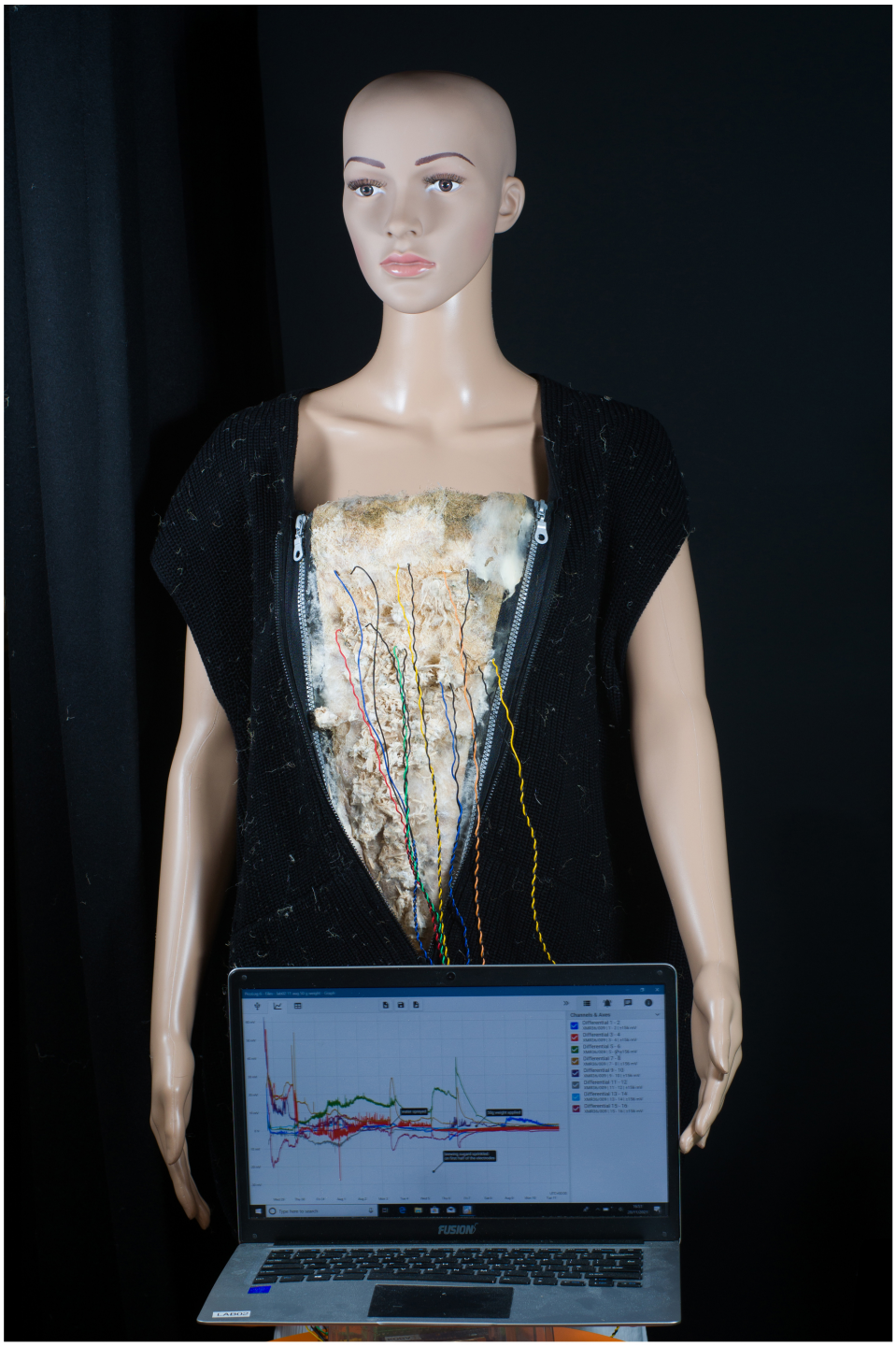


Figure 6.7: Fungal wearable prototype. Photo by Irina Petrova

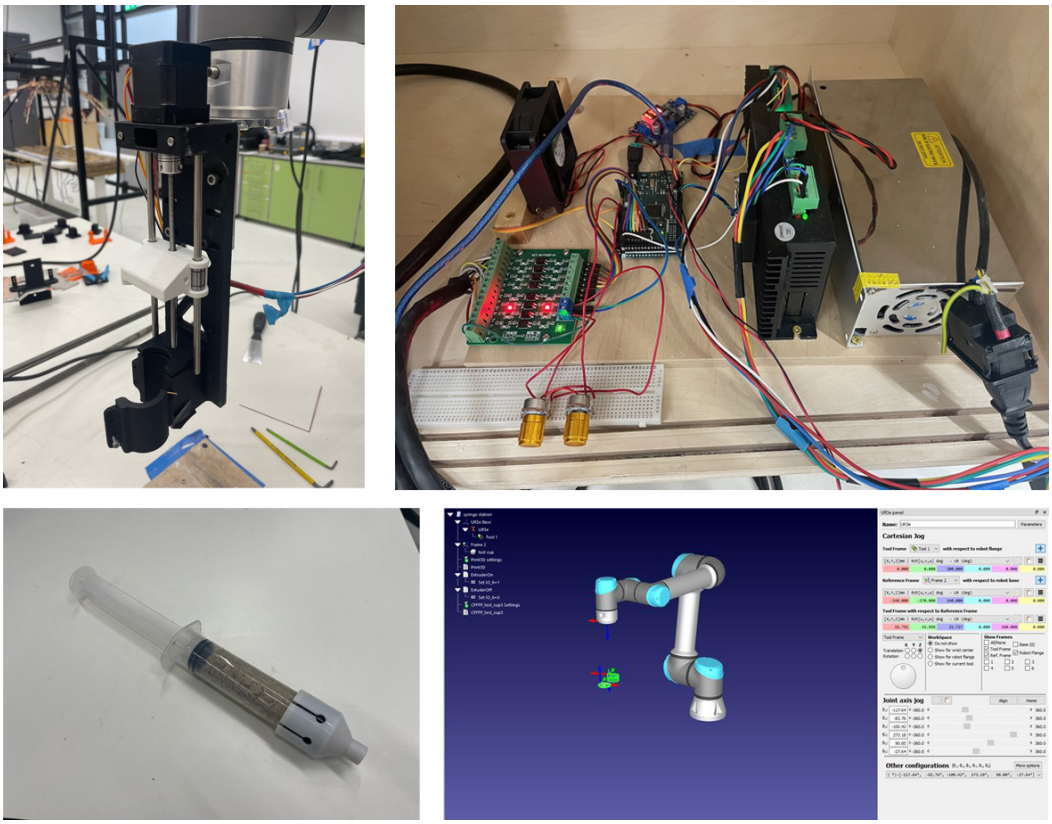


Figure 6.8: Digital fabrication of bio-receptive substrates that can support and sustain the growth of living communities. The images show the robotic 3D printing test system used for paste printing. In collaboration with Centre for Print Research, UWE, Bristol.

Manufacturing- digital fabrication

Novel digital fabrication processes that allow the creation of unique geometries and structures, capable of accommodating nutrients and water uptake to host and support the growth of the targeted living microbiomes, can be explored. The studies may focus on size control, scalability, and responsive potentials. Initial work in this direction has been conducted with paste 3D printing and can be found in the Appendix section/ Supporting Output 3.

Materials as living computers- computation

Further research may be conducted on the computation capabilities of the living hybrid materials. In addition to utilising logic operations, such as duplicate gates, ternary logic gates could be explored to increase computing efficiency. Machine learning techniques may also be employed to interpret correlations between electrical activity response patterns and external stimuli.



Figure 6.9: Robotic 3D printing of bioreceptive substrate for lichen inoculation. In collaboration with Centre for Print Research, UWE, Bristol.

7 Publications

ROYAL SOCIETY OPEN SCIENCE

royalsocietypublishing.org/journal/rsos

CC BY

Research

Cite this article: Nikolaidou A, Mougkogiannis P, Adamatzky A. 2024 Electroactive composite biofilms integrating Kombucha, Chlorella and synthetic proteinoid Proto–Brains. *R. Soc. Open Sci.* **11**: 240238.
https://doi.org/10.1098/rsos.240238

Subject Category:
Engineering

Subject Areas:
materials science/biomaterials/robotics

Keywords:
thermal proteins, proteinoids, unconventional computing, Kombucha cellulose biofilms, memristors, soft robotics

Author for correspondence:
Anna Nikolaidou
e-mail: anna.nikolaidou@uwe.ac.uk

Electronic supplementary material is available online at https://doi.org/10.6084/m9.figshare.c.7214477.

THE ROYAL SOCIETY PUBLISHING

Downloaded from https://royalsocietypublishing.org/ on 29 May 2024

Electroactive composite biofilms integrating Kombucha, Chlorella and synthetic proteinoid Proto–Brains

Anna Nikolaidou[1,2], Panagiotis Mougkogiannis[1] and Andrew Adamatzky[1]

[1]Unconventional Computing Laboratory, and [2]School of Architecture and Environment, University of the West of England, Bristol, UK

AN, 0000-0002-2787-8986; PM, 0000-0003-1710-4917; AA, 0000-0003-1073-2662

In this study, we present electroactive biofilms made from a combination of Kombucha zoogleal mats and thermal proteinoids. These biofilms have potential applications in unconventional computing and robotic skin. Proteinoids are synthesized by thermally polymerizing amino acids, resulting in the formation of synthetic protocells that display electrical signalling similar to neurons. By incorporating proteinoids into Kombucha zoogleal cellulose mats, hydrogel biofilms can be created that have the ability to efficiently transfer charges, perform sensory transduction and undergo processing. We conducted a study on the memfractance and memristance behaviours of composite biofilms, showcasing their capacity to carry out unconventional computing operations. The porous nanostructure and electroactivity of the biofilm create a biocompatible interface that can be used to record and stimulate neuronal networks. In addition to *in vitro* neuronal interfaces, these soft electroactive biofilms show potential as components for bioinspired robotics, smart wearables, unconventional computing devices and adaptive biorobotic systems. Kombucha-proteinoids composite films are a highly customizable material that can be synthesized to suit specific needs. These films belong to a unique category of 'living' materials, as they have the ability to support cellular systems and improve bioelectronic functionality. This makes them an exciting prospect in various applications. Ongoing efforts are currently being directed towards enhancing the compositional tuning of conductivity, signal processing and integration within hybrid bioelectronic circuits.

© 2024 The Authors. Published by the Royal Society under the terms of the Creative Commons Attribution License http://creativecommons.org/licenses/by/4.0/, which permits unrestricted use, provided the original author and source are credited.

Downloaded from https://royalsocietypublishing.org/ on 29 May 2024

1. Introduction

There is a growing interest in using electrically conductive biofilms for applications that involve the interaction between electronic devices and biological tissues. Conductive biofilms, which consist of microbial communities and biopolymers, are a highly appealing choice for coating materials in implantable electrodes and biosensors. This is primarily due to their biocompatibility and sustainability, which make them superior to synthetic polymers [1,2]. These electroactive biofilms can function as flexible, adaptable coatings that transmit signals between electronic components and electrically excited cells. In microbial fuel cells, for instance, the natural redox and conductive properties of microbial biofilms have been used to improve the power output [3,4]. The incorporation of conductive biocomponents in the development of synthetic bio-electronic biofilms has the potential to facilitate the creation of advanced hybrid bioelectronic systems that can interface with both living and non-living elements.

Thermal proteinoids are abiotic polypeptides that were initially synthesized by Sidney Fox in early 1970s. They are formed by heating mixtures of amino acids, which leads to the formation of sequences that are not directly coded by genes [5]. Proteinoids possess electrical conductivity and memristive properties that can be used in the field of bioelectronics [6,7]. Furthermore, proteinoids have the ability to self-assemble into microspheres that resemble cells, which makes them a fascinating material for bioinspired engineering [8–10].

Kombucha is a beverage made by the process of fermentation, when a symbiotic culture of bacteria and yeasts (SCOBY) is introduced into tea [11]. The tea components are metabolized by the microbial community, resulting in the production of organic acids and a biofilm made of cellulose [12]. Bacteria and yeasts lead a symbiotic life in the cellulosic film layer [13] which increases in thickness as fermentation progresses, providing the necessary oxygen for microorganisms [14]. Microbial metabolism has been used in microbial fuel cells development for electron generation and transfer [15]. For the Kombucha biofilm-forming process, the cellulose serves as an immobilization matrix, resulting in enhanced electron transfer [16].

In this study, we have combined the bioelectronic properties of proteinoids with the matrix-forming ability of Kombucha. Electrically conductive and flexible biocomposite films were created by combining proteinoids and Kombucha. The hybrid material displayed enhanced mechanical strength and electrochemical responses in comparison to the separate components, indicating the presence of synergistic interactions.

The mixture of proteinoids with Kombucha results in a composite material that exhibits unique electrical properties derived from proteinoids, while also benefiting from the matrix-forming, self-growing and self-repairing capabilities of the Kombucha biofilm. The combination of proteinoids and Kombucha in this composite material forms a biofilm that exhibits electrical conductivity, making it a promising candidate for bioelectronic interfaces.

Proteinoids play a significant role in enabling signal transmission through their memristive, memcapacitive and conductive properties. In the interim, the Kombucha culture synthesizes a cellulose membrane that serves as a flexible and cohesive framework for immobilization. Each separate component contributes complementing advantages, resulting in the production of an electroactive biofilm that surpasses the capabilities of each component on its own.

The application of conductive biofilms has great promise in the field of neuronal tissues. The hydrogel-based matrix has favourable characteristics for the application of uniform coating on implantable electrodes, facilitating efficient transmission of signals between electronic devices and excitable cells without interruption. The application of composites presents a viable and environmentally sustainable option for electrode coating, in contrast to the use of synthetic polymers. Moreover, the inherent biocompatibility has the potential to enhance the integration of neurons with electrodes and contribute to sustained performance over an extended period of time.

To summarize, the combination of proteinoids' distinct bioelectronic properties with Kombucha's ability to form biofilms shows great potential for creating adaptable conductive interfaces between living and non-living systems. The combination of the two biocomponents has the potential to facilitate the development of sophisticated hybrid bioelectronic devices.

Proteinoids were synthesized through the process of thermal polymerization of amino acids and subsequently introduced into Kombucha during the fermentation process, resulting in the formation of biofilms with conductive properties.

The objectives were:

— To maximize biofilm conductivity and electrochemical activity, it is important to optimize the proteinoid composition and fermentation parameters.
— Analyse various electrical behaviours such as I–V sweeps, transfer functions, coulometry, capacitance and impedance.

Downloaded from https://royalsocietypublishing.org/ on 29 May 2024

— To showcase the proof-of-concept of neuronal interfacing, we will coat microelectrodes and measure the signalling activity using model neurons.

Our hypothesis proposed that the composite material would exhibit a synergistic effect by combining the complimentary advantages of its components, hence facilitating improved communication between neurons and electrodes. The present work aims to provide a comprehensive understanding of the processes involved in biofilm formation, as well as the electrochemical properties associated with it. Additionally, the study explores the potential of using biofilms for interacting with neurons.

2. Methods

A Kombucha mat (SCOBY) initially obtained from Freshly Fermented Ltd (Lee-on-the-Solent, PO13 9FU, UK) was used for the production of the Kombucha-proteinoid biofilms. We prepared an infusion of 5 l of boiled tap water, 500 g of white granulated sugar (Tate & Lyle, UK) and 10 tea bags (Taylors Yorkshire Teabags 125 g, UK) in a plastic container. After the solution reached room temperature, the Kombucha mat was placed in the container and stored at 20–23°C in the absence of light. The solution was changed every 10 days and monitored for the production of daughter Kombucha mats. When ready, two daughter mats were transferred from the container and the samples were placed in 12 cm diameter Petri dishes with 20 ml solution each. To enhance the functional properties of the Kombucha biofilm, 10 ml of Chlorella Vulgaris (Blades Biological Ltd) were added to the solution of one sample. Chlorella Vulgaris is a microalgae with a spherical microscopic cell of 2–10 µm diameter [17–19]. We selected Chlorella Vulgaris due to its robustness to changing environmental conditions, fast growth rate [20], its ability to photosynthesize [21] and the presence of proteins in its composition which represents 42–58% of the biomass dry weight [22–26] with 30% migrating in and out of the cell [27]. In addition to this, it has already been demonstrated that Chlorella Vulgaris can act as living biosensor media by exhibiting periodic electrical activity in the form of spikes [28]. The biofilms were kept in the Petri dishes for a week. The proteinoids used in this study were synthesized using the thermal condensation protocol that was previously described in [29]. In this experiment, the amino acids L-glutamic acid and L-arginine were used. These amino acids were purchased from Sigma Aldrich and had a purity level of over 99%. To begin, the amino acids were heated to a temperature of 180°C for a duration of 60 min. This process resulted in the formation of a homogeneous mixture consisting of polypeptide chains. Afterwards, the mixture was dissolved in water to achieve a concentration of 10 mg ml^{-1}. The proteinoids were dried using lyophilization. The proteinoids that were obtained were used without undergoing any additional purification steps. A $3 \times 3\ cm^2$ section of the biofilms was used for the production of the kombucha-proteinoid (KP) biofilm. Two millilitre proteinoid solution were injected in the kombucha biofilm and applied to the surface. The biofilm was then placed back to the Petri dish for 24 h.

Various instruments were employed to perform dynamic current–voltage (I–V) profiling, impedance, capacitance and resistance measurements for the electrical evaluation of the proteinoid-microbial composite samples. The experimental configuration consisted of platinum-iridium wire electrodes, which were positioned at a distance of 10 mm from each other. These electrodes were in direct contact with the sample material, allowing for the application of voltages and the measurement of currents. An LCR meter (Model 891, BK) was used to conduct impedance spectroscopy within the frequency range of 1 kHz to 300 kHz. The experimental setup involved doing I–V sweep measurements using a Keithley 2450 source meter, where the voltage range varied from −1 V to +1 V. The BK Precision 4053B 10 MHz dual channel function generator was used to supply input waveforms for the purpose of conducting experiments on frequency-dependent capacitance and resistance. The measurements were conducted at ambient temperature with specialized test setups designed to facilitate the connection between the samples and the electrode probes. We used a Picolog ADC-24 high impedance data logger (figure 1) to analyse the electrical activity of the kombucha biofilms. The proteinoid-microbial samples that have been obtained were subjected to characterization using scanning electron microscopy (SEM) with an FEI Quanta 650 field emission SEM.

3. Results

3.1. Structural characterization of Kombucha-proteinoids complexes by SEM

SEM was employed to analyse the structural properties of the integrated system comprising Kombucha and proteinoids. The analysis of the data depicted in figure 2 reveals the presence of yeast cells measuring around 1.4 µm in diameter in close proximity to bigger Chlorella microspheres with a diameter of 4.76 µm. These

Downloaded from https://royalsocietypublishing.org/ on 29 May 2024

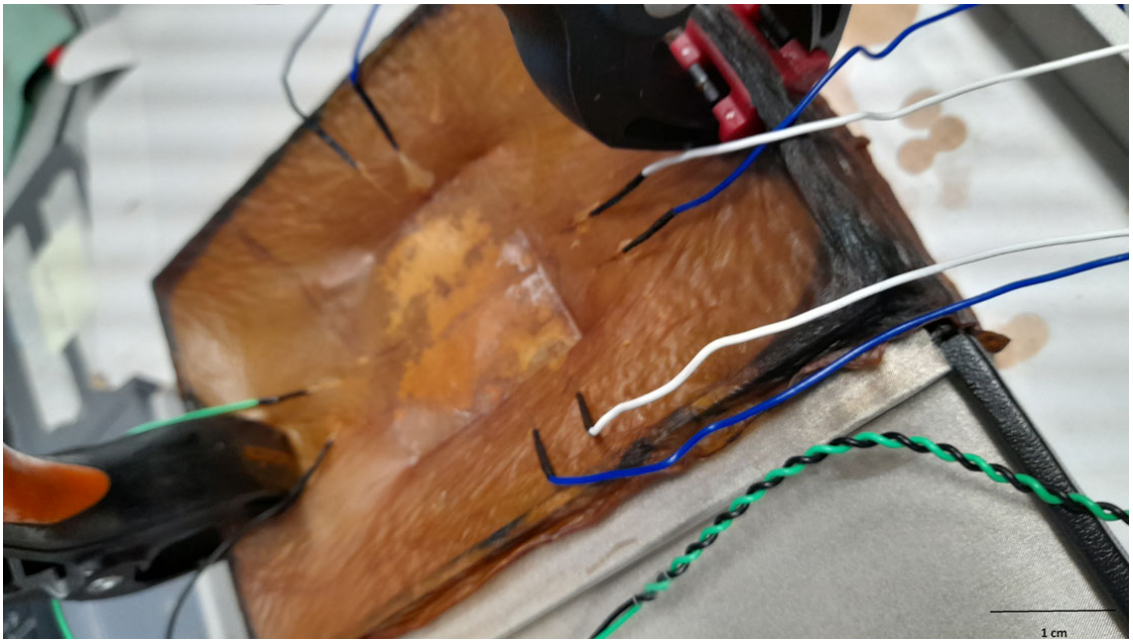


Figure 1. The experimental setup employed for the analysis of electrical spikes in Kombucha using Picolog electrodes. The growth of the Kombucha biofilm proceeds in a sugared tea infusion enriched with the necessary nutrients. Platinum–irhidium wire electrodes are inserted into the Kombucha matrix. The electrodes are linked to a Picolog ADC-24 data logger with high impedance capabilities in order to facilitate the capture and storage of electrical signals. The photograph given depicts a magnified perspective wherein the working electrodes are observed to be entering the Kombucha sample. The experimental configuration enables the application of stimulation to the Kombucha culture using the Picolog hardware, while simultaneously measuring the dynamic variations in current and the characteristics of spikes, which serve as indicators of the electrophysiological activity of the biofilm. The scale bar in the image represents a length of 1 cm, providing a reference for the size of the experimental setup and the Kombucha biofilm sample is in a wet state.

microspheres are encompassed by proteinoids nanospheres measuring 105 nm in diameter, which are made of L-Glu and L-Arg. Furthermore, it was observed that proteinoid nanospheres were distributed uniformly inside the sample, with a particular concentration observed in the vicinity of yeast cells. The findings presented in this study illustrate the effective reorganization of Kombucha with L-Glu:L-Arg proteinoids, resulting in the formation of a composite structural framework that encompasses both microbial and peptide components. The results of the SEM study indicate that the proteinoid nanospheres are not simply located on the surface of the Kombucha biofilm, but rather they are closely integrated with the microbial and microalgal components. The presence of invasive three-dimensional integration of proteinoids inside the architecture of the Kombucha biofilm requires unique molecular recognition and interaction between the proteinoids and the biofilm components.

The observed integration and adherence of proteinoid nanospheres to the Kombucha biofilm architecture, as detected using SEM, is believed to be assisted by several intermolecular interactions. Electrostatic interactions might potentially arise between the charged amino acid residues, such as glutamate and arginine, located in the polypeptide chains of proteinoids, and the many anionic functional groups found in the extracellular polymeric substances (EPS) of the Kombucha matrix, which are rich in polysaccharides [30]. Furthermore, the proteinoids possess non-polar domains that are dispersed throughout their structure. These non-polar domains have the ability to insert themselves into hydrophobic regions found on the microbial cell walls or penetrate into the EPS matrix through hydrophobic interactions [31]. The proteinoid-Kombucha interface exhibits several hydrogen bonding possibilities, which stem from the hydroxyl, carboxyl and amino groups present on both proteinoid and Kombucha components. In addition, weak van der Waals forces can also contribute to the interactions mentioned above by facilitating a general attraction between the proteinoids and the biofilm surface at close range. The proteinoids and morphological features of the biofilm may exhibit conformational compatibility, which can enhance multivalent bindings and promote increased surface networking [32]. The close association between proteinoids and Kombucha, as discovered in this study, suggests the potential for creating a bio-abio hybrid system that can emulate certain functions of the brain, thereby forming a basic 'Kombucha-proto brain.' Proteinoid nanonetworks possess the capacity to function as distributed computing components similar to neurons, facilitating the exchange of impulses throughout a

Downloaded from https://royalsocietypublishing.org/ on 29 May 2024

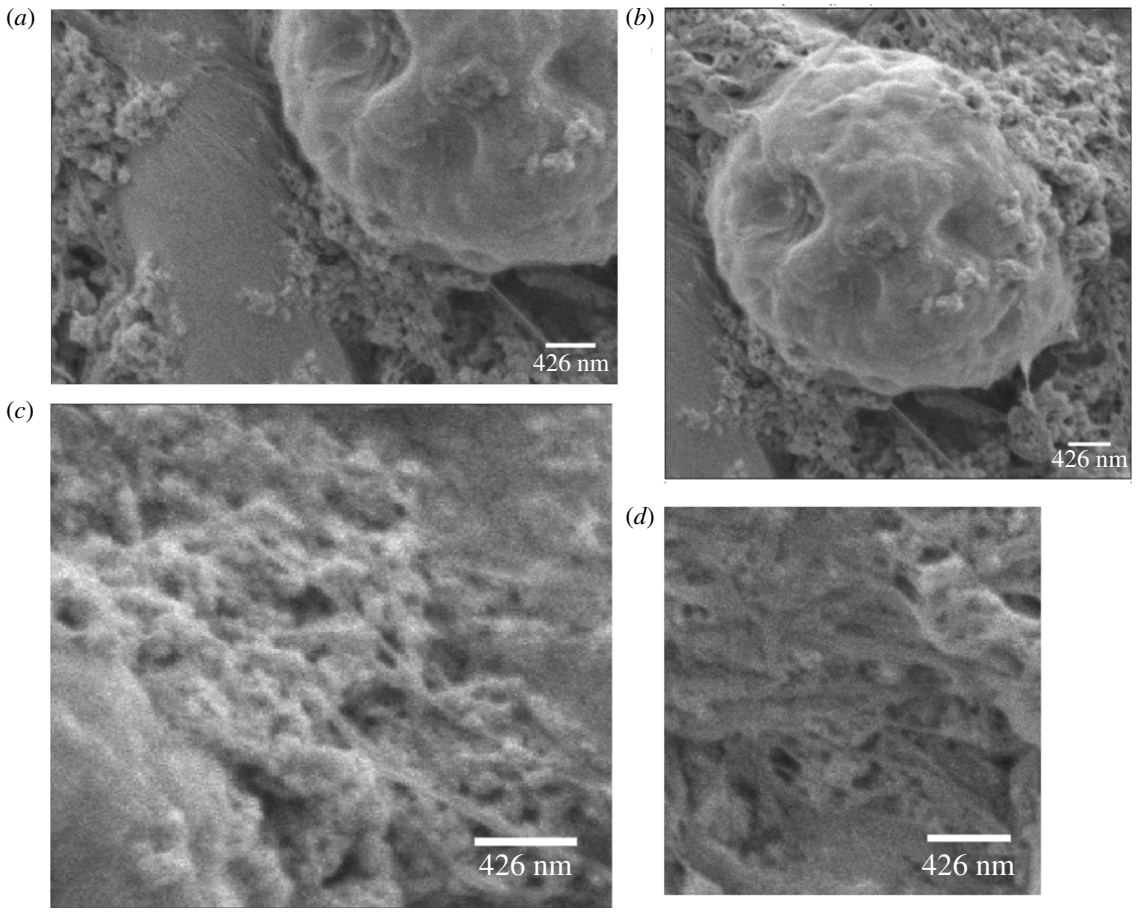


Figure 2. A SEM analysis of the integrated KPs system. (*a*) SEM image of yeast with a diameter of 1394 nm in close proximity to a Chlorella microsphere (4.76 µm in diameter) surrounded by L-Glu:L-Arg proteinoids with a diameter of 104.6 nm. (*b*) SEM image of a complete microsphere of Chlorella. (*c*) The SEM image depicts proteinoids nanospheres. (*d*) A SEM image depicting yeast surrounded by proteinoids nanospheres. All SEM images were captured at 2.00 kV, x27 234 magnification, with a scale bar of 426 nm.

linked polysaccharide matrix facilitated by the Kombucha. The cooperative biomolecular network integrates the information processing and signalling capacities of proteinoids with the structural scaffolding provided by microbial cellulose. Similar to the emergence of the brain, which originated from ancient biochemical transformations such as lipid membranes and protein ion channels, the theory of the 'Kombucha-proto brain' uses the self-assembly of abiotic peptides and microbial fluids to imitate the complex processes of excitation, conduction and cognition. The reported bioelectronic functionalities, adaptivity and learning capacities exhibited by 'Kombucha-proto brains' embody fundamental characteristics essential for the development of primitive synthetic brains and bio-nervous systems. The continued development of this process of biosynthetic integration could potentially facilitate the development of engineered living materials that possess cognitive abilities, adaptive characteristics and computational capabilities [33–37].

The diverse morphologies seen using SEM offer visual validation of the production of biofilms composed of KPs, exhibiting distinct structural organization. Additional investigation is necessary to thoroughly assess the potential of these integrated biofilms for applications involving neural interface, specifically in terms of their electrical conductivity and stimulatory capacity.

3.2. Elucidating the dynamic behaviour of Kombucha-proteinoids networks using sinusoidal inputs

When the proteinoids system was exposed to input signals, it showed a decrease in amplitude along with slight changes in frequency (figure 3). On the other hand, the composites that consisted of proteinoids and Kombucha mixtures exhibited increased output amplitudes and enhanced frequency consistency when compared with the input data (table 1). As an example, after examining sample A composed of 40% proteinoids and 60% Kombucha-Chlorella (KC), it was seen that there was an approximate 35-fold increase in amplitude while the input frequency remained constant. The system consisting solely

Downloaded from https://royalsocietypublishing.org/ on 29 May 2024

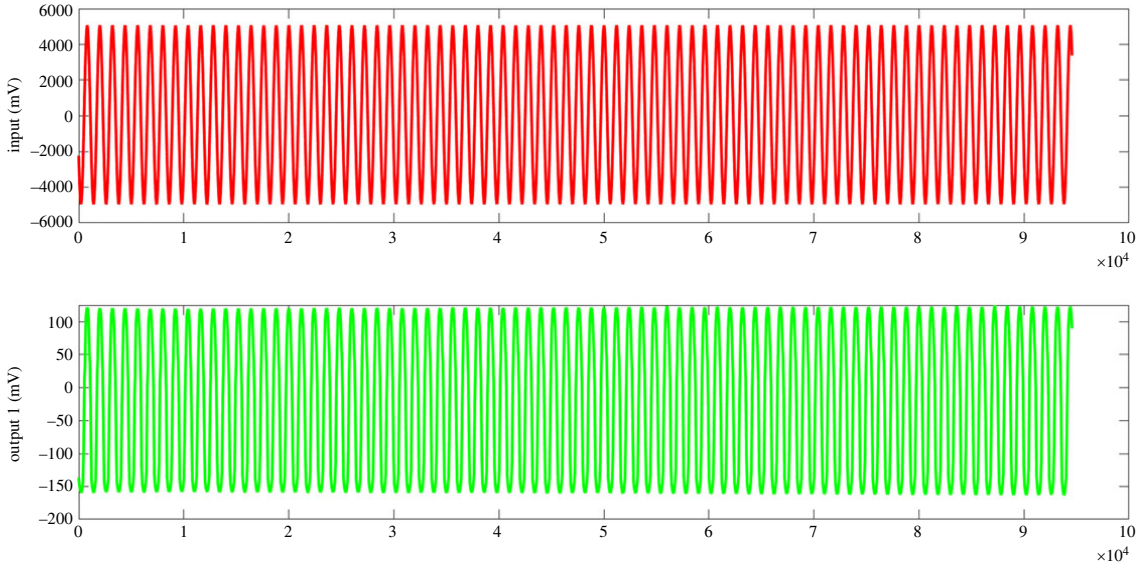


Figure 3. Response characteristics of L-Glu:L-Arg proteinoids. The proteinoids were subjected to an input signal with an amplitude of 5.05 mV and a frequency of 0.056 Hz. (*b*) Signal recorded from the proteinoids as a result of the input signal. Compared to the input values, the measured output signal exhibited a significant decrease in amplitude, measuring 288.55 mV, and a corresponding shift in frequency, measuring 0.119 Hz.

Table 1. Response characteristics of proteinoids-Kombucha biofilms.

sample	% proteinoids	% Kombucha	input amplitude (mV)	input frequency (Hz)	output amplitude (mV)	output frequency (Hz)
A	40%	60% Kombucha-Chlorella	10.04	0.055	352.28	0.114
B	40%	60% Kombucha	9.96	0.055	26.13	0.256
C	25%	75% Kombucha-Chlorella	10.06	0.055	360.59	0.120
D	25%	75% Kombucha	9.98	0.056	27.41	0.272

of proteinoids demonstrated a nonlinear connection between input and output, with a decrease in amplitude observed at higher input amplitudes (figure 4). This indicates the presence of inherent amplitude-dependent filtering capabilities. On the other hand, the proteinoids-Kombucha biofilms exhibited signalling behaviours that were more optimized, as illustrated in figure 5. A linear correlation between input and output was observed for all samples of proteinoids-Kombucha biofilms with samples containing Kombucha and Chlorella generating higher output potentials than samples containing only Kombucha when the same input potentials are applied (figure 6).

The proteinoids-KC composites exhibit enhanced signalling behaviours compared to proteinoids alone, suggesting that there are synergistic interactions taking place between the components of the mixture. The Kombucha and Chlorella are likely to contain a significant amount of hydrophilic polysaccharides and cell surfaces. These elements have the ability to retain higher densities of proteinoids through electrostatic and hydrogen bonding forces. As a result, the conductivity is increased. Furthermore, the cellulosic and microbial nanowires found in Kombucha have the potential to enable the direct connection between neighbouring proteinoid nanostructures. This would establish interconnected pathways for electron transfer throughout the composite network. Chlorella's endogenous redox proteins and metabolites have the potential to interact with proteinoids, creating novel intramolecular charge transfer pathways. In addition, the three-dimensional matrix formed by the proteinoids, Kombucha and Chlorella components is highly organized. This matrix enhances the connection between nearby domains, allowing signals to be transmitted accurately and effectively. The binding of Kombucha and Chlorella to proteinoids leads to conformational changes, which may lead

Downloaded from https://royalsocietypublishing.org/ on 29 May 2024

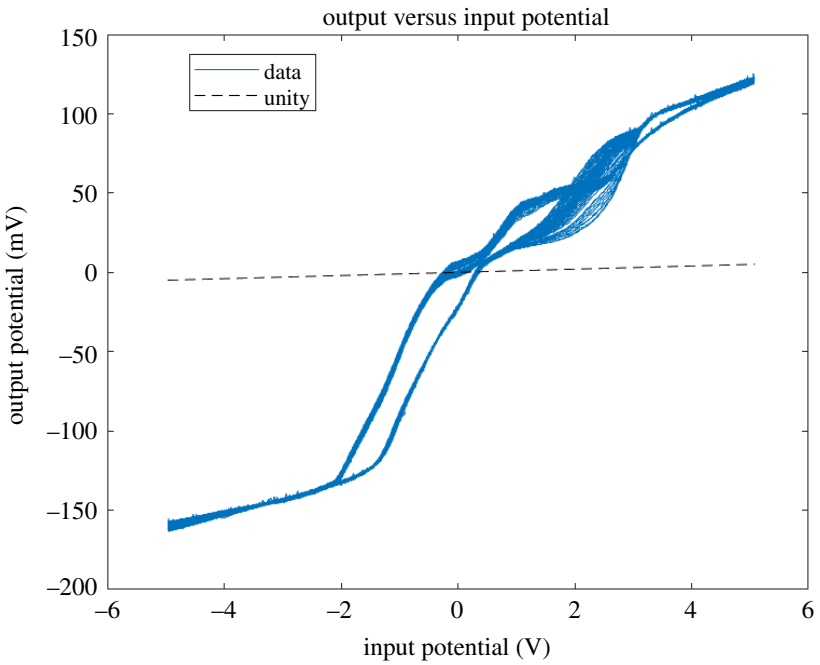


Figure 4. Potential output versus input for the proteinoids system. The output potential of the proteinoids is compared to the input potential of the system. The dashed unity line indicates an input-to-output ratio of one-to-one. The proteinoids' nonlinear response suggests that they have amplitude-dependent filtering properties.

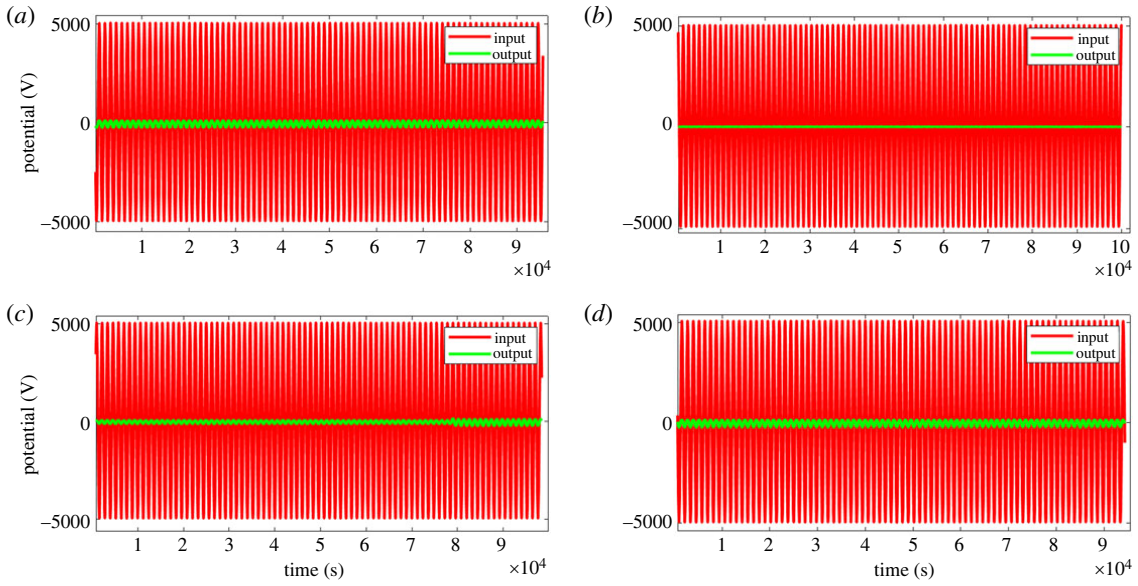


Figure 5. Response characteristics of proteinoids-Kombucha biofilms. (*a*) Sample A with 40% proteinoids, 60% KC showed input amplitude of 10.04 mV, input frequency of 0.055 Hz, output amplitude of 352.28 mV and output frequency of 0.114 Hz. (*b*) Sample B with 40% proteinoids, 60% Kombucha exhibited input amplitude of 9.96 mV, input frequency of 0.055 Hz, output amplitude of 26.13 mV and output frequency of 0.256 Hz. (*c*) Sample C with 25% proteinoids, 75% KC displayed input amplitude of 10.06 mV, input frequency of 0.055 Hz, output amplitude of 360.59 mV and output frequency of 0.120 Hz. (*d*) Sample D with 25% proteinoids, 75% Kombucha showed input amplitude of 9.98 mV, input frequency of 0.056 Hz, output amplitude of 27.41 mV and output frequency of 0.272 Hz. The results demonstrate tuning of the output response based on proteinoids-microbial composition, with KC samples showing higher output amplitudes and minor frequency shifts.

to the unlocking of alternative conductivity states. These states can have improved transmission efficiency. In summary, the cooperative molecular interactions among the proteinoid, microbial and microalgal constituents seem to work together to enhance electron mobility, charge transfer and conductivity. This allows for the efficient transmission of input signals with amplification.

Downloaded from https://royalsocietypublishing.org/ on 29 May 2024

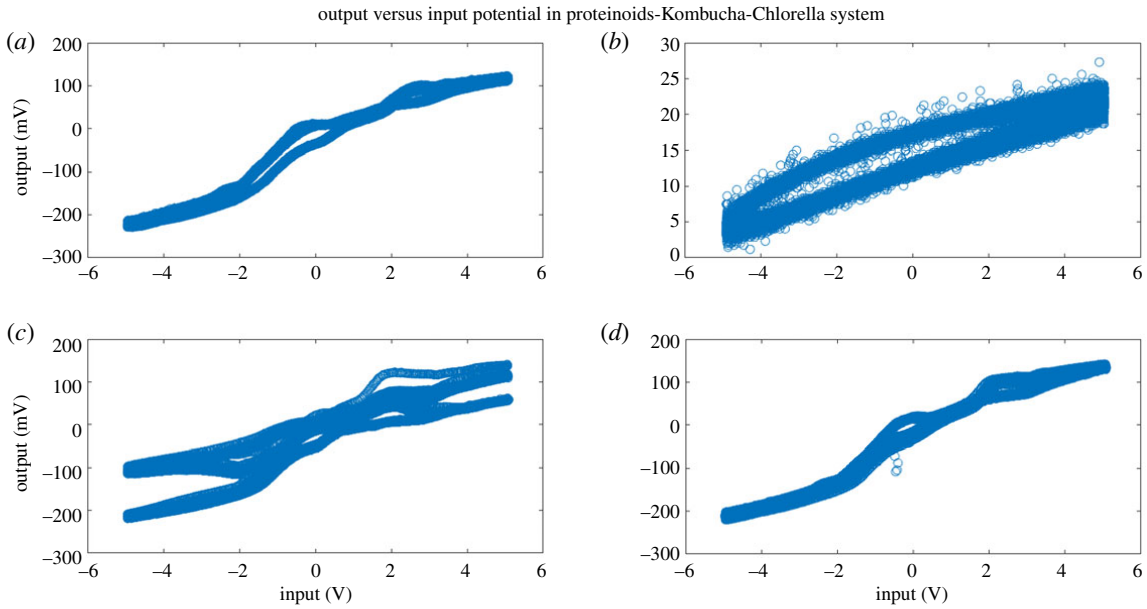


Figure 6. The plot demonstrates the relationship between the input potential and the output potential for four distinct samples of proteinoids-Kombucha biofilms. The samples demonstrate a linear correlation between the two variables. However, it is important to note that the slopes vary depending on the composition of the biofilms. Samples A and C, which contain KC, exhibit steeper slopes compared to samples B and D, which solely contain Kombucha. This implies that samples A and C have the ability to generate higher output potentials than samples B and D, even when given the same input potentials. The plot showcases how proteinoids-Kombucha biofilms can be adjusted to improve signal transmission in various input conditions. This is supported by the observed effects that vary in magnitude depending on the amplitude.

The findings of this study indicate that the integration of proteinoids with microbial components such as Kombucha modifies the signalling characteristics, resulting in great properties such as increased amplification and a wider range of frequency response. The ability to adjust the input–output relationships allows for the optimization of composition in order to achieve predicted response characteristics. To better understand the signalling behaviours in these integrated biomolecular composites, it is necessary to conduct additional spectroscopic and microscopic experiments. Such research will help us uncover the precise structure-function mechanisms that are responsible for these interactions.

3.3. Elucidating the adaptive performance of a 'Kombucha-Proto Brain' via multi-frequency impedance and capacitance measurements

Capacitance measurements across a range of input frequencies were implemented to examine the adaptive properties of the KP proto-brain system (figure 7). The composite biofilms exhibited voltage-dependent characteristics in their capacitance profiles, wherein an overall decrease in capacitance was noted as the frequency increased. The observed decrease in capacitance is likely attributed to the influence of dielectric polarization occurring within the microbial and proteinoid components. At higher frequencies, the applied field can induce molecular dipole oscillations which do not fully align, lowering the composite permittivity and thereby the measured capacitance [38–40]. The presence of irregular peaks and troughs observed in the capacitance-frequency graphs indicates the occurrence of distinct channels for charge transfer within the architecture of the proto-brain, which are activated when specific frequency resonances are reached. A variable external input signal causes frequency-dependent capacitance variations in the KP proto brain system. Capacitance modulation in response to varied input frequencies shows that the KP network actively adapts and reconfigures its structure and characteristics dependent on the stimuli. This property is an essential feature of adaptive systems. The composite 'architecture' undergoes molecular and morphological adaptations as the input frequency changes. These adaptations result in changes to its dielectric properties and charge storage capacity. The tunable capacitance is likely a result of dynamic polarization mechanisms occurring within the proteinoid nanonetworks and their interfaces with the polysaccharide matrix. The conformation and alignment of proteinoids can be altered at various frequencies, thereby

Downloaded from https://royalsocietypublishing.org/ on 29 May 2024

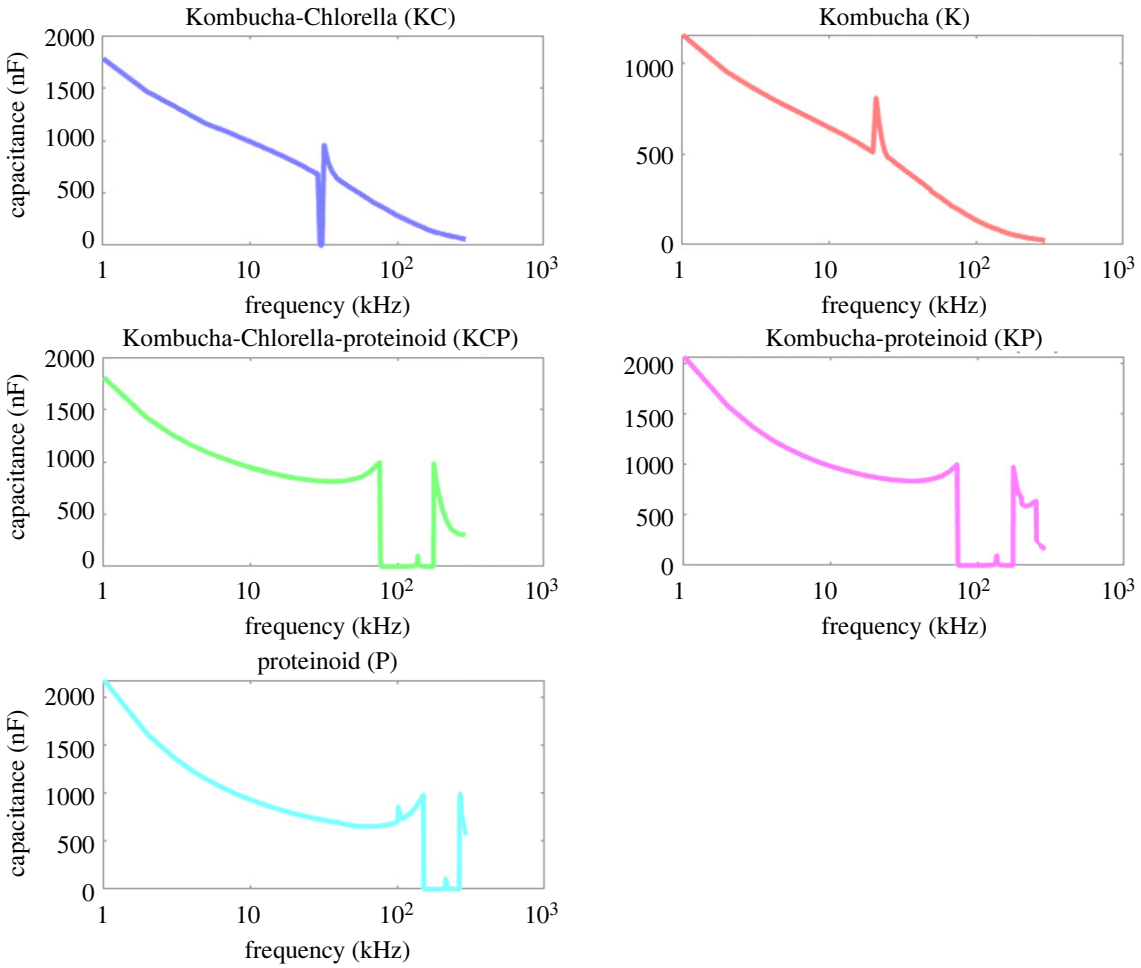


Figure 7. The capacitance as a function of frequency is measured for five different samples: Kombucha-Chlorella (KC), Kombucha (K), Kombucha-Chlorella-proteinoid (KCP), Kombucha-proteinoid (KP) and proteinoid (P). The plot of capacitance is represented on a linear scale, while the frequency is represented on a logarithmic scale. At a frequency of 1 kHz, KC, KCP, KP and P all have a similar initial capacitance of approximately 2000 nF. However, K has a lower starting capacitance of 1150 nF. In general, the capacitance of all samples decreases in a linear manner as the frequency increases. There are some significant deviations from linearity that are worth mentioning. Specifically, there are spikes in capacitance observed for KC at 29 kHz and K at 21 kHz. Additionally, there are capacitance wells observed between 72 and 269 kHz for KCP, KP and P samples. The complex impedance spectra of capacitance demonstrate the presence of frequency-dependence and nonlinear characteristics. This indicates that changes in the microstructures and interfaces within the composite biofilms are influenced by voltage. The capacitance wells observed between 72 and 269 kHz for the KCP, KP and P samples suggest the presence of frequency-dependent and nonlinear characteristics in these composite biofilms. These characteristics are likely influenced by the complex microstructures and interfaces within the biofilms, which can be sensitive to voltage changes. It is important to note that the capacitance drop around 100 Hz is not observed in the KC and K samples, which do not contain proteinoids. This suggests that the presence of proteinoids in the KCP, KP and P samples may contribute to the distinct electrical behaviour and capacitance response at lower frequencies.

modulating dipolar interactions. In addition, the Kombucha component may experience changes in cell wall permeability, hydration and interior conductivity due to voltage, which collectively affect the overall capacitance of the system. The outcome is a versatile material that has the ability to process information in a 'context'-dependent manner, similar to natural neural systems [41–45].

Furthermore, the frequency-dependent impedance of the samples offered valuable insights into their adaptive response, as depicted in figure 8. The impedance spectra mirrored capacitive trends, showing an early decrease followed by the attainment of plateau values. These plateau values suggest the presence of a frequency threshold beyond which the passive electrical properties remain stable. Nevertheless, the proteinoid sample exhibited distinct impedance modulation throughout the frequency range of 34–278 kHz, which corresponds to the reported oscillations in capacitance that are exclusively associated with samples containing proteinoids. The changes in capacitance and impedance that are

Downloaded from https://royalsocietypublishing.org/ on 29 May 2024

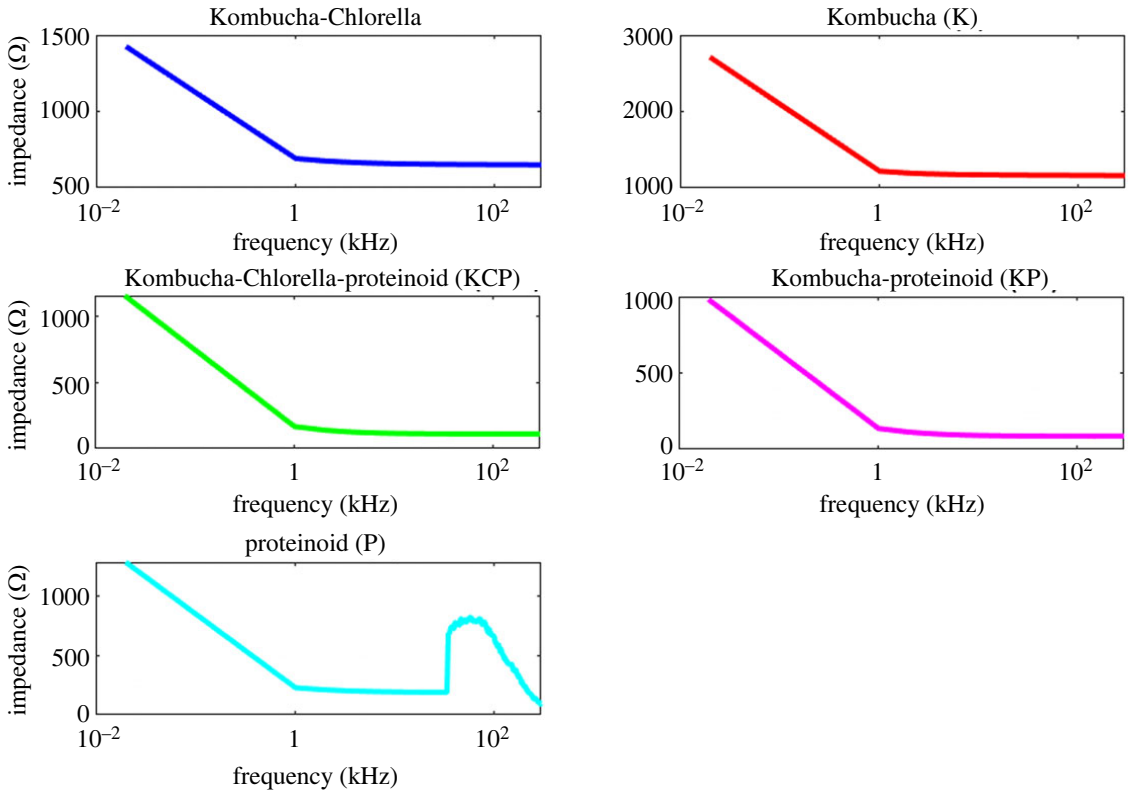


Figure 8. The impedance spectra were obtained for samples of Kombucha-Chlorella (KC), Kombucha (K), Kombucha-Chlorella-proteinoid (KCP), Kombucha-Proteinoid (KP) and Proteinoid (P). At a frequency of 0.02 kHz, the impedance values are as follows: 1425 Ω for KC, 2711 Ω for K, 1150 Ω for KCP, 981.4 Ω for KP and 1285 Ω for P. The impedance decreases in a linear manner until it stabilizes at 1.02 kHz. At this frequency, the impedance values are as follows: 691 Ω (KC), 1220 Ω (K), 165.8 Ω (KCP), 136.5 Ω (KP) and 228 Ω (P). This plateau indicates frequency-independent impedance above 1 kHz. One notable exception is the P sample, which exhibits a significant increase in impedance from 189.5 to 821.1 Ω within the frequency range of 34–278 kHz. The spectra provide insights into passive electrical properties that are dependent on voltage. These properties are likely a result of structural changes occurring at the interfaces of microbial and proteinoid components. Equivalent circuit modelling could determine specific conductive pathways obtained at different input frequencies [46,47].

correlated at specific resonant frequencies indicate the activation of particular conductive pathways and charge transfer processes. The passive electrical characteristics of the proto-brain samples were statistically compared through boxplots of the impedance and capacitance distributions (figure 9).

Table 2 provides a summary of the capacitance measures for each type of sample. An analysis of the median values reveals a discernible pattern of escalating capacitance among the different samples, ranging from Kombucha (K) to proteinoid (P). Notably, the proteinoid sample demonstrates the greatest median capacitance, measuring at 658.6 nF. This suggests that the incorporation of proteinoids with microbial components leads to an enhancement of the dielectric permittivity on a broader scale. Furthermore, it is worth noting that the KPC sample exhibited a substantial range of 8681.994 nF in capacitance, indicating a notable modulation of capacitance in response to voltage. On the other hand, the sample containing just Kombucha (K) exhibited the most limited range of 2009.1 nF. The observed differences in the median and range of values demonstrate the collaborative influence of proteinoid and microbial constituents on the overall dielectric properties at all levels. A noteworthy characteristic observed in the capacitance data is the presence of a low capacitance value of –850.1 nF, which was recorded for the Kombucha (K) sample. The presence of negative capacitance in microbial biofilm networks indicates the occurrence of active voltage-dependent processes. This stems from dynamic feedback mechanisms that counteract the applied AC field through nonlinear molecular conformations or charge injections. The membrane potential of Kombucha is likely to have an effect in conjunction with proton and ion fluxes, which can temporarily reverse the field response [49,50].

Downloaded from https://royalsocietypublishing.org/ on 29 May 2024

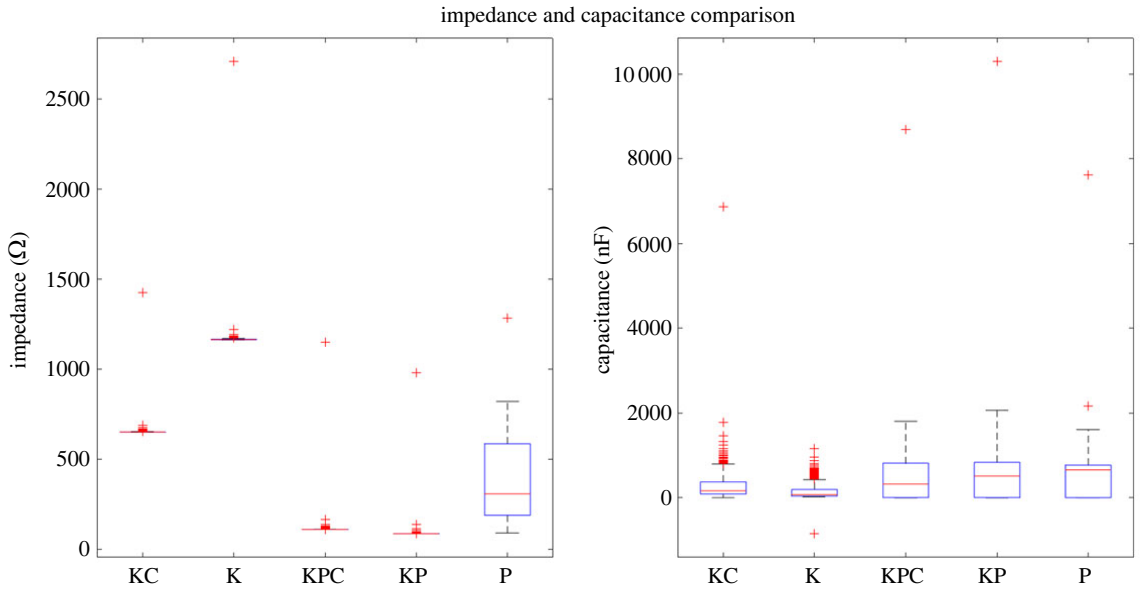


Figure 9. A boxplot comparison is conducted to analyse the impedance and capacitance of different samples, including Kombucha-Chlorella (KC), Kombucha (K), Kombucha-Chlorella-proteinoid (KCP), Kombucha-proteinoid (KP) and proteinoid (P). The box represents the values of the first quartile, median and third quartile, while the whiskers show the variability beyond the upper and lower quartiles. Individual points outside the whiskers represent outliers. The marks on the graph indicate the median confidence interval. The impedance measurement shows that K has the highest median value, while KCP has the lowest spread. In the context of capacitance, the variable P exhibits the highest median value, while KP demonstrates the widest range of variation.

Table 2. Capacitance statistics for each sample type. The presence of negative capacitance values, particularly in the K sample, suggests the occurrence of phenomena similar to those observed in ZnO thin films [48]. The loss of metal/semiconductor interface charge states under forward bias conditions, along with the presence of oxygen vacancies and piezoelectric/electrostriction effects, may contribute to the negative capacitance behaviour in the composite biofilms. This negative capacitance phenomenon has the potential to be exploited for reducing the limiting effects in the downscaling of electronic devices and going beyond the Boltzmann limit, as demonstrated in ZnO thin-film-based field-effect transistors [48].

sample	median (nF)	min (nF)	max (nF)	spread (nF)
KC	164.7	1.091	6874	774.9
K	73.38	−850.1	1159	2009.1
KPC	325.8	1.006	8683	8681.994
KP	515.3	1.004	10 300	10298.996
P	658.6	1.002	7623	7621.998

Examining the impedance metrics across varieties of samples reveals distinct tendencies (table 3). The Kombucha (K) sample displayed the maximum median impedance of 2655.5 Ω, reflecting greater resistive properties. In contrast, the Kombucha-proteinoid (KP) combination had the lowest median impedance at 945.5 Ω, indicating complexes more conducive to charge transport. Due to conformational changes, the Kombucha (K) sample exhibited the widest spread between minimum and maximum impedance values of 181 Ω. This indicates greater impedance variability. By contrast, KPC had the smallest dispersion of 148 Ω, indicating a more stable and ordered conductive network. The impedance profiles of Kombucha-Chlorella (KC) and Kombucha-Chlorella-proteinoid (KCP) samples were intermediate.

The conductivity profiles of the proto-brain samples, which vary depending on frequency, offer additional insights into their adaptive electrical response characteristics. The conductivity σ was determined by using the measured capacitance values and applying the following relation:

$$\sigma = \frac{1}{\omega C\sqrt{1+\tan^2(\phi)}}. \tag{3.1}$$

Downloaded from https://royalsocietypublishing.org/ on 29 May 2024

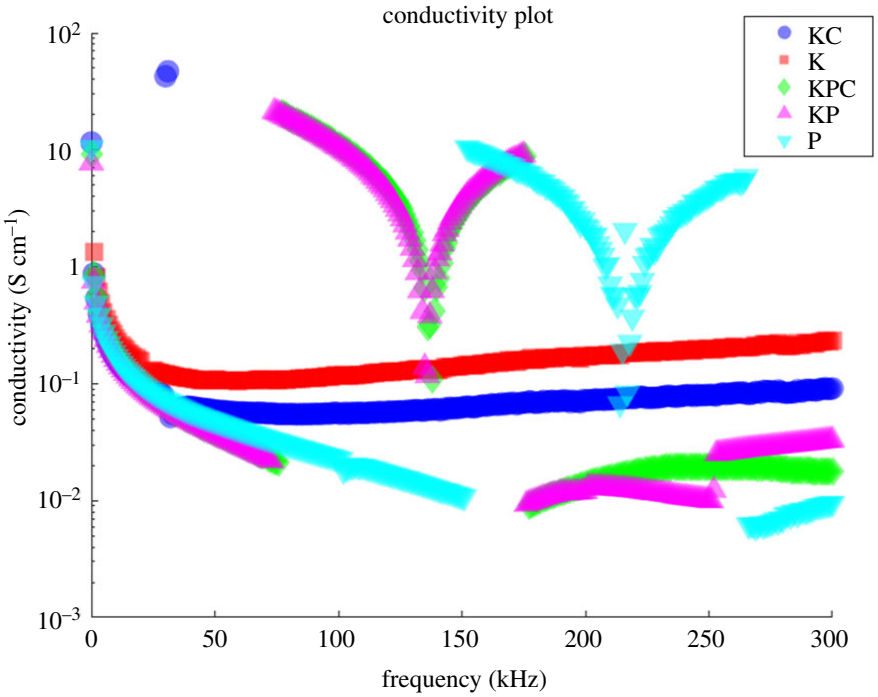


Figure 10. The conductivity profiles for various mixtures of components in Kombucha are as follows: Kombucha-Chlorella (KC), Kombucha (K), Kombucha-Chlorella-proteinoid (KCP), Kombucha-proteinoid (KP) and proteinoid (P). These patterns of conductivity (S cm^{-1}) vary depending on the frequency (kHz). The conductivity was obtained by taking the inverse of the capacitance measurements and converting the units. The KC, KPC and P samples exhibited the highest conductivity across a wide range of frequencies, indicating a higher level of charge mobility. The samples showed a decrease in conductivity as the frequency increased. However, the KPC and KP samples showed significant increases in conductivity, with rises of over three orders of magnitude between 74 and 178 kHz. The conductivity rose from 0.03 to 20 S cm^{-1}. The P sample exhibited a comparable increase in conductivity within the frequency range of 152–259 kHz. The occurrence of these unusual increases implies that there is activation of enhanced conduction mechanisms at specific frequency resonances. The conductivity spectra demonstrate the adjustable charge transport properties of the composite biofilms. These properties can be specifically controlled by varying the frequency of the input signal.

Table 3. Impedance statistics for each sample type.

sample	median (Ω)	min (Ω)	max (Ω)	spread (Ω)
KC	1408.5	1256	1510	254
K	2655.5	2500	2820	320
KPC	1102	1050	1198	148
KP	945.5	869	1023	154
P	1215	1120	1301	181

The symbol ω represents the angular frequency, C represents the capacitance and ϕ represents the phase angle between the current and voltage. This model takes into consideration both resistive and reactive contributions across a frequency range of 0–300 kHz [6]. The conductivity profiles provide additional information to the capacitive trends, so presenting an in-depth understanding of the proto-brain's ability to effectively transport charge and reduce signal attenuation. Conductivity is also directly influenced by molecular-level factors including ion mobility, membrane permeability and structural order [51–54]. A closer look at the frequency dependency may thus provide valuable mechanistic insights into the dynamic reorganization of conductive components within the proteinoid-microbe matrix (figure 10). Multi-modal electrical analysis provides a comprehensive understanding of how the emerging proto-brain network adjusts its properties to encode and transmit information.

The conductivity metrics for each sample are presented in table 4. Upon examining the median conductivity, it is evident that the Kombucha-proteinoid (KP) and Kombucha-Chlorella (KC) samples

Downloaded from https://royalsocietypublishing.org/ on 29 May 2024

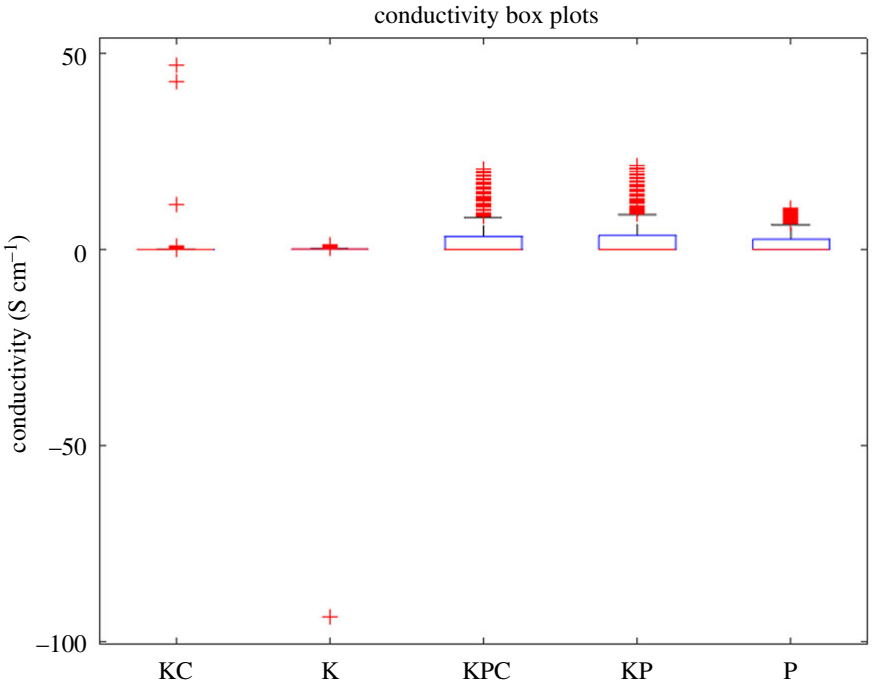


Figure 11. A boxplot comparison is conducted to analyse the conductivity values for five different samples: Kombucha-Chlorella (KC), Kombucha (K), Kombucha-Chlorella-proteinoid (KCP), Kombucha-proteinoid (KP) and proteinoid (P). The K and P samples exhibited the highest median conductivities. The KPC demonstrated the largest difference between the first and third quartiles, which suggests that it has a wide range of tunable conductivity. The KC sample exhibited the highest number of outliers, suggesting that it had greater variability in its conduction properties. In general, the composites that included proteoinoids (KPC, KP) showed higher conductivity when compared with Kombucha alone.

Table 4. Conductivity statistics for each sample type. The minimum conductivity value for the K sample is negative. One possible explanation for this outlier is the presence of charge carrier trapping or scattering phenomena at the electrode-sample interface, leading to a temporary reduction in the measured current and a consequent negative conductivity value.

sample	median (S cm^{-1})	min (S cm^{-1})	max (S cm^{-1})	spread (S cm^{-1})
KC	0.069348	0.051857	47.027684	46.975827
K	0.156378	−93.609542	1.346284	94.955825
KPC	0.038001	0.009141	20.543528	20.534387
KP	0.038905	0.009258	21.288726	21.279469
P	0.063023	0.005958	10.449820	10.443863

displayed the highest values, suggesting a higher degree of charge mobility. The presence of a significantly negative minimum conductivity in the Kombucha (K) sample suggests that there are active processes taking place within the microbial network. Furthermore, the composites of Kombucha-proteinoid (KP), Kombucha-Chlorella-proteinoid (KCP) and Kombucha-Chlorella (KC) exhibited conductivity spreads exceeding 20 S cm^{-1}, indicating their ability to achieve a wide range of tunable conductivity. In general, the combination of proteinoids with the microbial components resulted in increased conductivity compared to using Kombucha alone (figure 11). The statistics on conductivity provide insights into how the cooperative interactions between components affect the overall conduction properties of these composite biosystems.

3.4. Realization of logic gates through signal mixing and thresholding in Proteinoids-Kombucha-Chlorella biofilms

On the output signals derived from 'Kombucha–proto Brain', fundamental logical operations were implemented. Samples A-D's input–output data was processed in MATLAB to generate AND, OR, XOR,

Downloaded from https://royalsocietypublishing.org/ on 29 May 2024

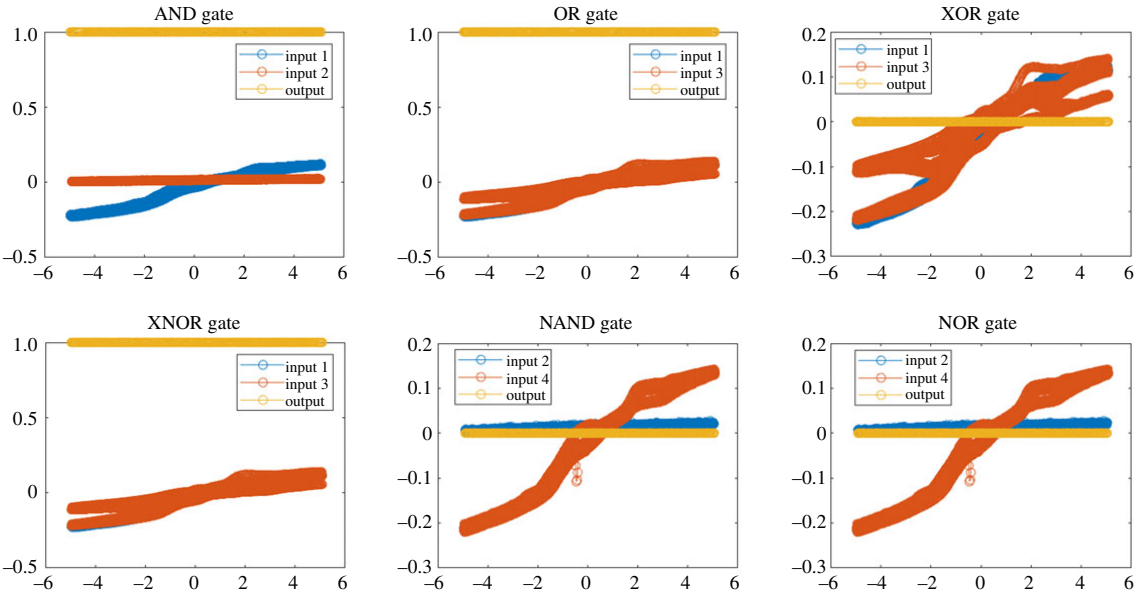


Figure 12. Implementation of fundamental logic operations on proteinoid-microbial biofilm output signals. The applied voltages for the input signals ranged from −4 to +4 V. The output signals that had been processed underwent thresholding to convert them into binary levels. Subsequently, bitwise operators such as AND, OR, XOR, XNOR, NAND and NOR were applied to achieve logical operations. The use of duplicate gates, denoted by subscripts 1 and 2, serves to illustrate the logical operation that is done to distinct output signal pairs originating from diverse biofilm samples. The ability to create logic gates demonstrates the promise of proteinoid-microbial biofilms in the field of biomolecular information processing and computation.

XNOR, NAND and NOR logic gates (figure 12). The continuous output voltages were initially converted into discrete binary levels with the application of a threshold value of 0.5V. The binary output signals were subsequently subjected to bitwise operations such as AND (&), OR (|) and NOT (~) in order to execute the logic functions. The construction of the AND gate involved the computation of the bitwise AND operation between Outputs 1 and 2. The NOR gate was derived through the application of bitwise negation (~) to the bitwise OR operation performed on Outputs 1 and 3. Various combinations of the four sample output signals were employed to evaluate the effectiveness of all logic gates, so demonstrating their broad applicability. The potential of using proteinoid-microbial biofilms for biomolecular computing has been demonstrated by their ability to execute signal processing and logic operations.

The basic logic gates can be represented mathematically using Boolean algebra notations. The AND gate performs a logical conjunction on the inputs, described by

$$y = x_1 \wedge x_2. \tag{3.2}$$

The OR gate performs a logical disjunction

$$y = x_1 \vee x_3. \tag{3.3}$$

Exclusive OR (XOR) outputs true when the inputs differ

$$y = x_1 \oplus x_3. \tag{3.4}$$

The XNOR gate is the inverse of the XOR operation

$$y = x_1 \leftrightarrow x_3. \tag{3.5}$$

The NAND and NOR gates represent AND and OR with negation. For NAND

$$y = \neg(x_2 \wedge x_4). \tag{3.6}$$

And NOR

$$y = \neg(x_2 \vee x_4), \tag{3.7}$$

where $\wedge$ is AND, $\vee$ is OR, $\oplus$ is XOR, $\leftrightarrow$ is XNOR and $\neg$ is NOT. These equations relate the input variables x_1, x_2, x_3, x_4 to the output y for each logic operation.

Downloaded from https://royalsocietypublishing.org/ on 29 May 2024

Table 5. A truth table is provided to concisely outline the input–output relationships for fundamental logic operations. The implementation of logic gates involves the use of discrete binary thresholding and mathematical bitwise operators on the output signals of the proteinoid-microbial biofilm. The logical operations of conjunction, disjunction and exclusive disjunction are implemented in computer systems using the bitwise operators &, | and $\oplus$. These operators perform the respective operations on binary input values [55]. The inherent nonlinearity and compositional diversity of proteinoid-microbial biofilms enable the processing of signals and execution of computational operations, as evidenced by the formation of digital logic patterns.

input 1	input 2	AND	OR	XOR	XNOR	NAND	NOR
0	0	0	0	0	1	1	1
0	1	0	1	1	0	1	0
1	0	0	1	1	0	1	0
1	1	1	1	0	1	0	0

The implementation of logic operations involved the use of discrete thresholding and bitwise operators on the output signals of the biofilm.

$$V'_{\text{out}} = \begin{cases} 1 & \text{if } V_{\text{out}} > 0.5\,\text{V} \\ 0 & \text{if } V_{\text{out}} \leq 0.5\,\text{V} \end{cases}. \tag{3.8}$$

The measured output voltage is denoted as V_{out}, whereas the discretized binary voltage used for logic operations is represented as V'_{out}.

The use of fundamental logical operations implies that proteinoid-microbial biofilms have the potential to function as biosynthetic materials for unconventional computing. The nonlinearity and structural diversity of these elements allow for intricate signal changes that can be compared to logic operations (table 5).

The proteinoid-microbial biofilm samples demonstrated intricate oscillatory signals, which serve as an essential precursor for chaotic dynamics (figure 13). By employing a process of extracting four signals and subsequently subjecting them to a simplistic chaotic mapping technique that merged them in a nonlinear manner, we successfully produced a novel composite signal characterized by randomized transitions between the inputs.

The previously mentioned combination technique brought key characteristics associated with chaos, including unpredictability, information encoding and heightened sensitivity to the initial conditions. Additional quantitative study is necessary in order to comprehensively characterize the chaotic qualities using methodologies such as Lyapunov exponents and fractal dimensions [56–58]. The incorporation of chaotic aspects has the potential to enhance security in communication systems, facilitate disruptive computation and offer fault-tolerance capabilities. The inherent biological intricacy present in these composite systems can be used for the development of bioinspired chaotic processors or reservoirs in the field of machine learning. The implementation of more sophisticated combination methods and recursive feedback loops has the potential to improve the observed chaotic behaviours. In simple terms, the use of proteinoid-microbial biofilms has the potential to offer a significant source of intricate multi-dimensional signals that can be harnessed for unconventional computing techniques by leveraging on the phenomenon of chaos [55,59–61].

3.5. Characterizing electrical spikes in Kombucha proto brain

Figure 14 provides a robust multivariate description of the oscillation patterns of KCP proto brains. Over time, the voltage trace reveals rhythmic spiking activity. The periodicity analysis reveals a mean surge interval of approximately 4000 s, or 1 h. The amplitude histogram reveals a normal distribution of spike peaks with a mean value of −45 mV. Fourier analysis uncovers the dominant frequencies contributing to the periodic spikes in voltage. Figure 15 illustrates the spiking response to a depolarizing pulse. Rapid depolarization of 50 mV causes repetitive spikes with a regular period of 6 min. The shape of the spike exhibits rapid rise and slower decline kinetics, with an amplitude of 25 mV. This reveals intrinsic oscillatory properties of the KCP proto brain system. Figure 16 further examines the spikes' higher-order statistics. Data with a left-skewed amplitude distribution indicates a high proportion of negative spike peaks. The leptokurtic periods suggest a distribution with heavy tails, with a high probability of extremely long and brief intervals. This demonstrates the variability and complexity of KCP spiking patterns.The results offer valuable insights into the emerging functionality of synthetic proto-brains made

Downloaded from https://royalsocietypublishing.org/ on 29 May 2024

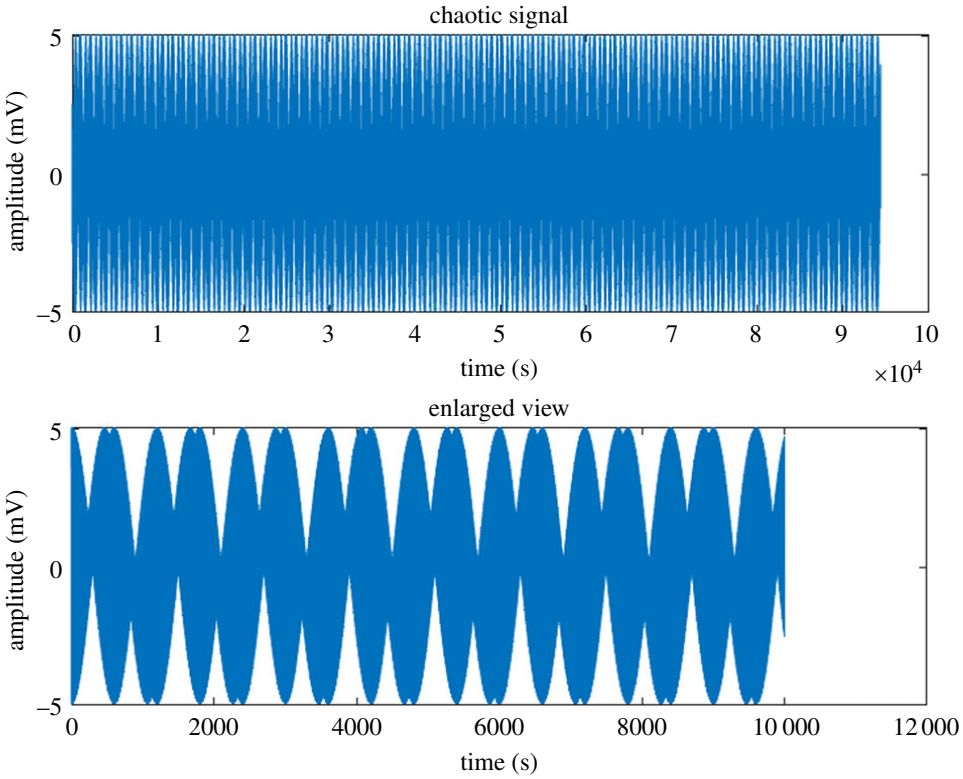


Figure 13. The proteinoid-microbial biofilms produce a chaotic fusion of signals. Chaotic signal synthesis by random switching of input signals. Subplot shows detailed view from $4 - 5 \times 10^4$ s. The subplot on enlargement provides additional information about the intricate and rapidly evolving nature of the chaotic signal during that specific time period. The phenomenon of random switching between input signals is associated with the introduction of unpredictability and information encoding, which are characteristic features of chaotic systems. The use of inherent disorder within proteinoid-microbial systems has the potential to facilitate the implementation of chaotic computing methodologies for encryption, resilience to noise and nonlinear information processing. The investigation of various combination schemes and feedback mechanisms has the potential to reveal emergent behaviours in evolving bio-computing architectures that use chaos.

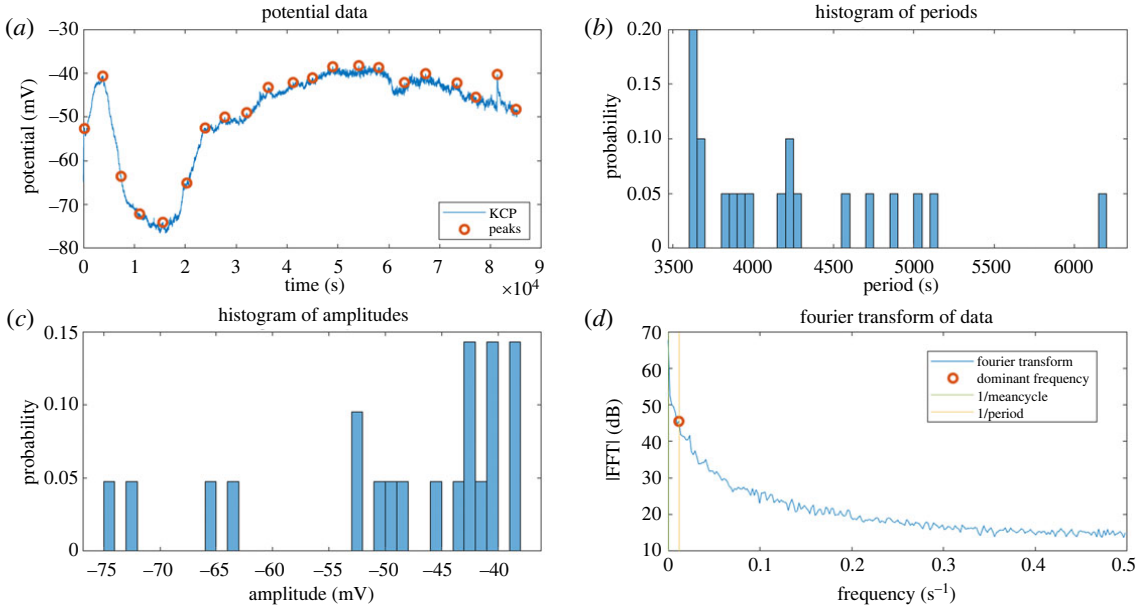


Figure 14. KCP oscillation patterns are statistically analysed. (*a*) Time-lapse voltage trace with rhythmic spikes in mV. (*b*) Histogram of oscillation times in seconds, with a mean of 4240.65 s and a median of 4068.50 s. (*c*) Histogram of spike amplitude peaks in mV, with a mean of −48.58 mV, a median of −43.25 mV and a standard deviation of 11.09 mV. (*d*) Fourier transform examination of the oscillatory signal reveals prominent frequencies. This multipanel image quantifies important periodicity and amplitude measures used to describe proteinoid spiking kinetics.

Downloaded from https://royalsocietypublishing.org/ on 29 May 2024

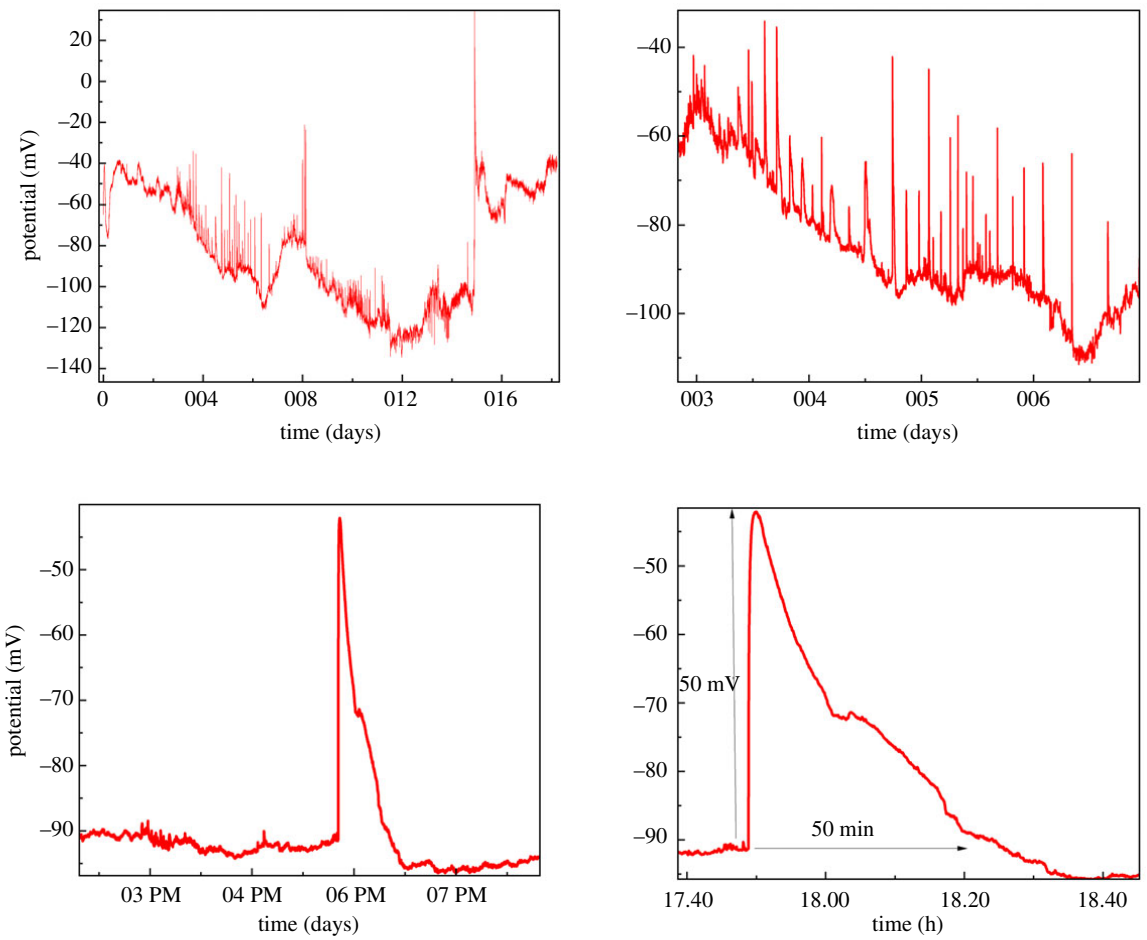


Figure 15. The dynamics of spiking in a KCP proto brain following an abrupt depolarization. Following an initial 50 mV depolarizing pulse disturbance, the voltage trace exhibits repeated spikes over time. The spikes display rapid depolarization upstrokes followed by delayed repolarization downstrokes, with an amplitude of about 50 mV above baseline. The periodicity of the surges is approximately 50 min on average. This activity reflects the proteinoid spiking response to a rapid depolarizing stimulus, revealing the spike shape, amplitude, kinetics and periodicity of oscillating voltages.

up of basic proteinoid components and Kombucha living skin. The KCP nanostructures exhibit neuron–like signalling behaviours, as evidenced by the observed voltage oscillations, spike statistics and response to perturbations. The rhythmic patterns, characterized by millisecond spike kinetics and periodicities ranging from minutes to hours, exhibit intrinsic excitability that is reminiscent of primitive neural networks. The dynamics exhibit complexity, as evidenced by the normal amplitude distributions and asymmetric periodicity statistics. The ability to regulate the activity of proteinoid spiking through stimuli such as rapid depolarization indicates the potential for transmitting information. By tuning parameters such as spike intervals and patterns, it becomes possible to encode signals.The combination of quantitative characterization and excitation of synthetic proto-brain dynamics holds great potential for advancing our understanding of the origins of cognition. Further investigation into the physical factors that influence proteinoid self-assembly and the formation of nanostructures could reveal principles for designing customized synthetic neural circuits.

3.6. Tracking electrical memory effects in microbial-proteinoid composites via dynamic I–V curves

Distinct pinched hysteresis loops, which are characteristic of memristive systems, were observed in the current–voltage characterization of the composite samples (figure 17). The I–V curves exhibited by the proteinoid-containing biofilms (KPC, KP and P) have a strong similarity to the ideal memristor behaviours, as evidenced by the extent of pinching seen. On the other hand, the samples containing simply microbes, namely K and KC, displayed memristive properties that were less prominent. However, the observation of electrical memory effects in all the mixed proteinoid-microbial compositions indicates

Downloaded from https://royalsocietypublishing.org/ on 29 May 2024

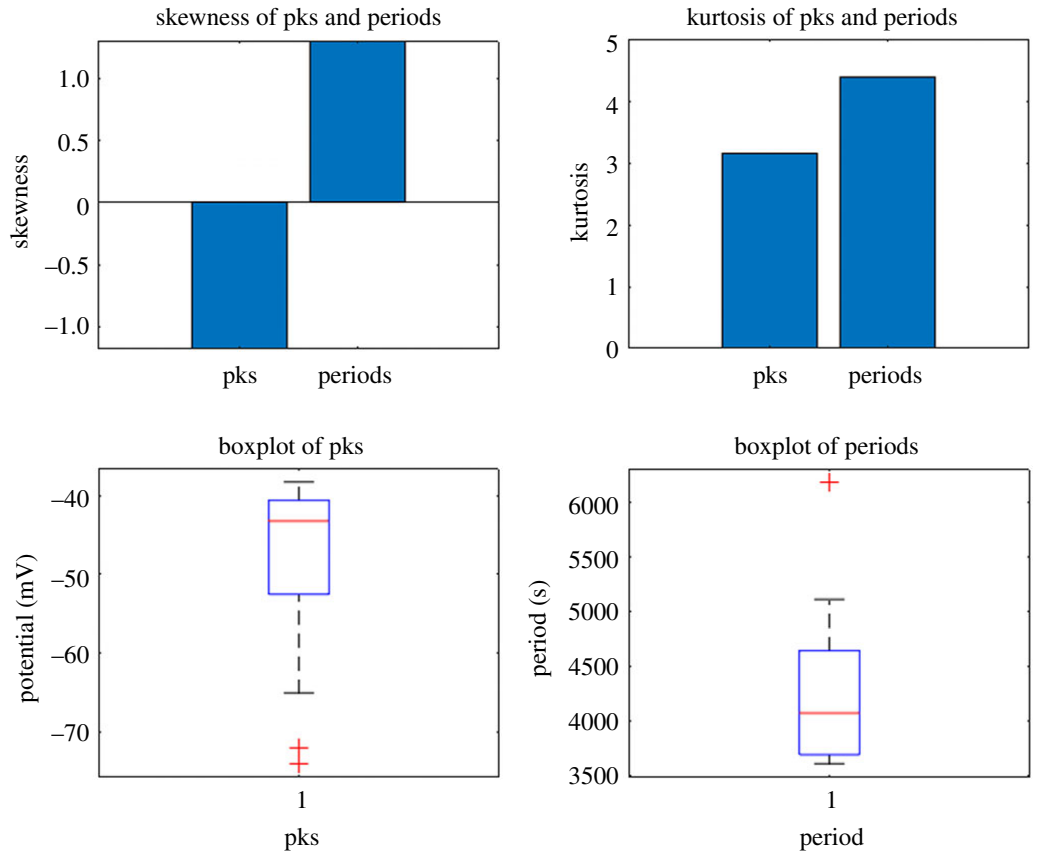


Figure 16. Higher-order statistical characterization of KCP sample spiking parameters. Peak values with a skewness of −1.18 indicate left-sided asymmetry. 3.15 kurtosis indicates a distribution that is near to normal. The positive skewness of 1.30 for periods indicates right-sided asymmetry. The increased kurtosis value of 4.38 indicates a leptokurtic distribution with heavier tails. The boxplots depict the data ranges, quartiles and outliers for the distributions of peak values and periods. This analysis provides a comprehensive multivariate description of the variability in proteinoid spiking peak and periodicity.

the existence of cooperative relationships within the hybrid biofilms. These interactions facilitate the regulation of conductivity, which is dependent upon 'remembering' of the applied voltage bias [62].

The analysis of the composite biofilms' current–voltage relationship demonstrated significant differences between the networks comprising proteinoids and those consisting only of microbes, as depicted in figure 18. During multiple voltage cycles, the KPC, KP and P samples exhibited habituation, characterized by a decrease in hysteresis, as well as memory, demonstrated by a return to a heightened conduction state after stimulation. On the other hand, KC and K demonstrated crossing I–V curves that were devoid of any memory effects. The observed I–V signals demonstrate a similarity between the forgetting characteristics of KC/K and the memory stability observed in the proteinoid-integrated biofilms. The proteinoids have a significant capacity for flexibility and adaptive conductivity, enabling the composite system to retain and encode information from previous inputs.

The proteinoid-microbial composites demonstrate dynamic electrical behaviours that indicate the presence of various adaptive molecular processes responsible for their learning and memory features (table 6). The observed hysteresis and memristive switching exhibit significant characteristics, which serve as evidence for voltage-mediated transitions between meta-stable conductive states. These transitions have the potential to facilitate transitory information storage. In the context of periodic stimulus response, the phenomenon of progressive habituation indicates that factors such as ion depletion may play a significant role. The capacity to computationally learn and remember past inputs is critical for engineering intelligent biosystems. The current results showcase the presence of important adaptive features in easily adjustable synthetic biofilms. These features are made possible through the combined interactions of biological components.

4. Discussion

This study showcases the potential of composite KP biofilms as adaptive and electroactive biosystems for interacting with neural cells, as depicted in the mind map illustration (figure 20). This type of effect encompasses memristive switching, intrinsic spiking patterns and dynamic conductive responses.

Downloaded from https://royalsocietypublishing.org/ on 29 May 2024

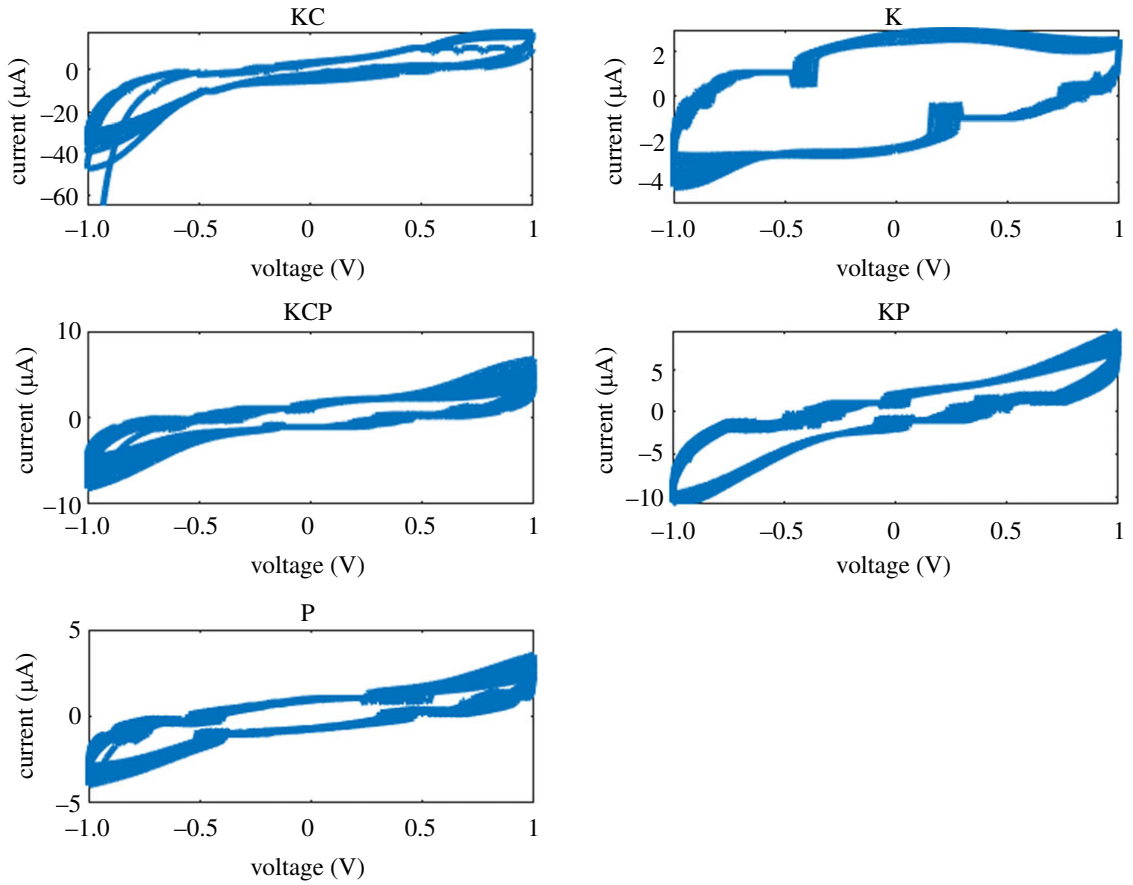


Figure 17. Current–voltage (I–V) profiles for Kombucha-Chlorella (KC), Kombucha (K), Kombucha-Chlorella-proteinoid (KPC), Kombucha-proteinoid (KP) and proteinoid (P) samples. The I–V curves indicate pinched hysteresis loops that are characteristic of memristive systems. Among them, KC demonstrates the broadest current range, spanning from −60 to 1 μA. K demonstrates a narrower semi-circular shape from −4 to 2 μA, while KPC, KP and P show similar intermediate current ranges on the order of −10 to 7 μA. The composites including proteinoids (KPC, KP and P) exhibit a high degree of resemblance to the ideal behaviour of memristors, as indicated by the extent of pinching observed. The dynamics observed in this figure demonstrate the modification of conductance dependent on voltage, which is a result of the interconnected networks between proteinoid and microbial networks.

The Kombucha-proteinoid biofilms include memristive switching characteristics that enable them to replicate the plasticity observed in biological synapses [70]. Similar to the way neurons adjust their connections in response to signals, these biofilms have the ability to regulate their conductivity by responding to voltage inputs. This gives them the ability to learn and store information over time. The spiking patterns relate to oscillations in voltage or current that have the ability to propagate across the biofilm, like action potentials observed in axons [37,71,72]. The dynamic electrical characterizations showed significant current fluctuations, spiking patterns and memristive hysteresis loops. These characteristics closely resemble the excitability and plasticity observed in biological neural networks.

Our findings show that Kombucha-Chlorella samples had increased conductivity, indicating semi-conducting behaviour. To explain doping effects in organic semiconducting materials, a granular model consisting of conductive areas linked by electrostatic forces was previously proposed (figure 19). This model may provide insights into the conductive mechanism observed in the KCP system. Electrical connections between these proteanoid-rich domains could potentially facilitate electron transit through the material, explaining the observed increase in conductivity [73].

Semiconductors are made up of small crystal grains packed together. In between these grains are regions called inter-grain boundaries. Here, the electrical properties change suddenly compared to inside the grains. This is because the charge density and band structure differs at these boundaries.

The inter-grain boundaries in the semiconductor can function as obstacles or barriers that impede the flow of electrical charges. The ability to block or trap charges is dependent upon factors such as the applied voltage, temperature and the presence of any magnetic field.

There are several factors that determine how charges can move past the inter-grain boundaries. These include the size and shape of the grains, which way they are oriented, what they are made of, and how

Downloaded from https://royalsocietypublishing.org/ on 29 May 2024

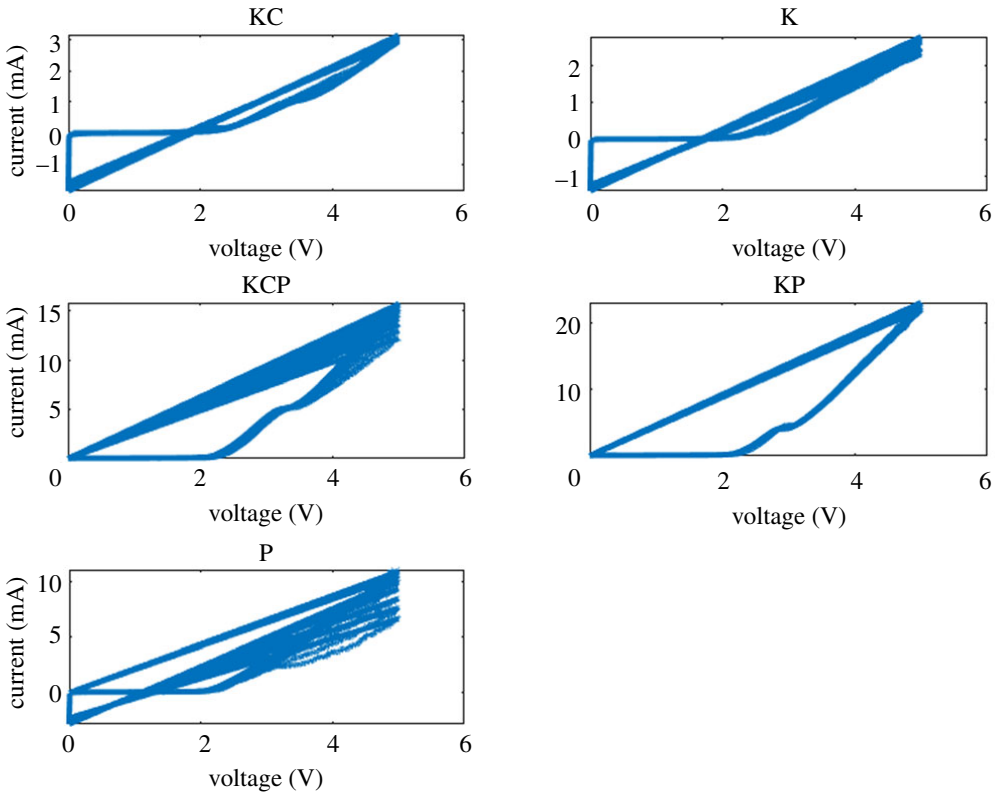


Figure 18. The current–voltage profiles of the Kombucha-Chlorella (KC), Kombucha (K), Kombucha-Chlorella-proteinoid (KCP), Kombucha-proteinoid (KP) and proteinoid (P) samples were monitored over a span of 20 cycles, ranging from 0 to 5 V. The composites KPC, KP and P, which are rich in proteinoids, demonstrate significantly higher maximum current values of 15 mA, 20 mA and 10 mA correspondingly. By contrast, the highest current values for KC and K are approximately 3 mA. Pronounced pinched hysteresis loops are seen in the KPC, KP samples, suggesting amplification in their memristive characteristics. By contrast, the I–V curves of KC, K and P do not exhibit memristive switching behaviours. The presence of proteinoid components facilitates significantly enhanced conductivities and notable electrical memory effects, which have great potential for the development of neurorobotic interfaces.

Table 6. Proposed adaptive mechanisms in proteinoid-microbial biofilms.

phenomena	potential molecular mechanisms
learning	the conformation and alignment of proteinoids undergo modifications in response to voltage stimulation, resulting in the alteration of conductivity channels and junctions between the various components [63–65]
remembering	meta-stable high conduction states can be achieved by applying voltages and are sustained through cooperative interactions and regenerative feedback mechanisms [66,67]
habituation	the process of repeated stimulation leads to the depletion of mobile ions and induces conformational relaxation, resulting in a decrease in hysteresis while maintaining its initial conductivity [62,68,69]

much surface area they share. The charges have to find ways to get around or jump over these boundaries between the grains [74].

The adaptive and electroactive properties of KP biofilms have potential implications in the field of neuromorphic computing, alongside their existing applications in medical and engineering fields. The cutting-edge approach aims to replicate the structure and functions of biological neural networks using synthetic materials and devices. The behaviours exhibited by these biofilms, such as conductivity modulation, plasticity and spiking activity, closely resemble the necessary characteristics for implementing artificial/biological neural networks in hardware.

This work sets the groundwork for engineering intelligent biosystems that can computationally mimic the brain's adaptive abilities in the future. The investigation of the precise interactions between proteinoids and

Downloaded from https://royalsocietypublishing.org/ on 29 May 2024

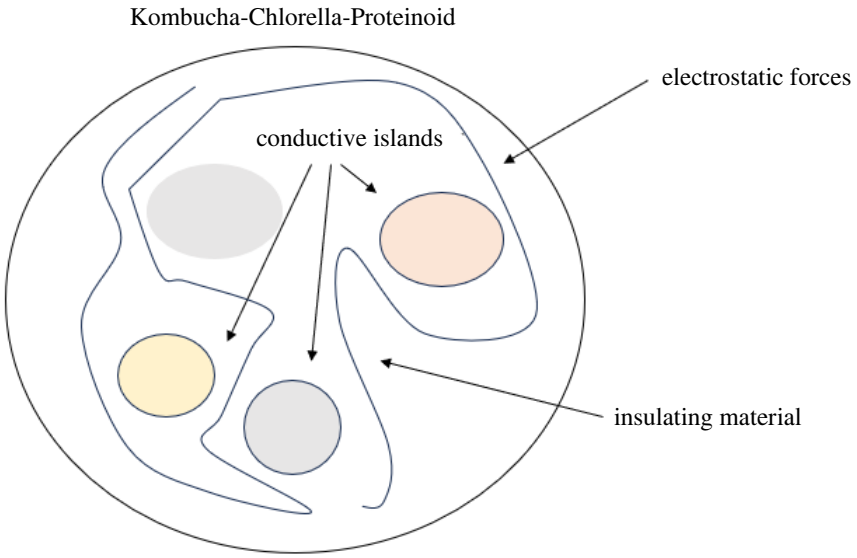


Figure 19. Granular structural model of Kombucha-Chlorella-Proteinoids sample. The large circle on the outside represents the Kombucha growing media. The cells produce proteinoids, which are shown as small coloured circles. Proteinoids are believed to create tiny conductive regions, and the dashed lines indicate the electrical connections between them. This model illustrates a granular semiconductor-like structure formed by proteinoids in the Kombucha-Chlorella system.

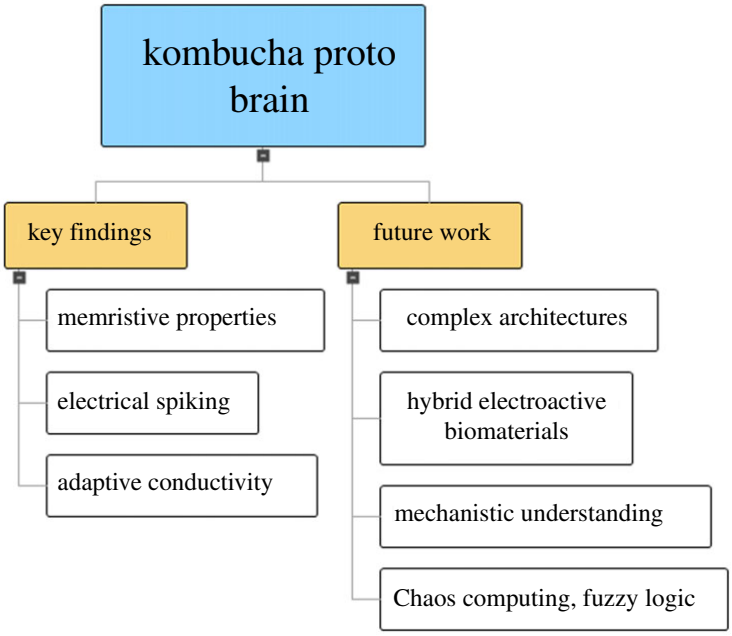


Figure 20. Key research findings highlighted include the emergent memristive properties, electrical spiking behaviours and adaptive conductivity exhibited by the Kombucha–proto brain. Several future research directions can be proposed, including the optimization of composition, the development of more complex architectures, the acquisition of mechanistic understanding, and the exploration of applications in unconventional computing.

microbes that influence the magnitude of conductivity and spiking dynamics has the potential to provide insights into ways for enhancing performance. The integration of additional nanoscale modifiers has the potential to reveal novel hybrid films that possess enhanced bioelectric capability [75–77].

In the realm of computer, the use of external stimulus patterns to train synthetic biofilms presents an opportunity for the integration of machine learning, enabling unconventional, biologically inspired information processing. In general, this study emphasizes potential avenues for integrating biological elements in order to develop intelligent biosystems that incorporate adaptivity, memory and problem-solving abilities. By delving into intricate and multi-faceted designs, as well as investigating the transmission of signals inside interconnected networks, researchers may reveal novel functionalities for unconventional computing systems inspired by biological processes [78].

Downloaded from https://royalsocietypublishing.org/ on 29 May 2024

Table 7. The essential criteria and conditions for using Kombucha-proteinoid biofilms as an alternative for conventional computing systems.

criteria	necessary conditions
connectivity	the ability to programme synaptic conductivity with a high number of connections per neuron
plasticity	dynamic modulation of synapse strength through memristive switching
spike patterns	action potential spikes and tunable oscillations
'Learning'	adaptive alterations in connectivity and conductivity in response to stimuli
biocompatibility	biodegradable, non-toxic materials and interfaces
scalability	architecture hierarchical across multiple dimension scales
stability	robust electroactive performance over the course of several months/years
integration	uniform interfaces between microorganisms and electronic components

In contrast to conventional metal electrodes, the KP biofilms exhibit enhanced biocompatibility and possess the ability to establish conformal contact with neural tissue. In relation to inflexible nanomaterials, biofilms have a malleable and organ-like texture. Nevertheless, there are still obstacles to overcome in relation to the ability to scale up and ensure the long-term durability of Kombucha-based biosystems prior to their extensive use in medical implants or bioelectronic applications.

Finally, integrating Kombucha biofilms with conventional semiconductor technology and programming their connectivity in an organized manner requires significant research. It will be crucial to carefully adjust the biofilm thickness, architecture, conductivity and spike patterns in order to effectively train and optimize their performance. If successfully developed, neuromorphic platforms based on Kombucha could offer more natural and efficient computing paradigms in comparison to traditional von Neumann architectures. This application showcases a thrilling new path for using these adaptive biosystems beyond the field of biomedicine.

The potential of KP biofilms for interacting with neural cells and neuromorphic computers is emphasized in the suggested applications, indicating the broad range of possibilities for these versatile biosystems beyond the field of biomedicine (figure 20). However, it is imperative that these biofilms satisfy a number of characteristics in order to successfully supplant traditional computing architectures, as outlined in table 7. The key factors encompass the attainment of programmable connectivity and plasticity, the ability to adjust spiking patterns, the capacity for learning, biocompatibility, scalability, long-term stability and uniform interface with electronic systems. To optimize these biosystems as biological neural networks for computation, it will be necessary to make significant advancements in other areas. The development of a mechanistic understanding of the electroactive characteristics and behaviours that arise from the hierarchical organization and symbiotic interactions of bacteria, yeasts and proteins within Kombucha biofilms presents both opportunities and challenges that are closely interconnected. Current research endeavours aim to uncover the complete capabilities of these living materials in order to advance bioelectronic technology for future generations.

5. Conclusion

In summary, this study showcases the potential of composite KP biofilms as versatile bioelectronic materials for connecting with neuronal networks. The proteinoid nanonetworks and Kombucha polysaccharide matrix collaborate to form a unified system that demonstrates emergent electrical excitability, resembling important characteristics observed in brain tissues found in nature. The proteinoid-Kombucha films exhibit dynamic electrical spikes, tunable conduction and intrinsic habituation, which contribute to their ability to mimic the signalling activities of biological neurons. This research offers a framework that combines the processability of biomolecular materials with the complexity of living systems.

Data accessibility. These data are accessible via the online database Zenondo https://doi.org/10.5281/zenodo.10037497 [79].

Supplementary material is available online [80].

Declaration of AI use. We have not used AI-assisted technologies in creating this article.

Authors' contributions. A.N.: conceptualization, investigation, methodology, validation, visualization; P.M.: conceptualization, investigation, methodology, validation, visualization; A.A.: conceptualization, investigation, methodology, supervision.

All authors gave final approval for publication and agreed to be held accountable for the work performed therein.

Downloaded from https://royalsocietypublishing.org/ on 29 May 2024

Conflict of interest declaration. We declare we have no competing interest.
Funding. The research was supported by EPSRC grant no. EP/W010887/1 'Computing with proteinoids'.
Acknowledgements. Authors are grateful to David Paton for helping with SEM imaging and to Neil Phillips for helping with instruments.

References

1. Conners EM, Rengasamy K, Bose A. 2022 Electroactive biofilms: how microbial electron transfer enables bioelectrochemical applications. *J. Ind. Microbiol. Biotechnol.* **49**, 012. (doi:10.1093/jimb/kuac012)
2. Bird LJ, Onderko EL, Phillips DA, Mickol RL, Malanoski AP, Yates MD, Eddie BJ, Glaven SM. 2019 Engineered living conductive biofilms as functional materials. *MRS Commun.* **9**, 505–517. (doi:10.1557/mrc.2019.27)
3. Leung DHL, Lim YS, Uma K, Pan GT, Lin JH, Chong S, Yang TCK. 2021 Engineering *S. oneidensis* for performance improvement of microbial fuel cell–a mini review. *Appl. Biochem. Biotechnol.* **193**, 1170–1186. (doi:10.1007/s12010-020-03469-6)
4. Angelaalincy MJ, Navanietha Krishnaraj R, Shakambari G, Ashokkumar B, Kathiresan S, Varalakshmi P. 2018 Biofilm engineering approaches for improving the performance of microbial fuel cells and bioelectrochemical systems. *Front. Energy Res.* **6**, 63. (doi:10.3389/fenrg.2018.00063)
5. Fox SW, Jungck JR, Nakashima T. 1974 From proteinoid microsphere to contemporary cell: formation of internucleotide and peptide bonds by proteinoid particles. *Orig. Life* **5**, 227–237. (doi:10.1007/BF00927027)
6. Mougkogiannis P, Raeisi Kheirabadi N, Chiolerio A, Adamatzky A. 2023 Electrical spiking activity of proteinoids-ZnO colloids. *bioRxiv*, pp. 2023–07.
7. Chua L, Sirakoulis GC, Adamatzky A. 2019 *Handbook of memristor networks*. London, UK: Springer Nature.
8. Kumar AM, Rao KP. 1998 Preparation and characterization of pH-sensitive proteinoid microspheres for the oral delivery of methotrexate. *Biomaterials* **19**, 725–732. (doi:10.1016/S0142-9612(97)00188-9)
9. Matsuno K. 1984 Electrical excitability of proteinoid microspheres composed of basic and acidic proteinoids. *BioSystems* **17**, 11–14. (doi:10.1016/0303-2647(84)90011-X)
10. Mougkogiannis P, Adamatzky A. 2023 Low frequency electrical waves in ensembles of proteinoid microspheres. *Sci. Rep.* **13**, 1992. (doi:10.1038/s41598-023-29067-0)
11. Marsh AJ, O'Sullivan O, Hill C, Ross RP, Cotter PD. 2014 Sequence-based analysis of the bacterial and fungal compositions of multiple kombucha (tea fungus) samples. *Food Microbiol.* **38**, 171–178. (doi:10.1016/j.fm.2013.09.003)
12. Goh W, Rosma A, Kaur B, Fazilah A, Karim A, Bhat R. 2012 Fermentation of black tea broth (Kombucha): I. Effects of sucrose concentration and fermentation time on the yield of microbial cellulose. *Int. Food Res. J.* **19**, 109–117.
13. Kayisoglu S, Coskun F. 2020 Determination of physical and chemical properties of kombucha teas prepared with different herbal teas. *Food Sci. Technol.* **41**, 393–397. (doi:10.1590/fst.12720)
14. Martínez Leal J, Valenzuela Suárez L, Jayabalan R, Huerta Oros J, Escalante-Aburto A. 2018 A review on health benefits of kombucha nutritional compounds and metabolites. *CyTA J. Food* **16**, 390–399. (doi:10.1080/19476337.2017.1410499)
15. Tommasi T, Chiolerio A, Crepaldi M, Demarchi D. 2014 A microbial fuel cell powering an all-digital piezoresistive wireless sensor system. *Microsyst. Technol.* **20**, 1023–1033. (doi:10.1007/s00542-014-2104-0)
16. Pradhan S, Prabhakar MR, Karthika Parvathy K, Dey B, Jayaraman S, Behera B, Paramasivan B. 2023 Metagenomic and physicochemical analysis of Kombucha beverage produced from tea waste. *J. Food Sci. Technol.* **60**, 1088–1096. (doi:10.1007/s13197-022-05476-3)
17. Yamamoto M, Fujishita M, Hirata A, Kawano S. 2004 Regeneration and maturation of daughter cell walls in the autospore-forming green alga *Chlorella vulgaris* (Chlorophyta, Trebouxiophyceae). *J. Plant. Res.* **117**, 257–264. (doi:10.1007/s10265-004-0154-6)
18. Illman AM, Scragg AH, Shales SW. 2000 Increase in Chlorella strains calorific values when grown in low nitrogen medium. *Enzyme Microb. Technol.* **27**, 631–635. (doi:10.1016/S0141-0229(00)00266-0)
19. Yamamoto M, Kurihara I, Kawano S. 2005 Late type of daughter cell wall synthesis in one of the Chlorellaceae, *Parachlorella kessleri* (Chlorophyta, Trebouxiophyceae). *Planta* **221**, 766–775. (doi:10.1007/s00425-005-1486-8)
20. Phukan MM, Chutia RS, Konwar B, Kataki R. 2011 Microalgae Chlorella as a potential bio-energy feedstock. *Appl. Energy* **88**, 3307–3312. (doi:10.1016/j.apenergy.2010.11.026)
21. Safi C, Zebib B, Merah O, Pontalier PY, Vaca-Garcia C. 2014 Morphology, composition, production, processing and applications of *Chlorella vulgaris*: a review. *Renew. Sustain. Energy Rev.* **35**, 265–278. (doi:10.1016/j.rser.2014.04.007)
22. Becker EW. 1994 *Microalgae: biotechnology and microbiology*, vol. **10**. Cambridge, UK: Cambridge University Press.
23. Morris HJ, Almarales A, Carrillo O, Bermúdez RC. 2008 Utilisation of Chlorellavulgaris cell biomass for the production of enzymatic protein hydrolysates. *Bioresour. Technol.* **99**, 7723–7729. (doi:10.1016/j.biortech.2008.01.080)
24. Safi C, Charton M, Pignolet O, Silvestre F, Vaca-Garcia C, Pontalier PY. 2012 Influence of microalgae cell wall characteristics on protein extractability and determination of nitrogen-to-protein conversion factors. *J. Appl. Phycol.* **25**, 523–529. (doi:10.1007/s10811-012-9886-1)
25. Servaites JC, Faeth JL, Sidhu SS. 2012 A dye binding method for measurement of total protein in microalgae. *Anal. Biochem.* **421**, 75–80. (doi:10.1016/j.ab.2011.10.047)
26. Seyfabadi J, Ramezanpour Z, Khoeyi ZA. 2011 Protein, fatty acid, and pigment content of *Chlorella vulgaris* under different light regimes. *J. Appl. Phycol.* **23**, 721–726. (doi:10.1007/s10811-010-9569-8)
27. Berliner MD. 1986 Proteins in *Chlorella vulgaris*. *Microbios* **46**, 199–203.
28. Phillips N, Mayne R, Adamatzky A. 2022 Chlorella sensors in liquid marbles and droplets. *Sens. Bio-Sens. Res.* **36**, 100491. (doi:10.1016/j.sbsr.2022.100491)
29. Mougkogiannis P, Phillips N, Adamatzky A. 2023 Transfer functions of proteinoid microspheres. *Biosystems* **227**, 104892. (doi:10.1016/j.biosystems.2023.104892)
30. Albano KM, Cavallieri ÂLF, Nicoletti VR. 2019 Electrostatic interaction between proteins and polysaccharides: physicochemical aspects and applications in emulsion stabilization. *Food Rev. Int.* **35**, 54–89. (doi:10.1080/87559129.2018.1467442)
31. Subbiahdoss G, Osmen S, Reimhult E. 2022 Cellulosic biofilm formation of *Komagataeibacter* in kombucha at oil-water interfaces. *Biofilm* **4**, 100071. (doi:10.1016/j.bioflm.2022.100071)
32. Van Oss C, Good R, Chaudhury M. 1986 The role of van der Waals forces and hydrogen bonds in 'hydrophobic interactions' between biopolymers and low energy surfaces. *J. Colloid Interface Sci.* **111**, 378–390. (doi:10.1016/0021-9797(86)90041-X)
33. Okereke MI, Akpoyomare A, Bingley M. 2014 Virtual testing of advanced composites, cellular materials and biomaterials: a review. *Compos. Part B: Eng.* **60**, 637–662. (doi:10.1016/j.compositesb.2014.01.007)
34. Xu J, Zhao X, Zhao X, Wang Z, Tang Q, Xu H, Liu Y. 2022 Memristors with biomaterials for biorealistic neuromorphic applications. *Small Sci.* **2**, 2200028. (doi:10.1002/smsc.202200028)
35. Walther A. 2020 From responsive to adaptive and interactive materials and materials systems: a roadmap. *Adv. Mater.* **32**, 1905111. (doi:10.1002/adma.201905111)
36. Xue K, Wang F, Suwardi A, Han MY, Teo P, Wang P, Wang S, Ye E, Li Z, Loh XJ. 2021 Biomaterials by design: harnessing data for future development. *Mater. Today Bio.* **12**, 100165. (doi:10.1016/j.mtbio.2021.100165)
37. Adamatzky A. 2021 Towards proteinoid computers. Hypothesis paper. *Biosystems* **208**, 104480. (doi:10.1016/j.biosystems.2021.104480)

Downloaded from https://royalsocietypublishing.org/ on 29 May 2024

38. Beebe SJ, White J, Blackmore PF, Deng Y, Somers K, Schoenbach KH. 2003 Diverse effects of nanosecond pulsed electric fields on cells and tissues. *DNA Cell Biol.* **22**, 785–796. (doi:10.1089/104454903322624993)
39. Zheng Y, Shojaei-Baghini E, Wang C, Sun Y. 2013 Microfluidic characterization of specific membrane capacitance and cytoplasm conductivity of singlecells. *Biosens. Bioelectron.* **42**, 496–502. (doi:10.1016/j.bios.2012.10.081)
40. Ohayon D, Inal S. 2020 Organic bioelectronics: from functional materials to next-generation devices and power sources. *Adv. Mater.* **32**, 2001439. (doi:10.1002/adma.202001439)
41. Dai C, Wan J, Geng W, Song S, Ma F, Shao J. 2017 KOH direct treatment of kombucha and in situ activation to prepare hierarchical porous carbon for high-performance supercapacitor electrodes. *J. Solid State Electrochem.* **21**, 2929–2938. (doi:10.1007/s10008-017-3631-2)
42. Baslak C, Demirel S, Kocyigit A, Alatli H, Yildirim M. 2022 Supercapacitor behaviors of carbon quantum dots by green synthesis method from tea fermented with kombucha. *Mater. Sci. Semicond. Process.* **147**, 106738. (doi:10.1016/j.mssp.2022.106738)
43. Adamatzky A. 2023 Electrical potential spiking of kombucha zoogleal mats: a symbiotic community of bacteria and yeasts. *Bioelectricity* **5**, 99–108. (doi:10.1089/bioe.2022.0030)
44. Hashemi SA *et al.* 2022 Bio-enhanced polyrhodanine/graphene Oxide/Fe_3O_4 nanocomposite with kombucha solvent supernatant as ultra-sensitive biosensor for detection of doxorubicin hydrochloride in biological fluids. *Mater. Chem. Phys.* **279**, 125743. (doi:10.1016/j.matchemphys.2022.125743)
45. Adamatzky A. 2022 Electrical potential spiking of kombucha zoogleal mats. *bioRxiv*, pp. 2022–08.
46. May C. 2020 *Passive circuit analysis with LTspice*. London, UK: Springer.
47. Jamnik J, Maier J. 1999 Treatment of the impedance of mixed conductors equivalent circuit model and explicit approximate solutions. *J. Electrochem. Soc.* **146**, 4183. (doi:10.1149/1.1392611)
48. Laurenti M, Verna A, Chiolerio A. 2015 Evidence of negative capacitance in piezoelectric ZnO thin films sputtered on interdigital electrodes. *ACS Appl. Mater. Interfaces* **7**, 24 470–24 479. (doi:10.1021/acsami.5b05336)
49. Khan AI, Chatterjee K, Wang B, Drapcho S, You L, Serrao C, Bakaul SR, Ramesh R, Salahuddin S. 2015 Negative capacitance in a ferroelectric capacitor. *Nat. Mater.* **14**, 182–186. (doi:10.1038/nmat4148)
50. Ershov M, Liu H, Li L, Buchanan M, Wasilewski Z, Jonscher AK. 1998 Negative capacitance effect in semiconductor devices. *IEEE Trans. Electron Devices* **45**, 2196–2206. (doi:10.1109/16.725254)
51. Guccini V, Carlson A, Yu S, Lindbergh G, Lindström RW, Salazar-Alvarez G. 2019 Highly proton conductive membranes based on carboxylated cellulose nanofibres and their performance in proton exchange membrane fuel cells. *J. Mater. Chem. A* **7**, 25 032–25 039. (doi:10.1039/C9TA04898G)
52. Liu Y, Tan X, Li K. 2006 Mixed conducting ceramics for catalytic membrane processing. *Catalysis Rev.* **48**, 145–198. (doi:10.1080/01614940600631348)
53. Jiang G, Zhang J, Qiao J, Jiang Y, Zarrin H, Chen Z, Hong F. 2015 Bacterial nanocellulose/Nafion composite membranes for low temperature polymer electrolyte fuel cells. *J. Power Sources* **273**, 697–706. (doi:10.1016/j.jpowsour.2014.09.145)
54. Khamwongsa P, Wongjom P, Cheng H, Lin CC, Ummartyotin S. 2022 Significant enhancement of electrical conductivity of conductive cellulose derived from bamboo and polypyrrole. *Comp. Part C: Open Access* **9**, 100314. (doi:10.1016/j.jcomc.2022.100314)
55. Motoike IN, Adamatzky A. 2005 Three-valued logic gates in reaction–diffusion excitable media. *Chaos Solitons Fractals* **24**, 107–114. (doi:10.1016/S0960-0779(04)00461-8)
56. Kinsner W. 2006 Characterizing chaos through Lyapunov metrics. *IEEE Trans. Syst. Man Cybern.* **36**, 141–151. (doi:10.1109/TSMCC.2006.871132)
57. Martinez GJ, Adamatzky A, Alonso-Sanz R. 2012 Complex dynamics of elementary cellular automata emerging from chaotic rules. *Int. J. Bifurcation Chaos* **22**, 1250023. (doi:10.1142/S021812741250023X)
58. Adamatzky A, Chen G. 2013 Chaos, Cnn, memristors and beyond: a festschrift For Leon Chua (With Dvd-rom, Composed By Eleonora Bilotta). Singapore: World Scientific. (doi:10.1142/8590)
59. Costello BDL, Adamatzky A. 2005 Experimental implementation of collision-based gates in Belousov–Zhabotinsky medium. *Chaos Solitons Fractals* **25**, 535–544. (doi:10.1016/j.chaos.2004.11.056)
60. Adamatzky A, Wuensche A, Costello BDL. 2006 Glider-based computing in reaction-diffusion hexagonal cellular automata. *Chaos Solitons Fractals* **27**, 287–295. (doi:10.1016/j.chaos.2005.03.048)
61. Adamatzky A, de Lacy Costello B, Shirakawa T. 2008 Universal computation with limited resources: Belousov–Zhabotinsky and Physarum computers. *Int. J. Bifurcation Chaos* **18**, 2373–2389. (doi:10.1142/S0218127408021750)
62. Mougkogiannis P, Adamatzky A. 2023 Learning in ensembles of proteinoid microspheres. (http://arxiv.org/abs/2306.14362)
63. Neftci EO, Averbeck BB. 2019 Reinforcement learning in artificial and biological systems. *Nat. Mach. Intell.* **1**, 133–143. (doi:10.1038/s42256-019-0025-4)
64. Slijepcevic P. 2021 Principles of information processing and natural learning in biological systems. *J. General Philos. Sci.* **52**, 227–245. (doi:10.1007/s10838-019-09471-9)
65. He J, Maltenfort MG, Wang Q, Hamm TM. 2001 Learning from biological systems: modeling neural control. *IEEE Control Syst. Mag.* **21**, 55–69. (doi:10.1109/37.939944)
66. Siuti P, Yazbek J, Lu TK. 2014 Engineering genetic circuits that compute and remember. *Nat. Protoc.* **9**, 1292–1300. (doi:10.1038/nprot.2014.089)
67. Squire LR. 2004 Memory systems of the brain: a brief history and current perspective. *Neurobiol. Learn. Mem.* **82**, 171–177. (doi:10.1016/j.nlm.2004.06.005)
68. Wu Z *et al.* 2020 A habituation sensory nervous system with memristors. *Adv. Mater.* **32**, 2004398. (doi:10.1002/adma.202004398)
69. Wang Y, Lv Z, Chen J, Wang Z, Zhou Y, Zhou L, Chen X, Han ST. 2018 Photonic synapses based on inorganic perovskite quantum dots for neuromorphic computing. *Adv. Mater.* **30**, 1802883. (doi:10.1002/adma.201802883)
70. Warraich Z, Kleim JA. 2010 Neural plasticity: the biological substrate for neurorehabilitation. *Pm&r* **2**, S208–S219. (doi:10.1016/j.pmrj.2010.10.016)
71. Schulz DJ. 2006 Plasticity and stability in neuronal output via changes in intrinsic excitability: it's what's inside that counts. *J. Exp. Biol.* **209**, 4821–4827. (doi:10.1242/jeb.02567)
72. Zhang A, Zhou H, Li X, Zhu W. 2019 Fast and robust learning in spiking feed-forward neural networks based on intrinsic plasticity mechanism. *Neurocomputing* **365**, 102–112. (doi:10.1016/j.neucom.2019.07.009)
73. Sakkopoulos S, Vitoratos E, Dalas E. 1998 Conductivity degradation due to thermal aging in conducting polyaniline and polypyrrole. *Synth. Met.* **92**, 63–67. (doi:10.1016/S0379-6779(98)80024-6)
74. Olimov L, Sokhibova Z, Abdurakhmanov B. 2019 Structure of inter grain boundaries in the granular semiconductors and the charge state. *Int. J. Res. Stud. Electr. Electron. Eng. (IJRSEEE)* **5**, 6–10. (doi:10.20431/2454-9436.0504002)
75. Wang YX, Li WQ, Zong WM, Su TY, Mu Y. 2019 Polyaniline-decorated honeycomb-like structured macroporous carbon composite as an anode modifier for enhanced bioelectricity generation. *Sci. Total Environ.* **696**, 133980. (doi:10.1016/j.scitotenv.2019.133980)
76. Campuzano S, Wang J. 2011 Nanobioelectroanalysis based on carbon/inorganic hybrid nanoarchitectures. *Electroanalysis* **23**, 1289–1300. (doi:10.1002/elan.201100186)
77. Wang YX, Hou N, Liu XL, Mu Y. 2022 Advances in interfacial engineering for enhanced microbial extracellular electron transfer. *Bioresour. Technol.* **345**, 126562. (doi:10.1016/j.biortech.2021.126562)
78. Adamatzky A, Bull L, Costello BDL. 2007 *Unconventional computing 2007*. London, UK: Luniver Press.
79. Nikolaidou A, Mougkogiannis P, Adamatzky A. 2023 Electroactive composite biofilms integrating Kombucha, Chlorella and synthetic proteinoid protobrains. Zenodo (doi:10.5281/zenodo.10037497)
80. Nikolaidou A, Mougkogiannis P, Adamatzky A. 2024 Electroactive composite biofilms integrating Kombucha, Chlorella and synthetic proteinoid Proto–Brains. Figshare. (doi:10.6084/m9.figshare.c.7214477)

ACS OMEGA

Open Access

This article is licensed under CC-BY 4.0

http://pubs.acs.org/journal/acsodf

Article

Functionalizing the Electrical Properties of Kombucha Zoogleal Mats for Biosensing Applications

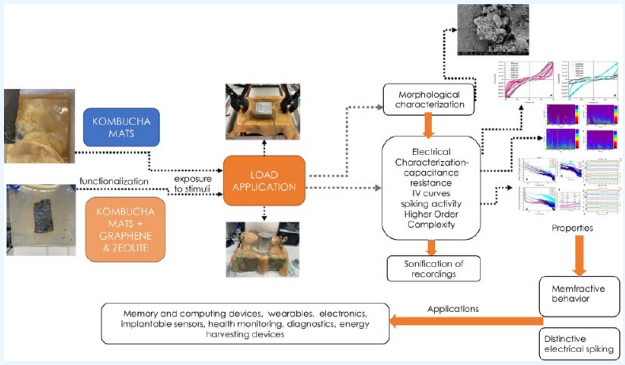
Anna Nikolaidou,* Alessandro Chiolerio, Mohammad Mahdi Dehshibi, and Andrew Adamatzky*

Cite This: https://doi.org/10.1021/acsomega.4c01227

Read Online

ACCESS | Metrics & More | Article Recommendations | Supporting Information

ABSTRACT: Kombucha is a type of tea that is fermented using yeast and bacteria. During this process, a film made of cellulose is produced. This film has unique properties such as biodegradability, flexibility, shape conformability, and ability to self-grow as well as be produced across customized scales. In our previous studies, we demonstrated that Kombucha mats exhibit electrical activity represented by spikes of the electrical potential. We propose using microbial fermentation as a method for *in situ* functionalization to modulate the electroactive nature of Kombucha cellulose mats, where graphene and zeolite were used for the functionalization. We subjected the pure and functionalized Kombucha mats to mechanical stimulation by applying different weights and geometries. Our experiments demonstrated that Kombucha mats functionalized with graphene and zeolite exhibit memfractive properties and respond to load by producing distinctive spiking patterns. Our findings present incredible opportunities for the *in situ* development of functionalized hybrid materials with sensing, computing, and memory capabilities. These materials can self-assemble and self-grow after they fuse their living and synthetic components. This study contributes to an emergent area of research on bioelectronic sensing and hybrid living materials, opening up exciting opportunities for use in smart wearables, diagnostics, health monitoring, and energy harvesting applications.



Downloaded via 91.141.34.125 on July 8, 2024 at 12:40:35 (UTC).
See https://pubs.acs.org/sharingguidelines for options on how to legitimately share published articles.

INTRODUCTION

There has been a significant increase in the use of cellulose as an alternative sustainable and renewable material in various fields such as medicine, packaging, food, and textiles. Cellulose is a natural biodegradable polymer and is considered to be one of the most abundant macromolecules in nature. It is produced by a wide range of living organisms, from bacteria to plants.[1−3] Bacterial cellulose is known to exhibit a higher purity, mechanical strength, water-holding capacity, chemical stability, and biological adaptability than cellulose produced by plants. This is due to a lack of lignin and hemicellulose polymers.[4] Acetic acid bacteria produce acetic acid by metabolizing carbon sources into acetic acid and ethanol through their oxidative fermentation pathways.[5] They are excellent producers of cellulose,[6] which can be obtained in a very short time.[7,8] Cellulose is organized in hydrogels and features interesting trains of spikes of extracellular electrical potential.[9] These potential spikes could be used to enable reactive sensing wearables by means of living colonies of bacteria.[10] When a community of bacteria, such as acetic acid bacteria and yeast, form a symbiotic relationship, they can enhance cellulose production through their combined microbial metabolism.[4] This synergy is found in Kombucha cellulose, which emerges during the fermentation of Kombucha tea. Kombucha tea is a popular probiotic beverage that is made by fermenting sugared tea with a SCOBY, a symbiotic culture of over 20 species of bacteria and yeast.[11−13] During fermentation, the microorganisms consume sucrose as the primary carbon source, while tea extract provides the nitrogen source. In the presence of oxygen, the SCOBY produces organic acids, carbon dioxide, and a floating biofilm composed of cellulose. The thickness of the film varies depending on the nutrients and breeding time.[14] Kombucha cellulose shows high biocompatibility due to its enhanced cell-matrix interactions, cell signaling pathways, and ability to maintain cellular homeostasis.[15] In our previous studies, we demonstrated that Kombucha cellulose mats show rich dynamics of electrical activity, represented by spikes of electrical potential. This makes them an exciting material for developing living bioelectronic materials with active electrical properties, sensing and computing capabilities.[16,17] The electroactive nature of the cellulose mats also makes them suitable for biosensing applications.

Received: February 7, 2024
Revised: June 7, 2024
Accepted: June 14, 2024

© XXXX The Authors. Published by American Chemical Society

Live Kombucha cellulose mats possess various chemical, electrical, and mechanical properties. They have a high production rate of cellulose, are cost-effective and flexible, and can take customized shapes while retaining the ability to self-grow. These mats can be produced in different sizes and thicknesses, making them ideal materials for scaffold production. They can be used to create biocomposites with targeted and enhanced functionalities suitable for applications such as smart wearables, soft robotics, and building materials.

To enhance the electrical properties and sensing capabilities of Kombucha cellulose mats, in this study we combine graphene and zeolite nanoparticles for the functionalization of the mats. The selection of zeolite-graphene nanoparticles as cell carriers within the Kombucha zoogleal mat was based on their distinct, but collaborative characteristics,[18−20] leading to the improvement of the mat's electrical conductivity, sensitivity, and stability. Graphene is a two-dimensional carbon nanomaterial with excellent electrical conductivity, mechanical strength, high thermal conductivity, and high electron mobility at room temperature.[21−26] These exceptional characteristics qualify graphene for the reinforcement of biopolymer matrixes.[27] The integration of graphene into the cellulose matrix enables the formation of electrical conductive pathways, facilitating effective electron transfer and thus improving the overall electrical conductivity of the material.[28,29] Additionally, Kombucha cellulose can strongly bind with graphene because of the many hydroxyl groups in the cellulose units, allowing for effective interactions between the cellulose and graphene such as hydrogen bonding.[27,30−33] Graphene is therefore an ideal candidate for functionalization and enhancement of the electrical properties of the Kombucha cellulose mats. Zeolites are a class of aluminosilicates with a crystalline lattice structure and pores of molecular dimensions.[34−39] They have been used for various applications including zeolite-based biosensors. Zeolite-based biosensors with different characteristics can be obtained by varying their properties such as ion exchange behavior, particle size, surface groups and pore size.[40] They have also been used for improving the performance of existing sensors due to their absorption, diffusion and catalytic properties.[41] Equal to graphene, zeolites present a multitude of benefits for functionalization. Due to their structure, they have a large surface area, high adsorption capacity, and high selectivity, enabling the absorption of various components.[37,42−44] Consequently, they can provide an expanded surface area which facilitates particle and cell immobilization and attachment. Additionally, zeolites facilitate a suitable environment for encapsulation, enabling immobilized biomolecules to have enhanced stability,[45] ensuring the material's durability and functionality. Taking advantage of the above complementary properties of zeolite and graphene nanoparticles, we aim to use them as carriers for integrated cells. Graphene contributes to exceptional electrical conductivity and mechanical strength, whereas the zeolite nanoparticles provide an expanded surface area to facilitate immobilization, adherence, and improved stability. Their unique combination into the cellulose fibers of the Kombucha mat allows for enhanced sensitivity, stability, and electrical responses to mechanical pressure.

This study presents new insights into the *in situ* fictionalization of Kombucha pellicles to enhance their electrical properties and introduce targeted responsive capabilities. We performed electrical measurements on both unmodified and functionalized cellulose mats under mechanical stimuli using weight load application and pattern projection. The results showed that the functionalized Kombucha cellulose mats exhibit significantly higher sensitivity to external input compared to the control unmodified cellulose mats. This work contributes to the emerging field of bioelectronic sensing and establishes Kombucha cellulose as an exciting, sustainable scaffold material for information recognition and transmission.

METHODS

Preparation of Pure and Functionalized Kombucha Cellulose. For modulating the electrochemical properties of Kombucha cellulosic mats, graphene and zeolite were used for *in situ* functionalization. For the production of the unmodified and functionalized Kombucha cellulose samples, a SCOBY culture of yeast and bacteria acquired from Freshly Fermented, Ltd. (Lee-on-the-Solent, PO13 9FU, UK) was inoculated in a sucrose tea infusion. For the infusion, black tea was selected as it has demonstrated higher levels of cellulose production.[4] The infusion was prepared with 5 L of boiled tap water, 500 g of white granulated sugar (Tate & Lyle, UK), and 10 black tea bags (Taylors Yorkshire Teabags, UK, 125 g) in a plastic container and left to reach room temperature (22 °C). The SCOBY mat was then placed in the solution, and the container was stored in darkness and maintained at static conditions of 19 °C. A lid with 8 × 0.5 mm^2 holes was used to fully enclose the plastic container. Film formation was observed on the sixth day as thin layers above and below the native SCOBY, and the thickness increased with the fermentation time. We replaced the solution every 12−14 days before the increase in cellulose production reached a plateau, following the same infusion protocol as that mentioned above. Our rationale was that a rapid decrease of sucrose has been reported from day 5 to day 15, which is attributed to the yeast extracellular enzyme production[4] resulting from the kinetic behavior that the Kombucha SCOBY exhibits, where yeasts hydrolyze sucrose for their own consumption, producing ethanol and carbon dioxide, and making available reducing sugars for bacterial metabolism.[11,46] After 8 weeks, the cellulose mats were transferred to a 240 × 240 mm^2 Petri dish each. 30 mL of newly made sucrose black tea solution was added to each Petri dish, instigating the fermentation process and allowing for the continuation of mat growth. After 7 days of inoculation, we proceeded with the experiments.

The two cellulose mats exhibited a high intensity of yellow and brown color. The yellowness can be attributed to the Maillard reactions taking place during the fermentation and film conditioning occurring between the sugars and amino acids in addition to colored phytochemicals.[4] The brown color has been reported to be caused by melanoidins, which are colored and nitrogen-containing compounds.[47,48] Some inhomogeneity observed in the visual appearance of the functionalized Kombucha mat is a typical feature of materials produced by microorganisms. Kombucha zoogleal mats are multispecies systems synthesized by variable natural symbiotes, yeast and bacteria. During the process of fermentation, cooperative and competitive interactions occur among the microbes. The nonuniformity observed in the growth of the modified Kombucha mat can be attributed to their ongoing interactions and metabolic activities. Additionally, the surface adherence properties of the mat can be directly affected by operational conditions such as the pH, temperature and sugar concentrations.[49,50] These factors account for the nonun-

https://doi.org/10.1021/acsomega.4c01227
ACS Omega XXXX, XXX, XXX−XXX

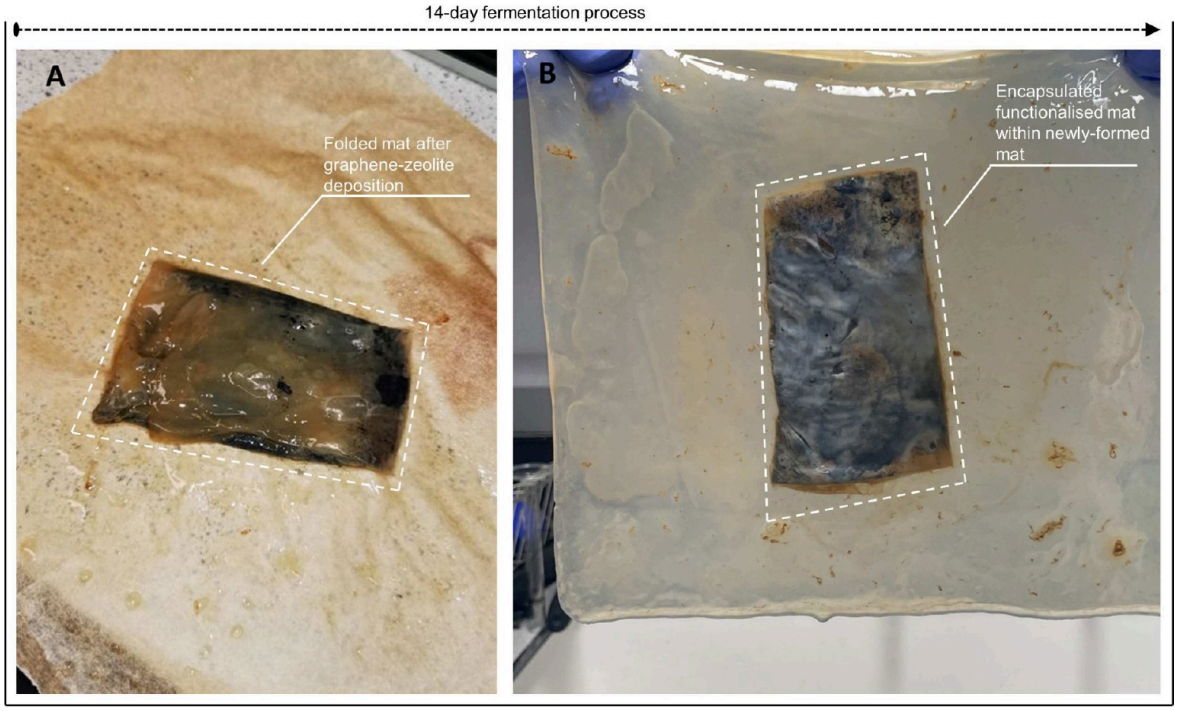


Figure 1. In situ preparation process of functionalized Kombucha mat. (A) The Kombucha cellulose mat after functionalization with graphene and zeolite Y nanoparticles. After homogeneous deposition, the mat was folded to avoid spillage of the mixture when entered back to the Kombucha solution. (B) Functionalized Kombucha cellulose mat after 14 days of growth.

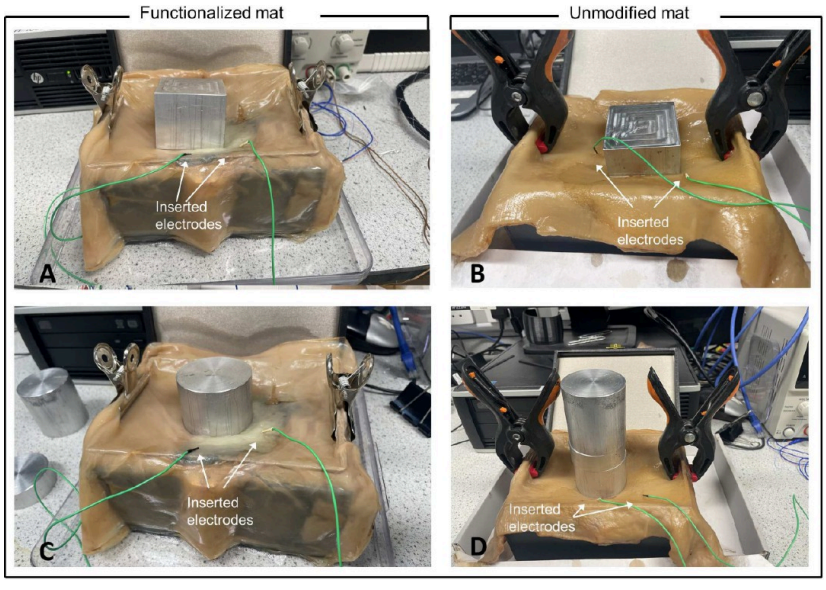


Figure 2. Electrical characterization of unmodified and modified Kombucha mats. A pair of iridium-coated stainless-steel subdermal needle electrodes was inserted into the mats for the performance of measurements. (A), (C) Impedance, capacitance, resistance, and $I-V$ measurements taken from functionalized Kombucha cellulose mat, 240 × 240 mm^2, under square and circular weights of 100, 200, 300, and 600 g. (B), (D) Impedance, capacitance, resistance, and $I-V$ measurements taken from functionalized Kombucha cellulose mat, 240 × 240 mm^2, under square and circular weights of 100, 200, 300, and 600 g.

iformity observed in the mat, which grows as multiple layers with strands suspended down. The inhomogeneity in growth may impact the experimental phenomena; however, these potential variations in the density, size, and porosity of the cellulose pellicles can enhance the distinct functions of the material, leading to tailored and controlled properties such as interactions with the functional nanomaterials (graphene and zeolite) and favorable mechanical properties. Microstructural characterization such as scanning electron microscopy and Fourier transformed infrared spectroscopy analysis as well as further analysis of the mat's properties via tensile tests and water vapor permeability could offer valuable information on correlations between inhomogeneity in growth, composition, and variations in the structure.[51] The thickness of the mats was 3.3 and 4.2 mm and was measured with an electronic digital caliper (accuracy ±0.2 mm, Vodlbov, China). The pH was

https://doi.org/10.1021/acsomega.4c01227
ACS Omega XXXX, XXX, XXX−XXX

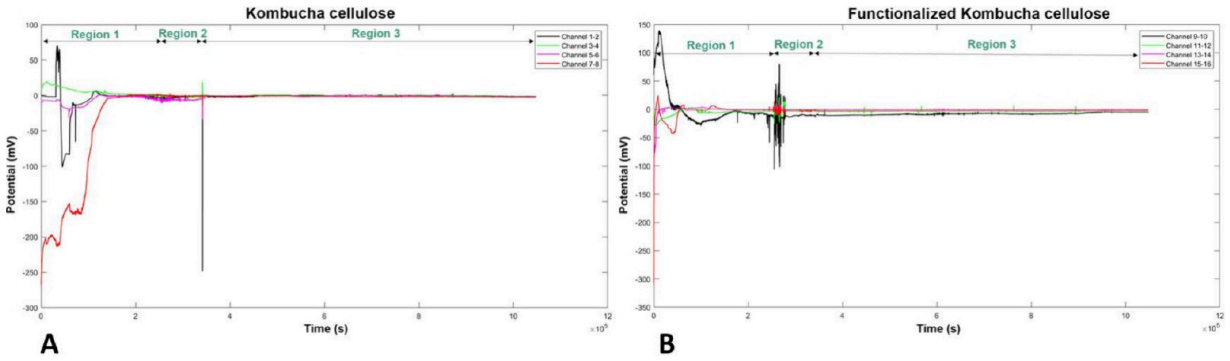


Figure 3. Spiking activity of 240 × 240 mm^2 samples when exposed to different loads. The graphs display the electrical activity over time, measured in potential (mV) versus time (sec), from both Kombucha (Ch1−Ch4) and Kombucha with graphene-zeolite Y cellulose mats (Ch5−Ch8). In (A), Region 1 shows the application of a 100 g box load, Region 2 represents the application of a 400 g box load, and Region 3 represents the application of a 300 g cylinder load. In (B), Region 1 represents the application of a 100 g cylinder load, Region 2 represents the application of a 400 g cylinder load, and Region 3 represents the application of a 300 g box load.

monitored starting from 6.49 and reducing to 3.02 using a digital pH meter (accuracy ±0.1% ± 2 digits, VWR pH110, Belgium).

One cellulose mat sample (thickness 3.3 mm) was functionalized with graphene and zeolite. For the functionalization, 5.372 g of graphene powder (HCG10000-P-1, Graphitene Energy Storage Series, https://www.graphitene.com) were mixed with 1.289 g of Zeolite Y powder (ThermoFisher Scientific UK, 045862.36). The thickness of graphene powder was 1−3 layers with a lateral size 0.5−5 μm, a surface area of 500 m^2/g, and an electrical conductivity >104 S/m. The surface area of zeolite Y was 927 m^2/g. To achieve good interfacial bonding between the graphene and zeolite molecules, we used PTFE solvent (Sigma-Aldrich, 665880), and the mixture was stirred until a homogeneous solution was achieved (the total mixture weight was 12.965 g). The graphene-zeolite Y mixture was deposited on the surface of the Kombucha cellulose film using a razor blade and dispersed homogeneously until it was fully coated. After coating the top surface, the film was folded in such a manner that the mixture remained enclosed within the film. For the in situ fabrication of the Kombucha-graphene-zeolite hybrid living material, the method of microbial fermentation was used and therefore, the functionalized film was placed back again into the Petri dish to allow further growth. After 14 days, a new cellulose mat was formed, fully encapsulating the functionalized cellulose mat (Figure 1). The size of the two samples was 240 × 240 mm^2.

Experimental Setup and Characterization. The unmodified and functionalized Kombucha cellulose mats were placed on top of a cardboard box with dimensions of $W \times L$ = 122 × 160 mm^2 and secured in place with plastic and metallic clamps prior to performing any measurements. To assess the response and mechanical properties of the samples when exposed to compression, we used a load application. For the mechanical stimulation of the samples, manually cut square aluminum weights of 100 g ($W \times L \times H$ = 51 ×51 × 14.2 mm^3), 200 g ($W \times L \times H$ = 51 × 51 × 28.4 mm^3), and 300 g ($W \times L \times H$ = 51 × 51 × 42.7 mm^3) and circular aluminum weights of 100 g ($D \times H$ = 51 × 18.1 mm^2), 200 g ($D \times H$ = 51 × 36 mm^2), and 300 g ($D \times H$= 51 × 54.4 mm^2) were employed. The weights were applied to both samples in different combinations to attain loads of 100, 200, 300, 400, and 600 g (Figure 2). Both patterns of weights (square and circular) were applied to the two cellulose samples.

Electrical characterization of the unmodified and functionalized mats prior to and during the application of 100, 200, 300, and 600 g loads was performed. A pair of iridium-coated stainless-steel subdermal needle electrodes (Spes Medica S.r.l., Italy), with twisted cables, was pierced through the mats with a distance between the electrodes of 50−60 mm. A Keithley 2450 SourceMeter was used for the provision of high-precision current−voltage ($I-V$) sweep measurements (type linear dual, voltage range from −1 to 1 V, step 10 mV, count finite 20, source limit 1A). Impedance, capacitance, and resistance measurements were taken using a BK Precision LCR Meter (model 891) within the frequency range of 20 Hz and 300 kHz. The experiments were repeated to ensure error elimination.

For the recordings of the electrical activity before and after the weight application, an ADC-24 (Pico Technology, UK) high-resolution data logger with a 24bit A/D converter was used. Weights of square and circular patterns of 100, 300, and 400 g were applied to the samples. Eight pairs of iridium-coated stainless-steel subdermal needle electrodes were inserted in the samples; the first 4 (channels 1−2, 3−4, 5−6, and 7−8) in the unmodified cellulose sample and the remaining 4 (channels 9−10, 11−12, 13−14, and 15−16) in the functionalized sample (Figure 3). We recorded electrical activity simultaneously, one sample per second, and each pair of electrodes reported a difference in the electrical potential between the electrodes. All readings were taken at a room temperature of 19 °C. During the recording, the logger undertook as many measurements as possible (typically up to 600 per second) and saved the average value. The distance between the electrodes was 10−20 mm.

The microstructure of the unmodified and functionalized Kombucha cellulose samples was analyzed by scanning electron microscopy and environmental scanning electron microscopy (FEI Quanta 650). For the preparation prior to imaging, the samples were air-dried and coated with a gold layer using an Emscope SC500 gold sputter coating unit. Images were acquired with a magnification range of 1300−20000× and a high voltage of 2 kV. To the best of our knowledge, this is the first time that Kombucha cellulose has been functionalized to evaluate its electrical properties and response to load application.

https://doi.org/10.1021/acsomega.4c01227
ACS Omega XXXX, XXX, XXX−XXX

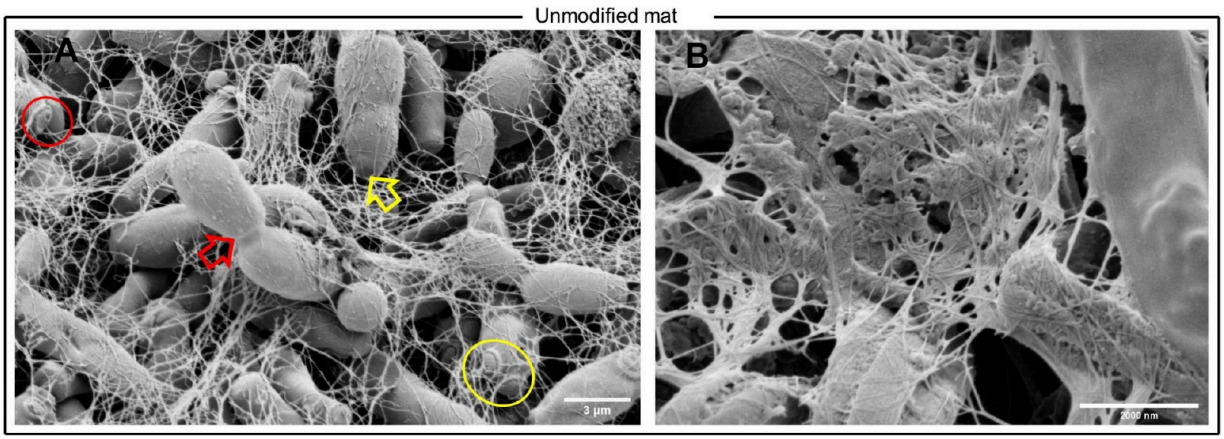


Figure 4. SEM images of the pure Kombucha mat. A) The presence of multiple-size yeast cells is identified, with lengths ranging from 1.93 to 7.76 μm. Cell bud scars, birth scars, multipolar budding, and bud−parent sites are marked in the image with red circles, yellow and red arrows, and a yellow circle accordingly. Image magnification is 8000×. B) Network of cellulosic fibers with a branching structure. Image magnification is 20000×.

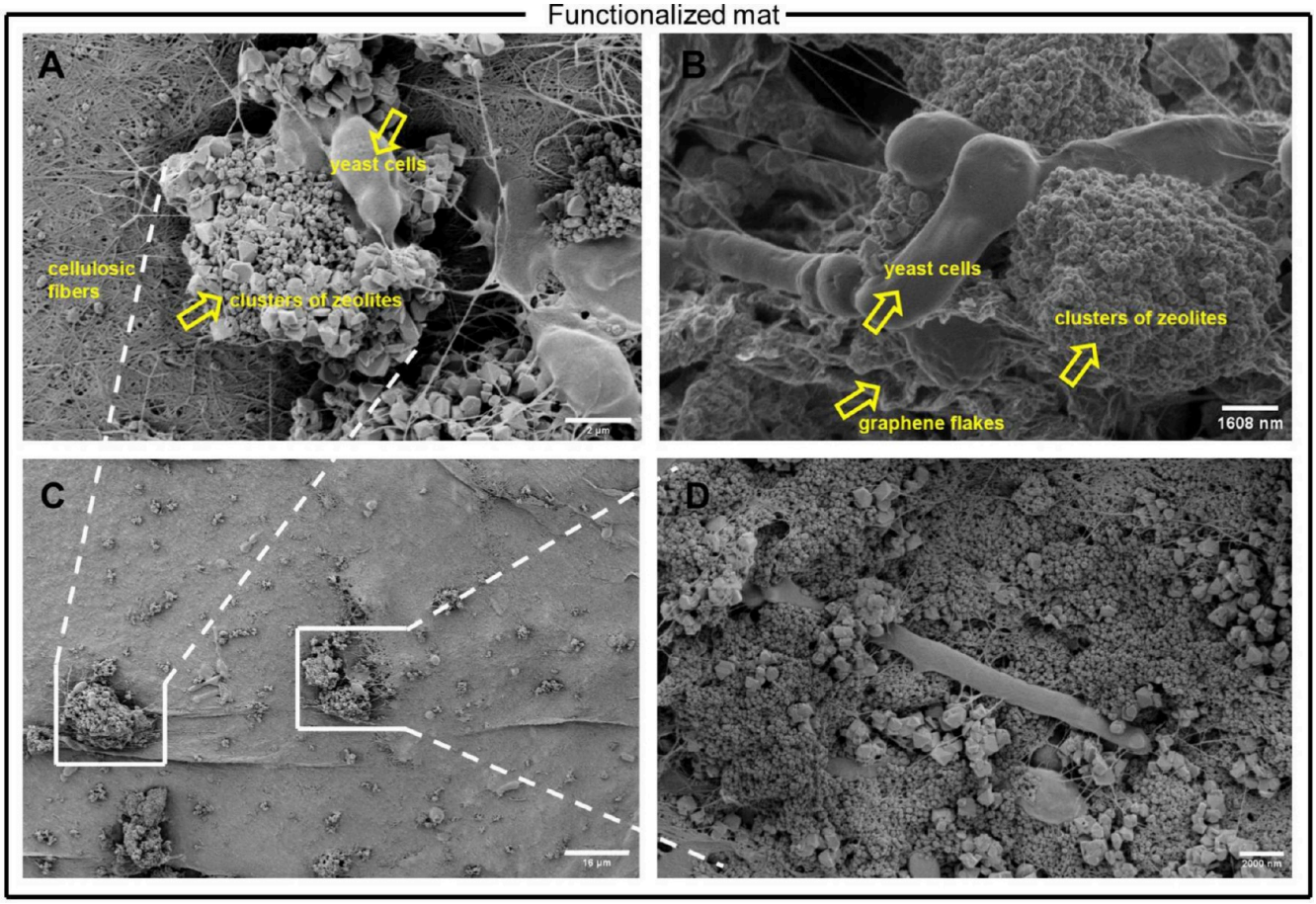


Figure 5. SEM images of functionalized Kombucha mat. A) Clusters of zeolite crystals entangled with microbes. Image magnification is 10000×. B) Graphene-zeolite assembly formations where graphene flakes attached to zeolite crystals and yeast cells are obsreved. Image magnification is 10000×. C) Lower magnification image showing distribution of nanoparticles. Image magnification is 1300×. D) Yeast cells integrated into zeolite-graphene nanoparticles. Image magnification is 7000×.

RESULTS

Morphological and Chemical Characterization. SEM imaging performed on pure and functionalized Kombucha-graphene-zeolite samples demonstrated that the structure of the pure Kombucha mat changes significantly with the integration of the graphene-zeolite particles. The morphological features of pure Kombucha reveal that the microbial community of yeast and bacterial cells present mostly ellipsoidal structures, are compactly and uniformly dispersed, and are entangled into a dense mesh of cellulosic fibers that form three-dimensional web-like structures. The presence of multiple-size yeast cells is observed, spanning from 1.93 to 7.76 μm in length. Chain yeast elongations are visible, and

https://doi.org/10.1021/acsomega.4c01227
ACS Omega XXXX, XXX, XXX−XXX

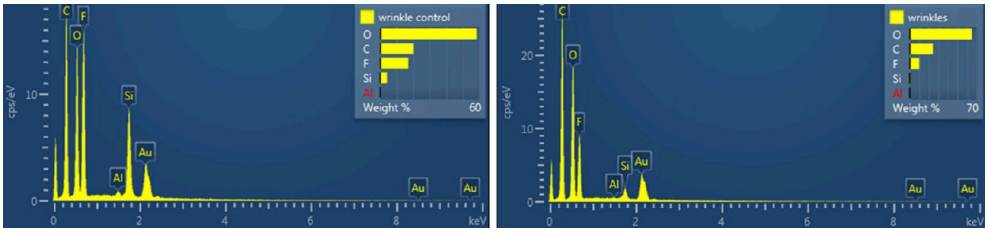


Figure 6. Energy-dispersive spectroscopy (EDS) graphs of two samples collected from different sites of the functionalized Kombucha mat, showing the distribution of elements. The graphs reveal the presence of silicon (Si), aluminum (Al), and carbon (C) peaks, indicating the integration of the zeolite and graphene nanoparticles within the Kombucha mat. Additionally, the presence of fluorine (F) is observed due to the use of PTFE solvent to achieve good interfacial bonding between the graphene and zeolite molecules. The gold (Au) peaks are attributed to the gold coating applied to the sample to increase its conductivity for improved scanning electron microscopy imaging. The peaks of elements in both EDS graphs follow a similar trend, indicating a homogeneous distribution of the graphene and zeolite nanoparticles in both samples and therefore, incorporation within the Kombucha matrix.

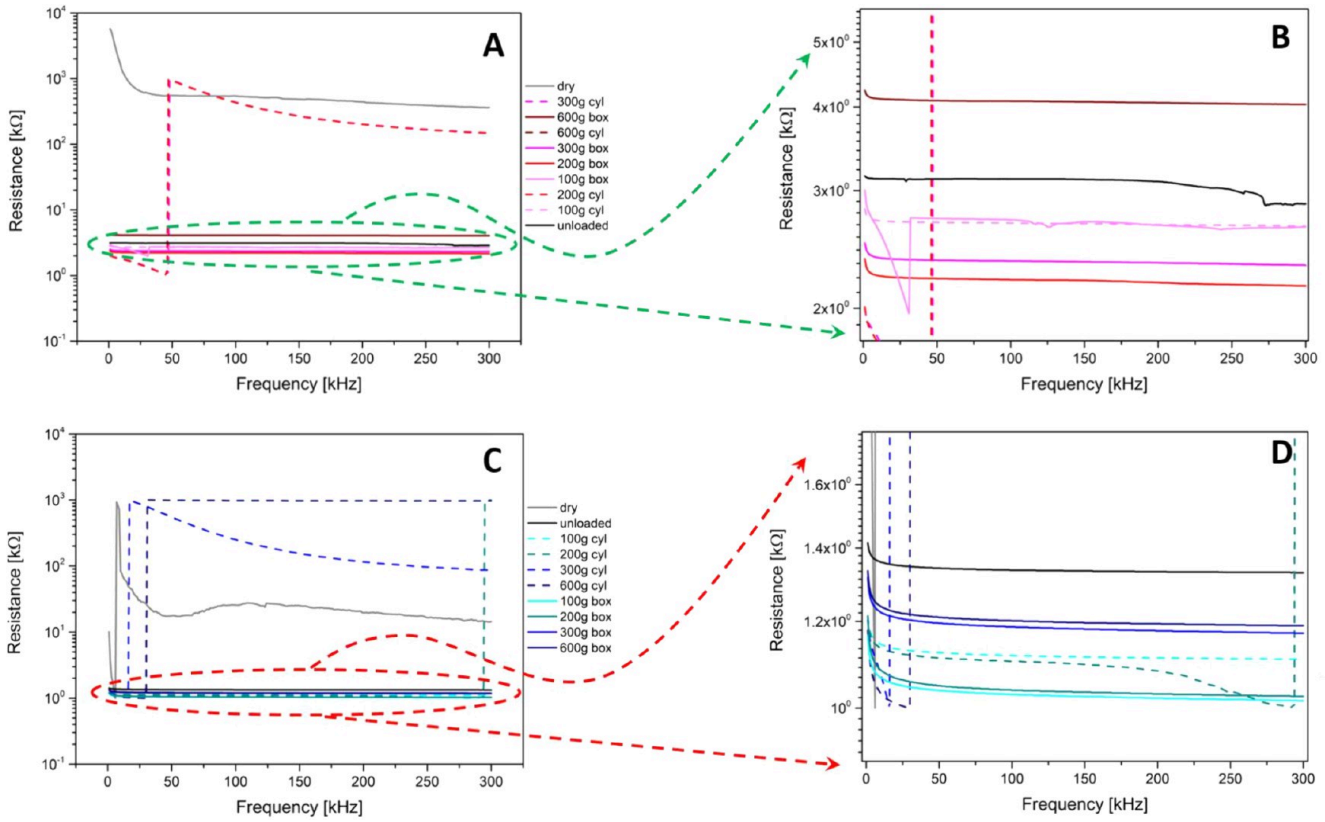


Figure 7. Series resistance as a function of the frequency. (A) Kombucha response to the different loads and (B) inset showing a zoomed-in view of the circled area. (C) The functionalized Kombucha response to the different loads and (D) inset showing a zoom of the circled area.

protrusions on the cell surfaces show cell budding mechanisms.[52] Figure 4 shows bud and birth scars as well as bud–parent junctions (marked with red circles and yellow and red arrows accordingly). Multipolar budding is also clearly identified on some cells (marked with a yellow circle).

Images of the functionalized sample revealed dense aggregations of zeolite crystals with morphologies of spherical agglomerates of tiny crystals next to larger polyhedrons surrounded by typical flakes of graphene particles[53] and integrated with scattered Kombucha microbes. The presented high-density configurations may be attributed to the high microporosity of the zeolite active sites, which provides space for the adsorption and exchange of cations, leading to the attachment of the graphene molecules. This connection could favor electron transport and contribute to the electrochemical performance of the functionalized Kombucha film. In addition to this, the cellulose fiber network appears to be less dense and finer, where the graphene-zeolite formations are present. The measured cluster assemblies have diameters of 9.61 and 7.75 μm (see Figure 5). Contrary to pure Kombucha images, microbial cells appear in lower densities in the functionalized Kombucha images, but elongations and birth scars are still present, suggesting that growth and replication mechanisms continue to take place after functionalization. The above findings indicate that the new structural formations may involve the microscopic movement of the microbial population due to the mechanical and physical forces built up from the graphene-zeolite encapsulation during in situ functionalization. Moreover, it is observed that the graphene-zeolite particles are found entangled with and attached to the microbial cells and in

https://doi.org/10.1021/acsomega.4c01227
ACS Omega XXXX, XXX, XXX−XXX

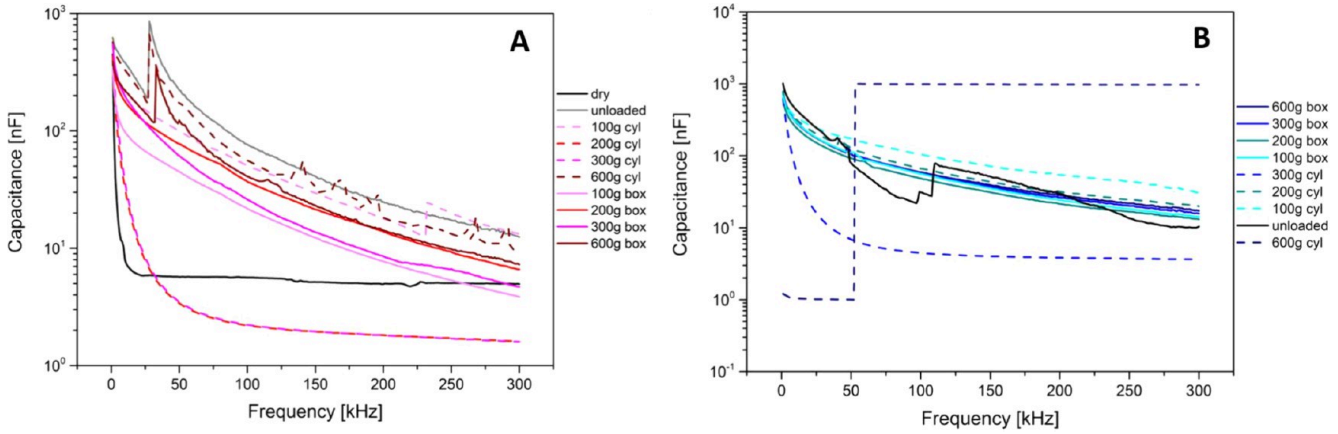


Figure 8. Capacitance as a function of the frequency. (A) Kombucha response to the different loads and (B) functionalized Kombucha response to the different loads.

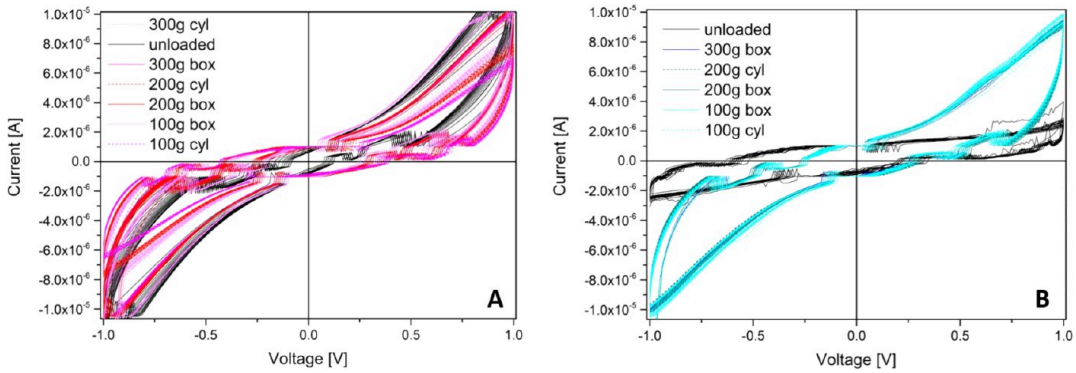


Figure 9. Hysteresis cycles showing the IV response of the mats. (A) Kombucha response to the different loads and (B) functionalized Kombucha response to the different loads.

parts enveloped by the cells, suggesting the integration of the living biological and synthetic components, therefore indicating the possible synthetic morphogenesis of a new and higher ordered structure. This may open up remarkable opportunities for the in situ development of functionalized hybrid materials that can self-assemble, self-replicate, self-generate, and self-grow after the fusion of their living and synthetic components.

Energy-dispersive spectroscopy (EDS) shows the distribution of elements within the functionalized Kombucha film (Figure 6). In the material distribution analysis, very low Al content is observed, demonstrating high hydrothermal stability.[54]

Direct Current and Impedance Properties. Measurements were carried out in the frequency range between 1 and 300 kHz. Series resistance as a function of the frequency is shown in Figure 7. The upper row shows the Kombucha mat in different conditions (dry, wet, and unloaded, and with cylinder and box loads from 100 to 600 g), while the bottom row shows functionalized mats. The dry condition is such that the functionalized mat features a resistance 1 order of magnitude lower than the pristine Kombucha mat due to the enhancement provided by graphene addition. The consecutive loading of the mat produces a reduction of the resistance that achieves a maximum with the intermediate loading of 200 g and then recovers back and eventually becomes even higher than the unloaded measure for the loading of 600 g. This effect might be due to pseudoelastic stretching of the matrix under the normal forces exerted by the loads with concurrent reduction of the section available for conduction. A remarkably similar trend might be found in the functionalized Kombucha mat, where the 100 and 200 g loads reduce the resistance and the 300 and 600 g loads increase it, to values lower than the unloaded case. Regarding the shape of the load, we note that the cylinder weight can produce very pronounced responses, particularly in the load range of 200−300 g for both mats. In Figure 7 we see that under some conditions the pristine Kombucha undergoes a transition and around 50 Hz its resistance increases by 3 orders of magnitude, featuring a response that is pretty similar to that of the dry mat. This happens for the 200 and 300 g cylinders, during a more severe deformation due to the smaller contact area in comparison to the box loads, which are more likely able to expel the extracellular fluids and produce a less conductive state. Similarly, the functionalized Kombucha mat shows a sudden jump in the resistance by 3 orders of magnitude during the application of 300 and 600 g cylinders, producing a response that is even less conductive than the dry mat, probably because of the zeolite dielectric contribution to resistance.

In Figure 8, the capacitance is shown in the same frequency range as that discussed above. The unloaded curve of the pristine mat versus the functionalized one shows that normally, the capacitance of the latter is approximately double that of the former, which can be due to the addition of zeolite compounds having a higher dielectric constant. Nevertheless, we should remember how much water content in a mat can influence this aspect, as the dielectric constant of water is very high: The dry

https://doi.org/10.1021/acsomega.4c01227
ACS Omega XXXX, XXX, XXX−XXX

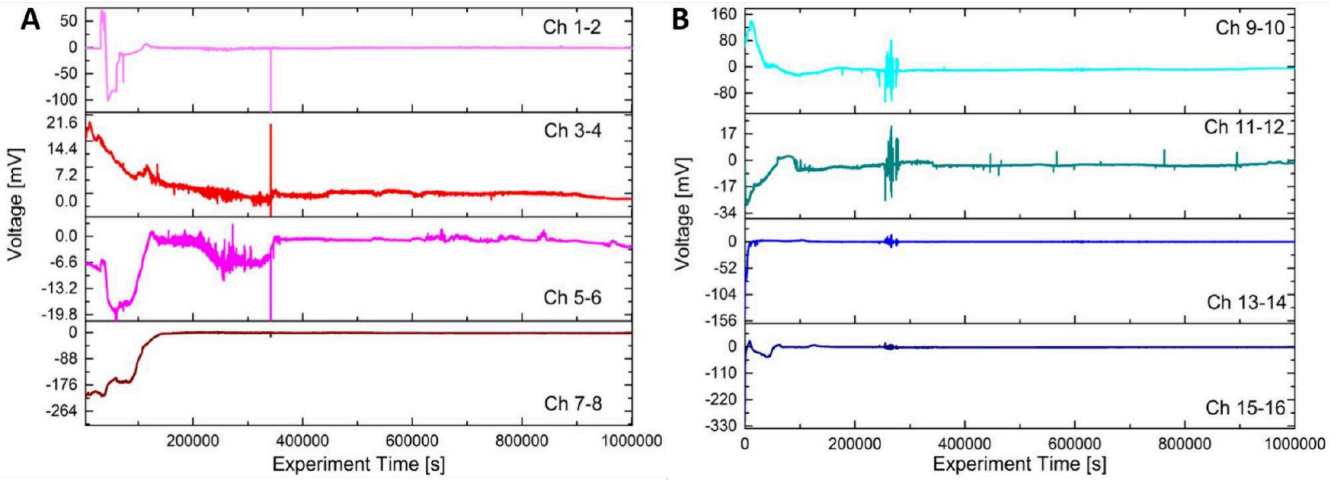


Figure 10. Recordings showing the spiking response of the mats. (A) Kombucha response to the different loads and (B) functionalized Kombucha response to the different loads.

mat curve shows how small its capacitance can be in the absence of water. Looking at the pristine mat curves, we cannot infer any specific pattern: the measurements cannot correlate with the load amount and/or its shape. On the contrary, the functionalized mat curves feature a more controlled behavior that perfectly maps the observations based on the resistance previously discussed: the deformation produced by 100 and 200 g loads reduces the capacitance, as the displacement of the hydrogel under the force exerted by the load reduces the surface of the dielectric layer incorporated in the capacitor. Other phenomena might occur, such as the capacitive coupling with the load materials (i.e., aluminum and polymers), making it difficult to infer the shape of the load from the measurements. In Figure 8 we can notice some sudden jumps of the capacitance, particularly the pristine Kombucha in dry conditions and after application of 600 g loads (both cylinder and box): Eventually squeezing out of the hydrogel more water by means of the highest loads produces a response that follows that of a dry material.

Another important analysis performed is the collection of $I-V$ curves along multiple hysteresis cycles to put in evidence typical current ranges and eventually a memristive behavior. Figure 9 shows that in the 1 V range, the currents are on the order of 10 μV for both the pristine and functionalized mats, but in the former case, all curves are very close, and the loading does not provide any strong variation. However, in the latter we can see how much the loaded curves differ from the unloaded one, having currents 5 times bigger. Therefore, loading the functionalized mat produces higher currents (lower resistances), while loading the pristine mat produces lower currents (higher resistances). An enhanced conductivity can explain this effect due to the percolation of the fillers added to the functionalized mat. The higher pressure creates more contact points between inorganic conductive fillers, such as the graphene flakes, and reduces the mat resistance.

Spiking Activity and Higher Order Complexity Analyses. The spontaneous spiking activity of two mats was continuously recorded while loads were being applied. The recorded profiles from four differential channels are shown in Figure 10 for the entire measurement period of 11 days. By examining each channel, we can observe a certain degree of correlation involving transitions and increased spiking activity with remarkably similar characteristics. Typically, the spontaneous activity range is around 20 mV. However, some channels exhibit a large baseline fluctuation of about 175 mV (for example, channels 1−2 and 5−6 of the pristine mat) and approximately 200 mV (for example, channels 9−10 of the functionalized mat). To gain a clearer understanding of what is happening in various situations, we used the fast Fourier transform (FFT) and higher order complexity (HOC) metrics[55−57] as shown in Figure 11.

The FFT analysis shows how the noise spectrum across the mat sensors is distributed over different frequencies, ranging from approximately 1 mHz up to 0.5 Hz, corresponding to half of the sampling frequency. The first row of graphs depicts data from "Region 1" when a 100 g load was positioned on the mats. The red lines (differential electrode couples 1−2, 3−4, 5−6, and 7−8) represent the pristine Kombucha, while the blue lines (differential electrode couples 9−10, 11−12, 13−14, and 15−16) represent the functionalized Kombucha. A fundamental oscillation mode occurs across all channels at 1 mHz, with visible superior harmonics at 2, 3, and 4 mHz. It is unclear whether the source of this ultralow frequency mode is an external noise disturbance or part of the mat's electrical oscillations. Notably, there is a broad peak spanning 0.1−0.2 Hz, a genuine signal component from the functionalized mat not observable in the pristine mat data. The complexity measures display consistent behavior where the curves either show a lower plateau for the first 500 min followed by recovery to higher levels for the remaining 4000 min (SE, TE, RE, SF, KE, LZC, and DI, where SE stands for Shannon entropy, TE represents Tsallis entropy, RE stands for Rényi entropy, SF represents space filling, KE represents Kolmogorov complexity, LZC represents Lempel−Ziv complexity, and DI represents diversity index) or an initial higher plateau followed by decay to lower values (SI, PCI, and FD, where SI represents Simpson index, PCI represents permuted complexity index, and FD represents fractal dimension). This demonstrates that implementing proper HOC measures makes it feasible to interpret the mat's spontaneous oscillations as a sensor response with long time scales.

Examining data from "Region 2", where a 200 g load was applied for 300 min, the shorter duration limits comparability to the complexity trends in Region 1. However, noteworthy FFT responses occur, including cleaner oscillation profiles and specific modes at 4.6, 7.3, 11.6, and 14.6 mHz visible on the

https://doi.org/10.1021/acsomega.4c01227
ACS Omega XXXX, XXX, XXX−XXX

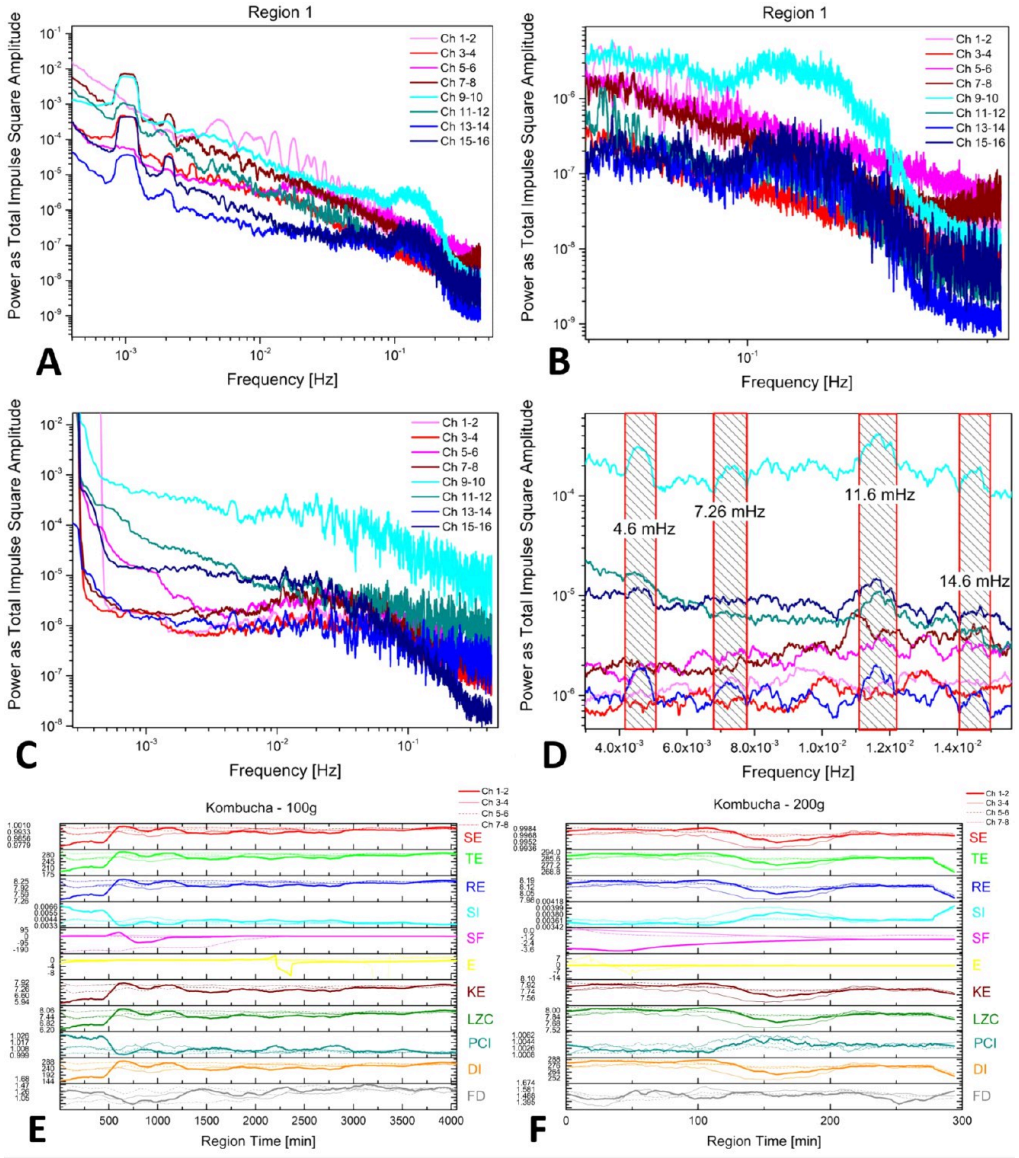


Figure 11. Regional details of the spiking activity features. (A) The fast Fourier transforms correspond to 100 g loading of the Kombucha mat and functionalized Kombucha mat. (B) A zoomed-in view highlights a broad peak structure. (C) The fast Fourier transforms for the region corresponding to 200 g loading of the Kombucha mat and functionalized Kombucha have been shown. (D) A zoomed-in view highlights a broad peak structure. (E) Higher-order complexity measures for the same region have been provided, pristine mat. SE stands for Shannon entropy, TE represents Tsallis entropy, RE stands for Rényi entropy, SI represents Simpson index, SF represents space filling, E represents expressiveness, KE represents Kolmogorov complexity, LZC represents Lempel−Ziv complexity, PCI represents permuted complexity index, DI represents diversity index, and FD represents fractal dimension. (F) Higher-order complexity measures for the same region, pristine mat, have been provided.

pristine mat. Similar modes at slightly shifted frequencies also emerge on the functionalized mat, generally skewed toward faster processes, potentially indicative of increased conductivity.

Further analysis using short time Fourier transforms (STFT) generates spectrograms with color-coded intensity fluctuations over time and frequency, depicted in Figure 12. When a specific spectral component (vertical axis, frequencies from direct current up to 500 mHz) carries a higher energy, its fingerprint appears with a color different from violet (stretching into blue, then green, yellow and red for the most energetic harmonics). The horizontal axis is associated with time and shows the evolution of the spectrum during long measurements. The top row shows the STFT for a functionalized mat differential couple (Region 1). A specific 5 h period exhibits multiple harmonics and a complex structure circled with a dashed ellipse and magnified in panel B, resembling a vocal signal with fundamentals around 30 mHz and harmonics approaching 200 mHz. Such a complex structure is composed by quasi-parallel bands; seven of them can be easily counted, starting from the strongest (fundamental at 30 mHz, red band) and extending up to the highest harmonic (200 mHz, cyan band that is 4 times less strong than the fundamental). Interestingly, a comparable 1 h fragment occurs in Region 2 data from the pristine mat with fundamentals around 30 mHz and a still visible fifth harmonic near 150 mHz, and this time the strength drop is much less pronounced (20% less). We might say that, by analogy, the electric melody provoked by spontaneous oscillations in pristine Kombucha carries a compact sound including both lower and higher frequencies,

https://doi.org/10.1021/acsomega.4c01227
ACS Omega XXXX, XXX, XXX−XXX

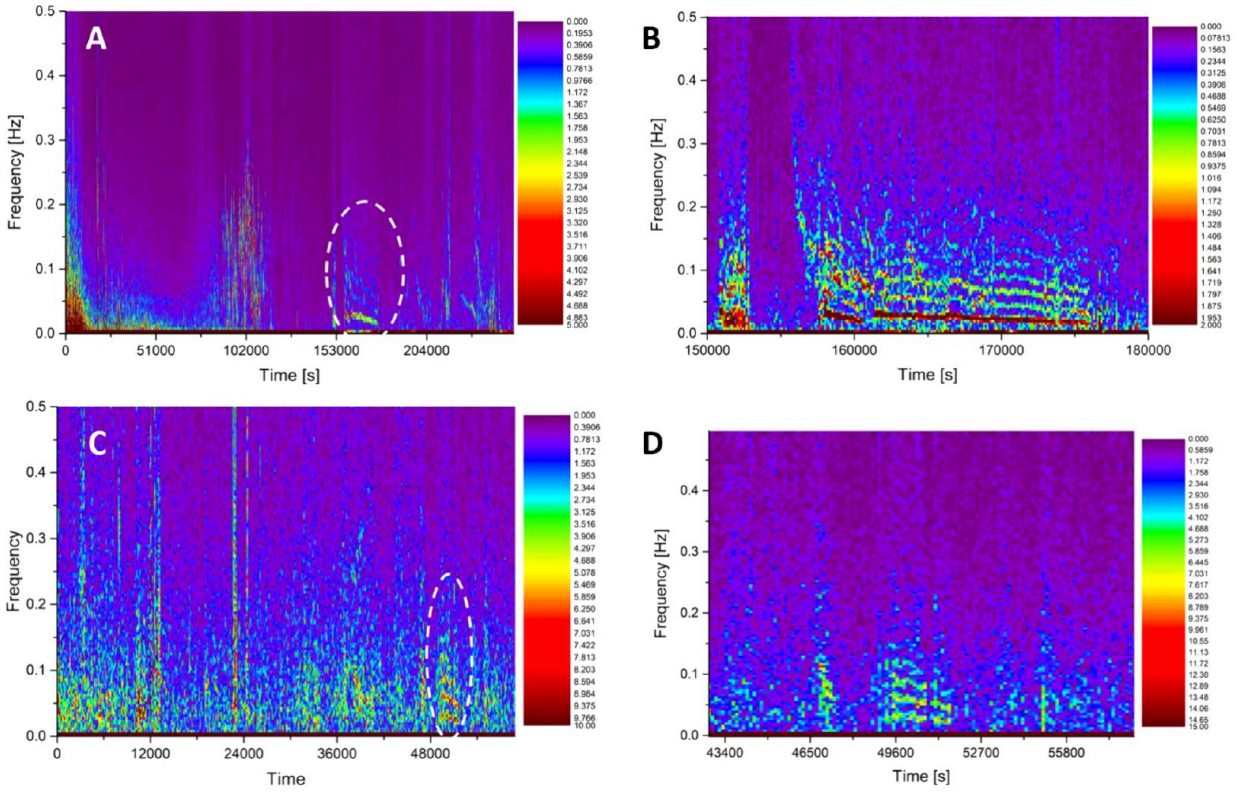


Figure 12. Regional details of the spiking activity features. (A) Short-time fast Fourier transforms on the region corresponding to 100 g loading of the differential channels 13−14 of the functionalized Kombucha mat. (B) A zoomed-in view highlights a peculiar feature, as indicated by the ellipse. (C) Short-time fast Fourier transforms on the region corresponding to 100 g loading of the differential channels 7−8 of the pristine Kombucha mat. (D) A zoomed-in view highlights a peculiar feature, as indicated by the ellipse.

while the one recorded in functionalized Kombucha carries a sound with a much lower timbre. Audio files were generated by the sonification of these recordings along with another excerpt from Region 3 using Melobytes software (Gardos Software Ltd. https://melobytes.com) and are provided as Supporting Information.

DISCUSSION

Kombucha mats are unique symbiotic systems where over 60 species of yeasts and bacteria cooperate. Pure Kombucha mats exhibit spiking activity due to the waves of depolarization traveling in the mats, emerging from metabolically triggered release of potassium.[58] Potassium has a role in biofilm formation,[59,60] and its release can generate changes in potential.[61] Action potential electrical signaling is mediated by ion channels,[62] and it is possible that the bacteria within the cellulosic matrix use potassium ion-channel-mediated electrical signals to coordinate metabolism.[61] Moreover, the yeast community identified in the Kombucha mats has demonstrated glicolytic oscillations which are reflected in oscillations of their resistance and capacitance,[63] possibly leading to electrical potential difference generated during the glycolysis process.[64] Although pure Kombucha mats exhibit spiking dynamics, their electrical conductivity is limited. To improve the electrical characteristics, graphene and zeolite nanoparticles were integrated into the cellulose network. The arrangement of the material's components, their interactions, and metabolic activity provide a unique fingerprint of electrical features and spiking activity. Two key findings are memfractive behavior and distinctive electrical spiking in response to mechanical loading. Memfractive materials combine properties of memristors, memcapacitors, and meminductors.[65] As a memristive material implied by its material nature,[66−69] Kombucha mats could enable various logic circuits,[70] stateful logic operations,[71] memory-aided logic circuits,[72] logic operations within passive crossbar arrays of memristors,[73] memory-aided logic circuits,[72] self-programmable logic circuits,[74] and memory devices.[75] Their memfractive nature also makes the mats suitable for integration into diverse memory and computing devices, including biocompatible electronics and biowearables.

CONCLUSION

In this study, we have demonstrated that Kombucha zoogleal mats, functionalized with graphene and zeolite particles, exhibit unique electrical properties. The observed electrical spiking from mechanical stimulation (i.e., applying loads) could be harnessed to create biocompatible sensors. Incorporating the mats into wearable devices or implantable sensors may facilitate the real-time detection of physiological changes in the human body or other biological systems with potential applications in real-time health monitoring. The electrical spiking could also be explored for energy harvesting purposes. If the spiking can be converted into a usable form of energy, then it might contribute to powering small electronic devices or sensors in remote or hard-to-reach locations. Combining Kombucha zoogleal mats with functional nanoparticles could lead to hybrid systems that leverage the strengths of both biological and synthetic elements.

This work demonstrates the early stage potential for hybrid systems combining Kombucha zoogleal mats with functional

https://doi.org/10.1021/acsomega.4c01227
ACS Omega XXXX, XXX, XXX−XXX

nanoparticles to leverage both biological and synthetic elements. This interdisciplinary approach could open up new possibilities in sustainable electronics and computing applications that are impossible with either system alone. Specifically, the biodegradable nature of Kombucha materials makes them well-suited for environmentally friendly devices and components aimed at reducing e-waste. Devices or components that naturally decompose after use could reduce electronic waste and positively impact sustainability.

■ ASSOCIATED CONTENT

Data Availability Statement

The data is accessible via the online database Zenodo and can be accessed at https://doi.org/10.5281/zenodo.10445665.

Supporting Information

The Supporting Information is available free of charge at https://pubs.acs.org/doi/10.1021/acsomega.4c01227.

Sonification of spectra from Region 2, channels 7−8, 13−14, and 15−16, respectively (MP3, MP3, and MP3)

■ AUTHOR INFORMATION

Corresponding Authors

Andrew Adamatzky − *Unconventional Computing Laboratory, University of the West of England, Bristol BS16 1QY, United Kingdom*; Email: andrew.adamatzky@uwe.ac.uk

Anna Nikolaidou − *Unconventional Computing Laboratory and Department of Architecture and Environment, University of the West of England, Bristol BS16 1QY, United Kingdom*; orcid.org/0000-0002-2787-8986; Email: anna.nikolaidou@uwe.ac.uk

Authors

Alessandro Chiolerio − *Bioinspired Soft Robotics, Istituto Italiano di Tecnologia, 16163 Genova, Italy*; orcid.org/0000-0001-9328-2999

Mohammad Mahdi Dehshibi − *Escuela Politécnica Superior, Departamento de Informática, Universidad Carlos III de Madrid, Leganés 28911, Spain*; orcid.org/0000-0001-8112-5419

Complete contact information is available at: https://pubs.acs.org/10.1021/acsomega.4c01227

Funding

This research did not receive any specific grant from funding agencies in the public, commercial, or not-for-profit sectors.

Notes

The authors declare no competing financial interest.

■ ACKNOWLEDGMENTS

The authors are grateful to David Patton for assisting with SEM imaging and Dr. Jun Yao for her advice on graphene and zeolites. The Supporting Information audio files were generated by the sonification of short time Fourier transform data to build a unique procedurally generated melody, using AI-powered Melobytes software (Gardos Software Ltd., https://melobytes.com).

■ REFERENCES

(1) Iguchi, M.; Yamanaka, S.; Budhiono, A. Bacterial cellulose−a masterpiece of nature's arts. *J. Mater. Sci.* **2000**, *35*, 261−270.

(2) Abeer, M. M.; Mohd Amin, M. C. I.; Martin, C. A review of bacterial cellulose-based drug delivery systems: their biochemistry, current approaches and future prospects. *J. Pharm. Pharmacol.* **2014**, *66*, 1047−1061.

(3) Thomas, B.; Raj, M. C.; B, A. K.; H, R. M.; Joy, J.; Moores, A.; Drisko, G. L.; Sanchez, C. Nanocellulose, a versatile green platform: from biosources to materials and their applications. *Chem. Rev.* **2018**, *118*, 11575−11625.

(4) Ramirez Tapias, Y. A.; Di Monte, M. V.; Peltzer, M. A.; Salvay, A. G. Bacterial cellulose films production by kombucha symbiotic community cultured on different herbal infusions. *Food Chem.* **2022**, *372*, 131346.

(5) Yamada, Y.; Yukphan, P. Genera and species in acetic acid bacteria. *International journal of food microbiology* **2008**, *125*, 15−24.

(6) Singh, A.; Walker, K. T.; Ledesma-Amaro, R.; Ellis, T. Engineering bacterial cellulose by synthetic biology. *International Journal of Molecular Sciences* **2020**, *21*, 9185.

(7) Cottet, C.; Ramirez-Tapias, Y. A.; Delgado, J. F.; de la Osa, O.; Salvay, A. G.; Peltzer, M. A. Biobased materials from microbial biomass and its derivatives. *Materials* **2020**, *13*, 1263.

(8) Laavanya, D.; Shirkole, S.; Balasubramanian, P. Current challenges, applications and future perspectives of SCOBY cellulose of kombucha fermentation. *Journal of Cleaner Production* **2021**, *295*, 126454.

(9) Chiolerio, A.; Adamatzky, A. Acetobacter biofilm: Electronic characterization and reactive transduction of pressure. *ACS Biomaterials Science & Engineering* **2021**, *7*, 1651−1662.

(10) Chiolerio, A.; Dehshibi, M. M.; Manfredi, D.; Adamatzky, A. Living wearables: Bacterial reactive glove. *Biosystems* **2022**, 104691.

(11) May, A.; Narayanan, S.; Alcock, J.; Varsani, A.; Maley, C.; Aktipis, A. Kombucha: a novel model system for cooperation and conflict in a complex multi-species microbial ecosystem. *PeerJ.* **2019**, *7*, e7565.

(12) Coelho, R. M. D.; de Almeida, A. L.; do Amaral, R. Q. G.; da Mota, R. N.; de Sousa, P. H. M. Kombucha. *Int. J. Gastronomy Food Sci.* **2020**, *22*, 100272.

(13) Delatorre, A. B.; Ribeiro, T. R. L.; Arcênio, N. M. C.; Mothé, G. P. B. Estudo sobre a adequação da normativa 41 para a produção e comercialização de Kombucha: estudo de caso em uma empresa de Macaé. *Congresso de Ensino Pesquisa e Extensão-CONEPE*; Instituto Federal Fluminense, 2020.

(14) Torgbo, S.; Sukyai, P. Bacterial cellulose-based scaffold materials for bone tissue engineering. *Applied Materials Today* **2018**, *11*, 34−49.

(15) Patra, S.; Singh, M.; Pareek, D.; Wasnik, K.; Gupta, P. S.; Paik, P. Advances in the Development of Biodegradable Polymeric Materials for Biomedical Applications. In *Encyclopedia of Materials: Plastics and Polymers*; Elsevier, 2022; pp 532.

(16) Adamatzky, A. Electrical potential spiking of kombucha zoogleal mats: A symbiotic community of bacteria and yeasts. *Bioelectricity* **2023**, *5*, 99−108.

(17) Adamatzky, A.; Tarabella, G.; Phillips, N.; Chiolerio, A.; D'Angelo, P.; Nikolaidou, A.; Sirakoulis, G. C. Kombucha electronics: electronic circuits on kombucha mats. *Sci. Rep.* **2023**, *13*, 9367.

(18) Bai, H.; Shi, G. Gas sensors based on conducting polymers. *Sensors* **2007**, *7*, 267−307.

(19) Adhikari, B.; Majumdar, S. Polymers in sensor applications. *Prog. Polym. Sci.* **2004**, *29*, 699−766.

(20) Ahuja, T.; Kumar, D.; et al. Recent progress in the development of nano-structured conducting polymers/nanocomposites for sensor applications. *Sens. Actuators, B* **2009**, *136*, 275−286.

(21) Papageorgiou, D. G.; Kinloch, I. A.; Young, R. J. Mechanical properties of graphene and graphene-based nanocomposites. *Prog. Mater. Sci.* **2017**, *90*, 75−127.

(22) Pattnaik, S.; Swain, K.; Lin, Z. Graphene and graphene-based nanocomposites: biomedical applications and biosafety. *J. Mater. Chem. B* **2016**, *4*, 7813−7831.

(23) Balandin, A. A.; Ghosh, S.; Bao, W.; Calizo, I.; Teweldebrhan, D.; Miao, F.; Lau, C. N. Superior thermal conductivity of single-layer graphene. *Nano Lett.* **2008**, *8*, 902−907.
(24) Novoselov, K. S.; Geim, A. K.; Morozov, S. V.; Jiang, D.; Katsnelson, M. I.; Grigorieva, I. V.; Dubonos, S. V.; Firsov, A. A. Two-dimensional gas of massless Dirac fermions in graphene. *Nature* **2005**, *438*, 197−200.
(25) Lee, C.; Wei, X.; Kysar, J. W.; Hone, J. Measurement of the elastic properties and intrinsic strength of monolayer graphene. *science* **2008**, *321*, 385−388.
(26) Zhu, Y.; Murali, S.; Cai, W.; Li, X.; Suk, J. W.; Potts, J. R.; Ruoff, R. S. Graphene and graphene oxide: synthesis, properties, and applications. *Advanced materials* **2010**, *22*, 3906−3924.
(27) Feng, Y.; Zhang, X.; Shen, Y.; Yoshino, K.; Feng, W. A mechanically strong, flexible and conductive film based on bacterial cellulose/graphene nanocomposite. *Carbohydr. Polym.* **2012**, *87*, 644−649.
(28) Guo, Z.; Ren, P.; Dai, Z.; Zong, Z.; Zhang, F.; Jin, Y.; Ren, F. Construction of interconnected and oriented graphene nanosheets networks in cellulose aerogel film for high-efficiency electromagnetic interference shielding. *Cellulose* **2021**, *28*, 3135−3148.
(29) Xing, J.; Tao, P.; Wu, Z.; Xing, C.; Liao, X.; Nie, S. Nanocellulose-graphene composites: a promising nanomaterial for flexible supercapacitors. *Carbohydr. Polym.* **2019**, *207*, 447−459.
(30) Bao, L.; Li, X. Towards textile energy storage from cotton T-shirts. *Advanced materials* **2012**, *24*, 3246−3252.
(31) Gao, K.; Shao, Z.; Li, J.; Wang, X.; Peng, X.; Wang, W.; Wang, F. Cellulose nanofiber-graphene all solid-state flexible supercapacitors. *Journal of Materials Chemistry A* **2013**, *1*, 63−67.
(32) Xie, X.; Yu, G.; Liu, N.; Bao, Z.; Criddle, C. S.; Cui, Y. Graphene−sponges as high-performance low-cost anodes for microbial fuel cells. *Energy Environ. Sci.* **2012**, *5*, 6862−6866.
(33) Nyholm, L.; Nyström, G.; Mihranyan, A.; Strømme, M. Toward flexible polymer and paper-based energy storage devices. *Adv. Mater.* **2011**, *23*, 3751−3769.
(34) Auerbach, S. M.; Carrado, K. A.; Dutta, P. K. *Handbook of Zeolite Science and Technology*; CRC Press, 2003.
(35) Auerbach, S. M.; Carrado, K. A.; Dutta, P. K. *Handbook of Layered Materials*; CRC Press, 2004.
(36) Cejka, J.; van Bekkum, H.; Corma, A.; Schueth, F. *Introduction to Zeolite Molecular Sieves*; Elsevier, 2007.
(37) Mintova, S.; Gilson, J.-P.; Valtchev, V. Advances in nanosized zeolites. *Nanoscale* **2013**, *5*, 6693−6703.
(38) Cejka, J.; Corma, A.; Zones, S. *Zeolites and Catalysis: Synthesis, Reactions and Applications*; John Wiley & Sons, 2010.
(39) Kulprathipanja, S. *Zeolites in Industrial Separation and Catalysis*; John Wiley & Sons, 2010.
(40) Soldatkina, O.; Kucherenko, I.; Soldatkin, O.; Pyeshkova, V.; Dudchenko, O.; Akata Kurç, B.; Dzyadevych, S. Development of electrochemical biosensors with various types of zeolites. *Applied Nanoscience* **2019**, *9*, 737−747.
(41) Zheng, Y.; Li, X.; Dutta, P. K. Exploitation of unique properties of zeolites in the development of gas sensors. *Sensors* **2012**, *12*, 5170−5194.
(42) Kadja, G. T.; Rukmana, M. D.; Mukti, R. R.; Mahyuddin, M. H.; Saputro, A. G.; Wungu, T. D. Solvent-free, small organic lactam-assisted synthesis of ZSM-5 zeolites. *Mater. Lett.* **2021**, *290*, 129501.
(43) Maghfirah, A.; Ilmi, M.; Fajar, A.; Kadja, G. A review on the green synthesis of hierarchically porous zeolite. *Materials Today Chemistry* **2020**, *17*, 100348.
(44) Azhari, N. J.; Nurdini, N.; Mardiana, S.; Ilmi, T.; Fajar, A. T.; Makertihartha, I.; Kadja, G. T.; et al. Zeolite-based catalyst for direct conversion of CO2 to C2+ hydrocarbon: A review. *Journal of CO2 Utilization* **2022**, *59*, 101969.
(45) Kucherenko, I.; Soldatkin, O.; Dzyadevych, S.; Soldatkin, A. Application of zeolites and zeolitic imidazolate frameworks in the biosensor development. *Biomaterials Advances* **2022**, *143*, 213180.
(46) Chakravorty, S.; Bhattacharya, S.; Chatzinotas, A.; Chakraborty, W.; Bhattacharya, D.; Gachhui, R. Kombucha tea fermentation: Microbial and biochemical dynamics. *International journal of food microbiology* **2016**, *220*, 63−72.
(47) Azeredo, H. M.; Barud, H.; Farinas, C. S.; Vasconcellos, V. M.; Claro, A. M. Bacterial cellulose as a raw material for food and food packaging applications. *Front. Sustain. Food Syst.* **2019**, *3*, 7.
(48) Dima, S.-O.; Panaitescu, D.-M.; Orban, C.; Ghiurea, M.; Doncea, S.-M.; Fierascu, R. C.; Nistor, C. L.; Alexandrescu, E.; Nicolae, C.-A.; Trică, B.; et al. Bacterial nanocellulose from side-streams of kombucha beverages production: Preparation and physical-chemical properties. *Polymers* **2017**, *9*, 374.
(49) Joseph, C. L.; Kumar, G.; Su, E.; Bisson, L. F. Adhesion and biofilm production by wine isolates of Brettanomyces bruxellensis. *American journal of enology and viticulture* **2007**, *58*, 373−378.
(50) Balasubramanian, P.; Praharaj, P. T. Principal component analysis revealed the key influencing factors of kombucha bacterial cellulose yield and productivity. *Bioresource Technology Reports* **2023**, *23*, 101539.
(51) Ramírez Tapias, Y. A.; Peltzer, M. A.; Delgado, J. F.; Salvay, A. G. Kombucha tea by-product as source of novel materials: Formulation and characterization of films. *Food and Bioprocess Technology* **2020**, *13*, 1166−1180.
(52) Watson, K.; Arthur, H. Cell surface topography of Candida and Leucosporidium yeasts as revealed by scanning electron microscopy. *J. Bacteriol.* **1977**, *130*, 312−317.
(53) Khenfouch, M.; Buttner, U.; Baïtoul, M.; Maaza, M. Synthesis and characterization of mass produced high quality few layered graphene sheets via a chemical method. *Graphene* **2014**, *3*, 7−13.
(54) Yokoi, T. Characterization of zeolites by advanced SEM/STEM techniques. *SI News* **2016**, *7*, 17−23.
(55) Dehshibi, M. M.; Adamatzky, A. Complexity of Electrical Spiking of Fungi. In *Fungal Machines: Sensing and Computing with Fungi*; Springer Nature Switzerland, 2023; pp 33−60.
(56) Dehshibi, M. M.; Adamatzky, A. Electrical activity of fungi: Spikes detection and complexity analysis. *Biosystems* **2021**, *203*, 104373.
(57) Dehshibi, M. M.; Chiolerio, A.; Nikolaidou, A.; Mayne, R.; Gandia, A.; Ashtari-Majlan, M.; Adamatzky, A. Stimulating Fungi Pleurotus Ostreatus with Hydrocortisone. *ACS Biomaterials Science & Engineering* **2021**, *7*, 3718−3726.
(58) Adamatzky, A. Dynamics of electrical resistance of kombucha zoogleal mats. *Biophysical Reviews and Letters* **2022**, *17*, 135−144.
(59) López, D.; Fischbach, M. A.; Chu, F.; Losick, R.; Kolter, R. Structurally diverse natural products that cause potassium leakage trigger multicellularity in Bacillus subtilis. *Proc. Natl. Acad. Sci. U. S. A.* **2009**, *106*, 280−285.
(60) Kinsinger, R. F.; Kearns, D. B.; Hale, M.; Fall, R. Genetic requirements for potassium ion-dependent colony spreading in Bacillus subtilis. *Journal of bacteriology* **2005**, *187*, 8462−8469.
(61) Prindle, A.; Liu, J.; Asally, M.; Ly, S.; Garcia-Ojalvo, J.; Süel, G. M. Ion channels enable electrical communication in bacterial communities. *nature* **2015**, *527*, 59−63.
(62) Gerstner, W.; Kistler, W. M. *Spiking Neuron Models: Single Neurons, Populations, Plasticity*; Cambridge University Press, 2002.
(63) Male, T.; Feder, J.; Giaever, G. N.; Giaever, I. Oscillations in yeast observed electrically. *Biological rhythm research* **1999**, *30*, 361−370.
(64) Adamatzky, A. Electrical potential spiking of kombucha zoogleal mats. *bioRxiv (Biophysics)*, August 5, 2022, 2022.08.03.502684, DOI: 10.1101/2022.08.03.502684.
(65) Abdelouahab, M.-S.; Lozi, R.; Chua, L. Memfractance: a mathematical paradigm for circuit elements with memory. *International Journal of Bifurcation and Chaos* **2014**, *24*, 1430023.
(66) Kvatinsky, S.; Satat, G.; Wald, N.; Friedman, E. G.; Kolodny, A.; Weiser, U. C. Memristor-based material implication (IMPLY) logic: Design principles and methodologies. *IEEE Transactions on Very Large Scale Integration (VLSI) Systems* **2014**, *22*, 2054−2066.
(67) Chen, Q.; Wang, X.; Wan, H.; Yang, R. A logic circuit design for perfecting memristor-based material implication. *IEEE Trans-*

https://doi.org/10.1021/acsomega.4c01227
ACS Omega XXXX, XXX, XXX−XXX

actions on Computer-Aided Design of Integrated Circuits and Systems **2017**, *36*, 279−284.
(68) Chua, L. Memristor-the missing circuit element. *IEEE Transactions on circuit theory* **1971**, *18*, 507−519.
(69) Strukov, D. B.; Snider, G. S.; Stewart, D. R.; Williams, R. S. The missing memristor found. *Nature* **2008**, *453*, 80−83.
(70) Vourkas, I.; Sirakoulis, G. C. Emerging memristor-based logic circuit design approaches: A review. *IEEE circuits and systems magazine* **2016**, *16*, 15−30.
(71) Sun, X.; Li, G.; Ding, L.; Yang, N.; Zhang, W. Unipolar memristors enable "stateful" logic operations via material implication. *Appl. Phys. Lett.* **2011**, *99*, 072101.
(72) Kvatinsky, S.; Belousov, D.; Liman, S.; Satat, G.; Wald, N.; Friedman, E. G.; Kolodny, A.; Weiser, U. C. MAGIC−Memristor-aided logic. *IEEE Trans. Circuits Syst., II* **2014**, *61*, 895−899.
(73) Linn, E.; Rosezin, R.; Tappertzhofen, S.; Böttger, U.; Waser, R. Beyond von Neumann−logic operations in passive crossbar arrays alongside memory operations. *Nanotechnology* **2012**, *23*, 305205.
(74) Borghetti, J.; Li, Z.; Straznicky, J.; Li, X.; Ohlberg, D. A.; Wu, W.; Stewart, D. R.; Williams, R. S. A hybrid nanomemristor/transistor logic circuit capable of self-programming. *Proc. Natl. Acad. Sci. U. S. A.* **2009**, *106*, 1699−1703.
(75) He, C.; Zhuge, F.; Zhou, X.; Li, M.; Zhou, G.; Liu, Y.; Wang, J.; Chen, B.; Su, W.; Liu, Z. Nonvolatile resistive switching in graphene oxide thin films. *Appl. Phys. Lett.* **2009**, *95*, 232101.

https://doi.org/10.1021/acsomega.4c01227
ACS Omega XXXX, XXX, XXX−XXX

scientific reports

Check for updates

OPEN

Responsive fungal insoles for pressure detection

Anna Nikolaidou[1,2]✉, Neil Phillips[1], Michail-Antisthenis Tsompanas[1] & Andrew Adamatzky[1]

Mycelium bound composites are promising materials for a diverse range of applications including wearables and building elements. Their functionality surpasses some of the capabilities of traditionally passive materials, such as synthetic fibres, reconstituted cellulose fibres and natural fibres. Thereby, creating novel propositions including augmented functionality (sensory) and aesthetic (personal fashion). Biomaterials can offer multiple modal sensing capability such as mechanical loading (compressive and tensile) and moisture content. To assess the sensing potential of fungal insoles we undertook laboratory experiments on electrical response of bespoke insoles made from capillary matting colonised with oyster fungi *Pleurotus ostreatus* to compressive stress which mimics human loading when standing and walking. We have shown changes in electrical activity with compressive loading. The results advance the development of intelligent sensing insoles which are a building block towards more generic reactive fungal wearables. Using FitzHugh-Nagumo model we numerically illustrated how excitation wave-fronts behave in a mycelium network colonising an insole and shown that it may be possible to discern pressure points from the mycelium electrical activity.

In-shoe sensor technologies have been widely used in the clinical domain for disease detection, diagnostics and therapeutic use. Smart insoles can detect impairments in balance, gait, posture, muscle strength and cognition, providing valuable information about the user's physical and mental health[1–3]. They most commonly integrate pressure or optical sensor technologies in relevant locations for monitoring the foot–ground interaction force[4], providing complex functions and exhibiting broad sensing range when exposed to mechanical stimuli. As detailed in[4] smart insoles can be divided into three subgroups: (1) passive smart insoles able to sense parameters including weight loading of user, local terrain topology, volatile organic compounds, (2) active or reactive smart insoles able to sense and react performing some actions, by integrating an actuator, (3) advanced smart insoles able to sense, react and tailor their behaviour to specific operating circumstances.

Integrating sensor technologies into insoles, patterns and strategies for executing different functional tasks can be assessed, capturing data that can form the basis for use in areas such as rehabilitation, prehabilitation, monitoring elderly people who have mobility problems, mitigating slipping and falling as well as assessing long-term chronic conditions such as Dementia, Parkinson's disease and stroke[5]. For example, smart insoles have been used for the measurement of the weight pressure distribution that a patient exerts on each foot, in addition to the gait time, swing time, and stance time of each leg while walking to diagnose several medical conditions[6].

Smart insoles have lately found new applications outside the clinical domain. The proliferation of consumer-grade smart wearables has further propelled the development of commercial in-shoe devices to assess health and wellness-related mobility parameters in activities of daily living[7–10] e.g., pressure mapping of insoles in footwear based on conventional sensor technology (e.g. dielectric layer) have been reported[11,12] and insoles with diagnostic capabilities are commercially available, for example NURVV Run Smart Insoles[13]. While the use of smart insoles in non-medical applications has recently attracted significant interest, there are important challenges to overcome.

Cost represents a limiting factor. The devices require a number of sensors and actuators driven by electrical circuit components, usually supplied by a battery, making them not only expensive to fabricate but also significantly contributing to the depletion of natural resources. Insoles based on conventional sensor technology have short battery life (e.g. 5 h[14]) and are available in a limited number of insole sizes/shapes (e.g. 6 sizes[15]). Moreover, the performance of smart insoles is directly linked to the number and distribution of the sensors integrated as well as the identification of optimal sensor locations that match areas subject to the highest plantar pressures during gait or standing[4]. These locations can vary depending on the foot sizes and gait patterns of different users and can therefore alter or limit the gait or standing event recognition accuracy.

Biomaterials, such as mycelium bound composites, present a promising alternative to conventional smart insoles. They exhibit sensing and responsive capabilities without requiring additional space (for support

[1]Unconventional Computing Laboratory, UWE, Bristol, UK. [2]Department of Architecture, UWE, Bristol, UK. ✉email: anna.nikolaidou@uwe.ac.uk

infrastructure) and external inputs (e.g., electrical power sources) to operate, using its own bioelectric activity. Fungal sensors offer increased biodegradability, they are self- sustainable as they can self-grow, self-repair and self-assemble, they are abundant and offer in situ low technology cultivation. Moreover, they present low capital requirements and are easily scalable for the production of customised insole sizes.

In our previous studies, we demonstrated that living blocks of colonised by filamentous polypore fungus *Ganoderma resinaceum* substrate (MOGU's collection code 19–18, Mogu S.r.l., Inarzo, Italy), showed immediate responses in the form of spikes of electrical potential when subjected to weight application (8 kg and 16 kg), recognising the application or removal of weight[16]. In this paper, we present an illustrative scoping study in which we research the response of mycelium composite insoles to pressure generated by the feet during gait or standing. The primary objective of the studies reported in this paper is to assess the performance and spiking activity of the fungal insoles when exposed to mechanical stimuli and in particular, weight shifting (shifting of weight from toe to heel). We present a prototype of pressure-sensitive fungal insoles, aiming to open up opportunities for further research and discussions on the novel field of responsive smart insoles from living material, with the objective of enabling real-time applications and providing a sustainable, cost efficient and accurate tool for posture, gait and activity recognition events.

Methods

An innovative new method of forming insoles colonised with fungi from capillary matting (rather than hemp) was developed through multiple iterations. In a sterilised hydroponic growing tent with a silver Mylar light proof inner lining (Green Box Tents, UK), 200 g slab of mixed (mostly Rye grain) seed substrate well colonised with *Pleurotus ostreatus* (Ann Miller's Speciality Mushrooms, UK, https://www.annforfungi.co.uk/shop/oyster-grain-spawn/) was placed in the bottom of a sterilised clean plastic container (5 L, 280 × 145 × 110 mm, Amazon, UK). Here, it is noteworthy that *P. ostreatus* was selected based on its higher rate of substrate colonisation and trivial cultivation procedure. Multi-layered, absorbent, capillary action matting, ~ 3 mm thickness, made from bonded, non-toxic, wool and acrylic fibres, 450 g m^{-2} (manufactured by Tech-Garden, UK) was manually cut into the shape of insoles (UK ladies size 10) using hemp scissors (manufactured by Pemmiproducts, Germany), see Fig. 1a. The bespoke insole was sprayed with deionized water (15 MΩ cm, model Essential, Millipore, UK) and placed on spawn bed, see Fig. 1b. The plastic container was placed inside a polypropylene bag (type 14A and 49.5 × 32 cm in size https://www.annforfungi.co.uk/shop/100-spawn-bags/) fitted with 0.5 µm air filter patch (Ann Miller's Speciality Mushrooms, UK) and sealed with food storage clip (model Bevara, IKEA, UK). The insole was kept at ambient room temperature 18–22 °C inside the growth tent (in darkness). The insole was checked for growth every 3 days and additional moisture was added as required (via manual spray bottle with de-ionised water) from a distance of c. 10 cm to maintain required humidity levels for keeping the insole healthy. The insole was kept within the sterile tent at all times and any sources of contamination were kept away from the tent. After c. 3 weeks, uniform mycelium growth throughout the capillary matting was observed, see Fig. 1b. The colonised insole was carefully lifted off the spawn bed, see Fig. 1c.

A bespoke test rig was developed to apply compressive loading to insoles to replicate the weight of a human when walking and standing. A prosthetic foot (ladies, UK size 10) was 3D printed in acrylonitrile butadiene styrene (with Ultimaker S5, UK), see Fig. 2. The top part of the prosthetic foot was intentionally printed flat. A pivot joint (with integrated locking mechanism) was positioned between the weight and aluminium plate on

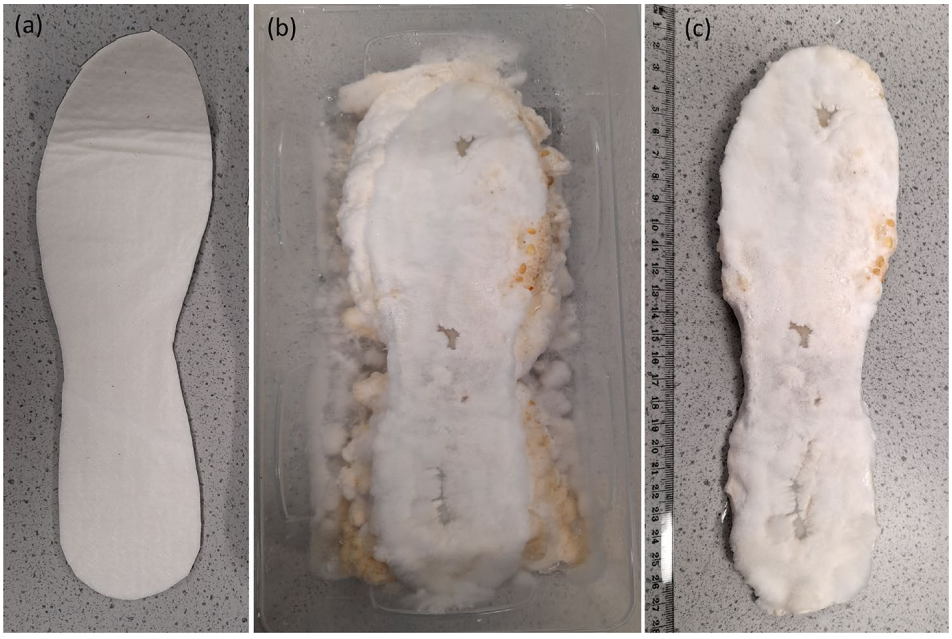


Figure 1. (**a**) capillary matting cut into insole pattern (**b**) insole on bed of spawn (**c**) well colonised insole.

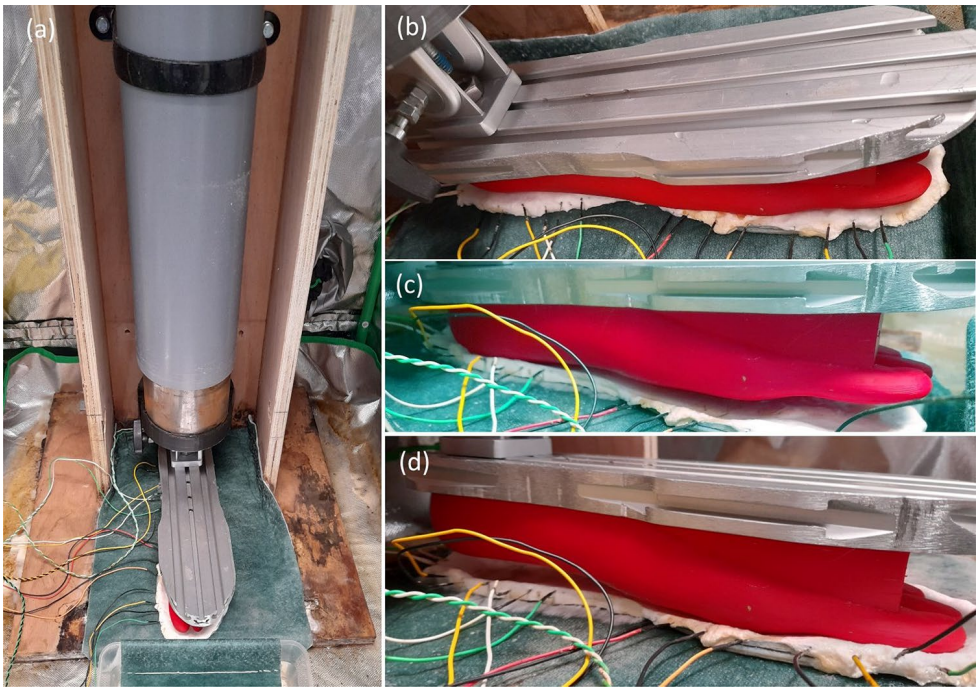


Figure 2. Bespoke insole test rig (**a**) setup inside growth tent (**b**) weight uniformly distributed via pivot joint on prosthetic foot (**c**) heel bias (**d**) toes bias.

top of the prosthetic foot to provide control over how the compressive load was distributed across the insole, see Fig. 2b. Test rig frame was assembled from plywood sheet (18 mm thickness) with plastic pipe (110 mm diameter). Mild steel bar (100 mm diameter) was free to move vertically inside the pipe to provide compressive loading on the insole at the bottom. For example, 500 mm length of steel bar weighs 35 kg which approximates a woman (with size 10 feet) standing on two feet (two 500 mm lengths can be used to replicate standing on one foot). The weight(s) could be raised and locked in the retracted position (by manual winch, fitted with a ratchet locking mechanism) to enable insoles to be interchanged and the load varied. To prevent the colonised insole slowly dehydrating over time (which might affect measurements) a sheet of capillary matting was placed under the insole, see Fig. 2a. The end of the capillary matting was left in a tray of de-ionised water which provided a source of moisture.The test rig was sterilised with 80% ethanol and placed in a sterilised hydroponic growing tent with a silver Mylar light proof inner lining (Green Box Tents, UK). Before and after the performance of each experiment, the rig and tent were sterilised with 80% ethanol.

Three modes of compressive loading were explored (i) toe bias, Fig. 2d (ii) heel bias, Fig. 2c and (iii) uniformly distributed, Fig. 2b.

Electrical activity of the mycelium colonising insoles was recorded using eight pairs of stainless steel subdermal needle electrodes (Spes Medica S.r.l., Italy), with twisted cables and ADC-24 (PICO Technology, UK) high-resolution data logger with a 24-bit A/D converter, galvanic isolation and software-selectable sample rates. The pairs of electrodes were pierced through the insole's edge as shown in Fig. 2. We recorded electrical activity one sample per second. During the recording, the logger has been doing as many measurements as possible (typically up to 10 per second) and saving the average value. We set the acquisition voltage range to 156 mV. Each pair of electrodes, called a channel (Ch), reported a difference of the electrical potential between the electrodes. Distance between electrodes was 1–2 cm.

Numerical modelling of the electrical activity was implemented as follows.

We used an artistic image of the mycelium network (Fig. 3a) projected onto a 364×985 nodes grid. The image was an integrative re-drawing of mycelium networks already grown in a surface. The original image $M = (m_{ij})_{1 \le j \le n_i, 1 \le j \le n_j}$, $m_{ij} \in \{r_{ij}, g_{ij}, b_{ij}\}$, where $n_i = 364$ and $n_j = 985$, and $1 \le r, g, b \le 255$ (Fig. 3a), was converted to a conductive matrix $C = (m_{ij})_{1 \le i,j \le n}$ (Fig. 3b) derived from the image as follows: $m_{ij} = 1$ if $r_{ij} > 170$, $g_{ij} > 170$ and $b_{ij} < 200$; a dilution operation was applied to C.

FitzHugh–Nagumo (FHN) equations[17–19] is a qualitative approximation of the Hodgkin–Huxley model[20] of electrical activity of living cells:

$$\frac{\partial v}{\partial t} = c_1 u(u-a)(1-u) - c_2 uv + I + D_u \nabla^2 \tag{1}$$

$$\frac{\partial v}{\partial t} = b(u-v), \tag{2}$$

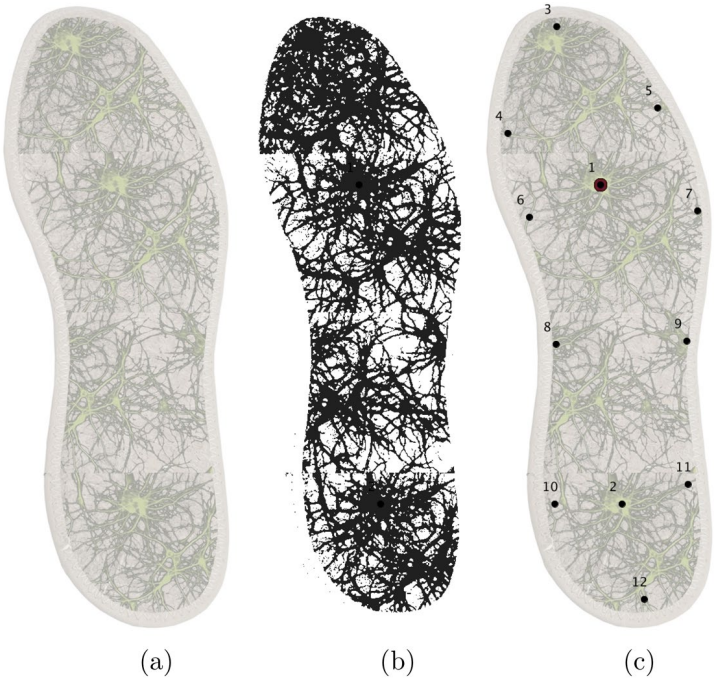


Figure 3. Image of the fungal colony, 1000 × 960 pixels used as a template conductive for modelling propagation of excitation in FitzHugh–Nagumo (FHN). (**a**) Original image, mycelium is seen as green pixels. (**b**) Conductive matrix *C*, conductive pixels are black. (**c**) Configuration of electrodes.

where u is a value of a trans-membrane potential, v a variable accountable for a total slow ionic current, or a recovery variable responsible for a slow negative feedback, I is a value of an external stimulation current. The current through intra-cellular spaces is approximated by $D_u\nabla^2$, where D_u is a conductance. Detailed explanations of the 'mechanics' of the model are provided in[21], here we shortly repeat some insights. The term $D_u\nabla^2 u$ governs a passive spread of the current. The terms $c_2u(u-a)(1-u)$ and $b(u-v)$ describe the ionic currents. The term $u(u-a)(1-u)$ has two stable fixed points $u=0$ and $u=1$ and one unstable point $u=a$, where a is a threshold of an excitation.

We integrated the system using the Euler method with the five-node Laplace operator, a time step $\Delta t = 0.015$ and a grid point spacing $\Delta x = 2$, while other parameters were $D_u = 1$, $a = 0.13$, $b = 0.013$, $c_1 = 0.26$. We controlled excitability of the medium by varying c_2 from 0.05 (fully excitable) to 0.015 (non excitable). Boundaries are considered to be impermeable: $\partial u/\partial \mathbf{n} = 0$, where $\mathbf{n}$ is a vector normal to the boundary.

To record dynamics of excitation in the network, as if in laboratory experiments, we simulated electrodes by calculating a potential p_x^t at an electrode location x as $p_x = \sum_{y:|x-y|<2}(u_x - v_x)$. Configuration of electrodes $1,\ldots,16$ is shown in Fig. 3c.

To imitate a pressure onto insole we perturbed the medium around electrodes E_1 or E_2 or both.

Time-lapse snapshots provided in the paper were recorded at every 100th time step, and we display sites with $u > 0.04$; videos and figures were produced by saving a frame of the simulation every 100th step of the numerical integration and assembling the saved frames into the video with a play rate of 30 fps. Videos are available at https://doi.org/10.5281/zenodo.5091807.

To examine the difference in responses of the insoles in more detail, the distribution of the weight across the insole was varied and applied in different regions (i.e., toe, heel, whole). That was designed in order to be similar to the way people change their weight distribution from heel to toe while walking. The number of spikes in each time period were automatically counted by utilising SciPy, an open-source collection containing mathematical algorithms and functions built on an extension of Python (https://docs.scipy.org). In specific, the function *find_peaks* was utilised to identify peaks with a prominence of 0.03 mV for this application. Then, a custom program was developed in Python to calculate the time difference between two spikes. Also, data visualization software Tableau was used to identify the potential (mV) differences under no load, even load, heel biased and toe biased load for every channel separately.

Results

Electrical activity was recorded for ~ 30 min immediately before, ~ 30 min during and ~ 30 min immediately after 35 kg was evenly distributed across the insole, see Fig. 4.

Electrical activity was recorded for ~24 h immediately before 35 kg was evenly distributed across the insole for ~72 h. The prosthetic foot was then tilted back to bias the weight onto the heel region of the insole for ~ 24 h. The prosthetic foot was then tilted forward to bias the weight onto the toe region of the insole for ~24 h.

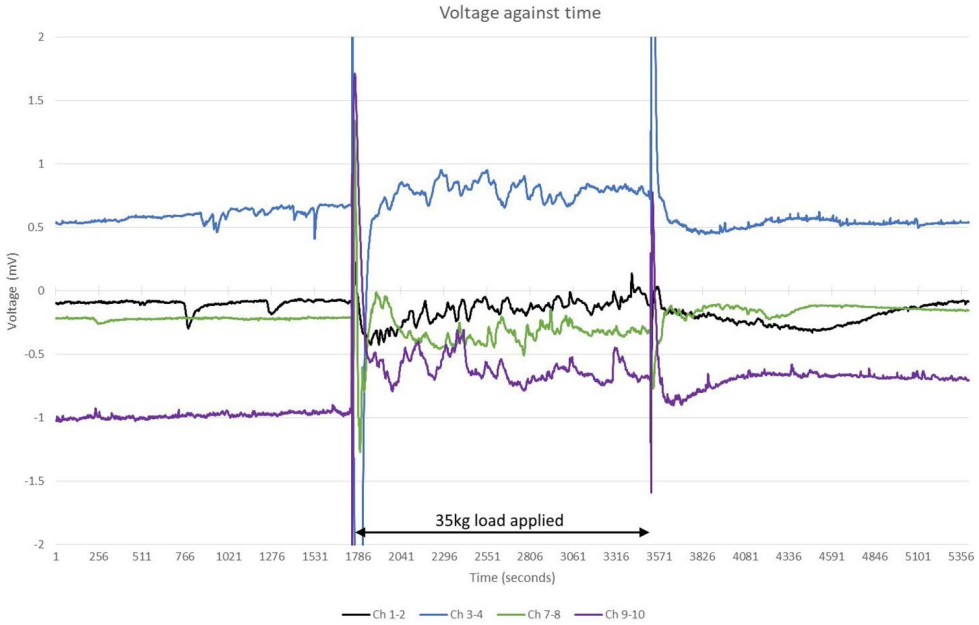


Figure 4. Electrical activity (recorded on Ch 1–2, Ch 3–4, Ch 7–8, Ch 9–10) before, during and after load (35 kg) was evenly distributed across insole.

Finally, the weight was removed for ~24 h. Eight pairs of needle electrodes were distributed along the side of the insole as shown in Fig. 5.

When a small area, c. 10 nodes, is perturbed the excitation starts propagating along the simulated mycelium network (Fig. 6a,b). With time, typically after 50–60 K iterations of the integration, the excitation wave fronts span all the mycelium network (Fig. 6c,d,e). Due to inhomogeneity of the network source so the spiral waves are formed. They become sources of oscillatory excitations. Repeated propagation of the spiral waves is reflected in the oscillatory activity levels on the mycelium network (Fig. 7).

Further we will demonstrate that it is possible to discern what loci of the insole pressure was applied based on electrical activity of the mycelium network. As evidenced in Fig. 7 the overall activity of the mycelium network depends on the site of pressure application (as imitated via exciting areas around electrodes E_1 or E_2 or both). When consider the three possible scenarios of the stimulation, the overall activity is lowest when area around electrode E_2 is excited ($E_1 = 0, E_2 = 1$). This is due to relatively lower number of mycelium strands in that part of the insole. The overall activity increases in the scenario where area round E_1 is excited ($E_1 = 1, E_2 = 0$). And the highest level of overall activity is evidenced for the scenario when areas around both electrodes ($E_1 = 1, E_2 = 1$).

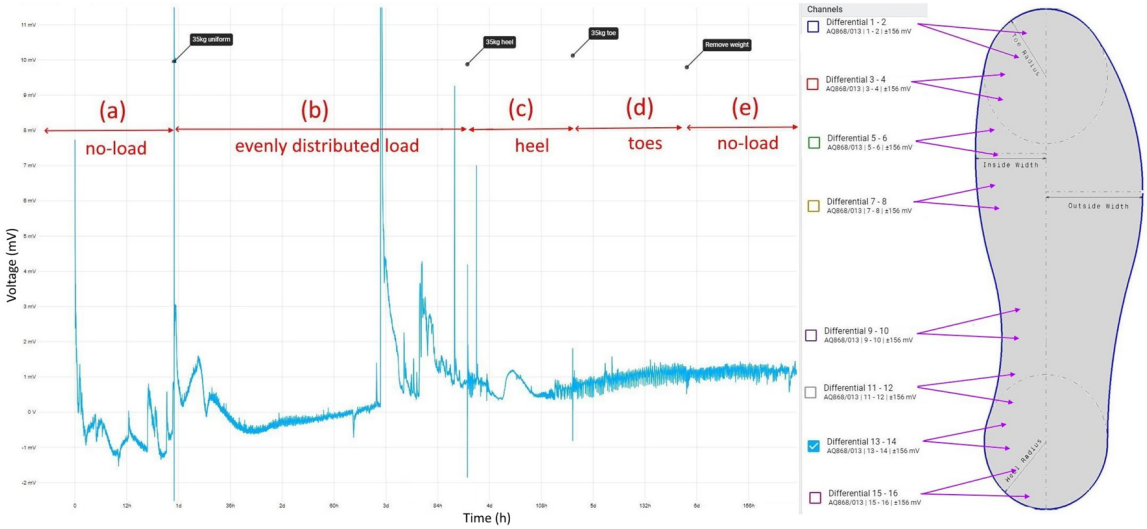


Figure 5. Exemplar of electrical activity recorded on Ch 13–14 (**a**) no load (**b**) load (35 kg) evenly distributed (**c**) load biased on heel region (**d**) load biased on toe region (**e**) no load.

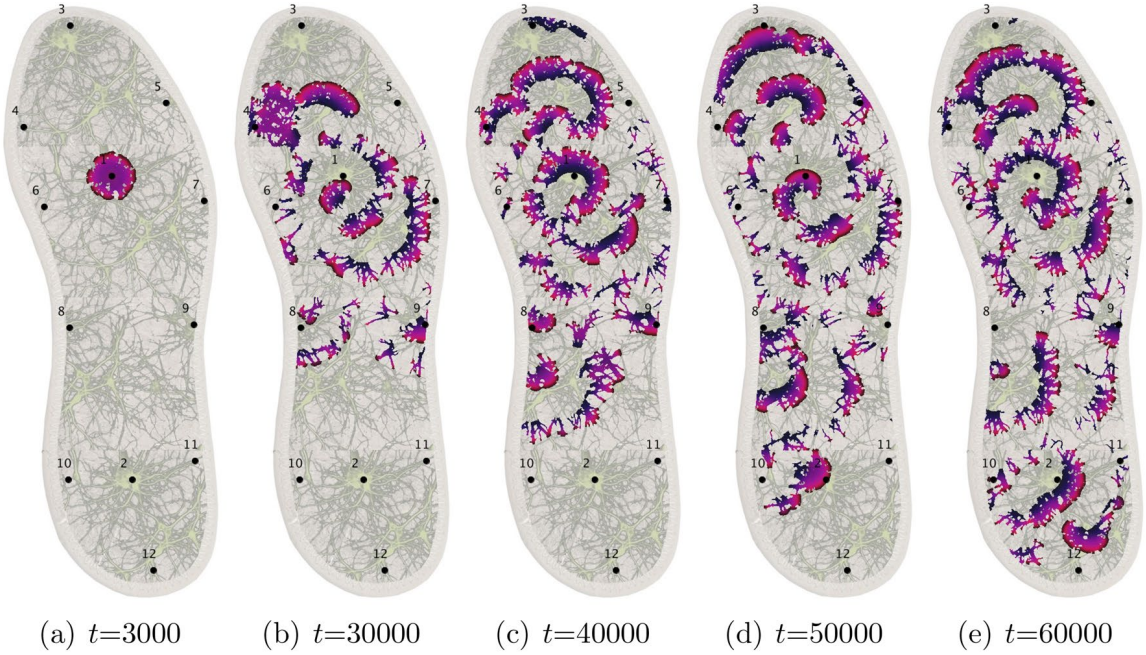


Figure 6. Snapshots of the excitation dynamics of the mycelium network colonising the insole produced from the computer simulations of FHN. Area around electrode E_1 has been excited originally.

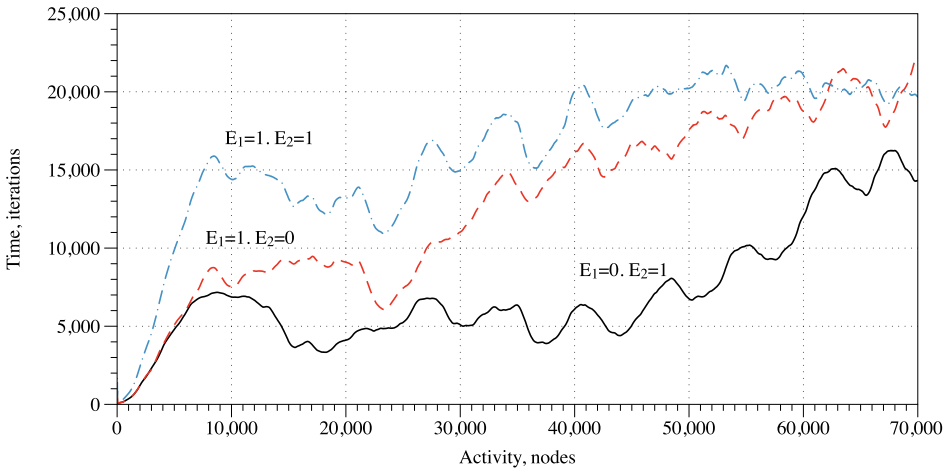


Figure 7. Activity of the mycelium network, for initial scenarios of excitation around electrode E_2, solid black, E_1, dashed red, E_1 and E_2, dot-dashed blue. The activity is measured in a number of nodes x with $u_x > 0.1$.

Coverage frequency could be another indicator to discern geometry of pressure. A coverage frequency at node x is a number of iterations values of excitation variable u_x exceeded 0.1, normalised by maximum coverage frequency amongst the nodes. The coverage frequency is illustrated in Fig. 8. The coverage frequency is maximum around the areas of pressure application and might even reflect a distance, not an Euclidean distance but a distance in the propagation metric of the mycelium networks, form the pressure application site.

A third measure applied to discern geometry of pressure would be spiking activity recorded on the electrodes. Examples of the spiking for all three scenarios of pressure application are shown in Fig. 9. The patterns of spiking activities might give us unique representations of the geometries of pressure applications. The formal representation of the spiking patterns could be done by distributions of Boolean gates in the spiking activity. This original technique has been developed by us in frameworks of cytoskeleton networks[22], fungal colony[23] and ensemble of proteinoid microspheres[24].

A spiking activity of the mycelium network shown in Fig. 9 in a response to stimulation, i.e. application of inputs $(E_1, E_2) = \{(0,1),(1,0),(1,1)\}$ via impulses at the electrodes E_1 and E_2, recorded from electrodes $E_1, \ldots, E_{12}$. We assume that each spike represents logical TRUE and that spikes occurring within less than $2 \cdot 10^2$ iterations are simultaneous. Then a representation of gates by spikes and their combinations can be implemented as shown in Table 1. By selecting specific intervals of recordings we can realise several gates in a single site of

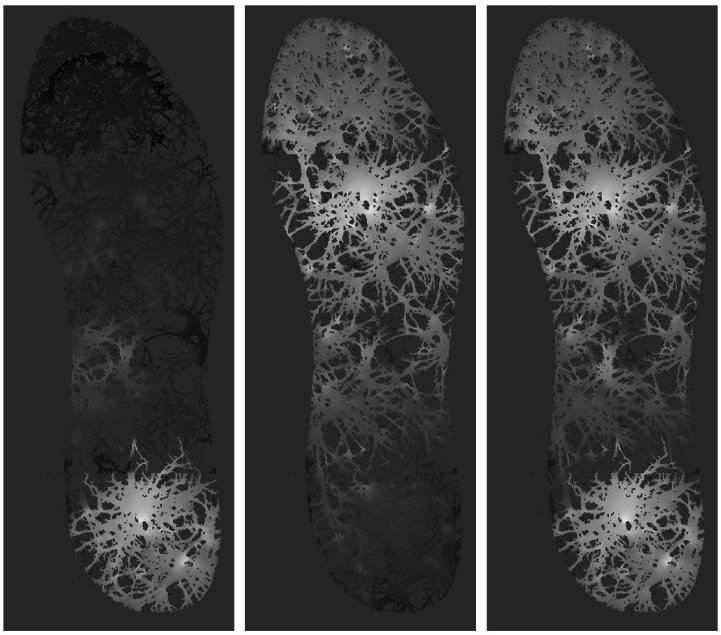


Figure 8. Coverage frequency, expressed in gradation of black. Areas never covered by excitation wave-fronts are black, areas covered most frequently are white. (**a**) Area around electrode E_2 have been excited initially. (**b**) Area around electrode E_1 have been excited initially. (**c**) Areas around electrodes E_1 and E_2 have been excited initially.

recording. In this particular case we assumed that spikes are separated if their occurrences are more than 10^3 iterations apart. In the simulated scenarios, we found that the following Boolean functions can be implemented on the electrodes $E_1, \ldots, E_{12}$. Three OR gates are realised on electrodes E_3, E_8 and E_{12}. Ten SELECTy, where y=TRUE signifies initial excitation around electrode E_2, are realised on electrodes E_3 and E_{12}. Fifty SELECTx, where x=TRUE signifies initial excitation around electrode E_1, are realised on the electrodes but E_1, E_9 and E_{11}. Five NOT-AND gate, in the form NOT x AND y, are realised on electrodes E_2, E_9 and E_{10}. The implementation of logical functions on the electrodes will allow for logical inference about geometries of pressure applied to insoles.

Discussion

Initially, off-the-shelf hemp insoles were used for inoculation with fungus *Pleurotus ostreatus*. The hemp insoles were sourced from different manufacturers (Hemp Made In UA, Ukraine, collection 100% natural hemp insoles) (HanfHaus, Denmark, collection organic hemp insoles) (Hemps, Ukraine, collection organic hemp multilayer therapeutic insoles with wormwood) (The Hemp Shop, Somerset, collection hemp organic insoles) and showed poor fungal colonisation, possibly due to unknown chemical processes to minimise bacterial growth which could lead to undesirable foot wear odour. Further testing of bespoke insoles cut from non-woven hemp matting (manufactured by Pemmiproducts, Germany) showed improved colonisation by fungi but inconsistent electrical activity (possibly due to inconsistent moisture level) and weak mechanical robustness. Capillary matting was tested and identified compatible with the biological organism being utilised and a strong candidate for the desired functionality.

It was observed that the risk of unwanted bacterial infection during colonisation of the insole could be reduced by keeping the insole inside a sealed local environment (for example, plastic bag fitted with sub-micron air filter) that mitigates airborne infection. Additionally, enclosing in a bag helps to prevent the insole dehydrating by maintaining a high local air humidity. Keeping the insole in darkness or low intensity light encourages its colonisation.

Optionally, forming the insole from two sheets of capillary matting allows a sandwich to be formed with nutrient layer (such as Rye grain seeds) between the top and bottom layer. This can allow the fungi to remain active for longer. Insoles infused with flour paste were prone to infection (even with sterilisation via autoclave).

The large internal volume and porous seals (long fabric zips) on the growth tent containing test rig was prone to low humidity, even with an open container of water present. It was found adding a sheet of capillary matting under the insole, see Fig. 2a, helped to maintain an adequate moisture level in the insole for fungal activity. The end of the sheet was left in a tray of de-ionised water which provided a source of moisture.

Oscillations in plant membrane are already known[25]. The physiological role of such oscillations has been the subject of much speculation. It has been hypothesised these oscillations are links to plants' adaptive response to environmental stresses[26].

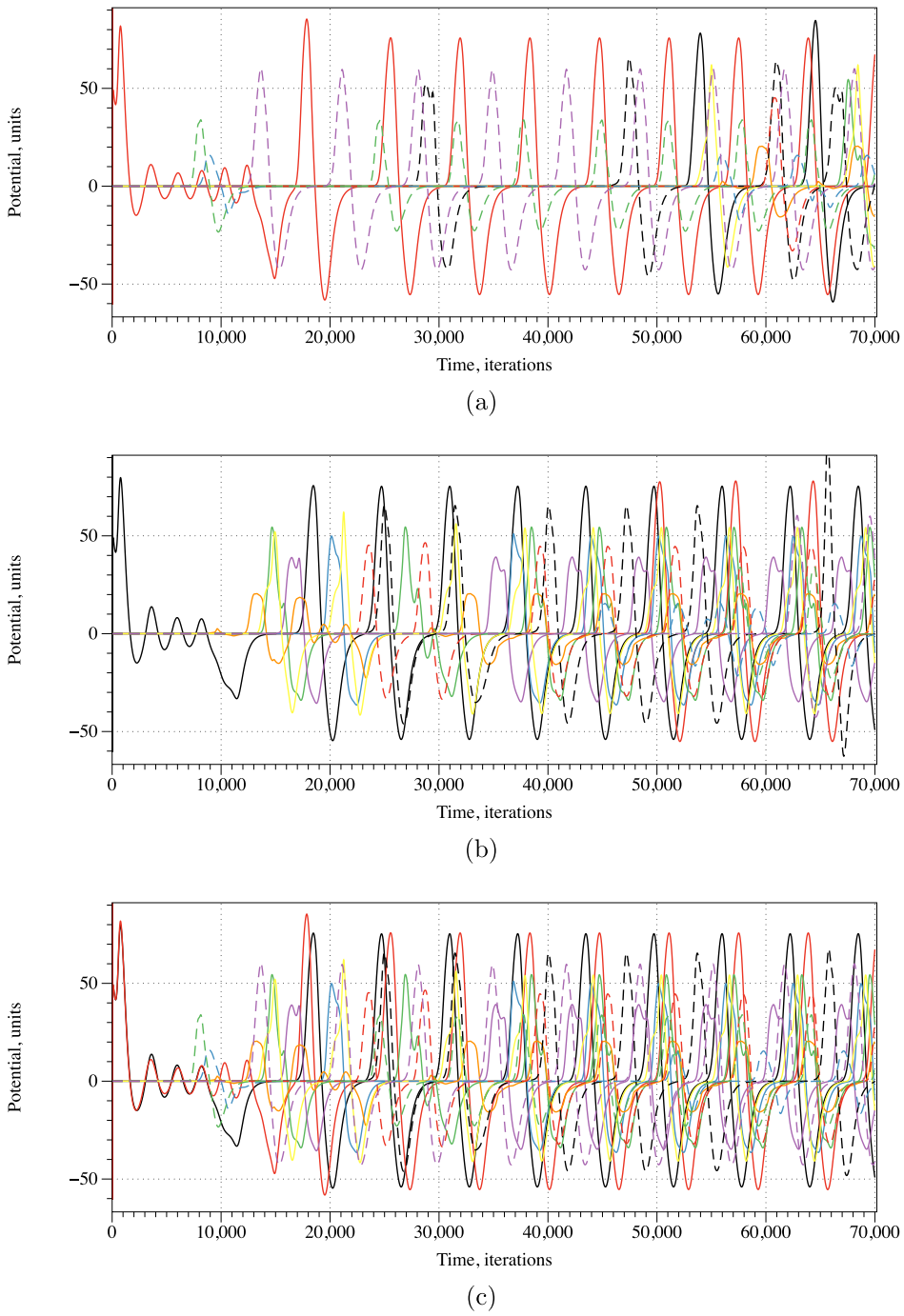


Figure 9. Potential recorded on electrodes $E_1, \ldots, E_{12}$ for initial scenarios of excitation around electrode (**a**) E_2, (**b**) E_1, (**c**) E_1 and E_2.

The number of spikes (< 0.1 mV) recorded over three ~30 m periods before, during after even compressive load are summarised in Table 2. Further, it was observed that periodicity of electrical spikes changed when the mycelium was under compressive load.

Measurements indicate a layer of mycelium integrated into an insole shows electrical response to mechanical stimulation with change in oscillatory activity. In particular, the number of spikes increases under compressive load. The response to removing weight is different to applying weight.

To examine the response of the distribution of the weight across the insole (i.e., toe, heel, whole, similar to the way people change their weight distribution from heel to toe while walking) the data were compared. Histograms of the distribution of time differences between spikes in each insole region under no load, heel biased and toe biased load were produced and they were drawn over the same axes to allow the comparison of the results as shown in Fig. 10. Moreover, the visualization to identify the potential differences under no load, even load,

spikes	gate	notations
	OR	$x + y$
	SELECT	y
	XOR	$x \oplus y$
	SELECT	x
	NOT-AND	$\overline{x}y$
	AND-NOT	$x\overline{y}$
	AND	xy

Table 1. Representation of gates by combinations of spikes. Black lines show the potential when the network was stimulated by input pair (01), red by (10) and green by (11). Adamatzky proposed this representation originally in[22].

Differential channels	30 min period before weight	30 min period during weight	30 min period after weight
Ch 1–2	2	10	1
Ch 3–4	2	6	0
Ch 7–8	0	8	3
Ch 9–10	0	7	2

Table 2. Electrical response to weight (electrical spikes < 0.1 mV).

heel biased and toe biased load for every channel separately is shown in Figs. 11 and 12. The amplitude of spikes decreases under even load application compared to no load application. No conclusions could be made regarding the electrical activity under heel biased and toe biased load. It was therefore, not possible to accurately discern the distribution of compressive loading across the insole from analysis of electrical responses.

Experimentation identified the rate of occurrence of spikes is lower than desirable to accurately infer the weight bearing when walking. However, when standing for a period, electrical activity can be collected and analysed to infer weight bearing which can be used for anatomical diagnostics[27,28]. Continuous monitoring of feet could offer numerous medical/health benefits[29–31]. For example, early detection of health related conditions (such as knee injury) or tiredness. It can also be useful for sports training[32–34].

In the experimental setup described, sensory mapping is limited to '1.5D' (8 pairs of differential electrodes in a row and limited vertical motion) however this could be expanded to '2.5D' by mapping with a 2D distributed array of electrodes across the insole. For example, needle electrodes replaced by thin/flexible wires integrated into the capillary matting such that uninsulated sections of the wires are spatially distributed and electrical connections are realised to the edge of the insole.

Direct conversion of mechanical energy into electricity offers potential as power source for various systems[35–37].

It was observed during the fabrication and testing of a diverse range of prototype wearables (including clothing) that capillary matting offer superior durability over hemp matting (in particular on flexible clothing joints, knees and elbows) and easy of interfacing to conventional fabrics (sewing and gluing). Therefore, capillary matting might be useful substrate for a range of smart fungal wearables.

Smart footwear offers benefits to safety footwear[38]. For example, automatic notification of injury to user and emergency services. Awareness of foot activity might also be beneficial in various environments such as driving (for example, enabling the vehicle to respond before the driver's foot has touched a pedal).

Simulation using FitzHugh–Nagumo model numerically illustrated how excitation wave-fronts behave in a mycelium network colonising an insole and shown that it is possible to discern pressure points from the mycelium electrical activity.

Conclusions

Electrical activity (spiking) was recorded in mycelium bound composites fabricated into insoles. The number and periodicity of electrical spikes change when the mycelium is subjected to compressive loading. We have shown that it might be possible to discern the loading from the electrical response of the fungi to stimuli. The results advance the development of intelligent sensing insoles which are a building block towards more generic reactive fungal wearables. Electrical activity changes in both spatial and temporal domains. Using FitzHugh–Nagumo

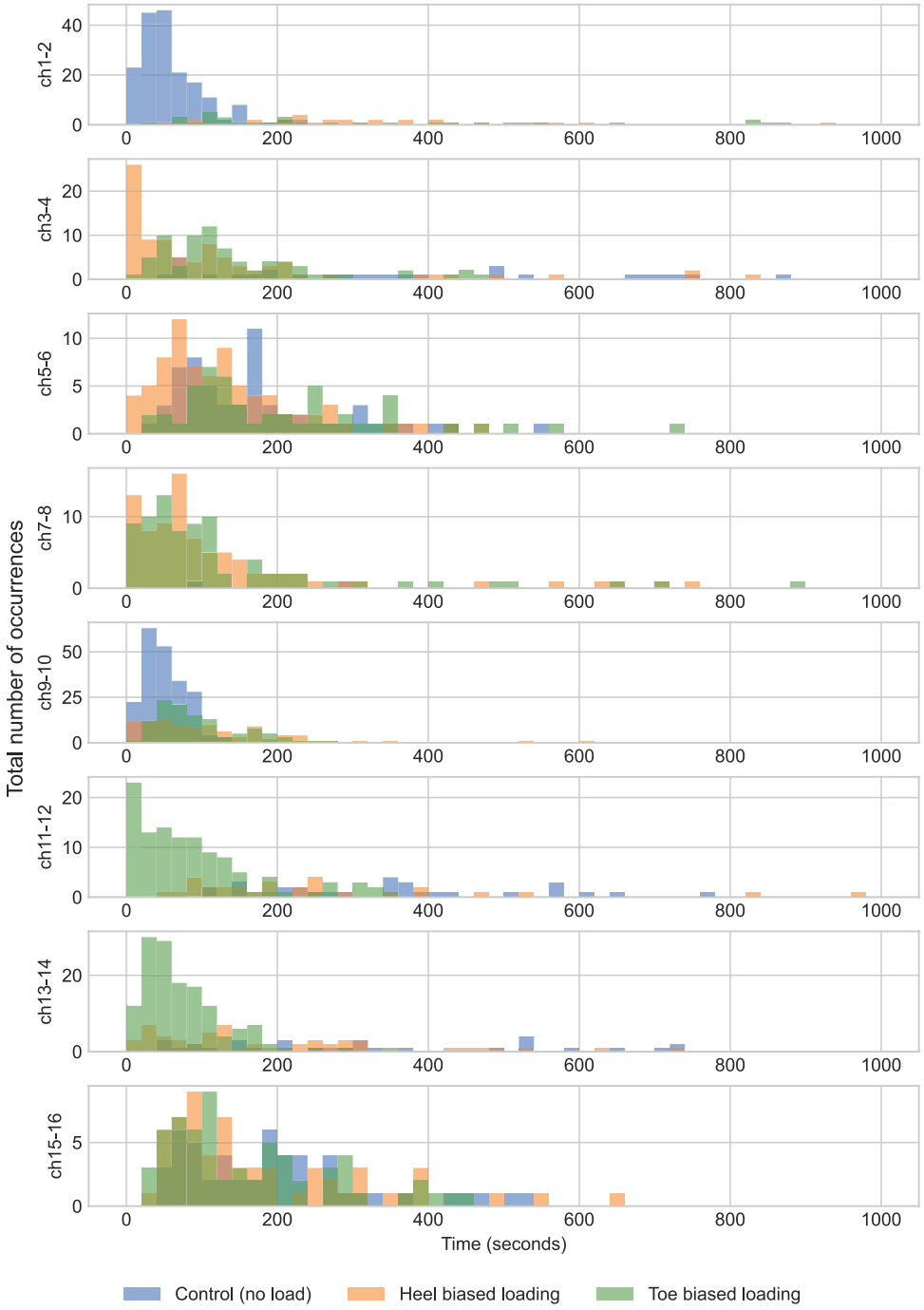


Figure 10. Histograms of the distribution of time differences between spikes in each insole region under a range of load condition.

model we numerically illustrated how excitation wave-fronts behave in a mycelium network colonising an insole and shown that it might be possible to discern pressure points from the mycelium electrical activity. Fungal based insoles offer augmented functionality (sensory) and aesthetic (personal fashion). We presented results of scoping experiments on living biowearables. The results open new horizons in exploring feasibility of living fungal materials in everyday life. Directions of future research will involve bench marking of the prototypes and testing them in real life.

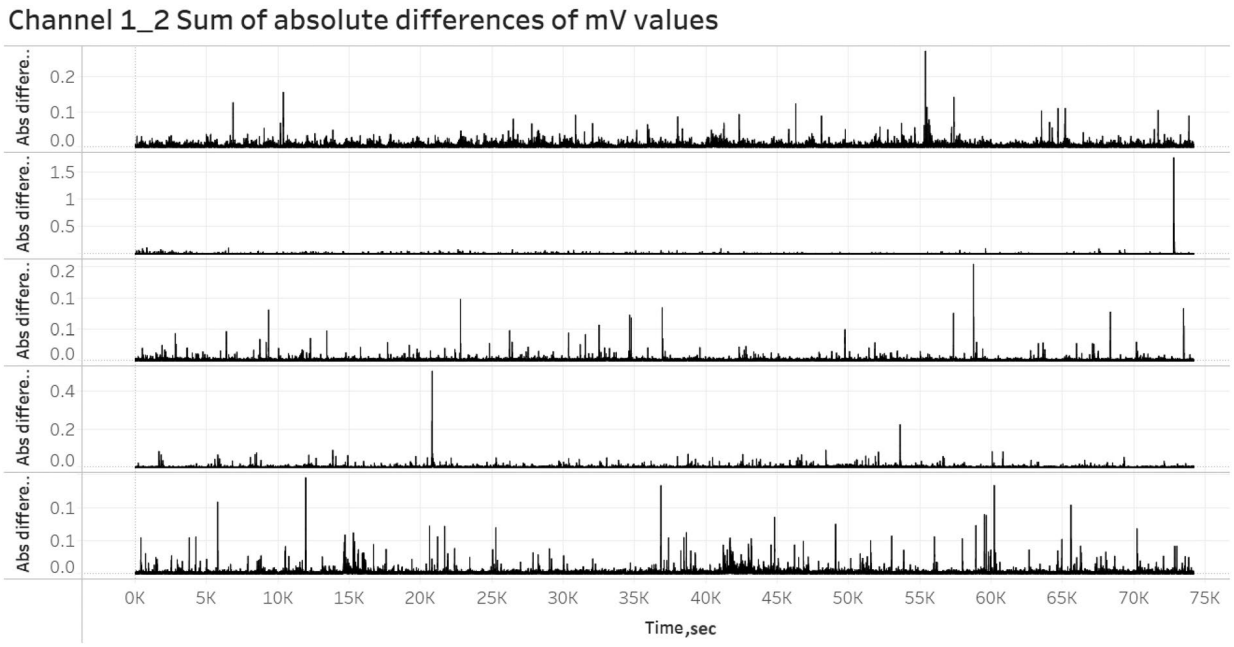


Figure 11. Graph showing decrease of amplitude when under even load compared to no load application for Channels 1–2.

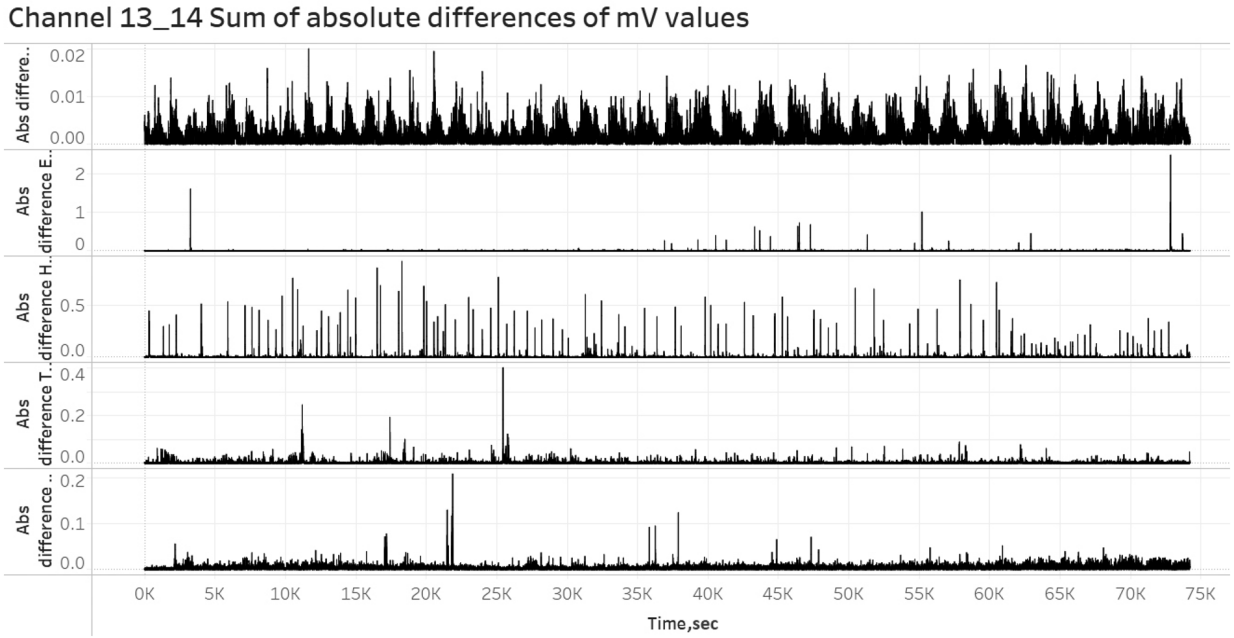


Figure 12. Graph showing decrease of amplitude when under even load compared to no load application for Channels 13–14.

Data availability

The datasets made and analysed during the current study are available from the corresponding author on reasonable request.

Received: 26 September 2022; Accepted: 14 March 2023
Published online: 21 March 2023

References

1. Tucker, M. R. *et al.* Control strategies for active lower extremity prosthetics and orthotics: A review. *J. Neuroeng. Rehabil.* **12**(1), 1–30 (2015).

2. Anabitarte-García, F. *et al.* Early diagnosis of frailty: Technological and non-intrusive devices for clinical detection. *Age. Res. Rev.* **70**, 101399 (2021).
3. Rajagopalan, R., Litvan, I. & Jung, T.-P. Fall prediction and prevention systems: Recent trends, challenges, and future research directions. *Sensors* **17**(11), 2509 (2017).
4. Martini, E. *et al.* Pressure-sensitive insoles for real-time gait-related applications. *Sensors* **20**(5), 1448 (2020).
5. Munoz-Organero, M., Parker, J., Powell, L. & Mawson, S. Assessing walking strategies using insole pressure sensors for stroke survivors. *Sensors* **16**(10), 1631 (2016).
6. Khoo, I.-H., Marayong, P., Krishnan, V., Balagtas, M. N., & Rojas, O. Design of a biofeedback device for gait rehabilitation in post-stroke patients. In *2015 IEEE 58th International Midwest Symposium on Circuits and Systems (MWSCAS)*, pp. 1–4. IEEE (2015).
7. Park, J., Na, Y., Gu, G. & Kim, J. Flexible insole ground reaction force measurement shoes for jumping and running. In *2016 6th IEEE International Conference on Biomedical Robotics and Biomechatronics (BioRob)*, pp. 1062–1067. IEEE (2016).
8. Ramirez-Bautista, J. A., Huerta-Ruelas, J. A., Chaparro-Cárdenas, S. L. & Hernández-Zavala, A. A review in detection and monitoring gait disorders using in-shoe plantar measurement systems. *IEEE Rev. Biomed. Eng.* **10**, 299–309 (2017).
9. Zhang, H., Zanotto, D. & Agrawal, S. K. Estimating cop trajectories and kinematic gait parameters in walking and running using instrumented insoles. *IEEE Robot. Autom. Lett.* **2**(4), 2159–2165 (2017).
10. Razak, A. H. A., Zayegh, A., Begg, R. K. & Wahab, Y. Foot plantar pressure measurement system: A review. *Sensors* **12**(7), 9884–9912 (2012).
11. Tao, J. *et al.* Real-time pressure mapping smart insole system based on a controllable vertical pore dielectric layer. *Microsyst. Nanoeng.* **6**, 62 (2020).
12. Gao, L. *et al.* Highly sensitive pseudocapacitive iontronic pressure sensor with broad sensing range. *Nano-Micro Lett.* **13**(1), 1–14 (2021).
13. Nurvv Ltd. NURVV Run Smart Insoles. https://www.nurvv.com/en-gb/products/nurvv-run-insoles-trackers/, 2022. Accessed 18 Sept 2022.
14. Nurvv Ltd. NURVV Run Smart Insoles operating time. https://www.nurvv.com/en-gb/products/nurvv-run-insoles-trackers/, 2022. Accessed 18 Sept 2022.
15. Nurvv Ltd. NURVV Run Smart Insoles. https://www.nurvv.com/en-gb/support/sizing/. 2022. Accessed 18 Sept 2022.
16. Adamatzky, A. & Gandia, A. Living mycelium composites discern weights via patterns of electrical activity. *J. Bioresour. Bioprod.* **7**(1), 26–32 (2022).
17. FitzHugh, R. Impulses and physiological states in theoretical models of nerve membrane. *Biophys. J* . **1**(6), 445–466 (1961).
18. Nagumo, J., Arimoto, S. & Yoshizawa, S. An active pulse transmission line simulating nerve axon. *Proc. IRE* **50**(10), 2061–2070 (1962).
19. Pertsov, A. M., Davidenko, J. M., Salomonsz, R., Baxter, W. T. & Jalife, J. Spiral waves of excitation underlie reentrant activity in isolated cardiac muscle. *Circ. Res.* **72**(3), 631–650 (1993).
20. Beeler, G. W. & Reuter, H. Reconstruction of the action potential of ventricular myocardial fibres. *J. Physiol.* **268**(1), 177–210 (1977).
21. Rogers, J. M. & McCulloch, A. D. A collocation-Galerkin finite element model of cardiac action potential propagation. *IEEE Trans. Biomed. Eng.* **41**(8), 743–757 (1994).
22. Adamatzky, A., Huber, F. & Schnauß, J. Computing on actin bundles network. *Sci. Rep.* **9**(1), 1–10 (2019).
23. Adamatzky, A. *et al.* On Boolean gates in fungal colony. *Biosystems* **193**, 104138 (2020).
24. Adamatzky, A. Towards proteinoid computers. arXiv:2106.00883 (2021).
25. Frantisek Baluska, D. V. & Mancuso, S. (eds) *Oscillations in Plants, Communication in Plants: Neuronal Aspects of Plant Life* 261–275 (Springer, 2006).
26. Shabala, S. *et al.* Oscillations in plant membrane transport: Model predictions, experimental validation, and physiological implications. *J. Exp. Bot.* **57**, 171–184 (2005).
27. Ghosh, A. K., Tibarewala, D., Mukherjee, P., Chakraborty, S. & Ganguli, D. S. Preliminary study on static weight distribution under the human foot as a measure of lower extremity disability. *Med. Biol. Eng. Comput.* **17**, 737–41 (1979).
28. Cavanagh, P. R. & Rodgers, M. M. *Pressure Distribution Underneath the Human Foot* 85–95 (Springer, Dordrecht, 1985).
29. Lin, F., Wang, A., Zhuang, Y., Tomita, M. R. & Xu, W. Smart insole: A wearable sensor device for unobtrusive gait monitoring in daily life. *IEEE Trans. Ind. Inf.* **12**(6), 2281–2291 (2016).
30. Xu, W., Huang, M.-C., Amini, N., Liu, J. J., He, L. & Sarrafzadeh, M. Smart insole: A wearable system for gait analysis. In *Proceedings of the 5th International Conference on PErvasive Technologies Related to Assistive Environments*, PETRA '12, (New York, NY, USA), Association for Computing Machinery (2012).
31. Wang, B., Rajput, K. S., Tam, W.-K., Tung, A. K. H. & Yang, Z. Freewalker: A smart insole for longitudinal gait analysis. In *2015 37th Annual International Conference of the IEEE Engineering in Medicine and Biology Society (EMBC)*, pp. 3723–3726 (2015).
32. Ziagkas, E., Loukovitis, A., Zekakos, D. X., Chau, T. D.-P., Petrelis, A. & Grouios, G. A novel tool for gait analysis: Validation study of the smart insole®. *Sensors*, **21**(17) (2021).
33. Tan, A. M., Fuss, F. K., Weizman, Y. & Troynikov, O. Development of a smart insole for medical and sports purposes. *Procedia Eng.*, **112**, 152–156 (2015). 'The Impact of Technology on Sport VI' 7th Asia-Pacific Congress on Sports Technology, APCST2015.
34. Oks, A., Katashev, A., Zadinans, M., Rancans, M. & Litvak, J. Development of smart sock system for gate analysis and foot pressure control. In *XIV Mediterranean Conference on Medical and Biological Engineering and Computing 2016* (eds Kyriacou, E. *et al.*) 472–475 (Springer, 2016).
35. Sun, J. *et al.* Enhanced mechanical energy conversion with selectively decayed wood. *Sci. Adv.* **7**(11), eabd9138 (2021).
36. de Fazio, R., Perrone, E., Velázquez, R., De Vittorio, M. & Visconti, P. Development of a self-powered piezo-resistive smart insole equipped with low-power BLE connectivity for remote gait monitoring. *Sensors*, **21**(13), 4539 (2021).
37. Wang, W. *et al.* Self-powered smart insole for monitoring human gait signals. *Sensors*, **19**(24), 5336 (2019).
38. Janson, D., Newman, S. & Dhokia, V. Next generation safety footwear. *Procedia Manufacturing*, **38**, 1668–1677 (2019). 29th International Conference on Flexible Automation and Intelligent Manufacturing (FAIM 2019), June 24–28, 2019, Limerick, Ireland, Beyond Industry 4.0: Industrial Advances, Engineering Education and Intelligent Manufacturing.

Acknowledgements

The research was supported by the funding from the European Union's Horizon 2020 research and innovation programme FET OPEN "Challenging current thinking" under Grant Agreement No 858132. We are grateful to Ann Miller's Speciality Mushrooms Ltd for information on their spawn.

Author contributions

A.N. and A.A. developed a concept. A.N. and N.P. undertook experiments and collection of data. A.A. developed the simulation using FitzHugh-Nagumo model. All authors contributed to information processing and data analysis. All authors wrote the main manuscript text and prepared the figures. All authors reviewed the manuscript.

Competing interests
The authors declare no competing interests.

Additional information
Correspondence and requests for materials should be addressed to A.N.

Reprints and permissions information is available at www.nature.com/reprints.

Publisher's note Springer Nature remains neutral with regard to jurisdictional claims in published maps and institutional affiliations.

Open Access This article is licensed under a Creative Commons Attribution 4.0 International License, which permits use, sharing, adaptation, distribution and reproduction in any medium or format, as long as you give appropriate credit to the original author(s) and the source, provide a link to the Creative Commons licence, and indicate if changes were made. The images or other third party material in this article are included in the article's Creative Commons licence, unless indicated otherwise in a credit line to the material. If material is not included in the article's Creative Commons licence and your intended use is not permitted by statutory regulation or exceeds the permitted use, you will need to obtain permission directly from the copyright holder. To view a copy of this licence, visit http://creativecommons.org/licenses/by/4.0/.

© The Author(s) 2023

BioSystems 199 (2021) 104304

Contents lists available at ScienceDirect

BioSystems

journal homepage: www.elsevier.com/locate/biosystems

Reactive fungal wearable

Andrew Adamatzky [a,*], Anna Nikolaidou [a,c], Antoni Gandia [b], Alessandro Chiolerio [a,d], Mohammad Mahdi Dehshibi [a,e]

[a] Unconventional Computing Laboratory, UWE, Bristol, UK
[b] Mogu S.r.l., Inarzo, Italy
[c] Department of Architecture, UWE, Bristol, UK
[d] Center for Sustainable Future Technologies, Istituto Italiano di Tecnologia, Torino, Italy
[e] Department of Computer Science, Universitat Oberta de Catalunya, Barcelona, Spain

ARTICLE INFO

Keywords:
Fungi
Wearables
Biosensing
Unconventional computing

ABSTRACT

Smart wearables sense and process information from the user's body and environment and report results of their analysis as electrical signals. Conventional electronic sensors and controllers are commonly, sometimes augmented by recent advances in soft electronics. Organic electronics and bioelectronics, especially with living substrates, offer a great opportunity to incorporate parallel sensing and information processing capabilities of natural systems into future and emerging wearables. Nowadays fungi are emerging as a promising candidate to produce sustainable textiles to be used as ecofriendly biowearables. To assess the sensing potential of fungal wearables we undertook laboratory experiments on electrical response of a hemp fabric colonised by oyster fungi *Pleurotus ostreatus* to mechanical stretching and stimulation with attractants and repellents. We have shown that it is possible to discern a nature of stimuli from the fungi electrical responses. The results paved a way towards future design of intelligent sensing patches to be used in reactive fungal wearables.

1. Introduction

Smart wearables are devices that extend the functionality of clothes and gadgets, they are responsive to the wearer and can act as an interface between the wearer and the environment producing a user responsive symbiotic system. The smart wearables have been developed as a result of the convergence between textiles and electronics (e-textiles). They integrate a high level of technology to provide complex functions and an easy operation and maintenance (Stoppa and Chiolerio, 2014). They can be divided into three subgroups: (1) passive smart wearables: able to sense the environment/user, (2) active or reactive smart wearables: able to sense the environment/user, and react performing some actions, therefore integrating an actuator, (3) advanced smart wearables: able to sense, react and adapt their behaviour to given circumstances. Sensors provide means to detect signals, actuators react upon stimuli either autonomously or after commands received from a central processing unit (Langereis et al., 2012). Textile-embedded sensing systems have been developed and commercially exploited in both the biomedical and safety communities (Custodio et al., 2012). Smart wearables have been used to record electrocardiography signals (Coosemans et al., 2003), electromyography signals (Scalisi et al., 2015), electroencephalography signals (Löfhede et al., 2010), temperature (Sibinski et al., 2010), biophotonic sensing (Omenetto et al., 2013), movement (Meyer et al., 2006), oxygen content, salinity, moisture, or contaminants (Coyle et al., 2010; Zadeh, 2006). Active functionalities might include power generation or storage capabilities (Vatansever et al., 2011), machine to human interface elements (Baurley, 2004), radio frequency communication capabilities (Black, 2007). Wearable intelligent systems, intrinsically soft and better compliant with extension, deformation and skin stiffness have been developed since a long time (Rajan et al., 2018).

The electronic wearables cannot self-grow and self-repair. This deficiency limits their application in the field of soft robotics and self-growing robots (Mazzolai, 2017; Sadeghi et al., 2017; Del Dottore et al., 2018; Sadeghi et al., 2020). We can overcome these limits by incorporating living fabric in the smart wearables. One of the solutions, explored by us previously, would be to grow slime mould *P. polycephalum* on a surface of the cloths or a body of a robot (Schubert et al., 2015). The slime mould is proven to be a biosensor for the chemical, mechanical and optical stimuli (Whiting et al., 2014; Adamatzky, 2013a,b). Despite the sufficient sensorial abilities, the slime mould is rather fragile, highly dependent on environmental conditions and requires particular sources of nutrients.

Fungi could, however, make a feasible alternative to the slime mould. Fungal materials – grow substrates colonised with mycelium

* Corresponding author.
E-mail address: andrew.adamatzky@uwe.ac.uk (A. Adamatzky).

https://doi.org/10.1016/j.biosystems.2020.104304
Received 15 September 2020; Received in revised form 29 October 2020; Accepted 18 November 2020
Available online 24 November 2020
0303-2647/© 2020 Published by Elsevier B.V.



Fig. 1. Experimental setup. (a) Overall view of the experimental setup. (b) Close up of the fungal wearable incorporated into real cloth. (c) Exemplar locations of electrodes.

of filamentous fungi – are emerging to be robust, reliable and ecologically friendly replacement for conventional building materials and fabrics (Travaglini et al., 2016; Haneef et al., 2017; Ross, 2018; Appels et al., 2019; Islam et al., 2017; Dahmen, 2017; Adamatzky et al., 2019; Chase et al., 2019; Meyer et al., 2020; Jones et al., 2020). Fungi "possess almost all the senses used by humans" (Bahn et al., 2007). Fungi sense light, chemicals, gases, gravity and electric fields. Fungi show a pronounced response to changes in a substrate pH (Van Aarle et al., 2002), mechanical stimulation (Kung, 2005), toxic metals (Fomina et al., 2000), CO_2 (Bahn and Mühlschlegel, 2006), stress hormones (Howitz and Sinclair, 2008). Thus, wearables made of or incorporating fabric colonised by fungi might act as a large distributed sensorial network. Fungi is known to respond to chemical and physical stimuli by changing patterns of its electrical activity (Olsson and Hansson, 1995; Adamatzky, 2018; Adamatzky et al., 2020a) and electrical properties (Beasley et al., 2020). This feature would allow to interface fungal wearables with conventional electronics. In view of their extension and interconnectivity, fungal networks represent certainly a sustainable infrastructure-forming substrate, able to wire loci separated by considerable space. Moreover, there are indications that mycelium networks not just sense the external stimuli but also process information, and that there is feasible opportunity to convert fungal responses into Boolean circuits, thus making fungal wearables parallel biological processing networks (Adamatzky et al., 2020b). Previously conducted experiments on sensorial properties of fungi have been using experimental laboratory setups where substrates colonised by fungi have been kept in 'comfortable' conditions of closed containers with preserved humidity (Dehshibi and Adamatzky, 2020). To assess the feasibility of a fungal wearable prototype in the real world we conducted experiments with a thin hemp-mycelium composite fabric incorporated on a t-shirt wore by a mannequin.

The paper is structured as follows. We introduce experimental techniques in Section 2. Section 3 analyses the fungal response to stimulation with chemo-attractants, chemo-repellents and mechanical stretching. In Section 4 we talk about mechanisms of the fungal wearable response and propose directions for further studies.

2. Methods

A commercial strain of the fungus *P. ostreatus* (Mogu's collection code 21-18), previously selected for its superior fitness growing on the targeted substrate, was cultured on a hemp bedding substrate in plastic boxes c. 35×20 cm^2 in darkness at ambient room temperature c. 22°C.

A hemp substrate well colonised by the fungus was spread on rectangular fragments, c. 12×12 cm^2, of moisturised hemp fabric. When the fragments were colonised, as visualised by white mycelial growth on surface, they were used for experiments. The colonised fabric was attached to a cloth, which in turn was placed on a mannequin (Fig. 1(a)). The mannequin was covered by a plastic sheet to prevent a quick decrease of moisture in the fungal fabric. The fabric was sprayed with distilled water once per two days. The humidity of the fungal fabric was 70%–80% (MerlinLaser Protimeter, UK). The experiments were conducted in a room with ambient temperature 21°C and illumination 30–150 LUX (ISO-Tech ILM 1332A).

Electrical activity of the colonised fabric was recorded using pairs of iridium-coated stainless steel sub-dermal needle electrodes (Spes Medica S.r.l., Italy), with twisted cables and ADC-24 (Pico Technology, UK) high-resolution data logger with a 24-bit A/D converter, galvanic isolation and software-selectable sample rates all contribute to a superior noise-free resolution. To keep electrodes stable we have been placing a polyurethane pad under the fabric. The pairs of electrodes were pierced through the fabric and into the polyurethane pad (Figs. 1(b) and 1(c)). We recorded electrical activity one sample per second, where the minimum and maximum logging times were 60.04 and 93.45 h, respectively. During the recording, the logger has been doing as many measurements as possible (typically up to 600 per second) and saving the average value. We set the acquisition voltage range to 156 mV with an offset accuracy of 9 μV at 1 Hz to maintain a gain error of 0.1%. Each electrode pair was considered independently with the noise-free resolution of 17 bits and conversion time of 60 ms. Each pair of electrodes, further called a Channel (Ch), reported a difference of the electrical potential between the electrodes. Distance between electrodes was 1–2 cm. In each trial, we recorded 5–8 electrode pairs (Ch) simultaneously. We stimulated the fungus with 96% ethanol, malt extract powder (Sigma Aldrich, UK) dissolved in distilled water, dextrose (Ritchie Products Ltd, UK) and by attaching weights (using foldback clips) to the hemp pads.

3. Results

A response of the fungal wearable to a chemo-attractant was studied using malt extract and dextrose. An exemplar response to application of malt extract is shown in Fig. 2(a). The immediate, first 3 hr, response is manifested in the spikes up to 15 mV and duration up to 140 min, and is due to a sudden increase in humidity of the substrate. Further response is attributed to fungi sensing malt extract as a chemo-attractant and a source of nutrients. The onset of the response is characterised by low frequency trains of spikes (Fig. 2(b)). There are 3–4 spikes, with amplitude over 2 mV, in each train. Average distance between spikes in each train is 291 s, $\sigma = 90$, average spike width is 273 s, $\sigma = 110$, average spike amplitude 2.6 mV, $\sigma = 0.15$. Average duration of a train is 31 min, $\sigma = 3$, a distance is up to one hour. Typically, a frequency of spike trains increases with time, a distance between trains decreases to 15 min in average, $\sigma = 5$ (Fig. 2(c)). Average amplitude of spike trains is 4.6 mV, $\sigma = 2.5$.

Results of experiments with malt extract echo in the experiments with application of dextrose (Fig. 2(d)). The fungi show low frequency oscillatory activity before stimulation: average distance between spikes is 197 min, $\sigma = 13.9$, average amplitude 0.3 mV, $\sigma = 0.2$. In first 5 h after the dextrose application the frequency of spikes substantially increases: average distance between spikes becomes 22 min, $\sigma = 13$ and amplitude increases to average 0.43 mV, $\sigma = 0.27$. In next 5 h average amplitude of spikes increases to 1.3 mV, $\sigma = 0.35$, and distance between spikes 20 min, $\sigma = 7$.

To assess a response to chemo-attractants we used ethanol. We applied 1 ml of 96 % ethanol on the colonised fabric near loci of Ch5. The response on one of the channel close to the application loci is shown in Fig. 2(e). We observed a drop by nearly 8 mV followed by further drop of the electrical potential by nearly 8 mV. The time to the peak of the response is c. 7 s. The drop in potential followed by repolarisation phase, which lasted c. 14 s. The potential remained c. 11 mV lower than that before stimulation. The response on channels further from the application loci is less pronounced, as seen in Fig. 2(f). The spikes of electrical potential recorded on the channels have the following amplitudes: 0.65 mV on Ch1, 0.34 mV on Ch3, 0.31 mV on Ch7, 0.5 mV on Ch11, and 0.3 mV on Ch13, where Ch1 is the closest to the application loci and Ch13 is the farthest one.

To uncover the fungal wearable's response to stretching we attached 50 g and 200 g weights to the bottom part of the fabric colonised by the fungus. A typical response to the application of 50 g weight is shown in Fig. 3(a). The response duration is 97 s in average, $\sigma = 37$ s with average response amplitudes is 1.3 mV, $\sigma = 0.74$ mV. Differential electrode pairs, labelled as channels in Fig. 3(a) have been arranged in a line from the top to the bottom (Fig. 1(c)), with Ch1 being closest to the top of the fabric and Ch13 to the bottom part. Most of the response spikes show action potential like depolarisation, repolarisation and hyperpolarisation phases. Ch1 and Ch13 show hyperpolarisation phases set up at higher, compared to that before stimulation, base potential.

On application of 200 g weight to lower part of the fabric, variety of response from differential electrodes pairs have been recorded. An exemplar response is shown in Fig. 3(b). The response has an average duration 38 min, $\sigma = 2$ min, and average amplitude 1.56 mV, $\sigma = 1.24$ mV. The response in the example consists of two trains of high ('high' in the frameworks of fungal temporal activity) frequency spikes. Average spike width is 80 s ($\sigma = 50$), average amplitude 0.31 mV ($\sigma = 0.32$), average distance between spike in each train is 71 s ($\sigma = 47$ s).

Overall reaction to the removal of the stretching stimuli is in the drift of the base potentials on electrodes towards zero, e.g. in Fig. 3(c) we see that the average based potential is -1.17 mV, $\sigma = 2$ mV, before stimulation was removed, and -0.8 mV, $\sigma = 1.3$ mV, after the weight was removed. A typical response, to removal of 200 g, recorded on a single Ch is shown in Fig. 3(d). The spike there has a duration of 9 s and amplitude 11 mV.

4. Discussion

We demonstrated that a fabric colonised by the fungus *P. ostreatus* shows distinctive sets of responses to chemical and mechanical stimulation. The response to 50 g load, Fig. 3(a), is in the range of c. 1.5 min which might indicate that rather purely electro-mechanical events take place than reactions involving propagation of calcium waves (Tuteja and Mahajan, 2007). A difference d between timing of the response spikes peaks at the electrodes pairs in the line is as follows: d(Ch1, Ch3) = 3.6 s, d(Ch1, Ch5) = 20 s, d(Ch1, Ch7) = 16 s, d(Ch1, Ch13) = 3 s. This might indicate that the mycelium networks closer to the fixed end (Ch1) and the end where the load is attached (Ch13) react to the stretching first, the reaction then propagates further into the interior parts of the fabric, thus delayed reactions are recorded on the channels Ch5 and Ch7.

The response to stimulation with ethanol is in a range of 7 s. This would rather indicate physico-chemical damages to hyphae walls and corresponding electrical responses. Would amplitude of a response spike reflect a distance to the stimulation loci? As seen in Fig. 2(f), on most channel the response amplitudes slightly decrease with increasing distance to the stimulation loci however more studies are required to give a certain answer. The response on the channels remote to the stimulation loci happens at the same time, as on the channel in proximity of the stimulation loci. This indicates that the response might be purely electrical (due to damage to cell walls impulse) and not due to diffusion in the fabric or volatile ethanol.

The increase of frequency of electrical potential oscillation in a response to application of chemo-attractants or nutrients is consistent with previous studies, where intracellular electrical potential of stimulated fungi was measured (Olsson and Hansson, 1995). Even if in the

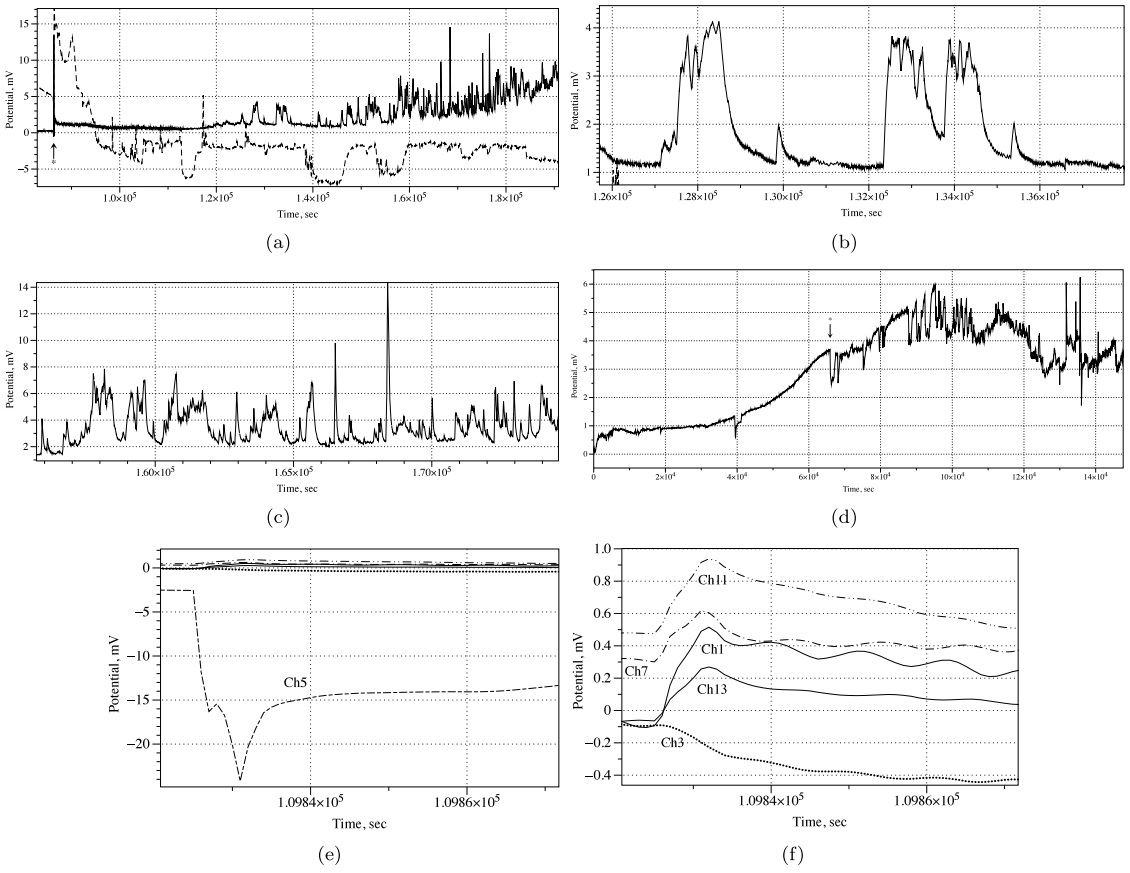


Fig. 2. (a) Response to application of malt extract. The moment of malt extract application is shown by asterisk. (b) Low frequency trains of spikes. (c) High frequency trains of spikes. (d) Response to application of dextrose. The moment of malt extract application is shown by asterisk. (ef) Response to stimulation with ethanol. An overall response is shown in (e) with some channels zoomed in (f).

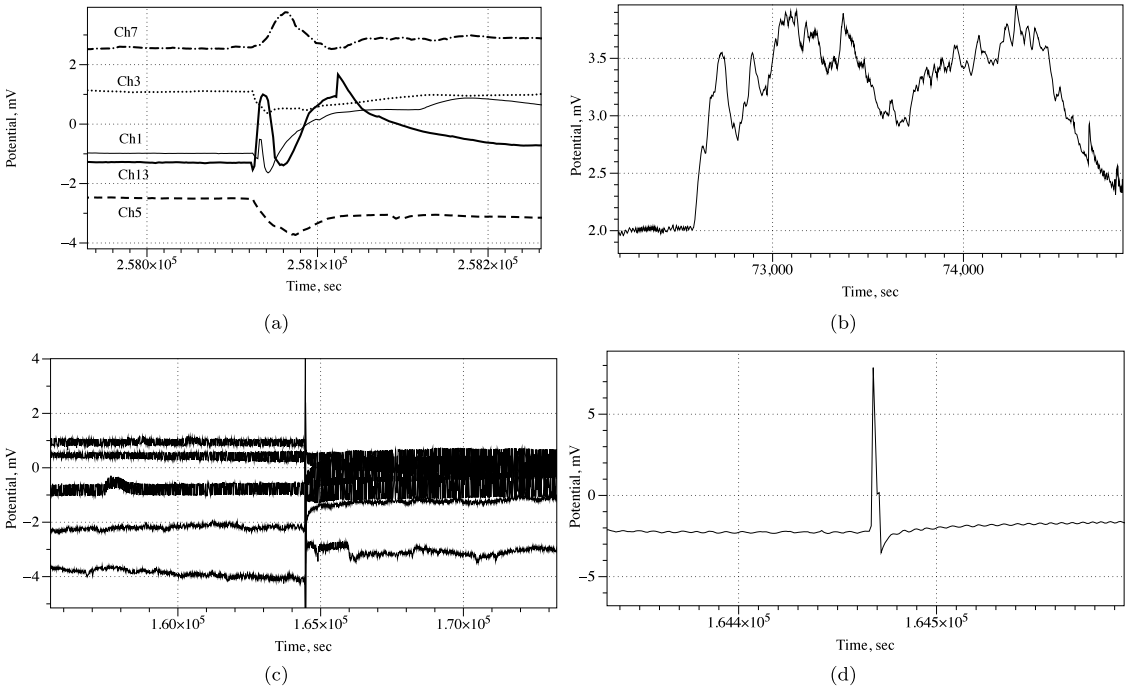


Fig. 3. Fungal wearable's response to stretching. (a) An exemplar response to stretching of the fabric by attaching 50 g weight to it. (b) Response to removal of 200 g weight recorded from five pairs of differential electrodes. (c) An exemplar response to removal of the weight recorded on one pair of differential electrodes. (d) Typical response to removal of 200 g weight, recorded on a one pair of differential electrodes.

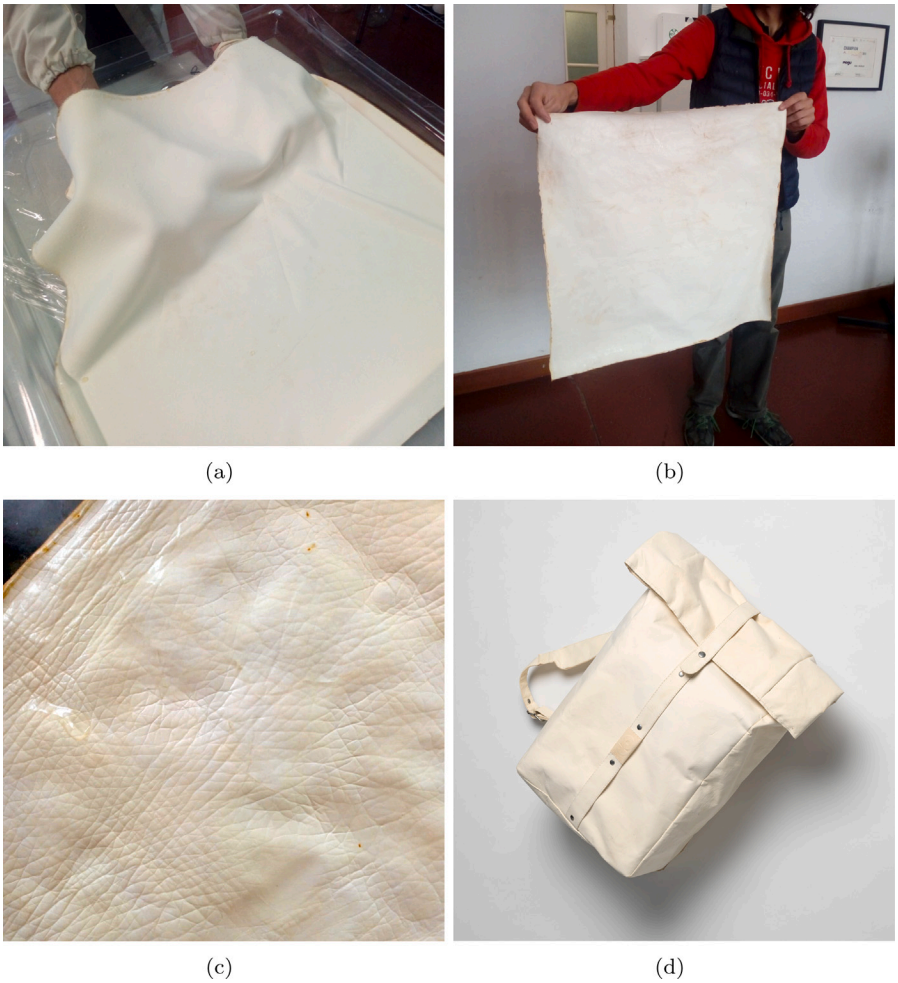


Fig. 4. Example of pure fungal flexible materials grown by Mogu S.rl. and branded as PURA Flex™. (a) Harvesting of a fungal skin, (b) size comparison with a human being, (c) texture detail resembling animal skin and (d) backpack prototype made with PURA Flex™ material.

case of malt extract solution increased spiking could be attributed to a water the experiments with dextrose, which was applied dry, show that the spiking shown increased frequency, and often amplitude, due to reaction to a chemoattractant or nutrient. The increase in amplitude of spiking five hours after the application of malt or dextrose might be due to the fungus ingesting the nutrients and transposing them across the wide mycelial network.

In laboratory conditions the fungal wearables survive for several months being kept in high humidity conditions. For practical future applications of the fungal wearables, preserving the moisture is fundamental. For example, the fragments of fungal materials could be coated with a breathable bioplastic.

Future developments in the field of fungal wearables may be along the following directions.

First direction is a computational one. We demonstrate in computational models that a fungal colony can implement a range of Boolean function (Adamatzky et al., 2020b). It might be possible to implement an experimental mapping between a set of stimuli and distribution of Boolean gates implemented by fungal wearables, as we demonstrated on sensing and computing organic liquid skin (Chiolerio and Adamatzky, 2020). In other words, in a response to a particular stimuli the fungal wearable will generate a unique set of Boolean function.

Second direction is in development of a large scale fabric made purely from mycelium — fungal skin (Fig. 4) and tailoring the fabric into wearables. Such mycelial tissue can be prepared using trimitic polypore fungal cultures, which are apparently preferred for the production of sturdy fungal skins, such as fungal leather or *mycoleather* (Jones et al., 2020). More specifically, a fungal fabric can be prepared by pouring a homogenised slurry of a liquid culture of *Ganoderma resinaceum* into a static fermentation tray and incubated for two weeks to allow the fungal hyphae to intermesh, forming a floating mat or skin (Adamatzky et al., 2020a). Examples of such type of fungal fabrics are shown in Fig. 4.

Third direction would be to culture fungi directly onto the pieces of clothing (Fig. 5(a)). This will allow us to achieve full response cloths and garments.

Fourth direction in the development of fungal wearables could be in using fungal hyphae (Fig. 5(b)) as wires and programmable (with e.g. light) resistor or electrically activated resistive switching devices in hybrid architectures incorporating conventional flexible electronics (Rajan et al., 2017) and live fungi. Routing the direction of the fungal wires can be done by arranging sources of attractants and repellents. Isolation of fungal wires, as well as localised connections when ordered arrays like the cross-bar array arrangement are required, could be done using inorganic materials, such as metal oxides of the proper work function deposited by means of atomic layer deposition (Porro et al., 2016), or digitally printed over a large scale, also in case of uneven surfaces (Bevione and Chiolerio, 2021).



(a) (b)

Fig. 5. (a) Part of the hemp glove colonised by fungus is visible in reflected light. (b) Stands of hyphae on the hemp fabric.

Declaration of competing interest

The authors declare that they have no known competing financial interests or personal relationships that could have appeared to influence the work reported in this paper.

Acknowledgement

This project has received funding from the European Union's Horizon 2020 research and innovation programme FET OPEN "Challenging current thinking" under grant agreement No 858132.

References

Adamatzky, A., 2013a. Slime mould tactile sensor. Sensors Actuators B 188, 38–44.
Adamatzky, A., 2013b. Towards slime mould colour sensor: Recognition of colours by Physarum Polycephalum. Org. Electron. 14 (12), 3355–3361.
Adamatzky, A., 2018. On spiking behaviour of oyster fungi Pleurotus djamor. Sci. Rep. 8 (1), 1–7.
Adamatzky, A., Ayres, P., Belotti, G., Wösten, H., 2019. Fungal architecture position paper. Int. J. Unconv. Comput. 14.
Adamatzky, A., Gandia, A., Chiolerio, A., 2020a. Fungal sensing skin. arXiv preprint arXiv:2008.09814.
Adamatzky, A., Tegelaar, M., Wosten, H.A., Powell, A.L., Beasley, A.E., Mayne, R., 2020b. On boolean gates in fungal colony. Biosystems 104138.
Appels, F.V., Camere, S., Montalti, M., Karana, E., Jansen, K.M., Dijksterhuis, J., Krijgsheld, P., Wösten, H.A., 2019. Fabrication factors influencing mechanical, moisture-and water-related properties of mycelium-based composites. Mater. Des. 161, 64–71.
Bahn, Y.-S., Mühlschlegel, F.A., 2006. CO_2 sensing in fungi and beyond. Curr. Opin. Microbiol. 9 (6), 572–578.
Bahn, Y.-S., Xue, C., Idnurm, A., Rutherford, J.C., Heitman, J., Cardenas, M.E., 2007. Sensing the environment: lessons from fungi. Nat. Rev. Microbiol. 5 (1), 57.
Baurley, S., 2004. Interactive and experiential design in smart textile products and applications. Pers. Ubiquitous Comput. 8, 274–281.
Beasley, A.E., Powell, A.L., Adamatzky, A., 2020. Fungal photosensors. arXiv preprint arXiv:2003.07825.
Bevione, M., Chiolerio, A., 2021. Benchmarking of inkjet printing methods for combined throughput and performance. Adv. Energy Mater. http://dx.doi.org/10.1002/adem.202000679.
Black, S., 2007. Trends in smart medical textiles. In: Smart Textiles for Medicine and Healthcare: Materials, Systems and Applications. University of Ghent, pp. 10–22.
Chase, J., Ross, P., Wenner, N., Morris, W., 2019. Fungal Composites Comprising Mycelium and an Embedded Material. Google Patents, US Patent App. 16/453, 791.
Chiolerio, A., Adamatzky, A., 2020. Tactile sensing and computing on a random network of conducting fluid channels. Flexible Print. Electron..
Coosemans, J., Hermans, B., Puers, R., 2003. Integrating wireless ECG monitoring in textiles. Sensors Actuators A 130, 48–53.
Coyle, S., Lau, K.-T., Moyna, N., O'Gorman, D., Diamond, D., Di Francesco, F., Costanzo, D., Salvo, P., Trivella, M., De Rossi, D., 2010. Flexible temperature sensors on fibers. IEEE Trans. Inf. Technol. Biomed. 14, 364–370.
Custodio, V., Herrera, F., López, G., Moreno, J., 2012. A review on architectures and communications technologies for wearable health-monitoring systems. Sensors 12, 13907–13946.
Dahmen, J., 2017. Soft futures: mushrooms and regenerative design. J. Archit. Educ. 71 (1), 57–64.
Dehshibi, M.M., Adamatzky, A., 2020. Electrical activity of fungi: Spikes detection and complexity analysis. arXiv preprint arXiv:2008.10276.
Del Dottore, E., Sadeghi, A., Mondini, A., Mattoli, V., Mazzolai, B., 2018. Toward growing robots: a historical evolution from cellular to plant-inspired robotics. Front. Robot. AI 5, 16.
Fomina, M., Ritz, K., Gadd, G.M., 2000. Negative fungal chemotropism to toxic metals. FEMS Microbiol. Lett. 193 (2), 207–211.
Haneef, M., Ceseracciu, L., Canale, C., Bayer, I.S., Heredia-Guerrero, J.A., Athanassiou, A., 2017. Advanced materials from fungal mycelium: fabrication and tuning of physical properties. Sci. Rep. 7 (1), 1–11.
Howitz, K.T., Sinclair, D.A., 2008. Xenohormesis: sensing the chemical cues of other species. Cell 133 (3), 387–391.
Islam, M., Tudryn, G., Bucinell, R., Schadler, L., Picu, R., 2017. Morphology and mechanics of fungal mycelium. Sci. Rep. 7 (1), 1–12.
Jones, M., Gandia, A., John, S., Bismarck, A., 2020. Leather-like material biofabrication using fungi. In: Nature Sustainability. Nature Research, pp. 1–8. http://dx.doi.org/10.1038/s41893-020-00606-1, URL https://www.nature.com/articles/s41893-020-00606-1.
Kung, C., 2005. A possible unifying principle for mechanosensation. Nature 436 (7051), 647.
Langereis, G., Bouwstra, S., Chen, W., 2012. Sensors, actuators and computing architecture systems for smart textiles. In: Smart Textiles for Protection, 7th Woodhead Publishing, pp. 190–213.
Löfhede, J., Martinez, S., Thordstein, M., 2010. Soft textile electrodes for EEG monitoring. In: Proceedings of 2010 the 10th IEEE International Conference on Information Technology and Applications in Biomedicine. ITAB, IEEE, pp. 1–4.
Mazzolai, B., 2017. Plant-inspired growing robots. In: Soft Robotics: Trends, Applications and Challenges. Springer, pp. 57–63.
Meyer, V., Basenko, E.Y., Benz, J.P., Braus, G.H., Caddick, M.X., Csukai, M., de Vries, R.P., Endy, D., Frisvad, J.C., Gunde-Cimerman, N., et al., 2020. Growing a circular economy with fungal biotechnology: a white paper. Fungal Biol. Biotechnol. 7, 1–23.
Meyer, J., Lukowicz, P., Tröster, G., 2006. Textile pressure sensor for muscle activity and motion detection. In: Proceeding of the 10th IEEE International Symposium on Wearable Computers. IEEE, pp. 11–14.

Olsson, S., Hansson, B., 1995. Action potential-like activity found in fungal mycelia is sensitive to stimulation. Naturwissenschaften 82 (1), 30–31.

Omenetto, F., Kaplan, D., Amsden, J., Dal Negro, L., 2013. Silk based biophotonic sensors. arXiv:2013.0330710.

Porro, S., Jasmin, A., Bejtka, K., Conti, D., Perrone, D., Guastella, S., Pirri, C., Chiolerio, A., Ricciardi, C., 2016. Low-temperature atomic layer deposition of TiO_2thin layers for the processing of memristive devices. J. Vac. Sci. Technol. A 34, 01A147.

Rajan, K., Bocchini, S., Chiappone, A., Roppolo, I., Perrone, D., Castellino, M., Bejtka, K., Lorusso, M., Ricciardi, C., Pirri, C., Chiolerio, A., 2017. WORM and bipolar inkjet printed resistive switching devices based on silver nanocomposites. Flexible Print. Electron. 2, 024002.

Rajan, K., Garofalo, E., Chiolerio, A., 2018. Wearable intrinsically soft, stretchable, flexible devices for memories and computing. Sensors 18 (2), 367.

Ross, P., 2018. Method for Producing Fungus Structures. Google Patents, US Patent 9, 951, 307.

Sadeghi, A., Del Dottore, E., Mondini, A., Mazzolai, B., 2020. Passive morphological adaptation for obstacle avoidance in a self-growing robot produced by additive manufacturing. Soft Robot. 7 (1), 85–94.

Sadeghi, A., Mondini, A., Mazzolai, B., 2017. Toward self-growing soft robots inspired by plant roots and based on additive manufacturing technologies. Soft Robot. 4 (3), 211–223.

Scalisi, R., Paleari, M., Favetto, A., Stoppa, M., Ariano, P., Pandolfi, P., Chiolerio, A., 2015. Inkjet printed flexible electrodes for surface electromyography. Org. Electron. 18, 89–94.

Schubert, T., Markert, M., Dreßler, M., Adamatzky, A., 2015. Bodymetries. Mapping the human body through amorphous intelligence. In: Experiencing the Unconventional: Science in Art. World Scientific, pp. 315–327.

Sibinski, M., Jakubowska, M., Sloma, M., 2010. Flexible temperature sensors on fibers. Sensors 10, 7934–7946.

Stoppa, M., Chiolerio, A., 2014. Wearable electronics and smart textiles: A critical review. Sensors 14, 11957–11992.

Travaglini, S., Dharan, C., Ross, P., 2016. Manufacturing of mycology composites. In: Proceedings of the American Society for Composites: Thirty-First Technical Conference.

Tuteja, N., Mahajan, S., 2007. Calcium signaling network in plants: an overview. Plant Signaling Behav. 2 (2), 79–85.

Van Aarle, I.M., Olsson, P.A., Söderström, B., 2002. Arbuscular mycorrhizal fungi respond to the substrate pH of their extraradical mycelium by altered growth and root colonization. New Phytol. 155 (1), 173–182.

Vatansever, D., Siores, E., Hadimani, R., Shah, T., 2011. Smart Woven Fabrics in Renewable Energy Generation. InTech, pp. 23–38.

Whiting, J.G., de Lacy Costello, B.P., Adamatzky, A., 2014. Towards slime mould chemical sensor: Mapping chemical inputs onto electrical potential dynamics of Physarum Polycephalum. Sensors Actuators B 191, 844–853.

Zadeh, E., 2006. Flexible biochemical sensor array for laboratory-on-chip applications. In: Proceeding of the International Workshop on Computer Architecture for Machine Perception and Sensing. pp. 65–66.

ACS Biomaterials SCIENCE & ENGINEERING

pubs.acs.org/journal/abseba

Article

Stimulating Fungi *Pleurotus ostreatus* with Hydrocortisone

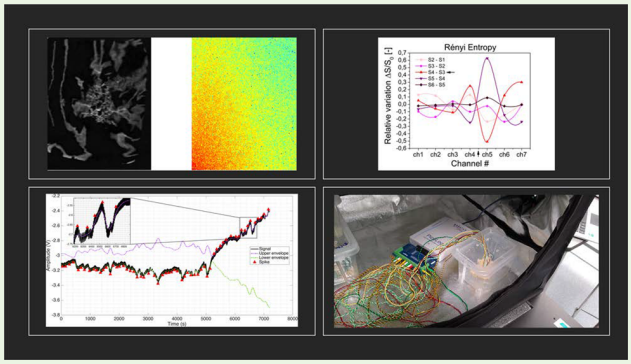
Mohammad Mahdi Dehshibi,* Alessandro Chiolerio, Anna Nikolaidou, Richard Mayne, Antoni Gandia, Mona Ashtari-Majlan, and Andrew Adamatzky*

Cite This: https://doi.org/10.1021/acsbiomaterials.1c00752

Read Online

ACCESS | Metrics & More | Article Recommendations

ABSTRACT: Fungi cells can sense extracellular signals via reception, transduction, and response mechanisms, allowing them to communicate with their host and adapt to their environment. They feature effective regulatory protein expressions that enhance and regulate their response and adaptation to various triggers such as stress, hormones, physical stimuli such as light, and host factors. In our recent studies, we have shown that *Pleurotus* oyster fungi generate electrical potential impulses in the form of spike events in response to their exposure to environmental, mechanical, and chemical triggers, suggesting that the nature of stimuli may be deduced from the fungal electrical responses. In this study, we explored the communication protocols of fungi as reporters of human chemical secretions such as hormones, addressing whether fungi can sense human signals. We exposed *Pleurotus* oyster fungi to hydrocortisone, which was directly applied to the surface of a fungal-colonized hemp shavings substrate, and recorded the electrical activity of the fungi. Hydrocortisone is a medicinal hormone replacement that is similar to the natural stress hormone cortisol. Changes in cortisol levels released by the body indicate the presence of disease and can have a detrimental effect on physiological process regulation. The response of fungi to hydrocortisone was also explored further using X-rays to reveal changes in the fungi tissue, where receiving hydrocortisone by the substrate can inhibit the flow of calcium and, as a result, reduce its physiological changes. This research could open the way for future studies on adaptive fungal wearables capable of detecting human physiological states and biosensors built of living fungi.



KEYWORDS: *fungi, hydrocortisone, biosensor, electrical activity*

Downloaded via Mohammad Mahdi Dehshibi on July 26, 2021 at 15:19:18 (UTC).
See https://pubs.acs.org/sharingguidelines for options on how to legitimately share published articles.

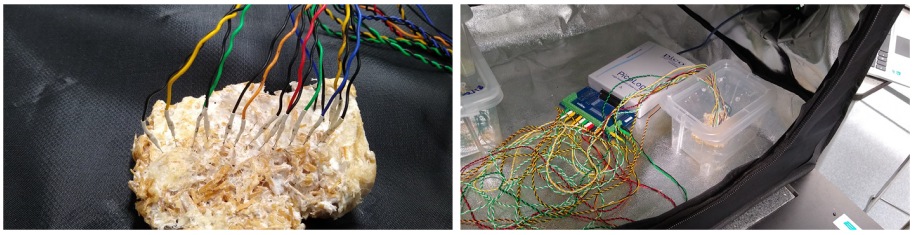
1. INTRODUCTION

All living organisms have evolved elaborate communication processes and mechanisms to sense, respond, and adapt to the surrounding environment in order to survive. These processes take place through reception, transduction, and response systems, which enable them to sense and adapt to their surroundings in response to a variety of cues such as nutrients, light, gases, stress, and host factors. Any form of communication requires the existence of three essential elements: a sender, a message, and a receiver. The process begins with a sender releasing a message and ends with a receiver understanding the message.[1] Fungi are composed of eukaryotic cells that report, react, and adapt to external stimuli primarily through signal transduction pathways.[2] They have extracellular and intracellular sensing mechanisms, as well as protein receptors that enable them to detect and respond to a variety of signals. *Pleurotus ostreatus*, a basidiomycete fungi, has effective regulatory protein expression that enhances its adaptation to stress triggers.[3]

In our previous studies, we reported that the oyster fungi *Pleurotus djamor* exhibit trains of electrical potential spikes similar to action potential spikes.[4−7] Our initial assumption was that spike trains might reflect increasing mycelium propagation in the substrate, nutrient and metabolite transport, and communication processes within the mycelium network. We investigated the information−theoretic complexity of fungal electrical activity[8−10] to pave the way for additional investigation into sensorial fusion and fungi decision making.[11−13] Later, in a series of laboratory experiments,[14,15] we demonstrated that fungal electrical activity patterns, specifically mycelium bound hemp composite, change in response to stimuli such as light, mechanical stretching, and attractants and repellents. Our findings demonstrated that fungi are a promising candidate for producing sustainable textiles for use as eco-friendly biowearables.

Received: June 7, 2021
Accepted: July 12, 2021

ACS Publications © XXXX American Chemical Society



(a) (b)

Figure 1. Experimental setup. (a) Exemplar locations of electrodes. (b) Electrode pairs and logging setup in the tent.

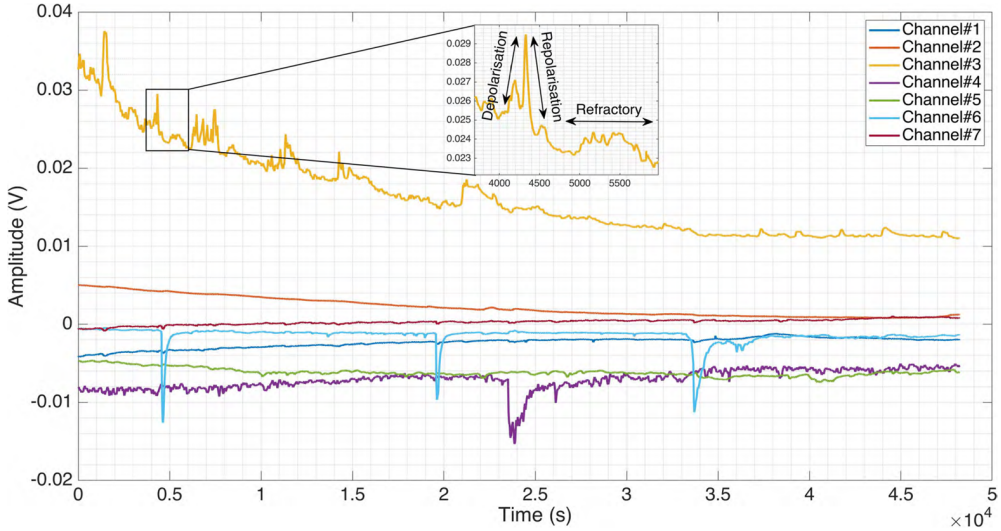


Figure 2. Example of electrical activity observed in seven channels of colonized hemp mats with fungi over 13.3 h. The insets are zoomed in on one channel to display a spike event with "depolarization", "repolarization", and "refractory" cycles. This spike has a duration of 2258 s and a refractory time of 1426 s. The rates of depolarization and repolarization are 54.85 and 45.75 μV/s, respectively.

We present an illustrative wide-ranging study in which we investigate the short- and long-term dynamics in mycelium of the oyster fungi *Pleurotus ostreatus* in response to stimulation with hydrocortisone. The purpose of this study is to encourage the scientific community to address the issue of fungi being able to sense animal hormones. The human body's adrenal glands release hormones such as cortisol and adrenaline. Cortisol levels in various bodily fluids can range from 4 to 70 pM.[16,17] Sweat cortisol levels have a strong correlation with salivary cortisol concentrations,[18] and the optimal cortisol level ranges from 0.02 to 0.5 M.[16,17] Monitoring cortisol levels in bodily fluids, which can be altered by chronic stress and disease, is critical for maintaining healthy physiological conditions. For this study, not only are the electrical activities investigated, but the substrate is also irradiated with an X-ray beam from multiple angles to produce cross-sectional images of the substrate.[19] This multimodal approach enables us to identify and track the dynamics of changes in the tissue of the mycelium anatomy.

We demonstrated that fungi's electrical responses and reconstructed computed tomography images can be used to detect the presence of stimuli. The findings could lead to the development of biosensing patches for use in organic electronics and bioelectronics, especially with living substrates, which offer a great opportunity to integrate natural systems' parallel sensing and information processing capabilities into future and emerging wearables.

The rest of this paper is structured as follows. Section 2 presents the experimental setup and details of the analysis. Experimental results are discussed in section 3. The discussion is given in section 4. Finally, the paper is concluded in section 5.

2. METHODS

2.1. Experimental Setup. A commercial strain of the fungus *Pleurotus ostreatus* (Mogu's collection code 21-18), preselected for showing superior fitness growth on different lignocellulosic substrates, was cultured on sterilized hemp shives contained in plastic boxes ca. 35 × 20 cm^2 in darkness at ambient room temperature ca. 22 °C. Particles of substrate well-colonized by the fungus were spread on rectangular fragments, ca. 12 ×12 cm^2, of moisturized nonwoven hemp fiber mats. When the mats were properly colonized, as visually confirmed by white and homogeneous mycelial growth on the surface, these were used in the experiments. The humidity of the hemp mats ranged from 70% to 80% (MerlinLaser Protimeter, U.K.). The experiments were carried out in a room with an ambient temperature of ca. 21 °C in the absence of light. It is worth mentioning that it takes approximately 25 days for the mats to be properly colonized, depending on the mat size, the ambient room temperature, and the lignocellulosic substrates chosen for the experiments. Figure 1 shows examples of the experimental setups.

Electrical activity of the colonized hemp mats was recorded using pairs of iridium-coated stainless steel subdermal needle electrodes (Spes Medica S.r.l., Italy) with twisted cables, via a high-resolution data logger with a 24-bit A/D converter, galvanic isolation, and software-selectable sample rates (Pico Technology, UK). The electrodes were placed in a straight line with a distance of 1−2 cm. To keep the electrodes stable, we put a polyurethane pad underneath

https://doi.org/10.1021/acsbiomaterials.1c00752
ACS Biomater. Sci. Eng. XXXX, XXX, XXX−XXX

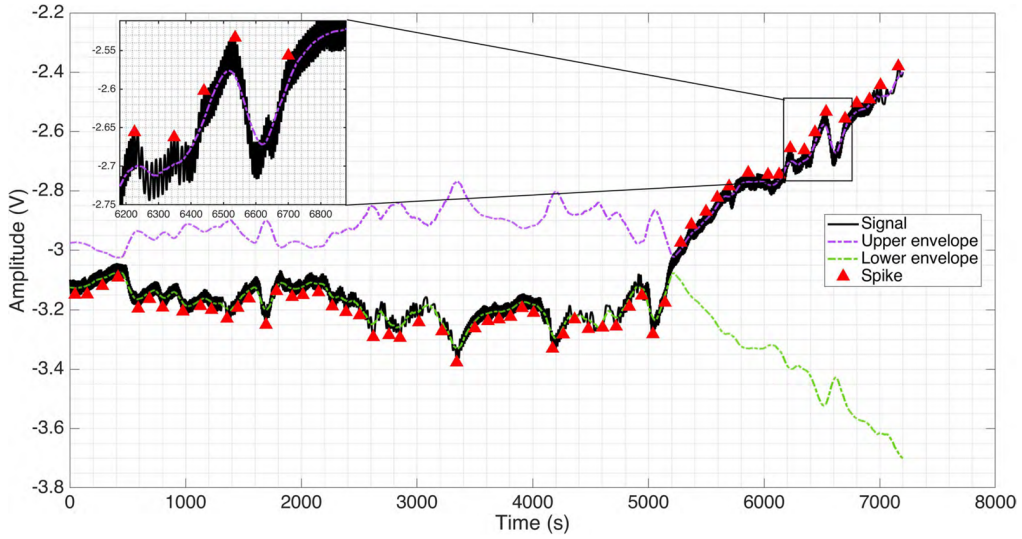


Figure 3. Construction of the intermediate representation of an input signal using eq 6, where the upper and lower envelopes are shown in violet and green dashed lines, respectively. We zoomed in on one chunk of electrical activity to highlight the identified spike events.

the fabric. As a result, the electrode pairs were inserted through the fabric and onto the polyurethane pad, as shown in Figure 1a.

In each trial, we recorded the electrical activity of seven electrode pairs simultaneously. Each pair of electrodes, termed a channel (Ch), reported a difference in the electrical potential between the electrodes. The electrical activity was recorded at a rate of one sample per second (1 Hz), with logging times ranging from 60.04 to 93.45 h for the different experiments. Throughout the recording, the logger took as many samples as it could (typically up to 600 per second) and saved the average value. We set the acquisition voltage range to 156 mV with an offset accuracy of 9 μV at 1 Hz to maintain a gain error of 0.1%. Each electrode pair was considered independently with a noise-free resolution of 17 bits and conversion time of 60 ms. We measured and logged a range of resistances 1−1.6 kΩ using a Fluke 8846A precision multimeter, with the test current being 1 ± 0.0013 μA, once per 10 s, 5×10^4 samples per trial.[7] Furthermore, the electrical resistance of the electrodes is always less than 10 Ω, making it minor in comparison to the resistance of the mycelium. Even employing pure gold electrodes would have no effect on the trials. Figure 1b shows one of the recording setups inside a light-proof growing tent.

For stimulation, we used hydrocortisone (Solu-Cortef trademark, 4 mL Act-O-Vial, Pfizer, Athens, Greece). We then applied 2 mL of the resulting solution to the surface of the colonized substrate in the loci surrounding Ch4 and Ch5.

The following was the rationale behind the dosage selection: human patients weighing 80 kg are typically given 20 mg of synthetic cortisol per day for a variety of diseases, such as maintenance therapy for patients with hypopituitarism. As a result, 20 mg divided by 80 kg yields 0.25 mg/kg. Hemp mats colonized with fungi weighed around 100−200 g each, so a 2 mL dose of 250 μg was needed.

2.2. Electrical Activity Analysis. Extracellular signals which surpassed a certain amplitude threshold with depolarization, repolarization, and refractory cycles are referred to as spike events (see Figure 2). Spike events represent the physiological and morphological processes of mycelium in the colonized hemp mat. We proposed a novel method for identifying spiking events, including three main stages: (1) splitting signal into chunks, (2) smoothing the chunk by mapping the constant amplitude to an instantaneous amplitude, and (3) detecting spike events.

Assume $\mathcal{X} = \{(t_i, x_i)\}_{i=1}^{\mathbb{C}}$ is a recording set of $\mathbb{C}$ channels with the entire length of T seconds and samplings rate of f_s Hz, where x defines the signal's sample value at time t, $1 \le t \le T$. Our objective is to detect the set of spike events $\mathcal{S} = \{s_1, s_2, ..., s_\eta\}$, where $\eta \ll T$. We segmented the signal $\mathcal{X}$ using the idea of the variable size sliding window to analyze its dynamics before and after hydrocortisone application in the same intervals. Each segment was then subdivided into chunks of $m = \{1, 2, 4, 8, 16\}$ hours. Note that the chunk $m = 16$ in all 16 experiments does not have the same length that resulted in 12−16 h of electrical activity recording.

The electrical activity of the colonized hemp mats with fungi displays diffraction patterns. The presence of these diffraction patterns from multiple slits can cause determining spike events to be distorted. The envelope of an oscillating signal can expand the concept of constant amplitude to instantaneous amplitude and, therefore, bypass multiple slits with a single slit diffraction pattern to outline significant extremes, i.e., spike events.[10]

To obtain the signal envelope (ξ), we used the discrete Fourier transform, as implemented in the Hilbert transform, to detect the analytical signal. Then, inspired by Marple et al.,[20] we set the negative frequency in half of each spectral period to zero, resulting in a periodic one-sided spectrum. More formally, using the sampling theorem,[21] we convert the input chunk,[a] $\mathcal{X}$, into a sequence of values with the sample period of $\tau \triangleq w\frac{T}{f_s}$ (see eq 1).

$$L[n] \triangleq \tau \cdot x(n\tau),\ 0 \le n \le N-1 \tag{1}$$

where N is an even number corresponding to the number of discrete-time analytical signal points. To obtain the N-point one-sided discrete-time analytic signal using the Hilbert transform,[20] we need to calculate the discrete-time Fourier transform of $L[n]$, with sampling at τ intervals to prevent aliasing (see eq 2). We take the second numerical signal derivation ($L = \frac{\partial^2 \mathcal{X}}{4\partial t^2}$) to highlight effective signal peaks and neutralize diffraction patterns.

$$F(\omega) = \tau \sum_{n=0}^{N-1} L[n] e^{-i2\pi\omega\tau n} \tag{2}$$

where $|\omega| \le \frac{1}{2\tau}$ Hz. To obtain a periodic one-sided spectrum ($Z[k]$), we set the negative frequency in half of each spectral period to zero and calculate the spectrum using eq 3.

$$Z[k] = \begin{cases} F[0], & \text{for } k = 0 \\ 2F[k], & \text{for } 1 \le k \le \frac{N}{2} - 1 \\ F\left[\frac{N}{2}\right], & \text{for } k = \frac{N}{2} \\ 0, & \text{for } \frac{N}{2} + 1 \le k \le N - 1 \end{cases} \tag{3}$$

https://doi.org/10.1021/acsbiomaterials.1c00752
ACS Biomater. Sci. Eng. XXXX, XXX, XXX−XXX

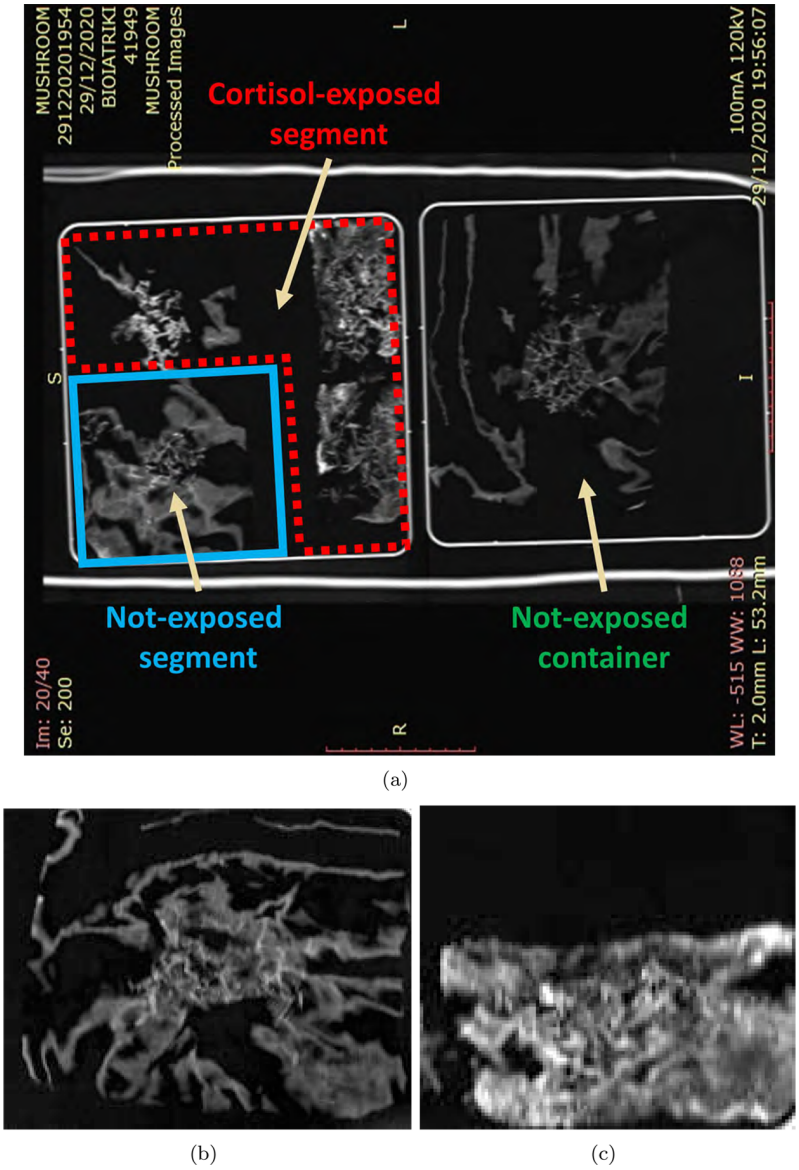


Figure 4. (a) CT image of two containers, with the substrate in the left container receiving hydrocortisone 2 h before being irradiated with the X-ray beam and the substrate in the right container receiving no stimulus. (b) The substrate segment in the left container that is not directly exposed to stimuli. (c) The cortisol-exposed segment of the substrate in the left container.

To obtain the envelope of the original signal $x(t)$, we need to calculate the inverse discrete-time Fourier transform of $F(\omega)$ and $Z[k]$ (see eq 4)

$$x_a[n] \triangleq \mathcal{F}^{-1}[F(\omega)], \quad z_a[n] \triangleq \mathcal{F}^{-1}[Z[k]] \tag{4}$$

where $\mathcal{F}^{-1}[\cdot]$ takes the inverse of the Fourier transform; x_a and z_a are the analytical signals, and $z_a[n] = \frac{1}{N_\tau}\sum_{k=0}^{N-1} Z[k]e^{i2\pi kn/N}$. By taking the root-mean-square value of the analytical signals as in eq 5, we can calculate ξ for the signal $\mathcal{X}$

$$e_a[n] = x_a[n] + jz_a[n],$$
$$\xi[n] = \sqrt{e_a[n] \times \overline{e}_a[n]} \tag{5}$$

where $\overline{e}_a$ is the complex conjugate of e_a and j refers to the imaginary part of the analytical signal. We construct an intermediate representation $(\tilde{x})$ of the input signal using the upper and lower envelopes to identify spike events. All amplitude values greater than or equal to the upper envelope and less than or equal to the lower envelope are replaced with the upper and lower envelope values, respectively, while all other amplitude values are preserved. Then, as in eq 6, we calculate the absolute differences between the input signal (x) and this intermediate representation $(\tilde{x})$

$$\tilde{x}[n] = \begin{cases} \xi_l[n], & x[n] \le \xi_l[n] \\ \xi_u[n], & x[n] \ge \xi_u[n] \\ x[n], & \text{otherwise} \end{cases}$$
$$\Phi[n] = |x[n] - \tilde{x}[n]| \tag{6}$$

where ξ_l and ξ_u are the lower and upper envelopes, respectively. We locate all local maxima (peaks) of the $\Phi[n]$ where the minimum peak prominence is γ. Here, γ is the 99% of confidence interval calculating using eq 7

$$\gamma = \bar{\Phi}[n] + z^* \frac{\sigma}{\sqrt{N}} \tag{7}$$

where $z^* = 2.576$,[22] and $\bar{\Phi}[n]$ and σ are the mean and standard deviation of $\Phi[n]$. The proposed spike detection algorithm has true-positive and false-positive rates of 76% and 16%, respectively,

https://doi.org/10.1021/acsbiomaterials.1c00752
ACS Biomater. Sci. Eng. XXXX, XXX, XXX−XXX

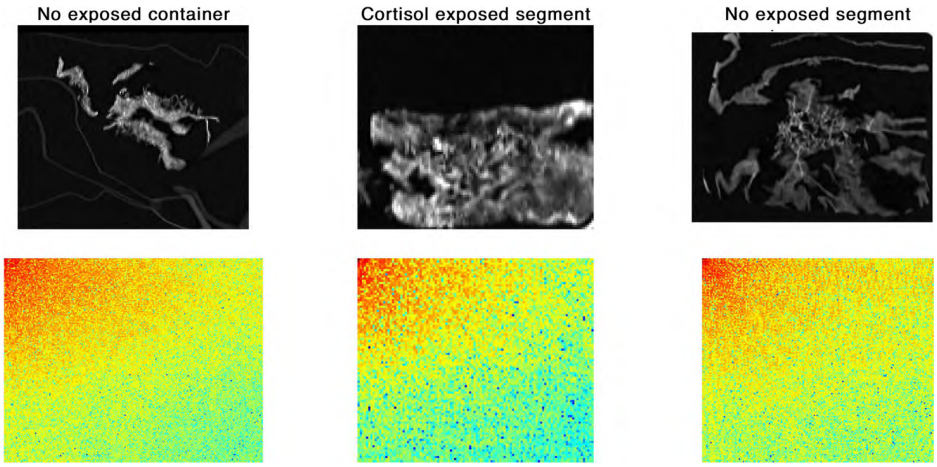


Figure 5. Results of applying DCT to CT images, where DCT expresses a finite sequence of data points as a sum of cosine functions oscillating at different frequencies. (a) On a nonexposed container, higher energies (red hue) are concentrated in the top left corner, while lower energies (green and blue hues) are concentrated in the bottom right corner. (b) The cortisol-exposed segment has a lower concentration of high energy in the top left corner and a higher dispersion of low energy (blue hue). (c) The no-exposed segment has a moderate energy distribution in comparison to the others, where the higher-energy spectral sub-bands are scattered rather than being concentrated in a few DCT coefficients.

implying that we missed 20% of the spike events. However, because this limitation applies to all trials, we report the amortized complexity analysis. Figure 3 shows an example of the proposed method's results.

2.3. CT Images Analysis. To gain a better understanding of the effect of stimuli on the fungal substrate, we prepared two containers. Two hours before being irradiated with an X-ray beam using the dual-energy Discovery City 750 HD CT scanner, one container received no stimuli, while the other received hydrocortisone. The detector provides for data acquisition with 64 detector rows of 0.625 mm collimation. Together with a z-flying focal spot, this allows simultaneous acquisition of data in 64 × 0.625 slices. The tubes were operated at 120 kVp. The gantry rotation time of the system is 0.35 s. CT images were reconstructed using Adaptive Statistical Iterative Reconstruction.[23] The image sets were reconstructed at a slice thickness of 1.25 mm, performing 128 slices per rotation (see Figure 4a). We used two different containers because the fungal colony retains its integrity through the flow of cytoplasm in the mycelium network, where calcium waves[24] and associated electrical potential waves change the propagation coordinate of this flow.

Therefore, we were able to analyze the stimuli spread across the flow of cytoplasm by comparing the CT image of the container that had not received any stimulus with the container that had only one segment exposed (see Figure 4b,c). When working with images in the spatial domain, we deal with changes in pixel values with respect to the scene. In the frequency domain, however, we are interested in the rate at which the pixel values in the spatial domain change, which provides us with a better understanding of the underlying distribution of changes and complexities. The discrete cosine transform (DCT) was used in this study (see eq 8) to transform the input CT image $I_{R\times C}$ from the spatial domain to the frequency domain, allowing us to divide the image into spectral sub-bands of varying significance. This transform can also concentrate the majority of the image's visually important details in just a few DCT coefficients. This property enables us to uncover changes in the substrate that are not apparent through visual inspection.

$$\mathrm{DCT}_{pq} = \alpha_p \alpha_q \sum_{r=0}^{R-1} \sum_{c=0}^{C-1} I_{rc} \cos\frac{\pi(2r+1)p}{2R} \cos\frac{\pi(2c+1)q}{2C},$$
$$\alpha_p = \begin{cases} 1/\sqrt{R} & p = 0 \\ \sqrt{2/R} & 1 \le p \le R-1 \end{cases} \quad \alpha_q = \begin{cases} 1/\sqrt{C} & q = 0 \\ \sqrt{2/C} & 1 \le q \le C-1 \end{cases} \tag{8}$$

where DCT_{pq} is the DCT coefficient in row p and column q of the DCT matrix; $I_{R\times C}$ is the intensity of the pixel in row R and column C. Figure 5 shows three examples of the results obtained by applying DCT to CT images.

2.4. Statistical and Information Theory Metrics. In statistics[25] and information theory,[26] the concept of entropy is essential. In statistics, entropy refers to the inference functional for an updating process, and in information theory, it specifies the shortest attainable encoding scheme. Recent advances in complex dynamical systems, on the other hand, have necessitated an extension of the entropy theory beyond the conventional Shannon−Gibbs entropy (H).[27] In this study, we used the Rényi (R_q)[28] and Tsallis (T_q)[29] additive entropy concepts, which are generalizations of the classical Shannon entropy. Regardless of the generalization, these two entropy measurements are used in conjunction with the principle of maximum entropy, with entropy's main application being in statistical estimation theory. Shannon, Tsallis, and Rényi entropy measurements are expressed as in eq 9.

$$H(\mathcal{S}) = -\sum_i p(s_i)\log p(s_i)$$
$$T_q(p_i) = \frac{k}{q-1}\left(1 - \sum_i p_i^q\right)$$
$$R_q(\mathcal{S}) = \frac{1}{1-q}\log\left(\sum_i p_i^q\right) \tag{9}$$

where $\mathcal{S}$ is a discrete random variable that represents spike events, with potential outcomes in the set $\mathcal{S} = \{s_1, s_2, ..., s_\eta\}$ and corresponding probabilities $p_i \doteq \Pr(\mathcal{S} = s_i)$ for $i = 1, ..., \eta$. p_i is a discrete set of probabilities with the condition $\sum_i p_i = 1$, and q is the *entropic-index* or Rényi entropy order with $q \ge 0$ and $q \ne 1$, which in our experiments was set to 2.

We take the logarithm to be in base 2, because we interpreted the entire recording duration T with bits, with "1s" indicating the availability of spike events and "0s" otherwise. To determine spike diversity across all channels, we represent recordings by a binary matrix with a row for each channel. We calculated the Lempel−Ziv complexity (LZc) over channels using the Kolmogorov complexity algorithm[30] to capture both temporal and spatial diversity. We then concatenated the rows of this binary matrix to form a single binary string and normalized LZc by dividing the raw value by the randomly shuffled value obtained for the same binary input sequence to obtain

https://doi.org/10.1021/acsbiomaterials.1c00752
ACS Biomater. Sci. Eng. XXXX, XXX, XXX−XXX

Table 1. Qualitative Description of Electrical Activity (1) 16 h before Hydrocortisone Exposure and (2) 1 h after Hydrocortisone Exposure

Ch no.	spike no.	length (s)	amplitude (V)	H(signal)	H(spike)	Γ	Δ	ϒ	Kolmogorov	PCIpK	T_q	R_q
16 h before the Trigger Event												
1	455	2.91	−1.20	−3.40	242.2	0.99	0.0078	3.07×10^4	0.055	3.86×10^{-03}	−3.230	−0.62
2	449	2.76	−0.32	−3.72	239.6	0.99	0.0077	3.07×10^4	0.052	3.64×10^{-03}	−2.498	−0.29
3	457	2.72	−0.02	−3.88	243.1	0.99	0.0079	3.06×10^4	0.053	3.66×10^{-03}	−0.001	12.52
4	449	3.40	−3.58	−3.74	239.6	0.99	0.0077	3.07×10^4	0.052	3.73×10^{-03}	−46.884	−3.70
5	460	2.23	1.18	−3.43	244.5	0.99	0.0079	3.06×10^4	0.055	3.64×10^{-03}	0.002	12.27
6	446	3.19	−1.09	−3.26	238.3	0.99	0.0077	3.08×10^4	0.052	3.69×10^{-03}	−6.544	−1.49
7	464	2.73	0.26	−3.58	246.2	0.99	0.0080	3.06×10^4	0.054	3.59×10^{-03}	0.102	4.30
1 h after the Trigger Event												
1	29	2.38	−1.08	−5.72	20.60	0.96	0.0080	2.55×10^3	0.062	0.048	−3.68	−0.78
2	28	2.97	−0.80	−5.49	20.01	0.96	0.0077	2.57×10^3	0.062	0.047	−1.93	0.04
3	30	2.52	−0.14	−5.38	21.18	0.96	0.0083	2.54×10^3	0.065	0.047	−0.12	4.43
4	27	3.15	−6.15	−5.56	19.41	0.96	0.0075	2.58×10^3	0.065	0.051	−47.67	−3.71
5	28	1.41	−0.22	−5.73	20.01	0.96	0.0077	2.57×10^3	0.062	0.045	−0.10	4.64
6	32	2.42	−2.43	−5.70	22.34	0.96	0.0088	2.51×10^3	0.075	0.049	−8.47	−1.79
7	29	2.03	0.25	−5.51	20.60	0.96	0.0080	2.55×10^3	0.068	0.050	0.23	1.83

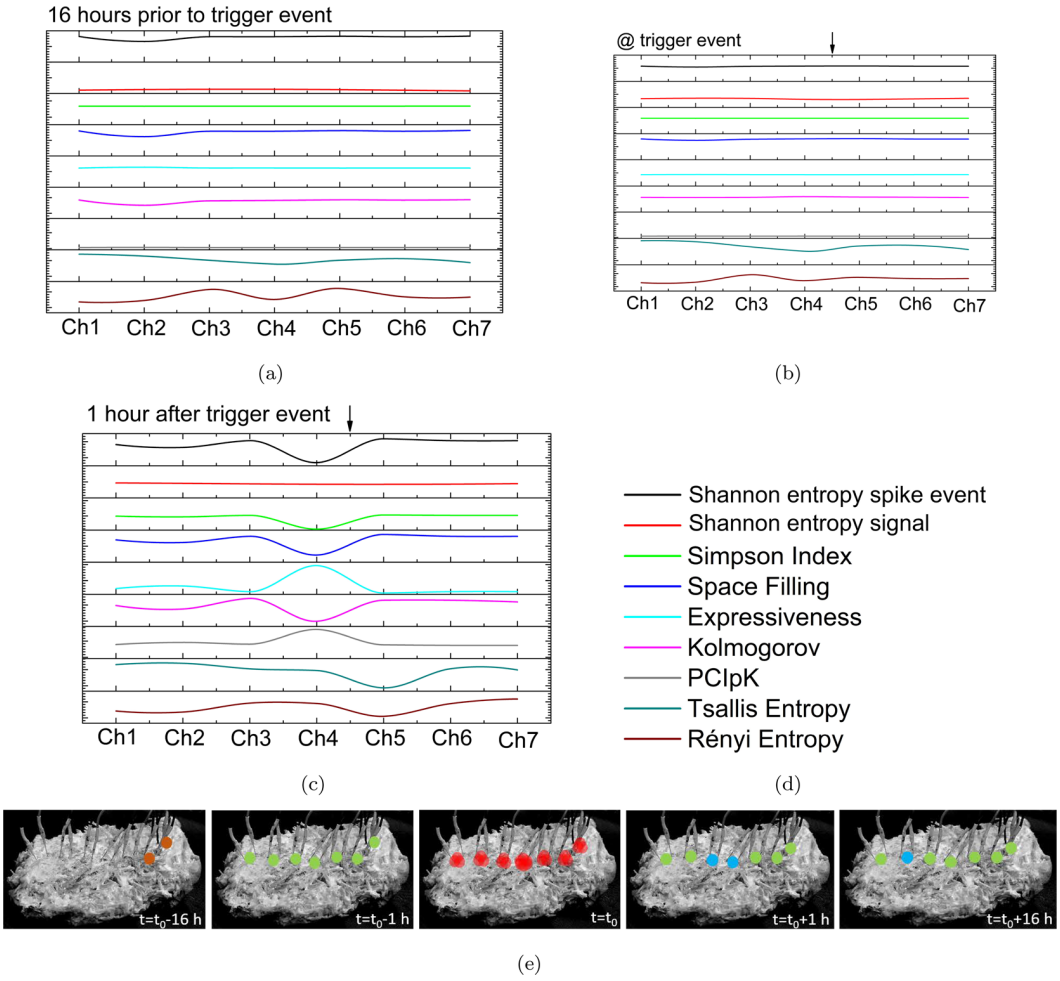


Figure 6. (a) Evolution related to a data segment recorded 16 h before hydrocortisone exposure. (b) Cortisol-exposed data segment (trigger event). (c) Evolution related to a data segment recorded 1 h after hydrocortisone exposure. (d) Merit figures of complexity measures performed on recorded potentials (legend). (e) Graphical representation of the living substrate with measurement electrodes and PCIpK complexity defined by a color code (light blue < −0.5; −0.5 < green < 0; 0 < orange < 0.5; red >0.5). In the inset, the reference time of each frame is specified.

PCIpK. Because the value of PCIpK for a fixed-length binary sequence is maximum when it is totally random, the normalized values reflect the degree of signal diversity on a scale of 0 to 1.

Other metrics that were used to quantify the complexity of spike events are Simpson's diversity, space-filling, and xpressiveness. Simpson's diversity is calculated as $\Gamma = \sum_i (p(s_i))^2$. For $H < 3$, it

https://doi.org/10.1021/acsbiomaterials.1c00752
ACS Biomater. Sci. Eng. XXXX, XXX, XXX−XXX

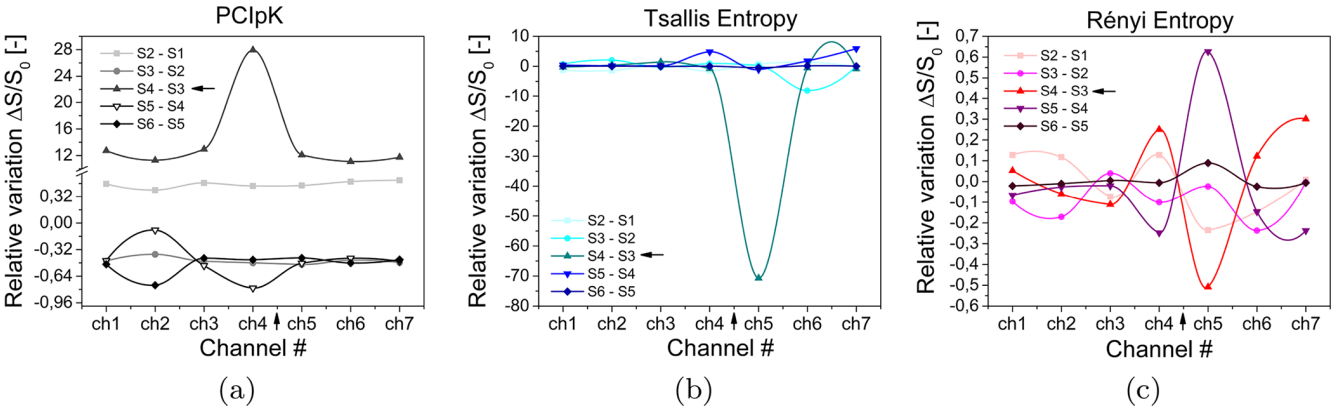


Figure 7. (a) PCIpK measured as a function of the measurement segments (which are time-dependent), with the arrows indicating both the spatial locus for hydrocortisone stimulation and the temporal segment corresponding to the trigger. The time interval used to compute the relative variance is denoted by $S(n + 1) - S(n)$. (b) Tsallis entropy. (c) Rényi entropy.

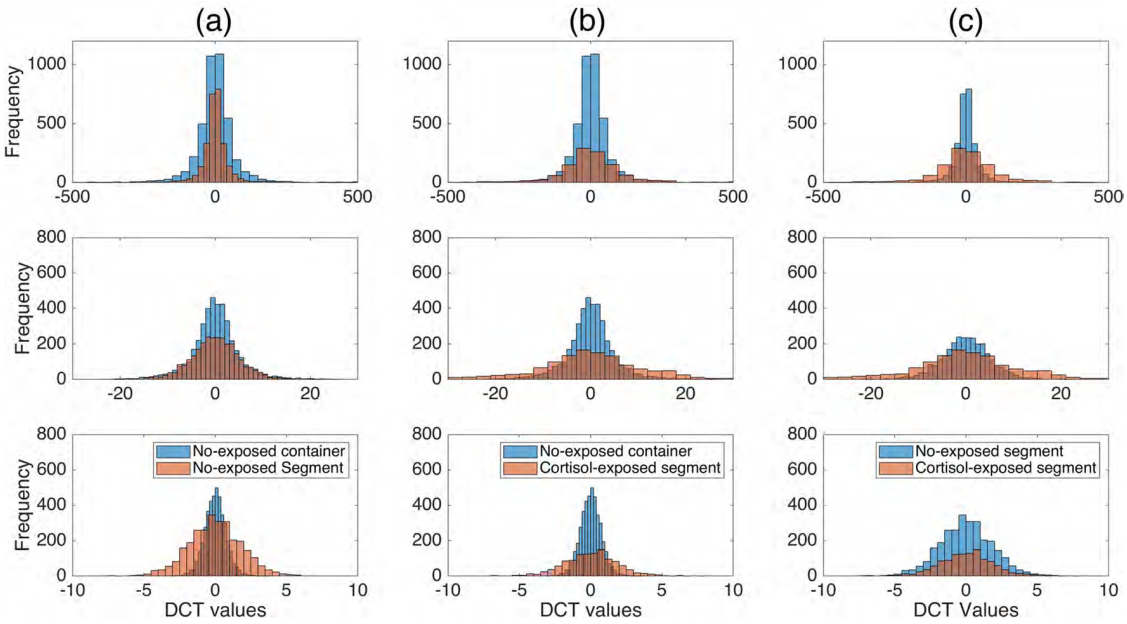


Figure 8. Comparison of the distribution of energy levels in the calculated DCT for (a) no-exposed container and no-exposed segment, (b) no-exposed container and cortisol-exposed segment, and (c) no-exposed segment and cortisol-exposed segment. The substrate that was not exposed to hydrocortisone had an energy frequency higher than that of the cortisol-exposed segment and the no-exposed segment adjacent to the cortisol-exposed segment.

correlates linearly with Shannon entropy, and the relationship becomes logarithmic for higher values of H. The value of Γ varies from 0 to 1, with 1 representing infinite diversity and 0 representing no diversity. Space-filling (Δ) is the ratio of nonzero entries in the binary representation of $\mathcal{X}$ to the total duration of the recording T. Expressiveness (Υ) is calculated as the Shannon entropy (H) divided by space-filling ratio (Δ), which represents the economy of diversity.

3. RESULTS

Table 1 presents a qualitative description of electrical activity for one of the trials, where all complexity metrics can be compared for the condition in which the substrate was exposed 16 h before hydrocortisone exposure and 1 h after hydrocortisone exposure.

Figure 6 graphically summarizes the qualitative description of electrical activity for all trials in a multicurve layout that can be used to easily identify those metrics that are more influenced by stimulation with hydrocortisone and can thus be used to track the impacts in electrical dynamics complexity. The different panels implicitly represent time, where Figure 6a refers to 16 h before exposure, Figure 6b to the exposure or trigger event, and Figure 6c to 1 h after exposure. The x-axis, where the channels are aligned, represents space. Those complexity metrics with no variation appear flat (for example, after trigger, the Shannon entropy for the signal; shown in red in the plots). Those influenced show positive or negative peaks, either to the left (Shannon entropy for the spike event, Simpson's diversity, space-filling, expressiveness, Kolmogorov complexity, and PCIpK) or toward the right of the sample (Tsallis and Rényi entropies). By superimposing complexity metrics on each channel and reconstructing the time evolution of the spiking dynamics of the mycelium, we can create a graphical representation of the excitatory or inhibitory state before, during, and after hydrocortisone exposure, demonstrating the formation of an electrical activity fingerprint that corresponds to that specific event (see Figure 6e).

https://doi.org/10.1021/acsbiomaterials.1c00752
ACS Biomater. Sci. Eng. XXXX, XXX, XXX−XXX

We found that the PCIpK, Tsallis, and Rényi entropies are the most relevant metrics for system analysis among all complexity measurements considered here (see Figure 7). The PCIpK measure provides an easy inspection of the substrate's evolution analysis, including its spatiotemporal features. Figure 7a shows that a hydrocortisone stimulus induces a much stronger response in the application locus. Following a stimulus, some excitation events can be seen propagating in the substrate at much lower potentials. Tsallis entropy, as shown in Figure 7b, is less sensitive but more accurate in tracking the evolution of the reference electrode signal. We can see from Figure 7c that Rényi entropy helps us to monitor peak evolution over time.

3.1. Internal Inspection of the Fungal Culture. The visual appearance of the substrates colonized by the fungi did not change after exposure to hydrocortisone. However, the impact of hydrocortisone exposure is visible in the distribution of energy levels as a result of applying DCT to CT images, as shown in Figure 8. The calculated DCT values for no-exposed container, no-exposed segment, and cortisol-exposed segment were divided into three parts, including the distribution of values for high, medium, and low energies, which are shown in the first, middle, and last rows, respectively. The substrate that was not exposed to hydrocortisone had a higher energy frequency than the cortisol-exposed segment and the no-exposed segment adjacent to the cortisol-exposed segment.

4. DISCUSSION

The integrity of the fungal colony is preserved by cytoplasm flow in the mycelium network, where calcium waves[24] change the flow's propagation coordination. Cortisol metabolism stimulates the production of receptor activator of nuclear factor-kappa-B ligand (RANKL), a type II membrane protein that regulates bone regeneration and remodelling in mammals.[31] The activity of cells responsible for calcium resorption from bone is inhibited when RANKL is stimulated.[32] The elevated circulating cortisol levels maintain stress levels, triggering physiological changes in the body's regulatory networks. Hog1 is a stress-activated mitogen-activated protein kinase (MAPK) in fungi that is homologous to the p38 MAPK pathways in mammals.[33] When exposed to stress conditions, Hog1 rapidly dephosphorylates and induces the appropriate cellular responses against the offending environmental stimuli.[34] We speculate that receiving cortisol by the substrate can inhibit the flow of calcium and, in turn, reduce its physiological changes.

5. CONCLUSION

We conclude that the effects of hydrocortisone exposure on a *Pleurotus ostreatus* mycelium can be demonstrated using a well-known combination of techniques in a proper interdisciplinary approach. The computed tomography shows a change in gray tones as a result of hydrocortisone exposure, which is associated with active ion transport triggered in the living mycelium in response to the hormone. Simultaneously, by capturing biopotential signals and extracting their numerical complexity, we could identify consistent metrics for tracing the stimulus and tracking the propagation of ionic waves in response to the hormone. Our research extends our understanding of living fungal colonies, which could be used in future wearable and architectural systems to benefit living species while also maximizing sustainability.

AUTHOR INFORMATION

Corresponding Authors

Mohammad Mahdi Dehshibi − *Department of Computer Science, Universitat Oberta de Catalunya, Barcelona, Spain;* orcid.org/0000-0001-8112-5419; Email: mohammad.dehshibi@yahoo.com, mdehshibi@uoc.edu

Andrew Adamatzky − *Unconventional Computing Laboratory, UWE, Bristol, U.K.;* orcid.org/0000-0003-1073-2662; Email: andrew.adamatzky@uwe.ac.uk

Authors

Alessandro Chiolerio − *Unconventional Computing Laboratory, UWE, Bristol, U.K.; Center for Sustainable Future Technologies, Istituto Italiano di Tecnologia, Torino, Italy;* orcid.org/0000-0001-9328-2999

Anna Nikolaidou − *Unconventional Computing Laboratory, UWE, Bristol, U.K.; Department of Architecture, UWE, Bristol, U.K.*

Richard Mayne − *Unconventional Computing Laboratory, UWE, Bristol, U.K.;* orcid.org/0000-0003-1915-4993

Antoni Gandia − *Institute for Plant Molecular and Cell Biology, CSIC-UPV, Valencia, Spain; Mogu S.r.l., Inarzo, Italy*

Mona Ashtari-Majlan − *Department of Computer Science, Universitat Oberta de Catalunya, Barcelona, Spain*

Complete contact information is available at: https://pubs.acs.org/10.1021/acsbiomaterials.1c00752

Notes

The authors declare no competing financial interest.

ACKNOWLEDGMENTS

This project has received funding from the European Union's Horizon 2020 research and innovation programme FET OPEN "Challenging current thinking" under Grant Agreement No. 858132. The authors thank Vasilis Mitsios and Stamatis Varvanikolakis for coordinating the scans at Bioiatriki, as well as Judith Gómez Cuyàs for her constructive suggestions.

ADDITIONAL NOTE

[a]Note that here we intentionally drop the *m* superscript to simplify mathematical notations.

REFERENCES

(1) Cottier, F.; Mühlschlegel, F. A. Communication in fungi. *Int. J. Microbiol.* **2012**, *2012*, 1−9.

(2) Alonso-Monge, R.; Román, E.; Arana, D.; Pla, J.; Nombela, C. Fungi sensing environmental stress. *Clin. Microbiol. Infect.* **2009**, *15*, 17−19.

(3) Hou, L.; Wang, L.; Wu, X.; Gao, W.; Zhang, J.; Huang, C. Expression patterns of two pal genes of pleurotus ostreatus across developmental stages and under heat stress. *BMC Microbiol.* **2019**, *19*, 231.

(4) Adamatzky, A. On spiking behaviour of oyster fungi pleurotus djamor. *Sci. Rep.* **2018**, *8*, 7873.

(5) Beasley, A. E.; Powell, A. L.; Adamatzky, A. Capacitive storage in mycelium substrate. *arXiv* **2020**, 2003.07816.

(6) Beasley, A. E.; Powell, A. L.; Adamatzky, A. Fungal photosensors. *arXiv* **2020**, 2003.07825.

(7) Adamatzky, A.; Chiolerio, A.; Sirakoulis, G. Electrical resistive spiking of fungi. *Biophys. Rev. Lett.* **2021**, *16*, 1−7.

(8) Adamatzky, A. Towards fungal computer. *Interface Focus* **2018**, *8*, 20180029.

(9) Adamatzky, A.; Goles, E.; Martinez, G. J.; Tsompanas, M.-A.; Tegelaar, M.; Wosten, H. A. *Fungal automata, Complex Systems* **2020**, *29*, 759−778.
(10) Dehshibi, M. M.; Adamatzky, A. Electrical activity of fungi: Spikes detection and complexity analysis. *BioSystems* **2021**, *203*, 104373.
(11) Adamatzky, A.; Ayres, P.; Belotti, G.; Wösten, H. Fungal architecture position paper. *Int. J. Unconventional Computing* **2019**, *14*, 397−411.
(12) Adamatzky, A.; Tegelaar, M.; Wosten, H. A.; Powell, A. L.; Beasley, A. E.; Mayne, R. On boolean gates in fungal colony. *BioSystems* **2020**, *193*, 104138.
(13) Goles, E.; Tsompanas, M.-A.; Adamatzky, A.; Tegelaar, M.; Wosten, H. A.; Martínez, G. J. Computational universality of fungal sandpile automata. *Phys. Lett. A* **2020**, *384*, 126541.
(14) Adamatzky, A.; Gandia, A.; Chiolerio, A. Towards fungal sensing skin. *Fungal Biology and Biotechnology* **2021**, *8*, 6.
(15) Adamatzky, A.; Nikolaidou, A.; Gandia, A.; Chiolerio, A.; Dehshibi, M. M. Reactive fungal wearable. *BioSystems* **2021**, *199*, 104304.
(16) Jang, H.-J.; Lee, T.; Song, J.; Russell, L.; Li, H.; Dailey, J.; Searson, P. C.; Katz, H. E. Electronic cortisol detection using an antibody-embedded polymer coupled to a field-effect transistor. *ACS Appl. Mater. Interfaces* **2018**, *10*, 16233−16237.
(17) Kaushik, A.; Vasudev, A.; Arya, S. K.; Pasha, S. K.; Bhansali, S. Recent advances in cortisol sensing technologies for point-of-care application. *Biosens. Bioelectron.* **2014**, *53*, 499−512.
(18) Russell, E.; Koren, G.; Rieder, M.; Van Uum, S. H. The detection of cortisol in human sweat: implications for measurement of cortisol in hair. *Ther. Drug Monit.* **2014**, *36*, 30−34.
(19) Gholami, N.; Dehshibi, M. M.; Adamatzky, A.; Rueda-Toicen, A.; Zenil, H.; Fazlali, M.; Masip, D. A novel method for reconstructing ct images in gate/geant4 with application in medical imaging: A complexity analysis approach. *Journal of Information Processing* **2020**, *28*, 161−168.
(20) Marple, L. Computing the discrete-time "analytic" signal via fft. *IEEE Transactions on signal processing* **1999**, *47*, 2600−2603.
(21) Shannon, C. E. Communication in the presence of noise. *Proc. IRE* **1949**, *37*, 10−21.
(22) Dekking, F. M.; Kraaikamp, C.; Lopuhaä, H. P., Meester, L. E. *A Modern Introduction to Probability and Statistics: Understanding why and how*; Springer Science & Business Media, 2005. DOI: 10.1007/1-84628-168-7.
(23) Barca, P.; Giannelli, M.; Fantacci, M. E.; Caramella, D. Computed tomography imaging with the adaptive statistical iterative reconstruction (asir) algorithm: dependence of image quality on the blending level of reconstruction. *Australas. Phys. Eng. Sci. Med.* **2018**, *41*, 463−473.
(24) Aramburu, J.; Heitman, J.; Crabtree, G. R. Calcineurin: a central controller of signalling in eukaryotes: Workshop on the calcium/calcineurin/nfat pathway: Regulation and function. *EMBO Rep.* **2004**, *5*, 343−348.
(25) Fan, J.; Farmen, M.; Gijbels, I. Local maximum likelihood estimation and inference. *Journal of the Royal Statistical Society: Series B (Statistical Methodology)* **1998**, *60*, 591−608.
(26) Petz, D. *Quantum Information Theory and Quantum Statistics*; Springer Science & Business Media, 2007. DOI: 10.1007/978-3-540-74636-2.
(27) Shannon, C. E. A mathematical theory of communication. *Bell Syst. Tech. J.* **1948**, *27*, 379−423.
(28) Rényi, A. On measures of entropy and information. In *Proceedings of the Fourth Berkeley Symposium on Mathematical Statistics and Probability, Vol. 1: Contributions to the Theory of Statistics*; University of California Press, 1961; pp 547−561.
(29) Tsallis, C. Possible generalization of boltzmann-gibbs statistics. *J. Stat. Phys.* **1988**, *52*, 479−487.
(30) Kaspar, F.; Schuster, H. Easily calculable measure for the complexity of spatiotemporal patterns. *Phys. Rev. A: At., Mol., Opt. Phys.* **1987**, *36*, 842.
(31) Chyun, Y. S.; Kream, B. E.; Raisz, L. G. Cortisol decreases bone formation by inhibiting periosteal cell proliferation. *Endocrinology* **1984**, *114*, 477−480.
(32) Davies, E.; Kenyon, C.; Fraser, R. The role of calcium ions in the mechanism of acth stimulation of cortisol synthesis. *Steroids* **1985**, *45*, 551−560.
(33) Hohmann, S. Osmotic stress signaling and osmoadaptation in yeasts. *Microbiol. Mol. Biol. Rev.* **2002**, *66*, 300−372.
(34) Bahn, Y.-S.; Kojima, K.; Cox, G. M.; Heitman, J. Specialization of the hog pathway and its impact on differentiation and virulence of cryptococcus neoformans. *Mol. Biol. Cell* **2005**, *16*, 2285−2300.

https://doi.org/10.1021/acsbiomaterials.1c00752
ACS Biomater. Sci. Eng. XXXX, XXX, XXX−XXX

8 Appendix

Supporting Outputs

The supporting outputs are not to be assessed as part of the examination but are intended to demonstrate additional work undertaken within the research field.

Living Kombucha Electronics with Proteinoids

Anna Nikolaidou[1], **Panagiotis Mougkogiannis**[1], **and Andrew Adamatzky**[1]

[1]UWE, Unconventional Computing Laboratory, Bristol, BS16 1QY, UK
[*]Panagiotis.Mougkogiannis@uwe.ac.uk

ABSTRACT

The work introduces a composite material that combines Kombucha cellulose mats with synthetic thermal proteinoids to create electroactive biofilms, capable for sensing and computation. The synthesis of proteinoids involves heating amino acid mixtures, which leads to the formation of proto–cell structures capable of biological electrical signalling. We demonstrate that these hybrid biofilms exhibit adjustable memristive and memfractance properties, which can be utilised for unconventional computing tasks. The potential applications of living biofilms extend beyond neural interfaces, encompassing bioinspired robotics, smart wearables, adaptive biorobotic systems, and other technologies that rely on dynamic bioelectronic materials. The composite films offer a wide range of options for synthesis and performance customisation. Current research is dedicated to customising the composition, nanostructure, and integration of proteinoids in hybrid circuits to achieve specific electronic functionalities. Overall, these cross–kingdom biofilms are an intriguing category of materials that combine the unique properties of biological organisms and smart polymers. The Kombucha–proteinoid composites are a significant step forward in the development of future technologies that bridge the gap between living and artificial life systems. These composites have the remarkable ability to support cellular systems and demonstrate adaptive bioelectronic behaviour.

Introduction

Origins and Evolution of Kombucha

Kombucha is a fermented tea beverage reported to have originated in Northeast China in around 220 BC and consumed extensively during the Qin Dynasty[1]. The fermented tea, referred to as “Manchurian mushroom" or “kombu tea"[2,3], was introduced to Japan in approximately 414 CE and employed for the purpose of alleviating Emperor Inkyo’s gastrointestinal ailments[4]. Kombucha spread over trade channels and eventually reached Russia and Eastern Europe during the next centuries[4].

Germany saw the introduction of Kombucha in the early 20th century. World War II facilitated the widespread introduction of it in Europe, leading to its increased popularity in France and North Africa due to its advantageous effects on health[5]. Nevertheless, the scarcity of tea and sugar during wartime resulted in the loss of its popularity[6]. In the 1950s, Swiss scientists sparked renewed interest by comparing Kombucha to yoghurt in terms of their ability to enhance gut microorganisms[7].

In the present day, the process of making Kombucha involves soaking tea and sugar, allowing it to cool, and then introducing a symbiotic culture of bacteria and yeast known as SCOBY[1]. The culture undergoes aerobic fermentation for a duration ranging from several days to weeks, resulting in the formation of cellulosic films.The exact composition of the SCOBY, the type and concentration of tea and sugar used[8,9], the oxygen concentrations, fermentation time[10,11], and temperature[10,12] can affect the composition of the Kombucha cellulose films. For the production of the Kombucha beverage, the completed Kombucha undergoes filtration, infusion of flavours, and is subsequently stored in a refrigerated environment [4]. Currently, the beverage, SCOBY cultures, and preparation kits are readily accessible for purchase in the market.

Bridging Prebiotic Conditions to Cellular Life: Proteinoids

Proteinoids, which were initially characterised by Sidney Fox in 1959, are abiotic synthetic polypeptides[13,14]. These are produced by heating mixtures of amino acids to trigger polymerization. The self-assembly of proteinoids, which are rich in glutamic and aspartic acid, leads to the formation of proteinoid microspheres.

The proteinoids microspheres demonstrate compartmentalization, selective permeability, and other lifelike qualities that resemble protocells. Their formation from easily accessible precursors supports models of early biological evolution progressing from simple to complex polymers. Proteinoids have a unique quality of being formed solely from amino acid precursors, setting them apart from other protocell models.

In addition to microspheres, proteinoids exhibit additional biomimetic capabilities such as catalytic activity, microtubule formation, and membrane generation[15–18]. Despite the changing environmental conditions on primitive Earth, their ability to self–organize in an orderly manner remained unaffected. Proteinoids provide a strong connection between prebiotic chemistry and the earliest minimal cells.

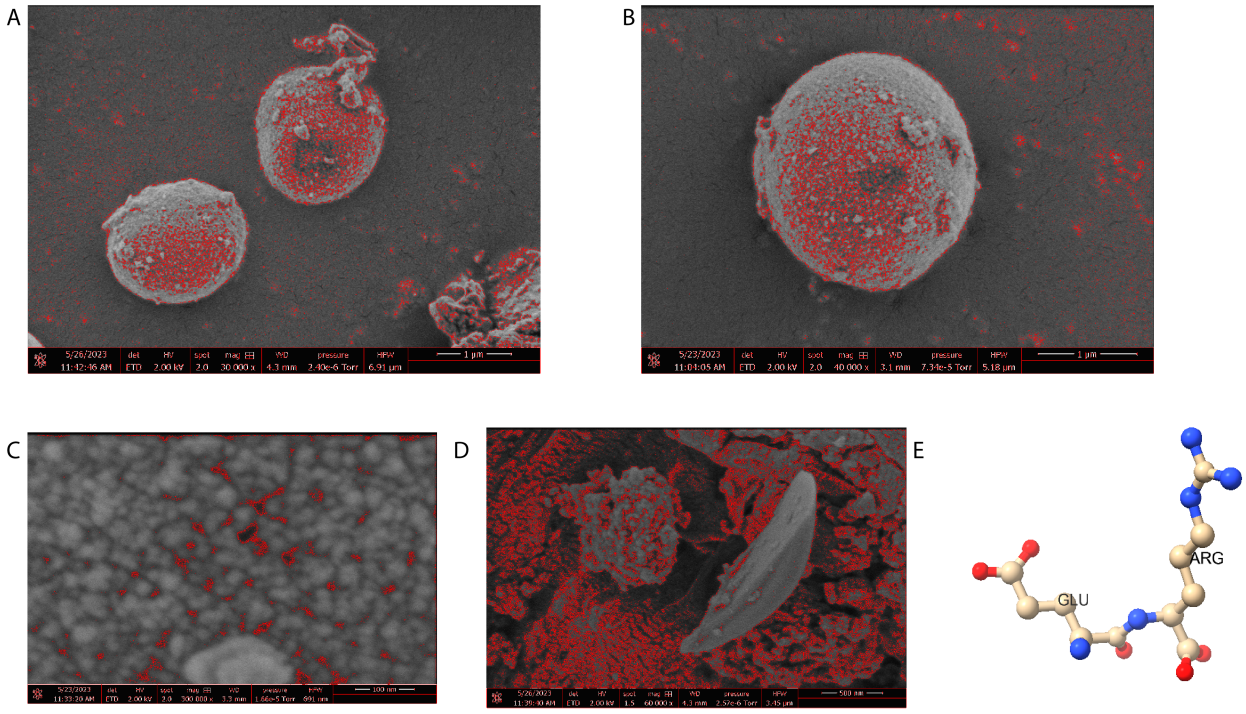


Figure 1. Scanning electron micrographs demonstrate the varied physical characteristics of proteinoid spheres that have formed through self–assembly, observed at different sizes. Image A depicts a pair of spherical twins, with a diameter of roughly 1.8 microns each, that are fused together in a manner simulating dividing cells. Image B depicts a solitary proteinoid sphere with a width of 2.4 microns, showcasing consistent and repeatable microscale structures. Upon closer examination of image C, it is evident that there are tightly packed nanospheres with a diameter of 23.5 nanometers on the surface of a larger microsphere. This arrangement showcases hierarchical self–organization at a submicron scale. Image D presents evidence of the fragmentation of these nanostructures, namely the partial breakage of nanospheres referred to as "protobrains," highlighting the dynamic nature of the assembly processes. These micrographs illustrate the diverse colloidal behaviours of synthetic proteinoids, ranging from micron–sized cellular imitations to bits of programmable nanomaterial with lifelike organisation and development. Additional examination of the collective interactions that govern the self–assembly of proteinoids may provide essential principles for designing intelligent biomaterials. To analyze the images computationally, techniques like segmentation, thresholding, and skeletonization facilitated by MATLAB can elucidate proteinoid boundaries, structures and interconnections within these complex bio–materials. Image E shows the chemical structure of a dipeptide L-glutamic acid and L-arginine (L-GLU:L-ARG), which is a crucial component of heat proteinoids.

The study of proteinoids offers valuable insights into potential pathways for the origins of life that cannot be obtained solely through modern biochemistry[19]. Researchers have been captivated by the elegance of their thermal polymerization and the intricate dynamics that arise from it for more than fifty years[20]. Continued research continues to uncover the lifelike capabilities and practical applications of proteinoids in the field of synthetic biology[21] and unconventional computing[22].

The proteinoids' synthesis in abiotic conditions, biomimetic characteristics, and complex assembly give hope that scientists can understand the progression from inanimate chemistry to evolving biology[23]. The synthetic polymers provide insights into the long path from primordial chaos to biological organisation[24].

The scanning electron micrographs displayed in Figure 1 provide a fascinating visual representation of the various morphological features of synthetic proteinoids. These images depict proteinoid particles undergoing spontaneous self–organization, resulting in a diverse range of biomimetic shapes and systems, spanning from the microscale to nanoscale constructs. Of particular interest is the lifelike characteristics on display across sizes—from near cell–like spherical twins to dense nanosphere colonies coating microsurfaces reminiscent of membranous tissue to fragmented nanostructures resembling prototypes of intracellular networks. When combined with computer analysis (as indicated in red), the intricate self–assembly process inherent in these proteinoids starts to resemble the microarchitecture observed in living cells. The concept proposed by Fox and Dose[20,25] of pseudo–metabolizing protocells arising from abiotic precursor chemistry inevitably brings to mind a

speculative vision. Despite being artificially created, these proteinoids demonstrate a strong tendency towards hierarchical arrangement and spatial programming, resembling biological systems. Additional investigation into their cross–linking interactions may reveal fundamental design patterns that can be applied to the development of adaptable biomaterials and bioelectronic systems.

Additional analysis using high–resolution structural techniques like digital optical microscopy could provide specific properties about the dynamic assembly process, which will assist in the development of bioinspired engineering projects. Proteinoids consistently show similarities between intentionally created artificial systems and the development of organisation in early prebiotic chemistry.

Electrical properties of kombucha and proteinoids

Both kombucha and proteinoids exhibit patterns of electrical activity similar to that of living neurons.

In[26] we demonstrated that Kombucha mats produce action potential like spikes of electrical potential, the spikes are often grouped in the trains of spikes[26]. We demonstrated that electrical responses of kombucha mats to chemical, electrical, and optical stimulation are distinctive and therefore the mats can be used as sensors, or even unconventional computing devices[26].

Proteinoids shows a wide spectrum of oscillations of electrical potential[27]. The electrical spiking activity of the proteinoids can modulated with light[21] and used to implement Boolean gates[28] and recognition of sounds[29].

Tailoring Kombucha with Proteinoids

Materials with sensing and information processing capabilities usually incorporate a substrate and a series of functional layers. The functional layers include the active elements where the main electrical activity takes place while the substrate is a solid substance where the functional layers are deposited[30,31]. Due to low production costs, easy accessibility, flexibility and shape conformability, customisation across various scales, renewability and degradability potentials, Kombucha cellulosic films present an excellent substrate candidate for functionalisation. On the other hand, proteinoids present unique electrical capabilities such as memristive, memcapacitive, and conductive properties [15] and are therefore suitable for utilisation as functional layers. Modulating the electrical properties of Kombucha[32] with proteinoids can lead to the production of a composite material with synergetic computational functionalities such as signalling dynamics, Boolean logic operations, adaptive learning behaviors and sensory transduction mechanisms. By optimising parameters such as the composition of the Kombucha substrate and functional proteinoid layers and the concentration of proteinoids in the substrate, the computational functionalities and electroactive activity of the Kombucha and proteinoid composites can be tailored.

The potential computational properties emerging from the Kombucha Proteinoid biofilms are summarized in the mind map shown in Figure 2[15,32]. As highlighted, the symbiotic living system exhibits capabilities spanning neural–like signaling dynamics, Boolean logic operations, adaptive learning behaviors, sensory transduction mechanisms, and potential for unconventional computing architectures. The mind map conveys relationships between these lifelike information processing properties arising synergistically through the hybrid fusion of proteinoids and electroactive bacterial cellulose.

Results

Electrical characterisation of proteinoid–microbial composite samples

To assess the electroactive properties of Kombucha–proteinoid composites, it is necessary to conduct electrical measurements using techniques such as current–voltage profiling, impedance spectroscopy, and capacitance recordings. The composites are interfaced with platinum-iridium wire electrodes, through which voltage ranges of -1V to +1V are applied.

High impedance data acquisition systems are widely used in various applications. Picolog loggers and Keithley source metres allow for the analysis of the electrical activity of the films. The recorded current–voltage curves offer valuable insights into conductivity, memristance, and spiking dynamics. The impedance and capacitance profiles provide insights into the response to alternating current and the ability to store charge.

The systematic characterization of electrical properties across various operating conditions uncovers valuable insights into the relationships between stimulus patterns and kombucha proteinoid network behaviours. Programming desired responses is made possible by adjusting stimulation parameters and material compositions. The input–output mappings in this text highlight the potential for information processing, learning, and logical operations.

Current research is focused on understanding how the nanostructure and integrated physiology of composites contribute to their emergent electronic properties. This knowledge will greatly contribute to the advancement of rational design for customised bioelectronic devices and systems. The combination of microbial matrix, synthetic polymers, and electronics demonstrates exciting potential at the intersection of biology and technology.

Electrical measurements are essential for understanding the intricate mechanisms of Kombucha–proteinoid protobrains. The understanding of stimulus-response couplings, signal transmission modes, and programmable behaviours in hybrid bioelectronics has greatly advanced both fundamental research and practical applications.

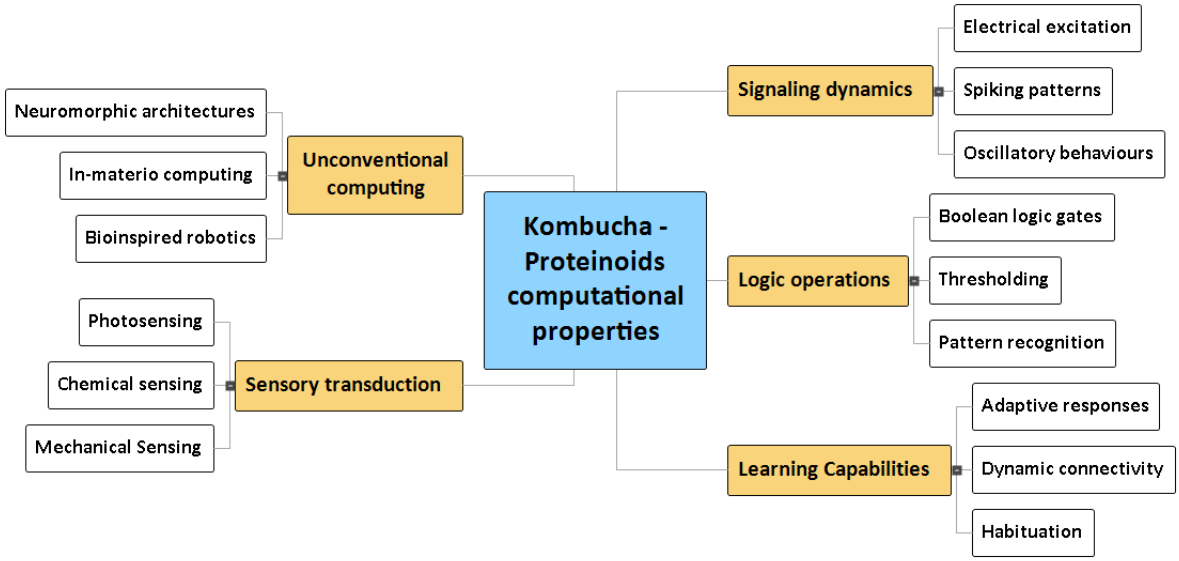


Figure 2. Computational features in Kombucha biofilms depicted in a mind map.The mind map emphasises the prominent signalling, reasoning, learning, sensory, and unconventional computing characteristics demonstrated by the living electronic composites. The hierarchical structure visually represents the connections between the emergent features of dynamic biomaterials, which are used for information processing and computation. The diverse capabilities emerge from the combination of proteinoids with the bacterial cellulose matrix. Additional clarification of the principles that govern the lifelike bionic behaviours of biofilms holds the potential for ongoing advancements in bioinspired technology.

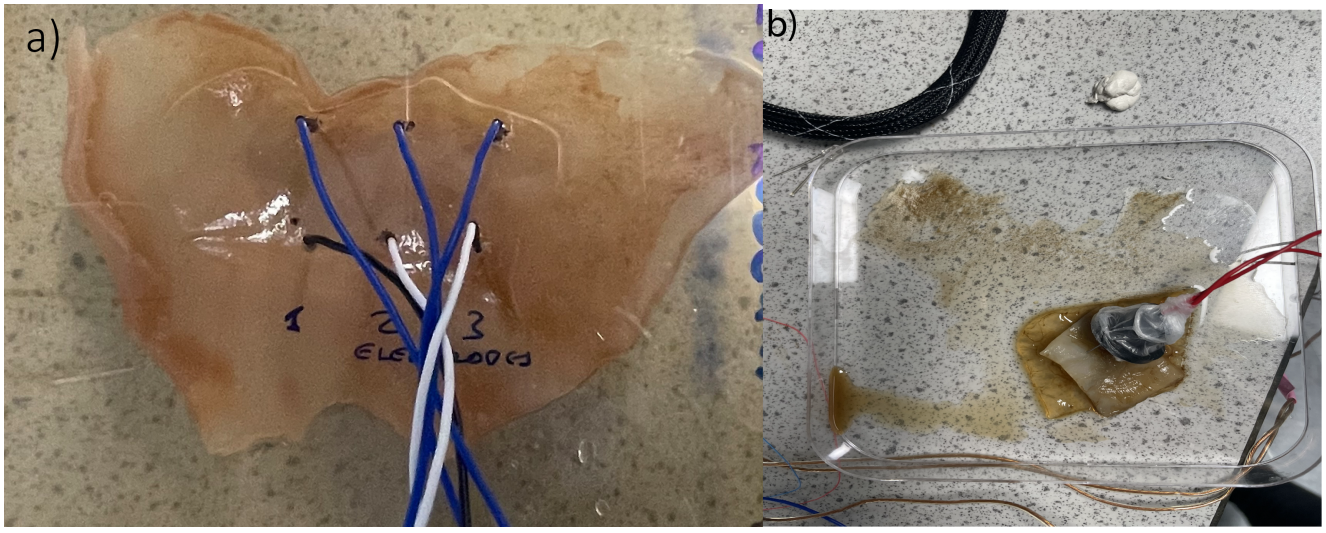


Figure 3. Experimental configurations for examining electrical activity in Kombucha-proteinoid protobrains.(a) Utilising platinum–iridium wire electrodes, a measurement configuration is employed to investigate the occurrence of electrical spikes in Kombucha films. (b) The objective is to analyse a composite Kombucha–proteinoid biofilm by employing wire electrodes in order to assess the impact of integrated proteinoids on the electrical signalling behaviours.Through systematic electrical testing, the correlations between stimuli, material compositions, and subsequent bioelectronic responses may be identified. This allows for the programming of certain traits and functionalities as required.

The experimental apparatus utilised to assess the protobrains' electrical activity is shown in Figure 3. The spike patterns in Kombucha films are examined in Figure 3a. The investigation of composite Kombucha–proteinoid biofilms is shown in Figure 3b, with the aim of assessing the impact of the proteinoids that are present.

Current—-Voltage Plots Show Signature of Memfractance

A memristor is an electrical component with two terminals that establishes a relationship between electric charge and magnetic flux connection. This concept was initially introduced by Leon Chua in 1971[33]. The memristor, along with the resistor, capacitor, and inductor, is one of the essential non–linear circuit components. Memristance is the measure of electrical resistance in a memristor, which is capable of changing depending on the past passage of current through the device[34].

Memfractance is a term used to describe the distinct set of characteristics exhibited by memristors, mem–capacitors, and mem–inductors[29]. Memristors are materials that demonstrate a type of material implication and can be employed in many applications. These applications encompass the development of logical circuits, stateful logic operations, passive crossbar arrays of memristors for logic operations, memory–aided logic circuits, self–programmable logic circuits, and memory devices. The investigation of mem–fractive characteristics in fungi arises from the possible advantages it presents[35].If the strands of fungal mycelium present in mycelium bound composites, along with the fruit bodies, have mem–fractive characteristics, it creates opportunities to include different memory and computer devices directly into architectural construction materials made from fungal substrates. In addition, the idea of wearable fungi that may be used as clothing is still in its initial phases but has demonstrated favourable characteristics including a sleek design, great flexibility, and minimal energy usage in comparison to traditional artificial wearable sensory devices[32]. Mycelium-bound composites, consisting of organic substrates that have been colonised by fungi, are very promising biomaterials with significant environmental sustainability. These materials are currently being used in applications such as providing acoustic and thermal insulation for wall cladding and packaging[36].

Memristors are passive components that demonstrate a memristive effect instead of possessing specific memristive functionality[37]. Practical memristor technologies, such as resistive random access memory (ReRAM), utilise nanoscale switches that can modify electrical resistance in a persistent manner[38]. Memristor components, when included into circuits, facilitate memory, learning, and self–adaptation capabilities. Memristors possess distinctive attributes that offer potential for groundbreaking utilisation in memory storage, neuromorphic computing, and other domains[39].

Although conceived of decades ago, the experimental realisation of optimal memristors has been a formidable obstacle. HP Laboratories documented the observation of memristive phenomena in titanium dioxide thin coatings in 2008[40]. The publication of this correlation between ReRAM devices and Chua's memristor suggested that memristors have the potential to revolutionise the field of electronics[41].

However, some researchers contend that it may be physically impossible to create ideal memristors[42]. Chua expanded the definition to encompass all non–volatile memory associated with resistance switching, asserting that memristors represent the most primal component of a circuit. However, there are ongoing scepticisms regarding the existence of reality as opposed to merely mathematical constructs. There have been propositions for experiments to determine whether a genuine memristor can be obtained[42–46].

In brief, although forward–thinking, the memristor continues to be a subject of debate. Enhancing the memorization capabilities of ReRAM and related technologies holds the potential to realise the theoretical potential of adaptive circuitry. Interdisciplinary cooperation among material scientists, circuit theorists, and device engineers is incentivized to address these fundamental inquiries in order to achieve a more comprehensive understanding of the scientific principles that underpin electronic innovations.

The unique electrochemical characteristics resulting from the integration of Kombucha and proteinoid are emphasised by a comparison of I–V measurements and statistical analysis, as depicted in Figure 4. The current–voltage (I–V) characteristics of pure L-Glu:L-Arg proteinoids and the Kombucha composite comprising L-Glu:L-Arg are represented in Figures 4a, b. Figures 4c, d present a statistical summary of the current distributions for each sample.

The Kombucha composite has a lower average current, but its standard deviation (3.25) is more than double that of the pure proteinoid sample (1.40). This suggests that the microbial–synthetic composite has a wider and more varied distribution and range of activity, which can be attributed to the combined and mutually enhancing actions of its two components. The enhanced bioelectronic behaviours highlight the advantages of combining biological and synthetic systems to achieve new and advanced functionalities.

To summarise, Figure 4 demonstrates notable statistical disparities in the I–V characteristics resulting from the incorporation of proteinoids into the microbial Kombucha matrix. This showcases adjustable electronic characteristics and enhanced functionalities compared to the separate components.

The analysis of higher order statistics provides valuable insights into the shape and symmetry of current distributions observed in the L–Glu:L–Arg proteinoid and Kombucha–proteinoid composite samples. The pure proteinoid sample exhibits a kurtosis value of 2.798, suggesting a distribution that is flatter with wider peaks in comparison to a normal distribution. The data also indicates a negative skewness of –0.39, indicating a slight left–skewed asymmetry.

On the other hand, the Kombucha composite shows a higher kurtosis of 4.53, which is much more similar to a Gaussian distribution. The skewness value of 0.40 indicates a relatively balanced current density distribution. The data suggests that the combination of Kombucha and proteinoid leads to a distribution that is more tightly concentrated around the mean, with less

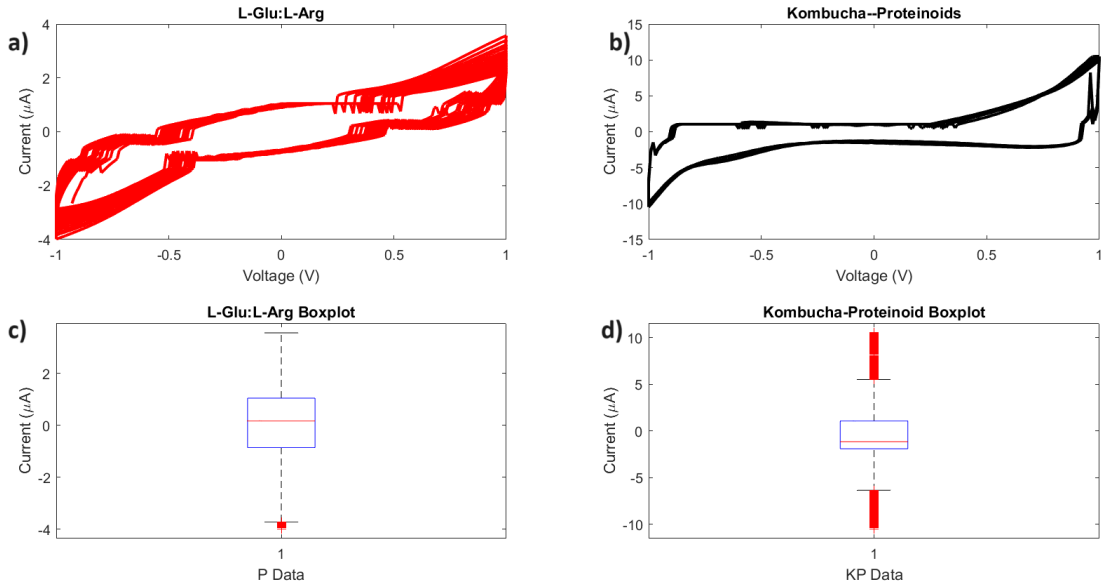


Figure 4. The current-voltage (I–V) characteristics and statistical metrics were analyzed for two samples - pure L–glutamic acid and L–arginine (L–Glu:L–Arg) proteinoid versus a composite of Kombucha microbes combined with L–Glu:L–Arg proteinoids. The proteinoids (P) displayed a reduced average current (–0.03 μA) in comparison to the Kombucha–proteinoids (KP) (–0.15 μA) during the recorded voltage sweeps. Nevertheless, the Kombucha–proteinoid composite exhibited a much higher standard deviation (3.25) compared to the pure proteinoids (1.40), suggesting a greater variability in the current values. This illustrates a mutually beneficial interaction between the artificial L–Glu:L–Arg substance and the active Kombucha microorganisms. In addition to the measures of central tendency and spread, the distributions exhibited distinct shapes. Specifically, the L–Glu:L–Arg sample displayed a slight negative skewness (–0.39), indicating a slight preference for positive currents. On the other hand, the Kombucha–proteinoid composite exhibited positive skewness (0.40), with a tail extending towards negative currents. The L–Glu:L–Arg proteinoid currents had a lower kurtosis value of 2.80 and were more similar to a normal distribution. On the other hand, the Kombucha–proteinoid currents had a higher kurtosis value of 4.53, indicating a distribution that is more likely to have outliers and a heavier tail. To summarise, the combination of synthetic proteinoids with microbial life not only changes electrical behaviours in general, but also greatly increases the range of nonlinear interactions between living and non–living components.

pronounced tails.

Conductivity Changes With Frequency

Understanding the electrical characteristics of Kombucha–proteinoid composite biofilms necessitates the use of precise methods for characterising charge transport. Conductivity measurements conducted on disordered organic systems are susceptible to experimental artefacts that have the potential to render the underlying models incorrect. For instance, the electrical characteristics of melanin were formerly believed to be due to its amorphous semiconductivity. However, further analysis has shown problems with the models that assume hydrated dielectric qualities[47].

To prevent these errors, it is necessary to apply strictness in aspects such as electrode arrangements, sample shape, biassing circumstances, and equilibrium dynamics. An in-depth analysis of the relationship between frequency and field strength in conduction across various time intervals provides a better understanding of transport mechanisms. It is crucial to take into account charge injection, trapping, recombination, and interfacial effects.

The presence of multiscale structure at the molecular, nano, micro, and macro levels adds complexity to the understanding of Kombucha-proteinoid conductivity. The diverse, structured, and water–rich biofilm morphology impacts the flow of electrical current and the spread of its effects. By combining spectroscopy, microscopy, and calculations with conduction testing, it becomes possible to establish a correlation between the structure and function.

The frequency–dependent conductivity profiles of the proto–brain samples provide insights into their tunable electrical

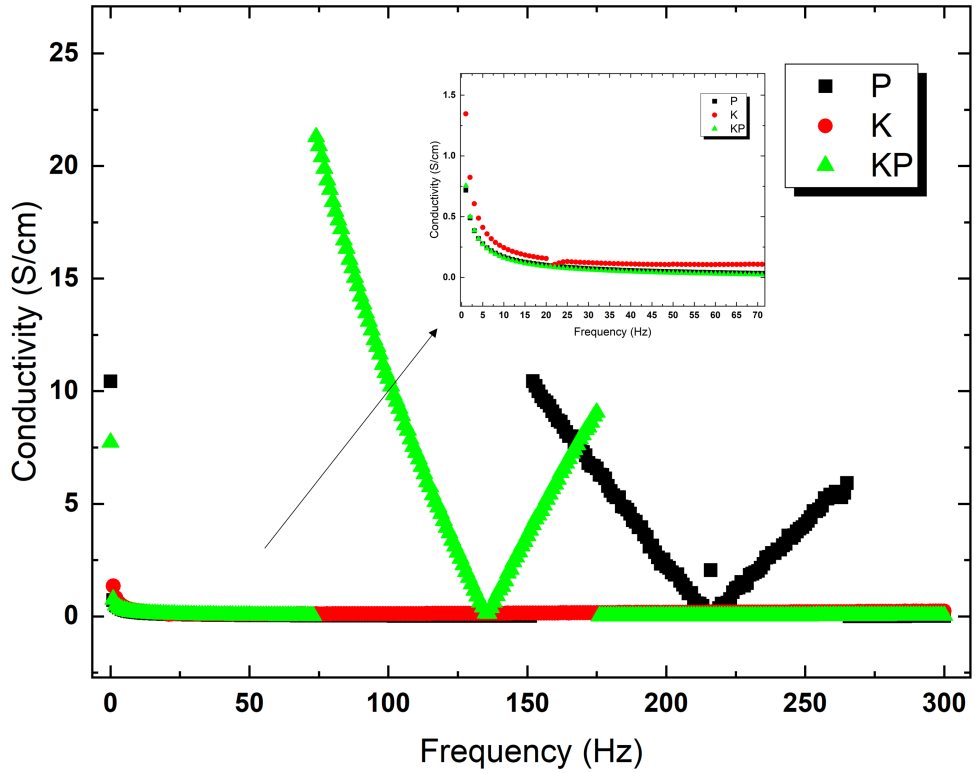


Figure 5. Frequency–dependent conductivity of Kombucha–proteinoid composite biofilms. Conductivity spectra are shown for samples with compositions including Kombucha (K), Kombucha-proteinoid (KP), and proteinoid (P). The KP and P sample exhibits the highest conductivity over the frequency range. Sharp increases in conductivity occur for the KP films between 74–178 kHz, rising over 1000x from 0.03 to 20 S/cm. A comparable spike occurs for sample P from 152–259 kHz. The tunable conductivity dynamics demonstrate activation of selective charge transport mechanisms at specific resonant frequencies.

behaviours. The conductivity σ was derived from the measured capacitance values using the following relation:

$$\sigma = \frac{1}{\omega C\sqrt{1+\tan^2(\phi)}} \tag{1}$$

Where ω is the angular frequency, C is the capacitance, and ϕ is the phase angle between current and voltage. This accounts for both resistive and reactive contributions over the test frequency range of 0 to 300 kHz[48].

The conductivity measurements of mixtures including Kombucha and proteinoids exhibited behaviours that were dependent on the composition and selective with respect to frequency. The Kombucha–proteinoid (KP) sample had the highest conductivity across frequencies, suggesting a higher degree of charge mobility. Typically, the conductivity decreased as the frequency increased due to hindered charge transport. Nevertheless, there were noticeable surges in conductivity seen for the Kombucha and Kombucha–proteinoid films throughout the frequency range of 150–250 kHz, exhibiting a remarkable rise of up to 1000 times from 0.03 to 20 S/cm. This suggests the initiation of heightened conduction processes at particular resonance frequencies. The proteinoid sample, in its pure form, demonstrated a distinct and rapid rise in conductivity between the frequencies of 152–259 kHz. The results emphasise the adjustable electrical conduction properties of the composite biofilms, which may be customised by manipulating input signal characteristics such as frequency. The conductivity spectra demonstrate the ability to choose control frequencies by assembling microbial and synthetic components in a modular manner. Additional clarification of the conduction mechanisms will assist in the logical design of bioelectronic devices with intentional, responsive functionality. The composition–dependent, frequency–selective conduction properties of the Kombucha–proteinoid biofilms are highlighted in Figure 5.

Probability distributions characterise the relative likelihood of variable values (Fig. 6A). Gaussian models offer useful reference predictions given by:

$$f(x|\mu,\sigma) = \frac{1}{\sigma\sqrt{2\pi}} e^{-\frac{(x-\mu)^2}{2\sigma^2}} \tag{2}$$

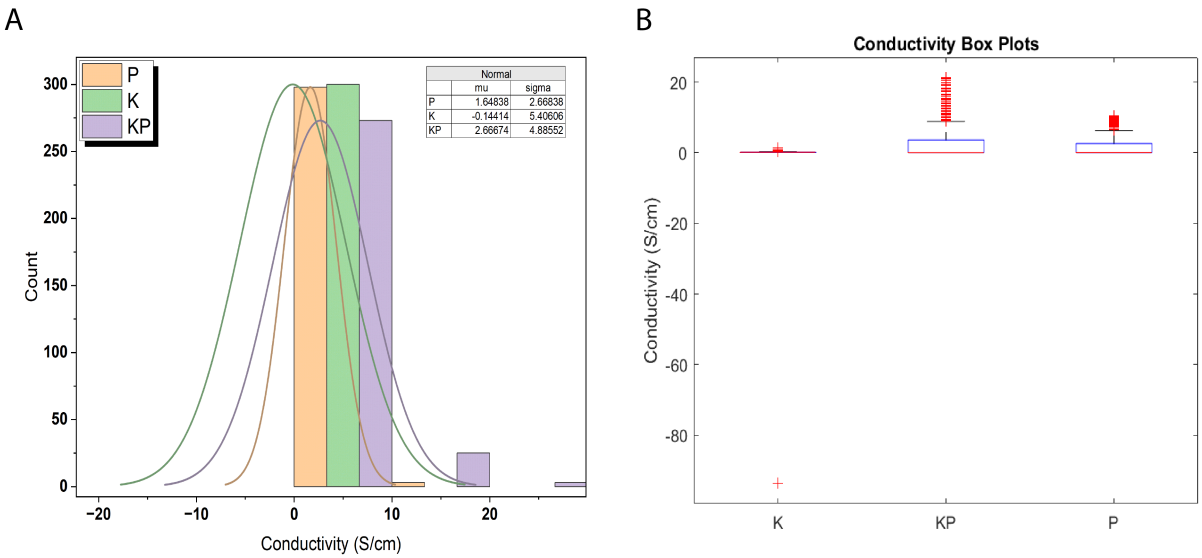


Figure 6. A) Fitting normal distributions allows quantification of central tendency and variability within the measured conductive responses across proteinoid (P), Kombucha (K), and composite (KP) samples. The proteinoid–only sample possesses a baseline mean conductivity of 1.65 S/cm with a standard deviation of 2.67 S/cm characterising its distribution spread. By contrast, the mixed Kombucha-proteinnoid sample has an elevated mean of 2.67 S/cm and increased variance with a standard deviation of 4.89 S/cm. This divergence demonstrates that interfacing the synthetic protocells with the living microbial biofilm significantly amplifies the diversity and range of resultant bioelectronic behaviour beyond either standalone system. However, the Kombucha sample exhibits an outlier distribution with comparable variance (σ=5.41 S/cm) yet inverted mean conductivity centered around –0.14 S/cm constituting a flipped response relative to the prototypical proteinoid profile. B) Quantiles of conductivity for compositions of Kombucha and proteinoids. The boxplots display the distribution of conductivity (S/cm) values for samples K, KP, and P. The 25th, 50th, and 75th percentile values are plotted, indicating that KP has the largest range, reaching approximately 20 S/cm, while K, and P are distributed below 2.62 S/cm. The extensive distribution ranges emphasise the adjustable conduction characteristics of KP biofilms resulting from the selective incorporation of both microbial and synthetic elements. Conductivity distributions can be statistically profiled to identify specific design approaches for customising bioelectronic response behaviours.

where μ and σ denote the mean and standard deviation, respectively. When comparing fitted normal distributions, differences in central tendency and dispersion properties emerge. The mean conductivity of the proteinoid–only sample (P) is 1.65 S/cm, with a standard deviation of 2.67 S/cm. In comparison, the Kombucha–proteinoid composite (KP) has a greater mean of 2.67 S/cm and a bigger variance with σ =4.89 S/cm. This suggests that combining proteinoids with the microbial Kombucha matrix greatly increases the diversity and extent of conductive responses. The Kombucha sample (K), on the other hand, has comparable variance but an inverted mean conductivity centred about –0.14 S/cm, indicating an outlier distribution. The goodness of fit test would determine whether Gaussian models accurately described the sample data. Further statistical analysis could evaluate the relevance of differences in conductivity distribution parameters among samples. Using probability density profiles to characterise emergent behaviours demonstrates how coupling synthetic biology with living microbial scaffolds alters the final bioelectronic phenotypes.

The research demonstrates a notable increase in conductivity achieved with the incorporation of proteinoids into the Kombucha matrices. The significant improvement in conductivity by selective hybridization (Fig. 6B) prompts the need for further optimisation in order to cater to specific bioelectronic applications. The distributions measure ways to modify emergent response behaviours by adjusting Kombucha–proteinoid ratios.

Controlling Material Functionality

The Kombucha–proteinoid composite films offer exciting possibilities for the development of low power analogue integrated systems, drawing inspiration from biology. These soft living electronic materials offer the unique benefits of biological intelligence, such as adaptation, autonomy, and fault tolerance, instead of relying on traditional rigid electronic components[44]. The integration of synthetic biology and semiconductor electronics opens up exciting possibilities for the development of advanced chip technologies.

The Kombucha–proteinoid composites have the remarkable capability to generate electrically excitable signals and adapt their conduction properties. Figure 5 clearly shows that the Kombucha-proteinoid composites display electrically excitable responses that are adjusted by stimulus frequency. The conductivity of the KP biofilms increases over 1000x when the input frequency is varied from 74 to 178 kHz, as seen by the spectra. This selective spiking demonstrates resonant activation of ionic transport pathways within these mixed microbial–abiotic networks. Similarly, sweeping the input frequency from 152 to 259 kHz causes a sharp conductivity amplification driven by frequency–dependent charge conduction pathways inherent in the proteinoids' assembly architecture. These tunable non–linear voltage enhancements confirm Kombucha–proteinoid systems' potential to electrically excite internal conductive regions in ways that increase output responsiveness. The emergent features go beyond the individual ingredients, with the interaction of the microbial cellulose matrix with synthetic protocell microspheres yielding complicated excitation dynamics analogous to excitable cells. In the same manner that neurons exhibit selective firing thresholds controlled by input stimulation patterns, mixed abiotic–biological composite networks self–organize complementary pathways that transform and relay external signals across a wide range of spatiotemporal regimes.

These networks can be used to create flexible analogue circuits. Characteristics like photosensitivity in circuits allow for the adjustment of their behaviour and performance based on inputs, much like the processes of natural synaptic plasticity. This provides a way to create hardware systems that closely mimic real–life systems and possess the capability to learn and optimise themselves.

Beyond components, Kombucha–proteinoid biofilms offer models to inspire wholly new bio–inspired device concepts. Studying the emergent complexity of microbial–abiotic symbiosis and specialized signaling cell types reveals design principles alternative to individual transistors.

The response dynamics of Kombucha–proteinoid biofilms can be tuned by their compositional ratios, as evidenced by characterization of input and output signals for films with varying proteinoid and Kombucha content.

In summary, Figure 7 highlights how modulating proteinoid–microbial ratios predicts tunable input–output transformations, enabling custom tailoring of response dynamics in these composite living materials. Figure 7 depicts the electrical responses of two distinct samples. Figure 7A depicts the first sample, which contained 40% proteinoids and 60% Kombucha. Figure 1B depicts the second sample, which contained 25% proteinoids and 75% Kombucha. The amplitude and frequency of the input and output signals were both measured. The input for the 40:60 ratio sample had an amplitude of around 10000 millivolts and a frequency of 14 Hertz. The output signal, on the other hand, was significantly weaker, with an amplitude of only 26 millivolts but a higher frequency of 4500 Hertz. The input in the 25:75 ratio sample had a similar amplitude of roughly 10000 millivolts but a frequency of –15 Hertz. Surprisingly, the output of this sample was stronger, with an amplitude of 360 millivolts and a frequency of 50 Hertz. Comparing the two samples reveals that the one containing less Kombucha and more proteinoids (25:75) produced a higher output amplitude and frequency. This shows that altering the mixture ratio has an effect on the proteinoid–Kombucha system's computational capability.

The entropy experiments indicated that the 25–75 % (v/v) KP mixture displayed a higher level of randomness in its voltage compared to the 40-60 % (v/v) KP sample, with a value of 1.02 bits vs 0 bits. However, while conducting cross–correlations, it was found that there was minimal similarity between the two signal traces. By utilising percentile cutoffs, the comparison of extremes highlighted the range of outputs between voltage spikes and troughs, encompassing a greater breadth from the 25th to the 75th percentile. By mapping the output paths across phase space, it was revealed that the 40–60 system exhibits more regular cycles compared to the extended and swirling chaos observed in its 25–75 "cousin". Collectively, our series of testing reveals that recipes with lower proteinoid content and improved Kombucha produce electrical fluctuations that are more chaotic and less predictable. In simpler terms, increasing the presence of microorganisms and reducing the amount of synthetic components seems to enhance the complexity of this mixture. The adjustment of biological and non–biological elements provides a means to potentially fine–tune the development of advanced cognitive abilities through the construction of next–generation biological systems.

Building Logic with Kombucha-—Proteinoid Proto Brain

Recent research has shown that Kombucha-proteinoid composite biofilms have the ability to carry out basic Boolean logic operations, including as AND, OR, XOR, XNOR, NAND, and NOR gates[26,49]. Converting the continuous electrical outputs into binary signals allows for performing bitwise operations using the basic logic operators.The integration of different network output signals enables the implementation of diverse gates, establishing a fundamental basis for bio–logic computation[32,36].

The logic functionality is derived from the intricate spatiotemporal signalling dynamics of the films[50]. Inputs, such as stimuli or proteinoid doping, undergo a transformation process that results in the formation of interaction patterns. These patterns then perform transfer functions that are similar to Boolean logic.

Thresholding is a process that turns continuous outputs into binary levels, which are essential for performing bitwise logic operations. This establishes the following equations that present the mathematical logic formulas.

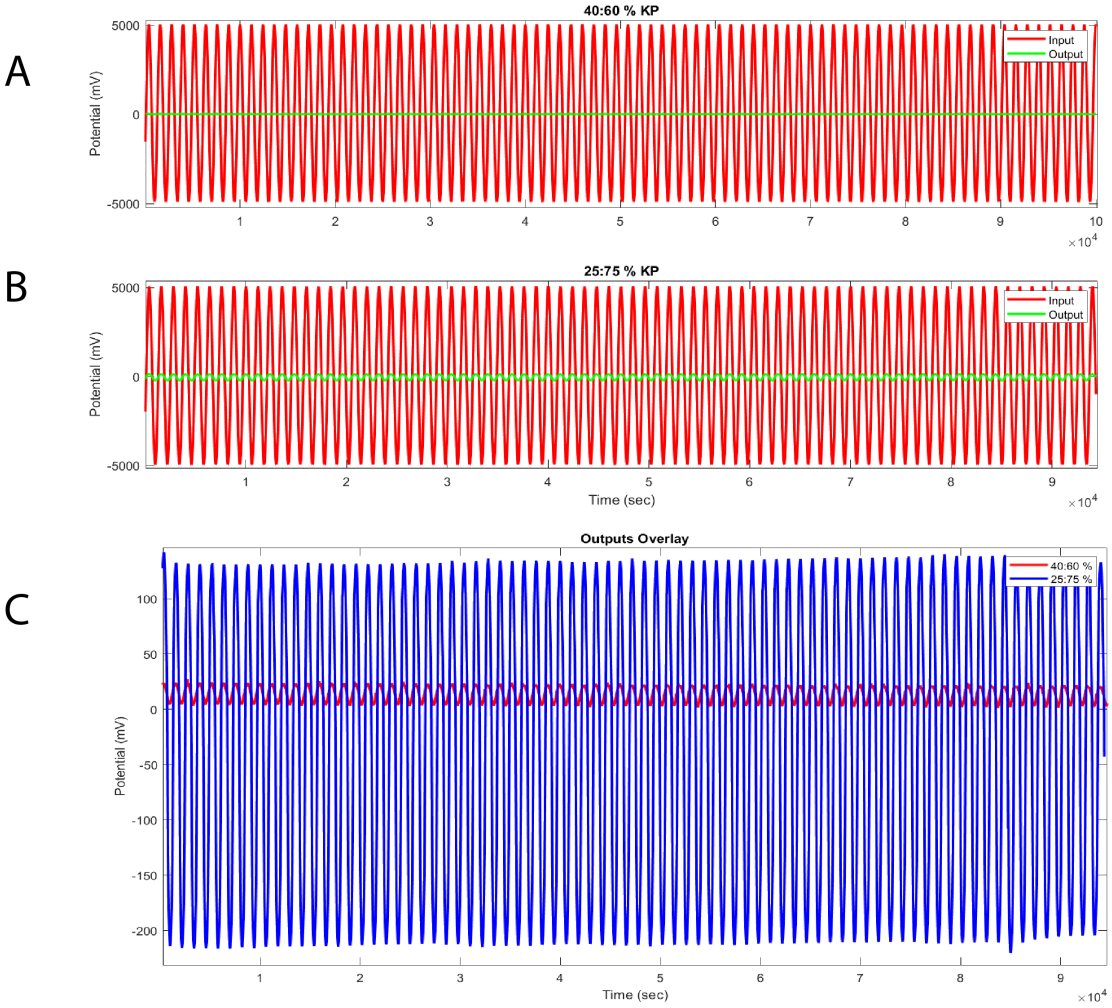


Figure 7. The plots depict the input and output signals for Kombucha–proteinoid biofilms with different composition: (A) 40% proteinoids and 60% Kombucha (KP), (B) 25% proteinoids and 75% Kombucha. The key input and output parameters derived from the signals encompass amplitude and frequency. The 40:60% KP sample had an input amplitude of 9963.07 mV and a frequency of 14.21 Hz. The output had a decreased amplitude of 26.13 millivolts, although a significantly elevated frequency of 4459.73 hertz. The 25:75% KP sample had an input with an amplitude of 10055.85 mV and a frequency of –15.40 Hz. The output had a greater magnitude of 362.62 millivolts and a frequency of 56.68 hertz. The increased amplitude and frequency of the 25:75% KP sample, in comparison to the 40:60% sample, indicates that the ratio of proteinoid–Kombucha (KP) composition affects the computational features of the system. C) The output potential signals (mV) were recorded over time with Kombucha:proteinoid ratios of 40:60 and 25:75 by volume.

The AND logic operation:

$$y = x_1 \wedge x_2 \tag{3}$$

The OR logic operation:

$$y = x_1 \vee x_3 \tag{4}$$

The XOR (exclusive OR) logic operation:

$$y = x_1 \oplus x_3 \tag{5}$$

The XNOR (exclusive NOR) logic operation:

$$y = x_1 \leftrightarrow x_3 \tag{6}$$

The NAND logic operation:

$$y = \neg(x_2 \wedge x_4) \tag{7}$$

The NOR logic operation:

$$y = \neg(x_2 \vee x_4) \tag{8}$$

Where $\wedge$ represents AND, $\vee$ represents OR, $\oplus$ represents XOR, $\leftrightarrow$ represents XNOR, and $\neg$ represents NOT. The input variables are denoted as x_1, x_2, etc. and the output is y. To convert the continuous output voltage V_{out} to binary levels for logic:

$$V'\text{out} = \begin{cases} 1 & \text{if } V\text{out} > 0.5\text{V} \\ 0 & \text{if } V_{\text{out}} \leq 0.5\text{V} \end{cases} \tag{9}$$

Where V'_{out} is the discretized binary voltage used for the logic operations.

Figure 8 illustrates the ability of Kombucha–proteinoid biofilms to conduct basic logical functions. Examples of AND, OR, XOR, XNOR, NAND, and NOR gates are displayed, which are accomplished by bitwise operators and thresholding the biofilm output signals at different input voltages. The strong logic functionality is demonstrated via duplicate gates in various sample output pairs. This basic logic realisation highlights the potential of hybrid bio–abiotic materials for information manipulation and biomolecular computing, an important first step towards bio–inspired unconventional computer systems. The goal of ongoing attempts to enhance the logic gates' generalizability and dependability is to fully use the rich processing capabilities of dynamic biomaterials, which are inspired by biological intelligence.

Investigating emergent dynamics in composite biotic–abiotic networks necessitates quantitative mapping of complicated recurring events. Figure 9 shows phase portraits reconstructed from time–delayed coordinates showing complicated attractors driving system dynamics. Phase space reconstruction is a well–established model for understanding processes using geometric coordinates encoded by:

$$x_i = [s(t), s(t+\tau), ..., s(t+(m-1)\tau)]^T \tag{10}$$

where $s(t)$ represents the bioelectric signal, τ dictates embedding lag, and m is the embedding dimension. Resultant attractor shapes sculpted by recursive patterns reveal multidimensional topology difficult to profile using linear statistics. The 40:60 % K–P depiction, for example, reveals a more complex structure, with wider spreads along orthogonal vectors indicating increased stochasticity. Quantitative Lyapunov exponents and entropic measurements support this difference, which is compatible with improved kinetics due to increased microbial input. Fractal Hausdorff estimates, on the other hand, approach an upper complexity bound for both compositions, indicating robust self–organised priority.

The largest Lyapunov Exponent (LE) measures the level of unpredictability in dynamical systems, where positive values indicate the presence of chaos. The Kombucha–proteinoid (K–P) sample with a 40:60 %v/v ratio yielded a slightly negative maximal LE of –0.026. The bioelectronic output signal of this suggests a higher degree of order, residing closer to stable fixed point or limit cycle attractor regimes. In contrast, the 25:75 % K–P output yielded a significant maximal Lyapunov Exponent of 0.035, indicating the presence of chaotic behaviours and trajectories that are more likely to diverge. The higher concentration of Kombucha enables the emergence of random influences, with small disturbances spreading unpredictably through the conductive composite network.

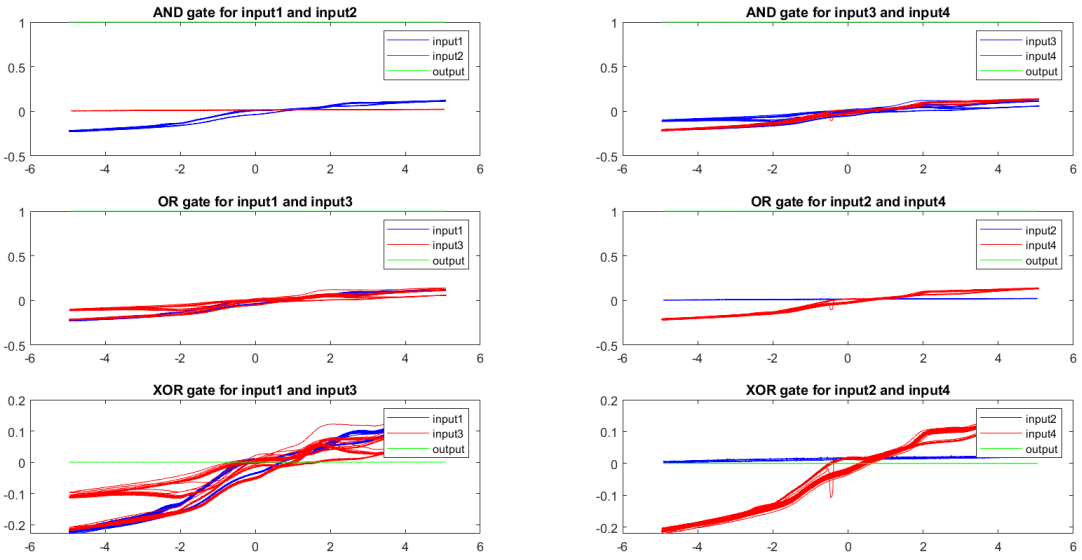


Figure 8. Utilising Kombucha–proteinoid biofilms, logic gates are realised. The charts demonstrate sample AND, OR, XOR, XNOR, NAND, and NOR logic operations carried out by bitwise and thresholding operators on Kombucha–proteinoid output signals for various input voltages ranging from -4 to +4 V. Logic applied to separate pairs of outputs from biofilm samples is highlighted by duplicate gates. The ability to modify signals logically highlights the potential of these living hybrid materials for information processing and biomolecular computing. Bio–inspired unconventional computing that uses lifelike dynamics is made possible by the continued development of reliable, generalizable logic gates.

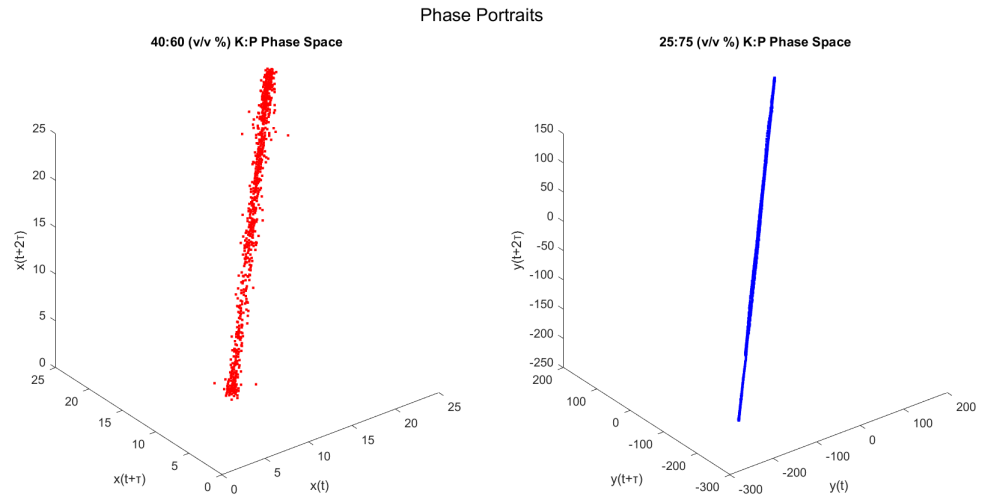


Figure 9. Through time–lagged coordinate analysis, visualising dynamical systems as phase space portraits reveals intrinsic recursive tendencies. The given results are from bio–hybrid composite samples, especially microbial Kombucha matrices merged with synthetic proteinoid micro–spheres at culture–to–additive ratios of 40:60 and 25:75 (v/v %), respectively. Tracking prior values against current signals reveals geometric attractors, which indicate the processing complexity of each live network. The shape differences between the two ratio scenarios show that the mix of biological and artificial components influences emergent activity profiles. The phase variables x(t) and y(t) represent the output signals at time t. The lag phase coordinates x(t+τ) and y(t+τ) represent the same signals offset by a constant delay (τ). Attractor shaping encodes information on the multidimensional state evolution of the system. Comparing phase pictures of 40:60 and 25:75 allows contrasting the dynamical response diversity for distinct K–P composition balances. Interpreting attractor geometry also helps with tuning.

Approximate entropy is a measure that helps us understand the level of randomness and unpredictability in time series data. The 40:60 K–P sample exhibited a higher entropy value of 0.105, suggesting the presence of more irregular signal patterns. In contrast, the 25:75 K–P system exhibited lower entropy, approximately 0.017, indicating a higher level of repeatability and predictability in its dynamics. Although both compositions exhibited nonlinear bioelectrical behaviour, the lower proteinoid fraction led to more orderly and less complex configurations. Adjusting the K–P balance has a significant effect on emergent signalling traits such as regularity and coordination, going beyond basic chaos measures.

Finally, the correlation dimension of Fractal Hausdorff[51] provides insights into the fractal properties of chaotic signals. Values generally fall within the range of 1 to 2 for fractional nonlinear systems. The correlation dimensions of both the 40:60 and 25:75 K-P samples were approximately 0.995. It suggests that there are certain patterns that exist between regular motion and chaotic trajectory divergence. Although the overall fractality remains intact, the lower proteinoid fraction causes a shift in informative signalling towards disruptive noise.

- How do the initial synaptic weights in temporally–coded neural networks, trained on Kombucha–Proteinoid data, shape the overall network architecture and its capacity for unconventional computing?

Figure 10 displays the initial synaptic weights in temporal coding neural networks that were trained using Kombucha–Proteinoid data. The heatmap plots illustrate the synaptic connections between pre–synaptic and post-synaptic neurons for two distinct compositions: Sample 1 (Kombucha–Proteinoid 40:60 % (v/v)) (Fig. 10a) and Sample 2 (Kombucha–Proteinoid 25:75 % (v/v)) (Fig. 10b). The heatmaps utilise colours to reflect the intensity of synaptic connections, with warmer hues denoting higher connectivity. The heatmaps demonstrate unique network structures for each composition scenario, emphasising the impact of the Kombucha–Proteinoid mixing ratio on the overall arrangement of the neural network.

According to Mougkogiannis et al., let $t \in \mathbb{R}^n$ represent a vector of time values measured in seconds, $p \in \mathbb{R}^{n\times 2}$ represent a matrix of potential values measured in volts for 2 different samples[52]. $N \in \mathbb{N}$ denotes the number of neurons in the Neural Network (NN), $T \in \mathbb{R}^+$ indicates the time window for temporal coding measured in seconds, and $\theta \in \mathbb{R}^+$ represents the threshold for spike detection measured in volts. Matrices $c \in \{0,1\}^{N\times n}$ and $W \in [-1,1]^{N\times N}$ symbolize the temporal codes for each neuron over time and the synaptic weights between neurons, respectively.

For each sample, denoted by $i = 1, \cdots, 2$, the temporal code $c_{j,i}$ will be equal to 1 if the corresponding potential value $p_{j,i}$ exceeds the threshold θ, and it will be multiplied by the time duration $(T - \min_{k\in[1,n]}\{p_{k,i} : p_{k,i} > \theta\})$. The indicator function $1_{p_{j,i}>\theta}$ returns 1 if the potential value $p_{j,i}$ is greater than θ, and 0 otherwise.

The neurons in the neural network are differentiated by their unique temporal coding, input parameters, and synaptic weights. When the temporal code (denoted as $c_{:,j}$) surpasses the threshold parameter (θ), the neuron produces an action potential similar to that of a real neuron, transmitting signals through its axonal connections. The proteinoid neurons bear a resemblance to the neurons in a biological nervous system. The synaptic weights (W) in the neural network control the strength of the connections between axons and dendrites, serving a similar function to synapses in natural neural systems.

Discussion

Kombucha–Proteinoid (KP) living electronics signify a significant advancement within the rapidly developing domain of biohybrid technologies, which involve the integration of organic constituents into conventional computational systems. Our findings indicate that the integration of these biotic and abiotic materials in a synergistic manner generates emergent functionality, which in turn stimulates innovation in a wide range of technological fields. Most notably, KP electronics demonstrate the intricate information processing capabilities that are essential for supplying power to adaptive robotics inspired by biology. KP devices have the potential to function as sensors that enable robots to react to environmental stimuli, in addition to circuits that facilitate advanced control systems that govern realistic movement and behaviour. These organic electronics would endow these devices with a capability comparable to that of cells, enabling them to perceive and adapt to their environment. Furthermore, the distinctive electrochemical characteristics of KP have the potential to significantly enhance synthetic biomedical apparatus by providing biocompatible interfaces for prosthetics. In addition, lab–on–a–chip devices could incorporate programmable KP sensors and microfluidic scaffolds to capture physiological dynamics, thereby transforming drug testing and disease diagnosis. Beyond the realm of biomedicine, the engineered protein nanostructures and exceptional electrical signalling behaviours that emerge from KP offer a flexible foundation for advancements in chemical synthesis, green electronics, and bio–imaging. Simulations of organs and tissues, biodegradable cables, circuits, and computer chips—-the scope of possibilities is astounding. Obviously, our exploration of the potential applications for biohybrid KP electronics is far from exhaustive. However, the vast array of functionalities that have been demonstrated already suggests that these living materials have the capacity to revolutionise technology by fusing the most advantageous aspects of the natural and synthetic realms[53–55].

- How can we design intelligent systems that imitate the information processing and adaptive behaviours of natural cognition?

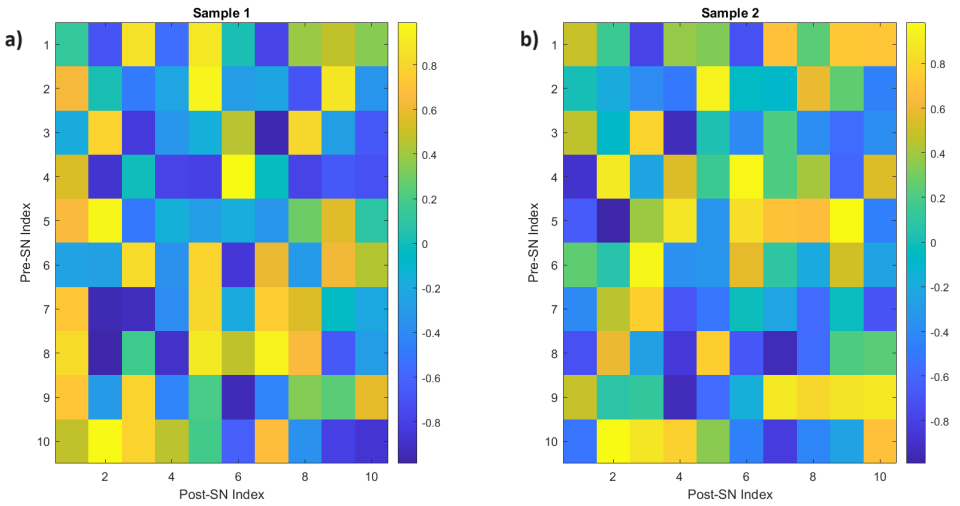


Figure 10. Visualising the initial synaptic weights in Temporal Coding Neural Networks that were trained using Kombucha-Proteinoid samples. Figure (a) displays the heatmap representation of the initial synaptic weights for Sample 1. This sample is the Kombucha–Proteinoid blend, which has a composition of 40% Kombucha and 60% Proteinoid, measured in volume. The heatmap facilitates a clear comprehension of the connection pattern between the pre–synaptic and post–synaptic neurons in the network. The heatmap in Figure (b) displays the initial synaptic weights for Sample 2, representing the composition ratio of Kombucha–Proteinoid as 25%:75% (v/v). This heatmap offers a clear depiction of the network structure involved in a diverse composition scenario. The plots utilise a colour gradient to represent the synaptic connections' strength, where warmer colours suggest stronger inter–neuronal communication. These heatmaps provide vital insights into the structure and arrangement of the neural network for various mixtures of Kombucha–Proteinoid proto–brains.

Robust information processing, adaptation, and emergent cognition are enabled by the integration of heterogeneous components in synthetic bio–computational systems. Proteinoids and Kombucha each bring their own unique set of properties that, when combined, form a foundation for advanced logic application and learning, as seen in Table 1. In particular, proteinoids operate as reconfigurable logic gates when they self–assemble into micro–networks that may carry electrical signals and execute Boolean logic operations (Table 1)[21]. In contrast to logic, which remains constant regardless of inputs, adaptive learning requires constant tuning as inputs change. The unique metabolic pathways of the microbial community in Kombucha are responsible for its reconfigurability. These pathways display synaptic plasticity, which is similar to long–term potentiation in neural networks (Table 1). In conclusion, by combining these two biocomponents, complex bio–logic circuits can be built, equipped with sensory processing capabilities and adaptive programming, and able to mimic important aspects of natural cognition in a computing living platform. Here, bottom–up synthetic biology and unconventional computation come together to show how designed biological systems can become more than the sum of their parts.

Table 1. Comparison of properties enabling computation and cognition.

	Proteinoids	**Kombucha**	**Kombucha-Proteinoids**
Structure	Assemblies and networks	Cellulose matrix	Embedded composites
Signaling Properties	Electrical spiking	Ion conduction	Tunable conductivity
Information Processing	Logic operations	Synaptic-like	Reconfigurable transforms
Adaptability	Learning	Metabolic pathways	Morphable networks
Emergent Cognition	Biological neural networks	Microbial intelligence	Bio-inspired computing

- Which complementary biomaterials can be synthesized into circuits capable of information processing and adaptation?
- How can predictive modeling and synthetic biology be integrated to enable robust emergent behaviors in bacteria–based biohybrid systems?

A recent study conducted by Leaman et al. presents a convincing illustration of how a data–driven statistical method may effectively describe the movement patterns in two distinct types of E. coli swarms[56]. Their model, in conjunction with a

collaborative gene expression scheme, identified variations in the time–frames for planned emergent behaviours among the bacterial groups. The study showcases the effectiveness of combining synthetic biology approaches with computational modelling to enhance engineered biological systems by discovering crucial factors that control their resilience and ability to emerge. As demonstrated in the research conducted by Buss et al., the swift movement and genetic adaptability of E. coli make it very suitable for drug delivery[57]

- What synergistic effects emerge from unifying proteinoids and Kombucha within a synthetic bio–system?

The hybrid system of microbial Kombucha networks interwoven with synthetic proteinoid microspheres shows promise for bio–inspired information processing and adaptive computation. The Kombucha SCOBY mat's cellulose–secreting properties provide a dynamic biotic scaffolding for housing and interfacing the proteinoids. This extracellular structure derived from self–organized bacteria and yeasts provides a living architecture ideal for proteinoid integration, with nutrient diffusion networks and signalling pathways ripe for coupling. Meanwhile, the proteinoids' customizability down to specific amino acid monomers allows for precise control of new characteristics and computing capacities. Proteinoids, which are polymerized using methods that mimic hypothesised prebiotic chemistry, are programmable protocells that can integrate modular and excitable computing features inside the microbial film ecology. Emergent computational and cognitive system behaviours appear at the interface of bottom–up synthetic biology and top–down living scaffold assembly. The interaction of SCOBY secreted cellulose, electron–transporting aceto–bacteria, spiking proteinoid micro–spheres, and shuttling molecular signals results in a dynamic bio–abiotic network with learning, adaptation, and information transformation characteristics far exceeding those of its isolated constituents. As the study of natural computing expands the substrates and architectures employed for processing, hybrid biosynthetic materials that balance intrinsic microbial intelligence with introducible synthetic block modularity will become increasingly powerful.

In order to thoroughly analyse the unconventional computing capabilities of the Kombucha–Proteinoid system, would necessitate several key lines of investigation. Experiments employing electrophysiology may shed light on the synaptic–like plasticity and electrical signalling characteristics of KP networks, thereby identifying bioelectric features that are conducive to learning and computation. In terms of speed, accuracy, and efficiency, logic implementations and architecture design that make use of the emergent topology may exhibit comparable performance to conventional computing on pattern recognition tasks. The study of information dynamics in KP circuits using biophysical models may yield valuable insights into the optimisation of computational capacities. By applying bilateral information and entropy metrics to the analysis of KP logic gate experiments, the extent of information processing in relation to biological cognition may be revealed. Furthermore, an investigation into the impacts of electrical, topological, and biochemical tuning protocols may reveal techniques for training substrates for high–performance KP computation. A thorough examination of the unconventional computing capabilities of the binary component Kombucha–Proteinoid system requires a multidisciplinary approach encompassing electrophysiology, bio–inspired engineering, biophysics, and information theory. Further effort is required to optimise KP composites for specialised applications; however, the underlying opportunity is evident: follow nature rather than resisting it.

- What further domains might benefit from this fusion of microbial scaffolds and synthetic biology?

The emergent conductive behaviours demonstrated by merging synthetic proteinoids with living Kombucha microbial scaffolds, as investigated in this study, demonstrate the vast potential of bio–hybrid materials for unconventional information processing. However, as illustrated in Figure 11, these bioelectronic devices represent only a small subset of the options available in the developing field of natural computing engineering. Myriad organic substrates, ranging from organisms such as lichen fungi to self–assembled structures such as cytoskeletal filaments and artificially–crafted components such as DNA–based logic gates, all provide fertile ground for the implementation of alternative modes of data representation, memory encoding, and computational operations.

Conclusion

Kombucha–proteinoid composite biofilms are an encouraging development in the field of engineering adaptive and multifunctional bioelectronic materials. This study showcases the potential of soft, dynamic films that incorporate synthetic biomolecular signalling components and a robust bacterial hydrogel matrix. These films are capable of performing critical functions such as biointerfaces and unconventional computation. The ability to modify the emergent electronic properties of the proteinoids and adjust their composition within the zoogleal nanostructure underscores the potential for customization of these biohybrid films to suit a wide range of applications. Beyond particular functionalities, the bioinspired approach integrates synthetic processing and resilience with realistic excitation, growth, and adaptation, which is critical for the development of next–generation technologies that exist at the interface of machines and organisms. Although additional work is required to completely implement these preliminary ideas into operational systems, the principles outlined in this study represent a promising advancement towards

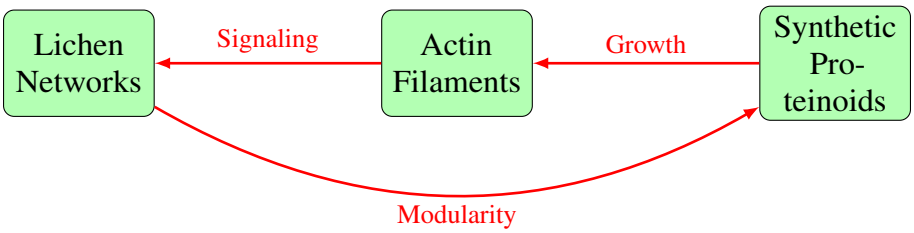


Figure 11. Substrates inspired by biological systems for the purpose of bio–computation. Organisms, natural structures, and synthetic analogues, such as lichen Networks, actin filaments, and synthetic proteinoids, can be used as initial models for developing unconventional information processing methods in engineering. Within these systems, Lichen Networks employ signalling routes to provide efficient communication and information exchange among many components. Actin filaments serve as a flexible structure that facilitates development and reorganisation, allowing for adaptation and responsiveness to stimuli. Synthetic proteinoids demonstrate emergent characteristics, including as modularity and self–assembly, that can be utilised for unconventional computing purposes. The interaction between signalling, growth, and modularity in these systems allows for the development of new types of bio–computation, which can be applied in areas such as biological intelligence and bioinformatics.

future integrated bio–abio systems based on the fundamental concepts of biological intelligence, organisation, and adaptability. The convergence of the technological advancements of humanity and the accomplishments of nature spanning billions of years continues to unveil profound scientific and engineering prospects.

Methods

Fabrication process for Kombucha-Proteinoid composites

Kombucha–Proteinoid protobrains are synthesized by integrating proteinoids within Kombucha cellulose pellicles. Kombucha films are first grown by infusing tea and sugar with boiled water, then inoculating with a SCOBY symbiotic culture and incubating at 20–23°C in darkness. Once a cellulosic biofilm forms, proteinoids are introduced by injecting proteinoid solutions into the mat and applying proteinoids to the surface. The composite is returned to the incubator for 24 hours to allow proteinoid diffusion and attachment (Fig. 12). Kombucha provides a robust scaffold with rapid growth, while proteinoids confer tailored functionality like signaling dynamics. Resulting composites exhibit periodic electrical activity reminiscent of spiking neurons. By pairing Kombucha's structural qualities with proteinoids' excitability, adaptable bioelectronic materials are produced. Their biotic–abiotic hybrid nature enables emergent capabilities. Studying factors influencing the integration process, including culture conditions, materials ratios, and assembly kinetics, will enable optimization of protobrain synthesis. Figure 13a depicts the modular biofabrication process, which starts with the cultivation of the Kombucha cellulose matrix. The hydrogel film demonstrates valuable characteristics such as fast growth, tunable scalability, and basic electrical conduction before the proteinoid is introduced. The introduction of proteinoids is facilitated through injection methods and surface attachment, enabling diffusion and interaction with the conductive scaffold (Fig. 13b). The figures clearly demonstrate the successful development of controlled Kombucha culture and the infusion of programmed proteinoids, allowing for the engineering of composite materials with specific characteristics. Continued refinement of growth conditions, culture durations, proteinoid compositions, and assembly kinetics is enhancing the precise integration of components in these hybrid living materials.

Electrical measurement and analysis

The experiment used a BK Precision 4053 MHz dual channel waveform generator to generate the electrical stimuli. To transmit the impulses and record the responses, platinum–iridium electrodes with a diameter of 0.2 mm and a spacing of 10 mm were inserted in the KP solutions. A Rigol oscilloscope (2 Channel, 100 MHz – 1GSa/s), PicoLog ADC–24, and Picoscope were used to acquire the data. Electrical measurements were also taken with a Keithley 2450 sourcemeter.

References

1. Dimidi, E., Cox, S. R., Rossi, M. & Whelan, K. Fermented foods: definitions and characteristics, impact on the gut microbiota and effects on gastrointestinal health and disease. *Nutrients* **11**, 1806 (2019).

2. Tietze, H. *Kombucha: The miracle fungus* (Harald Tietze Publishing P/, 1996).

3. Greenwalt, C., Steinkraus, K. & Ledford, R. Kombucha, the fermented tea: microbiology, composition, and claimed health effects. *J. food protection* **63**, 976–981 (2000).

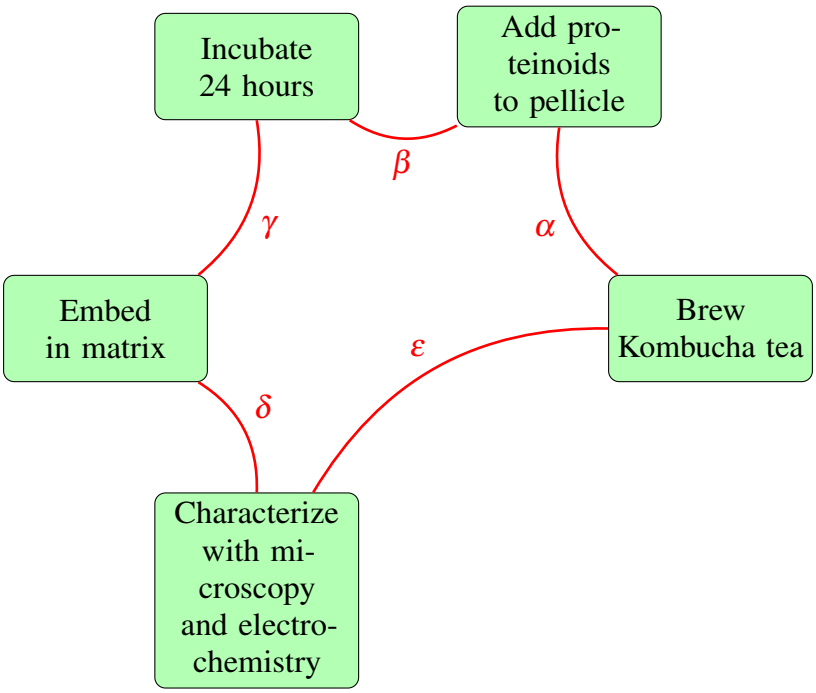


Figure 12. Kombucha–Proteinoid protobrains are synthesized through a five-step process. A dynamic structure is produced where yeasts and bacteria coexist within cellulose fibres. Proteinoid microspheres are inserted into the tiny structure and attach to the biofilm. After incubating for one day, the proteinoids get embedded within the gelatinous microbial mesh, allowing for integration. Ultimately, composites undergo analysis using microscopes and voltmeters, which unveil neural-like signalling patterns. Cycling arrows denote iterative refinement of preparation protocols.

4. Santos, M. J. d. *Kombucha: caracterização da microbiota e desenvolvimento de novos produtos alimentares para uso em restauração*. Ph.D. thesis (2016).
5. Coelho, R. M. D., de Almeida, A. L., do Amaral, R. Q. G., da Mota, R. N. & de Sousa, P. H. M. Kombucha. *Int. J. Gastron. Food Sci.* **22**, 100272 (2020).
6. Jayabalan, R., Malbasa, R. & Sathishkumar, M. Kombucha. reference module in food science, 11, 422 (2016).
7. Frank, G. W. *Kombucha: healthy beverage and natural remedy from the Far East; its correct preparation and use* (Ennsthaler, 1991).
8. Fu, C., Yan, F., Cao, Z., Xie, F. & Lin, J. Antioxidant activities of kombucha prepared from three different substrates and changes in content of probiotics during storage. *Food Sci. Technol.* **34**, 123–126 (2014).
9. Gaggìa, F. *et al.* Kombucha beverage from green, black and rooibos teas: A comparative study looking at microbiology, chemistry and antioxidant activity. *Nutrients* **11**, 1 (2018).
10. Lončar, E., Djurić, M., Malbaša, R., Kolarov, L. & Klašnja, M. Influence of working conditions upon kombucha conducted fermentation of black tea. *Food Bioprod. Process.* **84**, 186–192 (2006).
11. Chen, C. & Liu, B. Changes in major components of tea fungus metabolites during prolonged fermentation. *J. applied microbiology* **89**, 834–839 (2000).
12. De Filippis, F., Troise, A. D., Vitaglione, P. & Ercolini, D. Different temperatures select distinctive acetic acid bacteria species and promotes organic acids production during kombucha tea fermentation. *Food microbiology* **73**, 11–16 (2018).
13. Fox, S. W. Thermal synthesis of amino acids and the origin of life. *Geochimica et Cosmochimica Acta* **59**, 1213–1214 (1995).
14. Fox, S. W. & Harada, K. The thermal copolymerization of amino acids common to protein1. *J. Am. Chem. Soc.* **82**, 3745–3751 (1960).
15. Mougkogiannis, P. & Adamatzky, A. Proto–neurons from abiotic polypeptides. (2023).
16. Przybylski, A. T. & Fox, S. W. Excitable artificial cells of proteinoid. *Appl. Biochem. Biotechnol.* **10**, 301–307 (1984).



Figure 13. The formation of Kombucha–proteinoid protobrains. (a) Kombucha cellulose cultivation before proteinoid integration. b) Injection and surface application of proteinoids into mature Kombucha mat.

17. Wolman, Y., Haverland, W. J. & Miller, S. L. Nonprotein amino acids from spark discharges and their comparison with the murchison meteorite amino acids. *Proc. Natl. Acad. Sci.* **69**, 809–811 (1972).

18. Przybylski, A. T., Stratten, W. P., Syren, R. M. & Fox, S. W. Membrane, action, and oscillatory potentials in simulated protocells. *Naturwissenschaften* **69**, 561–563 (1982).

19. Fox, S. W. & Dose, K. Molecular evolution and the origin of life. *(No Title)* (1977).

20. Fox, S. W., Jungck, J. R. & Nakashima, T. From proteinoid microsphere to contemporary cell: formation of internucleotide and peptide bonds by proteinoid particles. *Orig. Life* **5**, 227–237 (1974).

21. Mougkogiannis, P. & Adamatzky, A. Light-induced spiking in proteinoids yields boolean gates. *Mater. & Des.* 112460 (2023).

22. Adamatzky, A. Towards proteinoid computers. hypothesis paper. *Biosystems* **208**, 104480 (2021).

23. HSU, L. H.-N. L. *PROTEINOID MICROSPHERES AS MODELS FOR PRIMORDIAL ORGANIC EVOLVING SYSTEMS.* (University of Miami, 1974).

24. Matsuno, K. *Molecular evolution and protobiology* (Springer Science & Business Media, 2012).

25. Dose, K. Chemical and catalytical properties of thermal polymers of amino acids (proteinoids). *Orig. Life* **5**, 239–252 (1974).

26. Adamatzky, A. Electrical potential spiking of kombucha zoogleal mats: A symbiotic community of bacteria and yeasts. *Bioelectricity* **5**, 99–108 (2023).

27. Mougkogiannis, P. & Adamatzky, A. Low frequency electrical waves in ensembles of proteinoid microspheres. *Sci. Reports* **13**, 1992 (2023).

28. Mougkogiannis, P. & Adamatzky, A. Logical gates in ensembles of proteinoid microspheres. *Plos one* **18**, e0289433 (2023).

29. Mougkogiannis, P. & Adamatzky, A. Recognition of sounds by ensembles of proteinoids. *bioRxiv* 2023–07 (2023).

30. Piro, B., Tran, H. V. & Thu, V. T. Sensors made of natural renewable materials: Efficiency, recyclability or biodegradability—the green electronics. *Sensors* **20**, 5898 (2020).

31. Cao, Y. & Uhrich, K. E. Biodegradable and biocompatible polymers for electronic applications: A review. *J. Bioact. Compatible Polym.* **34**, 3–15 (2019).

32. Adamatzky, A. *et al.* Kombucha electronics: electronic circuits on kombucha mats. *Sci. Reports* **13**, 9367 (2023).

33. Chua, L. Memristor-the missing circuit element. *IEEE Transactions on circuit theory* **18**, 507–519 (1971).

34. Chua, L. O. & Kang, S. M. Memristive devices and systems. *Proc. IEEE* **64**, 209–223 (1976).

35. Beasley, A. E. *et al.* Mem-fractive properties of mushrooms. *Bioinspiration & Biomimetics* **16**, 066026 (2022).

36. Adamatzky, A. Electrical potential spiking of kombucha zoogleal mats. *bioRxiv* 2022–08 (2022).

37. Isah, A., Tchakoutio Nguetcho, A., Binczak, S. & Bilbault, J. Polarity reversal effect of a memristor from the circuit point of view and insights into the memristor fuse. *Front. Commun. Networks* **2**, 647528 (2021).

38. Wang, Z. *et al.* Memristors with diffusive dynamics as synaptic emulators for neuromorphic computing. *Nat. materials* **16**, 101–108 (2017).

39. Pershin, Y. V. & Di Ventra, M. A simple test for ideal memristors. *J. Phys. D: Appl. Phys.* **52**, 01LT01 (2018).

40. Mellor, C. Hp 100tb Memristor drives by 2018 – if you're lucky, admits tech titan. https://www.theregister.com/2013/11/01/hp_memristor_2018/ (2013).

41. Williams, R. S. How we found the missing memristor. *IEEE spectrum* **45**, 28–35 (2008).

42. Meuffels, P. & Soni, R. Fundamental issues and problems in the realization of memristors. *arXiv preprint arXiv:1207.7319* (2012).

43. Di Ventra, M. & Pershin, Y. V. On the physical properties of memristive, memcapacitive and meminductive systems. *Nanotechnology* **24**, 255201 (2013).

44. Kim, J., Pershin, Y. V., Yin, M., Datta, T. & Di Ventra, M. An experimental proof that resistance-switching memory cells are not memristors. *Adv. Electron. Mater.* **6**, 2000010 (2020).

45. Sundqvist, K. M., Ferry, D. K. & Kish, L. B. Memristor equations: Incomplete physics and undefined passivity/activity. *Fluctuation Noise Lett.* **16**, 1771001 (2017).

46. Abraham, I. The case for rejecting the memristor as a fundamental circuit element. *Sci. reports* **8**, 10972 (2018).

47. Bernardus Mostert, A., Powell, B. J., Gentle, I. R. & Meredith, P. On the origin of electrical conductivity in the bio-electronic material melanin. *Appl. Phys. Lett.* **100** (2012).

48. Mougkogiannis, P., Raeisi Kheirabadi, N., Chiolerio, A. & Adamatzky, A. Electrical spiking activity of proteinoids-zno colloids. *bioRxiv* 2023–07 (2023).

49. Adamatzky, A. Dynamics of electrical resistance of kombucha zoogleal mats. *Biophys. Rev. Lett.* **17**, 135–144 (2022).

50. Ramírez Tapias, Y. A., Peltzer, M. A., Delgado, J. F. & Salvay, A. G. Kombucha tea by-product as source of novel materials: Formulation and characterization of films. *Food Bioprocess Technol.* **13**, 1166–1180 (2020).

51. Hausdorff (Box-Counting) Fractal Dimension. https://uk.mathworks.com/matlabcentral/fileexchange/30329-hausdorff-box-counting-fractal-dimension (2013).

52. Mougkogiannis, P. & Adamatzky, A. Proteinoid microspheres as protoneural networks. *ACS Omega* **8**, 35417–35426, DOI: 10.1021/acsomega.3c05670 (2023). https://doi.org/10.1021/acsomega.3c05670.

53. Lin, Z., Jiang, T. & Shang, J. The emerging technology of biohybrid micro-robots: a review. *Bio-Design Manuf.* 1–26 (2022).

54. Menciassi, A., Takeuchi, S. & Kamm, R. D. Biohybrid systems: Borrowing from nature to make better machines. *APL bioengineering* **4** (2020).

55. Patino, T., Mestre, R. & Sanchez, S. Miniaturized soft bio-hybrid robotics: a step forward into healthcare applications. *Lab on a Chip* **16**, 3626–3630 (2016).

56. Leaman, E. J. *et al.* Data-driven statistical modeling of the emergent behavior of biohybrid microrobots. *APL bioengineering* **4** (2020).

57. Buss, N., Yasa, O., Alapan, Y., Akolpoglu, M. B. & Sitti, M. Nanoerythrosome-functionalized biohybrid microswimmers. *APL bioengineering* **4** (2020).

Acknowledgements

The research was supported by EPSRC Grant EP/W010887/1 "Computing with proteinoids". Authors are grateful to David Paton for helping with SEM imaging and to Neil Phillips for helping with instruments.

Author contributions statement

Anna Nikolaidou contributed to the writing and editing of the paper, as well as the synthesis of Kombucha and analyzing the results. Panagiotis Mougkogiannis performed experiments on the proteinoids and contributed to the writing of the paper. Andrew Adamatzky supervised the research and edited the final paper.

Competing Interests

We, the authors Anna Nikolaidou, Panagiotis Mougkogiannis and Andy Adamatzky, declare that we don't have conflicts of interest associated with the article.

Data availability

The datasets generated and/or analysed during the current study are available in the zenodo repository, [https://zenodo.org/records/10206807].

Turing Machine Universality of the Game of Life, Cham, Springer, 2016.

[25] S. J. Martínez, I. M. Mendoza, G. J. Martínez, & S. Ninagawa, "Universal One-dimensional Cellular Automata Derived from Turing Machines," *op. cit.*

[26] *Ibidem*.

[27] N. Margolus, T. Toffoli & G. Vichniac, "Cellular-automata super- computers for fluid-dynamics modeling," *Physical Review Letters 56(16)*, 1986, 1694; S. Wolfram, "Cellular automaton supercomputing," Center for Complex Systems Research, 1987, online: https://content.wolfram.com/uploads/sites/34/2020/07/cellular-automaton-supercomputing.pdf; A. Adamatzky, *Computing in nonlinear media and automata collectives*, Boca Raton, CRC Press, 2001.

[28] A. Adamatzky & G. J. Martinez (eds), *Designing Beauty: the Art of Cellular Automata*, Cham, Springer, 2016.

[29] C. H. Bennett, "Logical reversibility of computation," *IBM journal of Research and Development 17(6)*, 1973, 525-532; K. Morita, "Reversible computing and cellular automata: A survey," *Theoretical Computer Science 395(1)*, 2008, 101-131.

[30] E. Fredkin & T. Toffoli, "Conservative logic," *International Journal of theoretical physics 21(3-4)*, 1982, 219-253; K. Morita, "A simple universal logic element and cellular automata for reversible computing," in M. Margenstern, Y. Rogozhin (eds), *International Conference on Machines, Computations, and Universality*, Berlin/Heidelberg, Springer, 2001, 102-113.

[31] L. O. Chua, "Chuas circuit: An overview ten years later," *Journal of Circuits, Systems, and Computers 4(02)*, 1994, 117-159.

[32] N. H. Margolus, "Crystalline computation," in A. Hey (ed.), *Feynman and Computation: Exploring the Limits of Computers*, Boca Raton, CRC Press, 1998, 267-305.

[33] T. Sienko, A. Adamatzky & N. Rambidi, *Molecular computing*, Cambridge, MIT Press, 2003.

[34] B. Grĭnbaum & G. C. Shephard, *Tilings and patterns*, Mineola, Courier Dover Publications, 1987.

[35] G. J. Martínez, A. Adamatzky, K. Morita & M. Margenstern, "Computation with competing patterns in Life-like automaton," in A. Adamatzky (ed.), *Game of Life Cellular Automata*, London, Springer, 2010, 547-572.

[36] M. Burgin, "Information Processing by Symmetric Inductive Turing Machines," *op. cit.*

[37] M. H. Jakubowski, K. Steiglitz & R. Squier, "Computing with solitons: a review and prospectus," in A. Adamatzky (ed.), *Collision-based computing*, London, Springer, 2002, 277-297.

[38] A. Adamatzky, "Slime mould computing," *International Journal of General Systems 44(3)*, 2015, 277-278.

*** Free software used to create the simulations in this paper.**

- Ready (Tim Hutton, Robert Munafo, Andrew Trevorrow, Tom Rokicki, https://github.com/gollygang/ready)
- CAviewer (José Antonio Jiménez Amador, Genaro J. Martínez, https:// www.comunidad.escom.ipn.mx/genaro/Papers/Thesis_files/CAviewer. tar.gz)
- CATM (Sergio Eduardo Juárez Martínez, César Iván Manzano Mendoza, https://www.comunidad.escom.ipn.mx/genaro/Papers/Thesis_files/maquinaTuring.java.tar.gz)

Living wearables from slime mould and fungi

Andrew Adamatzky,[1] Anna Nikolaidou,[2] Antoni Gandia,[3] and Alessandro Chiolerio[4]

Smart wearables, augmented with soft and liquid electronics, can display sensing, responsive and adaptive capabilities, but they cannot self-grow or self-repair. Living organisms colonising a fabric could be a viable alternative. In the present article we briefly review our ideas on implementing living wearables with slime mould and fungi. The living networks of slime mould protoplasmic tubes and fungal mycelium networks can act as distributed sensorial networks, fuse sensorial inputs from wearers and environment, process information in a massive parallel manner and provide responses in benefit of the consortium human-microbe.

Most living creatures have plenty of living wearables: skin, mites, fungal and bacterial colonies colonising the skin, and critters living our hairs. Skin is out living wearable number one. The skin senses, transmit information and, more likely, is capable of distributed decision making. Limitations of the skin are that the skin is not disposable, we cannot change our skin as easy as we can change the pants or socks, sensorial and computational properties of the skins are not easily tunable, attempts to integrate soft and liquid electronics into human skins pose health risks and incompatibility issues. Also it is not acceptable in many cultures to appear in public naked, so a substantial area of our skin should be covered by fabric and thus renders useless for immediate environmental sensing. Traditionally, wearables have acted as covering tools aiming to provide comfort and protection from the elements. They have also constituted semiotic devices, machines for communication[5] and functioned as social mediators and interfaces between our bodies and society.[6] With the emergence of novel and smart materials, the functionality of wearables has been extended, offering new opportunities. Smart materials can be defined as highly engineered materials that respond intelligently to their environment.[7] They are characterized by their ability to detect and respond to stimuli from the environment (such as stress, temperature, moisture, pH, electric or magnetic fields), by a specific change of behaviour, as for instance a colour or shape or form change.[8] Smart materials are often embedded in more conventional materials and applied in a system with microelectronic components and miniaturized technologies.[9]

Smart wearables are devices that are responsive to the wearer, they can sense and process information from the user's body and environment and report results of their analysis as electrical signals.[10] In the last decade, electronics and textiles (e-textiles) have been a fundamental part of smart wearables. Integrating electronics into textile products enables the development of wearable electro-textiles for sensing / monitoring body functions, delivering communication facilities, data transfer, control of the environment, and many other applications.[11] For example, a material surface, such as a common fabric that embeds a nitinol wire (a smart material), can become sensitive and responsive (with visual or kinetic response) according to an external stimulus, like a rise in temperature. This may happen when you wear it, and the increase in body temperature causes the expansion of the fabric.[12] One of the most impacting issues regarding both electron devices and nanocomposite materials is represented by their poor capability to self-repair and grow, to self-organize and adapt to changing environmental conditions.

Although smart wearables can display sensing, responsive and adaptive capabilities, they cannot self-grow and self-repair. In addition to



Fig. 1. Live slime mould *Physarum polycephalum* growing on a doll. Experiments conducted with A. A.'s daughter, Adriana Adamatzky, in 2010.



Fig. 2. A polyurethane mannequin head colonised by slime mould *Physarum polycephalum*.



Fig. 3. Imitation of scalp innervation with *Physarum polycephalum*.

this, the materials usually used to create the electronic components of the wearables such as metals, plastics and other petroleum-based materials are derived from natural resources, which are limited and non-renewable. Electronic waste or e-waste is one of the emerging problems in developed and developing countries worldwide as it comprises a multitude of components with valuable materials, some containing toxic substances, that can have an adverse impact on human health and the environment.[13] Living organisms could be a viable alternative.

Back in the 2010s we proposed a concept of *extralligence* by growing living slime *Physarum polycephalum* on models of human bodies.[14] We designed, and partly implemented in laboratory conditions with slime mould *Physarum polycephalum*, an intelligent adaptive living network wearable by humans and robots. When grown on 3D bodies (living or inanimate) the living *Physarum* network provides a highly-distributed sensorial structure (light-, electro-magnetic, chemical and tactile sensitivity) with embedded dynamic architecture of massive-parallel computing processors based on geometry of proximity graphs. We have chosen an acellular slime mould *Physarum polycephalum* as amorphous living substrate because Physarum is a living, dynamical reaction diffusion pattern formation mechanism; Physarum may be considered as equivalent to a membrane bound sub excitable system (excitation stimuli provided by chemo-attractants and chemo-repellents); Physarum may be regarded as a highly efficient and living micro-manipulation and microfluidic transport device; Physarum is sensitive to illumination and AC electric fields and therefore allows for parallel and non-destructive input of information; Physarum represents results of computation by configuration of its body. In experimental laboratory studies, we showed that when inoculated on bare plastic surfaces, Physarum successfully develops an optimal network of protoplasmic tubes spanning sources of attractants while avoiding domains with over threshold concentration of repellents. When exposed to attractants and repellents, Physarum changes patterns of its electrical activity. We experimentally derived a unique one-to-one mapping between a range of selected bioactive chemicals and patterns of oscillations of the slime mould's extracellular electrical potential. This direct and rapid change demonstrates detection of these chemicals in a similar manner to a biological contactless chemical sensor. We believe results could be used in future designs of slime mould based chemical sensors and computers. We also evaluated feasibility of slime-mould based colour sensors

by illuminating Physarum with red, green, blue and white colours and analysing patterns of the slime mould's electrical potential oscillations. We defined that the slime mould recognises a colour if it reacts to illumination with the colour by a unique changes in amplitude and periods of oscillatory activity. In laboratory experiments we found that the slime mould recognises red and blue colour. The slime mould does not differentiate between green and white colours. The slime mould also recognises when red colour is switched off. We also mapped colours to diversity of the oscillations: illumination with a white colour increases diversity of amplitudes and periods of oscillations, other colours studied increase diversity either of amplitude or period.

As a proof of concept we designed an experimental laboratory implementation of a slime mould based tactile bristles, where the slime mould responds to repeated deflection of bristle by an immediate high-amplitude spike and a prolonged increase in amplitude and width of its oscillation impulses. We demonstrated that signal strength of the Physarum tactile bristle sensor averages near six for an immediate response and two for a prolonged response. Despite the sufficient sensorial abilities, the slime mould is rather fragile, highly dependent on environmental conditions and requires particular sources of nutrients. Fungi could, however, make a feasible alternative to the slime mould for the following reasons. Fungal composite materials, normally in form of solid lignocellulosic substrates colonised with the mycelium of filamentous fungi (e.g. *Ganoderma* spp., *Pleurotus* spp., *Trametes* spp.), are an emerging type of biomaterial known by being a robust, reliable and ecologically friendly replacement for conventional building materials and fabrics.[15] Fungi possess almost all the senses used by humans.[16] Fungi sense light, chemicals, gases, gravity and electric fields. Fungi show a pronounced response to changes in a substrate pH,[17] mechanical stimulation,[18] toxic metals,[19] CO2,[20] and stress hormones.[21] Fungi are known to respond to chemical and physical stimuli by changing patterns of its electrical activity[22] and electrical properties.[23] Thus, wearables made of or incorporating a cellulosic fabric colonised by fungi might act as a large distributed sensorial network.

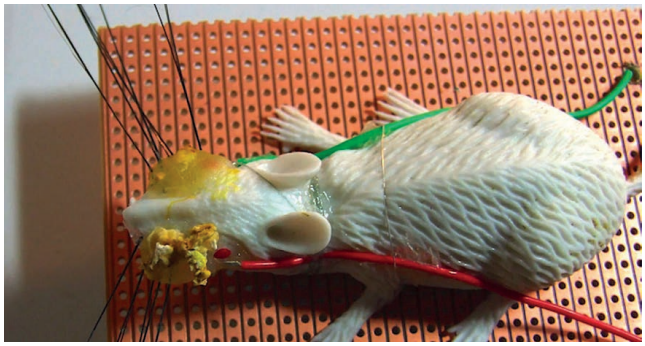


Fig. 4. Rat whiskers made of living slime mould *Physarum polycephalum*.

To evaluate feasibility of the living fungal wearables, we conducted two sets of laboratory experiments.
In the first set, to assess the sensing potential of fungal wearables, we undertook laboratory experiments on electrical response of a hemp fabric colonised by oyster fungus *Pleurotus ostreatus* to mechanical stretching and stimulation with attractants and repellents.[24] A fabric colonised by the fungus *P. ostreatus* shows distinctive sets of responses to chemical and mechanical stimulation. The response to 50 g load is in the range of 1.5 min which might indicate that rather purely electro-mechanical events take place than reactions involving propagation of calcium waves. The response to stimulation with ethanol is in a range of 7 sec. This would rather indicate physico-chemical damages to hyphae walls and corresponding electrical responses. The increase of frequency of electrical potential oscillation in a response to application of chemo-attractants or nutrients is consistent with previous studies. The increase in amplitude of spiking hours after the application of malt or dextrose might be due to the fungus ingesting the nutrients and transposing them across the wide mycelial network.
In the second set of experiments[25] we experimented with fungal skin. A fungal skin is a thin flexible sheet of a living interwoven, homogeneous, and continuous mycelium made by a filamentous fungus. The skin could be used in future living architectures of adaptive buildings and as a sensing living skin for soft self-growing/adaptive robots. In experimental laboratory studies, we demonstrated that the fungal skin is capable of recognising mechanical and optical stimulation. The skin reacts differently to loading of a weight, removal of the weight,

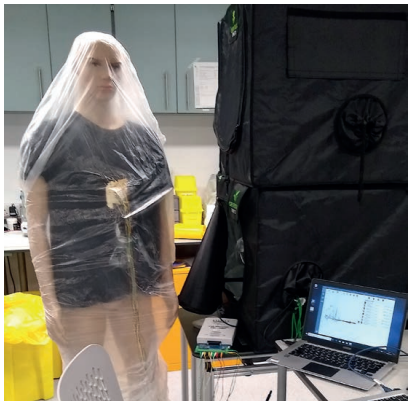


Fig. 5. A photo of experimental setup showing a hemp pad colonised with fungi, attached to a T-shirt with electrodes and recording equipment.

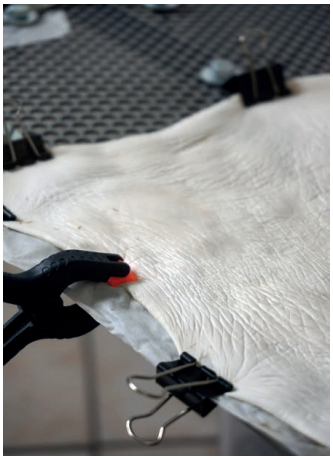


Fig. 6. The fungal skin shows animal type wrinkles.

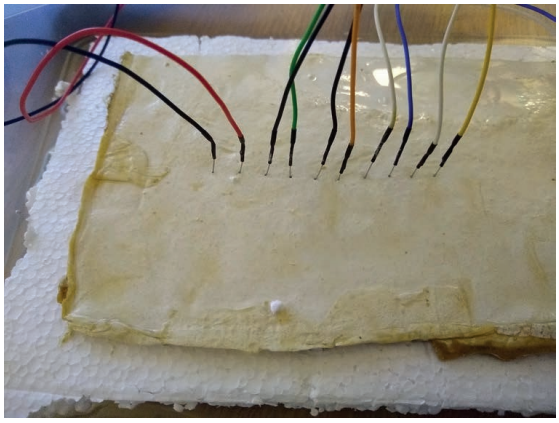


Fig. 7. Pairs of differential electrodes inserted in the fungal skin to record electrical response of the fungal skin to mechanical and optical stimulation.

and switching illumination on and off. These are the first experimental evidences that fungal materials can be used not only as mechanical skeletons in architecture and robotics but also as intelligent skins capable of recognition of external stimuli and sensorial fusion.
Living wearables offer a new spectrum of performance possibilities such as reactiveness, adaptiveness, and sensing capabilities. They are harmless to the environment, biodegradable and they can even nurture the cultivation of new materials in their end of life. The living material provides a unique opportunity for the wearables to be programmable by guiding the growth, controlling the nutrients and setting up the conditions in which the wearable can be created. Their ability to self-repair and self-grow makes them one of the most promising. Future studies can be focused on better understanding of electrical communication and stimulation in fungi and other microbes (advancements in biocomputation), development of biological sensors able to report slight changes in physico-environmental conditions and biochemical traces, biological sentient clothing that responds to the environment, self-sustaining and self-healing clothing and parchments grown *in situ*, exoskins and exoskeletons that symbiotically interact with the user, cross-over synergistic interactions between biological entities and electronic circuits or machines (advancements in biorobotics and biomechanoids).

[1] Professor in Unconventional Computing, UWE, Bristol, UK.
[2] Senior Lecturer in Architecture, UWE, Bristol, UK.
[3] Leading Researcher at MOGU, Italy.
[4] Leading Researcher at IIT, Torino, Italy.
[5] U. Eco, *Travels in Hyperreality*, New York, Mariner Books, 1986.
[6] M. Barnard, *Fashion Theory: An Introduction*, London, Routledge, 2014.
[7] M. Addington, D. Schodek, *Smart Materials and New Technologies. For Architecture and Design Professions*, Oxford, Architectural Press-Elsevier, 2005.
[8] M. Ferrara, M. Bengisu, *Materials that Change Color. Smart Materials, Intelligent Design*, Cham, Springer, 2013.

[9] M. Ferrara, "Smart Experience in Fashion Design: A speculative analysis of smart material systems applications," *Arts Basel 8*, 2019, 1-11.
[10] A. Adamatzky, A. Nikolaidou, A. Gandia, A. Chiolerio, and M. M. Dehshibi," Reactive fungal wearable," arXiv preprint arXiv:2009.05670 (2020).
[11] X. T Tao, *Wearable Electronics and Photonics*, Cambridge, Woodhead Publishing Limited and Textile Institute Abington, 2005.
[12] M. Ferrara, M. Bengisu, *Materials that Change Color*, *op. cit.*
[13] S. Needhidasan, M. Samuel, R. Chidambaram, "Electronic waste – an emerging threat to the environment of urban India," *Journal of Environmental Health Science and Engineering 12(1)*, 2014, 36.
[14] A. Adamatzky & T. Schubert, "Slime Extralligence: Developing a Wearable Sensorial and Computing Network with Physarum polycephalum," UWE Research Repository 927012, 2013.
[15] F. V. Appels, S. Camere, M. Montalti, E. Karana, K. M. Jansen, J. Dijksterhuis, P. Krijgsheld, H. A. Wosten, "Fabrication factors influencing mechanical, moisture-and water-related properties of mycelium-based composites," *Materials & Design 161*, 2019, 64-71; M. Jones, A. Gandia, S. John, A. Bismarck, "Leather-like material biofabrication using fungi," *Nature Sustainability*, 2020. https://doi.org/10.1038/s41893-020-00606-1
[16] Y.-S. Bahn, C. Xue, A. Idnurm, J. C. Rutherford, J. Heitman, M. E. Cardenas, "Sensing the environment: lessons from fungi," *Nature Reviews Microbiology 5*, 2007, 57.
[17] I. M. Van Aarle, P. A. Olsson, B. Soderstrom, "Arbuscular mycorrhizal fungi respond to the substrate ph of their extraradical mycelium by altered growth and root colonization," *New Phytologist 155*, 2002, 173-182.
[18] C. Kung, "A possible unifying principle for mechanosensation," *Nature 436(7051)*, 2005, 647.
[19] M. Fomina, K. Ritz, G. M. Gadd, "Negative fungal chemotropism to toxic metals," *FEMS Microbiology Letters 193*, 2000, 207-211.
[20] Y.-S. Bahn, F. A. Muhlschlegel, "Co2 sensing in fungi and beyond," *Current opinion in microbiology 9*, 2006, 572-578.
[21] K. T. Howitz, D. A. Sinclair, "Xenohormesis: sensing the chemical cues of other species," *Cell 133*, 2008, 387-391.
[22] S. Olsson, B. Hansson, "Action potential-like activity found in fungal mycelia is sensitive to stimulation," *Naturwissenschaften 82*, 1995, 30-31; A. Adamatzky, "On spiking behaviour of oyster fungi pleurotus djamor," *Scientific reports 8*, 2018, 1-7; A. Adamatzky, A. Gandia, A. Chiolerio, "Fungal sensing skin," arXiv preprint arXiv:2008.09814 (2020).
[23] A. E. Beasley, A. L. Powell, A. Adamatzky, "Fungal photosensors," arXiv preprint arXiv:2003.07825 (2020).
[24] A. Adamatzky, A. Nikolaidou, A. Gandia, A. Chiolerio, and M. M. Dehshibi, "Reactive fungal wearable," *op. cit.*
[25] *Ibidem*.

Brain Lego
Toy Computing with Lego Bricks

Stefan Höltgen[1]

"HIRNLEGOHIRNLEGOHIRNLEGOLEGOLEGO
HIRNLEGOLEGOLEHIRNLEGOLEGOLEGO
HIRNLEGOLEGOLEGOHIRNLEGOLEGOLEGO"
(*Einstürzende Neubauten*, Hirnlego, 1989)

"I have always had a predominantly visual approach to my environment. This is also probably why I never pursued music. This perhaps one-sided talent was also evident in the construction of my computer models; here, too, I preferred mechanical and electromechanical constructions and left the electronics to others who were better qualified."[2]
In this quote, computer pioneer Konrad Zuse describes his tinkering with construction kits he played with as a boy and a teenager from his viewpoint as an engineer. He used those kits in the 1920s to build all sorts of things with them: (award winning) models of cranes and excavators, spare parts for his bike, and mechanical household aids. Later on, when his computers were already working electronically, he used the thought pattern for a new system of self-reproducing machines.[3]

This mechanical thinking of computer functions has a long tradition reaching back into the Middle Ages: from Ramon Llullu's book *Ars Magna* published in 1305 where a theological 'converter' for Muslims to become Christians is drafted, to Leibniz' *Machina arithmeticae dyadicae* from 1679 (a mechanism to calculate with binary numbers) — both remained "paper machines" — through to the mechanical and electromechanical logical machines of the 19th and 20th centuries,[4] culminating in Claude Shannon's switching algebra from 1937. All of these drafts were based on the idea to make calculation and computation not only logically but also mechanically constructible.
From our present-day perspective, some of these drafts appear more like toys than serious calculators; toys that merely show the principles of computation but are not very suitable for actual usage. This view also has to do with the fact that those prototypes show their material and epistemological toy characteristics: they are often built from construction kits (for children and youth) or from everyday objects — according to the "Baukastenprinzip" ("kit principle"),[5] using heuristic design procedures, trial and error, and learning by doing.
The invitation to *think while tinkering* ("thinkering")[6] seems to be a basic principle of both logic and kit toying because both make it possible to comprehend/handle complex phenomena. This logic (the two-valued sentential logic, inaugurated in the 3rd century B.C. from Aristotle) is the timeless and non-spatial basis of all our thinking. It provides the transcendental basic structure of truth-apt propositions which are the foundation of our everyday thinking, actions, science, playing, … This reality is formalized in logics: propositions become tokens that can hold a truth value (true/false — no third option) and can be combined with junctors (and, or, if-then, not, …) to complex sentences.
A sentence like "*Tonight I'll go to the movies or I will read a book*" can be formalized as *p*

PLEA 2024 WROCŁAW
(Re)thinking Resilience

Robotic additive manufacturing of lichen composites for air quality monitoring

Digital fabrication of responsive and resilient material systems from lichens

Anna Nikolaidou[a,b] Tavs Jorgensen[c]

[a]*Unconventional Computing Laboratory, UWE, Bristol, UK*
[b]*School of Architecture and Environment, UWE, Bristol, UK*
[c]*Centre for Print Research, UWE, Bristol, UK*

ABSTRACT: In the light of an unprecedented climate emergency, there is an urgent need to reconsider the materials we use for the construction of our buildings and to explore alternative material systems that are abundant, easy to source, and exhibit increased climate resilience and adaptability. Materials with these attributes have been developed by living systems. We propose the development of hybrid materials from living lichens and abiotic components for air pollutant sensing, using a 3D digitally driven paste delivery system. Lichens are excellent indicators of air pollutants, they present resilience to extreme environmental conditions and are abundant, can self-grow and self-regulate. The lichen species Flovoparmelia caperata, Parmotrema perlatum and Xanthoria parietina were used for the production of the samples. We employed a robust photographic recording system that allowed the morphological monitoring of the samples. We assessed colonisation tendencies and performed statistical analysis of changes in pigmentation distribution to understand substrate-lichen correlations and the metabolic activity change over time. Our findings demonstrated that three combinations of lichen species-substrates presented optimal integration and were selected as most suitable for 3D printing. We also report that one sample demonstrated excellent colonisation behaviour and less changes in its metabolic activity over time.
KEYWORDS: hybrid living materials, lichens, robotic 3D printing, biosensing, sustainability

1. INTRODUCTION

The building industry accounts for one of the largest negative impacts on the planet, significantly contributing to the depletion of natural resources and raw materials. In addition to this, we are already experiencing pressure on living conditions and an increase in damage to buildings from extreme weather events, attributed to climate change [1]. In the light of this unprecedented climate emergency, there is an urgent need to reconsider the materials we use for the construction of our buildings, their production and assembly processes. We therefore need to explore alternative material systems and fabrication processes that allow the use of materials that are not only abundant in our planet, readily available and easy to source, but also exhibit increased climate resilience and adaptability, mitigating the impact of extreme climate change events and responding to the ever-changing environmental conditions.

Materials with responsive capabilities have already been developed by living systems over the last 4.5 billion years, as they have created biological structures for the modification of their environment and survival [2]. Natural biological systems are capable of sensing environmental conditions and responding to them on multiple scales [3]. Living systems possess distinctive features that endow them with intrinsic advantages for the manufacture of responsive materials such as their ability to grow autonomously into structured bulk materials without human effort, to self-regenerate and degrade the components that they make, thereby possessing a sustainable life cycle for the entire material and to provide complex responses to environmental stimuli [4]. In addition to the above features, they exhibit living attributes such as self-growth, self-regulation, self-repair and self-replication, making them excellent candidates for the development of materials with reduced environmental impact as compared to conventional materials. The above exceptional properties and capabilities make living materials attractive as functional components for the development of responsive materials.

An emerging area of materials that has attracted interest in the scientific community is Living Hybrid

Materials. This class of materials can be defined as materials composed of living cells that form or assemble the material itself, or modulate the functional performance of the material in some manner [2]. Living hybrid materials contain both living organisms and abiotic components. They retain the living attributes while the incorporated abiotic materials enhance the material structure and performance such as responsive and sensing functionalities [4]. Living hybrid materials with sensing and information processing capabilities usually incorporate a substrate, and functional or active layers [5]. The functional layers include the active elements where the main activity takes place while the substrate is a solid substance upon which the functional layers are deposited [6, 7].

This research project aims to contribute to an emerging and growing body of work that recognises the potential of living cells as functional layers for the development of materials with responsive capabilities such as sensing external stimuli. We propose the development of hybrid living materials from lichens, using a novel robotic additive manufacturing process for paste 3D printing of the lichen substrate matrix.

Lichens are symbiotic organisms, usually composed of a fungal partner and one or more photosynthetic partners [8]. They are found on trees, rocks and in soils [9] and are perennial, resilient and able to live for many years in extreme conditions [10,11]. They are abundant, providing easy accessibility, they can self-grow, self-repair and they are self-regulating. Unlike plants, lichens lack vascular organs to directly control their water loss or uptake [12], their water content equilibrates with atmospheric conditions and as a result, lichens range between desiccated and water-saturated states on a daily basis throughout much of their lifetime [13]. Lichens can survive in harsher environments compared to their constituting fungi and algae as individual living microorganisms due to passing nutrients and metabolites to each other which ensures better adaptability [14]. This astonishing capability to survive and remain living and healthy under extreme environmental changes, makes them promising candidates to be used as a sustainable alternative to conventional materials currently used in the building industry.

In addition to exhibiting resilience to extreme environmental conditions, lichens are excellent biomonitors for air pollutants. The use of lichens as biomonitors is attributed to their ability to respond to air pollutants at different levels, their slow growth rate, longevity as well as their ability to indicate the presence and the concentrations of these pollutants [15,16]. Although lichens have been used extensively in the field for the detection and monitoring of air pollutants such as metals and organic air pollutants, to our best knowledge, integration of lichens into substrates for the development of building material composites has not been reported yet. We therefore present a scoping study in which we investigate the integration of lichens into various substrate matrices using a digitally driven paste delivery system.

2. HYPOTHESIS AND OBJECTIVES

Drawing from the existing literature demonstrating lichen's ability to respond to extreme environmental changes as well as sense and report the presence of air pollutants, we hypothesise that it might be possible to 3D print lichen composites that can perform the above functions. Our aim is to develop living hybrid material systems from lichens that exhibit responsive capabilities when exposed to environmental pollutants, using a novel digital fabrication method of paste delivery.

The hypothesis is sought to be verified through the following objectives:

- To assess and establish protocols of lichen/substrate colonisation for the development of the hybrids.
-To 3D print substrates that present optimal colonisation behaviour using a digitally driven paste delivery system.
-To evaluate gas absorption rates of hybrid materials upon exposure to pollutants.
-To develop a framework for deploying lichen hybrid material systems.

3. METHODS

3.1 Experimental set up and material synthesis

The lichen species Flovoparmelia caperata, Parmotrema perlatum and Xanthoria parietina were collected from three tree trunks of an outdoor area with average pollution levels in Bristol, United Kingdom. For each of the species, the same tree trunk site was used for the collection. The rationale for this decision was that since the same site was used, it was most likely that the specific lichen species benefitted from the same secondary metabolites such as nutrients and water intake, environmental stress, moisture content and sun exposure, allowing the development of conclusions by excluding these parameters when performing morphological characterisation and statistical analysis.

Seventeen samples of different substrates- lichen species combinations were produced (Fig. 1). The substance choice and concentrations were based on an already established protocol of material mixture and concentrations used for 3D printing. The materials used were Cellulose Fibre Scarva, Methyl cellulose, Chitosan, Glycerin, Agar, Coffee grounds, Rice Starch, Sodium alginate, Hemp Shive and Clay (Smooth Terracotta). Table 1 shows the composition and quantities of the developed substrate samples.

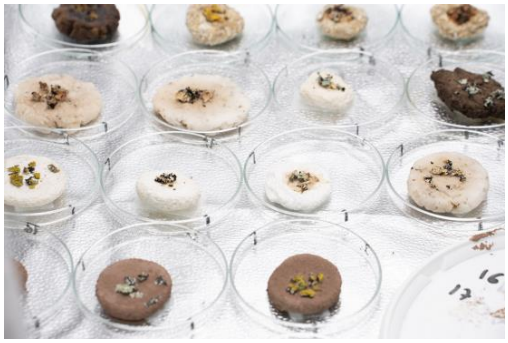


Figure 1: Inoculated substrate samples. Flovoparmelia caperata, Parmotrema perlatum and Xanthoria parietina lichen species were used for the inoculation. *Photograph by Simon Regan 2023.*

The samples were kept at ambient room temperature in a hydroponic growing tent with the provision of artificial daylight (Fig. 2) and monitored every 2-3 days. Additional moisture was added manually as required with de-ionised water.

3.2 Pigmentation distribution

A photographic recording system incorporating a customised 3D printed base for the positioning of a camera at an angle and distance that allows the morphological monitoring and characterisation of the samples was established.

Sample 8
Lichen species: Parmotrema perlatum

Material	Weight (g)
Cellulose Fibre Scarva	10
Methyl cellouse	50 dry
Chitosan	80
Glycerin	40

Sample 10
Lichen species: Flovoparmelia caperata

Material	Weight (g)
Cellulose Fibre Scarva	12
Sodium alginate	50
Rice Starch	4
Glycerin	20
Cellulose Fibre Scarva	12

Samples 9
Lichen species: Parmotrema perlatum

Material	Weight (g)
Cellulose Fibre Scarva	5
Bio bean	20
Chitosen	30
Additive 5	40
Fine Hemp Shive	5

Samples 11, 12
Lichen species: Xanthoria parietina, Parmotrema perlatum

Material	Weight (g)
Cellulose Fibre Scarva	12
Sodium alginate	50
Rice Starch	4
Agar	20
Cellulose Fibre Scarva	5

Sample 13
Lichen species: Flovoparmelia caperata

Material	Weight (g)
Cellulose Fibre Scarva	10
Methyl cellulose	30
Sodium alginate	20

Samples 14, 14a
Lichen species: Parmotrema perlatum, Flovoparmelia caperata

Material	Weight (g)
Cellulose Fibre Scarva	10
Methyl cellouse	50 dry
Chitosan	80
Glycerin	40

Samples 15, 16, 17
Lichen species: Flovoparmelia caperata, Parmotrema perlatum, Xanthoria parietina,

Material	Weight (g)
Clay [Valentines Smooth Terracotta VC1D]	200
Hemp Shiv	5

Table 1: Substances and concentrations used for the development of the substrate samples.

Images of each sample were taken for 6 consecutive weeks prior to the implementation of data analysis (Fig. 3).

We performed colour distribution statistical analysis. The rationale behind the selection of this method is the described below



Figure 3: Recordings of sample 16 for 6 consecutive weeks. Pigmentation distribution changes have been analysed to understand correlations between lichen species and substrate composition.

The parameters that may affect the distribution of the lichen pigmentation over time can be attributed to the following factors: 1. Fungal partner pigments 2. Algal or cyanobacteria pigments 3. Secondary metabolites 4. Interaction of lichens with the substrate 5. Type of lichens 6. Environmental stress 7. Moisture content. Since the inoculation of the substrates was performed in controlled conditions, factors 3, 6 and 7 remain the same for all samples and therefore can be eliminated from the parameters taken into consideration. Changes to pigmentation distribution over time may therefore be attributed to the interaction of the lichens with the different substrates as well as the composition of the fungal and photosynthetic partners in each sample. Conclusions may lead to a better understanding of how lichens interact with the substrates and which lichen species- substrate combinations could lead to integration and adherence of the lichens to the substrate substances and therefore to self-assembly formation mechanisms. For the interpretation of the data set depicting pigmentation change over time, the data of the same lichen species samples were analysed and compared to allow the elimination of the impact of factor 5 on our possible conclusions. MATLAB was used for the analysis.



Figure 2: Hydroponic tent used for the lichen-substrate inoculation to allow controlled conditions of light, humidity and temperature for all samples. Photograph by Simon Regan 2023.

3.3 Robotic 3D printing test system

The Robotic 3D printing test system used in this research project consists of an UR collaborative Robotic Arm which is connected to an Arduino based micro controller hardware unit. This unit operates a stepper motor which is integrated within Poseidon open-source syringe pump fixture that facilitate the delivery of the paste, synchronised with the movement of the robotic arm. The Poseidon fixture has been modified to fit the UR end-effector bracket and adapted to hold a 60ml syringe tightly. The syringe itself has been modified with a set of interchangeable set of nozzles 3D printed in 5, 8 and 10mm diameter.

The workflow of processing test prints starts with forms designed in a CAD software and saved in the STL format. The STL files are then sliced into 3D printing paths using the CURA software. These paths are saved as G code data, which can be interpreted by the integrated robot arm and paste delivery system. To facilitate the interpretation, the CURA G-code commands are loaded into the RobotDK software running on a laptop which is connected to the UR control box via an ethernet cable – enabling real time data flow. Data is relayed from the UR control box to an Arduino microcontroller which in turn send commands to stepper motor driver that controls movement of the stepper motor which pushes the plunger of the syringe and ultimately deliver the paste in amounts that are synchronised with the movement of the robotic arm (Fig. 4).

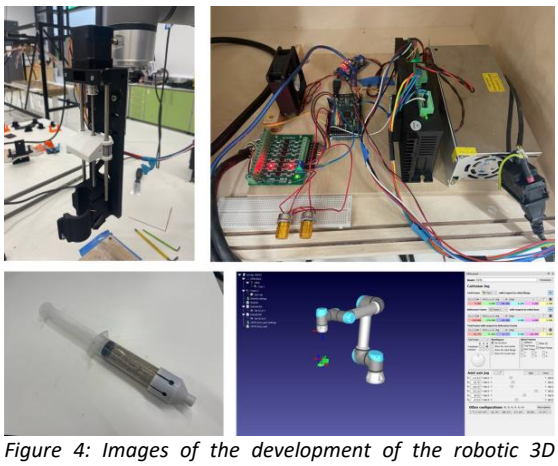


Figure 4: Images of the development of the robotic 3D printing test system. The system consists of an UR collaborative Robotic Arm connected to an Arduino based micro controller hardware unit using a syringe paste delivery printing process.

3. RESULTS

Samples 1, 2 and 11 presented optimal colonisation and the lichen species were fully integrated with the substrate, forming a hybrid material from the fusion of the living and synthetic particles. By optimal colonisation, we refer to the binding and attachment of the lichen species to the substrate in such a manner that the components are coalesced and cannot be separated.

It is worth noting that for the image classification via statistical analysis of changes in pigmentation distribution implemented in the analysis below, the red, green and blue mean values are the average values of the red, green and blue channels of the image pixels. In regard to the species Xanthoria parietina and for the course of 6 weeks, sample 2 presented the highest red and green mean values of 177.9 and 170.9 with standard deviation values of 49.4 and 55.0, skewness of 2.52 and 2.47 and kurtosis 8.97 and 8.55. This indicates that the sample presents leptokurtic distribution and the kurtosis is therefore positive. Additionally, the skewness is negative. On the other hand, sample 1 showed the lowest red and green mean values of 157.2 and 150.2, with 70.3 and 76.2 standard deviation values, skewness of 2.56 and 2.48 and kurtosis 8.77 and 8.53, also presenting leptokurtic distribution with positive kurtosis and negative skewness. Sample 11 showed the highest blue mean value of 158, 48.6 standard deviation value, with skewness 0.86 and kurtosis 2.60. This may be interpreted as negative skewness but the kurtosis is platykurtic. In contrast, sample 1 demonstrated the lowest blue value of 140.2 with standard deviation of 78.5 and 1.97 skewness and 6.05 kurtosis with leptokurtic distribution. The above statistical analysis indicates that for sample 1 (Fig. 5), modification in pigmentation distribution remains the lowest compared to the other samples inoculated with the Xanthoria parietina species which may be attributed to the living cells retaining their nutrients and functional exchanges between the fungal and photosynthetic components. Sample 2 contains cellulose fibre scarva, methyl cellouse and chitosan, same particles used in sample 1. In addition to the above particles, sample 1 substrate also contains glycerine and additive. It may therefore be possible that the glycerine and additive contributed to the living cells presenting lowest pigmentation modifications and thus retaining their original living state and metabolic activity.

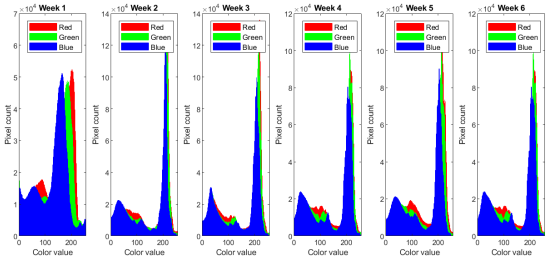


Figure 5: Plots depicting pigmentation distribution changes over 6 consecutive weeks for sample 1.

A similar trend can be observed in regard to the species Parmotrema perlatum. Sample 14 presented the highest red mean value of 169.6, standard deviation of 58.3, a negative skewness of 1.65 and a positive kurtosis of 4.46 with leptokurtic distribution. Sample 8 showed the highest green mean value of 165.4, standard deviation of 45.1, a negative skewness of 1.69 and a positive kurtosis of 5.80 with leptokurtic distribution. Finally, sample 12 showed the highest blue mean value of 157.2, standard deviation of 45.8, a negative skewness of 0.86 and a kurtosis of 2.22 with platykurtic distribution. On the contrary, sample 9 displayed the lowest red, green and blue mean values of 155.2, 148.7 and 139.9 (Fig. 6). The standard deviation values were 73, 78.3 and 79 respectively, with negative skewness of 2.84, 2.62 and 2.44 and positive kurtosis of 10.67, 9.45 and 8.92, also with leptokurtic distribution. From the above analysis, it is demonstrated that from the substrates inoculated with Parmotrema perlatum lichen species, sample 9 displayed the lowest pigmentation distribution modifications and therefore its substrate might have contributed to the living lichens maintaining their original state and metabolic activity in comparison to the other samples. By comparison of the substances used in the samples, it may be possible that this behaviour is attributed to Bio bean and Additive and/or Fine Hemp Shive.

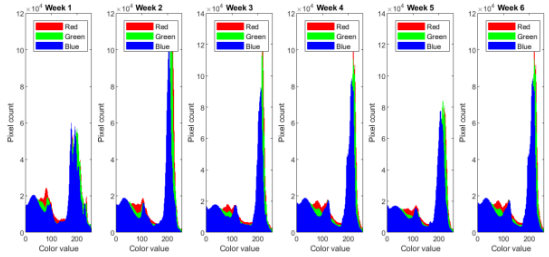


Figure 6: Plots depicting pigmentation distribution changes over 6 consecutive weeks for sample 9.

Lastly, for the species Flovoparmelia caperata, sample 14a showed the highest red mean value of 173, standard deviation of 46.7, a negative skewness of 1.08 and a negative kurtosis of 2.73 with platykurtic distribution. These findings are consistent with sample 14 discussed above, where the same substrate is inoculated with the lichen species Parmotrema perlatum and also show the highest red mean value. It is therefore possible that the particles used in substrates 14 and 14a have a maximum impact on the lichen species and more specifically on their metabolic activity. Table 1 shows in detail the substances used for each sample. Sample 14a also presents the highest green mean value which is 167.1 with 49.2 standard deviation, a negative skewness of 0.70 and a negative kurtosis of 2.16 with platykurtic distribution. Finally, three samples showed the same blue mean value of 156.2 which was the highest between the discussed samples of this lichen type. These samples are 3, 13 and 14. Standard deviation is 59.3, 45.1 and 53 respectively. The skewness is negative for all three samples and is 1.58, 1.43 and 0.45 respectively. The kurtosis is positive for samples 3 and 13 and is 4.28, 3.80 with a leptokurtic distribution and negative for sample 14 with a value of 2.34 and platykurtic distribution. It is therefore evident that the substrate components of sample 14 may impact most the metabolic activity of the lichens and therefore exhibit highest change of the pigmentation distribution. Regarding the lowest mean values, sample 5 demonstrated the lowest mean values for all three pigments (Fig. 7). These are 154.5, 148.9 and 141, showing standard deviation of 74.1, 79.8 and 80.9 respectively. The skewness is negative and the values are 2.99, 2.87 and 2.50 for red, green and blue pigments. The kurtosis is positive and is 12.20, 11.39 and 9.11 with a leptokurtic distribution.

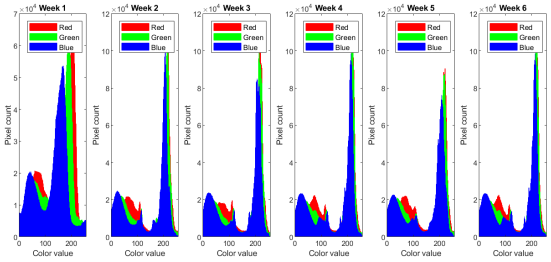


Figure 7: Plots depicting pigmentation distribution changes over 6 consecutive weeks for sample 5.

4. DISCUSSION

Our findings demonstrated that three combinations of lichen species-substrates presented optimal colonisation (1, 2, 11) and were therefore selected as most suitable for 3D printing using the system mentioned above (Fig. 8). Additionally, the data analysis contributed to a better understanding of the substrate-lichen correlation and more specifically the metabolic activity change over time. We can report that the three samples that showed lowest change of the pigmentation distribution are 1, 5, 9 and therefore their metabolic activity was more similar to

their initial state than the other samples. On the other hand, most pigmentation distribution changes were observed in samples 2, 11, 14, 14a, 3 and 13 indicating that the metabolic activity of the living cells has been most impacted. We can therefore report that from the data analysis and physiological monitoring, sample 1 presents the most ideal candidate for the development of the new hybrid living material since it exhibits excellent colonisation behaviour and less changes in its metabolic activity over time. Further research needs to be undertaken to better understand the impact of the concentrations of the substrate components on the metabolic activity, the implication of metabolic changes to the living cells and substrate as well as the specifics of the substances used so that a more accurate mapping can be achieved.

5. CONCLUSION

This research project marks a ground-breaking investigation of incorporating lichens into substrate matrices aimed at robotic 3D printing. To our best knowledge, this is the first time that such approach has been tested, opening up exciting opportunities for the development of a new class of hybrid materials using living components that are truly resilient to environmental stress, sustainable, can self- assemble, self-heal and self-regenerate. Our findings so far contribute to a better understanding of lichen species- substrates correlations as well as 3D printing approaches that can lead to the production of lichen hybrid living materials with scalability potentials for applications in the building industry through integration and self- assembly of their components.

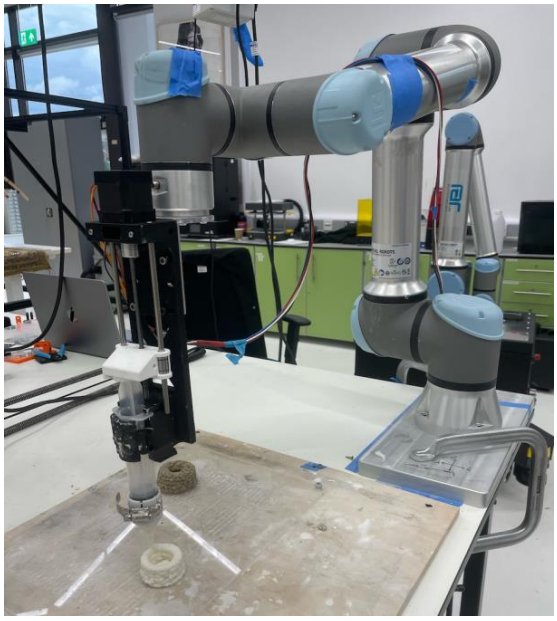


Figure 8: Small scale 3D printing studies of optimal substrates for lichen inoculation.

Following the above studies, we will use our findings for the next phase of this research project which includes the assessment of the responsiveness of the developed hybrid living materials to air pollutants exposure. For assessing gas absorption, the inoculated 3D printed hybrid living materials will be subjected to distinct gases in bespoke chambers and quantitative data will be collected for analysis of absorption. The findings of this phase will be included in the conference presentation. Challenges that need to be considered in this next research phase is minimising contamination risks and deterioration of the substrate material as well as monitoring the lichen hybrid materials for any pathogen growth.

REFERENCES

1. United Nations Environment Programme (2021). A Practical Guide to Climate-resilient Buildings & Communities. [Online], Available: https://www.unep.org/resources/practical-guideclimate-resilient-buildings [28 August 2023].
2. Nguyen, P. Q., Courchesne, N. M. D., Duraj-Thatte, A., Praveschotinunt, P., & Joshi, N. S. (2018). Engineered living materials: prospects and challenges for using biological systems to direct the assembly of smart materials. Advanced Materials, 30(19), 1704847.
3. Teague, B. P., Guye, P., & Weiss, R. (2016). Synthetic morphogenesis. Cold Spring Harbor perspectives in biology, 8(9), a023929.
4. Wang, Y., Liu, Y., Li, J., Chen, Y., Liu, S., & Zhong, C. (2022). Engineered living materials (ELMs) design: From function allocation to dynamic behavior modulation. Current Opinion in Chemical Biology, 70, 102188.
5. Li, W., Liu, Q., Zhang, Y., Li, C. A., He, Z., Choy, W. C., ... & Kyaw, A. K. K. (2020). Biodegradable materials and green processing for green electronics. Advanced materials, 32(33), 2001591.
6. Piro, B., Tran, H. V., & Thu, V. T. (2020). Sensors Made of Natural Renewable Materials: Efficiency, Recyclability or Biodegradability—The Green Electronics. Sensors, 20(20), 5898.
7. Cao, Y., & Uhrich, K. E. (2019). Biodegradable and biocompatible polymers for electronic applications: A review. Journal of Bioactive and Compatible Polymers, 34(1), 3-15.
8. Nash, T. (2008). Introduction. In T. Nash, III (Ed.), Lichen Biology (pp. 1-8). Cambridge: Cambridge University Press.
9. M.E. Hale, M.E. (1974) The Biology of Lichens, 2nd ed., Edward Arnold, London.
10. L. Bergamaschi, L. et.al. (2003) Determination of baseline element composition of lichens using samples from high elevations, Chemosphere 55, p. 933–939.
11. Maphangwa, K.W. et.al. (2012) Differential interception and evaporation of fog, dew and water vapour and elemental accumulation by lichens explain their relative abundance in a coastal desert, J. Arid Environ. 82, p.71–80.
12. Proctor MCF, Tuba Z (2002) Poikilohydry and homoihydry: antithesis or spectrum of possibilities? New Phytol 156(3), pp. 327–349.

13. ten Veldhuis, MC., Ananyev, G. and Dismukes, G.C. (2020) Symbiosis extended: exchange of photosynthetic O2 and fungal-respired CO2 mutually power metabolism of lichen symbionts. Photosynth Res. 143, 287–299.
14. Wöstemeyer, J. (1997) MT Madigan, JM Martinko, J. Parker, Biology of Microorganisms, Prentice Hall International Inc.
15. Sloof, J.E., de Bruin, M., Wolterbeek, H. (1988) Critical evaluation of some commonly used biological monitors for havy metal air pollution, in: Environmental Contamination: Proceedings of the international Conference Venice (Italy), Edinburgh, pp. 296–298.
16. Nimis, P.L. et al. (1993) Lichens as bioindicators of heavy metal pollution: a case study at La Spezzia, VHC, New York, pp. 265–284.

Rethinking living matter

Animate behaviours of fungal composites

Anna Nikolaidou[1,2] **Andy Adamatzky** [1,2]

[1]*Department of Architecture, University of West of England, Faculty of Environment and Technology, Bristol, BS16 1QY, United Kingdom*
[2]*Unconventional Computing Laboratory, University of West of England, Bristol, BS16 1QY, United Kingdom*

Keywords: biosensing, fungi, sustainability, electrical activity.

ABSTRACT

Smart materials integrating conventional soft electronics e.g. sensors and actuators, are widely used in the building and wearable industries, contributing to the depletion of natural resources and having a vast environmental impact. In this paper, a novel method using living fungi for the development of responsive materials for smart architectural and wearable skins is discussed. Living fungi composites exhibit remarkable self-sustainable properties: self-growth, self- repair and self-assembly. They present responsive capabilities to environmental, chemical and mechanical stimuli, allowing the implementation of sensorial fusion and decision making. We inoculated hemp mat substrates with the fungus Pleurotus ostreatus and cultured until a coating of white mycelial growth was observed. We performed a series of laboratory experiments on the fungal composites, exposing them to various environmental, chemical and mechanical stimuli and we explored their communication protocols and smart capabilities. We found that living fungi composites employ precise responsive mechanisms by generating distinct electrical potential impulses in the form of spike events, presenting a promising alternative to conventional smart materials. The results open up new possibilities for the development of the next generation of smart materials for the building and wearable industries, allowing large scale implementation and production.

1.INTRODUCTION

Smart materials are highly engineered materials, often embedded in more conventional materials, that respond intelligently to their users and environment. They integrate microelectronic components and technologies that enable them to perceive surrounding events, process them and then deploy suitable responses (Addington and Schodek, 2005). They can display intrinsic or implanted intelligent capabilities (Ikechukwu and Moses, 2019) and different degrees of complexity. Smart materials can integrate three types of technologies that can define their behaviour and performance: (1) sensing technologies, most commonly in the form of sensors, which enable them to receive information from the environment and users, (2) actuating technologies that convert input in the form of a signal into an action (Addington and Schodek, 2004) and (3) control technologies that translate input signals perceived from permanent and temporary environmental data and users preferences

into actuation commends based on pre-programmed control logics (Barozzi et al. 2016). The systems integrating smart materials exhibit key attributes such as flexibility (Loonen et al., 2013), adaptability (Aelenei, et al., 2016), multi-functionality (Khoo, 2013), scalability (Decker, 2013) and controllability (Ogwezi et al., 2011).

Over the last decade, smart materials integrating one or more of the above technologies have been extensively used in buildings and wearables to improve performance, efficiency and wellbeing through sensing and responding to control parameters such as environmental stimuli, the user's preferences and needs. This exponential use of electronic components has vastly contributed to an evolving environmental problem, the accumulation of Electrical and Electronic Equipment waste (EEE) in the environment. In 2019, the world generated 53.6 metric tons of e-waste, an average of 7.3 kg per capita. On average, the total weight of global EEE consumption increases annually by 2.5 million metric tons (Forti et al., 2020). Moreover, the above technologies require the use of materials such as metals, ceramics, semiconductors etc. leading to supply risks and the depletion of natural resources. It is therefore, an absolute priority to find alternative materials with the required attributes and capabilities of smart materials but with limited environmental impact. The next generation of intelligent materials must include smart functional properties that surpass existing capabilities, such as the ability to be self-sustained.

2.ANIMATE INTELLIGENCE

Living materials can be defined as those that are sensitive to their environment and able to adapt to it in a number of ways to better fulfil their function. These materials may be understood in relation to three principles of animacy: (1) they are 'active', in that they can change their properties or perform actions, often by taking energy, material or nutrients from the environment, (2) they are 'adaptive' in sensing changes in their environment and responding through action to a specific prompt so that they maintain or promote their function (3) they are 'autonomous' in being able to select an appropriate response to stimuli without any kind of external control or guidance and showing versatility in combining various inputs to generate a suitable behaviour from a diverse repertoire (Royal Society, 2021). Although smart materials integrating any or all of the technologies mentioned in the introduction (sensing, actuating and control technologies) can be classified as active and often adaptive, they are lacking the third principle of animacy as they require the existence of external control or guidance and therefore, rarely display autonomous capabilities. In addition to this, smart materials are not self-sustainable and ecologically friendly.

Fungal material presents a feasible alternative to conventional smart materials. It is renewable, abundant and can quickly decompose. It can self-grow and self-repair, lessening the impact on resources and targeting challenges such as natural resources depletion. Fungi exhibit all three animate qualities because of the way they interact with their environment and can be produced across multiple length scales, making them a promising candidate for use as an intelligent material in the building and wearables industries.

In this paper, we present an illustrative scoping study based on feasibility studies undertaken in laboratory setting in which we assess the animate capabilities of living fungi composites when exposed to environmental, chemical and mechanical stimuli.

The rest of the paper is structured as follows. Section 3 presents the bio-fabrication of fungi composites and the experimental set up of the studies. In Section 4 we present the results, followed by a discussion on the opportunities, challenges and limitations in Section 5. Finally, we conclude in Section 6 by proposing potential applications and directions for future studies.

3.METHODS

3.1 Bio-fabrication of fungal composites

Bio-fabrication can be defined as the production of complex living and non-living biological products from raw materials such as living cells or molecules (Adamatzky, et al., 2021). Biological material assembly can occur under mild conditions, driven by sustainable energy sources, and resulting in the production of biodegradable products (Gilbert, 2019).

Over the last decade, the vegetative growth of filamentous fungi, called mycelium, has attracted increasing academic and commercial interests as a new form of low energy bio-fabrication and waste upcycling (Jones, 2017, Holt, et al., 2012, Pelletier et al., 2013, Nawawi, 2020). Mycelium binds organic matter through a network of hyphal micro-filaments in a natural biological process (Jones, 2017, Holt et al., 2012, Pelletier et al., 2013, Haneef et al., 2017, Islam et al., 2017), utilising biological growth than expensive energy intensive manufacturing processes to convert low-cost substrates such as hemp, wood- chips, straws into environmentally friendly material composites. The fungal hyphae grow on these substrates, forming a fibrous mycelium matrix, surrounding, covering and binding together all the substrate particles and forming a composite solid material (Adamatzky, et al., 2021).

To fabricate the fungal composites, we cultured a commercial strain of the fungus *Pleurotus ostreatus* (Mogu's collection code 21-18), on hemp bedding substrate in plastic boxes c. 35 x 20 cm^2 in darkness at ambient room temperature c. 22^oC. The substrate was placed in a hydroponic growing tent with a silver Mylar light proof inner lining (Green Box Tents, UK). P. ostreatus represents an ideal candidate for use due to its rapid growth rate and tolerance to environmental conditions. When a coating of white mycelial growth was observed, particles of the colonised fungus substrate were spread on rectangular fragments of moisturised hemp fibre pads (c. 12 x 12 cm^2). After the hemp pads were colonised by white and homogeneous mycelial growth on the surface, we proceeded to the experiments, testing the responsive capabilities of the fungal pads during and after exposure to environmental, chemical and mechanical stimulants.



(a) (b) (c) (d)

Figure 1. Bio-fabrication of fungal composites. (a) inoculated hemp bedding and mat substrate (b) colonised fungal composite (c) inoculated hemp mat with particles of colonised fungus substrate for the fabrication of fungal textile (d) fungal wearable, photo credit: Irina Petrova.

3.2 Experimental set up

The electrical activity of the colonised fungal composites was recorded using pairs of iridium-coated stainless-steel subdermal needle electrodes (Spes Medica SRL, Italy) with twisted cables, via an ADC-24 (Pico Technology, UK) high- resolution data logger with a 24-bit A/D converter, galvanic isolation and software-selectable sample rates, contributing to a superior noise-free resolution. The electrodes were inserted with a distance of 1-2 cm. For each study, we recorded the electrical activity of five to eight electrode pairs simultaneously. Each pair of electrodes, referred to as a Channel (Ch), reported a difference in the electrical potential between the electrodes. The electrical activity was recorded at a rate of one sample per second (1 Hz), with logging times ranging from 60.04 to 93.45 hours for the different experiments. Throughout the recording, the logger took as many samples as it could (typically up to 600 per second) and saved the average value. We set the acquisition voltage range to 156~mV with an offset accuracy of 9 mV at 1~Hz to maintain a gain error of 0.1%. Each electrode pair was considered independently with the noise-free resolution of 17 bits and conversion time of 60 ms. In the experiments, the electrode pairs were arranged either randomly or in lines.

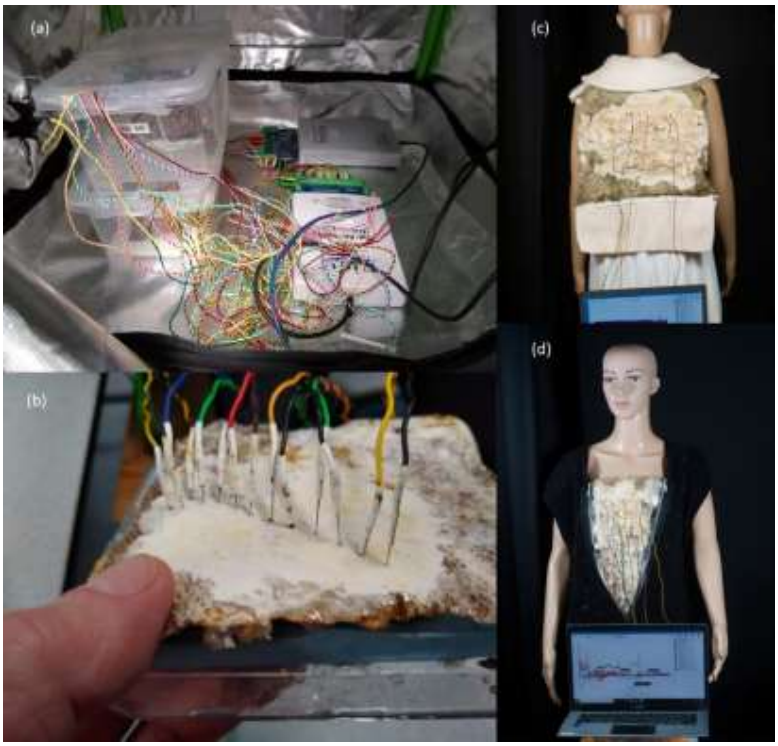


Figure 2. Experimental setup. (a) growth tent (b) exemplar location of electrodes in colonised fungal substrate (c) (d) insertion of electrodes in fungal wearable, photo credit: Irina Petrova.

Oscillation of electrical potential of fungi has been reported through intracellular recording (Slayman et al., 1976, Stefan, 1995) and extra-cellular recordings by inserting

electrodes in fruit bodies (Adamatzky, 2018) and in substrates colonised by fungi (Adamatzky,2021).

3.3 Exposure to control parameters

We exposed the fungal composites to environmental, chemical and mechanical stimulants as below:

1. Malt extract powder (Sigma Aldrich, UK) dissolved in distilled water
2. Dextrose (Ritchie Products Ltd, UK)
3. Ethanol (1 ml of 96% ethanol)
4. Attachment of weights (50 g and 200 g)
5. Hydrocortisone solution (2 mL of Solu-Cortef trademark, 4 mL Act-O-Vial, Pfizer, Athens, Greece)

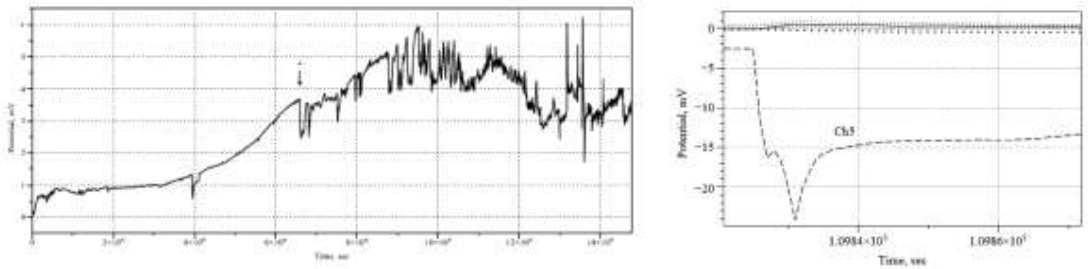
Malt extract is a chemo-attractant and source of nutrients while dextrose and ethanol are chemo-attractants. The weight application was undertaken to assess the fungal composite's response to mechanical stretching.

Hydrocortisone is a medical replacement hormone similar to the natural stress hormone cortisol. Changes in cortisol levels released by the body indicate the presence of disease and stress. Human patients weighing 80 kg are typically given 20 mg of synthetic cortisol per day for a variety of diseases. As a result, 20 mg divided by 80 kg yields 0.25 mg/kg. Fungal composites used in this feasibility study weighed 100-200 g each, so a 2 mL dose of 250 µg was applied (Dehshibi et al., 2021).

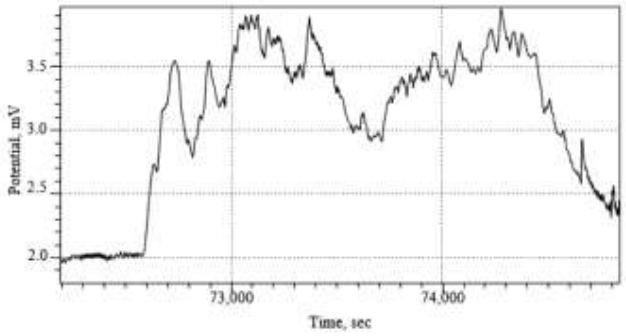
We recorded the electrical activity of the fungal composites during and after exposure to the above stimulants using the method described in the 3.2 section to assess their responsive capabilities. To investigate any changes in the fungal tissue of the fungal composites, we performed a series of scans using X-Rays, CT and MRI scans on the composite exposed to hydrocortisone.

4.RESULTS

The experiments performed using the malt extract powder and dextrose stimulants showed distinctive patterns of electrical activity with a substantial increase in the spiking activity after exposure compared to prior being exposed. For example, in the first 5 hours after the dextrose application, the frequency of spikes substantially increased (Fig. 3 (a)): the average distance between the spikes became 22 min, σ = 13 and the amplitude increased to average 0.43 mV, σ = 0.27. In next 5 hours, the average amplitude of spikes increased to 1.3 mV, σ = 0.35, and the distance between spikes 20 min, σ = 7.



(a) (b)



(c)

Figure 3. (a) Response to application of dextrose. (b) Response to application of ethanol (c) Response to removal of 200 g weight.

Exposure to ethanol (Fig. 3 (b)) showed a drop by nearly 8 mV followed by a further drop of the electrical potential by nearly 8 mV. The potential remained c. 11 mV lower than that before stimulation. Responses to application and removal of the weights, showed distinctive trains of spikes. Example Fig. 3 (c) demonstrates a response to removal of 200 g weight of an average duration of 38 min, σ=2 min, and average amplitude 1.56 mV, σ=1.24 mV. The response in the example consists of two trains of high frequency spikes. Average spike width is 80 sec (σ = 50), average amplitude 0.31 mV (σ=0.32), average distance between spike in each train is 71 sec (Adamatzky et al., 2021) Therefore, living fungi material can detect and respond to chemical, environmental and mechanical stimulants, paving the way to the construction of buildings and wearables that exhibit intelligence, sensorial fusion and decision-making capabilities. In the building industry, such material can be an exceptional sustainable replacement to conventional materials and conventional sensing technologies currently widely used.

Similarly, exposure to hydrocortisone stimulant showed the formation of an electrical activity fingerprint that corresponds to the specific event, inducing a strong response. The impact of hydrocortisone exposure was also visible in the distribution of energy levels resulting from the analysis of the scans. The substrate that was not exposed to hydrocortisone had a higher energy frequency than the cortisol-exposed segment and the no-exposed segment adjacent to the cortisol-exposed segment (Dehshibi et al., 2021). To the authors' knowledge, responsive behaviour of fungi upon exposure to

hormones has not been reported before. This could open up exciting possibilities for the use of living fungi composites in the building industry, enabling our buildings to detect and report disease as well as capture data about the users' health and wellbeing.

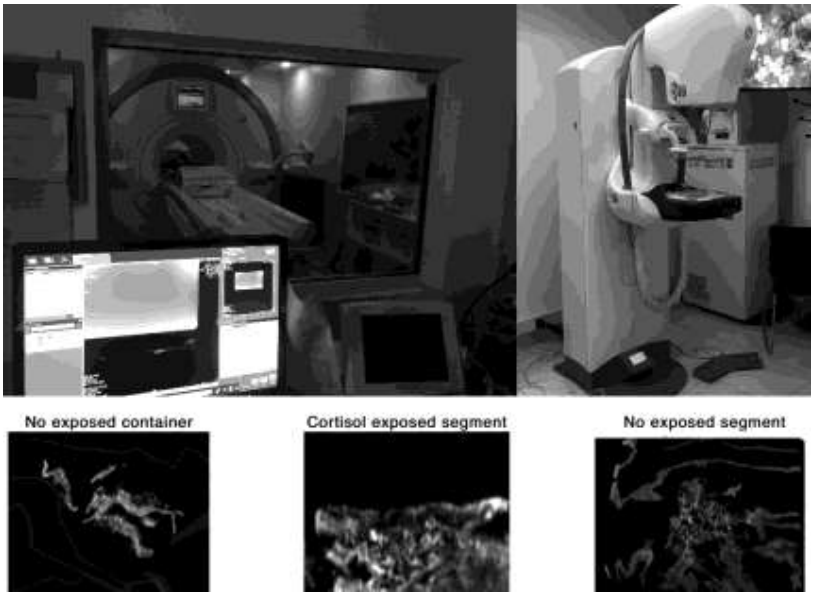


Figure 4. Use of X-ray, MRI and CT scans to study changes in fungi composite tissue before/ during and after exposure to hydrocortisone.

DISCUSSION

The above feasibility studies demonstrated that fungal composites show distinctive sets of responses when exposed to chemical and mechanical stimulation. They sense their environment by generating distinctive trains of electrical spikes when exposed to stimulants and cues without the need of any external control or intervention. They therefore meet all three principles of animacy as discussed in section 2, opening up exciting possibilities for the fabrication of intelligent and sustainable materials. Deriving to a unique one-to-one mapping between a range of selected environmental, chemical and mechanical stimulants and electrical responses, could allow our buildings and wearables to detect air pollutants, toxic substances, hormone changes etc. leading to prevention of disease and long-term conditions. Moreover, our buildings could respond and react to environmental stimulants such as exposure to light or humidity, improving their efficiency, performance, thermal comfort and energy saving. Our findings demonstrated that fungal substrates are a promising candidate for producing sustainable smart composites.

To realise the full potential of the fungal composites, it will be necessary to overcome two main challenges. Firstly, in laboratory conditions, the fungal composites can survive for several months as they are being kept in high humidity conditions and in a controlled environment (e.g. temperature, light etc.). The longevity of the fungal composites is dependent on stable moisture levels. To ensure viability, coating systems should be

tested e.g. the use of a hydrogel external layer. Secondly, fungal composites are prone to the development of pathogens and contamination. Assessing the influence of the environmental conditions that support the growth of infection is vital.

CONCLUSION

Our research shows that fungal composites present intriguing possibilities that could lead to a step-change in sustainable smart material design and development. The building industry is one of the primary consumers of environmental resources, leading to a catastrophic environmental impact and the depletion of natural resources. This applies to both the building construction and to the resource consumption during its occupation and use. It is therefore necessary to address this grand societal challenge and explore approaches that envision a paradigm shift in how material is sourced, processed and assembled, address the magnitude of these challenges in a truly sustainable way. This research proposes the development of a structural substrate by using living mycelium that can detect, sense and adapt to its environment in a similar manner to humans. We envision the construction of buildings that can self-grow and self-repair, adapt to their environment and self-regulate themselves efficiently. By taking advantage of the remarkable properties of fungi, a new paradigm for material production could be developed leading to self-sustainable and environmentally responsive materials that are cost-effective and have reduced environmental impact as compared to conventional materials. Applications such as air quality and health monitoring could lead to early disease detection and prevention of chronic conditions. Mechanical sensing and detection of weight application or removal could open up new possibilities for load detection in buildings. Responding to the presence of chemical substances such as VOCs and smoke could protect the occupants and provide real-time data.

ACKNOWLEDGEMENT

This project has received funding from the European Union's Horizon 2020 research and innovation programme FET OPEN "Challenging current thinking" under grant agreement No 858132.

REFERENCES

Adamatzky, A., Nikolaidou, A., Gandia, A., Chiolerio, A. and Dehshibi,M. (2021) Reactive fungal wearable. *Biosystems*, 199, 104304.

Adamatzky, A., Gandia, A., Ayres, P., Wösten, H. and Tegelaar, M. (2021) Adaptive Fungal Architectures. *LINKs-series*, vol. 5-6 (10), pp. 66-77.

Adamatzky, A. (2018) On spiking behaviour of oyster fungi Pleurotus djamor. *Sci Rep* 8**,** 7873.

Addington, M. and Schodek, D. (2005) Smart Materials and New Technologies: For the Architecture and Design Professions. *Architectural Press*, Boston.

Addington, M., and Schodek, D. (2004) Smart Materials and Technologies in Architecture. 1 ed. Amsterdam: Architectural Press.

Aelenei, D., Aelenei, L. and Vieira, C. P. (2016) Adaptive Façade: Concept, Applications, Research Questions. Energy Procedia 91 (Supplement C), pp. 269–275.
Barozzi, M., et al. (2016) The Sustainability of Adaptive Envelopes: Developments of Kinetic Architecture. The Proceeding of Engineering Conference. 155, pp. 275–284.
Decker, M. (2013) Emergent Futures: Nanotechnology and Emergent Materials in Architecture. The proceeding of conference of tectonics of teaching: building technology educators society. Newport: Rhode Island.
Dehshibi, M., Chiolerio, A., Nikolaidou, A., Mayne, R., Gandia, A., Ashtari-Majlan, M. and Adamatzky, A, (2021) Stimulating Fungi Pleurotus ostreatus with Hydrocortisone. ACS Biomaterials Science & Engineering, 7 (8), 3718-3726.
Forti V., Baldé C.P., Kuehr R., Bel G. (2020) The Global E-waste Monitor 2020: Quantities, flows and the circular economy potential. United Nations University (UNU)/United Nations Institute for Training and Research (UNITAR) – co-hosted SCYCLE Programme, International Telecommunication Union (ITU) & International Solid Waste Association (ISWA), Bonn/Geneva/Rotterdam.
Gilbert, C. and Ellis, T. (2019) Biological Engineered Living Materials: Growing Functional Materials with Genetically Programmable Properties. *ACS Synthetic Biology*. 8 (1), pp. 1-15
Haneef, M., Ceseracciu, L., Canale, C., Bayer, I.S., Heredia-Guerrero, J.A. and Athanassiou, A. (2017) Advanced materials from fungal mycelium: fabrication and tuning of physical properties. *Sci. Rep*., 7 (1), 41292.
Holt, G., Mcintyre, G., Flagg, D., Bayer, E., Wanjura, J. and Pelletier, M. (2012) Fungal mycelium and cotton plant materials in the manufacture of biodegradable molded packaging material: evaluation study of select blends of cotton byproducts. *J. Biobaased Mater. Bioenergy*. 6 (4), pp. 431-439.
Ikechukwu, O. and Moses, O. (2019) Conceptual Issues in the Qualification of Intelligent Buildings. *Open Journal of Energy Efficiency*, 8 (2), pp. 52-63.
Islam, M., Tudryn, G., Bucinell, R., Schadler, L., and Picu, R. (2017) Morphology and mechanics of fungal mycelium. Sci. Rep., 7 (1), 13070.
Jones, M., Mautner, A., Luenco, S., Bismarck, A. and John, S. (2020) Engineered mycelium composite construction materials from fungal biorefineries: A critical review. *Materials & Design*. 187, 108397.
Jones, M., Huynh, T., Dekiwadia, C., Daver, F. and John, S. (2017) Mycelium composites: a review of engineering characteristics and growth kinetics. *Journal of Bionanoscience*, 11 (4), pp. 241-257.
Khoo, C. (2013) Morphing architecture: with responsive material system. *Thesis, architecture and design school*, RMIT University, Australia.
Loonen, R. C. G. M., et al. (2013) Climate Adaptive Building Shells: State-of-the- art and Future Challenges. *Renewable and Sustainable Energy Reviews*. 25, pp. 483–493.
Matin, N. H. and Eydgahi, A. (2019) Technologies used in responsive facade systems: a comparative study. Intelligent Buildings International.
Nawawi, W., Jones, M., Murphy, R.J., Lee, K.-Y., Kontturi, E. and Bismarck, A. (2020) Nanomaterials Derived from Fungal Sources—Is It the New Hype? *Biomacromolecules*. 21 (1), pp 30-55.

Ogwezi, B., et al. (2011) Multifunctional, Adaptable Facades. *The proceeding of TSBE*.
Pelletier, M.G., Holt, G.A., Wanjura, J.D., Bayer, E. and McIntyre, G. (2013) An evaluation study of mycelium based acoustic absorbers grown on agricultural by-product substrates*. Ind. Crop. Prod*. 51 (1), pp. 480-485.
Slayman, C.L., Long, W.S., Gradmann, D (1976) "Action potentials" in NEUROSPORA CRASSA, a mycelial fungus. *Biochimica et Biophysica Acta (BBA) – Biomembranes* 426(4), pp. 732-744.
Stefan, O. and Hansson, B. (1995). Action Potential-Like Activity Found in Fungal Mycelia Is Sensitive to Stimulation. *Naturwissenschaften*. 82 (1), pp. 30-31.
The Royal Society (2021) *Animate Materials* [online]. London: The Royal Society. Available from: royalsociety.org/animate-materials. [Accessed 1 June 2022].

References

Abadi, P. P., Garbern, J. C., Behzadi, S., Hill, M. J., Tresback, J. S., Heydari, T., Ejtehadi, M. R., Ahmed, N., Copley, E., Aghaverdi, H., et al. (2018). Engineering of mature human induced pluripotent stem cell-derived cardiomyocytes using substrates with multiscale topography. *Advanced Functional Materials*. 28.19, p. 1707378.

Abbott, L. F. and Nelson, S. B. (2000). Synaptic plasticity: taming the beast. *Nature neuroscience*. 3.11, pp. 1178–1183.

Abdelouahab, M.-S., Lozi, R., and Chua, L. (2014). Memfractance: a mathematical paradigm for circuit elements with memory. *International Journal of Bifurcation and Chaos*. 24.09, p. 1430023.

Abeer, M. M., Mohd Amin, M. C. I., and Martin, C. (2014). A review of bacterial cellulose-based drug delivery systems: their biochemistry, current approaches and future prospects. *Journal of Pharmacy and Pharmacology*. 66.8, pp. 1047–1061.

Adamatzky, A. (2011). Topics in reaction-diffusion computers. *Journal of Computational and Theoretical Nanoscience*. 8.3, pp. 295–303.

Adamatzky, A. (2018). On spiking behaviour of oyster fungi Pleurotus djamor. *Scientific reports*. 8.1, p. 7873.

Adamatzky, A. (2019a). A brief history of liquid computers. *Philosophical Transactions of the Royal Society B*. 374.1774, p. 20180372.

Adamatzky, A. (2019b). Plant leaf computing. *Biosystems*. 182, pp. 59–64.

Adamatzky, A. (2021a). *Handbook Of Unconventional Computing (In 2 Volumes)*. World Scientific.

Adamatzky, A. (2021b). Language of fungi derived from electrical spiking activity. *arXiv preprint arXiv:2112.09907*.

Adamatzky, A. (2022a). Dynamics of electrical resistance of kombucha zoogleal mats. *Biophysical Reviews and Letters*. 17.04, pp. 135–144.

Adamatzky, A. (2022b). Language of fungi derived from their electrical spiking activity. *Royal Society Open Science*. 9.4, p. 211926.

Adamatzky, A. (2023). Electrical potential spiking of kombucha zoogleal mats: A symbiotic community of bacteria and yeasts. *Bioelectricity*. 5.2, pp. 99–108.

Adamatzky, A., Chiolerio, A., and Sirakoulis, G. (2020). On resistive spiking of fungi. *arXiv preprint arXiv:2009.00292*.

Adamatzky, A., Costello, B. D. L., and Asai, T. (2005). *Reaction-diffusion computers*. Elsevier.

Adamatzky, A., Gandia, A., Ayres, P., Wösten, H., and Tegelaar, M. (2021). Adaptive fungal architectures. *LINKs-series*. 5, pp. 66–77.

Adamatzky, A., Lacy Costello, B. de, Rozenberg, G., Bäck, T., and Kok, J. (2012). Reaction-Diffusion Computing. *Handbook of natural computing*. 4, p. 1898.

Adamatzky, A., Schunselaar, E., Wösten, H. A., and Ayres, P. (2023). Multiscalar electrical spiking in Schizophyllum commune. *Scientific Reports*. 13.1, p. 12808.

Adhikari, B. and Majumdar, S. (2004). Polymers in sensor applications. *Progress in polymer science*. 29.7, pp. 699–766.

Agate, S., Joyce, M., Lucia, L., and Pal, L. (2018). Cellulose and nanocellulose-based flexible-hybrid printed electronics and conductive composites–A review. *Carbohydrate polymers*. 198, pp. 249–260.

Ahuja, T., Kumar, D., et al. (2009). Recent progress in the development of nano-structured conducting polymers/nanocomposites for sensor applications. *Sensors and Actuators B: Chemical*. 136.1, pp. 275–286.

Albano, K. M., Cavallieri, Â. L. F., and Nicoletti, V. R. (2019). Electrostatic interaction between proteins and polysaccharides: Physicochemical aspects and applications in emulsion stabilization. *Food Reviews International*. 35.1, pp. 54–89.

Albu, M. G., Vuluga, Z., Panaitescu, D. M., Vuluga, D. M., Căşărică, A., and Ghiurea, M. (2014). Morphology and thermal stability of bacterial cellulose/collagen composites. *Central European Journal of Chemistry*. 12, pp. 968–975.

Almeida, M. C. and Brand, A. C. (2017). Thigmo responses: the fungal sense of touch. *Microbiology spectrum*. 5.2, pp. 10–1128.

Amao, Y., Shuto, N., Furuno, K., Obata, A., Fuchino, Y., Uemura, K., Kajino, T., Sekito, T., Iwai, S., Miyamoto, Y., et al. (2012). Artificial leaf device for solar fuel production. *Faraday Discussions*. 155, pp. 289–296.

Anand, S. V., Ali, M. Y., and Saif, M. T. A. (2015). Cell culture on microfabricated one-dimensional polymeric structures for bio-actuator and bio-bot applications. *Lab on a Chip*. 15.8, pp. 1879–1888.

Andres, D. S. (2015). The language of neurons: theory and applications of a quantitative analysis of the neural code. *International Journal of Medical and Biological Frontiers*. 21.2, p. 133.

Annabi, N., Selimović, Š., Cox, J. P. A., Ribas, J., Bakooshli, M. A., Heintze, D., Weiss, A. S., Cropek, D., and Khademhosseini, A. (2013). Hydrogel-coated microfluidic channels for cardiomyocyte culture. *Lab on a Chip*. 13.18, pp. 3569–3577.

Ansari, S. and Giannelis, E. P. (2009). Functionalized graphene sheet—Poly (vinylidene fluoride) conductive nanocomposites. *Journal of Polymer Science Part B: Polymer Physics*. 47.9, pp. 888–897.

Armstrong, R. (2023). Towards the microbial home: An overview of developments in next-generation sustainable architecture. *Microbial Biotechnology*.

Arrieta, J., Barreira, A., Chioccioli, M., Polin, M., and Tuval, I. (2017). Phototaxis beyond turning: persistent accumulation and response acclimation of the microalga Chlamydomonas reinhardtii. *Scientific reports*. 7.1, p. 3447.

Asadian, E., Ghalkhani, M., and Shahrokhian, S. (2019). Electrochemical sensing based on carbon nanoparticles: A review. *Sensors and Actuators B: Chemical*. 293, pp. 183–209.

Asally, M., Kittisopikul, M., Rué, P., Du, Y., Hu, Z., Çağatay, T., Robinson, A. B., Lu, H., Garcia-Ojalvo, J., and Süel, G. M. (2012). Localized cell death focuses mechanical forces during 3D patterning in a biofilm. *Proceedings of the National Academy of Sciences*. 109.46, pp. 18891–18896.

Auerbach, S. M., Carrado, K. A., and Dutta, P. K. (2003). *Handbook of zeolite science and technology*. CRC press.

Auerbach, S. M., Carrado, K. A., and Dutta, P. K. (2004). *Handbook of layered materials*. CRC press.

Avnir, D., Coradin, T., Lev, O., and Livage, J. (2006). Recent bio-applications of sol–gel materials. *Journal of Materials Chemistry*. 16.11, pp. 1013–1030.

Azeredo, H. M., Barud, H., Farinas, C. S., Vasconcellos, V. M., and Claro, A. M. (2019). Bacterial cellulose as a raw material for food and food packaging applications. *Frontiers in Sustainable Food Systems*. 3, p. 7.

Azhari, N. J., Nurdini, N., Mardiana, S., Ilmi, T., Fajar, A. T., Makertihartha, I., Kadja, G. T., et al. (2022). Zeolite-based catalyst for direct conversion of CO2 to C2+ hydrocarbon: A review. *Journal of CO2 Utilization*. 59, p. 101969.

Bae, S., Kim, H., Lee, Y., Xu, X., Park, J.-S., Zheng, Y., Balakrishnan, J., Lei, T., Ri Kim, H., Song, Y. I., et al. (2010). Roll-to-roll production of 30-inch graphene films for transparent electrodes. *Nature nanotechnology*. 5.8, pp. 574–578.

Bahn, Y.-S., Xue, C., Idnurm, A., Rutherford, J. C., Heitman, J., and Cardenas, M. E. (2007). Sensing the environment: lessons from fungi. *Nature Reviews Microbiology*. 5.1, pp. 57–69.

Bai, H. and Shi, G. (2007). Gas sensors based on conducting polymers. *Sensors*. 7.3, pp. 267–307.

Ball, P. (2021). *Animate materials*.

Bao, L. and Li, X. (2012). Towards textile energy storage from cotton T-shirts. *Advanced materials*. 24.24, pp. 3246–3252.

Barr, M. C., Rowehl, J. A., Lunt, R. R., Xu, J., Wang, A., Boyce, C. M., Im, S. G., Bulović, V., and Gleason, K. K. (2011). Direct monolithic integration of organic photovoltaic circuits on unmodified paper. *Advanced Materials*. 23.31, pp. 3500–3505.

Barroso, Á., Landwerth, S., Woerdemann, M., Alpmann, C., Buscher, T., Becker, M., Studer, A., and Denz, C. (2015). Optical assembly of bio-hybrid micro-robots. *Biomedical microdevices*. 17, pp. 1–8.

Barud, H. S., Regiani, T., Marques, R. F., Lustri, W. R., Messaddeq, Y., Ribeiro, S. J., et al. (2011). Antimicrobial bacterial cellulose-silver nanoparticles composite membranes. *Journal of Nanomaterials*. 2011.

Baslow, M. H. (2009). The languages of neurons: an analysis of coding mechanisms by which neurons communicate, learn and store information. *Entropy*. 11.4, pp. 782–797.

Baumgartner, M., Coppola, M. E., Sariciftci, N. S., Glowacki, E. D., Bauer, S., and Irimia-Vladu, M. (2017). Emerging "green" materials and technologies for electronics. *Green Materials for Electronics*. 101.1.

Beasley, A. E., Abdelouahab, M.-S., Lozi, R., Powell, A. L., and Adamatzky, A. (2020). On memfractance of plants and fungi. *arXiv preprint arXiv:2005.10500*.

Beasley, A. E., Powell, A. L., and Adamatzky, A. (2020). Capacitive storage in mycelium substrate. *arXiv preprint arXiv:2003.07816*.

Belkin, S., Yagur-Kroll, S., Kabessa, Y., Korouma, V., Septon, T., Anati, Y., Zohar-Perez, C., Rabinovitz, Z., Nussinovitch, A., and Agranat, A. J. (2017). Remote detection of buried landmines using a bacterial sensor. *Nature biotechnology*. 35.4, pp. 308–310.

Ben-Jacob, E., Cohen, I., Shochet, O., Tenenbaum, A., Czirók, A., and Vicsek, T. (1995). Cooperative formation of chiral patterns during growth of bacterial colonies. *Physical Review Letters*. 75.15, p. 2899.

Ben-Jacob, E., Schochet, O., Tenenbaum, A., Cohen, I., Czirok, A., and Vicsek, T. (1994). Generic modelling of cooperative growth patterns in bacterial colonies. *Nature*. 368.6466, pp. 46–49.

Berridge, M. J., Bootman, M. D., and Roderick, H. L. (2003). Calcium signalling: dynamics, homeostasis and remodelling. *Nature reviews Molecular cell biology*. 4.7, pp. 517–529.

Bettinger, C. J., Bruggeman, J. P., Misra, A., Borenstein, J. T., and Langer, R. (2009). Biocompatibility of biodegradable semiconducting melanin films for nerve tissue engineering. *Biomaterials*. 30.17, pp. 3050–3057.

Bingley, M. (1966). Membrane potentials in Amoeba proteus. *Journal of Experimental Biology*. 45.2, pp. 251–267.

Bird, L. J., Kundu, B. B., Tschirhart, T., Corts, A. D., Su, L., Gralnick, J. A., Ajo-Franklin, C. M., and Glaven, S. M. (2021). Engineering wired life: synthetic biology for electroactive bacteria. *ACS Synthetic Biology*. 10.11, pp. 2808–2823.

Blake, P., Brimicombe, P. D., Nair, R. R., Booth, T. J., Jiang, D., Schedin, F., Ponomarenko, L. A., Morozov, S. V., Gleeson, H. F., Hill, E. W., et al. (2008). Graphene-based liquid crystal device. *Nano letters*. 8.6, pp. 1704–1708.

Bonfante, P. and Genre, A. (2010). Mechanisms underlying beneficial plant–fungus interactions in mycorrhizal symbiosis. *Nature communications*. 1.1, p. 48.

Bose, S., Kuila, T., Uddin, M. E., Kim, N. H., Lau, A. K., and Lee, J. H. (2010). In-situ synthesis and characterization of electrically conductive polypyrrole/graphene nanocomposites. *Polymer*. 51.25, pp. 5921–5928.

Böttcher, H., Soltmann, U., Mertig, M., and Pompe, W. (2004). Biocers: ceramics with incorporated microorganisms for biocatalytic, biosorptive and functional materials development. *Journal of Materials Chemistry*. 14.14, pp. 2176–2188.

Branda, S. S., González-Pastor, J. E., Ben-Yehuda, S., Losick, R., and Kolter, R. (2001). Fruiting body formation by Bacillus subtilis. *Proceedings of the National Academy of Sciences*. 98.20, pp. 11621–11626.

Branda, S. S., Vik, Å., Friedman, L., and Kolter, R. (2005). Biofilms: the matrix revisited. *Trends in microbiology*. 13.1, pp. 20–26.

Bray, D. (2009). *Wetware: a computer in every living cell*. Yale University Press.

Cantley, L. C., Hunter, T., Sever, R., and Thorner, J. W. (2014). *Signal transduction: principles, pathways, and processes*. Cold Spring Harbor Laboratory Press Cold Spring Harbor, NY, USA:

Cao, Y. and Uhrich, K. E. (2019). Biodegradable and biocompatible polymers for electronic applications: A review. *Journal of Bioactive and Compatible Polymers*. 34.1, pp. 3–15.

Carlier, A., Pessi, G., and Eberl, L. (2015). Microbial biofilms and quorum sensing. *Principles of Plant-Microbe Interactions: Microbes for Sustainable Agriculture*, pp. 45–52.

Cejka, J., Bekkum, H. van, Corma, A., and Schueth, F. (2007). *Introduction to zeolite molecular sieves*. Elsevier.

Cejka, J., Corma, A., and Zones, S. (2010). *Zeolites and catalysis: synthesis, reactions and applications*. John Wiley & Sons.

Ceylan, H., Giltinan, J., Kozielski, K., and Sitti, M. (2017). Mobile microrobots for bioengineering applications. *Lab on a Chip*. 17.10, pp. 1705–1724.

Chakraborty, A., Alam, M., Dey, V., Chattopadhyay, A., and Mukhopadhyay, D. (2021). A survey on adversarial attacks and defences. *CAAI Transactions on Intelligence Technology*. 6.1, pp. 25–45.

Chen, C. and Liu, B. (2000). Changes in major components of tea fungus metabolites during prolonged fermentation. *Journal of applied microbiology*. 89.5, pp. 834–839.

Chen, H.-H., Chen, L.-C., Huang, H.-C., and Lin, S.-B. (2011). In situ modification of bacterial cellulose nanostructure by adding CMC during the growth of Gluconacetobacter xylinus. *Cellulose*. 18, pp. 1573–1583.

Chen, X. J., Wang, B., Thompson, I. P., and Huang, W. E. (2021). Rational design and characterization of nitric oxide biosensors in E. coli Nissle 1917 and Mini SimCells. *ACS Synthetic Biology*. 10.10, pp. 2566–2578.

Cheng, K.-C., Catchmark, J. M., and Demirci, A. (2009). Enhanced production of bacterial cellulose by using a biofilm reactor and its material property analysis. *Journal of biological engineering*. 3.1, pp. 1–10.

Choi, S., Lee, H., Ghaffari, R., Hyeon, T., and Kim, D.-H. (2016). Recent advances in flexible and stretchable bio-electronic devices integrated with nanomaterials. *Advanced materials*. 28.22, pp. 4203–4218.

Chua, L. (1971). Memristor-the missing circuit element. *IEEE Transactions on circuit theory*. 18.5, pp. 507–519.

Chua, L. (2014). If it's pinched it'sa memristor. *Semiconductor Science and Technology*. 29.10, p. 104001.

Chua, L., Sirakoulis, G. C., and Adamatzky, A. (2019). *Handbook of Memristor Networks*. Springer Nature.

Chua, L. O. and Kang, S. M. (1976). Memristive devices and systems. *Proceedings of the IEEE*. 64.2, pp. 209–223.

Chuapradit, C., Wannatong, L. R., Chotpattananont, D., Hiamtup, P., Sirivat, A., and Schwank, J. (2005). Polyaniline/zeolite LTA composites and electrical conductivity response towards CO. *Polymer*. 46.3, pp. 947–953.

Clementi, E. A., Marks, L. R., Roche-Håkansson, H., and Håkansson, A. P. (2014). Monitoring changes in membrane polarity, membrane integrity, and intracellular ion concentrations in Streptococcus pneumoniae using fluorescent dyes. *Journal of Visualized Experiments: JoVE*. 84.

Cocatre-Zilgien, J. and Delcomyn, F. (1992). Identification of bursts in spike trains. *Journal of neuroscience methods*. 41.1, pp. 19–30.

Costenoble, O. O. (2016). Standards and Regulations for the Bio-based Industry-STAR4BBI.

Cox, D. D. and Dean, T. (2014). Neural Networks and Neuroscience-Inspired Computer Vision. *Current Biology* [online]. 24.18, R921–R929. ISSN: 0960-9822. DOI: https://doi.org/10.1016/j.cub.2014.08.026. Available from: https://www.sciencedirect.com/science/article/pii/S0960982214010392.

Cvetkovic, C., Rich, M. H., Raman, R., Kong, H., and Bashir, R. (2017). A 3D-printed platform for modular neuromuscular motor units. *Microsystems & Nanoengineering*. 3.1, pp. 1–9.

Das, A. A., Bovill, J., Ayesh, M., Stoyanov, S. D., and Paunov, V. N. (2016). Fabrication of living soft matter by symbiotic growth of unicellular microorganisms. *Journal of materials chemistry B*. 4.21, pp. 3685–3694.

Davidson, M. D., Ban, E., Schoonen, A. C., Lee, M.-H., D'Este, M., Shenoy, V. B., and Burdick, J. A. (2020). Mechanochemical adhesion and plasticity in multifiber hydrogel networks. *Advanced Materials*. 32.8, p. 1905719.

Davies, D. G., Parsek, M. R., Pearson, J. P., Iglewski, B. H., Costerton, J. W., and Greenberg, E. P. (1998). The involvement of cell-to-cell signals in the development of a bacterial biofilm. *Science*. 280.5361, pp. 295–298.

Davies, R., Teall, O., Pilegis, M., Kanellopoulos, A., Sharma, T., Jefferson, A., Gardner, D., Al-Tabbaa, A., Paine, K., and Lark, R. (2018). Large scale application of self-healing concrete: Design, construction, and testing. *Frontiers in Materials*. 5, p. 51.

De Belie, N. and Wang, J. (2016). Bacteria-based repair and self-healing of concrete. *Journal of Sustainable Cement-Based Materials*. 5.1-2, pp. 35–56.

De Filippis, F., Troise, A. D., Vitaglione, P., and Ercolini, D. (2018). Different temperatures select distinctive acetic acid bacteria species and promotes organic acids production during Kombucha tea fermentation. *Food microbiology*. 73, pp. 11–16.

Delatorre, A. B., Ribeiro, T. R. L., Arcênio, N. M. C., and Mothé, G. P. B. (2020). "Estudo sobre a adequação da normativa 41 para a produção e comercialização de Kombucha: estudo de caso em uma empresa de Macaé". In: *Congresso de Ensino Pesquisa e Extensão-CONEPE*.

Di Ventra, M., Pershin, Y. V., and Chua, L. O. (2009). Circuit elements with memory: memristors, memcapacitors, and meminductors. *Proceedings of the IEEE*. 97.10, pp. 1717–1724.

Dima, S.-O., Panaitescu, D.-M., Orban, C., Ghiurea, M., Doncea, S.-M., Fierascu, R. C., Nistor, C. L., Alexandrescu, E., Nicolae, C.-A., Trică, B., et al. (2017). Bacterial nanocellulose from side-streams of kombucha beverages production: Preparation and physical-chemical properties. *Polymers*. 9.8, p. 374.

Dimidi, E., Cox, S. R., Rossi, M., and Whelan, K. (2019). Fermented foods: definitions and characteristics, impact on the gut microbiota and effects on gastrointestinal health and disease. *Nutrients*. 11.8, p. 1806.

Distler, T., Solisito, A. A., Schneidereit, D., Friedrich, O., Detsch, R., and Boccaccini, A. R. (2020). 3D printed oxidized alginate-gelatin bioink provides guidance for C2C12 muscle precursor cell orientation and differentiation via shear stress during bioprinting. *Biofabrication*. 12.4, p. 045005.

Eckert, R., Naitoh, Y., and Friedman, K. (1972). Sensory mechanisms in Paramecium. *Journal of Experimental Biology*. 56.3, pp. 683–694.

Edwards, M. R., Wright Carlsen, R., and Sitti, M. (2013). Near and far-wall effects on the three-dimensional motion of bacteria-driven microbeads. *Applied Physics Letters*. 102.14.

Eroglu, E., Agarwal, V., Bradshaw, M., Chen, X., Smith, S. M., Raston, C. L., and Iyer, K. S. (2012). Nitrate removal from liquid effluents using microalgae immobilized on chitosan nanofiber mats. *Green Chemistry*. 14.10, pp. 2682–2685.

Fan, H., Wang, L., Zhao, K., Li, N., Shi, Z., Ge, Z., and Jin, Z. (2010). Fabrication, mechanical properties, and biocompatibility of graphene-reinforced chitosan composites. *Biomacromolecules*. 11.9, pp. 2345–2351.

Feinberg, A. W. (2015). Biological soft robotics. *Annual review of biomedical engineering*. 17, pp. 243–265.

Feng, Y., Zhang, X., Shen, Y., Yoshino, K., and Feng, W. (2012). A mechanically strong, flexible and conductive film based on bacterial cellulose/graphene nanocomposite. *Carbohydrate Polymers*. 87.1, pp. 644–649.

Fernandez-Rodriguez, J., Moser, F., Song, M., and Voigt, C. A. (2017). Engineering RGB color vision into Escherichia coli. *Nature chemical biology*. 13.7, pp. 706–708.

Fijałkowski, K., Żywicka, A., Drozd, R., Junka, A. F., Peitler, D., Kordas, M., Konopacki, M., Szymczyk, P., and Rakoczy, R. (2017). Increased water content in bacterial cellulose synthesized under rotating magnetic fields. *Electromagnetic Biology and Medicine*. 36.2, pp. 192–201.

Flemming, H.-C., Wingender, J., Szewzyk, U., Steinberg, P., Rice, S. A., and Kjelleberg, S. (2016). Biofilms: an emergent form of bacterial life. *Nature Reviews Microbiology*. 14.9, pp. 563–575.

Fortunato, E., Correia, N., Barquinha, P., Pereira, L., Gonçalves, G., and Martins, R. (2008). High-performance flexible hybrid field-effect transistors based on cellulose fiber paper. *IEEE Electron Device Letters*. 29.9, pp. 988–990.

Fox, S. W. (1992). Thermal proteins in the first life and in the "mind-body" problem. In: *Evolution of Information Processing Systems: An Interdisciplinary Approach for a New Understanding of Nature and Society*. Springer, pp. 203–228.

Fox, S. W., Jungck, J. R., and Nakashima, T. (1974). From proteinoid microsphere to contemporary cell: formation of internucleotide and peptide bonds by proteinoid particles. *Origins of Life*. 5, pp. 227–237.

Fox, S. W. and Nakashima, T. (1980). The assembly and properties of protobiological structures: The beginnings of cellular peptide synthesis. *BioSystems*. 12.3-4, pp. 155–166.

Freyman, M. C., Kou, T., Wang, S., and Li, Y. (2020). 3D printing of living bacteria electrode. *Nano Research*. 13, pp. 1318–1323.

Fromm, J. and Lautner, S. (2007). Electrical signals and their physiological significance in plants. *Plant, cell & environment*. 30.3, pp. 249–257.

Fu, C., Yan, F., Cao, Z., Xie, F., and Lin, J. (2014). Antioxidant activities of kombucha prepared from three different substrates and changes in content of probiotics during storage. *Food Science and Technology*. 34, pp. 123–126.

Gaggıa, F., Baffoni, L., Galiano, M., Nielsen, D. S., Jakobsen, R. R., Castro-Mejía, J. L., Bosi, S., Truzzi, F., Musumeci, F., Dinelli, G., et al. (2018). Kombucha beverage from green, black and rooibos teas: A comparative study looking at microbiology, chemistry and antioxidant activity. *Nutrients*. 11.1, p. 1.

Gale, E., Adamatzky, A., and Lacy Costello, B. de (2015). Slime mould memristors. *BioNanoScience*. 5, pp. 1–8.

Gale, E., Costello, B. D. L., and Adamatzky, A. (2012). "Observation and characterization of memristor current spikes and their application to neuromorphic computation". In: *AIP Conference Proceedings*. Vol. 1479. 1. American Institute of Physics, pp. 1898–1901.

Gale, E., Lacy Costello, B. de, and Adamatzky, A. (2014). Emergent spiking in non-ideal memristor networks. *Microelectronics Journal*. 45.11, pp. 1401–1415.

Gale, E., Mayne, R., Adamatzky, A., and Lacy Costello, B. de (2014). Drop-coated titanium dioxide memristors. *Materials Chemistry and Physics*. 143.2, pp. 524–529.

Gallego, G., Delbrück, T., Orchard, G., Bartolozzi, C., Taba, B., Censi, A., Leutenegger, S., Davison, A. J., Conradt, J., Daniilidis, K., et al. (2020). Event-based vision: A survey. *IEEE transactions on pattern analysis and machine intelligence*. 44.1, pp. 154–180.

Gao, K., Shao, Z., Li, J., Wang, X., Peng, X., Wang, W., and Wang, F. (2013). Cellulose nanofiber–graphene all solid-state flexible supercapacitors. *Journal of Materials Chemistry A*. 1.1, pp. 63–67.

Gao, W., Emaminejad, S., Nyein, H. Y. Y., Challa, S., Chen, K., Peck, A., Fahad, H. M., Ota, H., Shiraki, H., Kiriya, D., et al. (2016). Fully integrated wearable sensor arrays for multiplexed in situ perspiration analysis. *Nature*. 529.7587, pp. 509–514.

Geim, A. K. and Novoselov, K. S. (2007). The rise of graphene. *Nature materials*. 6.3, pp. 183–191.

Gelin, K., Bodin, A., Gatenholm, P., Mihranyan, A., Edwards, K., and Strømme, M. (2007). Characterization of water in bacterial cellulose using dielectric spectroscopy and electron microscopy. *Polymer*. 48.26, pp. 7623–7631.

Gerber, L. C., Koehler, F. M., Grass, R. N., and Stark, W. J. (2012). Incorporating microorganisms into polymer layers provides bioinspired functional living materials. *Proceedings of the National Academy of Sciences*. 109.1, pp. 90–94.

Gilbert, C., Tang, T.-C., Ott, W., Dorr, B. A., Shaw, W. M., Sun, G. L., Lu, T. K., and Ellis, T. (2021). Living materials with programmable functionalities grown from engineered microbial co-cultures. *Nature materials*. 20.5, pp. 691–700.

GK, J. et al. (2010). Memristance in human skin.

Gooch, J., Daniel, B., Parkin, M., and Frascione, N. (2017). Developing aptasensors for forensic analysis. *TrAC Trends in Analytical Chemistry*. 94, pp. 150–160.

Goodfellow, I., Bengio, Y., and Courville, A. (2016). *Deep learning*. MIT press.

Grimm, D. and Wösten, H. A. (2018). Mushroom cultivation in the circular economy. *Applied microbiology and biotechnology*. 102, pp. 7795–7803.

Gullo, M., La China, S., Falcone, P. M., and Giudici, P. (2018). Biotechnological production of cellulose by acetic acid bacteria: current state and perspectives. *Applied microbiology and biotechnology*. 102, pp. 6885–6898.

Guo, J., Luo, X., Tan, S., Ogunseitan, O. A., and Xu, Z. (2020). Thermal degradation and pollutant emission from waste printed circuit boards mounted with electronic components. *Journal of hazardous materials*. 382, p. 121038.

Guo, Z. and Tong, Y. W. (2014). The interactions between Chlorella vulgaris and algal symbiotic bacteria under photoautotrophic and photoheterotrophic conditions. *Journal of Applied Phycology*. 26, pp. 1483–1492.

Hahn, M. S., Taite, L. J., Moon, J. J., Rowland, M. C., Ruffino, K. A., and West, J. L. (2006). Photolithographic patterning of polyethylene glycol hydrogels. *Biomaterials*. 27.12, pp. 2519–2524.

Hammock, M. L., Chortos, A., Tee, B. C.-K., Tok, J. B.-H., and Bao, Z. (2013). 25th anniversary article: the evolution of electronic skin (e-skin): a brief history, design considerations, and recent progress. *Advanced materials*. 25.42, pp. 5997–6038.

Hamouche, H., Makhlouf, S., Chaouchi, A., and Laghrouche, M. (2018). Humidity sensor based on keratin bio polymer film. *Sensors and Actuators A: Physical*. 282, pp. 132–141.

Han, T., Nag, A., Mukhopadhyay, S. C., and Xu, Y. (2019). Carbon nanotubes and its gas-sensing applications: A review. *Sensors and Actuators A: Physical*. 291, pp. 107–143.

Haneef, M., Ceseracciu, L., Canale, C., Bayer, I. S., Heredia-Guerrero, J. A., and Athanassiou, A. (2017). Advanced materials from fungal mycelium: fabrication and tuning of physical properties. *Scientific reports*. 7.1, p. 41292.

Hanson, A. (2021). Spontaneous electrical low-frequency oscillations: a possible role in Hydra and all living systems. *Philosophical Transactions of the Royal Society B*. 376.1820, p. 20190763.

Hasebe, A., Suematsu, Y., Takeoka, S., Mazzocchi, T., Vannozzi, L., Ricotti, L., and Fujie, T. (2019). Biohybrid actuators based on skeletal muscle-powered microgrooved ultrathin films consisting of poly (styrene-block-butadiene-block-styrene). *ACS Biomaterials Science & Engineering*. 5.11, pp. 5734–5743.

Hawksworth, D. L. (2001). The magnitude of fungal diversity: the 1· 5 million species estimate revisited. *Mycological research*. 105.12, pp. 1422–1432.

Heßler, N. and Klemm, D. (2009). Alteration of bacterial nanocellulose structure by in situ modification using polyethylene glycol and carbohydrate additives. *Cellulose*. 16, pp. 899–910.

Higgins, M. J., Molino, P. J., Yue, Z., and Wallace, G. G. (2012). Organic conducting polymer–protein interactions. *Chemistry of Materials*. 24.5, pp. 828–839.

Hileman, B. (2002). Electronic waste. *Chem. Eng. News*. 80.26, pp. 15–18.

Holt, G. A., Mcintyre, G., Flagg, D., Bayer, E., Wanjura, J., and Pelletier, M. (2012). Fungal mycelium and cotton plant materials in the manufacture of biodegradable molded packaging material: Evaluation study of select blends of cotton byproducts. *Journal of Biobased Materials and Bioenergy*. 6.4, pp. 431–439.

Hosseini, N. R. and Lee, J.-S. (2015). Biocompatible and flexible chitosan-based resistive switching memory with magnesium electrodes. *Advanced Functional Materials*. 25.35, pp. 5586–5592.

Hrymak, A. and Margaritis, A. (2017). Recent developments in the production and applications of bacterial cellulose fibers and nanocrystals AU-Reiniati, Isabela. *Crit. Rev. Biotechnol*. 37.4, pp. 510–524.

Hu, W., Chen, S., Yang, J., Li, Z., and Wang, H. (2014). Functionalized bacterial cellulose derivatives and nanocomposites. *Carbohydrate polymers*. 101, pp. 1043–1060.

Hu, Y., Rehnlund, D., Klein, E., Gescher, J., and Niemeyer, C. M. (2020). Cultivation of exoelectrogenic bacteria in conductive DNA nanocomposite hydrogels yields a programmable biohybrid materials system. *ACS applied materials & interfaces*. 12.13, pp. 14806–14813.

Huang, J. and Gu, Y. (2011). Self-assembly of various guest substrates in natural cellulose substances to functional nanostructured materials. *Current opinion in colloid & interface science*. 16.6, pp. 470–481.

Humphries, J., Xiong, L., Liu, J., Prindle, A., Yuan, F., Arjes, H. A., Tsimring, L., and Süel, G. M. (2017). Species-independent attraction to biofilms through electrical signaling. *Cell*. 168.1, pp. 200–209.

Iguchi, M., Yamanaka, S., and Budhiono, A. (2000). Bacterial cellulose—a masterpiece of nature's arts. *Journal of materials science*. 35.2, pp. 261–270.

Illman, A., Scragg, A., and Shales, S. (2000). Increase in Chlorella strains calorific values when grown in low nitrogen medium. *Enzyme and microbial technology*. 27.8, pp. 631–635.

Inda, M. E. and Lu, T. K. (2020). Microbes as biosensors. *Annual Review of Microbiology*. 74, pp. 337–359.

Irimia-Vladu, M., Głowacki, E. D., Troshin, P. A., Schwabegger, G., Leonat, L., Susarova, D. K., Krystal, O., Ullah, M., Kanbur, Y., Bodea, M. A., et al. (2012). Indigo-A natural pigment for high performance ambipolar organic field effect transistors and circuits. *Advanced Materials*. 24.3, pp. 375–380.

Ul-Islam, M., Khattak, W. A., Kang, M., Kim, S. M., Khan, T., and Park, J. K. (2013). Effect of post-synthetic processing conditions on structural variations and applications of bacterial cellulose. *Cellulose*. 20, pp. 253–263.

Iwamura, T. (1949). Correlations between protoplasmic streaming and bioelectric potential of a slime mold, Physarum polycephalum. *Shokubutsugaku Zasshi*. 62.735-736, pp. 126–131.

Jasinski, D., Haque, F., Binzel, D. W., and Guo, P. (2017). Advancement of the emerging field of RNA nanotechnology. *ACS nano*. 11.2, pp. 1142–1164.

Jasti, S., Sieracki, M. E., Poulton, N. J., Giewat, M. W., and Rooney-Varga, J. N. (2005). Phylogenetic diversity and specificity of bacteria closely associated with Alexandrium spp. and other phytoplankton. *Applied and Environmental Microbiology*. 71.7, pp. 3483–3494.

Jayanthi, V. S. A., Das, A. B., and Saxena, U. (2017). Recent advances in biosensor development for the detection of cancer biomarkers. *Biosensors and Bioelectronics*. 91, pp. 15–23.

Jones, M., Huynh, T., Dekiwadia, C., Daver, F., and John, S. (2017). Mycelium composites: a review of engineering characteristics and growth kinetics. *Journal of Bionanoscience*. 11.4, pp. 241–257.

Jones, M., Mautner, A., Luenco, S., Bismarck, A., and John, S. (2020). Engineered mycelium composite construction materials from fungal biorefineries: A critical review. *Materials & Design*. 187, p. 108397.

Jonkers, H. M., Thijssen, A., Muyzer, G., Copuroglu, O., and Schlangen, E. (2010). Application of bacteria as self-healing agent for the development of sustainable concrete. *Ecological engineering*. 36.2, pp. 230–235.

Kadja, G. T., Rukmana, M. D., Mukti, R. R., Mahyuddin, M. H., Saputro, A. G., and Wungu, T. D. (2021). Solvent-free, small organic lactam-assisted synthesis of ZSM-5 zeolites. *Materials Letters*. 290, p. 129501.

Kamiya, N. and Abe, S. (1950). Bioelectric phenomena in the myxomycete plasmodium and their relation to protoplasmic flow. *Journal of Colloid Science*. 5.2, pp. 149–163.

Kandimalla, V. B., Tripathi, V. S., and Ju, H. (2006). Immobilization of biomolecules in sol–gels: biological and analytical applications. *Critical Reviews in Analytical Chemistry*. 36.2, pp. 73–106.

Kang, S.-K., Koo, J., Lee, Y. K., and Rogers, J. A. (2018). Advanced materials and devices for bioresorbable electronics. *Accounts of chemical research*. 51.5, pp. 988–998.

Kang, S., Zhao, K., Yu, D.-G., Zheng, X., and Huang, C. (2022). Advances in biosensing and environmental monitoring based on electrospun nanofibers. *Advanced Fiber Materials*. 4.3, pp. 404–435.

Kempaiah, R., Chung, A., and Maheshwari, V. (2011). Graphene as cellular interface: Electromechanical coupling with cells. *Acs Nano*. 5.7, pp. 6025–6031.

Khenfouch, M., Buttner, U., Baıtoul, M., and Maaza, M. (2014). Synthesis and characterization of mass produced high quality few layered graphene sheets via a chemical method.

Khurana, B., Gierlich, P., Meindl, A., Gomes-da-Silva, L. C., and Senge, M. O. (2019). Hydrogels: soft matters in photomedicine. *Photochemical & Photobiological Sciences*. 18.11, pp. 2613–2656.

Kim, D.-H., Kim, Y.-S., Amsden, J., Panilaitis, B., Kaplan, D. L., Omenetto, F. G., Zakin, M. R., and Rogers, J. A. (2009a). Silicon electronics on silk as a path to bioresorbable, implantable devices. *Applied physics letters*. 95.13.

Kim, J. and Hayward, R. C. (2012). Mimicking dynamic in vivo environments with stimuli-responsive materials for cell culture. *Trends in biotechnology*. 30.8, pp. 426–439.

Kim, K. S., Zhao, Y., Jang, H., Lee, S. Y., Kim, J. M., Kim, K. S., Ahn, J.-H., Kim, P., Choi, J.-Y., and Hong, B. H. (2009b). Large-scale pattern growth of graphene films for stretchable transparent electrodes. *nature*. 457.7230, pp. 706–710.

Klemm, D., Kramer, F., Moritz, S., Lindström, T., Ankerfors, M., Gray, D., and Dorris, A. (2011). Nanocelluloses: a new family of nature-based materials. *Angewandte Chemie International Edition*. 50.24, pp. 5438–5466.

Klemm, D., Schumann, D., Kramer, F., Heßler, N., Hornung, M., Schmauder, H.-P., and Marsch, S. (2006). Nanocelluloses as innovative polymers in research and application. *Polysaccharides ii*, pp. 49–96.

Knierim, C., Enzeroth, M., Kaiser, P., Dams, C., Nette, D., Seubert, A., Klingl, A., Greenblatt, C. L., Jérôme, V., Agarwal, S., et al. (2015). Living composites of bacteria and polymers as biomimetic films for metal sequestration and bioremediation. *Macromolecular Bioscience*. 15.8, pp. 1052–1059.

Ko, J., Nguyen, L. T., Surendran, A., Tan, B. Y., Ng, K. W., and Leong, W. L. (2017). Human hair keratin for biocompatible flexible and transient electronic devices. *ACS applied materials & interfaces*. 9.49, pp. 43004–43012.

Kopeček, J. and Yang, J. (2012). Smart self-assembled hybrid hydrogel biomaterials. *Angewandte Chemie International Edition*. 51.30, pp. 7396–7417.

Kosta, S. P., Kosta, Y. P., Bhatele, M., Dubey, Y., Gaur, A., Kosta, S., Gupta, J., Patel, A., and Patel, B. (2011). Human blood liquid memristor. *International Journal of Medical Engineering and Informatics*. 3.1, pp. 16–29.

Koster, S. A. de, Mors, R. M., Nugteren, H. W., Jonkers, H. M., Meesters, G. M., and Ommen, J. R. van (2015). Geopolymer coating of bacteria-containing granules for use in self-healing concrete. *Procedia Engineering*. 102, pp. 475–484.

Kranner, I., Beckett, R., Hochman, A., and Nash III, T. H. (2008). Desiccation-tolerance in lichens: a review. *The Bryologist*. 111.4, pp. 576–593.

Krawczyk, K., Xue, S., Buchmann, P., Charpin-El-Hamri, G., Saxena, P., Hussherr, M.-D., Shao, J., Ye, H., Xie, M., and Fussenegger, M. (2020). Electrogenetic cellular insulin release for real-time glycemic control in type 1 diabetic mice. *Science*. 368.6494, pp. 993–1001.

Kucherenko, I., Soldatkin, O., Dzyadevych, S., and Soldatkin, A. (2022). Application of zeolites and zeolitic imidazolate frameworks in the biosensor development. *Biomaterials Advances*. 143, p. 213180.

Kuila, T., Bose, S., Hong, C. E., Uddin, M. E., Khanra, P., Kim, N. H., and Lee, J. H. (2011). Preparation of functionalized graphene/linear low density polyethylene composites by a solution mixing method. *Carbon*. 49.3, pp. 1033–1037.

Kulprathipanja, S. (2010). *Zeolites in industrial separation and catalysis*. John Wiley & Sons.

Kuncová, G., Ishizaki, T., Solovyev, A., Trögl, J., and Ripp, S. (2016). The repetitive detection of toluene with bioluminescence bioreporter Pseudomonas putida TVA8 encapsulated in silica hydrogel on an optical fiber. *Materials*. 9.6, p. 467.

Kyaw, A. K. K., Jamalullah, F., Vaithieswari, L., Tan, M. J., Zhang, L., and Zhang, J. (2016a). Thermally stable and sterilizable polymer transistors for reusable medical devices. *ACS Applied Materials & Interfaces*. 8.15, pp. 9533–9539.

Kyaw, A. K. K., Lay, L. S., Peng, G. W., Changyun, J., and Jie, Z. (2016b). A nanogroove-guided slot-die coating technique for highly ordered polymer films and high-mobility transistors. *Chemical Communications*. 52.2, pp. 358–361.

Lam, T., Dehne, T., Krüger, J. P., Hondke, S., Endres, M., Thomas, A., Lauster, R., Sittinger, M., and Kloke, L. (2019). Photopolymerizable gelatin and hyaluronic acid for stereolithographic 3D bioprinting of tissue-engineered cartilage. *Journal of Biomedical Materials Research Part B: Applied Biomaterials*. 107.8, pp. 2649–2657.

Leavitt, S. D., Kraichak, E., Nelsen, M. P., Altermann, S., Divakar, P. K., Alors, D., Esslinger, T. L., Crespo, A., and Lumbsch, T. (2015). Fungal specificity and selectivity for algae play a major role in determining lichen partnerships across diverse ecogeographic regions in the lichen-forming family Parmeliaceae (Ascomycota). *Molecular Ecology*. 24.14, pp. 3779–3797.

LeCun, Y., Bottou, L., Bengio, Y., and Haffner, P. (1998). Gradient-based learning applied to document recognition. *Proceedings of the IEEE*. 86.11, pp. 2278–2324.

Lee, K.-Y. and Bismarck, A. (2012). Susceptibility of never-dried and freeze-dried bacterial cellulose towards esterification with organic acid. *Cellulose*. 19, pp. 891–900.

Legendy, C. and Salcman, M. (1985). Bursts and recurrences of bursts in the spike trains of spontaneously active striate cortex neurons. *Journal of neurophysiology*. 53.4, pp. 926–939.

Leonat, L., White, M. S., Głowacki, E. D., Scharber, M. C., Zillger, T., Rühling, J., Hübler, A., and Sariciftci, N. S. (2014). 4% efficient polymer solar cells on paper substrates. *The Journal of Physical Chemistry C*. 118.30, pp. 16813–16817.

Letnik, I., Avrahami, R., Rokem, J. S., Greiner, A., Zussman, E., and Greenblatt, C. (2015). Living composites of electrospun yeast cells for bioremediation and ethanol production. *Biomacromolecules*. 16.10, pp. 3322–3328.

Li, R., Wang, L., and Yin, L. (2018). Materials and devices for biodegradable and soft biomedical electronics. *Materials*. 11.11, p. 2108.

Li, S., Huang, D., Zhang, B., Xu, X., Wang, M., Yang, G., and Shen, Y. (2014). Flexible supercapacitors based on bacterial cellulose paper electrodes. *Advanced Energy Materials*. 4.10, p. 1301655.

Li, W., Liu, Q., Zhang, Y., Li, C., He, Z., Choy, W. C., Low, P. J., Sonar, P., and Kyaw, A. K. K. (2020a). Biodegradable materials and green processing for green electronics. *Advanced materials*. 32.33, p. 2001591.

Li, X., Zhu, X.-q., Okuda, K., Zhang, Z., Ashida, R., Yao, H., and Miura, K. (2017). Preparation of carbon fibers from low-molecular-weight compounds obtained from low-rank coal and biomass by solvent extraction. *New carbon materials*. 32.1, pp. 41–47.

Li, X., Wang, X., Zhang, L., Lee, S., and Dai, H. (2008). Chemically derived, ultrasmooth graphene nanoribbon semiconductors. *science*. 319.5867, pp. 1229–1232.

Li, X., Ding, C., Li, X., Yang, H., Liu, S., Wang, X., Zhang, L., Sun, Q., Liu, X., and Chen, J. (2020b). Electronic biopolymers: From molecular engineering to functional devices. *Chemical Engineering Journal*. 397, p. 125499.

Li, X., Cai, W., An, J., Kim, S., Nah, J., Yang, D., Piner, R., Velamakanni, A., Jung, I., Tutuc, E., et al. (2009). Large-area synthesis of high-quality and uniform graphene films on copper foils. *science*. 324.5932, pp. 1312–1314.

Li, Z., Seo, Y., Aydin, O., Elhebeary, M., Kamm, R. D., Kong, H., and Saif, M. T. A. (2019). Biohybrid valveless pump-bot powered by engineered skeletal muscle. *Proceedings of the National Academy of Sciences*. 116.5, pp. 1543–1548.

Lin, Z., Jiang, T., and Shang, J. (2022). The emerging technology of biohybrid micro-robots: a review. *Bio-Design and Manufacturing*, pp. 1–26.

Lind, J. U., Busbee, T. A., Valentine, A. D., Pasqualini, F. S., Yuan, H., Yadid, M., Park, S.-J., Kotikian, A., Nesmith, A. P., Campbell, P. H., et al. (2017). Instrumented cardiac microphysiological devices via multimaterial three-dimensional printing. *Nature materials*. 16.3, pp. 303–308.

Liu, J., Prindle, A., Humphries, J., Gabalda-Sagarra, M., Asally, M., Lee, D.-y. D., Ly, S., Garcia-Ojalvo, J., and Süel, G. M. (2015). Metabolic co-dependence gives rise to collective oscillations within biofilms. *nature*. 523.7562, pp. 550–554.

Liu, X., Tang, T.-C., Tham, E., Yuk, H., Lin, S., Lu, T. K., and Zhao, X. (2017). Stretchable living materials and devices with hydrogel–elastomer hybrids hosting programmed cells. *Proceedings of the National Academy of Sciences*. 114.9, pp. 2200–2205.

Liu, X., Yuk, H., Lin, S., Parada, G. A., Tang, T.-C., Tham, E., Fuente-Nunez, C. de la, Lu, T. K., and Zhao, X. (2018). 3D printing of living responsive materials and devices. *Advanced Materials*. 30.4, p. 1704821.

Lončar, E., Djurić, M., Malbaša, R., Kolarov, L., and Klašnja, M. (2006). Influence of working conditions upon kombucha conducted fermentation of black tea. *Food and Bioproducts Processing*. 84.3, pp. 186–192.

López, D. and Kolter, R. (2010). Extracellular signals that define distinct and coexisting cell fates in Bacillus subtilis. *FEMS microbiology reviews*. 34.2, pp. 134–149.

Ma, X., Xu, H., Li, G., Wang, M., Chen, H., and Chen, S. (2006). Gas-Response Studies of Polyaniline Composite Film Containing Zeolite to Chemical Vapors. *Macromolecular Materials and Engineering*. 291.12, pp. 1539–1546.

Maghfirah, A., Ilmi, M., Fajar, A., and Kadja, G. (2020). A review on the green synthesis of hierarchically porous zeolite. *Materials Today Chemistry*. 17, p. 100348.

Maicas, S. (2020). *The role of yeasts in fermentation processes*.

Mani, G., Feldman, M. D., Patel, D., and Agrawal, C. M. (2007). Coronary stents: a materials perspective. *Biomaterials*. 28.9, pp. 1689–1710.

Markx, G. H., Andrews, J. S., and Mason, V. P. (2004). Towards microbial tissue engineering? *Trends in biotechnology*. 22.8, pp. 417–422.

McGILLIVRAY, A. M. and Gow, N. A. (1986). Applied electrical fields polarize the growth of mycelial fungi. *Microbiology*. 132.9, pp. 2515–2525.

McNeil, B. and Harvey, L. (2008). *Practical fermentation technology*. John Wiley & Sons.

Mehmood, A., Liu, G., Wang, X., Meng, G., Wang, C., and Liu, Y. (2019). Fungal quorum-sensing molecules and inhibitors with potential antifungal activity: a review. *Molecules*. 24.10, p. 1950.

Mei, Y., He, C., Zeng, W., Luo, Y., Liu, C., Yang, M., Kuang, Y., Lin, X., and Huang, Q. (2022). Electrochemical biosensors for foodborne pathogens detection based on carbon nanomaterials: Recent advances and challenges. *Food and Bioprocess Technology*. 15.3, pp. 498–513.

Mintova, S., Tsapatsis, M., and Valtchev, V. (2009). *Ordered porous solids: recent advances and prospects*. Elsevier Science.

Miodownik, M., Morris, R., et al. (2021). Animate Materials.

Molaei, M., Barry, M., Stocker, R., and Sheng, J. (2014). Failed escape: solid surfaces prevent tumbling of Escherichia coli. *Physical review letters*. 113.6, p. 068103.

Moon, R. (2011). J.; Ashlie, M.; Nairn, J.; Simonsen, J.; Youngblood. *Chem. Soc. Rev*. 40, pp. 3941–3994.

Morales, N. M. and McClean, M. N. (2017). Engineered bacteria self-organize to sense pressure. *Nature Biotechnology*. 35.11, pp. 1045–1047.

Morimoto, Y., Onoe, H., and Takeuchi, S. (2019). Biohybrid device with antagonistic skeletal muscle tissue for measurement of contractile force. *Advanced Robotics*. 33.5, pp. 208–218.

Mougkogiannis, P. and Adamatzky, A. (2023). Morphologies of proteinoids. *Available at SSRN 4539346*.

Mougkogiannis, P., Nikolaidou, A., and Adamatzky, A. (2024). On Transducing Properties of Kombucha–Proteinoid Complexes. *ACS Applied Bio Materials*.

Mougkogiannis, P., Raeisi Kheirabadi, N., Chiolerio, A., and Adamatzky, A. (2023). Electrical spiking activity of proteinoids-ZnO colloids. *bioRxiv*, pp. 2023–07.

Munoz-Organero, M., Parker, J., Powell, L., and Mawson, S. (2016). Assessing walking strategies using insole pressure sensors for stroke survivors. *Sensors*. 16.10, p. 1631.

Nadell, C. D., Xavier, J. B., Levin, S. A., and Foster, K. R. (2008). The evolution of quorum sensing in bacterial biofilms. *PLoS biology*. 6.1, e14.

Nakajima-Shimada, J., Iida, H., Tsuji, F. I., and Anraku, Y. (1991). Monitoring of intracellular calcium in Saccharomyces cerevisiae with an apoaequorin cDNA expression system. *Proceedings of the National Academy of Sciences*. 88.15, pp. 6878–6882.

Nassif, N., Roux, C., Coradin, T., Rager, M.-N., Bouvet, O. M., and Livage, J. (2003). A sol–gel matrix to preserve the viability of encapsulated bacteria. *Journal of Materials Chemistry*. 13.2, pp. 203–208.

Natali, M., Campana, A., Posati, T., Benvenuti, E., Prescimone, F., Ramirez, D. S., Varesano, A., Vineis, C., Zamboni, R., Muccini, M., et al. (2019). Engineering of keratin functionality for the realization of bendable all-biopolymeric micro-electrode array as humidity sensor. *Biosensors and Bioelectronics*. 141, p. 111480.

Nations, U. (2020). *The Sustainable Development Goals Report 2020. United Nations; 2020*.

Nations, U. (1998). Kyoto protocol to the united nations framework convention on climate change.

Nawawi, W. M., Jones, M., Murphy, R. J., Lee, K.-Y., Kontturi, E., and Bismarck, A. (2019). Nanomaterials derived from fungal sources—is it the new hype? *Biomacromolecules*. 21.1, pp. 30–55.

Nelson, G., Kozlova-Zwinderman, O., Collis, A., Knight, M., Fincham, J., Stanger, C., Renwick, A., Hessing, J., Punt, P., Van Den Hondel, C., et al. (2004). Calcium measurement in living filamentous fungi expressing codon-optimized aequorin. *Molecular Microbiology*. 52.5, pp. 1437–1450.

Nguyen, P. Q., Courchesne, N.-M. D., Duraj-Thatte, A., Praveschotinunt, P., and Joshi, N. S. (2018). Engineered living materials: prospects and challenges for using biological systems to direct the assembly of smart materials. *Advanced Materials*. 30.19, p. 1704847.

Nieminen, L., Webb, S., Smith, M. C., and Hoskisson, P. A. (2013). A flexible mathematical model platform for studying branching networks: experimentally validated using the model actinomycete, Streptomyces coelicolor. *PloS one*. 8.2, e54316.

Noback, C. R. and Demarest, R. J. (1981). The human nervous system: basic principles of neurobiology. *(No Title)*.

Novoselov, K. S., Geim, A. K., Morozov, S. V., Jiang, D.-e., Zhang, Y., Dubonos, S. V., Grigorieva, I. V., and Firsov, A. A. (2004). Electric field effect in atomically thin carbon films. *science*. 306.5696, pp. 666–669.

Nyholm, L., Nyström, G., Mihranyan, A., and Strømme, M. (2011). Toward flexible polymer and paper-based energy storage devices. *Advanced Materials*. 23.33, pp. 3751–3769.

Olsson, S. and Hansson, B. (1995). Action potential-like activity found in fungal mycelia is sensitive to stimulation. *Naturwissenschaften*. 82, pp. 30–31.

Ooyama, S. and Shibata, T. (2011). Hierarchical organization of noise generates spontaneous signal in Paramecium cell. *Journal of theoretical biology*. 283.1, pp. 1–9.

Paine, K., Alazhari, M., Sharma, T., Cooper, R., and Heath, A. (2016). "Design and performance of bacteria-based self-healing concrete". In: *The 9th International Concrete Conference 2016: Environment, Efficiency and Economic Challenges for Concrete*, pp. 545–554.

Papagianni, M. (2004). Fungal morphology and metabolite production in submerged mycelial processes. *Biotechnology advances*. 22.3, pp. 189–259.

Paredes-Vallés, F., Scheper, K. Y., and De Croon, G. C. (2019). Unsupervised learning of a hierarchical spiking neural network for optical flow estimation: From events to global motion perception. *IEEE transactions on pattern analysis and machine intelligence*. 42.8, pp. 2051–2064.

Park, S. J., Lee, Y. K., Cho, S., Uthaman, S., Park, I.-K., Min, J.-J., Ko, S. Y., Park, J.-O., and Park, S. (2015). Effect of chitosan coating on a bacteria-based alginate microrobot. *Biotechnology and bioengineering*. 112.4, pp. 769–776.

Park, S. J., Park, S.-H., Cho, S., Kim, D.-M., Lee, Y., Ko, S. Y., Hong, Y., Choy, H. E., Min, J.-J., Park, J.-O., et al. (2013). New paradigm for tumor theranostic methodology using bacteria-based microrobot. *Scientific reports*. 3.1, p. 3394.

Parker, R. and Snyder, M. (1964). Electrical potentials of the dental plaque. *Life Sciences*. 3.11, pp. 1275–1279.

Parlak, O. (2021). Portable and wearable real-time stress monitoring: A critical review. *Sensors and Actuators Reports*. 3, p. 100036.

Pataranutaporn, P., Vujic, A., Kong, D. S., Maes, P., and Sra, M. (2020). "Living bits: Opportunities and challenges for integrating living microorganisms in human-computer interaction". In: *Proceedings of the augmented humans international conference*, pp. 1–12.

Patra, S., Singh, M., Pareek, D., Wasnik, K., Gupta, P. S., and Paik, P. (2022). Advances in the Development of Biodegradable Polymeric Materials for Biomedical Applications.

Peláez, E. C., Estevez, M.-C., Portela, A., Salvador, J.-P., Marco, M.-P., and Lechuga, L. M. (2018). Nanoplasmonic biosensor device for the monitoring of acenocoumarol therapeutic drug in plasma. *Biosensors and Bioelectronics*. 119, pp. 149–155.

Pelletier, M., Holt, G., Wanjura, J., Bayer, E., and McIntyre, G. (2013). An evaluation study of mycelium based acoustic absorbers grown on agricultural by-product substrates. *Industrial Crops and Products*. 51, pp. 480–485.

Peng, B., Ren, X., Wang, Z., Wang, X., Roberts, R. C., and Chan, P. K. (2014). High performance organic transistor active-matrix driver developed on paper substrate. *Scientific reports*. 4.1, p. 6430.

Phillips, N., Mayne, R., and Adamatzky, A. (2022). Chlorella sensors in liquid marbles and droplets. *Sensing and Bio-Sensing Research*. 36, p. 100491.

Phumman, P., Niamlang, S., and Sirivat, A. (2009). Fabrication of Poly (p-Phenylene)/Zeolite composites and their responses towards ammonia. *Sensors*. 9.10, pp. 8031–8046.

Piraner, D. I., Abedi, M. H., Moser, B. A., Lee-Gosselin, A., and Shapiro, M. G. (2017). Tunable thermal bioswitches for in vivo control of microbial therapeutics. *Nature chemical biology*. 13.1, pp. 75–80.

Piro, B., Tran, H. V., and Thu, V. T. (2020). Sensors Made of Natural Renewable Materials: Efficiency, Recyclability or Biodegradability—The Green Electronics. *Sensors*. 20.20, p. 5898.

Prindle, A., Liu, J., Asally, M., Ly, S., Garcia-Ojalvo, J., and Süel, G. M. (2015). Ion channels enable electrical communication in bacterial communities. *nature*. 527.7576, pp. 59–63.

Pruszynski, J. A. and Zylberberg, J. (2019). The language of the brain: real-world neural population codes. *Current opinion in neurobiology*. 58, pp. 30–36.

Puangprasert, S. and Prueksasit, T. (2019). Health risk assessment of airborne Cd, Cu, Ni and Pb for electronic waste dismantling workers in Buriram Province, Thailand. *Journal of environmental management*. 252, p. 109601.

Raman, R., Grant, L., Seo, Y., Cvetkovic, C., Gapinske, M., Palasz, A., Dabbous, H., Kong, H., Pinera, P. P., and Bashir, R. (2017). Damage, healing, and remodeling in optogenetic skeletal muscle bioactuators. *Advanced healthcare materials*. 6.12, p. 1700030.

Ramanathan, T., Abdala, A., Stankovich, S., Dikin, D., Herrera-Alonso, M., Piner, R., Adamson, D., Schniepp, H., Chen, X., Ruoff, R., et al. (2008). Functionalized graphene sheets for polymer nanocomposites. *Nature nanotechnology*. 3.6, pp. 327–331.

Ramírez Tapias, Y. A., Peltzer, M. A., Delgado, J. F., and Salvay, A. G. (2020). Kombucha tea byproduct as source of novel materials: Formulation and characterization of films. *Food and Bioprocess Technology*. 13, pp. 1166–1180.

Ramón-Azcón, J., Ahadian, S., Estili, M., Liang, X., Ostrovidov, S., Kaji, H., Shiku, H., Ramalingam, M., Nakajima, K., Sakka, Y., et al. (2013). Dielectrophoretically aligned carbon nanotubes to control electrical and mechanical properties of hydrogels to fabricate contractile muscle myofibers. *Advanced materials*. 25.29, pp. 4028–4034.

Raut, S. H., Sarode, D., and Lele, S. (2014). Biocalcification using B. pasteurii for strengthening brick masonry civil engineering structures. *World Journal of Microbiology and Biotechnology*. 30, pp. 191–200.

Ray, T. R., Choi, J., Bandodkar, A. J., Krishnan, S., Gutruf, P., Tian, L., Ghaffari, R., and Rogers, J. A. (2019). Bio-integrated wearable systems: a comprehensive review. *Chemical reviews*. 119.8, pp. 5461–5533.

Reeksting, B. J., Hoffmann, T. D., Tan, L., Paine, K., and Gebhard, S. (2020). In-depth profiling of calcite precipitation by environmental bacteria reveals fundamental mechanistic differences with relevance to application. *Applied and Environmental Microbiology*. 86.7, e02739–19.

Ricotti, L. and Fujie, T. (2017). Thin polymeric films for building biohybrid microrobots. *Bioinspiration & biomimetics*. 12.2, p. 021001.

Rivera-Tarazona, L. K., Campbell, Z. T., and Ware, T. H. (2021). Stimuli-responsive engineered living materials. *Soft Matter*. 17.4, pp. 785–809.

Rosenblatt, F. (1958). The perceptron: a probabilistic model for information storage and organization in the brain. *Psychological review*. 65.6, p. 386.

Roshanbinfar, K., Mohammadi, Z., Mesgar, A. S.-M., Dehghan, M. M., Oommen, O. P., Hilborn, J., and Engel, F. B. (2019). Carbon nanotube doped pericardial matrix derived electroconductive biohybrid hydrogel for cardiac tissue engineering. *Biomaterials science*. 7.9, pp. 3906–3917.

Rudge, T. J., Federici, F., Steiner, P. J., Kan, A., and Haseloff, J. (2013). Cell polarity-driven instability generates self-organized, fractal patterning of cell layers. *ACS synthetic biology*. 2.12, pp. 705–714.

Ruiz-Hitzky, E., Darder, M., Aranda, P., and Ariga, K. (2010). Advances in biomimetic and nanostructured biohybrid materials. *Advanced materials*. 22.3, pp. 323–336.

Sadasivuni, K. K., Kafy, A., Kim, H.-C., Ko, H.-U., Mun, S., and Kim, J. (2015). Reduced graphene oxide filled cellulose films for flexible temperature sensor application. *Synthetic Metals*. 206, pp. 154–161.

Safi, C., Zebib, B., Merah, O., Pontalier, P.-Y., and Vaca-Garcia, C. (2014). Morphology, composition, production, processing and applications of Chlorella vulgaris: A review. *Renewable and Sustainable Energy Reviews*. 35, pp. 265–278.

Saibuatong, O.-A. and Phisalaphong, M. (2010). Novo aloe vera–bacterial cellulose composite film from biosynthesis. *Carbohydrate Polymers*. 79.2, pp. 455–460.

Salama, A. M. (2019). Methodological research in architecture and allied disciplines: philosophical positions, frames of reference, and spheres of inquiry. *Archnet-IJAR: International Journal of Architectural Research*. 13.1, pp. 8–24.

Salek-Maghsoudi, A., Vakhshiteh, F., Torabi, R., Hassani, S., Ganjali, M. R., Norouzi, P., Hosseini, M., and Abdollahi, M. (2018). Recent advances in biosensor technology in assessment of early diabetes biomarkers. *Biosensors and Bioelectronics*. 99, pp. 122–135.

Sánchez, J. A., Lasker, H. R., Nepomuceno, E. G., Sánchez, J. D., and Woldenberg, M. J. (2004). Branching and self-organization in marine modular colonial organisms: a model. *The American Naturalist*. 163.3, E24–E39.

Schnepp, Z. (2013). Biopolymers as a flexible resource for nanochemistry. *Angewandte Chemie International Edition*. 52.4, pp. 1096–1108.

Scholes, N. S. and Isalan, M. (2017). A three-step framework for programming pattern formation. *Current opinion in chemical biology*. 40, pp. 1–7.

Schulz, D. J. (2006). Plasticity and stability in neuronal output via changes in intrinsic excitability: it's what's inside that counts. *Journal of Experimental Biology*. 209.24, pp. 4821–4827.

Schwarz, L., Medina-Sánchez, M., and Schmidt, O. G. (2017). Hybrid biomicromotors. *Applied Physics Reviews*. 4.3.

Sexton, L. T., Horne, L. P., Sherrill, S. A., Bishop, G. W., Baker, L. A., and Martin, C. R. (2007). Resistive-pulse studies of proteins and protein/antibody complexes using a conical nanotube sensor. *Journal of the American Chemical Society*. 129.43, pp. 13144–13152.

Shah, N., Ul-Islam, M., Khattak, W. A., and Park, J. K. (2013). Overview of bacterial cellulose composites: a multipurpose advanced material. *Carbohydrate polymers*. 98.2, pp. 1585–1598.

Sharma, S., Shukla, S., Vaid, D., et al. (1983). Shellac-structure, characteristics & modification. *Defence Science Journal*. 33.3, pp. 261–271.

Shea, K., Moreau, J., Loy, D., Corriu, R., Boury, B., Gomez-Romero, P., and Sanchez, C. (2004). Functional hybrid materials. *Edited by*.

Shi, X., Shi, Z., Wang, D., Ullah, M. W., and Yang, G. (2016). Microbial cells with a Fe3O4 doped hydrogel extracellular matrix: manipulation of living cells by magnetic stimulus. *Macromolecular Bioscience*. 16.10, pp. 1506–1514.

Shimizu, M., Miyamoto, K., Asano, T., Yoshinobu, T., Yawo, H., Ogura, T., Ishiguro, A., Hosoda, K., et al. (2013). Muscle tissue actuator driven with light-gated ion channels channelrhodopsin. *Procedia CIRP*. 5, pp. 169–174.

Singh, A. V. and Sitti, M. (2016). Patterned and specific attachment of bacteria on biohybrid bacteria-driven microswimmers. *Advanced healthcare materials*. 5.18, pp. 2325–2331.

Singh, R., Lin, Y.-T., Chuang, W.-L., and Ko, F.-H. (2017). A new biodegradable gate dielectric material based on keratin protein for organic thin film transistors. *Organic Electronics*. 44, pp. 198–209.

Slayman, C. L., Long, W. S., and Gradmann, D. (1976). "Action potentials" in Neurospora crassa, a mycelial fungus. *Biochimica et Biophysica Acta (BBA)-Biomembranes*. 426.4, pp. 732–744.

Stankovich, S., Dikin, D. A., Dommett, G. H., Kohlhaas, K. M., Zimney, E. J., Stach, E. A., Piner, R. D., Nguyen, S. T., and Ruoff, R. S. (2006). Graphene-based composite materials. *nature*. 442.7100, pp. 282–286.

Steinberg, M. S. (2007). Differential adhesion in morphogenesis: a modern view. *Current opinion in genetics & development*. 17.4, pp. 281–286.

Strubell, E., Ganesh, A., and McCallum, A. (2019). Energy and policy considerations for deep learning in NLP. *arXiv preprint arXiv:1906.02243*.

Su, Y., McCuskey, S. R., Leifert, D., Moreland, A. S., Zhou, L., Llanes, L. C., Vazquez, R. J., Sepunaru, L., and Bazan, G. C. (2021). A living biotic–abiotic composite that can switch function between current generation and electrochemical energy storage. *Advanced Functional Materials*. 31.6, p. 2007351.

Subbiahdoss, G., Osmen, S., and Reimhult, E. (2022). Cellulosic biofilm formation of Komagataeibacter in kombucha at oil-water interfaces. *Biofilm*. 4, p. 100071.

Suh, K. Y., Seong, J., Khademhosseini, A., Laibinis, P. E., and Langer, R. (2004). A simple soft lithographic route to fabrication of poly (ethylene glycol) microstructures for protein and cell patterning. *Biomaterials*. 25.3, pp. 557–563.

Suk, J. W., Piner, R. D., An, J., and Ruoff, R. S. (2010). Mechanical properties of monolayer graphene oxide. *ACS nano*. 4.11, pp. 6557–6564.

Sun, B., Xiao, M., Zhou, G., Ren, Z., Zhou, Y., and Wu, Y. (2020a). Non–zero-crossing current-voltage hysteresis behavior in memristive system. *Materials Today Advances*. 6, p. 100056.

Sun, T., Shi, Q., Liang, Q., Yao, Y., Wang, H., Sun, J., Huang, Q., and Fukuda, T. (2020b). Fabrication of vascular smooth muscle-like tissues based on self-organization of circumferentially aligned cells in microengineered hydrogels. *Lab on a Chip*. 20.17, pp. 3120–3131.

Surya, S. G., Raval, H. N., Ahmad, R., Sonar, P., Salama, K. N., and Rao, V. R. (2019). Organic field effect transistors (OFETs) in environmental sensing and health monitoring: A review. *TrAC Trends in Analytical Chemistry*. 111, pp. 27–36.

Swanson, R. A. and Holton, E. F. (2005). *Research in organizations: Foundations and methods in inquiry*. Berrett-Koehler Publishers.

Tanaka, N., Yamashita, T., Yalikun, Y., Amaya, S., Sato, A., Vogel, V., and Tanaka, Y. (2019). An ultrasmall fluid oscillation unit for pumping driven by self-organized three-dimensional bridging of pulsatile cardiomyocytes on elastic micro-piers. *Sensors and Actuators B: Chemical*. 293, pp. 256–264.

Tapias, Y. A. R., Di Monte, M. V., Peltzer, M. A., and Salvay, A. G. (2022). Bacterial cellulose films production by Kombucha symbiotic community cultured on different herbal infusions. *Food Chemistry*. 372, p. 131346.

Teague, B. P., Guye, P., and Weiss, R. (2016). Synthetic morphogenesis. *Cold Spring Harbor perspectives in biology*. 8.9, a023929.

Teichert, I., Steffens, E. K., Schnaß, N., Fränzel, B., Krisp, C., Wolters, D. A., and Kück, U. (2014). PRO40 is a scaffold protein of the cell wall integrity pathway, linking the MAP kinase module to the upstream activator protein kinase C. *PLoS genetics*. 10.9, e1004582.

Thomas, B., Raj, M. C., Joy, J., Moores, A., Drisko, G. L., and Sanchez, C. (2018). Nanocellulose, a versatile green platform: from biosources to materials and their applications. *Chemical reviews*. 118.24, pp. 11575–11625.

Thomson, D. D., Wehmeier, S., Byfield, F. J., Janmey, P. A., Caballero-Lima, D., Crossley, A., and Brand, A. C. (2015). Contact-induced apical asymmetry drives the thigmotropic responses of C andida albicans hyphae. *Cellular microbiology*. 17.3, pp. 342–354.

Tobjörk, D. and Österbacka, R. (2011). Paper electronics. *Advanced materials*. 23.17, pp. 1935–1961.

Torgbo, S. and Sukyai, P. (2018). Bacterial cellulose-based scaffold materials for bone tissue engineering. *Applied Materials Today*. 11, pp. 34–49.

Tran, T., Grandvalet, C., Winckler, P., Verdier, F., Martin, A., Alexandre, H., and Tourdot-Maréchal, R. (2021). Shedding light on the formation and structure of kombucha biofilm using two-photon fluorescence microscopy. *Frontiers in Microbiology*. 12, p. 725379.

Trebacz, K., Dziubinska, H., and Krol, E. (2006). Electrical signals in long-distance communication in plants. *Communication in plants: Neuronal aspects of plant life*, pp. 277–290.

Tulliani, J.-M., Inserra, B., and Ziegler, D. (2019). Carbon-based materials for humidity sensing: A short review. *Micromachines*. 10.4, p. 232.

Valentini, L., Bittolo Bon, S., Signetti, S., and Pugno, N. M. (2016a). Graphene-based bionic composites with multifunctional and repairing properties. *ACS Applied Materials & Interfaces*. 8.12, pp. 7607–7612.

Valentini, L., Bon, S. B., and Pugno, N. M. (2016). Microorganism nutrition processes as a general route for the preparation of bionic nanocomposites based on intractable polymers. *ACS Applied Materials & Interfaces*. 8.34, pp. 22714–22720.

Valentini, L., Bon, S. B., Signetti, S., Tripathi, M., Iacob, E., and Pugno, N. M. (2016b). Fermentation based carbon nanotube multifunctional bionic composites. *Scientific Reports*. 6.1, p. 27031.

Van Oss, C., Good, R., and Chaudhury, M. (1986). The role of van der Waals forces and hydrogen bonds in "hydrophobic interactions" between biopolymers and low energy surfaces. *Journal of colloid and Interface Science*. 111.2, pp. 378–390.

Vandermeulen, G. W. and Klok, H.-A. (2004). Peptide/protein hybrid materials: enhanced control of structure and improved performance through conjugation of biological and synthetic polymers. *Macromolecular Bioscience*. 4.4, pp. 383–398.

Vannozzi, L., Ricotti, L., Cianchetti, M., Bearzi, C., Gargioli, C., Rizzi, R., Dario, P., and Menciassi, A. (2015). Self-assembly of polydimethylsiloxane structures from 2D to 3D for bio-hybrid actuation. *Bioinspiration & biomimetics*. 10.5, p. 056001.

Vaswani, A., Shazeer, N., Parmar, N., Uszkoreit, J., Jones, L., Gomez, A. N., Kaiser, Ł., and Polosukhin, I. (2017). Attention is all you need. *Advances in neural information processing systems*. 30.

Vega, K., Kalkum, M., et al. (2012). Chitin, chitinase responses, and invasive fungal infections. *International journal of microbiology*. 2012.

Vert, M., Doi, Y., Hellwich, K.-H., Hess, M., Hodge, P., Kubisa, P., Rinaudo, M., and Schué, F. (2012). Terminology for biorelated polymers and applications (IUPAC Recommendations 2012). *Pure and Applied Chemistry*. 84.2, pp. 377–410.

Vitta, S. and Thiruvengadam, V. (2012). Multifunctional bacterial cellulose and nanoparticle-embedded composites. *Current science*, pp. 1398–1405.

Vlamakis, H., Aguilar, C., Losick, R., and Kolter, R. (2008). Control of cell fate by the formation of an architecturally complex bacterial community. *Genes & development*. 22.7, p. 945.

Volkov, A. and Markin, V. (2017). Electrochemistry of Gala apples: Memristors in vivo. *Russian Journal of Electrochemistry*. 53, pp. 1011–1018.

Volkov, A. G., Tucket, C., Reedus, J., Volkova, M. I., Markin, V. S., and Chua, L. (2014). Memristors in plants. *Plant signaling & behavior*. 9.3, e28152.

Walker, K. T., Goosens, V. J., Das, A., Graham, A. E., and Ellis, T. (2019). Engineered cell-to-cell signalling within growing bacterial cellulose pellicles. *Microbial biotechnology*. 12.4, pp. 611–619.

Wan, X., Volpetti, F., Petrova, E., French, C., Maerkl, S. J., and Wang, B. (2019). Cascaded amplifying circuits enable ultrasensitive cellular sensors for toxic metals. *Nature chemical biology*. 15.5, pp. 540–548.

Wang, G., Yang, J., Park, J., Gou, X., Wang, B., Liu, H., and Yao, J. (2008). Facile synthesis and characterization of graphene nanosheets. *The Journal of Physical Chemistry C*. 112.22, pp. 8192–8195.

Wang, J., Van Tittelboom, K., De Belie, N., and Verstraete, W. (2012). Use of silica gel or polyurethane immobilized bacteria for self-healing concrete. *Construction and building materials*. 26.1, pp. 532–540.

Wang, J. (2005). Carbon-nanotube based electrochemical biosensors: A review. *Electroanalysis: An International Journal Devoted to Fundamental and Practical Aspects of Electroanalysis*. 17.1, pp. 7–14.

Wang, L., Zhang, Q., Chen, S., Xu, F., Chen, S., Jia, J., Tan, H., Hou, H., and Song, Y. (2014). Electrochemical sensing and biosensing platform based on biomass-derived macroporous carbon materials. *Analytical chemistry*. 86.3, pp. 1414–1421.

Wang, L., Lou, Z., Wang, K., Zhao, S., Yu, P., Wei, W., Wang, D., Han, W., Jiang, K., and Shen, G. (2020). Biocompatible and biodegradable functional polysaccharides for flexible humidity sensors. *Research*.

Wang, W. and Yao, e. a. (2017). Harnessing the hygroscopic and biofluorescent behaviors of genetically tractable microbial cells to design biohybrid wearables. *Science advances*. 3.5, e1601984.

Wang, X., Kong, D., Zhang, Y., Wang, B., Li, X., Qiu, T., Song, Q., Ning, J., Song, Y., and Zhi, L. (2016). All-biomaterial supercapacitor derived from bacterial cellulose. *Nanoscale*. 8.17, pp. 9146–9150.

Wang, Y., Wu, H., Wang, Z., Zhang, J., Zhu, J., Ma, Y., Yang, Z., and Yuan, Y. (2019). Optimized synthesis of biodegradable elastomer pegylated poly (glycerol sebacate) and their biomedical application. *Polymers*. 11.6, p. 965.

Wang, Y., Liu, Y., Li, J., Chen, Y., Liu, S., and Zhong, C. (2022). Engineered living materials (ELMs) design: From function allocation to dynamic behavior modulation. *Current Opinion in Chemical Biology*. 70, p. 102188.

Wannatong, L. and Sirivat, A. (2008). Polypyrrole and its composites with 3A zeolite and polyamide 6 as sensors for four chemicals in lacquer thinner. *Reactive and Functional Polymers*. 68.12, pp. 1646–1651.

Warraich, Z. and Kleim, J. A. (2010). Neural plasticity: the biological substrate for neurorehabilitation. *Pm&r*. 2.12, S208–S219.

Watson, K. and Arthur, H. (1977). Cell surface topography of Candida and Leucosporidium yeasts as revealed by scanning electron microscopy. *Journal of Bacteriology*. 130.1, pp. 312–317.

Webb, J. S., Givskov, M., and Kjelleberg, S. (2003). Bacterial biofilms: prokaryotic adventures in multicellularity. *Current opinion in microbiology*. 6.6, pp. 578–585.

Weng, Z., Liu, W., Yin, L.-C., Fang, R., Li, M., Altman, E. I., Fan, Q., Li, F., Cheng, H.-M., and Wang, H. (2015). Metal/oxide interface nanostructures generated by surface segregation for electrocatalysis. *Nano letters*. 15.11, pp. 7704–7710.

Wood, T. K., Hong, S. H., and Ma, Q. (2011). Engineering biofilm formation and dispersal. *Trends in biotechnology*. 29.2, pp. 87–94.

Xie, S., Jiao, N., Tung, S., and Liu, L. (2016). "Novel algae guiding system to robotize algae cells". In: *2016 IEEE International Conference on Manipulation, Manufacturing and Measurement on the Nanoscale (3M-NANO)*. IEEE, pp. 64–68.

Xie, X., Yu, G., Liu, N., Bao, Z., Criddle, C. S., and Cui, Y. (2012). Graphene–sponges as high-performance low-cost anodes for microbial fuel cells. *Energy & Environmental Science*. 5.5, pp. 6862–6866.

Yamamoto, M., Fujishita, M., Hirata, A., and Kawano, S. (2004). Regeneration and maturation of daughter cell walls in the autospore-forming green alga Chlorella vulgaris (Chlorophyta, Trebouxiophyceae). *Journal of plant research*. 117, pp. 257–264.

Yamamoto, M., Kurihara, I., and Kawano, S. (2005). Late type of daughter cell wall synthesis in one of the Chlorellaceae, Parachlorella kessleri (Chlorophyta, Trebouxiophyceae). *Planta*. 221, pp. 766–775.

Yan, T., Wang, Z., and Pan, Z.-J. (2018). Flexible strain sensors fabricated using carbon-based nanomaterials: A review. *Current Opinion in Solid State and Materials Science*. 22.6, pp. 213–228.

Yan, Z., Chen, S., Wang, H., Wang, B., and Jiang, J. (2008). Biosynthesis of bacterial cellulose/multi-walled carbon nanotubes in agitated culture. *Carbohydrate Polymers*. 74.3, pp. 659–665.

Yáñez-Sedeño, P., Agüí, L., Villalonga, R., and Pingarrón, J. (2014). Biosensors in forensic analysis. A review. *Analytica chimica acta*. 823, pp. 1–19.

Yáñez-Sedeño, P., Agüí, L., Campuzano, S., and Pingarrón, J. M. (2019). What electrochemical biosensors can do for forensic science? Unique features and applications. *Biosensors*. 9.4, p. 127.

Yang, C., Aslan, H., Zhang, P., Zhu, S., Xiao, Y., Chen, L., Khan, N., Boesen, T., Wang, Y., Liu, Y., et al. (2020). Carbon dots-fed Shewanella oneidensis MR-1 for bioelectricity enhancement. *Nature communications*. 11.1, p. 1379.

Yang, G.-Z., Bellingham, J., Dupont, P. E., Fischer, P., Floridi, L., Full, R., Jacobstein, N., Kumar, V., McNutt, M., Merrifield, R., et al. (2018). The grand challenges of science robotics. *Science robotics*. 3.14, eaar7650.

Yano, S., Maeda, H., Nakajima, M., Hagiwara, T., and Sawaguchi, T. (2008). Preparation and mechanical properties of bacterial cellulose nanocomposites loaded with silica nanoparticles. *Cellulose*. 15, pp. 111–120.

Yi, Z., Lian, J., Liu, Q., Zhu, H., Liang, D., and Liu, J. (2023). Learning rules in spiking neural networks: A survey. *Neurocomputing*. 531, pp. 163–179.

Yokoi, T. (2016). Characterization of zeolites by advanced SEM/STEM techniques. *SI News*. 7, pp. 17–23.

Yong, Y.-C., Yu, Y.-Y., Zhang, X., and Song, H. (2014). Highly active bidirectional electron transfer by a self-assembled electroactive reduced-graphene-oxide-hybridized biofilm. *Angewandte Chemie International Edition*. 53.17, pp. 4480–4483.

Yuan, X., Wei, Y., Chen, S., Wang, P., and Liu, L. (2016). Bio-based graphene/sodium alginate aerogels for strain sensors. *RSC advances*. 6.68, pp. 64056–64064.

Yuan, Y., Zhou, S., Yang, G., and Yu, Z. (2013). Electrochemical biomemory devices based on self-assembled graphene–Shewanella oneidensis composite biofilms. *RSC advances*. 3.41, pp. 18844–18848.

Zelter, A., Bencina, M., Bowman, B. J., Yarden, O., and Read, N. D. (2004). A comparative genomic analysis of the calcium signaling machinery in Neurospora crassa, Magnaporthe grisea, and Saccharomyces cerevisiae. *Fungal Genetics and Biology*. 41.9, pp. 827–841.

Zhang, K., Zhang, L. L., Zhao, X., and Wu, J. (2010). Graphene/polyaniline nanofiber composites as supercapacitor electrodes. *Chemistry of Materials*. 22.4, pp. 1392–1401.

Zhao, X., Zhang, Q., Chen, D., and Lu, P. (2010). Enhanced mechanical properties of graphene-based poly (vinyl alcohol) composites. *Macromolecules*. 43.5, pp. 2357–2363.

Zheng, Y., Li, X., and Dutta, P. K. (2012). Exploitation of unique properties of zeolites in the development of gas sensors. *Sensors*. 12.4, pp. 5170–5194.

Zhou, Y., Kong, D., Wang, X., Yu, G., Wu, X., Guan, N., Weber, W., and Ye, H. (2022). A small and highly sensitive red/far-red optogenetic switch for applications in mammals. *Nature Biotechnology*. 40.2, pp. 262–272.

Zhu, B., Wang, H., Leow, W. R., Cai, Y., Loh, X. J., Han, M.-Y., and Chen, X. (2016). Silk fibroin for flexible electronic devices. *Advanced Materials*. 28.22, pp. 4250–4265.

Zhu, L., Dong, S., Li, J., Huang, T., and Tian, Y. (2022). Ultra-high temporal resolution visual reconstruction from a fovea-like spike camera via spiking neuron model. *IEEE Transactions on Pattern Analysis and Machine Intelligence*. 45.1, pp. 1233–1249.

Zhuang, J., Park, B.-W., and Sitti, M. (2017). Propulsion and chemotaxis in bacteria-driven microswimmers. *Advanced Science*. 4.9, p. 1700109.

Zimmermann, M. R. and Mithöfer, A. (2013). Electrical long-distance signaling in plants. *Long-distance systemic signaling and communication in plants*, pp. 291–308.

Zschieschang, U., Yamamoto, T., Takimiya, K., Kuwabara, H., Ikeda, M., Sekitani, T., Someya, T., and Klauk, H. (2011). Organic electronics on banknotes. *Advanced Materials*. 23.5, pp. 654–658.